PETROLEUM RESEARCH JOURNAL

Journal of the
Libyan Petroleum Institute
Tripoli
State of Libya

NATIONAL OIL CORPORATION
LIBYAN PETROLEUM INSTITUTE

Chairman
DR. MANSOUR EMTIR

Editor-in-Chief
MAHMOUD T. ELBAKAI

Associate Editors
MOHAMMED S. ELBOUSAIFI
AMMAR M. GAMMUDI
OMAR A. MKHATRESH

Co-ordinator
ABDULMAGID A. ELMRYED

TECHNICAL PAPERS

A Case Study of Reservoir Souring Despite Injection of Low-sulphate Seawater 1

Tidal Influnced Eocene Deposits of Dur At Talah (Libya) Compared with Present Day Tidal Sediments from the Bay of MT St Michel (France)..... 13

Triassic and Creataceouse Palynomorphose from Well A2-045 /01 Offshore Libya 33

Systematic Description Ostracods Fauna from the Lower Tar Member (Zimam Formation) Northern Ghadamis Basin 41

Palynological Analysis of cutting samples from Well: A1-177/01, Murzuq Basin .. 67

Magnetic Data for Delineating Subsurface Structures and Estimating Magnetic Sources Depth of Magnetic Intrusive in Farigh Area, Sirt Basin 85

Petroleum System and Play Concept in the Area 113-3&4, Southern Margin of the Ghadames Basin, Libya 95

Geochemical Evaluation of Thermal Maturity and Depositional Palaeoenvironment of Seven Cretaceous Formations from the East Sirt Basin, Libya 107

Effect of Pore Geometry on Reservoir Rock Properties 119

Log Derived Saturation Functions for Giant Carbonate Reservoirs in the Middle East 125

Predication of Shear Velocity at Shaly Sand Reservoir Rock 129

Neural Network Approach to Predict Average Reservoir Pressure 137

Analytical Study for Physicochemical Characteristics of Bentonite Clay in Libya 143

Evaluation of the Total Quality Factors Based on Deming Management Model in Oil Industry in Libya - An Empirical Study 153

Effect of Plastic Deformation on the Corrosion Behavior of Super1Duplex Stainless Steel 163

Incompatibility of Injection Water with Formation Waters from Different Depths 171

TQM Implementation in Libyan Oil and Gas Sector 179

Characterization of Post-Pyrolysis Tyre Char as a pigment in Aqueos Ink-Jet Printing Inks: Using Different Analytical and Spectroscopy Technique 191

Rheology and Pipeline Start up Pressure of Raguba Crude Oil 195

Study of Paraffin Wax Effect on Base oil flow Behavior 205

Thermodynamic Analysis for Nitric Acid Plant 215

A Study of Precipitation and Flocculation of Calcium Carbonate and Magnesium Hydroxide in Alkaline Flooding 221

A Case Study of Reservoir Souring Despite Injection of Low-sulphate Seawater

Keith Robinson* and Eivind Samuelsen**

Abstract: The use of sulphate rejection membrane (SRM) technology to generate low-sulphate seawater (LSSW) for water injection is becoming more commonplace, primarily to avoid severe barium sulphate scaling problems but it is also being increasingly applied to avoid reservoir souring.

This paper presents some operational data and results of an investigation into hydrogen sulphide appearance in Hess's South Arne production facilities. The field produces from a 115°C chalk reservoir, and is located in the Danish sector of the North Sea.

In addition to achieving the primary objective of barium sulphate scaling control, 10 years of historical data from South Arne show that the injection of LSSW also significantly reduced the severity of reservoir souring to levels acceptable for the metallurgy used in the field's wells and production facilities. This is important information for oilfields in general, and especially for deep-sea fields where high-strength steel risers must be used, but which are susceptible to sulphide stress corrosion cracking.

Despite using SRM technology since December 2000, South Arne production facilities saw increasing concentrations of H_2S in late 2008, up to 15 ppm in the bulk gas and 35 ppm in gas from individual wells. Analyses of the produced water's ionic composition and H_2S concentrations in oil, water and gas showed that approximately 50% of the remaining sulphate introduced into the reservoir in the injection water was converted to H_2S.

Stable isotope measurements of sulphide in H_2S were consistent with sulphate-reducing prokaryotes metabolizing a high proportion of the available sulphate. Molecular microbiological methods (MMM) showed high concentrations of sulphate-reducing archaea (a group of thermophilic microorganisms producing H_2S, but genetically very different to sulphate-reducing bacteria) present in the produced fluids.

Although some H_2S was produced, despite use of LSSW from the very beginning of water injection, one study conclusion was that the residual microbiological sulphate reduction may have minimized the field's barium sulphate scaling risk by lowering the sulphate concentrations in the waterflood water below those achievable by SRM alone.

Overall, the use of SRM to enable injection of LSSW was very successful in the control of potentially severe barium sulphate scaling and reservoir souring, although not entirely eliminating souring.

Keywords: Reservoir Souring, Low Sulphate Sea Water, Barium Sulphate Scaling, Molecular Microbiology, Sulphate Reducing Prokaryotes, Nano-filtration

INTRODUCTION

The South Arne Field is located in the North Western area of the Danish North Sea, and is operated by Hess Denmark. The oil reservoir is in the Tor and Ekofisk chalk formations, at approximately 115°C reservoir temperature.

The field development plan changed significantly as more reservoir data became available, beginning in 1997 with a depletion case, but with an option to install seawater injection for secondary oil recovery, and that option was decided upon in 1998. However the inorganic scale risks were unknown at that time due to very limited sampling of the formation water, and also because the high barium and strontium contents of the formation water were unexpected since they did not occur in any other Danish chalk reservoirs, even one as close as 5 km away. In 1999, new wells showed very high barium and strontium concentrations in the formation water samples and so the decision was made to install a sulphate-removal plant to treat the injection seawater.

*Oil Plus Ltd, Dominion House, Kennet Side, Newbury, Berkshire, RG14 5PX, England. E-mail: k.robinson@oilplus.co.uk
**Hess Corporation

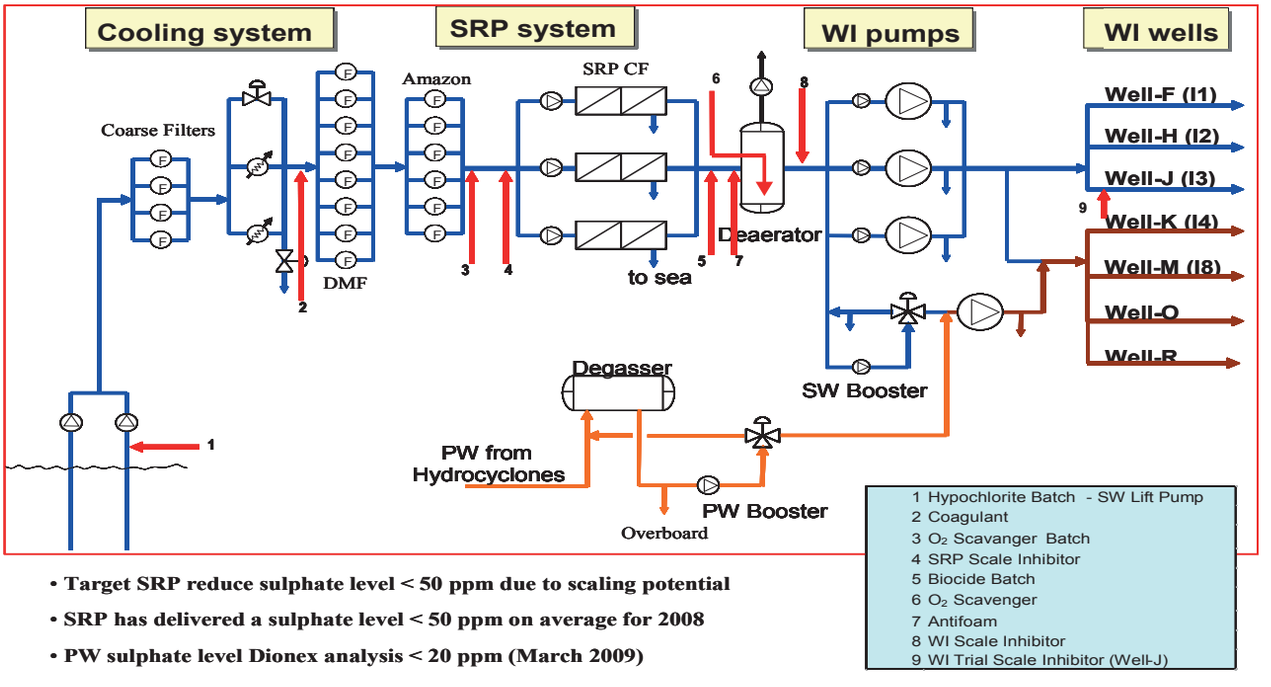
The sequential decisions and the limited platform space available had an impact on the seawater treatment process train in that the sulphate-removal unit (SRU) had to be installed upstream of the deaerator, rather than downstream which is more common, although there are advantages and disadvantages to both options, as described further below.

Water injection began in 2000 using de-sulphated seawater, sometimes described as low-sulphate seawater (LSSW), from the onset, but as produced water became available this was sent to separate injection wells, to those injecting LSSW, although now (2010) all wells receive a mixture of treated produced water and deaerated LSSW. The sequence of events was that LSSW injection commenced in December 2000, initially into the northern area of the field, then in mid-2001 into the southern area. A produced water re-injection (PWRI) trial began in 2004 into a southern area well and, as this was successful, PWRI was extended into all southern area wells, and then into all wells in mixture with deaerated LSSW in 2009; see Fig. 1 (Robinson *et al* 2010).

Sulphate removal from seawater is used primarily to reduce the risk of barium and strontium sulphate scale precipitation, which could result from mixture of normal-sulphate seawater with the formation/produced water, and that is a notably high risk with South Arne formation water due to its barium ion concentration of approx. 900 mg/l, and a similar strontium concentration (approx. 800mg/l). The LSSW would also reduce any risks of calcium sulphate scales (gypsum and/or anhydrite) and of calcium carbonate too as the membrane process also removes some of the natural bicarbonate ion from the seawater.

Initial oil and gas production, which began in 1999, was sweet (<3 ppm H_2S in gas) but increased concentrations of H_2S have been observed recently, starting in late 2008, although routine monitoring was not comprehensive in the years between, until a high value was reported during one offloading operation from the platform's oil storage tank to the shuttle tanker. That high value was speculated to be either a result of microbial activity within the oil storage tank, or within the topsides process train, or from reservoir souring associated with seawater injection. All three possibilities could involve sulphate-reducing bacteria (SRB) and/or sulphate-reducing archaea (SRA), together identified as sulphate-reducing prokaryotes (SRP) (Larsen *et al* 2009). The implementation of sulphate-removal can be expected to greatly the reduce the potential for reservoir souring (Alkindi *et al* 2007, and Walsh *et al* 2008), but may not entirely prevent it, depending on the level of sulphate reduction achieved by the sulphate rejection membranes (SRM) in the sulphate removal unit (SRU).

In addition to reservoir souring, the possibilities of H_2S generation by SRP in the topsides vessels,



- **Target SRP reduce sulphate level < 50 ppm due to scaling potential**
- **SRP has delivered a sulphate level < 50 ppm on average for 2008**
- **PW sulphate level Dionex analysis < 20 ppm (March 2009)**

Fig. 1. Process flow diagram for the South Arne Water Injection System Showing the Points of Chemical Injection

pipe-work and process vessels had been suggested as contributory factors to the observed H_2S concentrations in produced fluids. Oil is stored in a concrete tank which forms the 'gravity base system' (GBS) of the platform, located on the seabed. In this, the stored crude oil is supported from below by (ballast) seawater, and is open to the sea such that 'new' seawater enters below the oil while oil is being offloaded to tanker (ship), typically every 20 days. The 'new' seawater is chlorinated, but not otherwise treated, as it enters the GBS system. That water is then displaced back to sea as the storage tank then gradually refills with oil from the production wells/ topside separation train. There were some concerns about H_2S development in the GBS, contributing to H_2S in the export oil

Twelve oil production wells are operated, each with gas-lift, using field (export) gas which contains low concentrations of H_2S, as the majority of the H_2S has been removed from the separated produced gas by liquid H_2S scavenger: see Fig. 2. The oil producing wells all have horizontal completion sections, some 2-3 km long from toe to heel, and all were acid-fractured for stimulation and with proppant injected.

In light of the above, Hess Denmark initiated a study with the primary objectives of determining the source(s) of the H_2S and its behaviour through the system. The study included an 8-day visit to South Arne in 2009 to sample a full round of production well tests and a tanker offload, and some key results are reported herein, with more details in reference papers (Lundgaard *et al* 2010; Robinson *et al* 2010).

SULPHATE REMOVAL PROCESS

The use of membrane filters, which are often described as nano-filters (NF) since they are intended to filter water down to nanometre specifications (10^{-9} m, or 0.001 micrometres), has been practiced in the offshore oil industry for over 20 years, since the first application on Marathon Brae platform in the North Sea in 1988, using membranes manufactured by Dow. That application was used, successfully, to prevent a severe barium sulphate scale problem developing in the oil production wells and topside facilities upon breakthrough of injected seawater along with formation/produced water. Since then over 50 offshore platforms and FPSOs are operating with SRUs (Walsh *et al* 2008), primarily to prevent that same scale problem, but also, and increasingly, to prevent or greatly limit the development of reservoir souring in sweet, deep-water oilfields, in which very high strength risers are required, as they

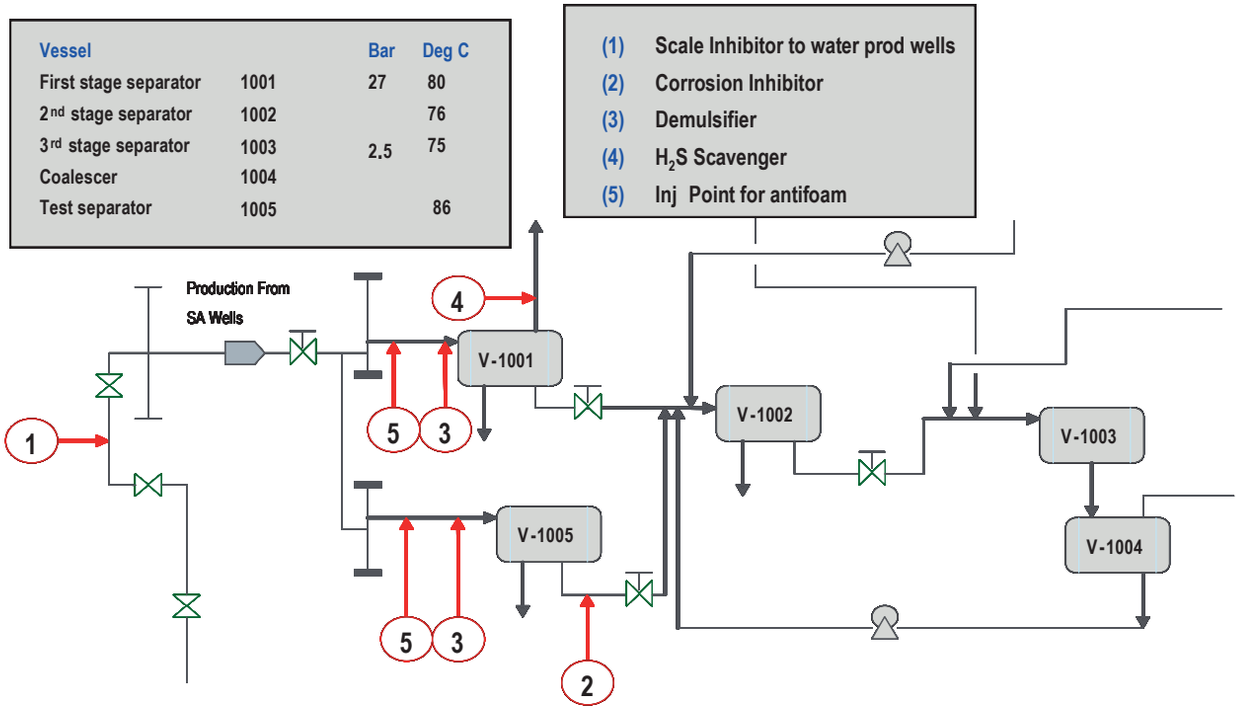


Fig. 2. Process flow diagram for the South Arne Production System Showing the Points of Chemical Injection

may be particularly susceptible to sulphide stress corrosion cracking (SSCC).

Although the South Arne field is not located in very deep seawater, concerns over SSCC and other forms of corrosion involving H_2S still apply, for wells, risers, topside process trains, oil storage GBS, and oil and gas export routes.

The nano-filters are highly selective for removal (rejection) of relatively large dissolved ions such as sulphate (SO_4^{2-}), which has 5 atoms and is divalent, whilst allowing through the smaller mono-element, monovalent ions sodium (Na^+) and chloride (Cl^-). Thus the filtered seawater is not desalinated but has a much lowered sulphate content, reduced from approx. 2800 mg/l typical of oceanic seawater to around 20 – 50 mg/l. The process is similar to the more widely known reverse osmosis, using spiral-wound membranes, but with a more permeable, larger pore size, and so the SRM can be operated at a lower feed pressure and higher flux rates than can RO membranes. That makes the process cost-effective and practicable for treatment of oilfield injection seawater in cases of very high barium sulphate ($BaSO_4$) and/or strontium sulphate ($SrSO_4$) scale potentials (Vu *et al* 2000).

In addition to removing almost all of the sulphate from seawater, the NF membranes also remove some of the other large or divalent ions which are naturally present in seawater, i.e. bicarbonate (HCO_3^-), calcium (Ca^{2+}) and magnesium (Mg^{2+}), and that may also be helpful in reducing the scaling potential of seawater injected into a hot oil reservoir, particularly of calcium carbonate, $CaCO_3$.

The field cases using SRUs to mitigate reservoir souring alone are relatively recent, but where their use can greatly reduce the potentials for both severe $Ba/SrSO_4$ scaling and reservoir souring too, then their inclusion in the seawater treatment process train is logical, as was the case for South Arne. However, it must be appreciated that there may still remain some potential for both the $BaSO_4$ scale, since it is extremely insoluble in water (only a few mg/l) and the 20 – 50 mg/l SO_4^{2-} residual typically achieved in the LSSW is sufficient to cause both some precipitation of it and perhaps also leave some SO_4^{2-} available for bacterial conversion to sulphide (HS^-/H_2S). As will be seen later in this paper, the two mechanisms may be competitive for the remaining sulphate ion in the LSSW in this case.

On South Arne, the LSSW sulphate ion concentration is rather higher than that reported on some other platforms, at ~ 50 mg/l, for a variety of reasons. In part, this stemmed from the need to install the SRU upstream of the deaerator which meant that, in effect, additional sulphate is added to the SRU-treated LSSW by way of injecting ammonium bisulphite oxygen scavenger into the deaerator to chemically remove any dissolved oxygen remaining after the vacuum stripping stage. The ammonium ion part of the oxygen scavenger also stays in the injection water going to the wells and reservoir. Had it been possible to install the SRU downstream of the deaerator then those ions (ammonium, excess bisulphite and sulphate formed from reaction of bisulphite ion with any dissolved oxygen remaining after vacuum stripping) would largely have been removed too. However, locating a deaerator upstream of the SRU does require the deaerator to be rated for approx. 33% greater water flow-rate to allow for the 25% reject (concentrate) stream of the SRU. That reject stream is necessary to keep the membrane units functioning correctly by carrying away, back to sea, the rejected sulphate ions plus the other large/divalent (scaling) ions and any suspended solids remaining in the water after the upstream filter stages.

Fig. 1 shows that on South Arne the upstream filters are coarse filters followed by DMF, which means Dual Media Filters (e.g. deep beds of anthracite granules above granules of fine garnet) and then a bank of (Amazon) disposable cartridge filters. Such a train of filtration is common where SRU are installed, because the membranes in the SRU are very prone to blockage if the feed water is not very clean, despite the cross-flow design (across the membrane's surface) being intended to carry away any remaining filterable suspended solids.

Fig. 1 also shows batch injection of sodium hypochlorite (for chlorination of the feed water as a primary control chemical for macro- and micro-organisms) which is somewhat unusual, as most water injection systems have continuous chlorination from on-board electrochlorinators. As the SRM are not tolerant at all to a strong oxidizing chemical such as chlorine/hypochlorite, the water must be de-chlorinated prior to contacting the membranes, and some ammonium bisulphite oxygen scavenger is injected for that purpose: it reacts more quickly with hypochlorite to remove it than it does with dissolved oxygen. As the hypochlorite is batch-injected, in this particular system, then so too must be the oxygen scavenger (but downstream, into the deaerator itself, there the main dose of oxygen scavenger is continuously injected).

MICROBIAL CONVERSION OF SULPHATE TO SULPHIDE

For decades it has been well known that sulphate-reducing prokaryotes (SRP) can, under favorable conditions, convert sulphate ion to hydrogen sulphide, and those conditions do exist in many oil reservoirs, as well as pipelines, storage tanks, tankers, etc.(Ollivier and Magot, 2005; Barton and Hamilton, 2007). However, culture-based methods of traditional microbiology (i.e. most probable number, MPN) applied to the microbiological processes involved in oilfield reservoir souring pose a threat of yielding inadequate and contradictory results (Larsen *et al* 2005). For that reason molecular microbiological methods (MMM) were applied in this study and showed high concentrations of sulphate-reducing archaea (SRA) in produced fluids while the traditional MPN techniques gave zero readings (Lundgaard *et al* 2010). It is generally accepted that any cultivation step, in bacterial analysis procedures, will, almost certainly, alter the population characteristics and thus the results upon which any evaluation will be based. Therefore, enumeration of microbes via the MPN method alone and decisions made based upon those results should be taken with great care (Skovhus *et al* 2007).

The general key chemical reactions responsible for souring and their stoichiometries are summarised below, where acetate, propionate and butyrate are volatile fatty acid (VFA) anions dissolved in the water phase, and which are the main carbon sources utilised by SRP (SRA and SRB) in reservoir souring.

$CH_3COO^- + SO_4^{2-} \rightarrow S^{2-} + H_2O + CO_2 + HCO_3^-$
Acetate
i.e. 1 acetate, 59 mg → 1 sulphide, 32 mg

$4CH_3CH_2COO^- + 7SO_4^{2-} \rightarrow 7S^{2-} + 12H_2O + 12CO_2$
Propionate
i.e. 1 propionate, 73 mg → 1.75 sulphide, 56 mg

$2CH_3(CH_2)_2COO^- + 5SO_4^{2-} \rightarrow 5S^{2-} + 8H_2O + 8CO_2$
Butyrate
i.e. 1 butyrate, 85 mg → 2.5 sulphide, 80 mg

Somewhat confusingly, VFAs are also known as non-volatile weak acids (NVWA), and in chemical terminology are all carboxylic acids or carboxylate ions from the -COO^- ending. The anions, such as acetate, will not be volatile at all, and so describing these nutrient carbon compounds as VFAs can be very misleading to those not versed in the subject as they are neither acids nor are they volatile, unless at much more acidic pH values than in oilfield waters. So, acetate, etc., anions should really be referred to as a NVWAAs, but most practitioners of oilfield microbiology and production chemistry realize what is meant when VFAs are mentioned.

HOW MUCH SULPHIDE COULD BE PRODUCED?

There were indications that the South Arne reservoir fluids contained a trace of H_2S from the very beginning of production in 1999, but at <3 ppm in the produced gas it was considered to be 'sweet'. It is possible that the traces of H_2S were erroneous measurements, or were as a result of minor contamination of the produced well(s) at the drilling stage (with some sulphate and SRP introduced in drilling fluids, say), or could have been falsely low readings as a consequence of somewhat higher natural reservoir H_2S reacting with the newly installed steel well tubulars. However, H_2S scavenger has been in continuous use since 2000 and its use may have masked any increases in H_2S concentrations because the gas export flow-rate has also decreased over that period, as described in the South Arne Results section below.

Since 2008, however, there has been a clear increase in H_2S concentrations, despite the installed SRU operating fully since the beginning of water injection. There was, therefore, a need to identify the source(s) of the H_2S and quantify the potential for further increases in produced fluids, and also in the export oil from the 'raw' seawater-displaced oil storage tank, especially as an export shuttle tanker had reported high H_2S concentrations in headspace gas.

Looking at how much H_2S could theoretically develop in the produced fluids, simple stoichiometry of sulphate to sulphide (a 3:1 molecular weight ratio, i.e. 96 → 32) shows the following maxima, in the water as that is where the microbes grow:

SO_4^{2-}	→	**S^{2-}**
MW 96	→	MW 32
e.g. 2840 mg/l	→	947 mg/l
or 25 mg/l	→	8.3 mg/l
or 50 mg/l	→	16.6 mg/l

These concentrations can be achieved in water provided that:

- There are no nutrient limits (assimilable carbon

e.g. acetate / propionate, N, P, trace elements);
- There is no temperature restriction (e.g. reservoir is too hot for SRP);
- There is no pressure restriction (e.g. reservoir pressure is not too high);
- There are no sulphide 'sinks' or scavenger minerals in the reservoir rocks (e.g. siderite, $FeCO_3$, or adsorbent clays);
- The generated sulphide has not reached a self-toxic limit to SRB and SRA;
- No souring control chemicals have been added (e.g. biocides, nitrate);
- Relevant strains of SRB and SRA are in place, and;
- 100% conversion of sulphate to sulphide.

It is also necessary to consider the varying mixtures of the seawater, whether full-sulphate or LSSW, with the reservoir formation water. This is because the seawater will be nutrient-limited (especially carbon) and so the reactions basically rely on obtaining nutrients from the formation water, via mixing/dilution, in order to obtain any assimilable carbon ,e.g. acetate, propionate, etc.

Nevertheless, if we use the 16.6 mg/l S^{2-} value from above (maximum generated from 50 mg/l SO_4^{2-}), how will that translate into an H_2S in gas concentration, as that is often the key parameter that operators often have limits on – rightly or wrongly, as from a corrosion perspective it is actually in the water phase that H_2S is corrosive, including SSCC.

As noted above, the microbial H_2S is generated in the water phase (injection water alone or mixture of injection and formation waters), but in passage through an oil zone in the reservoir there will be some exchange, or partitioning, of H_2S into the oil, and/or partitioning will occur in the oil production well(s), flowlines, and surface/topside separation vessels. The amount of partitioning will depend upon pH, pressure, temperature, salinity (or Total Dissolved Salts, TDS) and oil & gas compositions, and the relative proportions of the three phases, i.e. gas: oil ratio (GOR) and water: oil ratio (WOR). The pH effect is very significant, and occurs because H_2S ionises, reversibly, in the water, i.e.:

$$H_2S \Leftrightarrow H^+ + HS^- \Leftrightarrow 2H^+ + S^{2-}$$

At lower pH values, <7, the reactions are 'driven' (as in Le Chatelier's Principle) to the left-hand side of this equation, because of the increased concentration of H^+ ions at lower pH, and that increases the partitioning of H_2S into the oil and gas phases, since ions can only exist in a water phase but molecular H_2S can dissolve in oil and transfer into gas.

The SRP generate the sulphide from sulphate absorbed into their cells, via specific pores in the cell membrane. Enzymes within the cells convert sulphate ions to sulphide ions, and the cells then 'pump out' the sulphide ions, again via pores in the cell membrane. Some fractionation of sulphur atoms occurs, from the absorbed sulphate ion, due to slightly more frequent binding by the enzymes to the lighter isotope ^{32}S, compared to the slightly heavier ^{34}S, such that the generated sulphide is slightly enriched in the lighter isotope ^{32}S. Conversely the generated sulphide is slightly depleted in ^{34}S, and this is often expressed in $\delta^{34}S$ ($^{o}/_{oo}$ vs CDT), i.e. parts per thousand relative to that found in the standard material of the Canon Diablo Troilite (a meteorite), and so bacterially produced H_2S is typically negative on this scale, often ranging from 0 to -40 $^{o}/_{oo}$ $\delta^{34}S$, which compares to the sulphur in sulphate of oceanic water at +20 $^{o}/_{oo}$ $\delta^{34}S$. This 'signature' can be a useful, but not necessarily conclusive, indicator that the detected H_2S was generated by SRP rather than being of geological origin. The considerable variation in the microbially generated $\delta^{34}S$ is dependent, in part, on the starting water's sulphate ion concentration (Sharp, 2007) as an excess of sulphate ion leads to a slow reaction rate and a larger fractionation, i.e. more negative $\delta^{34}S$, whereas when sulphate is limited then the sulphur isotope fractionation will be smaller. Other factors such as temperature, nutrients, types of microbes, etc., doubtless have an influence too. The low sulphate content in LSSW may result in a $\delta^{34}S$ signature in SRP-generated H_2S which is different to that from oceanic seawater, but any value below zero is well below the +20 $^{o}/_{oo}$ $\delta^{34}S$ value of seawater and so a strong indicator of any H_2S being of microbial origin. However it should also be recognised that if all the sulphate in the original water was converted to sulphide then the total sulphide must have the same $\delta^{34}S$ as the starting water, or +20 $^{o}/_{oo}$ $\delta^{34}S$ for oceanic (including North Sea) water.

The pH of the water outside of the SRP cells then governs how much stays as S^{2-}, or ionises to HS^- or forms molecular H_2S, or, indeed, precipitates as FeS, say, or converts $FeCO_3$ to FeS or FeS_2. The water pH will depend almost entirely on the natural pH values of the water in that local environment, be that deaerated LSSW, formation water, or those two waters in various mixture ratios within the oil reservoir pores or fracture network, or in the

produced water or the ballast seawater in the GBS, say. Furthermore, some H_2S, and only the molecular H_2S but not ionic S^{2-} or HS^- , may partition into any hydrocarbon phases present, i.e. oil and/or gas, either locally near the SRP or more distantly wherever the sulphidic water and oil/gas come together, e.g. in the producing wells and oil/gas/water separation process train.

The concentrations of H_2S in gas, which is often the high-focus parameter in any oilfield, depend very strongly on the relative volumes of gas, oil and water, plus physico-chemical parameters such as partitioning coefficients, pressures and temperatures, To illustrate the effects of gas: oil ratio (GOR) alone on H_2S in gas concentrations consider the following example, which has used water, oil and gas compositions not detailed here:

The following conditions were used in a proprietary H_2S partitioning model:

TDS = 35,000 mg/l
Separator Pressure, P = 30 psig/44.7 psia (2 barg/3 bara)
Separator Temperature, T = 60°C
Separator Water pH = 7
Liquid Rate (oil and water) = 10,000 bpd (417 m^3/h)
Water Cut = 80%

Calculated H_2S concentrations from 16.6 mg/l S^{2-} in water were:

Variable GOR, scf/stb	H_2S Mass Rate, kg/d	H_2S in Water at P,T, mg/l	H_2S in Oil at P,T, mg/l	H_2S in Gas at P, T, ppm (v/v)
10	22.4	14.4	10.9	781
500	22.4	6.0	4.6	326
2000	22.4	2.2	1.6	117

Note: liquid concentrations in mg/l; gas concentrations in ppm (v/v).

As can be seen, the total mass rate of H_2S (generated) is the same for each GOR used in the example and the differences seen in calculated H_2S concentrations in each of the three phases is due to establishing equilibrium conditions, with appropriate transfers of H_2S from the oil and water phases into the gas phase. Thus a higher GOR dilutes the molecular H_2S (gas) but also gives a greater transfer from the oil and water phases to reach the equilibrium condition. Whether, or not, equilibrium is reached, during passage from the reservoir, up the wells, through valves and separators, will depend on the amount of turbulence experienced and on the phase contact times. It will also depend on many other factors, e.g. oil- or water-continuous flow, phase viscosities, laminar or turbulent flow, etc.

In the case of South Arne, the use of gas lift in the producing wells will give increased turbulence and so probably lead to equilibrium being established between the three phases before the fluids reach the individual wellheads. It is, of course, necessary to allow for the lift gas mass flow and its H_2S content in any mass balance calculations, although with only 2 ppm (v/v) H_2S in the lift gas (which has been prior-treated with a 'scavenger' chemical to remove H_2S) its contribution to well-flow H_2S is very small.

The above example is a simple equilibrium calculation and prediction of real well and field H_2S development profiles ideally involves the use of sophisticated 3D souring simulators coupled to the output of the specific oil reservoir simulator, or at least combinations of multiple well-pair 2D simulations. Combining reservoir and souring simulators allows for the very considerable complexities of real oil reservoirs in terms of multiple layers, say, or fractures, well positions, well orientations, well production histories, etc.

From the above example, it may be appreciated that even low concentrations of sulphate in injection water may lead to sufficient sulphide generation by SRP to give potentially unacceptable concentrations of H_2S in gas (above 5 ppm can give SSCC conditions to susceptible steels at high pressures, according to the NACE/ISO standard MR0175/ISO15156, dependent on the *in-situ* water pH).

In addition, the potential for microbiologically-influenced corrosion (MIC) should not be ignored as biofilm/colonies of SRP can extract sulphate from low concentrations in almost any water and generate under-deposit corrosion and the pitting which is a well-known characteristic of SRB

SOUTH ARNE RESULTS AND DISCUSSIONS

The field audit involved sampling all 12 oil production wells via test separators, and then throughout the oil processing train. A variety of on-site analytical techniques was used in order to obtain valid data, as sample preservation and much later analysis in onshore laboratories often renders results questionable.

For example, pH measurements were conducted on-line and still under pressure, to avoid loss of the acidic gases CO_2 and H_2S, since their loss would lead to a rise in the measured pH, as shown by Fig. 3, in which the pressure was deliberately reduced during tests on produced fluids flowing through

test separators from two wells, Well-B and Well-E, and from the production train first and second stage separators.

Similarly, special techniques were used for H_2S measurements in the oil and water phases, using what is known as the 'double-bomb' method to depressurise the samples, taken at system pressure in Teflon-lined sample cylinders, and strip out the H_2S using oxygen-free nitrogen. The total stripped H_2S was then measured using a series of the standard (ASTM, 2005) length-of-stain detector tubes (Gastec type): the results for the wells are shown on Fig. 4, with the distribution between phases illustrated more clearly on Fig. 5.

For the process train, the H_2S concentrations are shown in Table 1, with calculated mass rate, in kg/d, given in Table 2, and that data was used to calculate the mass balance as shown on Fig. 6. With regards to the high H_2S value reported in an offload to tanker, that was correlated with re-starting production from Well-L (see Fig. 4) after a 2-year shut-in and successful water shut-off work-over, and during that time the near well-bore area had been cooled due to dump-flooding from Well-F, so creating a local reservoir environment perhaps suited to growth of SRA and/or SRB.

In addition to the pH and H_2S measurements,

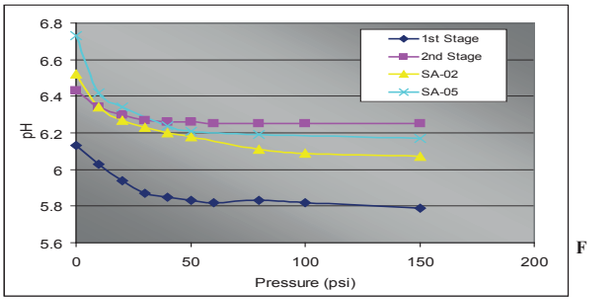


Fig. 3. pH vs. Pressure – Separators and Selected Wells

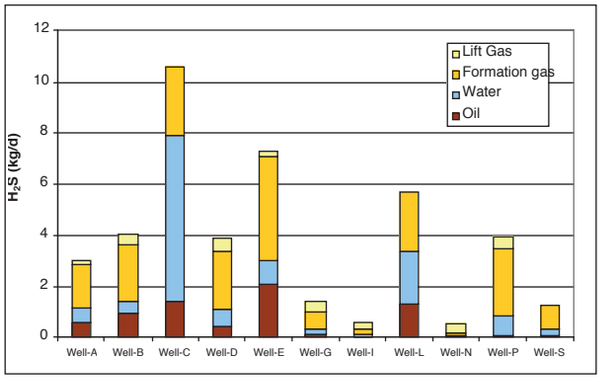


Fig. 4. H_2S Mass Flow Rates from Production Well Tests

Table 1 H_2S Concentrations in Process System

	1st Stage	2nd Stage	3rd Stage	Coalescer	Degasser
Pressure (barg)	26.4	11	2.6	2.6	0.1
Temp (°C)	76	71	70	70	53
H_2S (gas, ppm)	14	53	75	-	190
H_2S in water (mg/l)	2.12	1.3	-	0.32	0.82
H_2S in oil (mg/l)	2.94	1.61	1.11	1.09	-

Table 2 H_2S Mass Rates in Process System

H_2S leaving 1st Stage Separator		H_2S leaving process system	
Gas	36.6 kg/d	1st stage gas	36.6 kg/d
Water	13.0 kg/d	2nd stage gas	2.1 kg/d
Oil	9.7 kg/d	3rd stage gas	3.3 kg/d
-		Rundown crude	3.5 kg/d
-		Degasser (water)	5.3 kg/d
Total:	59.3 kg/d	Total:	50.8 kg/d

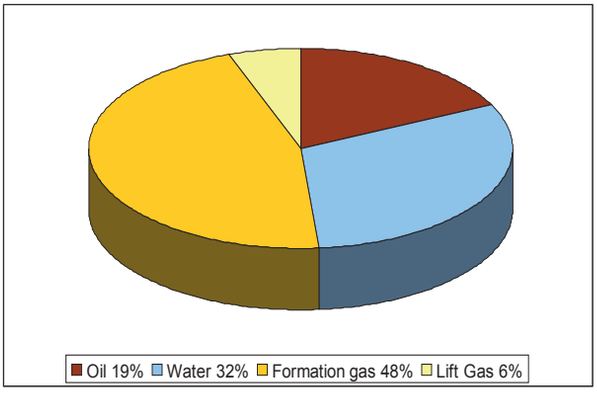


Fig. 5. H_2S Distribution between Phases from Well Tests

many other parameters were measured on site or on samples suitably preserved for onshore analysis. The following parameters were measured, although not all data is given here since only some is relevant to this paper on reservoir souring involving LSSW:

- CO_2 in gas.
- Total Suspended Solids.
- Bacteria and Archaea.
- Cations in water: barium; calcium; iron; lithium; magnesium; potassium; sodium; strontium.
- Anions in water (excluding NVWAA): bicarbonate; borate; bromide; chloride; silicate;

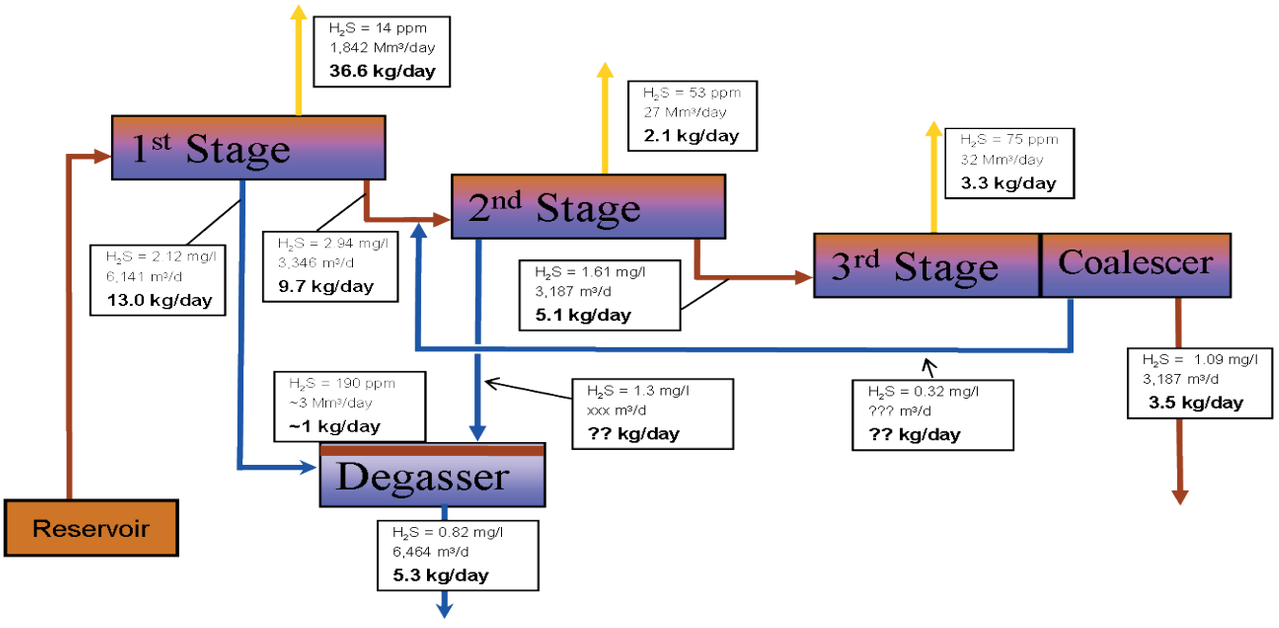


Fig. 6. H_2S Mass Balance for South Arne Process

sodium; sulphate.

- NVWAA: acetate, butyrate, formate; iso-valerate; propionate.
- Sulphur isotopes.

Of particular relevance to the study were the barium (Ba), strontium (Sr) and sulphate concentrations, plus the archaea and bacteria (SRP), and, of course, the H_2S and pH values.

The sulphur isotope results were somewhat inconclusive, in that they were below the +20 $^{o}/_{oo}$ $\delta^{34}S$ standard value for oceanic seawater, at 7.6 to 10.2 $^{o}/_{oo}$ $\delta^{34}S$ in three samples, but were not below zero, which is often the case for microbially-generated H_2S. However, as noted above, the apparently high conversion percentage of the sulphate remaining in LSSW (especially when 'diluted' by much lower-sulphate formation water) would tend to move the values towards the more positive end of the spectrum. The isotope results are, therefore, consistent with SRP metabolising a significant proportion of the available sulphate.

A variety of MMM techniques were used during this study: DAPI staining, FISH (Fluorescent *In-Situ* Hybridisation), qPCR (quantitative Polymerase Chain Reaction), and the traditional MPN technique (Serial Dilution to Extinction). The latter failed to give any positive results for the (hot) well and process train water samples, although did give useful results for the cooler samples from the GBS. Although the qPCR technique does not currently allow distinction to be made between active, inactive and dead microorganisms (see Fig. 7), the technique was particularly valuable for this study as it clearly showed that there were a great many of the extremophilic SRA present in the upstream, hotter parts of the production train, with no SRB in the test and first stage separators, but then almost equal numbers of SRA and SRB in the further downstream degasser and coalescer (in the produced water treatment train); see Fig. 8.

Interestingly, no SRA were found, using qPCR, in the LSSW deaerator outlet water, nor in the ballast water from the GBS.

Using the FISH technique to identify active bacteria, the results did indicate active SRB and not only SRA in the test separator sample, but no

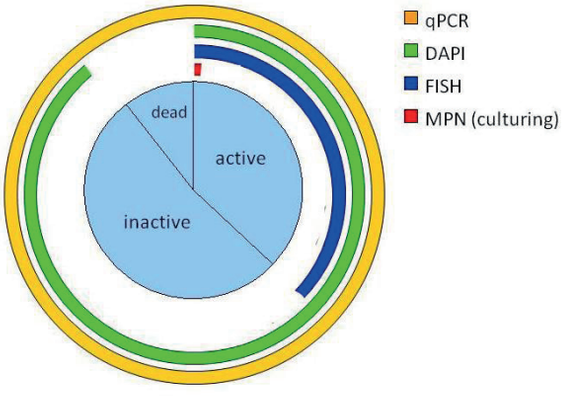


Fig. 7. An illustration of the different pools of microbes (active, inactive, and dead) that are included when employing different microbiological techniques (Lundgaard et al, 2010)

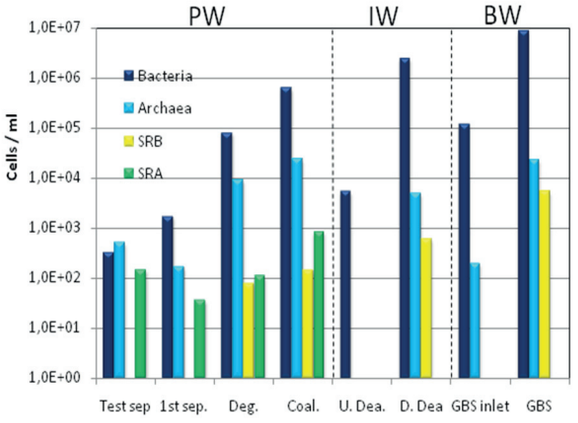


Fig. 8. qPCR data from eight sampling points in the South Arne water systems: Produced water (PW), injection water (IW) and ballast water (BW) (Lundgaard et al, 2010)

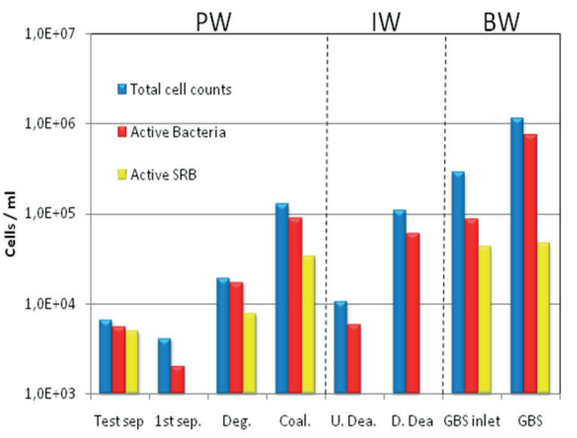


Fig. 9. Microscopy data (FISH/DAPI) from eight sampling points throughout South Arne water systems: Produced water (PW), injection water (IW) and ballast water (BW) (Lundgaard et al, 2010)

SRB in the continuously flowing, hot (75-85°C) first stage separator. SRB were found throughout the cooler (45-50°C) produced water train (degasser and coalescer) and the GBS ballast water, but not into or out of the LSSW deaerator, thus indicating that the SRM process achieves a useful degree of microbial control, which is not surprising of course for nano-filtration; see Fig. 9. Nevertheless, high counts of active non-SRB were still detected in the LSSW.

Interestingly, the traditional MPN techniques did give low, but positive, SRB results downstream of the deaerator. The MPN technique was used both just before and just after a biocide treatment to the deaerator, and showed that this was effective in reducing planktonic SRB in water counts from 95 to 4.5 per ml (those are statistical most-probable numbers): the effectiveness of the biocide treatment to any sessile biofilms within the deaerator could not be assessed during this brief audit.

Overall, the results suggest that microorganisms able to produce H_2S are thriving in the reservoir and the topside oil production system despite high temperature and relatively low sulphate availability. Furthermore, signs of microbial growth were observed in all examined water systems. Data also suggested that a shift in population takes place through the production system, very likely due to a shift in temperature.

The ionic water chemistry data of particular significance to the study are the potential microbial nutrient anions, specifically the NVWAA (= VFA anions), and the potential scaling barium and sulphate ions. In addition, the chloride ion concentrations of the individual well waters, compared to a virgin formation water composition provided by Hess, were used to calculate a percentage content of the LSSW in each one. The assumption was that the LSSW had a constant content of 50 mg/l sulphate ion. The results were then used to calculate predicted sulphate ion contents should no sulphate have been 'lost' in passage through the reservoir. The solid line on Fig. 10 represents the amount of sulphate that would be expected if there were no loss of sulphate during the injection water's transit through the reservoir. The amount by which the measured value falls below this line represents the amount of sulphate lost in the reservoir.

The proportions of sulphate converted to H_2S are quite high, ranging from 32% to 76%. This suggests that SRB are acting on the sulphate before other major removal mechanisms (e.g. scaling with formation water barium) come into play. It also, significantly, suggests that without souring higher sulphate levels could be seen at the producers, which would bring an increased $BaSO_4$ scaling risk.

CONCLUSIONS

South Arne field has been injecting deaerated, low-sulphate seawater (LSSW) for 10 years, and mixtures of LSSW with produced water in part of the field since 2004 and into all wells since 2009. Although the formation water contains significant concentrations of available carbon in a form suitable for use by sulphate-reducing bacteria (SRB), e.g. acetate anion, the amount of H_2S that could be generated is stoichiometrically

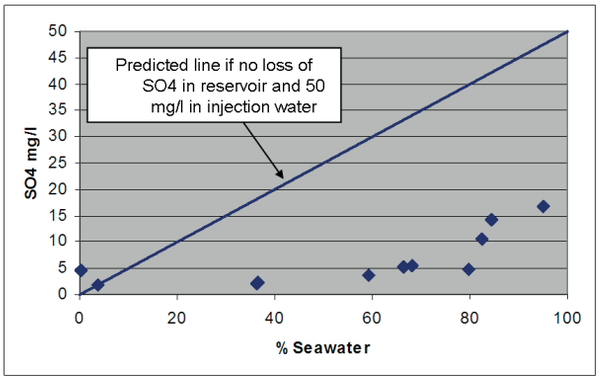


Fig. 10. Sulphate in Produced Water vs. Seawater Cut (Different Wells)

limited by the amount of sulphate ion injected, which is typically < 50 mg/l in the LSSW and < 10 mg/l in the produced water. Other operators which have described the use of sulphate-removal membrane (SRM) filters, primarily for the control of severe barium sulphate scaling potentials, have not reported on the development of reservoir souring, and so it was somewhat unexpected when Hess Denmark, the operator of South Arne, saw increasing concentrations of H_2S in produced fluids.

This study has shown, by modern molecular microbiological techniques (MMM), supported by sulphur isotope analyses, that the H_2S seen is a result of microbial reduction of sulphate to sulphide in the oil reservoir, although not by sulphate-reducing bacteria (SRB) but by sulphate-reducing archaea (SRA). The SRA are extremophiles and are tolerant to, and indeed prefer in this case, high temperatures. The SRA were found in fluids from production wells and in first stage process separators at 75-85°C, and SRB were only found in cooler (45-50°C), downstream parts of the process train.

The traditional SRB detection method of most probable number (MPN) by serial dilution to extinction in culture media did not detect these SRA, although the method still proved useful in lower temperature parts of the production and water injection process trains, including demonstrating that biocide injection is still needed to control bacteria, and so potential corrosion, in the produced fluids and even in the LSSW.

Despite the appearance of reservoir souring the use of LSSW has greatly limited how much H_2S can be generated, as well as meeting its primary objective of limiting the potential for barium sulphate scaling. The H_2S concentrations are low enough that the *in situ* 13% Cr steel well tubulars and completions remain acceptable.

Somewhat ironically, it is considered that the sulphate reduction to H_2S which is occurring is actually reducing any residual $BaSO_4$ scaling potential which would otherwise occur even with 50 mg/l sulphate ion in the injection water.

The produced H_2S is removed from the export gas using conventional liquid H_2S scavenger chemicals, at an acceptable cost because the H_2S mass rate (approx. 50 kg/d) is quite small, and much less than if normal-sulphate seawater had been injected.

Overall the injection of LSSW has been a big success for Hess Denmark and the South Arne Field partners and operations staff in greatly limiting both a severe barium sulphate scaling potential and a quite substantial reservoir souring potential, which otherwise would have given much higher operating costs, in chemicals and well work-overs, and increased hazards from high H_2S concentrations.

ACKNOWLEDGEMENTS

The authors wish to thank Hess, DONG Energy, Noreco and Danoil for permission to publish this paper, and the Danish Technological Institute (especially Torben Lund Skovhus and Thomas Lundgaard) plus William (Bill) Ginty, formerly at Hess but now at DONG Energy, for their substantial contributions to the studies leading to this paper.

REFERENCES

Alkindi, A., Prince-Wright, R., Moore, W., Walsh, J., Morgenthaler, L. and Kuijvenhoven, C. (2007). Challenges for Water flooding in a Deepwater Environment, OTC paper 18523, presented at 2007 Offshore Technology Conference, Houston, Texas, USA.

ASTM D4913–00 (2005). Standard Practice for Determining Concentration of Hydrogen Sulfide by Direct Reading, Length of Stain, Visual Chemical Detectors. *ASTM*, USA.

Barton, L. L. and Hamilton, W. A. (2007). Editors. Sulphate-Reducing Bacteria: Environmental and Engineered Systems, *Cambridge University Press, ISBN* 978-0-521-85485-6.

Larsen, J., Sorensen, K., Hojris, B., and Skovhus, T. L. (2009). Significance of Troublesome Sulfate-Reducing Prokaryotes (SRP) in Oil Field Systems, *NACE paper 09389, NACE Corrosion & Expo, Houston*, Texas, USA.

Larsen, J., Zwolle, S., Kjellerup, B. V., Frolund, B., Nielsen, J .L., and Nielsen, P. H. (2005). Identification of Bacteria Causing Souring and Biocorrosion in the Halfdan Field by Application of New Molecular Techniques", *NACE Paper 05629, National Association of Corrosion Engineers conference, Corrosion*.

Lundgaard, T., Sorensen, K., Holmkvist, L., Thomsen, U., Skovhus, T. L., Tuck, J., Ginty, B., and Samuelsen, E. (2010). Investigation of Significant Microorganisms Responsible for Souring in a Hot Oil Reservoir in the North Sea. *TEKNA Oilfield Chemistry Symposium, Geilo, Norway*.

NACE MR0175/ISO 15156. Petroleum and natural gas industries—Materials for use in H_2S-containing environments in oil and gas production. *National Association of Corrosion Engineers*, USA.

Ollivier, B. and Magot, M. (2005). Editors. *Petroleum Microbiology*, ASM Press, ISBN 1-55581-327-5.

Robinson, K., Ginty, W., Samuelsen, E., Lundgaard, T. and Skovhus, T. L. (2010). Reservoir Souring in a Field with Sulphate Removal: A Case Study", *SPE Paper 132697, SPE ATCE*, Florence, Italy.

Skovhus, T. L., Hojris, B., Saunders, A. M., Thomsen, T. R., Agerbaek, M. and Larsen, J. (2005). Practical Use of New Molecular Tools in Oil Production. *SPE Paper 109104, Offshore Europe* 2007, Aberdeen, UK.

Sharp, Z. (2007). Principles of Stable Isotope Geochemistry. Pearson Prentice Hall, ISBN 0-13-009139-1.

Vu, V. K., Hurtevent, C., Davis, R. A. (2000). Eliminating the Need for Scale Inhibition Treatments for Elf Exploration Angola's Girassol Field. *SPE paper 60220, presented at Second International Symposium on Oilfield Scale*, Aberdeen, UK, 26-27 Jan 2000.

Walsh, J., McElhiney, J., Maxwell, S., Burger, E. and Davis, R. (2008). Adoption of a Process to Prevent souring Associated with Seawater Waterflooding in the Ursa-Princess Fields, deepwater Gulf of Mexico. *SPE paper 113317, presented at 2008 SPE International Oilfield Corrosion Conference*, Aberdeen, UK.

Tidal Influnced Eocene Deposits of Dur At Talah (Libya) Compared with Present Day Tidal Sediments from the Bay of MT St Michel (France)

Abouessa A.*, Duringer Ph., Pelletier J., Schuster M., Rubino J. L., Salem M. J and Hlal O

Abstract: Dur At Talah escarpment is located in south central Libya, the southern peripheries of Sirt Basin. The escarpment (height ≈ 130m and length ≈ 150 km.) can generally be considered as the exposed part of Abu Tumayam Trough. The outcrop is built up with marine to deltaic clay, silty clay and various sandstones, it is attributed to the Upper and uppermost Eocene time. Only a few field studies have previously been carried out to this area, those were mainly attracted to its vertebrate fossil-content. For the moment, sedimentology and depositional environment are poorly documented.

Taking into consideration the importance of Dur At Talah escarpment outcrop, at the southern fringes of the large hydrocarbon bearing Sirt Basin, this paper aimed at defining the main facies, encountered in the exposed sequence. Sedimentological investigation suggested that the greatest part of the outcrop, which is the lower and the middle (approx. the lower 100 m.) parts, are strongly tidal dominated. The upper part therefore, appears to show smooth changing from tidal to 'pure' fluvial, probably includes mouth bar environments. In order to compare the Libyan tidal facies exposed in this outcrop, to modern ones, several field trips were conducted to the modern "macrotidal" environment of the Bay of Mont St Michel, France. The comparison would contribute to the understanding of the sedimentological sequence encountered in Dur At Talah area. Main results, especially the comparison between fossil and modern environments are presented in this paper.

Keywords: Macrotidal, tide-dominated facies, comparing sedimentary structure, Mont Saint Michel, Dur At Talah Escarpment

INTRODUCTION

Present is the key to the past is a principle (e.g. Charles Lyell) used among geologists since about two centuries. This principle has been applied to study the ancient sediment compared with the present analogs. In this article, the ancient example is Dur At Talah Formation, that is exposed (Fig. 1) as a large E-W stretching escarpment, of about 130 m in thickness located in the southern fringes of Sirt Basin, south central Libya. Particularly, the study involves a comparison of sedimentary structures and features from ancient deposits of Dur At Talah, with the active present day tidal-environment's sediment, as a modern analog. The Dur At Talah is attributed to the Late Eocene (Jaeger *et al* 2010a,b). In the Bay of Mont Saint Michel (Fig. 2), the tidal rang which is the difference between highest and lowest sea level of two successive tides, reaches a vertical distance of 15.5 m between the low sea level (low tide) and the successive high sea level (high tide).

Field work has been conducted to the Bay of Mont Saint Michael, Western coast of France, and to Dur At Talah escarpment, the southern periphery of Abu Tumayam trough (Vasic and Sherif, 2007). The escarpment is striking along latitude ≈25° 45′ N for approximately 150 km. To the west it interrupted by the southwestern corner of Al Haruj Basaltic complex. Best access to the escarpment is from the North that permits a direct access to the top of the cliff and from there to a multitude of small thalweg and Wadis. Access from the base as well as prospection on the foot of the escarpment is especially difficult because of the occurrences of soft, powder-like soil called "Fesh- Fash" composed of windblown clay and fine sand (Wight 1980). Previous geological field studies to the area were mainly attracted to the presence of interesting varieties of continental and marine fossil-vertebrates (Savage 1971; Wight, 1980; Rasmussen *et al* 2008; Duringer *et al* 2008; and Jaeger *et al* 2010a,b) embedded in their sediments.

*Corresponding author: abuissaashour@yahoo.com

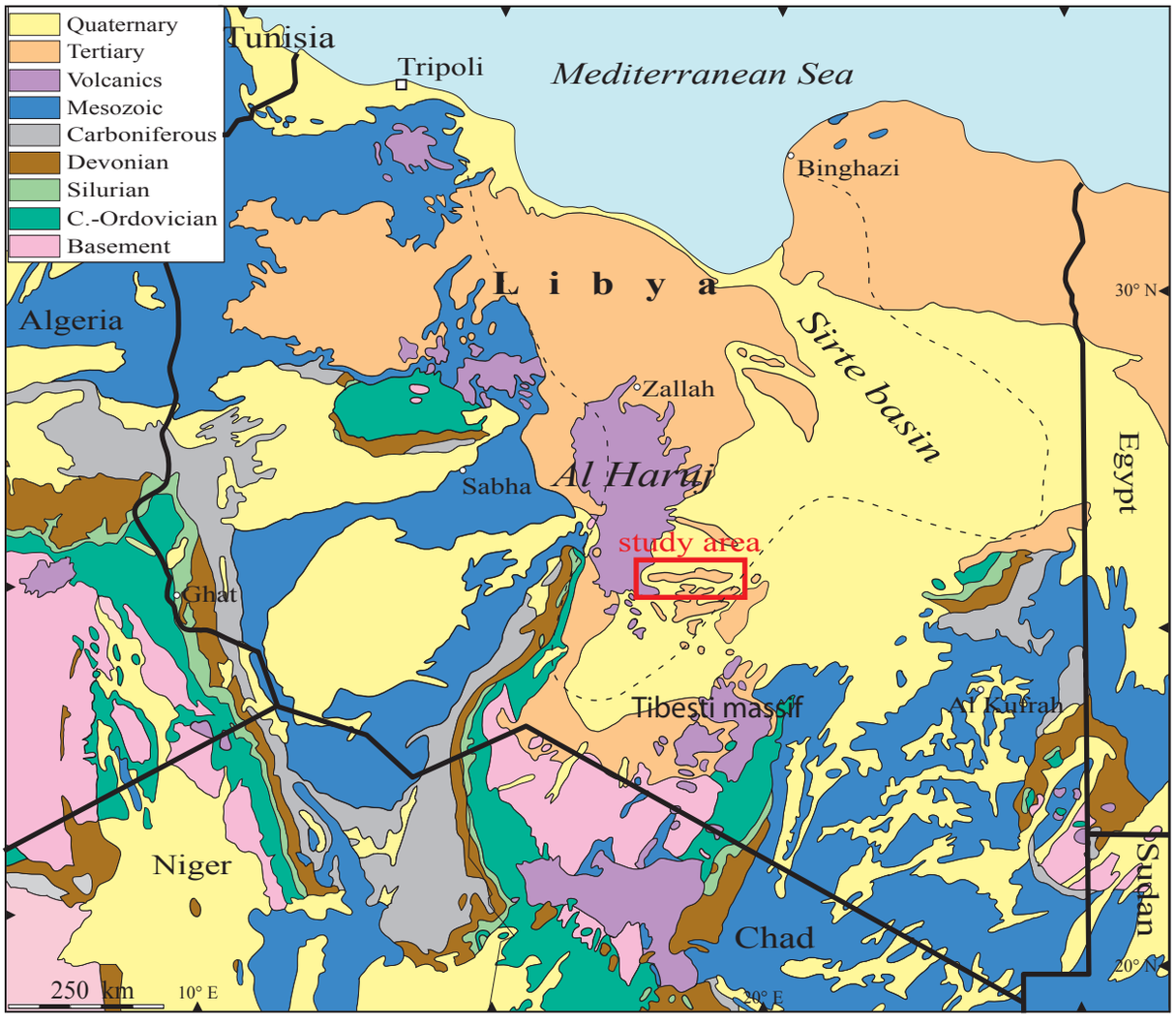


Fig. 1. Location map of Dur At Talah escarpment (red rectangle) south western flanks of Sirt Basin; the escarpment stretches east-west, to the west of Haruj basaltic complex, and to the north of Sarir Tibisti.

The Importance of the area increased in response to the continuous exploration activities devoted to discover more hydrocarbon occurrences in Sirt Basin. Late Cretaceous and Early Tertiary rocks of Sirt Basin contain large accumulations of hydrocarbon which have been the target of numerous exploration wells drilled in the region since oil discovery up to date. The study area can be considered as one of the best outcrops located in the southern Sirt Basin, the Abu Tumayam Trough. Understanding geology of this outcrop therefore, is of vital importance to understanding counterparts in the subsurface of the basin center to the north.

In the year 2007 Industrial Research center (IRC; Vasic and Sherif, 2007) produced the first 1: 250,000 general geological map with explanatory guide booklet (named ″Dur At Talah Sheet″) covering the study area and utilizing its name. By accepting the name “Dur At Talah” IRC puts an end to the differences in the spelling concerning the name of this area, and introduced the name to their new ″Dur At Talah″ Formation. Sediments exposed in this sheet area are dominantly marine carbonate in the south, located beneath the clastic deposits that dominate the northern parts including the escarpment.

During their mapping campaign, Vasic and Sherif (2007) established an overall geological description of Dur At Talah escarpment area; subdividing sedimentary rocks exposed in the sheet area including the escarpment, from older to younger (south to north) into three formations: (i) Al Jir (Gir) formation, (ii) Wadi Thamat and (iii) Dur At Talah Formations. The former two formations exposed south of the escarpment, the later (Dur At Talah Formation, which is the main objective of this study), occupies the whole body of the escarpment.

Most previous studies focus mainly on

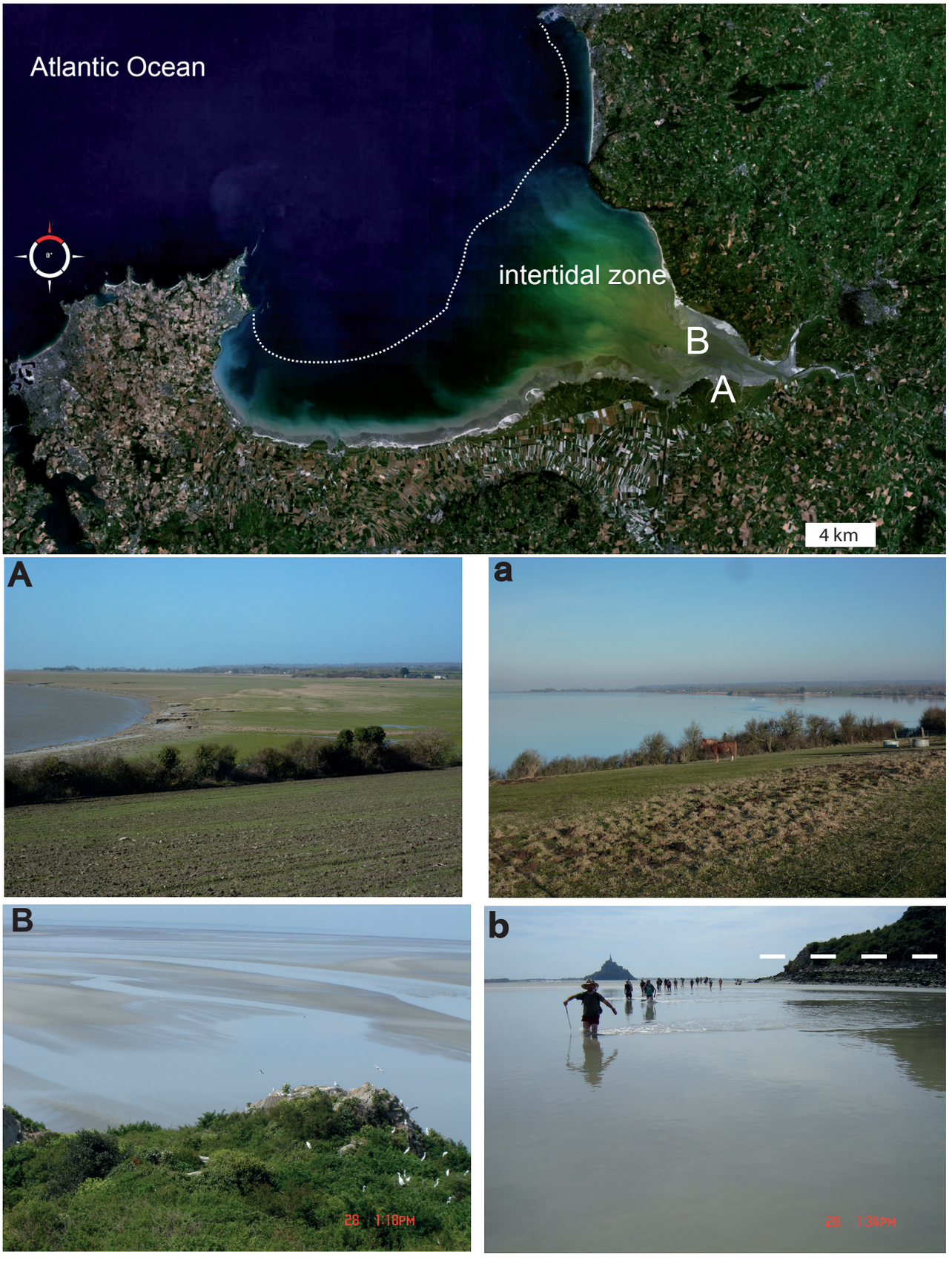


Fig. 2. Satellite image of the Mont Saint Michael Bay, the western coast of France. Dashed line refers to the low-tide limit, characters (A and B) on the image show the locations of the photos: Example from the supratidal zone during ebb (A) and flood after 6 hours (a) in the same location, (B) large size tidal channels as appear during low-tide and (b) closer view of the tidal channel observed in (B), dashed line marks water level during high tide.

paleontology. The present work attempts to consider sedimentological aspects of Dur At Talah escarpment succession. Special attention is given to the tidal sedimentary features, and the comparison of those features and structures with the ones from the present day macro-tidal environment operating today in the Bay of Mont Saint Michel, France.

During our last field work carried out in 2009, field observations and data (paleocurrent measurement) were collected, in order to define and describe the main facies successions encountered in Dur At Talah escarpment. Several locations have been investigated and described, including review of some sites mentioned by previous workers, such as Wight (1980) and Vasic and Sherif (2007).

Four major (large scale) facies successions (Fig. 3) have been recognized, each of those successions are genetically related.

1 The lower most facies of these are clay-dominated facies intercalated by several horizons of oyster shell accumulation (oyster bank).
2 The second facies succession is the thickest constitute of bioturbation-dominated, heterolithic, argillaceous succession, manifested with tidal characteristics, it occurs in the gently sloping, lower part of the escarpment
3 The third facies succession is of medium to coarse grained cross bedded sandstone intercalated by subordinate amount of mudstone, this succession forms the main part of the ledge of the cliff, and it displays less tide characteristics than the underlaying bioturbation-dominated facies.
4 The uppermost facies which shows absence of tidal criteria, is represented by very coarse to microconglomeritic sandstone, contain variable occurrences of fossil roots and large silicified wood trunks.

Sedimentary structures which are known to be tide generated are presented by the middle two facies successions. Therefore, they will take the greater attention of this article.

IMPORTANT ASPECTS OF TIDAL FACIES

Tidal current commonly have sufficient velocity to move sand and gravel on the bed, and silt and clay in suspension (Bridge and Demicco, 2008). Tidal currents are known to be generated as a result of the gravitational force acted on the earth by mainly the moon and, to a lesser extent by the sun (Reineck and Singh, 1980). As result water on the oceans and seas moves forward (flood) and backward (ebb) in a harmonic motion one time, twice times a day, or more complicated according to geographic area. Due to the increasing volume of water tidal range and therefore energy increases, as the water passes into narrow areas such as bays (embayment; the Bay of Mont Sainte Michael is a worldwide example) and funnel shaped coastal regions. This fact explains why tidal range is specifically high in relatively restricted areas.

In tidal environments, traction currents are commonly bidirectional. Maximum flood and ebb currents commonly follow different pathways; result in characteristic sediment transport path for which there is net sediment transportation in a given direction (e.g. Harris *et al* 1995). In many cases, only one water directions is recorded, though, It is usual to observe a high asymmetry in recording of the sedimentary features. Thus, tidal megaripples are often associated with reverse small ripples, each representing one direction of water flow (Ashley, 1990). Tidal deposits therefore is known by its systematic (rhythmic) variations in the thickness of lamina, this have been related to periodic variations in current strength and deposition rate over tidal cycles Dalrymble (1992).

Tidal flat in the Bay of Mont Sainte Michel are flooded and exposed at regular intervals twice times a day. Reshaping of tidal bars and tidal channel can be visualized within several hours. The objective of the field work to the Bay was to practically understanding tidal processes and to find a set of criteria within the recent sediments, that can be applied to compare with the fossil counterpart of Dur At Talah deposits. The tidal flats of Mont Saint-Michel Bay, in France belong to the macro-tidal flat of very high tidal range (15.5 m.; Reineck and Singh, 1980; Bonnot-Courtois, *et al* 2002).

Tides in this region are semidiurnal; two tidal cycle each 24 hours.; In each cycle the water flood landward up to (high sea level) the high tide level, then short period of stagnation (slack water period), followed by ebb back towards the sea until the low tide, short period of stagnation and so on. The horizontal distance of tidal flat between low sea level and high sea level exceeds 15 Kilometers, and water speed is capable of transporting sand-size and even coarser sediments several meters per second.

Small and large scale sedimentary processes have been observed operating on the sediments of the Mont Saint Michael Bay, large scale processes include: (i) active tidal channels (of straight and meander types; Fig. 2) cutting across muddy to

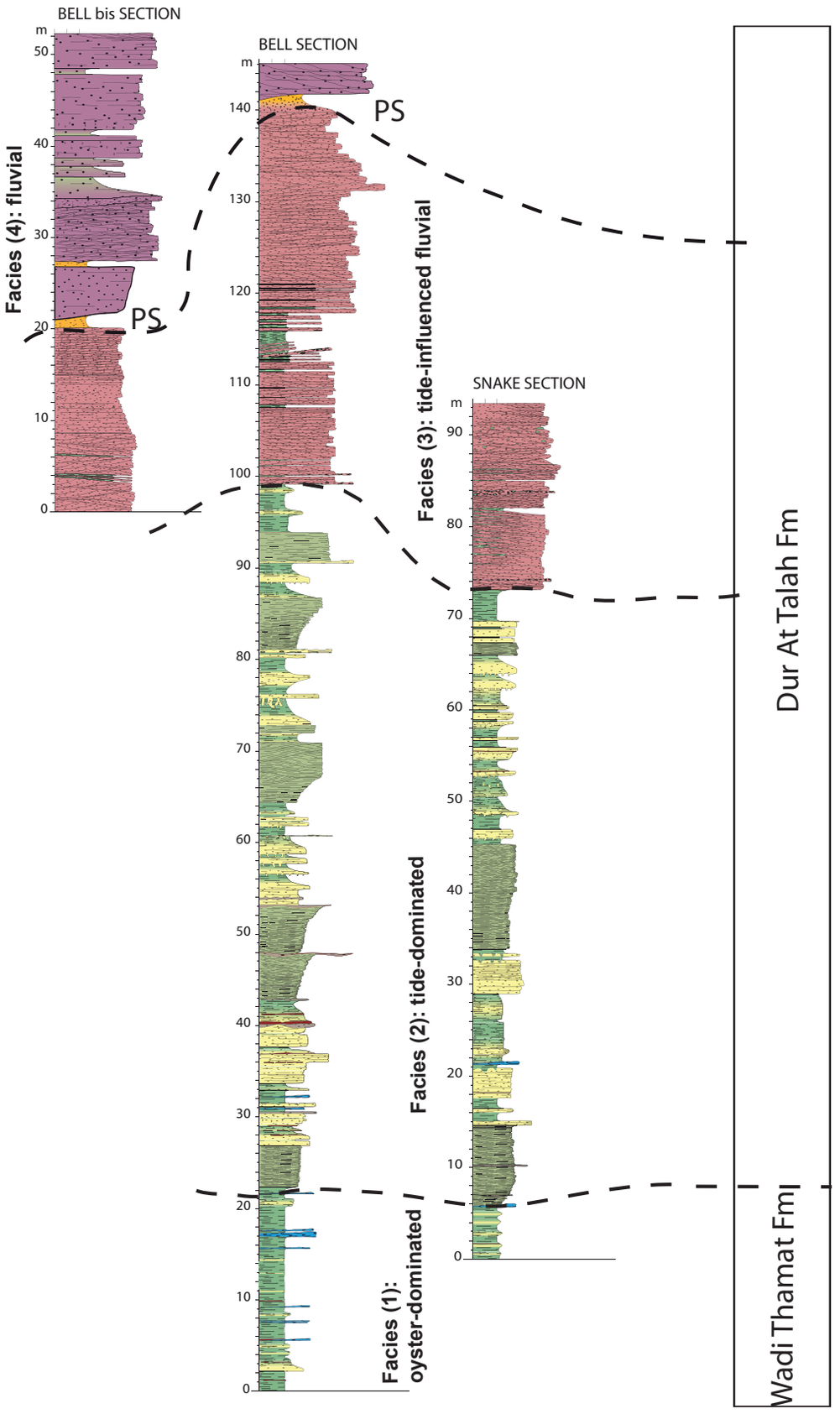


Fig. 3. Sedimentological log representing the main facies encountered in Dur AT Talah (escarpment) Formation. This section if pieced out from three adjacent (few kilometers apart) location at the western part of the escarpment. PS for paleosoil, and dashed line, separates the main facies.

sandy tidal flat, (ii) tidal channel lateral shifting and eroding previously deposited, unconsolidated sand and mud flats, (iii) mud deposition in abandoned channels, and (iv) landward sand transportation during flood tides and seaward sand transportation during ebb tides. The smaller scale features include but not limited to: deposition of mud from suspension during slack water periods to produce mud drapes on sand (e.g., Dalrymple and Choi, 2007), formation of ripple mark during ebb as well as flood, sediments burrowing by worms, crabs and bivalves.

DUR AT TALAH ESCARPMENT GEOLOGICAL SETTING

The Dur at Talah escarpment represents the southern extension of Abu Tumayam Trough of Sirt Basin. Sirt Basin or Embayment (Conant and Goudarzi, 1967; Goudarzi, 1980) has long been considered as part of the Tethyan rift system. The Basin reflects significant rifting in the Early Cretaceous and syn-rift sedimentary filling during Cretaceous through Eocene times, and post-rift deposition in the Oligocene and Miocene (e.g. Ahlbrandt, 2001 and Abadi *et al* 2008).

Geomorphologically, Dur At Talah area in general consists of three prominent morphological elements (Fig. 4): (1) the escarpment extends East-West around latitude ≈25° 45′ N; between 18° 00′ and ≈19° 30′ E; (2) the lower low- relief plain to the south; and (3) the upper, capping plateau to the north of the escarpment. Rocks forming Dur At Talah escarpment (equivalent to IRC's Dur At Talah Formation) are the main target of this study. These rocks are made up mainly of siliciclastic sediments shows coarsening and thickening up trend; clay, sandy clay, and fine sand at the base grads up into coarse to microconglomeratic sandstones at the top. The southern adjacent vicinity to the escarpment, represented by the lower plain, is occupied by sediments of uppermost member of Wadi Thamat Formation, and to which our lower facies (1) is included, Vasic and Sherif, (2007). This is composed of dominantly claystones, interbedded with oyster shell. The capping plateau has relatively lower

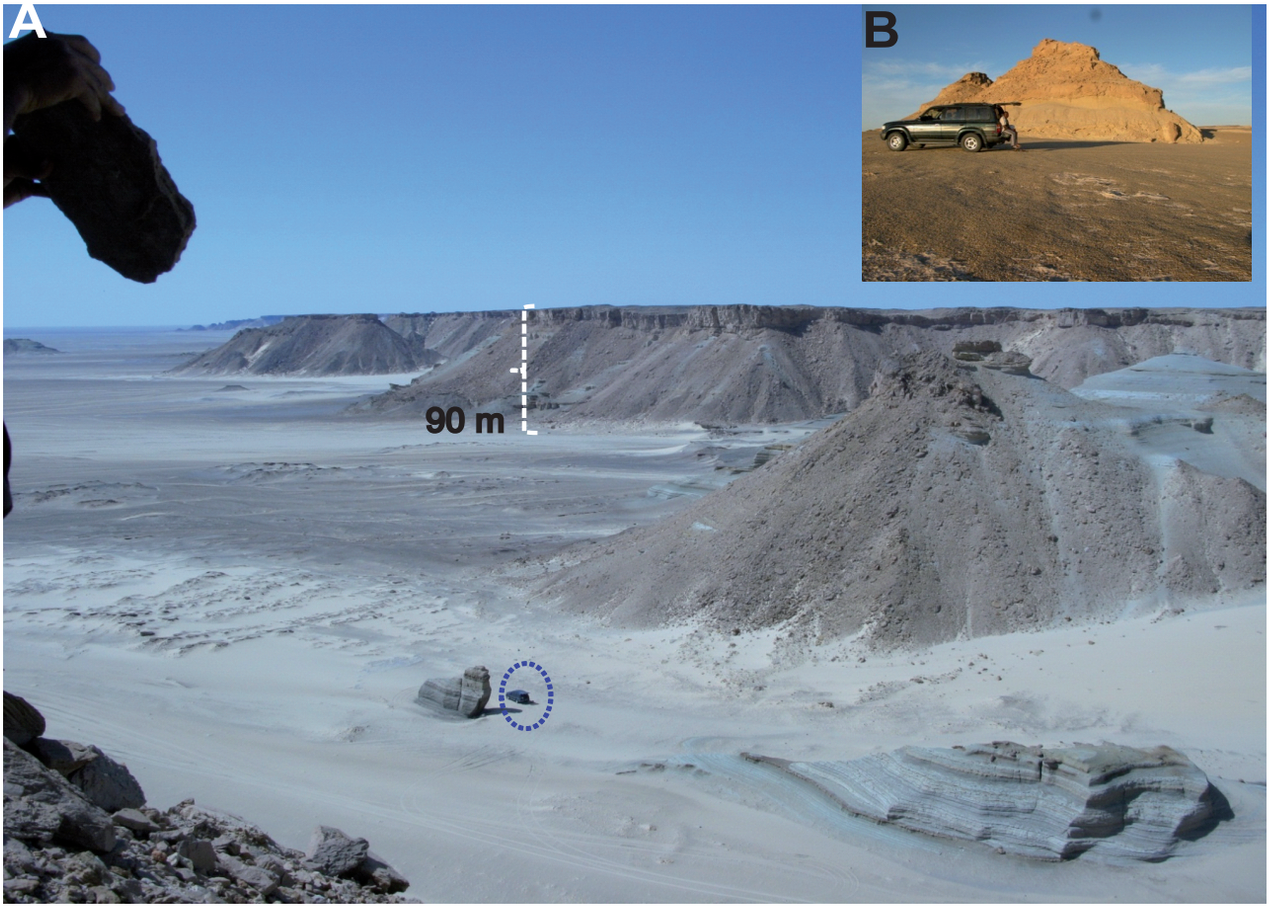


Fig. 4. Photo shows the major morphological elements of Dur At Talah Escarpment area. The escarp is stretching East-West for 150 km. total height about 130 m, starting from the footwall until the top of the hills on the capping plateau (the inset photo).

relief, it constitute scattered hills of maximum 20m high, composed mainly of very coarse to microconglomeratic sandstones.

The chronological framework of the Dur At Talah Formation is still in progress. Eocene to Early Oligocene ages have been first proposed in comparison with equivalent formations in the Sirt Basin, as well as to what thought to be equivalent outcrops adjacent to the area (e.g. Peregi *et al* 2003). Biochronology, based on large mammal fauna suggested a latest Eocene age (Savage, 1971 and Wight, 1980). Biochronology based on micromammals and paleomagnetic studies suggested an upper Eocene age (Jaeger *et al* 2010a,b).

There is a common agreement among local geologists that the source of clastic sediment supplied to the basin was the higher land to the south around Tibesti Massif. A major marine transgression in the Paleocene and Eocene times extended southward from the basin center south into its deep embayment, which by the late Eocene had reached the Tibesti area and possibly beyond (e.g. Barr and Wegeer, 1972; Benfield and Wright, 1980). Such transgression is well recorded by the marine fossil-dominated carbonate rocks, exposed to the south of the study area. Paleocurrent measurements from various locations, confirm that the main trend of sedimentary transport is from the South to the North. Nevertheless, as a result of tidal currents, many outcrops show local paleocurrent measurements.

Structurally, Dur At Talah rock sequence shows very low dip angle (1-2°), that is generally northward. Except of very widely spaced, typical normal and reverse faults, the area can be considered structurally undisturbed. The vertical displacement of those faults does not exceed one meter, with almost no horizontal displacement. Exceptionally, the western extremity of the escarpment, which is bordering the Haruj basaltic Massif (Pliocene to Late Pleistocene; Busrewil *et al* 1996) is displaying a small scale and localized folding, which might be attributed to doming effect during the generation of the basalt.

DUR AT TALAH FORMATION, GEOLOGICAL CONSIDERATIONS

Vasic and Sherif (2007) comprehensively described all the rocks exposed in Dur At Talah mapped area, starting from the rocks exposed in the lower plain (south of 25° 45′ N) extending north to the capping plateau into three formations, summarized hereunder.

Al Jir (Gir) Formation: Al Jir Formation Is the oldest (Lower Eocene, Ypersian-Lutetian), in the sheet area, it has more than 45 m thickness, and consists of marine carbonate rocks, occasionally contain concretions of silica. The Jir formation has a much greater thickness in the subsurface of Sirt Basin (Barr and Wegeer, 1972) the formation is oil-producing in Ed Dib and Facha fields.

Wadi Thamat Formation: The Wadi Thamat Formation (Middle Eocene, Lutetian-Priabonian), its thickness varies from160 m to-200m thick, and is divided into three Members: (i) Al Gata Member, the oldest, chiefly consists of bioclastic limestone with nummulites, (ii) Thmed Al Qusur Member, composed of limestone and chalky limestone, marlstone, gypsum, and dolomite varieties, and (iii) Qarart Al Jifah Member which is made up of sequences of green claystone, marly claystone, bioclastic limestone with frequent oyster (lumachelles) layers. Vertebrate bones have been mentioned (Vasic and Sherif, 2007) and observed in the top of Qarart Al Jifah Member. The Middle Eocene in the subsurface of the Sirt basin is represented by the Gedari Formation and its lateral equivalent Gailo formation, Wadi Thamat Formation is equivalent to the Gedari Formation (Tawadros, 2001).

According to our observations, the uppermost oyster bank is situated several meters above the foot of the scarp, that was considered as the boundary between Wadi Thamat Formation and the overlaying Dur At Talah Formation (Vasic and Sherif, 2007). Such boundary therefor is just an arbitrary, since the oyster banks are common in the lower part of the escarpment. It is worth mentioning that, up to date, there is no visible physical discontinuity separating the Wadi Thamat Formation from the overlying Dur At Talah formation.

Dur At Talah Formation: The name Dur At Talah Formation was first introduced by Vasic and Sherif (2007). The succession has been split into two members. The lower member is composed of alternation of fine sediments (mud, silt and fine sand), and is rich in marine vertebrates. The upper member is made up of coarse sandstone dominated with silicified tree trunks. Details about the major facies composing Dur At Talah Formation will be presented in the next section. In the subsurface of Sirt Basin the Oligocene-aged Arida and Diba

Formations described by Barr and Wager (1972) bears nearly similar lithological characteristics with the IRC's upper member of the Dur At Talah formation.

Dur At Talah Formation of Vasic and Sherif (2007), is equivalent to the Wight's (1980) three units: The Evaporite, the Idam, and Sarir units. The Evaporite unit therefore, is not primarily an evaporite, because the gypsum proportion is low compared with the clay and sand content, and in fact this gypsum is diagenetic rather than depositional (Duringer *et al* 2008). The term Idam unit was not suitable and shortly abandoned, as it is confusing with the Lidam Formation of Upper Cretaceous. Idam unit is included in the undifferentiated Eocene sediments in the geological map of Libya (1985). It can be inferred that Wight's Evaporite and Idam units is more or less equivalent to lower member of Dur At Talah formation of Vasic and Sherif (2007). Meanwhile the Sarir unit of Wight is, more or less, equivalent to the upper Member of Dur At Talah formation.

MAIN FACIES OF DUR AT TALAH FORMATION

Based on numerous field observations along and across the escarpment outcrop, and taking into consideration the outcrop scale sedimentological variations in the rocks composing Dur At Talah (Escarpment) Formation. This formation has been split (Fig. 3) into four vertical successions (or main facies), from bottom to top, these are:

1 Clay- oyster banks interbedded facies (marine-dominated facies)
2 Bioturbated fine sand to mud facies (Tide-dominated facies)
3 Cross bedded coarse sandstone facies (Transitional or tide-influenced facies)
4 Micro-conglomeritic sandstone facies (Fluvial facies)

In this study special attention has been given first two facies (1 and 2) as they own a characteristic sedimentary structures and features which are directly related to tidal sediments and processes. these structures are analogous to the one observed in the Bay of Mont Saint Michael tidal flat, which represents one of the best modern environment showing tidal dynamics. In other word, the sediments of facies (2 and 3) possess numerous features and sedimentary structures that are common and highly similar to the one occurring today in the Bay of Mont Sainte Michael. Meanwhile the Fluvial facies shows characteristic sedimentary structures which have not be observed in the Modern tidal Bay. The next section will illustrate the main characteristic features of each facies in correlation with their modern counterpart.

Clay-Oyster Banks Interbedded Facies (Marine-Dominated Facies): This facies is composed of green clay interbedded with shell accumulation known as oyster bank (wight, 1980; Vasic and Sherif, 2007). It is occurred in the lowermost part of the escarpment and extends far to the south, with a very gentle sloping terrain, where it is generally poorly exposed and covered by ″Fesh-Fash″. The topmost few meters of this clay-dominated facies, show better outcrop at the foot of the escarpment. This interbedding facies has a minimum thickness of 15 m, and was considered as the upper part of Wadi Thamat Formation (Vasic and Sherif, 2007)

Bioturbated Facies (Tide-Dominated Facies): This facies occupies the lower (65-70 m; Fig. 3) of the section; it displays a thinly stratified, commonly heavily bioturbated succession, forming the gentle to moderate sloping, lower part of the escarpment. Compared to the sediments in Mont Saint Michael Bay, this facies embraces characteristic tidal features very similar and sometimes identical with those observed operating today, in the tide-dominated Bay of Mont Saint Michel tidal. For this reason it named ″Tide-dominated facies″. A very prominent, easily distinguishable oyster bank of 50 cm thick (Fig. 5) can be considered as the lower contact with the

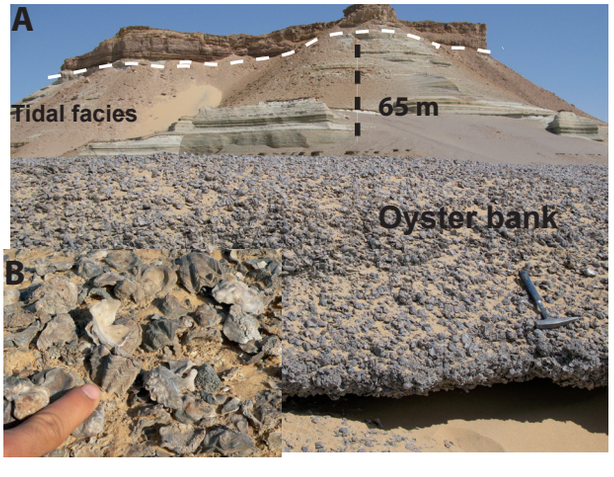


Fig. 5. composite photo from Dur At Talah, illustrates an example of the oyster bank occurrences, at the base of the bioturbated (tide-dominated) succession. The solid white line shows the location of the contact with the overlying cross bedded sandstone facies. Small photo in the corner (B) shows closer view of the oyster bank.

underlying clay-oyster bank dominated facies. This contact marks the onset of typical tidal sedimentary structures. It is important to mention that this bank is not a chrono-stratigraphic marker. Similar oyster banks (shell accumulation) are currently occurring in the Bay of Mont Saint Michel (Fig. 6) and interpreted as a wash over fans.

Sedimentary structures of the bioturbated facies include but not limited to the biogenic (mainly bioturbation) structures, and the small scale intra-bed sedimentary structures, such as ripple laminations and mud-sand alternation, flaser-, wavy- and lenticular-bedding, climbing ripples, and occasionally bi-polar cross lamination. As well as, large scale structures such as tidal bundles, (Reineck and Wünderlich 1968; Dalrymple 1992) composed of systematic silt-mud alternations, and larger scale structured as channels and channel filling including frequent reactivation surfaces followed by rip up clasts. The small scale structures such as climbing ripples are well preserved and displayed within the large scale structures such as channels. The upper contact (Fig. 7) of the bioturbated facies are erosional and has a wide lateral extent along the escarpment. It is usually marked by well cemented ferruginous sandstone layer. Morphologically it is represented by a break in the slope, from gentle and moderate below to cliff and steep sloping above.

Bioturbated facies versus modern tidal flat: Apart from the various types of sedimentary structures preserved in the bioturbated (tide-dominated) facies succession, this succession has been split into three alternating subfacies, based on grain size variations. Accordingly, the tide-dominated facies succession can simply be described as an alternations of three interbedding (lithofacies) subfacies. All three lithofacies display characteristic sedimentary structures that are encountered today in the sediments of Mont Saint Michel Bay. In Dur At Talah therefore, the distribution of bioturbation content (Fig. 8) is not yet well elaborated, and bioturbation could be expected to occur in a variable

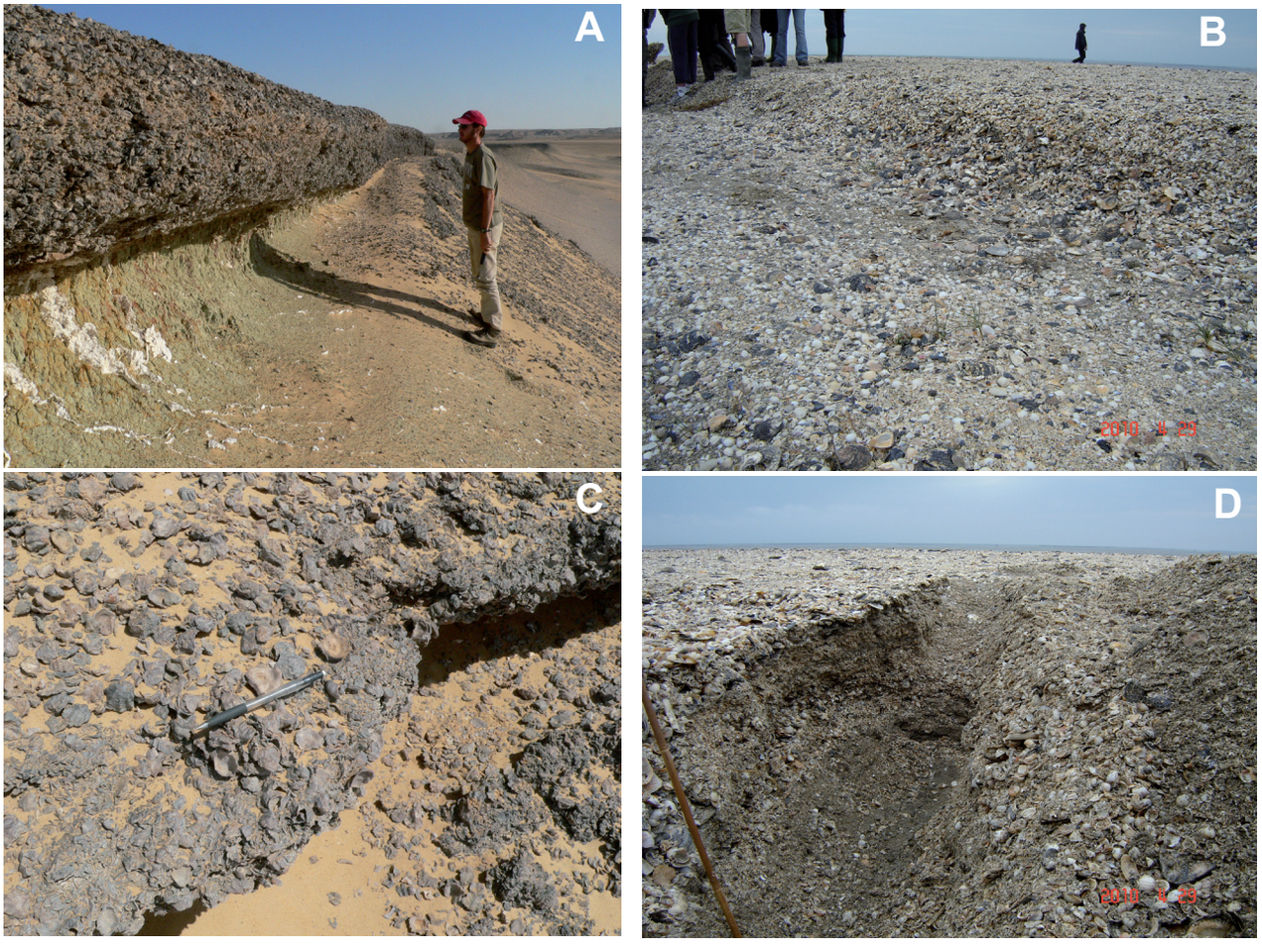


Fig. 6. photos (A to D) shows the comparison between the ancient (A and C, left side, from Dur At Talah) and the modern (right side, B and D, from the Bay of Mont Saint Michael) oysters accumulation or banks. Note the similarity between both ancient and modern oyster banks morphology.



Fig. 7. Photo from Dur At Talah formation shows the erosional contact between the bioturbated facies (gray mud) below and cross bedded sandstone facies above. The contact is usually marked by a ferruginous sandstone layer (above the dashed line), which indicated permeability barrier between muddy deposits below and sandy above.

intensity at any level, within these three lithofacies. The following section will define and describe each of these three lithofacies individually:

- Heterolithic (Mud-sand dominated) lithofacies
- Mud dominated lithofacies,
- Fine sand dominated lithofacies.

Sometimes the three lithofacies appear to be arranged in a set of finning up Parasequences. In fact they appear to be interbedding vertically, and interplaying laterally in a kilometric-scale distances.

Heterolithic (Mud-sand dominated) lithofacies: This lithofacies is made of packages of sand-mud interbedding bundles, arranged in a rhythmical sequence, which occasionally contain intraformational conglomerate lenses (Fig. 9). Individual beds of this facies has a thickness varies from 1m up to several meters. It exhibits two morphologies; the most common is horizontal parallel stratified appearance, and second is the inclined clinoform-like appearance. The latter is thought to be a cross sectional view of channel infill. Those are the most commonly observed features in the tide-dominated unit, and in both cases they are built up of alternating beds of fine sand, silt and clay layers. The thickness of each individual layer varies from less than one to five centimeters.

In correlation with the recent sediments in the Bay of Mont Sainte Michael, the heterolithic lithofacies possess many sedimentary structures diagnostic of tidal environment, these include but not limited to: tidal bundles (Fig. 10), represented by systematically organized sand-mud layers reflecting variation in tide energy attributed to semidiurnal and/or neap-spring variations. Visser (1980) suggested that tidal bundles associated with mud couplets are the best criteria of estuarine subtidal environment. Ripple lamination, cross lamination, and climbing ripples, as well as flaser to lenticular bedding of Reineck and Wünderlich (1968), and bipolar (herringbone) cross lamination are well preserved in the sediments of this lithofacies. Comparatively, the same structures are observed in modern intertidal sediments.

Mud dominated lithofacies: This lithofacies consists of beds of light gray to green mud (clay and/or silt). It varies in thickness from several decimeters to less than 3 m. in most cases internal (intra-bed; Selley, 1992) sedimentary structures are barely observed in this lithofacies, especially when the clay is dominating. Nevertheless, they occasionally appear as laminated and cross laminated when the silt is dominating. In many situations, small leave prints, as well as some Skolithos and other undifferentiated burrow are observed. Exceptionally, accumulation of plants (silicified wood fragments and fossil fruits) and a variety of fossil vertebrate bones are preserved in a level located in the middle of the bioturbated beds. Features, Such as tree trunks, fruits, and bones have been observed in the intertidal sediments of Mont Saint Michael Bay. Unlike the heterolithic lithofacies above, and fine sand lithofacies below, bioturbation are uncommon in mud dominated lithofacies.

Fine sand dominated lithofacies: This lithofacies is composed of light gray to white very fine to fine grained, occasionally argillaceous sandstone. It has thickness range between few decimeters to two meters. Bioturbation of various shapes and sizes are abundant and well preserved in this lithofacies. Such abundance (Fig. 11) can also be compared with that occurring in the sand flat of the Mont Saint Michel. Frequently, bioturbation in this lithofacies is intensive, so that it obscures the primary sedimentary structures. Furthermore, bioturbation are sometimes large sized (up to 70 cm deep, 20 cm diameter; Fig. 8 A and B). This large bioturbation is thought to be a combination of both roots and fossil traces. Distinguishable sedimentary structures are laminations, centimeter scale cross laminations and climbing ripples (Fig. 12). Presence of fossil fish and crocodilian skulls and remains are confirmed in many beds of this lithofacies. Uncommon horizons of this sandstones display a green color which thought to be due to the presence of glauconite.

Cross Bedded Medium Sandstone Facies (Tide-

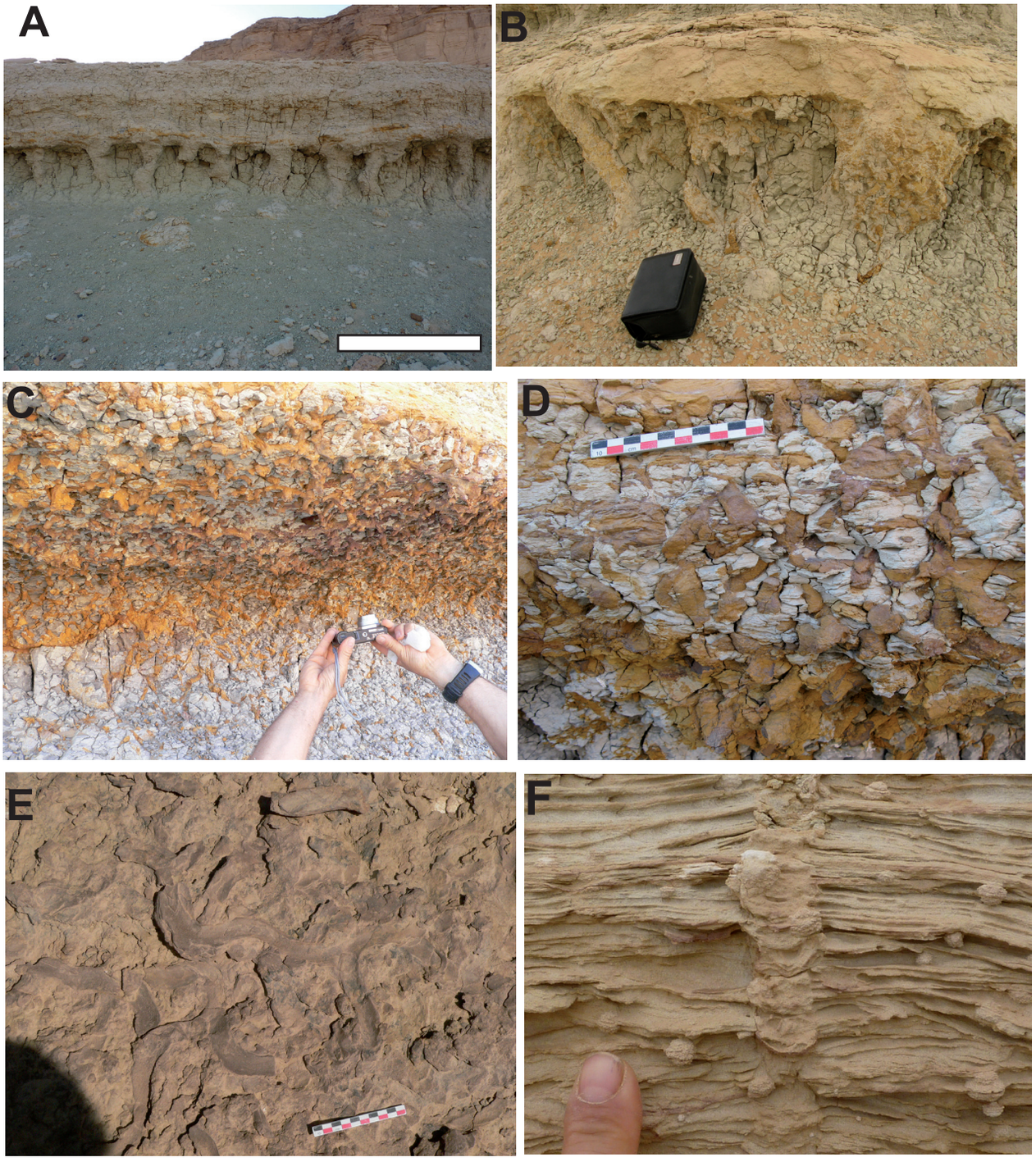


Fig. 8. photos A to F from Dur At Talah Formation, show various occurrences of bioturbation found in the bioturbated facies. In A (scale bar 1 m) and B the burrow are very intensive and shows multiple generations. Its morphology appears like a combination of roots traces and burrows. (B) is a closer view of (A); (C) shows domination of small size burrows, Thalassinoides in some levels, and to a lesser extent Skolithos; (D) a closer view of C, notes that sedimentary structures are no more distinguishable due such biogenic activities. (E) Shows plane view of fine sandstone with Teichichnus ichnospecies, and photo (F) shows Teichichnus cross-sectional view.

Influenced Facies):Unlike the bioturbated facies which is composed of fine sand and finer sediments, this facies (≈30 m.) is made up of yellow, medium to coarse, cross bedded sandstones. This sandstone is intercalated with subordinate amount of thin and irregular beds of light gray to white mudstones. Abrupt erosional contact separates this relatively large scale cross bedded sandstone from the underlying tide-dominated facies. In most locations where this contact is observed, it cuts (Fig. 7)

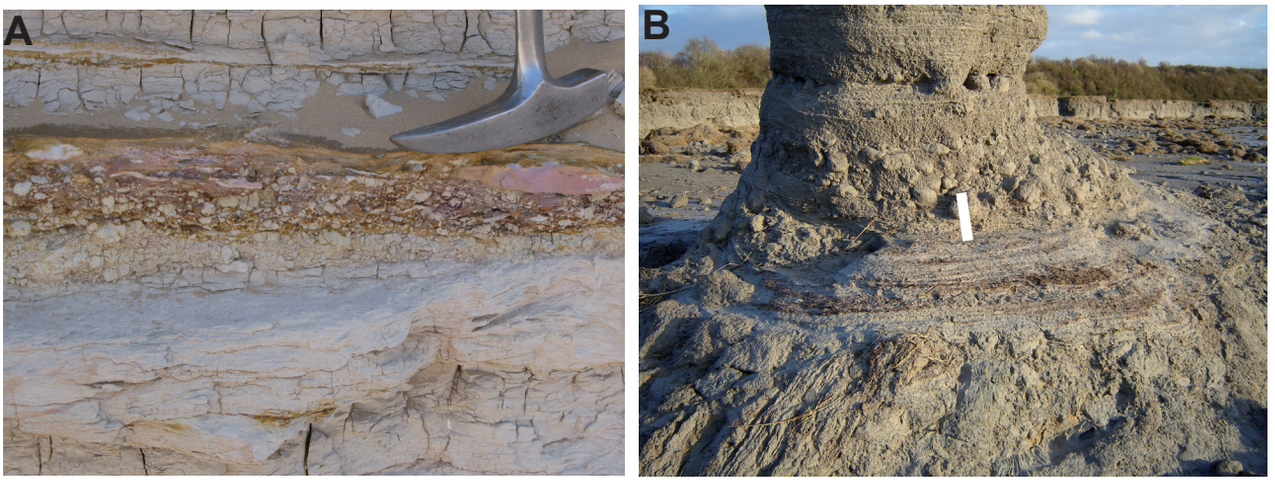


Fig. 9. photos (A) and (B) illustrate the comparison of intrabasinal conglomerate in the ancient (A; Dur At Talah) and the recent (B; Mont Saint Michel Bay, scale bar 10 cm), such conglomerate is resulted from the erosion when tidal channel cuts through mud flat.

into the mud of the underlying bioturbated facies, and it marks the end of all kinds of fossil fauna, ichnofossils intensity is also highly diminished.

In spite of this great change, typical signs of tidal influence are still preserved in this coarsely sandstone facies, especially within its lower part. The tidal influence compared with what has been documented in the present day tidal environment is well displayed by the presence of mud drapes (Dalrymple, 1992) between forests of the cross bedded sandstone (Fig. 13). In modern tidal environment, such drapes of mud are deposited from suspension during periods of slack water (Allen, 1990) culminating each tide cycle. Sometimes double mud drapes also preserved, recording (semi-diurnal) two tidal cycles per day. Superimposed cross bedding cosets display bipolar palaeocurrent directions is another evidence of tidal action, such diversity in current directions is uniquely documented in ancient and witnessed in modern tidal environments (e.g. Selley, 1992; Dalrymple and Choi, 2003).

The cross bedded sandstone of this facies can preliminarily be described as an amalgamation of prograding sand-bars complex, intersected by abandoned channel fill . In many locations distinctive large scale packages of fine sand-mud alternations (Fig. 14) occupied the abandoned channels. Small pieces of petrified wood is uncommonly scattered here. Understanding the sedimentary processes resulted in occurrences of such sand-mud alternations, requires more field investigations to be well elaborated. In the cross bedded sandstone facies therefore, tidal action appear to decrease gradually upward, in the contrary fluvial influence appear to be increasing, as suggested by the local abundance of cross stratified sandstone beds containing silicified tree trunks.

Microconglomeratic Sandstone Facies (Fluvial Facies): This facies occupy the uppermost part of the Dur Attallah Formation (or escarpment). It has a thickness that exceeds 30 meters. In the western side of the escarpment it is represented by an isolated hills and small outliers attached to the escarpment. This facies is more or less equivalent to the Sarir unit of Wight (1980). To the east, it has less thickness and (in part) disconnected far away to the north of the escarpment body. The decreasing in thickness is possible attributed to differential erosion. This facies is composed of very coarse, occasionally microconglomeratic sandstones. It lacks any kind of tidal sedimentary structures, and possesses features that are diagnostic of fluvial environment: large scale trough cross bedding, graded bedding, and the onset of sandstone bars with intensive roots network. The contact of this unit with the lower facies is not well defined, but there is a zone of several meters marks the first appearance of thick irregular beds of paleosoil. These paleosoil horizons are channelized with thick well cemented beds of microconglomeratic sandstone. Laterally, this zone is changed into sandstone probably with in situ vertically positioned silicified trunks. Above the contact zone, the sandstone is mostly very coarse and pebbly, poorly sorted, trough cross bedded occasionally with basal conglomeratic layers. This sandstone is gray to white in color, and intercalated with lenticular beds of green sandy mudstone.

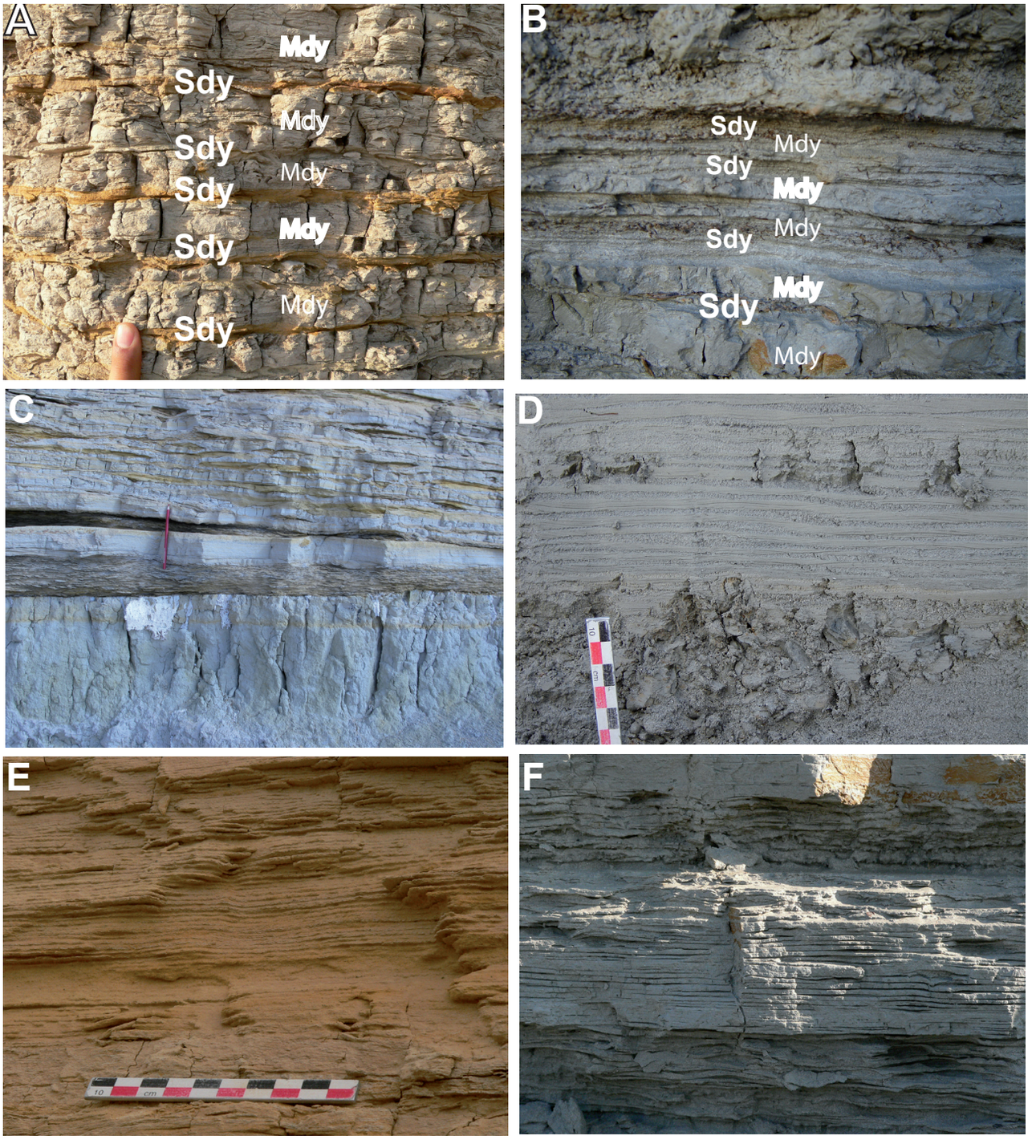


Fig. 10. photos (A to F) illustrate three different examples of tidal bundles from Dur At Talah deposits (left side photos: A, C, and E), compared with the modern analog in Mont Saint Michael Bay (the right side photos: B, D, F). Note the muddy (mdy)-sandy (Sdy) alternation of layers, resulted from diurnal and neap-spring variations in tidal energy.

DISCUSSION AND INTERPRETATIONS

In correlation with the modern tidal processes acting at the sediments of the Bay Mont Saint Michael in the present time, the 130 meter's rock sequence composing Dur At Talah escarpment (formation) is possibly interpreted to be deposited as a result of two major environments: (a) Tidal environment certainly acted in variable degrees on the lower 100 meters of the sequence; and (b) in the uppermost (30 m) a fluvial environment is evident, due to the presence of the in situ silicified wood and paleosoil horizons, supported by the absence of any tidal sedimentary structure.

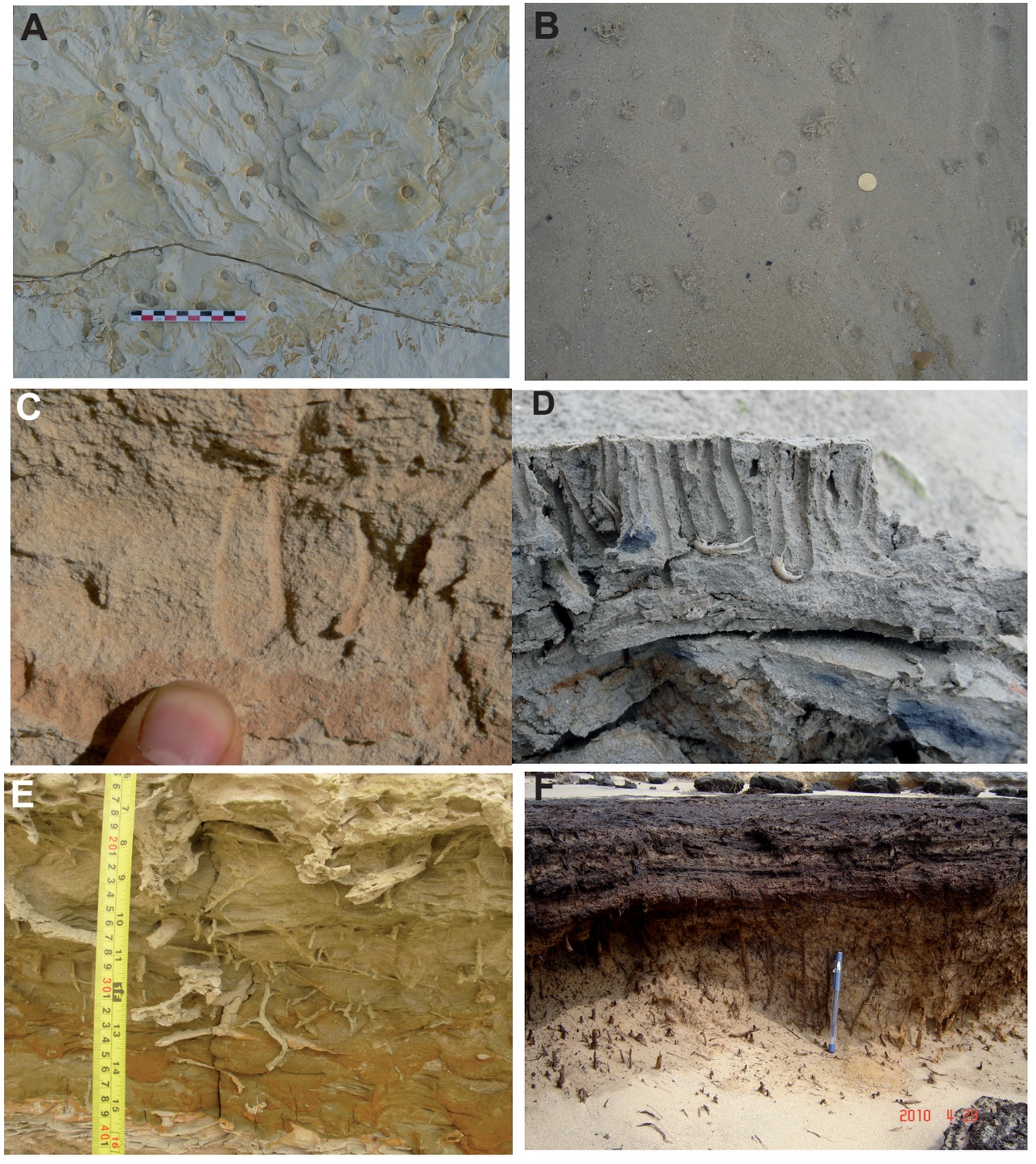


Fig. 11. plate show comparison of trace fossils from Dur At Talah (photos A, C, and E) with their modern counterparts from the Bay of Mont Saint Michael (photos B, D, and F). A and B are examples of burrowing worms. U-shaped trace in C and D is a burrows of crabs, the animal is still exist in D. in photos E and F sediments is roots dominated, with the presence some Skolithos?, sediments in photo F is several hundred years old.

Tide-domination: Tide dominance occurs if tidal currents are responsible for more sediment transport than river currents or waves and they determine the large geomorphology (Gallawy, 1975). The lower two facies namely the bioturbated facies, and cross bedded sandstone facies, (70) and (30) meters respectively possess a common characteristic sedimentary features which has been closely correlated with the currently active tidal settings. Numerous tidal features recorded in the

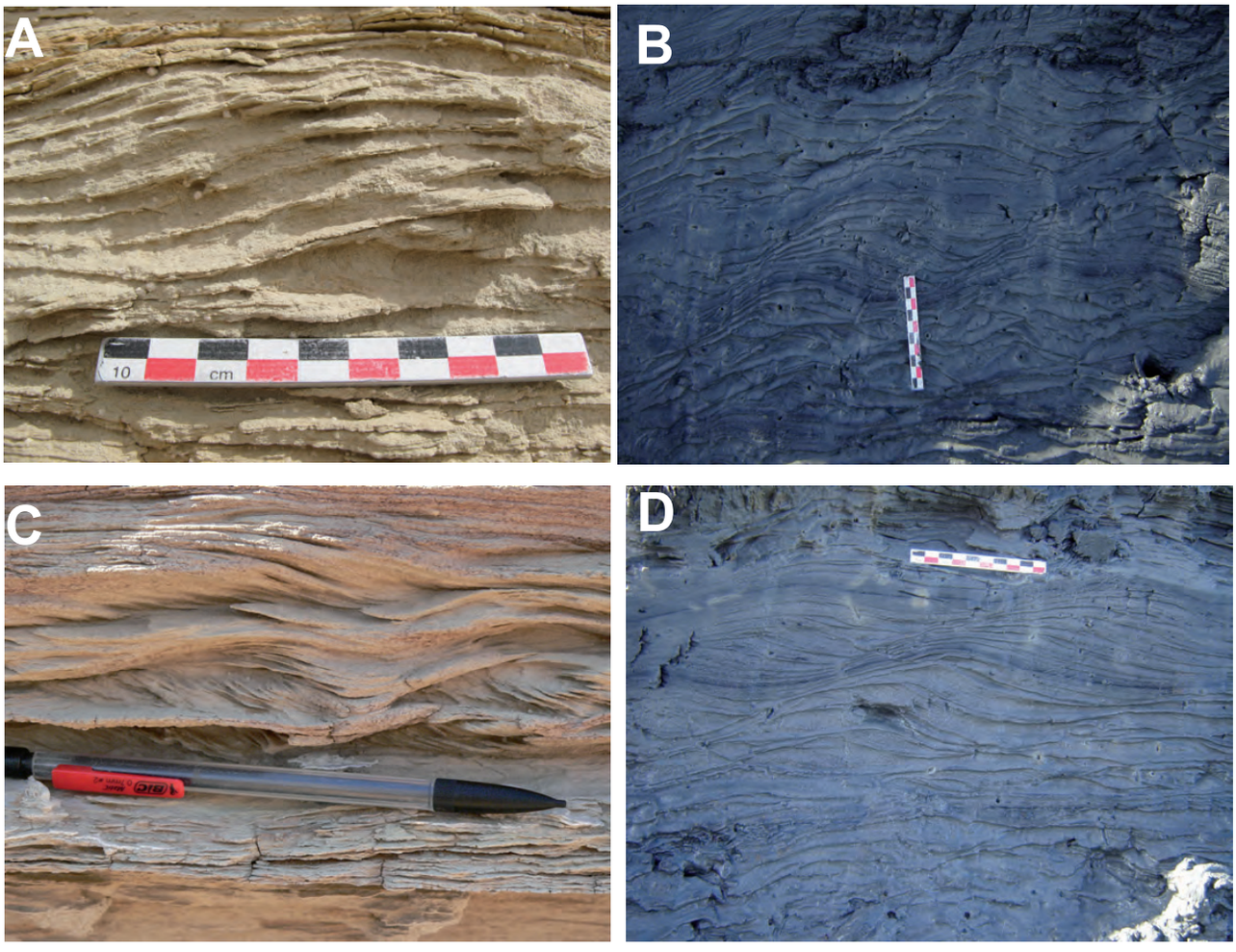


Fig. 12. photos A to D shows the occurrences of climbing ripple in ancient- (A and C, Dur At Talah) and modern- (B and D, Mont Saint Michael) tidal environments. Note, mud drapes (and double drapes as in A) separating successive sand ripples in both ancient and modern examples. The pencil head in C points to the current direction. The ripples in both modern and fossil examples are built upward in overlapping series rather than migrating in a forward direction, indicating rapid rate of sedimentation.

bioturbated facies of the Dur At Talah sequence, the most common of which are the rhythmic sand-mud layers alternation (e. g., Dalrymple and Choi, 2003; Fig. 15). Reactivation surfaces caused by tidal flow reversal (Klein, 1970; Allen 1973) are common as well. In addition, purely continental evidence is uncertain in this facies. Accordingly, it is termed ″ tide-dominated″ facies.

It can be concluded that tide-dominating succession is displayed as a lateral and vertical alternations of tidal (mud and sand) flat intersected/ amalgamated with a simple and complex tidal channels. Similar channeling features have been documented by Schumacher *et al* (2010) in the Eocene Green River Formation, Uinta Basin, within the Tide-dominated succession with certain evidence of tidal dominance. Moreover, there are many criteria that emphasize a continual, uninterrupted, and relatively rapid sedimentation rate, characteristic of tidal setting. Most important of those criteria are: (i) the presence of very common, well preserved climbing ripple structure. The development of climbing-ripple from ripples requires that abundant sedimentation is continually available to a current or wave so that the ripple are built upward in an overlapping series rather than merely migrating in a forward direction (e. g. Allen 1963); (ii) This interval possess a common similarity among the type of sediments which embraces identical trace fossil assemblages such as Thalassainoides and variety of Skolithos, and other fossil such as large skulls of crocodilian , intact part of fish skeleton and other vertebrate remains (e. g. Wight, 1980; Rasmussen *et al* 2008). Fig. 16 shows some examples of such fossil assemblages; and (iii) the common occurrences of well-preserved, soft sediment deformation. The tide-dominated succession, therefore, can be considered as an

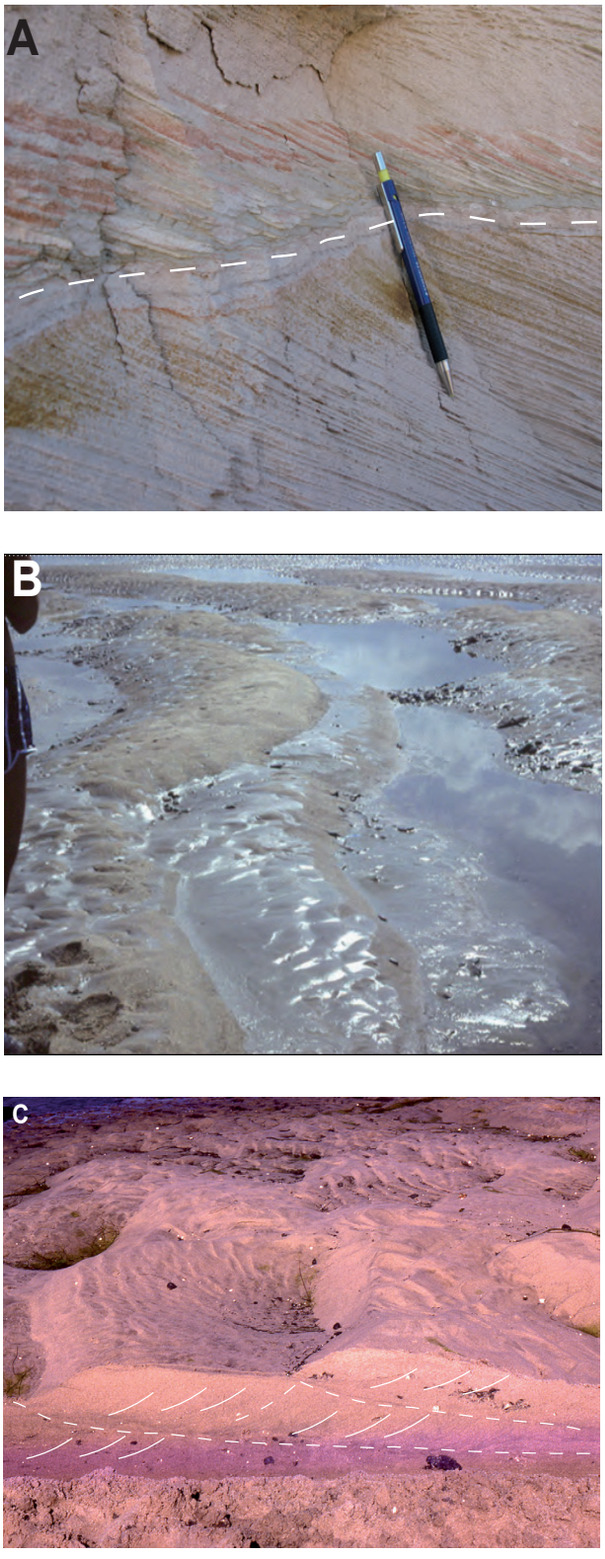


Fig. 13. photos A to C, show (A; Dur At Talah) mud drapes which appear in green, coating the cross bedded sandstone forests. In (B) Mont Saint Michael) the mud is draping the sandstone's current megaripple. In (C, Mont Sainte Michael)) mud drapes occurrences are very similar to that in (A), the white inclined lines represent foresets, the drapes appears as a greenish shade on the foreset. Dashed line in A indicates the reactivation surface between two sets of cross bedding.

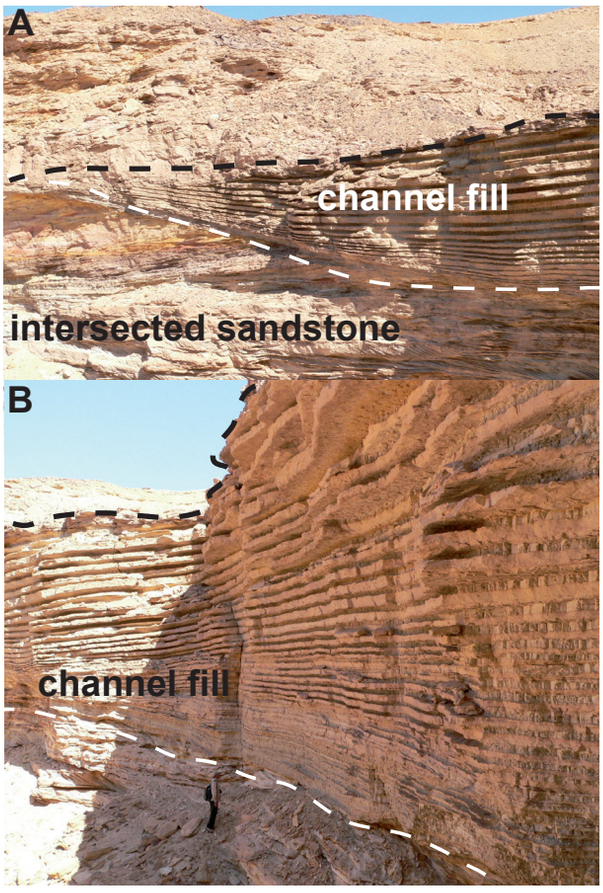


Fig. 14. photos (A and B) from Dur At Talah Formation show locally existed channel infilling morphology. Photo A shows general view indicating the channel base and top and the alternating sand and mud beds occupying the channel (width of the photo about 50 m). B is another view of the same package to the right of photo A (the center of the channel), regular thickening up of the bed is observed.

aggrading phase involves equilibrium between sedimentation rate and accommodation space availability.

Tide-influence: The deposition of transitional or tidal influenced (cross bedded medium to coarse sandstone) facies has occurred after a remarkable rapid and strong erosion of the underlying tide-dominated sediments, this is proven by the presence of erosional relics (Fig. 17) from the tidal unit floating in the transitional facies above the prominent erosional surface. Those relics are in form of pebbles and cobbles of intrabasinal mud clasts and, occasionally, in form of erosional remnants (with depositional sedimentary structures preserved) embedded within the cross bedded sandstone. Similar erosional remnants are observed also in Mont Saint Michael Bay. The presence of such remnants indicate two facts: (i) stronger energy acted on that unit, than that acted in the tide-dominated unit below,

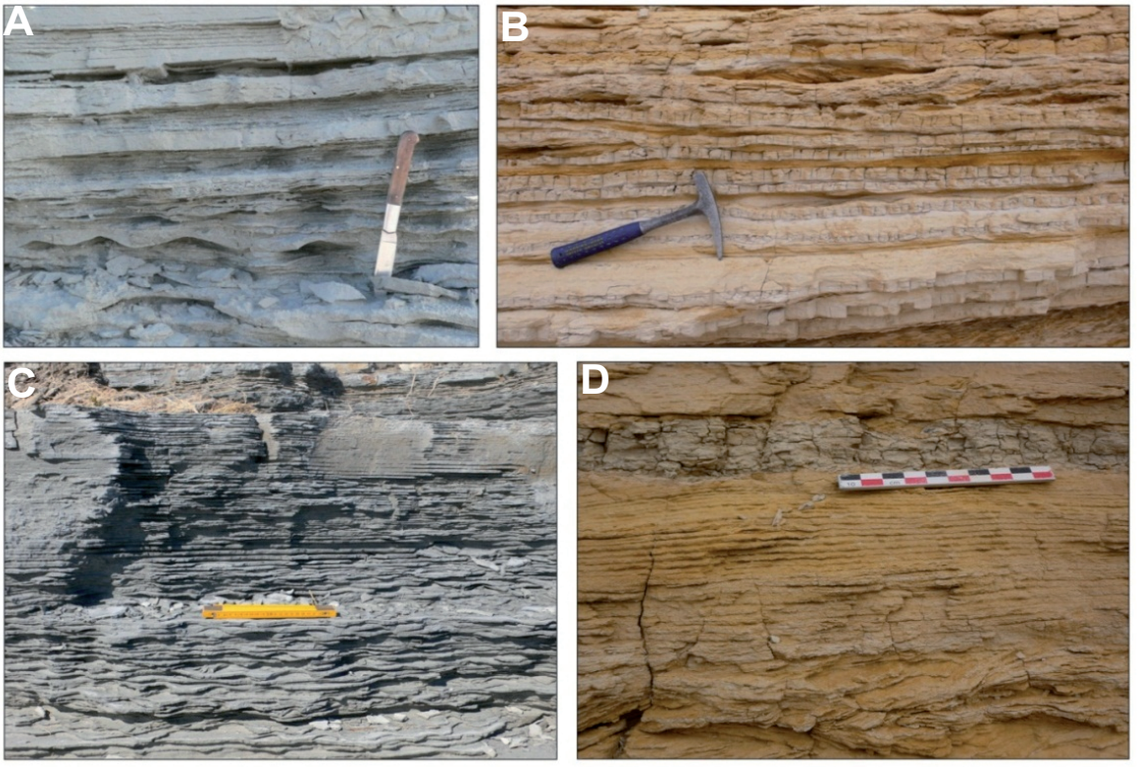


Fig. 15. Photos A to D illustrate mud-sand alternation which is common in the bioturbated (mud-dominated) facies succession, Dur At Talah formation (B and D, Eocene). Structures in B and D are closely comparable with those in A and C from the intertidal zone of Mont Saint Michael. The photos above shows neap spring tide variations, the photos below shows ebb aggradation.



Fig. 16. photos (A to D) show examples of vertebrate fossils from Dur At Talah Formation: (A) well preserved crocodilian skull, (B) well preserved fish, (C) vertebra of fish, and (D) large bone probably from whale body. These fossils are known for nearshore environments.

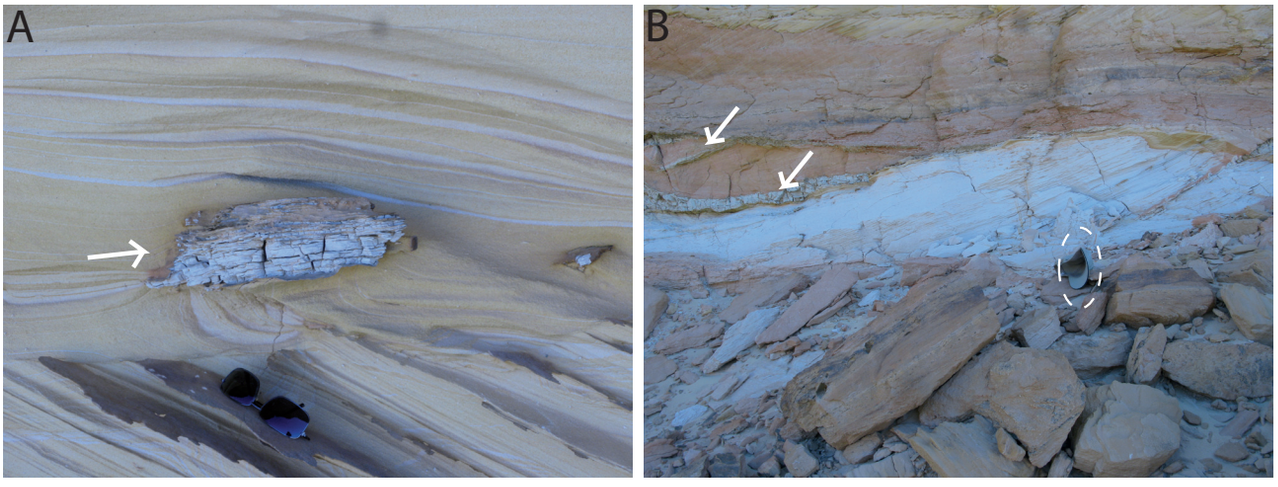


Fig. 17. photos A and B from cross bedded (tide-influenced) sandstone facies of Dur At Talah Formation: (A) shows small remnant (arrow) from the underlying tide-dominated facies, floating in the younger sandstone. Photo B is another example shows larger erosional remnant composed of muddy sediments (arrows; the hat inside the circle for scale). The presence of such erosional relics would indicate rapid sedimentation, and it also indicates that the deposition of the sandstone is shortly after the mud of the lower unit.

(ii) short or no time gap between the depositions of both facies. In spite of this increase in the energy spectrum, tidal processes are still acting as evidenced by sedimentary structures illustrated in Figs. (10-14 in the previous section) such as mud drapes on sandy foresets (Selly, 1992; Darymple and Choi, 2003), mud couplet (Dalrymple, 1992) and bidirectional cross bedding.

This unequivocal change in sedimentary features between the tide-dominated and the tide-influenced facies suggests three alternatives: (i) change of the environment from narrow embayment to less restricted more open marine (closely resemble to the Lower Cretaceous Woburn sand in Southern England; Yoshida *et al* 2002) side of the Sirt embayment; (ii) the second alternative suggested occurrences of a pulse of transgression (i.e., relative see level rise) which allowed change from more muddy intertidal zone to more sandy subtidal setting. The later situation is comparable with the modern macrotidal environments of Mont Saint Michael, and that of the Bay of Foundy in the Canadian coast (e.g. Dalrymple and Choi, 2003).

Fluvial setting: The contact of the transitional facies with the overlying fluvial facies is irregular and complex; it requires more field investigation to be well defined. Nevertheless, a zone of pebbly sandstone beds amalgamated with paleosoil appears to be located above the contact zone. In some places, there is an intensive silicified wood bearing sandstone bed lies above the tidal influenced sandstone facies. This sandstone bed with dominating, large size wood trunk marks the onset of completely terrestrial environment that certainly bears fluvial characteristics. This interval therefore, is probably represents a forced regression and northward shoreline retreat.

CONCLUSIONS

Sediments composing Dur At Talah escarpment are made up, from bottom to top, of three different packages of facies: (i) the clay-oyster bank interbedded facies, (ii) the bioturbated fine sand to mud facies, (iii) the medium to coarse sandstone facies, and (iv) the micro conglomeratic sandstone facies.

Facies (i) correspond to marine environment, facies (ii and iii) correspond to tidal environment, and facies (iv) is a typical fluvial environment.

Both the bioturbated facies and the cross bedded sandstone facies (ii and iii) bear sedimentary structures that are operating in modern tidal environment of Mont Saint Michael Bay.

Many described sedimentary structures suggested that the studied sequence has been deposited rapidly without indications of major interruption of sedimentation, and because the sequence display coarsening upward trend it might suggest an overall regressive trend, interrupted by transgressive pulses.

ACKNOWLEDGMENTS

I would like to thank the Libyan Petroleum institute for allowing me to accomplish this study. Thanks go also to Dr. M. Al Bakai for his useful corrections of the manuscript.

REFERENCES

Abadi, A. M., Van Wees, J., Van Dijk, M. P, and Cloetingh S. A. (2008). Tectonic and subsidence evolution of the Sirt Basin, Libya. AAPG Bulletin, v. 92: 993-1027.

Ahlbrandt, T. S. (2001). The Sirte Basin Provinces of Libya-Sirte-Zelten total petroleum system. U.S. Geological survey Pulltin 2202-F: 1-29.

Allen, J. R. L. (1973). Features of cross-stratified units due to random and other changes in bed forms. Sedimentology 20: 189-202.

Allen, J. R. L. (1990). The Severn Estuary in southwest Britain: its retreat under marine transgression, and fine-sediment regime. Sedimentary Geology 66: 13-28.

Arambourg C. (1963). Continental vertebrate faunas of the Tertiary of North Africa. In: Howell F.C, Bourliere F. (eds), African ecology and human evolution. Chicago, IL: 55–60.

Ashley, G. M. (1990). Classification of large-scale subaqueous bed-forms: a new look at an old problem. Jour. Sedim. Petro. 60: 160-172.

Barr, F. and Weegar, A. A. (1972). Stratigraphic Nomenclature of the Sirt Basin, Libya. Pet. Expl. Soc. Libya, Tripoli. p179.

Benfield, A. C. and Wright, E. P. (1980), Post-Eocene sedimentation in the Eastern Sirt Basin, Libya. Sec. Symp. Geol. Libya, V 2 : 463-499.

Bonnot-Courtois, C., Caline, B., L'Homer, A. and L. E. Vot. (2002). (ed). La Baie du Mont-Saint-Michel et l'estuaire de la Rance. Environnements sédimentaires, aménagements et évolution récente. Bull. Centre Rech. Elf Explor. Prod., Mém. 26: p256.

Bridge, S. J and Demicco, R. V. (2008). Earth Surface Processes, Landforms and Sediment Deposits. The University press, Cambridge, UK. p815.

Busrewil, M. T., Mriheel, I., Al-Fasatwi, Y. (1996). Volcanism, Tectonism, and hydrocarbon potential of parts of Al Haruj area, SW Sirt Basin, Libya. In: Sedimentary Basins of Libya, First Symposium "The Geology of Sirt Basin", Ed. by: Salem M. J. et al. Vol. III: 317-329.

Conant, L. C and Goudarzi, G. H. (1967). Geological Map of Libya, 1: 2000000 scale. U. S. Geological survey. Misc. Geol. Invest. Map, 1-350A. Washington.

Dalrympe, R. W. (1992). Tidal depositional systems. In: Walker, R. G. and James, N. P. (eds), Facies Models: response to sea level change. Geological association of Canada, St. John's: 195-218.

Dalrympe, R. W., Zaitlin, B. A. and Boyd, R. (1992). Estuarine facies model: Conceptual basis and stratigraphic implications. Jour. Sedi. Petr., 62: 1130-1146.

Dalrympe, R. W. and Choi, K. (2003). Sediments transport by tidal currents. In: Middleton, G. V. (Ed.), Encyclopedia of Sediments and sedimentary rocks. Kluwer Academic publisher, Dordrecht: 606-609.

Dalrympe, R. W. and Choi, K. (2007). Morphologic and facies trends through the fluvial-marine transition in tide-dominated depositional system: A schematic for environmental and sequence stratigraphic interpretation. Earth-Science Reviews 81: 135–174.

Duringer P., Schuster M., Métais E. Benammi M., Salem M. J. and Jaeger J-J. (2008). New insight into the sedimentary record of the Dur At-Talah (Paleogene, Libya). In: The Geology of Southern Libya, Sedimentary Basins of Libya, Fourth Symposium (Ed. By: M. J. Salem *et al*). In press.

Gallawy, W. E. (1975). Process framework for describing the morphologic and stratigraphic evolution of deltaic depositional systems. In: Deltas, Models for exploration (ed. By: M. L. Broussard). Huston, TX: Houston Geological Society: 87-98.

Goudarzi, G. H. (1980). Structure-Libya. In: Geology of Libya (ed. By: Salem, M. J. and, M. T. Busrewil). Tripoli, Libya, Al-Fatah University, III: 879-892.

Gruenwald, R. (2001). The Hydrocarbon prospectivity of the Lower Oligocene deposits in the Maragh trough, SE Sirt Basin, Libya. Journal of Petroleum Geology, v. 24 (2), p. 213-231.

Harris, P. T. Pattiaratchi, C. B., Collins, M. B. and Dalrymple, R. W. (1995): what is a bed load partings? In: Tidal signatures in Modern and ancient sediments (ed. By: B. W. Flemming and A. Bartholoma), Oxford: Blackwells: 3-18.

Jaeger, J. J., Marivaux, L., Salem, M., Bilal, A. A., Benammi, M., Chaimanee, Y., Duringer, P., Marandat, B., Métais, E., Schuster, M., Valentin, X. and Brunet, M., (2010a). New rodent assemblages from the Eocene Dur At-Talah escarpment (Sahara of central Libya): systematic, biochronological, and Palaeobiogeographical implications. Zoological Journal of Linnean Society,160: 195-213.

Jaeger, J. J., Beard, K. C., Chaimanee, Y., Salem, M. J., Benammi, M., Hlal, O., Coster, P., Bilal, A. A., Duringer, P., Schuster, M., Valentin X.,

Marandat B., Marivaux L., Métais E., Hammuda, O. and Brunat, M. (2010b). Late middle Eocene epoch of Libya yields earliest known radiations of African anthropoids. Nature 467, 1095-1099.

Klein G. de V. (1970). Depositional and dispersal dynamics of intertidal sand bars. Jour. Sedi. Petr. 40: 1095-1127.

Peregi, Z., Les Gy., Konard, Gy., Fodor, L., Gulaesi, Z., Gyalog L., Turki, S. M., Swesi, S., Sherif, K. H., and Dalub H. (2003). Geological Map of Libya 1: 250000, sheet Al Haruj – Al Abyad (NG 33-8). Explanatory Booklet, Industrial Research Centre, Tripoli: p250.

Rasmussen, D. T., Tshakreen, O. S., Abugares, M. M., and Smith, B J. (2008). Return to Dor al-Talha: Paleontological Reconnaissance of the Early Tertiary of Libya. In: A Search for Origins, (Edt. By: J. G. Fleagle, C. C.) Gilbert Elwyn Simons.

Reineck, H. E., and Wünderlich, F. (1968). Classification and origin of flaser and lenticular bedding. Sedimentology 11: 99-104.

Reinek H. E and Singh I. B. (1980). Depositional Sedimentary Environment. Second edition. Berlin, Germany: Springer-Verlag: P540.

Schumacher E. R., Kjemperud, A. V, Nystuen, P. J., Jhren, J. S. (2010). Recognation and significance of sharp-based mouth-bar deposits in Eocene Green River Formation, Unita Basin, Utah. Sedimentology, 57: 1069-1087.

Savage, R. J. G. (1971). Review of the fossil mammals of Libya. In: Symposium on Geology of Libya (Edt. By: Gray, C.). University of Libya, Tripoli: 215-226.

Selley, C. R. (1992). Applied Sedimentology. Academic Press, Harconrt Brace Jovanorich, Publishers: p. 446.

Tawadros, E. E. (2001). Geology of Egypt and Libya, publication of A. A. Balkema, USA: p468.

Vasic, N. and Sherif, K. A. (2007). Geological map of Libya 1: 250,000, Sheet Dur At Talah (NG 34-9). Explanatory booklet, Industrial Research Centre, Tripoli: p180.

Visser, M. J. (1980). Neap-Spring cycles reflected in Holocene subtidal large-scale bed form deposits: a preliminary note. Geology 8: 543-546.

Wight, A. W. R. (1980). Paleogene vertebrate fauna and regressive sediments of Dur At Talaha, southern Sirt Basin, Libya. In: Geology of Libya (Edt. By: M. J. Salem and M. T. Busrewil), Academic Press, London, V1: 309-325.

Triassic and Creataceouse Palynomorphose from Well A2-045 /01 Offshore Libya

Rajab El-Zaroug*

Abstract: Triassic and Cretaceous palynomorphs have been recovered from twenty three ditch cutting samples of borehole A2-054/01 located in the most northern part of Sirt Basin (Offshore), Libya.

Microscope investigations revealed moderately rich assemblages consisting only miospores in the Triassic section and mixed palynomorphs (dinocysts, miospores & algae) in the Cretaceous section. The recovered palynomorphose from the studied samples enabled to erect two distinctive palynological assemblages. These assemblages range from Early Triassic to Early Cretaceous in age. The ages assigned to these assemblages have been determined by comparing the palynomorphs assemblages with similar assemblages recorded from Mesozoic sequences in other nearby regions in Africa, North America and Europe.

Paleoenvironmental interpretation of the investigated sediments revelled that Cretaceous sediments were mostly deposited in shallow marine environment; other investigated rocks (Triassic) were deposited either in non-marine environment or in marginal marine environment.

Keywords: Triassic, Cretaceous, Palynomorphs, Offshore Sirt Embayment.

INTRODUCTION

Hot shot Playonological study have been utilized in order to define age and depositional environments of selected twenty three cutting samples from well A2-054/01 located in the Offshore Sirt Embayment, Libya (Fig. 1), which belongs to Hess Libya, located in the Offshore Libya.

The study based on selected of twenty three cutting samples (Table 1), and despite of difficulties caused by caved palynomorphs from younger strata and highly carbonised of palynomorphs in the last two samples (10660-10675), which may be caused by either continental environment or/and affected by heat of volcanic rocks. Palynological recovery in general was fair in most samples.

Microscope investigations revealed fair assemblages consisting of pollen grains, dinoflagelates cysts and few spores. Palynodebris (amorphose organic matter & woody derbies) are heavely counted in the investigated samples. The extracted palynomorphs assemblages range from Early Triassic – Late Cretaceous in age. The ages assigned to these assemblages have been determined by comparing the palynomorphs assemblages with similar assemblages recorded from Mesozoic sequences in other nearby regions such as Sirt Basin, north east Libya region, south east Libya (Al Kufrah Basin) and from other parts of Africa and also from North America and Europe. Paleoenvironmental interpretation is based on interpreted lithological and palynological criteria.

MATERIAL AND METHODS

Samples: Twenty three cutting samples from well A2-054/04 were selected by HESS geologists (Table 1).

Laboratory Techniques: The Samples were prepared according to standard palynological procedures. The preparation stages can be summarized as following:

Cleaning sample: Samples were washed using tap water and 150 µm mesh sieve to remove drilling mud.

Picking: All selected samples were sieved in 2 mm mesh sieve to eliminate any possible caved material (material larger than 2mm assumed to be caved)

*Geological Department, Faculty of Engineering, Tripoli University
rzaroug@yahoo.com

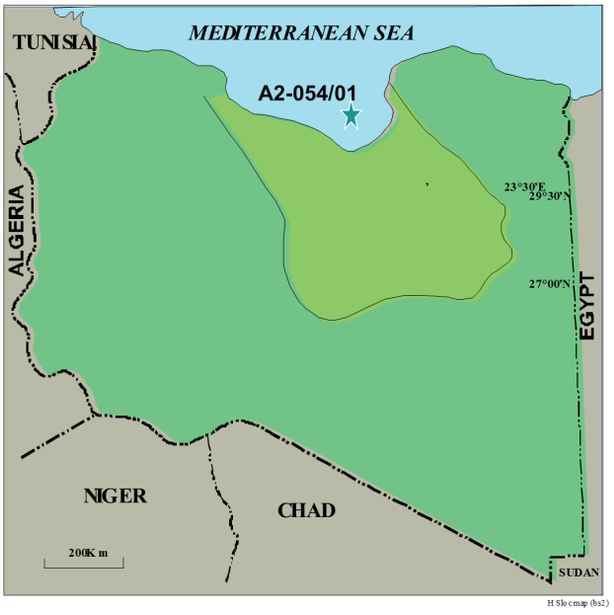


Fig.1. Location of the studied well A2-054/04

Table 1: Samples Selected for Palynological Analyses

S/N	Depth/feet
1	10000-10020
2	10020 - 10040
3	10040 - 10060
4	10060 - 10080
5	10080 - 10100
6	10100 - 10120
7	10120 - 10140
8	10140 - 10160
9	10160 - 10180
10	10180- 10200
11	10200 - 10220
12	10220- 10240
13	10240 - 10260
14	10260 - 10280
15	10280 - 10300
16	10300 - 10320
17	10320 - 10340
18	10340 - 10360
19	10360 - 10380
20	10380 - 10400
21	10400 - 10420
22	10660 - 10670
23	10675

Demimeralization:

- Carbonate removal using hydrochloric acid (HCI 18%).
- Silicate removal using hydrofluoric acid (HF 40%).
- Sieving using 10, 18 and 64 micron sieve as appropriate
- Oxidation to remove unwanted organic matter using nitric acid (HNO3 65%) for about 3-5 minutes (applied for some samples)
- Removal of minerals (separation the inorganic mineral from the organic matter by using zinc chloride (ZnBr) with specific gravity 2.00.
- The cleaned and neutralized residue is mixed with few drops of the dispersing solution (PVA) to prevent coagulation of the organic residue on the slide. This mixture spread on two 24X50mm cover slips using pipettes and allowed to dry on hot plate (25˚C). Mounting was achieved by placing one or two drops of the resin on to a clean microscope slide (76 X 26mm).

PALYNOLOGICAL RESULTS

Interval (ft.): 10000–10280
Samples analyzed: 14 Cutting samples.
Age: Early–Mid Cretaceouse (Albian-Cenomanian).

Remarks: Mixed land derived and marine palynomorphs, were recovered from this interval. Herbaceous debris also was highly counted in many samples of this interval.

Age of this interval based on the presence of the following palynomorphs:

Dinocyst: *Florentinia mantellii, Oligospheridium pulcherrimum, Oligospheridium complex, Odontochitina operculata, Subtilisphaera zawia, S. Cheit, Cyclonephelium* spp., and *Coronifera sp.* Cf. *C. tubulosa*.

Miospores: *Afropollis operculatus, Concavisporites spp., Ephedripites* spp., *Classopollis brasiliensis, Balmeisporites holodictyus, Elaterosporites castelainii* and *Cicatricosisporites* spp.

Similar assemblages were reported by Thusu & Van Der Eem (1985), Batten & Uwins (1985) and Uwins & Batten (1988) from Early – Mid Cretaceous sediments of North East Libya region.

Paleoenvironment: The mixed presence of land derived organic matter (miospores & woody derbies) and marine Dinocysts suggest deposition in shallow marine environments. However high abundance of herbaceous debris in number of samples suggest

close proximate toward the shore line. The presence of fresh water algae (*Pediastrum palaeogenites*) indicates fresh water influences.

Interval (ft.): 10280 – 10420
Samples analyzed: 7 Cutting samples.
Age: Early Cretaceous (late Neocomian-Aptian).

Remarks: Sparsely land derived organic matter, dominated by miospores and herbaceous debris were recovered from this interval. Age of this interval based on the presence of Miospores; *Chomotriletes minor, Dicheiropollis etruscus, Perotrilites* sp. & *Trilobosporites* cf. *Bernissartensis, along with Dinocysts; Pseudoceratium retusum, Muderongia simplex* and *Aptea securigera*.

The above assemblages indicate an age no younger than Early Cretaceous (Aptian). Almost similar assemblages were reported from early Cretaceous sediments, NE Libya by Batten (1996); Batten & Uwins (1985), Uwins & Batten (1988) and Thusu *et al* (1988).

Paleoenvironment: The predominance of land derived material in which herbaceous debris were the most common, few marine palynomorphs (few specimens of dinoflagelate cysts, most of them can be of younger cretaceouse strata), suggest deposition in marginal to shallow marine environment.

Interval (ft.): 10480 – 10675
Samples analyzed: 10 Cutting samples.
Age: ?Early–Mid Triassic (Scythian-Karnian).

Remarks: Land derived organic matter, dominated by pollen grains and herbaceous debris was recovered from this interval. Age of this interval based on the presence of (if insitu) *Lunatisporites pellucidus, Alisporites australis, A. Robusta, Aratrisporites centatus, A. Scabrates, A. Composites, Platysaccus leschikii, P. Papilionis, Protohaploxypinus* spp., and *Voltziaceaesporites heteromorphus.*

Similar assemblages were reported from Early Triassic sediments, Northwest Libya by (Adloff *et al* 1986). Almost similar assemblages were recorded by Brugman & Visscher (1988), from Early Triassic sediments in Northeast Libya

Paleoenvironment: The predominance of land derived organic matter in which pollen grains and herbaceous debris was the most common and almost absent of marine palynomorphs (few Acritarchs were observed, but regarded to be either caved or recycled and also few caved dinocysts from younger strata), suggest deposition in a non marine environment.

Table 2: Summary of the Stratigraphy

Top Depth/feet	Series	Stage
10000-10280	Mid-Cretaceous	Albian-Cenomian
10300-10460	Early Cretaceouse Unconformity	Neocomian Aptian
10480 – 10675 (TD)	Early-Mid Triassic	Scythian-Karnian

The following summary tables are based on data obtained from the analyses of ditch cuttings samples. The boundaries quoted are either the bottom depths of sampled intervals or have been adjusted to suitable wire line log break.

CONCLUSION

Two distinctive palynological zones have been established. These from the Triassic and Cretaceous sediments of the studied well A2-054/04, on the basis of miospores and acritarchs, ranging in age from Early Triassic to Early Cretaceous (Fig. 2). These zones are assemblage zones and are correlatable with similar assemblages recorded from Mesozoic sequences in other nearby regions in Africa, North America and Europe.

Paleoenvironmental interpretation of the investigated sediments revelled that Cretaceous sediments were mostly deposited in shallow marine environments; other investigated rocks (Triassic) were deposited either in non-marine environments or in marginal marine environments.

REFERENCES

Adloff, M. C., Doubinger, J., Massa, D. & Vachard, D. (1986). Trias de Tripolitain (Libya), Nouvelles Donnees Biostratigraphiques et Palynologiques. Rev. Inst. Fr. Petrole, 40(6): 27-63.

Batten, D. J. (1996). Mesozoic–Tertiary Spores and Pollen Introduction. In: Palynology: Principal and application, (ed. by: J. Jansonius and D. C. Mcgregor) V. 2: 751-753.

Batten, D. J. & Uwins, P. J. R. (1985). Early to Late Cretaceous (Aptian–Cenomanian) Palynomorphs. In: The Palynostratigraphy of North-East Libya, (ed. by: B. Thusu and B. Owens). V. 4(1): 151-168.

Brugman, W.A. and Visscher, H. (1988). Permian and Triassic Palynostratigraphy of Northeast Libya. In: Subsurface Palynostrati-Graphy of Northeast Libya, (ed. by:A. El-Arnauti, B. Owens and B. Thusu). Research Centre, Garyounis University, Benghazi: 157-169.

Thusu, B. and Van dereem, J. G. L. A. (1985). Early Cretaceous (Neocomian-Cenomanian) Palynomorphs. In: The Palynostratigraphy of North-East Libya, (ed. by: B. Thusu and B. Owens). Journ. Micropalaeontology, V. 4: 131-150.

Thusu, B., Van Dereem, J. G .L. A., El-Mehdawi, A. and Bu-Argoub, F. (1988). Jurassic-Early Cretaceous Palynostratigraphy in Northeast Libya. In: Subsurface palynostratigraphy of northeast Libya, (ed. by: A. El-Arnauti, B. Owens and B. Thusu). Research Centre, Garyounis University, Benghazi: 171-213.

Uwins, P. J. R. and Batten, D. J. (1988). Early to Mid-Cretaceous Palynology of Northeast Libya. In: Subsurface palynostratigraphy of northeast Libya, (ed. by: A. El-Arnauti, B. Owens and B. Thusu). Research Centre, Garyounis University, Benghazi: 215-258.

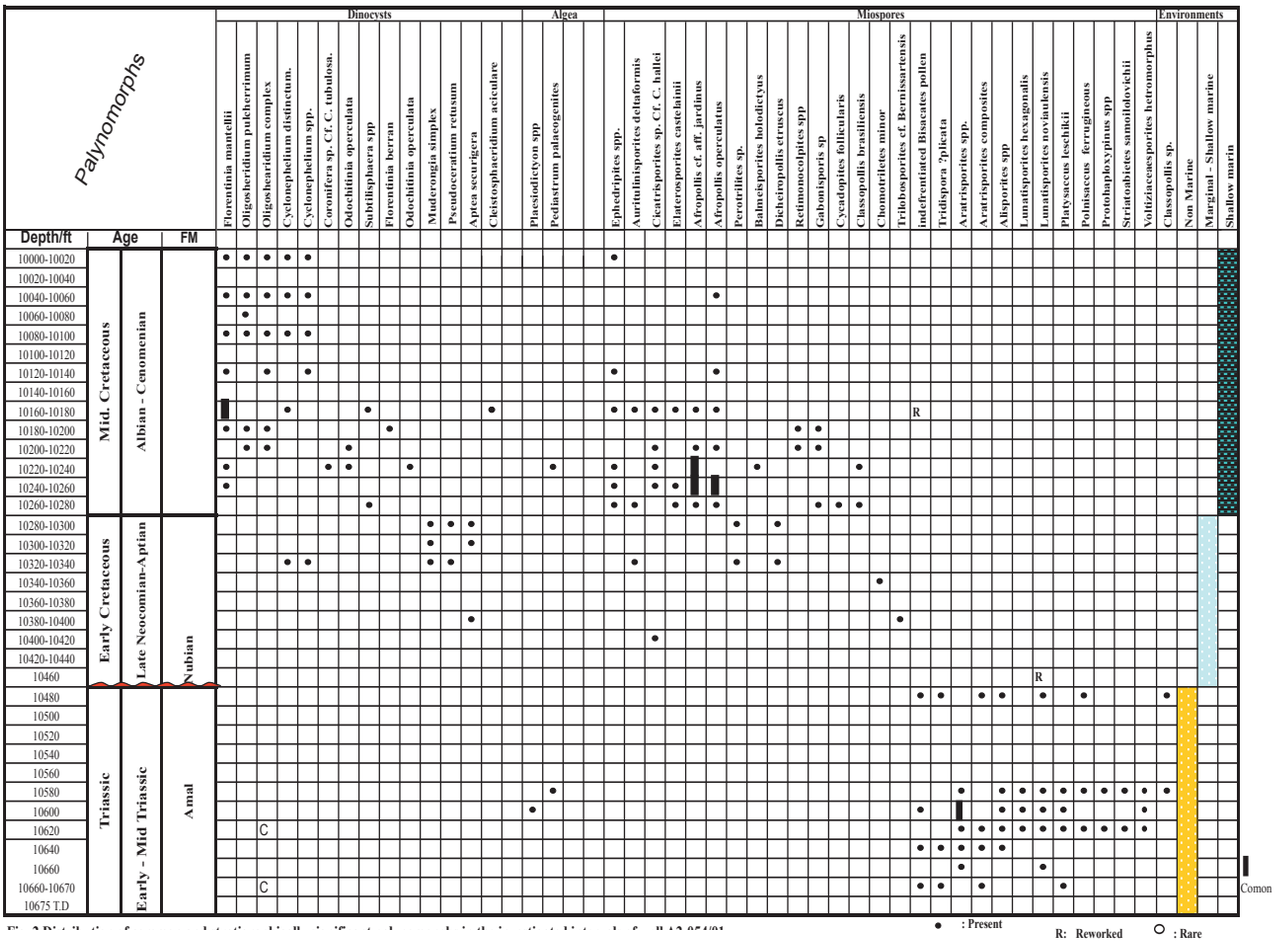


Fig.2. Distribution of common and stratigraphically significant palynomorphs in the investigated intervals of well A2-054/01.

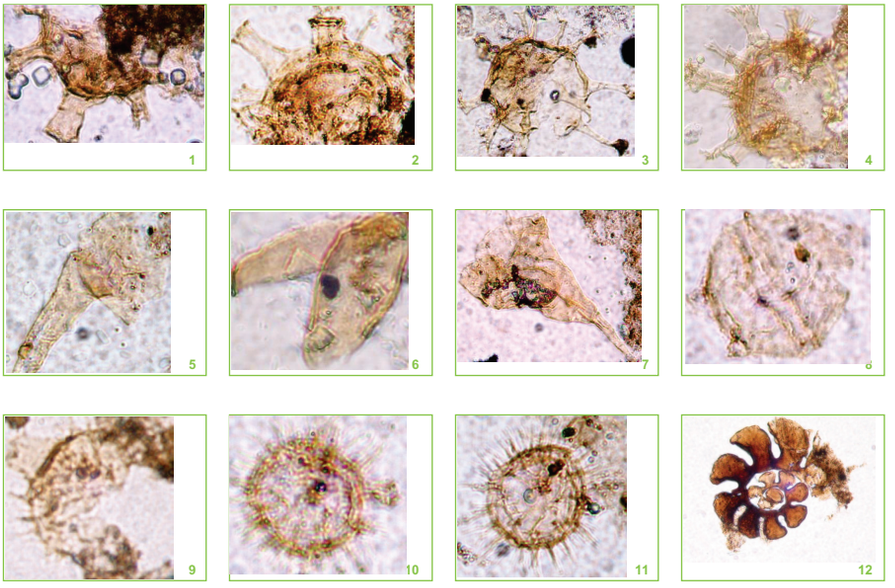


PLATE I

Early and Mid Cretaceous Dinocysts
The species name is followed by the sample depth in feet. All figures are X800 unless otherwise indicated

Plate I - 1, 2 Florentinia mantellii @ 10160-10180
Plate I - 3, 4. Oligospheridium complex @ 10080-10100
Plate I - 5 - 7 Odontochitina operculata @ 10200-10220
Plate I - 8. Subtilisphaera zawia @ 10260-10280
Plate I - 9. Florentinia berran.
Plate I - 10, 11 Coronifera sp. Cf. C. tubulosa @ 10220-10240
Plate I - 12. Foram lining @ 10040-10060

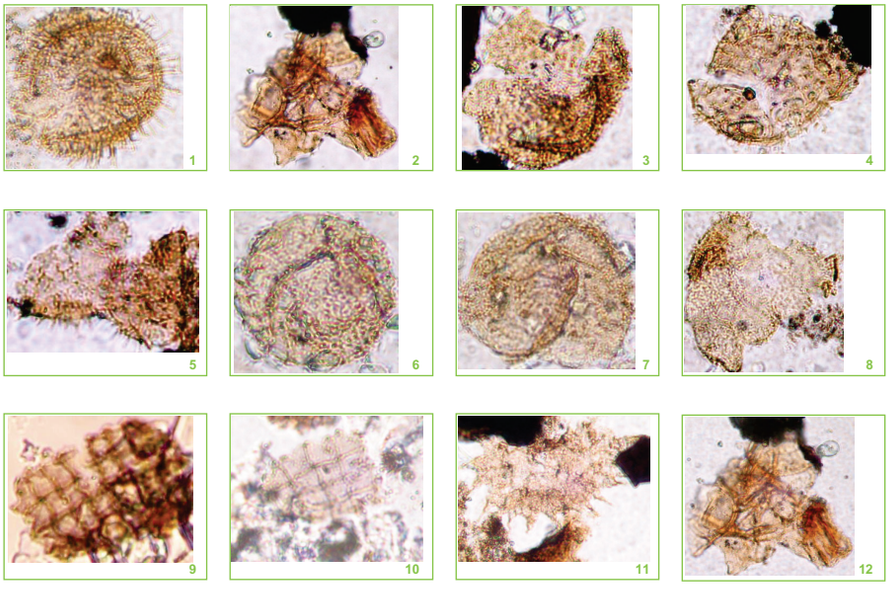


PLATE II

Early and Mid Cretaceous Dinocysts & Algea

Plate II - 1. Cleistosphaeridium aciculare @ 10340-10360
Plate II - 2, 12 Muderongia simplex @ 10320-10340
Plate II - 3, 4. Cyclonephelium distinctum @ 10340-10360
Plate II - 5, 8 Pseudoceratium retusum @ 10340-10360
Plate II - 6, 7 Cyclonephelium sp@ 10300-10320
Plate II - 9, 10 Plaesiodictyon spp (Algae) @ 10675
Plate II - 11 Pediastrum palaeogenites (fresh water algae) @ 10220-10240

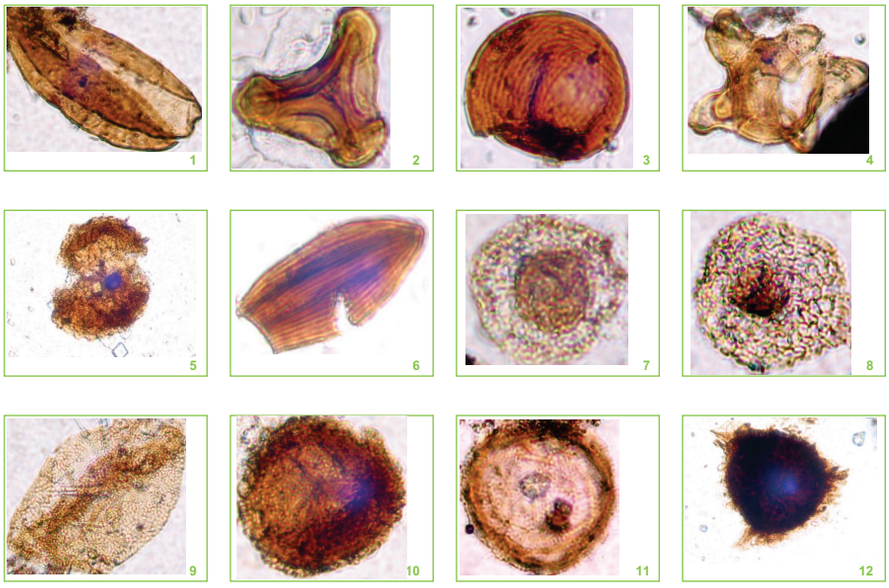


PLATE III

Early and Mid Cretaceous Miospores

Plate III - 1, 6 Ephedripites spp @ 10160-10180
Plate III - 2 Auritulinisporites deltaformis. @ 10160-10180
Plate III - 3 Cicatrisporites sp. Cf. C. hallei @ 10160-10180
Plate III - 4 Elaterosporites castelainii@ 10200-10220
Plate III - 5 Dicheiropollis etruscus @ 10320-10340
Plate III - 7 Afropollis operculatus @ 10160-10180
Plate III - 8 Afropollis cf. aff. jardinus @ 10320-10340
Plate III - 9 Retimonocolpites spp @ 10180-10200
Plate III - 10 Gabonisporis sp. @ 10220-10240
Plate III - 11 Chomotriletes minor @ 10340-10360
Plate III - 12 Perotrilites sp.. @ 10320-10340

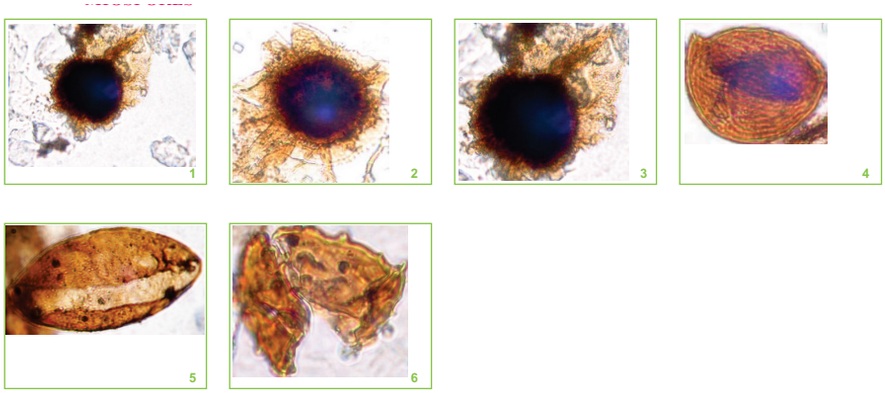


PLATE IV

Early and Mid Cretaceous Miospores

Plate IV - 1 - 3. Balmeisporites holodictyus @ 10220-10240
Plate IV - 4. Classopollis brasiliensis @ 10220-10240
Plate IV - 5. Cycadopites follicularis @ 10300-10320
Plate IV - 6. Trilobosporites cf. Bernissartensis@ 10380-10400

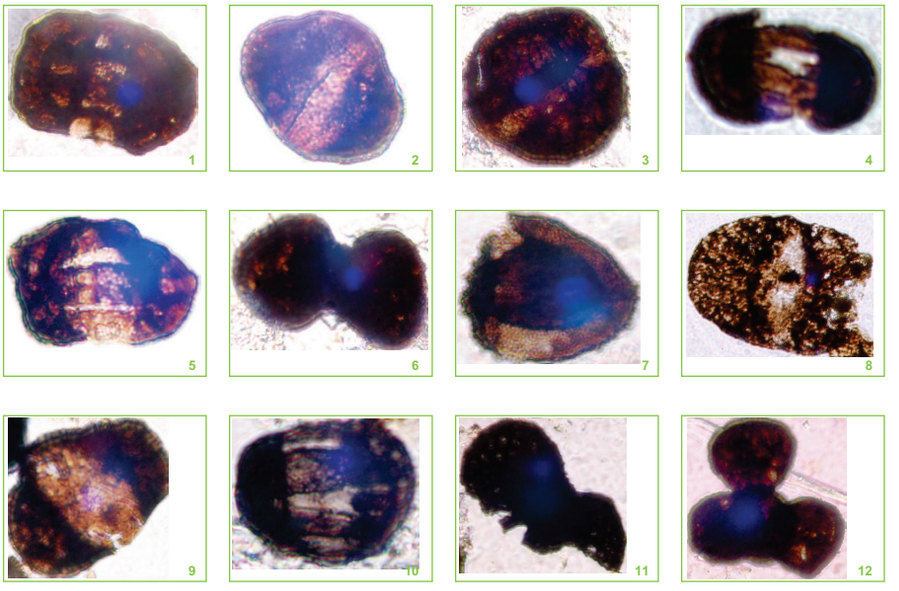


PLATE V

Triassic Miospores

Plate V - 1	Lunatisporites hexagonalis@ 10660
Plate V - 2	Triadispora plicata @ 10580
Plate V - 3	Polnisaccus ferrugineous @10660
Plate V - 4	Protohaploxypinus spp @10600
Plate V - 5	Striatoabietes samoilolovichii @10660
Plate V - 6	Platysaccus leschikii @10660
Plate V - 7	Aratrisporites composites @ 10620
Plate V - 8	Voltziaceaesporites hetromorphus @ 10600
Plate V - 9	Alisporites spp., @10600
Plate V - 10	Lunatisporites noviaulensis @10660
Plate V - 11	Indiferentiated Bisaccates pollen @ 10600
Plate V - 12	Classopollis sp. @ 10600

Systematic Description Ostracods Fauna from the Lower Tar Member (Zimam Formation) Northern Ghadamis Basin

Meloud Zedan Entat* and Amar Gammudi**

Abstract: Ostracods are widely used for geological studies due to their small size, widely distributed, and have had rapidly evolving lineage, so that we have studied these creatures from Zimam Formation (Lower Tar Member) exposed on the southern edge of the Ghadamis Basin in order to systematic accounts of Upper Cretaceous ostracods.

Twenty seven samples were collected and processed from outcrop section north of Al Qaryat Al Sharqhia which belongs to the Lower Tar Member. Lithologically consists of marl, Clay, limestone, and dolomitic limestone with gypsum in parts.

Eighteen species recorded belong to fourteen genera, four species has wide geological distribution in North Africa and the Middle East, one new species proposed (Cytherelloidea dabai) and the remaining species left under open nomenclature, although they shows similarities to earlier described fauna which reported from North Africa and the Middle East.

The ostracods species recording from the Lower Tar Member indicate deep to shallow marine environments.

Keywords: Ostracods, Zimam Formation, Ghadamis Basin, Cretaceous.

INTRODUCTION

Our purpose of this study is to find out systematic description of the Ostracoda fauna of the Maastrichtian Lower Tar Member (Zimam Formation) in Ghadamis Basin North West.

Location of the study section: The material which forms the basis of this study was collected from the outcrop 20 km north of Alqaryat Alsharghia northern Ghadamis Basin (Fig. 1), between:

Longitude	30°	33’	47’’	N
Latitude	13°	34’	93’’	E

General geology of Ghadamis Basin: The Ghadamis Basin is one of several “interior sag” basins on the North African craton. These basins are dominated by Paleozoic clastics and unconformably overlain by Mesozoic sands, carbonate and evaporites.

The Ghadamis Basin is a large basin located in northwestern Libya and extends westward into parts of southern Tunisia and eastern Algeria, where it is known as Berkine and Illizi basins respectively. This basin is bounded from the east by the Hun Graben, north by Nafusah Uplift, south by the Gargaf Arch and to the west by the Themboka High.

Basin evolution: The Ghadamis Basin was affected by three post-Ordovician orogenies. These are the Caledonian, Hercynian, and Albian, summarized by (Anketell, 1996; Guiraud, 1998 and klitzsch, 2000). The Caledonian Orogeny is the first tectonics caused deformation of strata, and

resulted in uplift and erosion of Silurian and older sediments over the NW-trending Tripoli-Tibesti Uplift. The effect of tectonics was formed sub-basins of the eastern part of the Ghadamis Basin (Zamzam Depression).

The Hercynian Orogeny was a major period of deformation and erosion during the Late Carboniferous and Permian. During this period the Nafusah Uplift emerged, reversing the regional dip and deeply eroded the Paleozoic, and formed the north side of the basin. There was also renewed uplift, along with erosion of the Gargaf Arch.

The Albian Orogeny took place during the end of Cretaceous-Early Paleocene. During this period all the western Libya became emergent, with termination of deposition in this area. This may have been the final uplift that affected the Gargaf Arch. There were however, further episodes of uplift and deformation

*Polytechnic Gharyan High Institute
**Libyan Petroleum Institute, Email: a_gammudi@yahoo.com

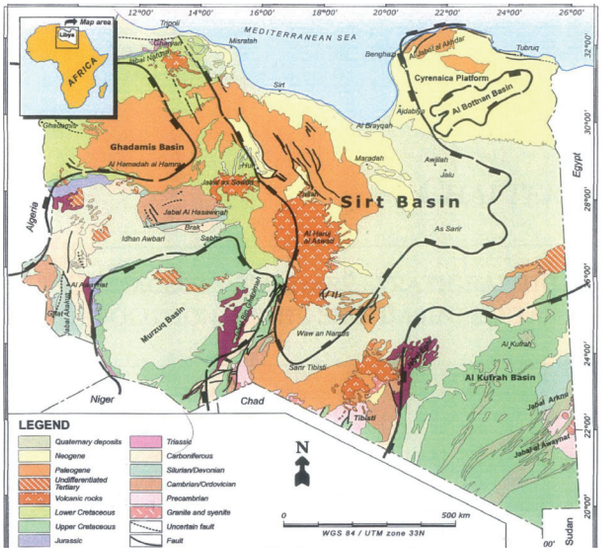


Fig. 1. Location map of the study section

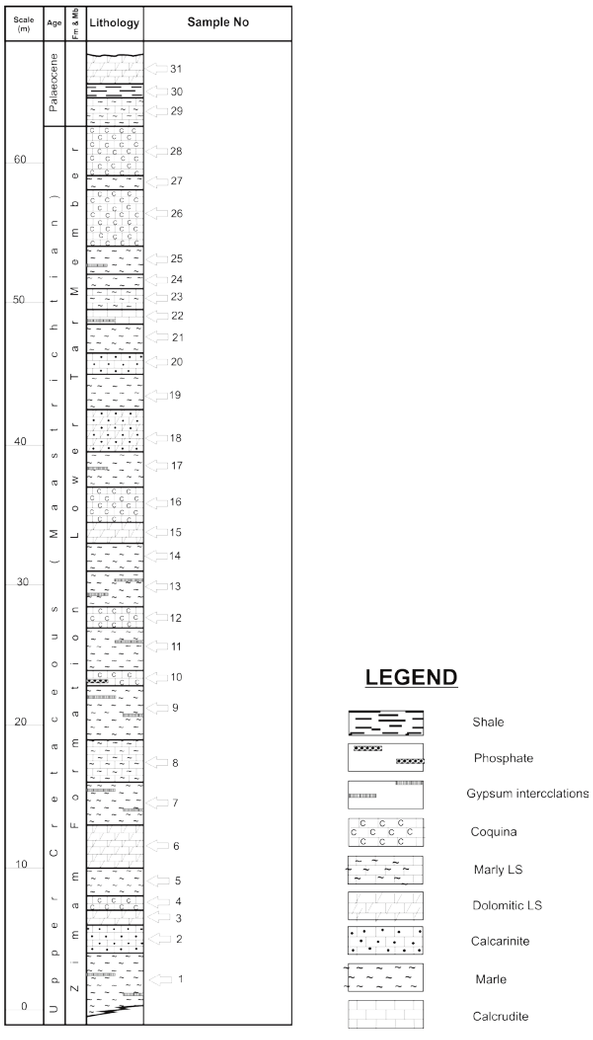


Fig. 2. Measured section and the position of the s

during the Tertiary, mainly strike-slip movements to the north and west, including the present offshore (Tripoli –Gabes Basin), these shaped the Nafusah Uplift.

ZIMAM FORMATION

Introduction: The section of Lower Tar Member has been studied and measured north of Al Qaryat Al Sharqhia (Fig. 2), and the samples were collected, processed and analysed following conventional method. This member considered to be Maastrichtian in age by previous workers. The Lower Tar considered as the oldest member in the Zimam Formation.

Jordi and Lonfat (1963) introduced the term Zimam Formation after Wadi Zimam which includes the claystone, marl, limestone and dolomitic limestone sequence of Maastrichtian-Danian age. The Lower Tar Member outcrops from the Hun graben to Wadi Suf Ajjin in the north and over a great part of Ghadamis Basin to the south of Mizda and extends to Tunisia and Algeria westward.

They subdivided Zimam Formation into Tar Marl and Had Limestone members (Fig. 3), which broadly correspond to Socna and Gheriat formations of Burollet's (1960). Subsequently, the Tar Marl Member was further divided into Lower and Upper Tar members, with a fossiliferous limy interval between them, termed as 'Socna Mollusc Bed'.

The type section of Zimam Formation originally described in an isolated hill, about 3.5 km north of Wadi At Tar Al Kabir (Lat. 29°22'30"N Long. 15°42'16"E) popularly known as Wadi Tar. A rounded SW part of the hill feature represents the type section for Lower Tar Member and the flat topped elongated feature represents the type section for the Upper Tar and Had members.

The Zimam Formation has a conformable relationship with the underlying Mizdah and overlying Shurfah formations, south of Jabal Assawda. The Lower Tar Member grades into a more clastic facies termed as Bin Affin Member by Furst (1964).

Gohrbandt (1966b) and Barr and Weegar (1972) following the definition of Jordi and Lonfat have added more data on the Zimam Formation. Eliagoubi (1975) has described a rich assemblage of planktonic foraminifera from the surface outcrops of the Lower Tar Member and its

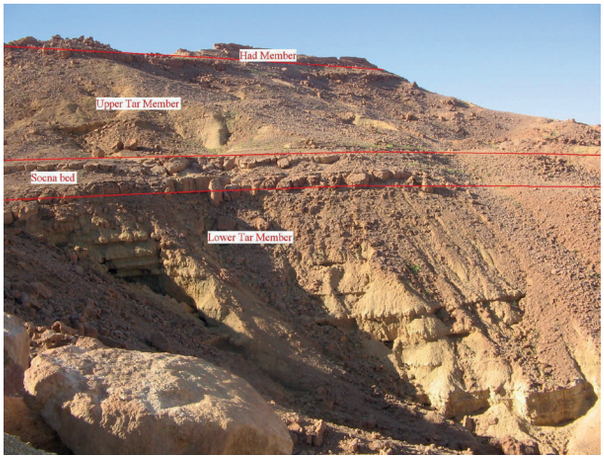


Fig. 3. Show thefour rock units of the Zimam Formation.

subsurface equivalent in Sirt Basin.

He has subdivided the Maastrichtian by planktonic foraminiferal assemblage into *Globotruncana fornicate* and *Globotruncana conica* zones , the *Globotruncana conica* zone has been further subdivided into *Globotruncana gansseri* and *Globotruncana contusa* subzones .

Energoprojekt (1975) subdivided the Zimam Formation into lower Tar Marl Unit, Socna Unit, Upper Tar Marl Unit and Had Limestone Unit.

The preserved thickness of Zimam Formation varies from 40 m in the western part (Djeneien sheet) to 265 m in the eastern part (Bani walid sheet). In the type area the exposed thickness averages 150 m.

The Zimam Formation is very rich in microfossils in the lower part, indicating deepening of the area of deposition with open sea connection, whereas, the upper part shows gradual shallowing as indicated by cross bedded Had Limestone which contains shallow water assemblage of Algae and foraminifera, suggesting littoral environment of deposition, extending up to the neritic zone.

Lower Tar Member: Jordi and Lonfat (1963) originally described the Lower Tar Member as a succession of marl and shale, dark green at the base, red very fossiliferous towards the top grading into 12 m of yellow lime-mudstone.

In the type area, the Lower Tar Member sequence starts with dark green gypsiferous clay alternating with greenish-yellow marl and few thin bands of marlstone together constituting the lower two third of 80 m thick succession. Macrofossils are rare in this part being represented by *Exogyra overwegi* and *Agerostrea ungulata,* but the rich microfaunal assemblage is dominated by planktonic foraminifera. This sequence gradually grades into the alternation of organodetrital limestone, calcilutite/calcarenite succession rich in fossils. The upper one third part of the exposed strata forms prominent dark red to brownish band which becomes buff to light brown towards the top and capped by a meter thick bed of unfossiliferous red brown calcarenite. The upper level of Lower Tar Member is characteristically developed with abundant fossils mostly represented by *Exogyra overwegi, Agerostrea ungulata, Omphalocyclus macroporus,* and others.

The unfossiliferous red brown layer, in a highly fossiliferous sequence, mark the top of the Lower Tar Member in the western part of Hun Graben, but is not traceable in the western part of Al Hammadah Al Hamra Plateau, where the last appearance of *Exogyra overwegi, Omphalocyclus macroporus* assemblage mark the top of Lower Tar Member.

The lower boundary with Thala Member is better exposed in the area of Wadi Zamzam and south of Wadi Suf Al Jin in Bani Walid and Al Qaryat Ash Sharqiyah Sheet, and can be traced into the Tunisian border in the west. The northern most outcrops of Lower Tar Member are traceable up to latitude 31°50'N in Bani Walid Sheet.

The boundary between Thala and Lower Tar Member is mostly gradational and has been marked at the top of the prominent calcarenite band which becomes porous and chalky in Nalut Sheet, and partly silicified and dolomitized in Al Qaryat Al Gharbiyah and Al Qaryat Ash Sharqiyah Sheets.

The Lower Tar Member exhibits facies variation from a predominantly gypsiferous-clay, marl sequence on the western part of Hun Graban (Hun Sheet) to marl calcarenite and gypsum alternations with some layers of gravel, conglomeratic material and slumped blocks interstratified in the middle part, with cross bedded calcarenites in the upper part of the sequence in Al Qaryat Al Gharbiyah and Al Qaryat Ash Sharqiyah Sheets. Further west and northwest the calcarenites become well stratified forming prominent scarps in Nalut, Ghadamis and Shawa Sheets. This part of the sequence was interpreted by Jordi and Lonfat (1963) as Had Limestone, leading him to conclude that the Had Limestone Member directly rests on the Lower Tar Member in the western part of Ghadamis Basin. In this part the Upper Tar Member and Had Member are preserved as small isolated slumped blocks, with greatly reduced thicknesses.

In the southern part of Ghadamis Basin the Lower Tar Member directly rests on the sandstones of Hasawnah Formation (Cambrian). In Jabal Al Hasawnah sheet it consists of a basal conglomeratic layer with rounded quartz pebbles and marly matrix. A thin fossiliferrous discontinous horizon is present near the base, overlain by marlstone, calcarenite intercalations with considerable amount of sand, about 4-6 m thick layer of chalky calcilutite with characteristic quartz geodes has also developed 10 m above the base of the sequence. The lower part dominated by hard cross bedded calcarenite-calculite alternation, contains rare fragments of *Inoceramus*. Gray green gypsiferous claystone appears in the middle part followed by marlstone and cross bedded calcarenite with *Omphalocyclus macroporus* and *Exogyra overwegi* locally developed as *lumachell*. This sequence laterally grades into predominantly sandy facies represented by Bin'Affin Member.

Generally, in the eastern and northeastern part of Ghadamis Basin the Lower Tar Member is represented by claystone and gypsiferous marl sequence in the lower part with common planktonic foraminiferal assemblage, and gradual shallowing in the upper part is reflected by the organodetrital

Limestone and calcarenites are rich with Oysters and larger foraminifera. In the central part of the basin the lower and middle levels of Lower Tar Member, contain a number of stratified gypsum horizons, and slumped blocks, gravel layers followed by cross bedded calcarenites in the upper level suggesting lagoonal to very shallow marine environment of deposition. In the southern part of Ghadamis basin the sand content increases appreciably till it develops into a distinct lithostratigraphic unit. The presence of a conglomeratic horizon at the base of the sequence in this part marks a major unconformable surface and confirms the transgressive nature of Zimam Formation over the underlying sediments.

The thickness of the Lower Tar Member in the western and southern part of the basin varies from 40 to 50 m (Djeneien and Jabal Al Hasawnah Sheets) increasing in the central part to 80-120 m (Al Qaryat Al Gharbiyah and Al Qaryat Ash Sharqiyah Sheets). A maximum thickness of 290 m is known from the subsurface (Eliagoubi, 1975).

Based on foraminifera assemblage a Maastrichtian age is assigned to the Lower Tar Member. The characteristic Upper Maastrichtian by index species such as *Abathomphalus mayaroensis* (Bolli) is rare in these beds as well as in other parts of NW Libya (Barr and Weeger 1972; Salaj 1979).

The pervious authors have recorded *Globotruncana falsocalcarata* from the upper part of the type section of Lower Tar Member. This species has been found to be restricted to the Upper Maastrichtian interval as evidenced from the record of this species from Egypt (Kerdany and Abdelsalam, 1969), Pakistan (Dorreen, 1974) and Iraq (Kassab, 1975). The Lower Tar Member represents the Maastrichtian interval in this region.

Salaj (1979) on the occurrence of planktonic foraminiferal assemblage of *Globotruncana acra rugosa* zone in association with *Neoflabellina rugosa* (d'Orb.), *Bolivina incrassata incrassata* (Reuss), from Al Qaryat Al Gharbiyah Sheet, suggests the possibility of extending the lower age limit of Lower Tar Member upto uppermost part of Campanian. On the other hand Gohrbandt (1966b) observes that the main part of Jordi and Lonfat's (1963) Lower Tar Member is known from the subsurface, and based on the presence of *Globorotalites michelinianus* (d'Orb.) may ranges down to Campanian-Santonian. These observations were not confirmed by Eliagoubi (1975) who studied the biostratigraphy of Lower Tar Member from the surface and subsurface and he suggested a Maastrichtian age for these beds. Salaj & Nairn, 1991 suggested a new formation and they named it Algarbiyah Formation (Upper Campanian–Upper Maastrichtian), previously called Lower Tar Member of the Zimam Formation. Algarbiyah Formation comprises three members , (Bir Bu al Ghurab Member, Lawdh Allaq Member and Lower Tar Member).

Bin'Affin Member: The term was originally introduced by Furst (1964) to include the facies change of Lower Tar Member into a predominantly sandy facies south of Jabal Assawda, which named after Sarir Bin' Affin. It crops out between latitude 26°30'N and longitude 28°30'N.

In the type area the Bin Affin Member is characterized by greenish yellow silty to fine sandy dolomitic marls containing a bone fragments bed with shark teeth and molluscan fossils, southwards dominantly poorly bedded sandy or clayey sandy facies has developed. A conglomeratic horizon has been recorded from bore holes. In the upper part of the sequence reddish brown to black brown

elongated iron oxide concretions perpendicular to the bedding plane are common. The lower contact with the underlying Palaeozoic Formations is sharp but the contact with Nubian Sandstone is marked by the absence of large scale cross bedding, and the presence of calcareous cement in the Bin'Afffn Sandstone which also contains rare molluscan shells and *Omphalocylus macroporus* The upper contact with the Upper Tar Member and their equivalents, the Dor El Gani Marl is marked by a prominent hard yellowish brown fossiliferous dolomitic limestone, occasionally sandy which is well developed throughout the region.

Furst (1964) had measured a composite type section for Bin' Affin Member, in two separate depressions between Dor El Gani and Wadi Kapir.

A maximum thickness ranges from 80-100 m has been recorded from surface and subsurface data. The Bin'Afffn Member directly rests on the marine Lower Carboniferous sequence in Wadi Kapir; southwards till at 26°25'N. It overlies the Nubian Sandstone, further south the contact is concealed but appears to rest directly on the basement rocks.

North of Lat 28°N, a small area in the SW part of Al Washkah and SE part of Jabal Al Hasawnah Sheet the Bin'Afffn Member sediments are exposed. Based on the record of fossils from Al Washkah and Jabal Al Hasawnah Sheet a Maastrichtian age has been assigned to this member.

Upper Tar Member: Jordi and Lonfat (1963) was first described this member as a succession of marl and lime mudstone, with thick shaly interrelations in the middle part and a fossiliferous limy interval in the lower part. In the type area the Upper Tar Member starts with about 4m thick bedded dark green to gray claystone grading into light yellow marlstone and followed by 8-10 m alternations of calcarenites and calcilutites. The calcarenites are rich with molluscan fossils, in some places appearing like *lumachelle*. The molluscan fossils mostly belong to the pelecypod families Carditidae and Tellinidae and gastropod superfamily Cerithiacea, with rare nautiloids, oysters and echinoids. This interval was referred by Jordi and Lonfat (1963) as 'Socna Mollusc Bed', due to its well development in the vicinity of Socna. This fossiliferous interval is followed by nearly 25 m thick, three bands of greenish yellow claystone with marly appearance, separated by less than one meter thick calcarenite bands containing few molluscan fossils. The claystones are poorly in fossils, but have yielded discorbis pseudoscopus (Nakkady), few rotalids and ostracods along with some reworked microfauna present in the Lower Tar Member. The uppermost 30 m succession consists of alternation of yellowish cream marly occasionally nodular limestone, calcilutite and fossiliferous calcarenites. These beds have yielded a shallow water foraminiferal and algal assemblage, and have undergone slight dolomitization, with resulting recrystallization of the contained fauna. These are in turn overlain by the cross bedded, cream coloured but weathering reddish brown limestones of Had Member (Megerisi & Mamgain 1980)

The exposed thickness of Upper Tar Member in the type area where both the lower and upper contacts are exposed averages 70 m, and shows little variation in the western part of Hun Graben, but gradually reduces in thickness towards Jabal Assawda averaging around 10 m south of it. Similarly the thickness of Upper Tar Member gradually reduces in the NW and SW parts of Ghadamis Basin, it does not cropout in Nalut Sheet.

Jordi and Lonfat (1963) stated that the Had Limestone directly rests on the Lower Tar Member could not be accepted by the work of Novovic (1977) who observed that the Zimam Formation in (Nalut Sheet) to be considered to represent the Lower Tar Member. In this area, the upper 10-15 m thick level is characterized by dark gray to yellowish and pinkish white dolomitic limestone, occasionally sandy and saccaroidal with interbeds of marly limestone, giving it an appearance of a condensed sequence of alternating hard and soft beds which characterize the Had Member. Novovic (1977) has recorded *Omphalocyclus macroporus* (Lamarck), *Exogyra overwegi* and *Inoceramus regularis,* etc. from these beds.

Socna Bed: Jordi and Lonfat (1963) informally used the term Socna Mollusc bed to distinguish the basal fossiliferous horizon of Upper Tar Member (Fig. 3). Because of its homonymy with the Socna Formation of Burollet (1960) and unconfirmed record of *Nerinea* sp from these beds; Energoprojekt (1975) expanded the concept of Jordi and Lonfat (1963) by including the uppermost fossiliferous interval of Lower Tar Member in these beds and terms the new combination as 'Socna Unit'. The main controversy however continues on the age of these beds.

The Upper fossiliferous interval of Lower Tar Member abounds in thick shelled oysters like *Exogyra overwegi, Agerostrea ungulata,* and larger foraminiferal genera *Omphalocyclus* and *Siderolites;* whereas the basal fossiliferous level of Upper Tar Member abounds in *Venericardia* and representatives of carditidae, tellinidae and cerithiacea and thin shelled oyster *Ostrea cellae.* Locally, as in the type section and near the mouth of Wadi Zimam, this interval also contains common *Siderolites* along with the above assemblage, some worn out and reworked specimens of *Omphalocyclus, Globotruncana, Rugoglobigerina, Pseudotextularia,* etc. were also recovered from these beds and the immediately overlying yellowish green claystones. The Maastrichtian elements present in this interval are reworked, though no characteristic Paleocene planktonic foraminiferal species were found in the type area, but *Globoconusa* has been recorded from the southern margin of Hun Graben in Al Washkah Sheet, represented by *Globoconusa daubgergensis* (Bronnimann), confirming the Paleocene age to this interval.

This fossiliferous interval, averaging 12 m in thickness in the type area shows a gradual thinning towards south, where the fossiliferous calcarenites average 2 m in thickness in the southern margin of Hun Sheet and continue with the same thickness in Al Washkah and Jabal Al Hasawnah Sheets. Their individuality is lost in the western and northwestern part of the Ghadamis` Basin where the calcarenites laterally merge into the claystone-marl succession.

The mapping teams of Industrial Research Centre do not consider this level as a distinct mappable unit, and the criteria to delimit the lower and Upper Tar Member boundary is based on a combination of factors including the last appearance of *Omphalocyclus - Exogyra* assemblage.

Based on fossil records, Danian (basal Paleocene) age is assigned to the Upper Tar Member, which was deposited in a shallow marine neritic to littoral environment of deposition (Megerisi & Mamgain 1980.

Had Member: Jordi and Lonfat (1963) introduced the name Had Limestone Member after Wadi Had, but the type section located in Wadi At Tar Al Kabir where the exposed thicknes about 50m of dolomite and dolomitic limestone with the intercalation of chalky marl.

In the type area the Had Member starts with a massive cavernous, creamy coloured, cross bedded dolomitic limestone, weathering reddish-brown, forming three prominent benches, separated by slightly dolomitize chalky limestone, rich in molluscan fossils. These hard dolomitic limestones form a prominent scarps and plateau surface in the western part of Hun Graben, covering large area of Ghadamis Basin. The middle limestone level is a thin bedded and contains Molluscan fossils, the top level is medium to coarse grained, creamy white on fresh surface, without visible fossils, but broken by huge columnar joints. The existence of joints in the Had Member has been explained by Antonovic (1977). He reported that due to the slumping of underlying soft marly horizons, affected by solution, resulting in large open fractures of the overlying hard resistant dolomitic limestones, aided by gravity sliding.

The thickness of Had Member ranges from 50 m in the type area to around 5 m south of Jabal Assawda, and together with Upper Tar Member averages 25 m in Ghadamis Sheet. The reduced thickness has eliminated the characteristic three prominent dolomitic limestone levels, which nearly merge into one, prominent brown weathering, grayish white crystalline dolomitic limestone with marly and occassionaly chalky intercalations (Megerisi & Mamgain 1980).

The chalky interval is very rich in macrofossils, mostly represented *by Tellina* sp, *Turrietella* sp, and *Nautilus* sp and *Echinods* etc. Ostracods are rare occasional ooids are present, but locally near Suknah, they have developed into dominant components of the dolomitic limestone. Based on the fossil record and its stratigraphic position of Paleocene (Montian) age has been assigned to this member, a shallow marine neritic to littoral environments.

Previous work on the upper Cretaceous Ostracoda from Libya: Literature survey shows that most micropaleontological work has been carried out on foraminifera. Few ostracods studies have been done by Salahi (1966) who investigated Upper Cretaceous, Palaeocene, Early Eocene and Oligocene ostracoda from the Zaltan region. He described sixty species of which forty-five were new but not nomenated due to their wide stratigraphic range.

El Waer (1992) studied the Tertiary and Upper Cretaceous ostracoda from NW Libya. He described one hundred and thirty species and sub-

species belong to fifty-five genera and sub-genera. El-Sogher (1996) investigated the Late Cretaceous and Paleocene ostracoda from the Waha Limestone and Hagfa Shale of the Sirt Basin.

Salaj & Nairn (1991) studied the Upper Cretaceoucs ostracoda from the northren Ghadamis Basin.

SYSTEMATIC DESCRIPTIONS

The systematic order used follows that of the Treatise (1961) on Invertebrate Palaeontology (Q).
Subclass Ostracoda Latreille,1806
Order Podocopida, Muller, 1894
Family Cytherllidae Sars, 1866

Cytherella sp1
Pl. 1, Figs. 4, 5, 6
Material: 30 carapaces and 22 valves.
Diagnosis: Carapace ovate to subrectangular in lateral view, right valve strongly overlapping the left valve except the antero-ventral and central-anterior, the surface of carapace is smooth.
Description: Carapace elongate to ovate in lateral outline, anterior margin well rounded, posterior margin obliquely rounded, dorsal margin almost straight in anterior, 2/3 posterior convex, ventral margin nearly straight in the left valve and slightly convex in the right valve, maximum height at 1/3 length from anterior, maximum length above center height, in dorsal view anterior margin tapered, surface of carapace is smooth, internal feature not seen, sexual dimorphism not distinct.
Dimension of figured specimens (in μm):

	Length	Height	L/H	Width
Male left carapace	480	425	1.13	----
Female right carapace	740	460	1.6	----

Remarks: The figured species is very similar in lateral outline to the *Cytherella saidi,* described from Shurfa Formation (Aburass Member) in Sirt Basin by Gammudi 1996, but the later species differ in having finely punctuate, also the studied species similar in lateral outline to *Cytherella sp* described from Eocene of Tripoli Basin, by Whatley and Arias (1993), but the later species differ in less overlapping left valve by right valve on the dorsal margin.
Occurrence: Occurs in the Lower Tar member (Zimam Formation) Ghadamis Basin.

Cytherella sp 2
Pl. 1, Figs. 1, 2, 8
Material: 32 carapaces and 15 valves.
Description: Carapace subrectangular in lateral view, anterior margin evenly rounded posterior margin rounded, dorsal margin nearly straight and sub parallel to ventral margin, maximum height at 1/3 length from posterior, maximum length at mid height, surface of carapace is smooth and slightly pronounced anterior rim, internal feature not known and sexual dimorphism well distinct male more elongate than female.
Dimension of figured specimens (in μm).

	Length	Height	L/H	Width
Male right carapace	660	330	2.0	---
Female right carapace	540	300	1.8	---
Female right carapace	611	345	1.77	---

Remarks: The figured species is very similar in lateral out line to *C. lagenalis* which described from late Paleocene to early Eocene of Egypt by Bassiouni and Luger (1990) apart from later species shows strong overlapping and more elongate, also the studied species shows similarities in lateral out line to *C. symmetrica* described from Paleocene-Eocene of Tarabulus Basin by Whately and Arias (1993), but later species differ in having small pits.
Occurrences: Occurs in outcrop of Lower Tar Member (Zimam Formation) Ghadamis Basin.

Cytherella sp3
Pl. 1, Fig. 7
Material: 2 carapaces.
Description: Carapace subrectangular in lateral outline, anterior margin broadly rounded, with pronounced anterior rim, posterior margin obliquely rounded, dorsal margin and ventral margin almost parallel, maximum height at 1/3 length from posterior, maximum length at the mid height, surface of carapace punctuate except central area of the carapace where weakly punctuate, the surface of carapace corroded.
Dimension of figured specimens (in μm):

	Length	Height	L/H	Width
Right carapace	520	290	1.79	---

Remarks: This is not well preserved carapace and has very week pits, the lateral outline of the figured specimens shows similarities to the *Cytherella joaalensis* described from shallow marine in West Africa by Witte (1993).
Occurrence: Occurs in Lower Tar Member (Zimam Formation) Ghadamis Basin

Genus *Cytherella* Jones, 1849
Type species: *Cytherina Ovate* Roemer,1840

***Cytherella mohamadi* Gammudi, 1996**
Pl. 1, Fig. 3, Pl. 2, Fig. 8
1996 *Cytherella Mohamadi* Gammudi,1996 p. 30, pl, 2, Fig. 4-9
Material: 2 carapaces.
Diagnosis: A species of *Cytherella* with distinct marginal rim around anterior, ventral and postero-ventral area anterior margin evenly rounded, ventral margin concave, dorsal margin centrally concave.
Dimension of figured specimens (in µm):

	Length	Height	L/H	Width
Left carapace	525	295	1.77	---
Right carapace	542	300	1.8	---

Remarks: This species is identical in lateral out line to *Cytherella mohamadi* originally described from Upper Paleocene Sirt Basin. But the studied species shows smaller size than the original species 540 µm cf 750 µm, (the small size refer to not reach to adult stage).
Occurrence: Occurs in outcrop of Lower Tar Member (Zimam Formation) and Upper Palaeocene in the Sirt Basin.

Genus *Cytherelloida* Alexander 1928
***Cytherelloida dabai* sp. nov**
PL. 2, Figs. 1-7, Pl. 3, Figs. 1-4
Material: 24 carapaces and 17 valves.
Derivation name: in honor of Ibrahim Daba a geologist who in comma since four years
Diagnosis: Carapace subrectangular in lateral outline, surface of the carapace is smooth, well distinct anterior marginal rim, and short ridge parallel to ventral margin lies on the 1/3 carapace length from ventral, with clear subcentral depression and vertical posterior rim clearly joined short dorsal margin ridge with sharp angle.
Holotype: Male left carapace Pl. 3, Fig. 3
Paratype: Seven specimens Pl. 2, Fig. 1-7
Type locality: Al Quariyat Al Sharghiah
Type horizon: Lower Tar Member.
Description: Carapace subrectangular in lateral view, anterior margin evenly rounded, posterior margin well rounded in the right valve and truncated in the left valve, dorsal margin straight to slightly concave at 1/3 length from anterior, ventral margin almost straight to slightly concave at the middle, surface of carapace is smooth with sub central depression and reticulated by anterior margin rim, and short horizontal ridge lies parallel to ventral margin at 1/3 high, with additional vertical posterior ridge ending with node at the postero-dorsal area while it is upper part bending interiorly.
Dimension of figured specimens in (µ m).

	Length	Height	L/H	Width
Male left carapace	666	365	1.82	---
Male right carapace	645	363	1.77	---
Female right carapace	590	355	1.66	---
Male right carapace	680	380	1.78	---
Female left carapace	680	375	1.81	---
Male right carapace	660	365	1.83	---
Female left carapace	675	400	1.68	---
Female right carapace	611	366	1.67	---
Male left carapace	666	360	1.85	---
Male left carapace	682	322	2.11	---
Female left carapace	675	400	1.68	---

Remarks: The figured species shows some similarities in lateral outline to *Cytherelloida ghorabi* which described from Middle Maastrichtian of Dakhla Formation, Egypt (Bassiouni and Luger, 1990). The later species differ in having nearly straight dorsal margin and less pronounced posterior rim and having median ridge.
Also the figured species differ from *Cytherelloida araromiensis* which described from Lower Tar Member by Salaj and Nairin 1991 in more pronounced dorsal ridge and truncated posterior margin, as well as having short median ridge.
Occurrences: Occurs in the outcrop of the Lower Tar Member (Zimam Formation) Ghadamis Basin.

Suborder *Podocopina* Sars, 1866
Superfamily *Bairdiacea* Sars, 1888
Family *Bairdiidae* Sars, 1888
Type Species *Bairdia sp 1*
Pl. 6, Figs. 1, 2, 3
Material: 42 carapaces and 60 valves.
Description: Large carapace with typical outline of the genus, posterior margin lower and narrower than anterior, left valve larger than right and clearly overlapping through dorsal margin postero-ventral and anterior, left valve slightly convex ventral margin while right valve straight, dorsal margin in the left valve broadly rounded, surface of carapace is smooth, the maximum height centrally, the maximum length at 1/3 from ventral margin, internal features not known, sexual dimorphism not distinct.
Dimension of figured specimens (in µm):

	Length	Height	L/H	Width
Left carapace	950	570	1.66	---
Right carapace	1000	662	1.51	---

Right carapace	1020	670	1.52	---

Remarks: The species *Bairdia sp.1* is very similar to *B. group ilaroensis* which described from Danian (Haghfa Shale) Sirt Basin Libya by keen *et al* (1994), but the later species differ in having highly arched dorsal margin, also our species shows similarities with *Bairdopilata ilaroensis*, Reyment and Reyment which described from Paleocene of Nigeria by Swain *et al* (1983), but the Nigerian species differ in more pointed posterior margin.
Occurrence: Occurs in outcrop of Lower Tar Member (Zimam Formation) Ghadames Basin.

Bairdia sp 2
Pl. 6, Figs. 4, 5, 6
Material: 8 carapaces and 19 valves.
Description: Large carapace subtriangular in lateral view, anterior margin obliquely rounded, pointed posterior end, dorsal margin broadly rounded, ventral margin nearly straight in the middle, greatest height at mid- length, maximum length about 1/3 of the height from ventral margin, the left valve strongly overlapping the right valve except in posterior end, internal feature not observed, sexual dimorphism not distinct.
Dimension of figured specimens (in µm):

	Length	Height	L/H	Width
Right carapace	1100	745	1.46	---
Left valve	960	560	1.71	---
Dorsal view	855	---	---	370

Remarks: Bairdia sp 2 shows some similarities to *Bairdia sp 1*, the later species more arched and the ventral margin more convex in the left valve.
Occurrences: Occurs in the outcrop of Lower Tar Member (Zimam Formation), Ghadames Basin.

Super Family *Cypirdacea* Baird, 1845
Family *Paracyprididea* Sars,1923
Genus *Pontocypris*
species A
Pl.7, Figs.1-8
Material: 24 carapaces and 20 valves.
Description: Carapace subtriangular in lateral view, anterior margin well rounded, posterior margin sharply pointed dorsal margin highly arched particularly left valve, ventral margin almost straight, maximum height about mid of the carapace, maximum length at 1/3 height from ventral, left valve strongly overlapping the right valve, surface of carapace is smooth, with distinct sexual dimorphism, the male been shorter than female, internal feature not been observed.

Dimension of figured specimens (in µm):

	Length	Height	L/H	Width
Male left carapace	922	420	2.19	---
Female right carapace	1050	525	2.0	---
Female left valve	975	500	1.95	---
Dorsal view	800	---	---	400
Male right carapace	925	416	2.22	---
Female left carapace	910	430	2.11	---
Female left valve	930	483	1.92	---
Female right carapace	910	450	2.02	---

Remarks: The figured species similar in lateral outline to *Paracypris trosliensis* Apostolescu,1956 which have been described from Paris Basin, but the later species differ in less arched dorsal margin and ventral margin slightly concave, also it is very similar in lateral view to *Paracypris paramaghaghaensis* which described from Eocene NW offshore Libya by El Waer (1992), but the figured species slightly differ in highly arched dorsal margin.
Occurrences: Occurs in outcrop of Lower Tar Member (Zimam Formation) Ghadamis Basin.

Genus *Pontocyprella recurva* Eskr,1968
Pl. 6, Figs. 7, 8 & Pl. 9, Fig. 6.
1968 *Pontocyprella recurva n. sp*. Eskar, p 323, pl 1,Figs 6,7, pl 4, Fig 7
1982 *Pontocyprella recurva*, Eskar, Donze *et al* p 281,pl.2, Figs 1,2
1992 *Pontocyprella recurva* Eskar, El-Waer,p 73,pl 57, Figs 1-3
1996 *Pontocyprella recurva* Eskar, Gammudi, p 62, pl 11, Figs 4-7
Material: 4 carapaces and 2 valves.
Description: Carapace elongate to ovate in lateral outline, with prominent overlapping convex left valve by the right in the antero-dorsal area, anterior margin obliquely rounded dorsally posterior margin pointed, ventral margin concave in the right valve and straight in the left valve, surface of carapace is smooth, no internal features been observed in the studied specimens, but original species has adont hinge as mentioned by Eskar (1968).

Dimenssion of figured specimens in (µm):

	Length	Height	L/H	Width
Male left valve	760	310	2.45	---
Female right carapace	625	258	2.42	---
Male right carapace	760	360	2.11	---

Remarks: This species was described from Danian (Zeubbeus Fm) near El-Kaf Tunisia by Eskar (1968) as well as recorded from Maastrichtian-

Danian of El Kaf section by Donze *et al*1982, the Maastrichtian-Paleocene of offshore Libya by El-Waer (1992) and Wathly *et al* (1993), also recorded this species from Eocene of offshore Tripoli Basin, their illustration shows difference from *P. recurva* in it is more tapered posterior margin and larger size (1.5 mm cf 0.7-0.94 mm).

Occurrences: Occurs in Maastrichtian–Paleocene of Libya and Tunisia.

Superfamily Cytheracea Baird, 1850
Family Brachcytheridae Puri, 1945
Brachycythere* cf *B. dakhlaensis

Pl.5, Figs.1-5

Material: 70 carapaces and 10 valves.

Description: Carapace subtriangular in lateral outline, anterior margin slightly obliquely rounded with prominent spines, posterior margin pointed with well prominent spines, dorsal margin arched with well pronounced eye spot clearly seen in the right valve, ventral margin slightly convex, maximum height nearly at the middle of carapace, maximum length at 1/3 length from ventral margin, surface of the carapace ornamented with weakly developed pits.

Dimension of figured specimens in (μm):

	Length	Height	L/H	Width
Male right carapace	800	47	1.70	---
Female left carapace	845	460	1.83	---
Female right carapace	880	480	1.83	---
Male left carapace	890	460	1.93	---
Dorsal view	820	---	---	420

Remarks: The figured species is very similar in lateral outline to the species have been described from Middle Maastrichtian of Egypt by Bassiouni and Luger (1990), the later species differ in more obvious pits in the posterior area, also our species shows similarities to the *Brachcythere angulata* described from Conacian-Maastrichtian in Pakestan, but the later species differ in well distinct pits of different size.

Occurrences: Occurs in outcrop of Lower Tar Member (Zimam Formation) Ghadamis Basin.

Family *Bythocytheridae Sars*, 1926
Genus *Monoceratina Roth*, 1928
Type species *Monoceratina Ventral Roth*, 1928
***Monoceratina Salemi* Gammudi, 1996**

Pl. 9, Figs. 3, 4, 5.

1996 *Monoceratina salmi* Gammudi, 1996 p. 72, pl. 13, figs. 11,12.

Material: 3 carapaces.

Diagnosis: A species of *Monoceratina* with distinct subcentral vertical sulcus, short caudal process and 2-3 weakly developed ribs in the swollen area.

Dimension of figured specimen in (μm):

	Length	Height	L/H	Width
Female right carapace	480	275	1.75	---
Female right carapace	512	280	1.82	---
Male right carapace	500	240	2.0	---

Remarks: This species is identical to *Monoceratin salmi* Gammudi, 1996, which described from the Paleocene outcrops (Bu Ras Member of Shurfa Formation) Sirt Basin in lateral outline and surface ornamentation, but slightly larger than *Monoceratina Salmi* (493μm cf 404μm).

Occurrences: Occurs in outcrop of Lower Tar Member (Zimam Formation) Ghadamis Basin and Palaeocene outcrop Bu Ras Member (Shurfa Formation) Sirt Basin.

Family: *Trachyleberididae* Sylvester-Bradley 1948
Subfamily *Buntonia* Aspostolescu, 1961
Genus *Protobuntonia* Grekoff,1954
Type species *Protobuntonia nakkadii* Bassiouni, 1970

Pl. 4, Figs. 5-8.

1971 *Protobountonia nakkadii* Bassiouni, p.23, pl. 2, Figs. 1-3.

1982 *Protobuntonia nakkadii* Bassiouni, Donz *et al* p. 295, pl. 12 Fig.1, pl. 14, Fig.6.

1990 *Protobuntonia nakkadii* Bassiouni, Bassiouni & Luger, p. 845, pl. 23, Figs.23,24.

1994 *Protobuntoni nakkadii* Bassiouni, Keen *et al* Pl.16.2, Fig.12.

Material: 20 carapaces and 3 valves.

Diagnosis: A species of *Protobuntonia* subtriangular in lateral view, surface of carapace smooth to finely punctate, 1-2 faint ribs parallel to ventral margin clearly seen in left valve with weakly eye tubercle.

Dimension of figured specimen (in μm):

	Length	Height	L/H	Width
Female left carapace	800	460	1.73	---
Male left carapace	915	480	1.90	---
Female right carapace	800	440	1.81	---
Male right carapace	820	440	1.86	---

Remarks: The studied species are typical to *P. Nakkadii* recorded from Maastrichtian Sirt Basin Libya, Keen *et al* 1993. the figured specimen slightly different in lateral outline to the specimens recorded from Late Maastrichtian-Paleocene of Tunisia by Donze *et al* (1982), and Lower Danian

by Said (1978) which have amore tapered posterior, also Basssiouni (1970) recorded larger specimens from Middle Paleocene of Jordan.
Occurrences: Occurs in outcrop of Lower Tar (Zimam Formation) Ghadamis Basin.

Genus *paracosta Siddiqi*, 1971
Type species *paracosta pervinquiri,* Donze *et al* 1982
Pl. 4, Figs. 1-4.
1982 - *Paleocosta pervinquiri* Donze and R. Said, n.sp,Donze *et al* p. 284, pl.3, Figs.4-10
1990 *Paracosta pervinquiri*, Bassiouni and Luger, p. 834, pl. 20, Figs. 7-10,12
1996 *Paracosta pervinquiri*, El Sogher, p. 323, pl. 30, Figs.1-5
Material: 45 carapaces and 10 valves**.**
Dimension of figured specimens (in µm):

	Length	Height	L/H	Width
Male right carapace	690	333	2.07	---
Female left carapace	625	320	1.95	---
Ventral view	680	---	---	285
Female right carapace	630	320	1.96	---

Discussion: Although being smaller, the present specimens agree very well with the description and figured given by Donze *et al* (1982), except for slight differences in details of reticulation in the antero- median and postero- median parts of the valve.

Remarks: The figured species in this study is the same species illustrated by Bassiouni and Luger 1990, in lateral outline, this species differ from Donze *et al* 1982, Bassiouni and Luger, 1990 and El Sogher, 1996, in smaller size and the longitudinal ridges not well pronounced may be due to environmental changes.
Occurrences: This species was first described from the late Maastrichtian to early Paleocene from Tunisia (Donze *et al* 1982) and Middle Maastrichtian of the Dakhla Formation Egypt (Bassiouni and Luger, 1990), and from Waha limestone (Maastrichtian) and Hagfa Shale (Danian) of Sirt Basin, also in the outcrop of Lower Tar Member (Zimam Formation), Ghadamis Basin.

Family *Krithidae* Mandelstam,1960
Subfamily *Krithinae* Mandelstam, 1960
Genus *Krithe* Brady Crosskey and Robertson, 1874
Krithe sp A
Pl. 10, Figs. 5-8
Material: 80 carapaces and 19 valves.
Description: Carapace subrectangular in lateral view, anterior margin evenly rounded, posterior margin obliquely rounded, dorsal margin convex, ventral margin slightly concave at the middle of the right valve, straight in the left valve, maximum height at 1/3 from posterior margin, maximum length below the middle of carapace, surface of carapace is smooth, the left valve strongly overlapping the right valve in particularly at anterior, posterior and dorsal areas, internal feature not known, sexual dimorphism is not distinct.
Dimension of figured specimens (in µm):

	Length	Height	L/H	Width
Male right carapace	570	280	2.03	---
Female left valve	560	280	2.0	---
Carapace dorsal view	535	---	---	245
Female left carapace	570	265	2.15	---

Remarks: The figured species shows some similarities to *Krithe aljurfae* which described from Maastrichtian of Tripoli Basin by El Waer, 1992 the later species differ in less arched dorsal margin and less overlapping left valve to right valve, also the studied species similar to *Krithe echlosa*, which described from Paleocene Sirt Basin by Gammudi (1996) but later species differ in having circular depression posterior and less arched dorsal margin.
Occurrences: Occurs in outcrop of the Lower Tar Member (Zimam Formation) Ghadames Basin.

Family *Xestoleberididae* Sars, 1928
Genus *Xestoleberis* Sars,1866
***Xestoleberis* sp A**
Pl. 10, Figs. 1-4
Material: 30 carapaces and 2 valves
Description: Carapace oval shaped in lateral outline, anterior margin rounded, posterior margin broadly obliquely rounded to sub truncated, dorsal margin highly arched, ventral margin slightly convex, carapace surface smooth and swollen, maximum height nearly at middle carapace, maximum length at 1/3 height from ventral, internal features not seen, sexual dimorphism not obvious.
Dimension of figured specimen in (µm):

	Length	Height	L/H	Width
Right carapace	400	300	1.33	---
Right carapace	430	310	1.38	---
Left carapace	425	300	1.41	---
Dorsal view	400	---	---	350

Remarks: The figured species is very similar in lateral out line to *Xestolebris Kiseibanesis* which described from Late Paleocene-Early Eocene of Egypt by Bassiouni & Luger (1990) the later species differ in having more truncated posterior margin and ventral margin almost straight.
Occurrences: Occur in outcrop of Lower Tar Member (Zimam Formation) Ghadamis Basin.

Family *Trachyleberididae*, Sylvester-Bradley, 1948
Genus Paragrenocythere Al-Furiah, 1975
Paragrenocythere. cf P. Gravis
Pl. 8, Figs. 1-8 and Pl. 9, Figs. 1,2.
Material: 48 carapaces and 10 valves.
Description: Carapace subrectangular in lateral view, anterior margin well rounded and decorated with small spines especially antero-ventral margin, posterior margin pointed with obvious posterior cardinal angle in postero-dorsal area, dorsal margin straight, ventral margin nearly straight, surface ornamentation with coarse reticulation, and has subcentral tubercle with ventral ridge starts from 1/3 length from anterior and nearly parallel ventral margin ending with coarse node at 1/3 length from posterior, eye tubercle well pronounced dorsal ridge starts behind eye tubercle ending with a node posteriorly clearly seen in the left valve, maximum height at eye tubercle and maximum length lies below subcentral tubercle, Sexual dimorphism distinct male been more elongate than female.
Dimensions of figured specimens (in μm):

	Length	Height	L/H	Width
Female left carapace	916	483	1.89	---
Male right carapace	1000	466	2.14	---
Ventral view	900	440	2.04	---
Male right carapace	1000	500	2.0	---
Left valve (inside)	860	410	2.09	---
Male left carapace	1000	450	2.22	---
Male right carapace	1000	450	2.22	---
Left carapace	916	500	1.83	---
Right carapace	966	416	2.32	---
Dorsal view	1000	---	---	500

Remarks: The figured species very similar in lateral out line to *Paragrenocythere gravis* which described from Maastrichtian–Upper Paleocene of Libya, the later species differ in having more pronounced dorsal ridge and shorter in length (778μm) also the studied species differ from *P.Gravis* which described by Al Furaih (1977) from Lower Paleocene in Saudi Arabia, the later species has subrounded posterior margin and shorter in length.
Occurrence: Occurs in the outcrop of Lower Tar Member (Zimam Formation) Ghadamis Basin.

Genus *Oertliella Pokorny* 1964
Oerteliella Khargensis
Pl. 5, Figs. 7,8.
1990 *Oertliella khargensis* Bassiouni & Luger, 1990. p.30, pl.18, Figs.1-5
Material: 34 carapace and 21 valves.
Diagnosis: This species charactrized by obliquely rounded posterior marginal and row of spines running in abroad curve below middle of carapace anteriorly to postero-ventral margin corner
Dimension of figured specimens (in μm):

	Length	Height	L/H	Width
Male left carapace	1000	486	2.05	---
Male right carapace	950	438	2.16	---

Remarks: The figure species differ from the original species described by Bassiouni & Luger (1990), in more prominent spines in the anterior and posterior area as well as larger size.
Occurrences: First described from Middle Mastrichtian of Egypt. In the present specimens it occurs in Lower Tar Member (Maastrichtian) Ghadamis Basin.

Genus A
Pl. 5, Fig. 6
Material: One carapace
Description: Carapace subrhomboidal in lateral view, anterior margin rounded, posterior margin with well pronounced caudal process directed upward, dorsal margin nearly straight, ventral margin almost straight anterior and curved upward posteriorly, carapace surface corroded with well pronounced postero-ventral ala, and weakly median sulcus starts from dorsal downward, and has slightly depression at antero-dorsal area, faint parallel ribs occurs at the ventral margin.
Dimension of figured specimens in (μm):

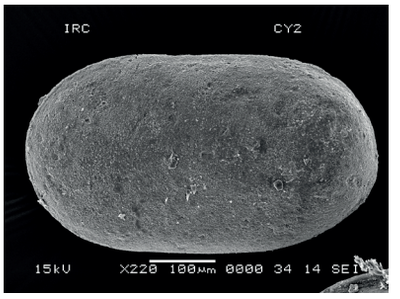
	Length	Height	L/H	Width
Right carapace	800	400	2.0	---

Remarks: This species is not very close to *Cytheropteron* except it has long caudal process, this makes it difficult to correlate with former genus, so it may be considered a new genus.
Occurrences: Occurs in outcrop of the Lower Tar Member (Zimam Formation) Ghadamis Basin.

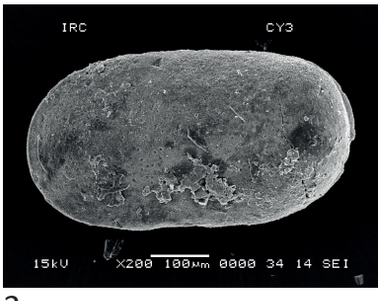
Sample no.	Thickness(in m)	Lithology
31	2	Calcilutite, yellow-light gray, medium hard, dolomitic in parts
30	1	Shale, gray- green, soft, fissil,
29	2	Calcilutite, yellow- light gray, medium hard,marly,with fossil fragment
28	3	Calcarenite, light gray- light brown, highly macrfossil content,medium hard,
27	1	Marl, light gray-light green, soft, fossilferous
26	3.5	Calcarenite, light brown-brown, rich with macrofossils, medium hard
25	2	Marl, light green- green, soft gypsiferous, fossilferous
24	1	Marl, light gray-light green,
23	1.5	Calcilutite, yellow- white, medium hard, marly,
22	1	Calcilutite, yellow- cream, soft- medium hard, marly in parts, slightly gypsiferous
21	2	Marl, light gray- light green, rich with macrofossils
20	1.5	Calcarenite,yellow- light gray, medium hard,with chert nodules
19	2	Marl, light gray- green,soft,
18	3	Calcarenite, yellow-white, hard,with fossil fragment, slightly dolomitic,
17	2	Marl, gray- light green, soft, gypsiferous
16	2.5	Calcarenite, light gray- light brown, fossiliferouce(exogari overge), highly fractured
15	1.5	Calcilutite, yellow-cream, hard, slightly dolometic.
14	2	Marl, white-yellow, soft with macrofossils.
13	2.5	Marl, as sample 11
12	1.5	Calcarenite, light brown –light gray, hard, rich in macrofossil,
11	3	Marl , yellow-light gren, soft, with gypsium streaks.
10	1	Calcarenite, light brown- red, medium hard, with phosphatic nodulls, and shell debris.
9	4	Marl, yellow, light green, soft, with shell fragment, gypsiferous in parts.
8	3	Calcilutite, cream to yellow, marly in parts,
7	3	Marl, light gray to light green, soft with streaks of gypsium, macrofossil are abundant.
6	3	Calciludite,white-cream, medium hard, slightly dolometic.
5	2	Marl, white-yellow, soft, gypsiferous.
4	1	Calcarenite , light gray, well sorted, subrounded shell fragment.
3	1	Calcilutite, white-yellow,slightly dolometic.
2	2	Calcarenite,yellow, hard, shell fragment observed, with gypsiferous marl in parts.
1	4	Marl,yellow-light green,gypsiferous.



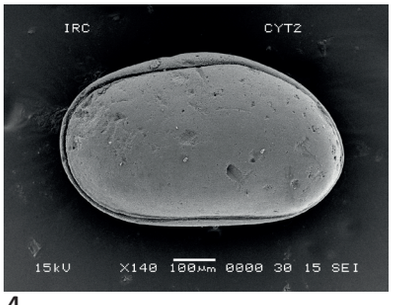
1



2



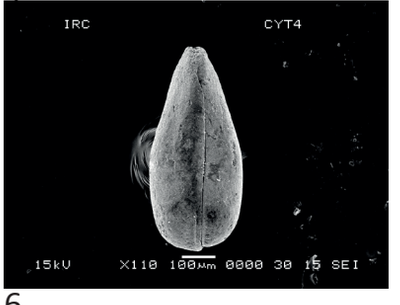
3



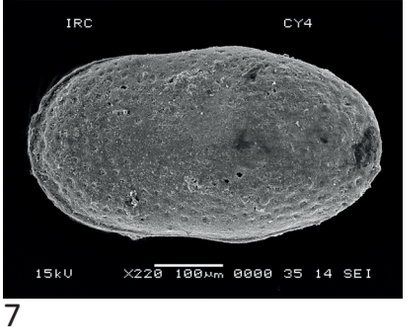
4



5



6



7



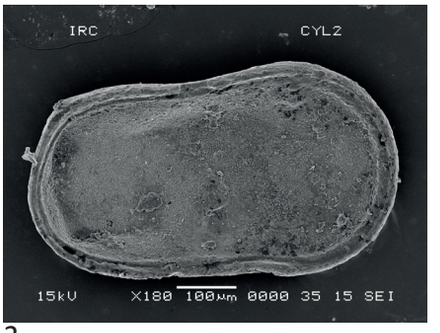
8

PLATE I

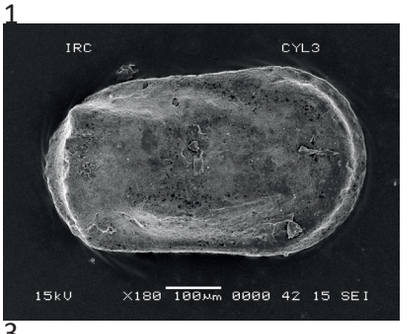
***Cytherella* sp. 2**
Plate I - 1 Male right carapace
Plate I - 2 Female right carapace
Plate I - 8 Female left carapace
Cytherella Mohamdi
Plate I - 3 Female left carapace
Cytherella sp. 1
Plate I - 4 Male left carapace
Plate I - 5 Female right carapace
Plate I - 6 Dorsal view
***Cytherella* sp. 3**
Plate I - 7 Female right carapace



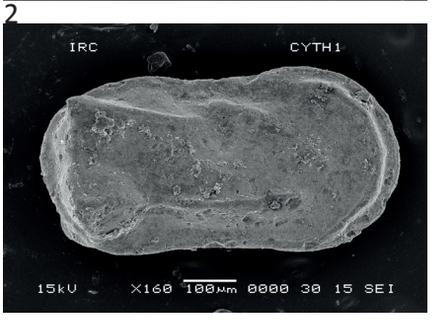
1



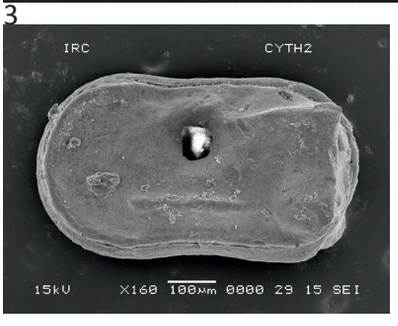
2



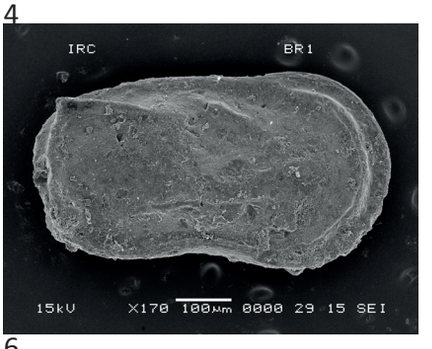
3



4



5



6



7



8

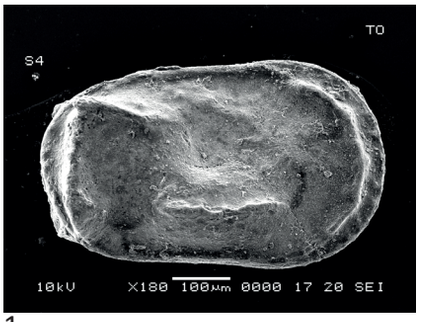
PLATE II

***Cytherelloida dabai* sp nov**

Plate II - 1	Male left carapace
Plate II - 2	Male right valve
Plate II - 3	Female right carapace
Plate II - 4	Male right carapace
Plate II - 5	Female left carapace
Plate II - 6	Male right carapace
Plate II - 7	Female left carapace

Cytherella mohamdi

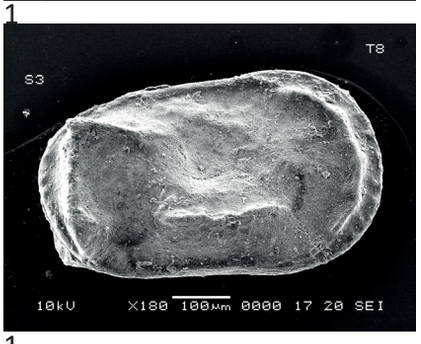
Plate II - 8	Female right carapace



1



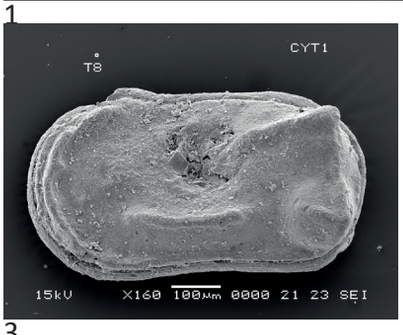
2



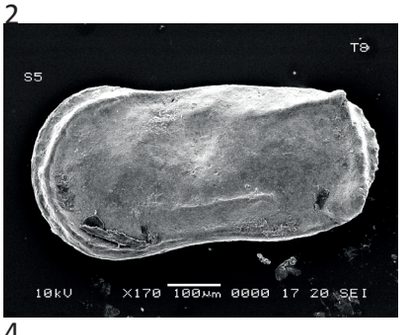
1



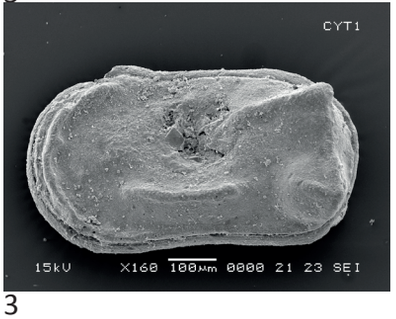
2



3



4



3

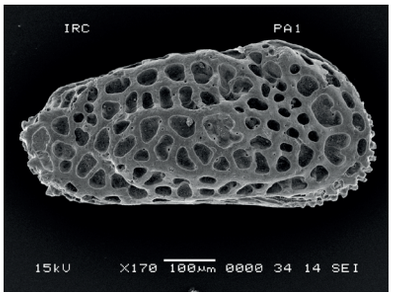


4

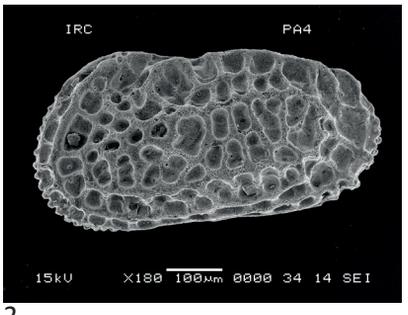
PLATE III

***Cytherelloida dabai* sp nov**

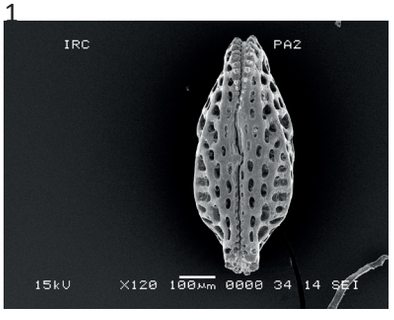
Plate III - 1 Female stereoscopic paired right carapace
Plate III - 2 Male stereoscopic paired left carapace
Plate III - 3 Female stereoscopic paired left carapace
Plate III - 4 Male stereoscopic paired left carapace



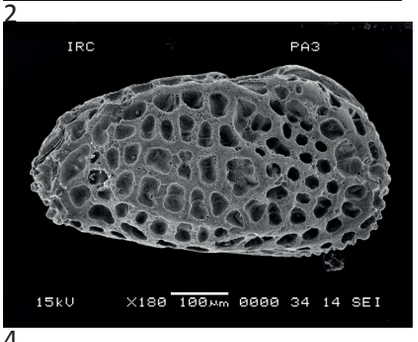
1



2



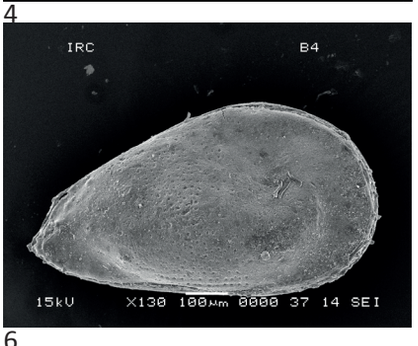
3



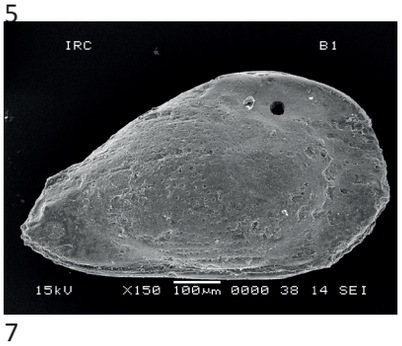
4



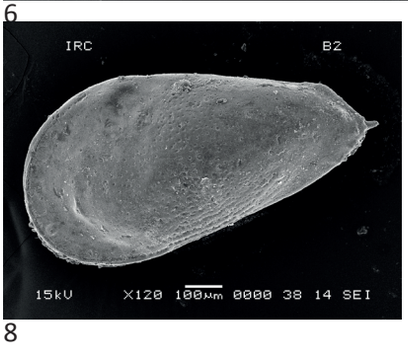
5



6



7



8

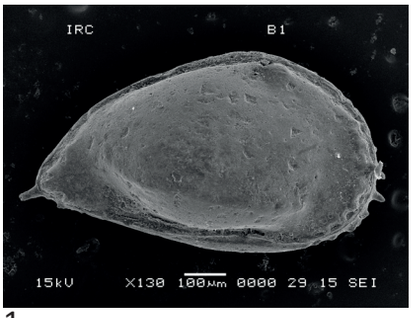
PLATE IV

Paracost a pervinquiri

Plate IV - 1 Male right carapace
Plate IV - 2 Female left carapace
Plate IV - 3 Ventral view
Plate IV - 4 Female right carapace

Protobuntonia nakkadii

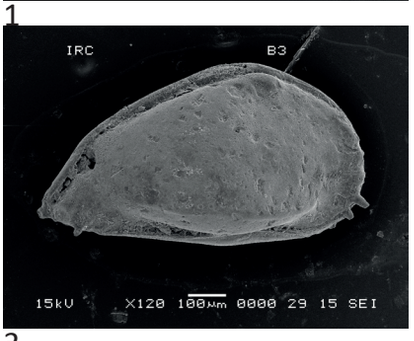
Plate IV - 5 Female left carapace
Plate IV - 6 Male right carapace
Plate IV - 7 Female right carapace
Plate IV - 8 Male right carapace



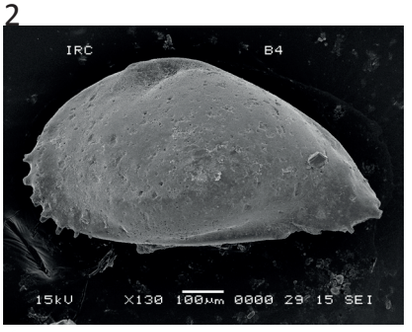
1



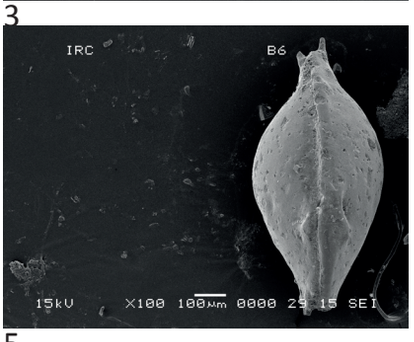
2



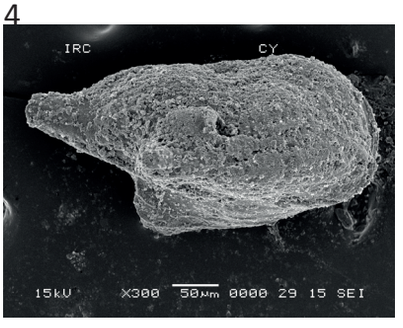
3



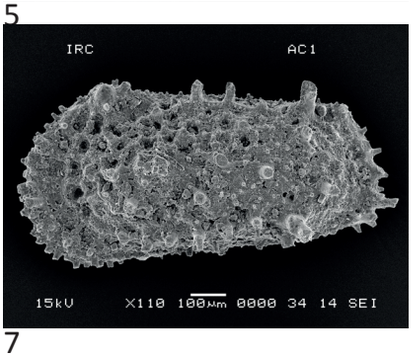
4



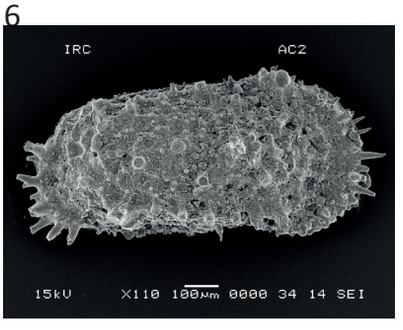
5



6



7



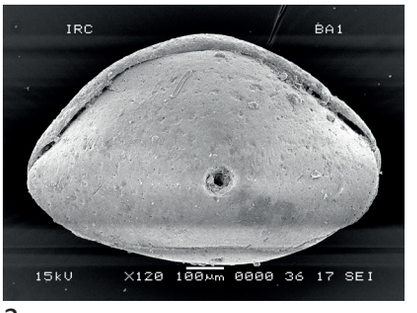
8

PLATE V

Brachycythere* cf. *B.dakhlaensis
Plate V - 1 Male right carapace
Plate V - 2 Female left carapace
Plate V - 3 Female right carapace
Plate V - 4 Male left carapace
Plate V - 5 Dorsal view
Genus A.
Plate V - 6 Right carapace
Oerteliella khargensis
Plate V - 7 Male left carapace
Plate V - 8 Male right carapace



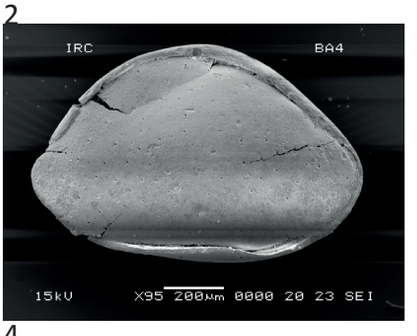
1



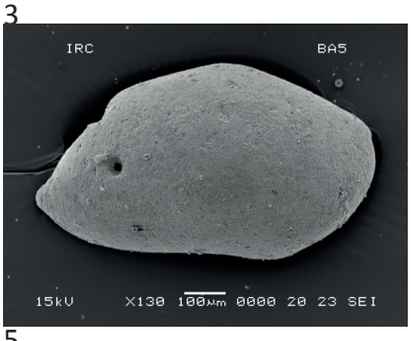
2



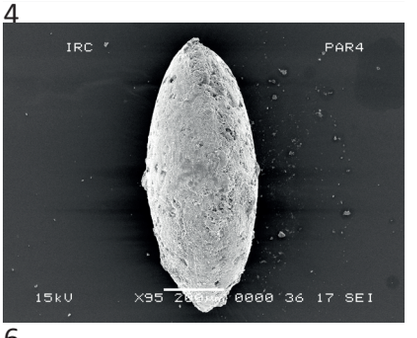
3



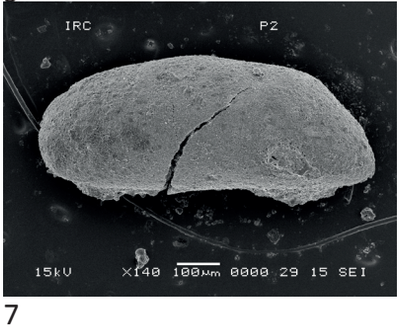
4



5



6



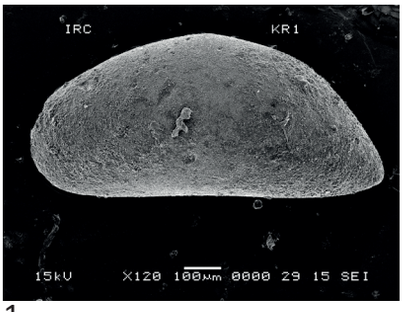
7



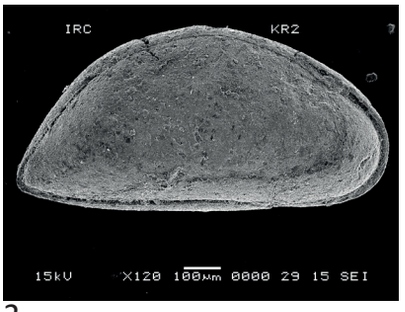
8

PLATE VI

***Bairdia* sp. 1**
Plate VI - 1 Left carapace
Plate VI - 2 Right carapace
Plate VI - 3 Left carapace
***Bairdia* sp. 2**
Plate VI - 4 Right carapace
Plate VI - 5 Left carapace
Plate VI - 6 Dorsal view
Pontocyprella recurva
Plate VI - 7 Left valve
Plate VI - 8 Right carapace



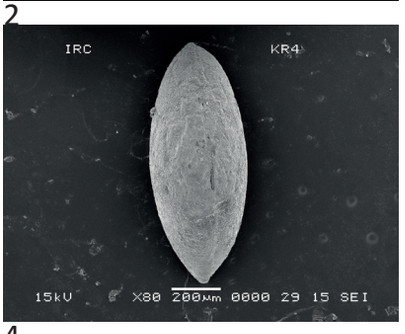
1



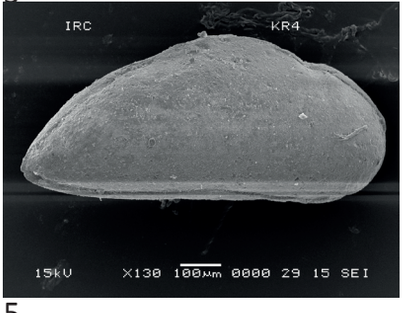
2



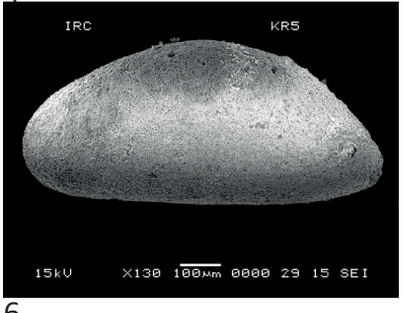
3



4



5



6



7

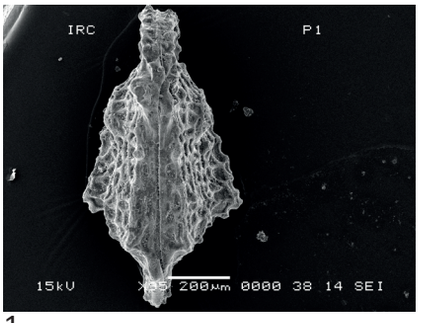


8

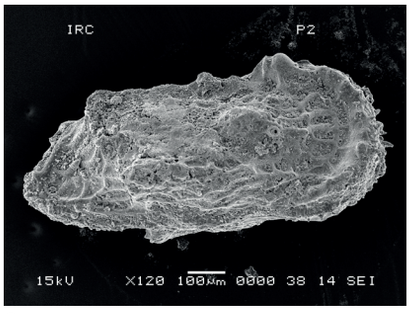
PLATE VII

***Pontocypris* sp. A**

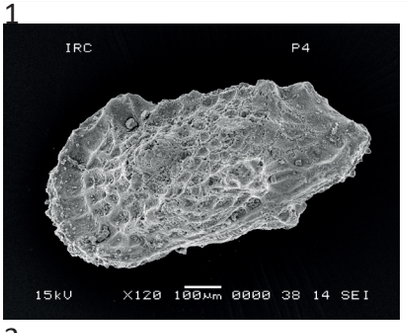
Plate VII - 1	Male left carapace
Plate VII - 2	Female right carapace
Plate VII - 3	Female left valve
Plate VII - 4	Dorsal view
Plate VII - 5	Male right carapace
Plate VII - 6	Female left carapace
Plate VII - 7	Female left carapace
Plate VII - 8	Female right carapace



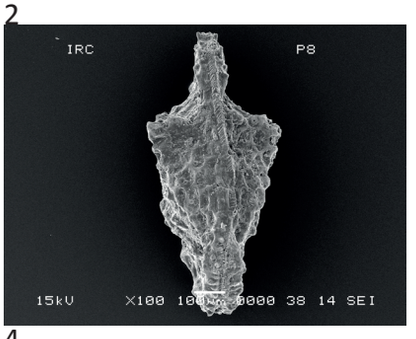
1



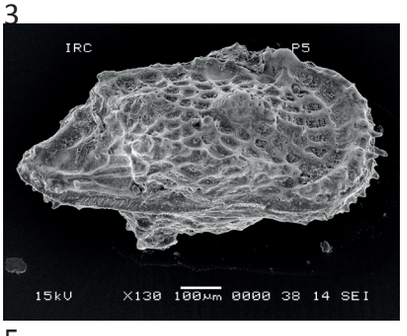
2



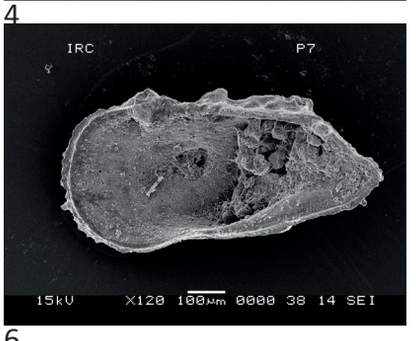
3



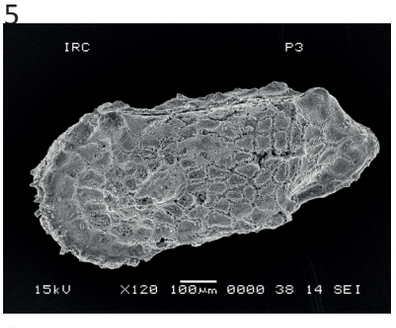
4



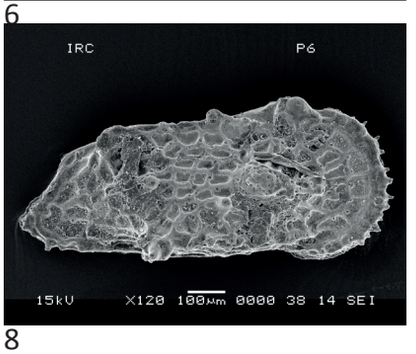
5



6



7



8

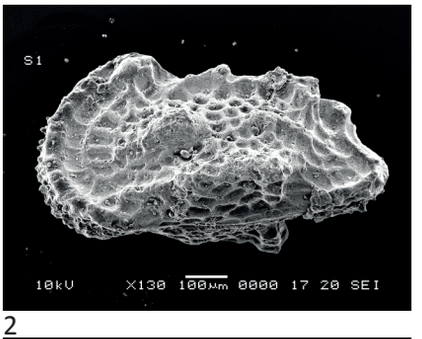
PLATE VIII

Paragrenocythere* cf. *P. gravis

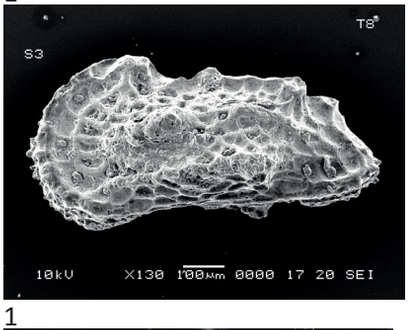
Plate VIII - 1 Dorsal view
Plate VIII - 2 Male right carapace
Plate VIII - 3 Female left carapace
Plate VIII - 4 Ventral view
Plate VIII - 5 Female right carapace
Plate VIII - 6 Male left valve
Plate VIII - 7 Male left carapace
Plate VIII - 8 Male right carapace



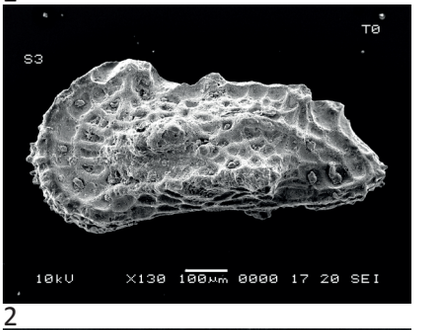
1



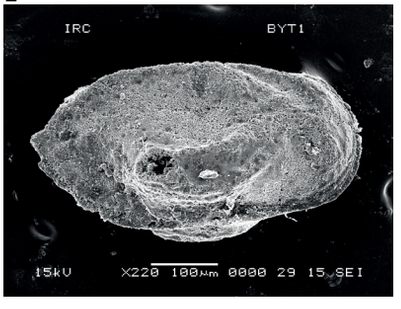
2



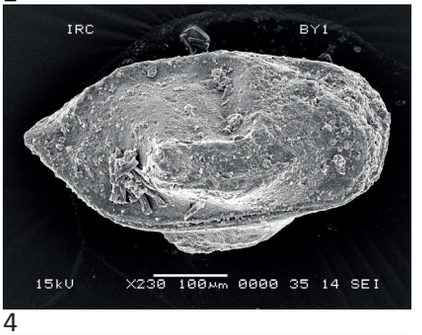
1



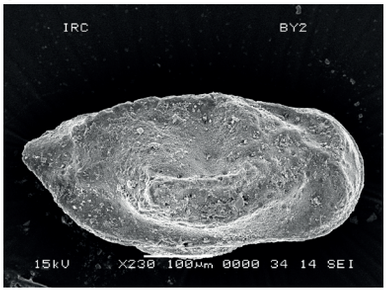
2



3



4



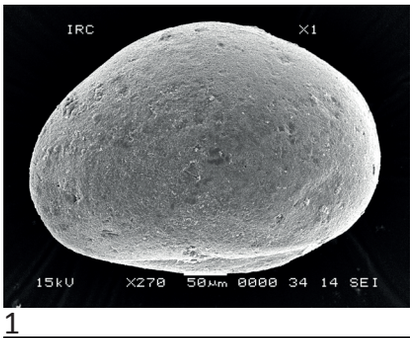
5



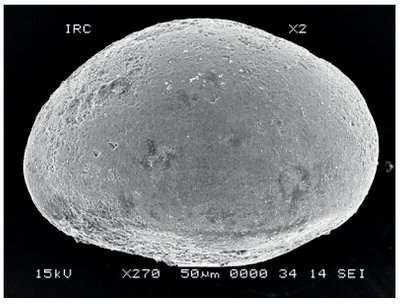
6

PLATE IX

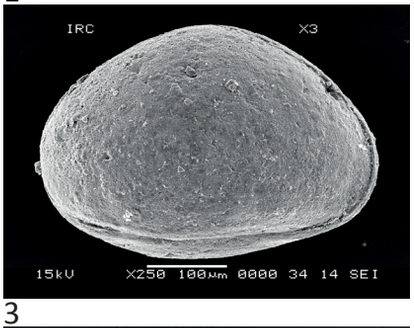
Paragrenocythere* cf. *P. gravis
Plate IX - 1 Female stereoscopic paired left carapace
Plate IX - 2 Male stereoscopic paired left carapace
Monoceratina salemi
Plate IX - 3 Female right carapace
Plate IX - 4 Female right carapace
Plate IX - 5 Male right carapace
Pontocyprella recurva
Plate IX - 6 Male right carapace



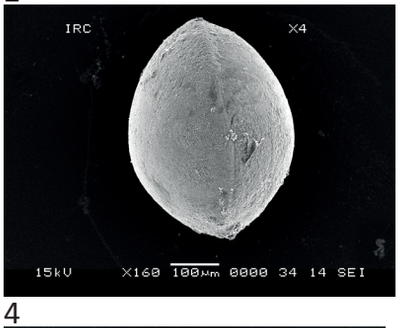
1



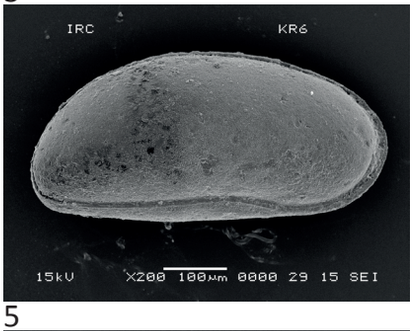
2



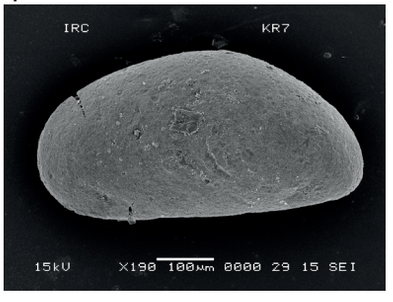
3



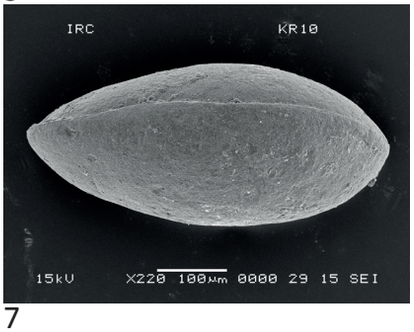
4



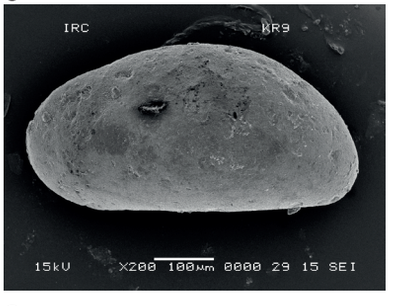
5



6



7



8

PLATE X

Xestoleberis

Plate X - 1	Right carapace
Plate X - 2	Right carapace
Plate X - 3	Left carapace
Plate X - 4	Dorsal view

***Krithe* sp. A**

Plate X - 5	Right carapace
Plate X - 6	Left valve
Plate X - 7	Dorsal view
Plate X - 8	Left carapace

CONCLUSION

Oil companies usually used fossils in order to estimate age dating of sediments, their paleoenvironments and paleogeography. The ostracoda is one of the tools have been employed in all over the world due to their cosmopolitan on worldwide and they can accommodate all kinds of environments from the poles to tropical areas. In this study we recorded eighteen ostracoda species which indicate Cretaceous age in the North Africa and Middle East and they represent the environment ranges from deeper to shallow marine species. Shallow species organisms such as *Oertilela*, *Paracosta* and deeper fauna like *krithe, Xestoleberis.* Only one species proposed as new and nominated (*Cytherella Dabai*).

Authors proposed byzone on the first appearance of species Pontooprella recurra which indicates Maastrechtian age in Tunisia and northern Libyan Offshore. In the northwest offshore Libya, this species associated with Ganssri zone and Apathomallus Mayoronsis zone Middle-Late Maastrechtian).

REFERENCES

AI-Furaih, A. A. F. (1977). On Paragrenochythere biclavat Al-Furaih gen et sp nov. Stereo-Atlas of Ostracoda shell, 2, 37 : 231-238.Cretaceous and Paleocene Species of the Ostracod *Hornibrokella* from Saudi Arabia. *Palaeontology.,* 20(3): 483-502, plts. 53-58.

Anketell, J. M. (1996). Structural History of Sirt Basin and Its Relationship to the Sabratah Basin and Cyrnaica Platform, Northern Libya. In: Geology of the Sirt Basin*,* (eds. M. J. Salem, M. T. Busrewil, A. A. Misillati, and M. A. Sola), Elsevier, Amsterdam, *First symposium on the Sedimentary Basins of Libya,* V.(3): 57-89.

Antonovic, A. (1977). Sheet Mizdah (NH 33-11). *Geological Map of Libya. Scale 1: 250,000, with Explanatory Booklet,* Industrial Research Center. Tripoli.

Apostolescu, V. (1955). Desciption du Quelques Ostracodes du Lutetien du Basin de Paris. *Cash, Geol. Thiary,* 28-29: 241-279, pls. 1-8.

Barr, F. T. and weegar, A. A. (1972). Stratigraphic Nomenclature of the Sirte Basin, Libya. *Petrol. Explor . Soc. Libya*: 129p.

Bassiouni, M, A. (1970). Ostracoda (Maastrichtian und Trachyleberidiae) und Ihre Bedeutung Fur die Biostratigraphie des Maastrichts und Alttertiarsvon Jordanien-Beith. Jb, 106: 5-52, Pls, hannover.

Bassiouni, M. A. and Luger, P. (1990). Maastrichtian to Early Eocene Ostracoda from Southern Egypt. *Paleontology, Paleoecology, Paleobiogeography and Biostratigraphy, Berliner geowiss. Abh.* (A) 120: 755-928.

Burolllet, P. F. (1960). Lexigue Stratigraphique International Afrique. *Fasc. IVa, Libye. Centre. Nat. de la Rech. Sci.*, Paris: 1-62.

Donze, P., Colin, J. P., Damorte, R., Oertli, H. J., Peypouquet, P.J., and Said, R. (1982). Les Ostracodes du Campanien Terminal à l Eocene Inferieur du la Coup du Kef, Tunisie Nord-Occidental. *Bull. du Center de Recherches Exploration Production Elf- Aquitaine,* 6(2): 273-335.

Dorreen. J. M. (1974). The Western Gaj River Section, Pakstan, and Cretaceous-Tertiary Boundary. *Micropaleontology,* V. 20(2): 178-193, Pl 1, tf.1-7.

Eliagoubi, B. A. H. (1975). Upper Cretaceous-Lower Tertiary Planktonic Foraminifera from the North Western Libya Offshore. *Jour. Afric. Earth Sci.,* 5(4): 423-449, pls.1-9, figs. 1-3.

EL-Sogher, A. (1996). Late Cretaceous and Paleocene Ostracoda from the Waha Limstone and Hagfa Shale Formations of the Sirt Basin, Libya. In: Geology of the Sirt Basin*,* (eds. M. J. Salem, A. J. Mouzughi and O. S. Hammuda), Elsevier, Amsterdam, *First symposium on the Sedimentary Basins of Libya,* V.(1): 287-382.

EL-Waer, A. (1992). Tertiary and Upper Cretaceous Ostracoda from Northest Offshore, Libya. Their Taxonomy, Biostratigraphy and Correlation with Adjacent Areas. Petroleum Research Center, Tripoli, Libya*, Special Publication* No.1: *445p.*

Esker, C. G. (1968). Danian Ostracoda from Tunisia. *Micropaleontology,* V. 14: 319-333, Pls. 1-4.

Ground Water Authority, Libya (1975). Wadi Sawfajjin-Wadi Zamzm–Aljufrah Regional Hydrogeological Study. *Energoprojekt Unpublished Report, Final Report Book–III-I.*

Furst, M., 1964, Die oberkreide Paleozoic_ Transgression in ostlichen Fezzan. *Geol. Rund.* V. 54(2): 1060 -1088.

Gammudi, A. (1990). Biostratigraphy and Ostracoda Faunas of the Miocene Marada Formation of the Eastren Sirt Basin, Libya*, M.Sc. Thesis. Glasgow University,* UK: 134p.

Gammudi, A. (1996). Lower Paleogene Ostracoda from the Sirt Basin of Libya, *Ph. D. Thesis, University of Glascow*, UK: 305p. Pls. 35.

Gohrbandt, K. H, A. (1966). Upper Cretaceous and Lower Tertiary Stratigraphy Along Westren and Southwestren Edge of the Sirt Basin, Libya. *Petrol. Explo. Soc. Libya, 8th Ann. Field Conf., 1966,* Southwestren Libya: 32-41.

Grekoff, N. (1969) Sur la Valuer stratigraphiques Ostracoda du Cretace du Paleocene et l Eocene infrerieur d´Algerie orientale. *3rd. Coll. Afr. Micropaleont; Cairo, 227-248,3 pls.*

Guiraud, R. (1998). Mesozoic Rifting and Basin Inversion Along the Northern African Tethyan Margin: An Overview. In: Petroleum Geology of North Africa. (ed. by: D. S. Macgreger, R. T. J. Mooody, D. D. Clark-Lowes). *Geol. Soc. Spec. Publ. No.132*: 217-230.

Jordi, H. A. and Lonfat, F. (1963). Stratigraphic Subdivision and Problems in Upper Cretaceous-Lower Tertiary Deposits in Northwestern Libya. *Revue de la Insitut Francais du Petrole,* 18(10 & 11): 1428- 1436.

Kassab, I. I. M. (1975). Globotruncana falsocalcarata Kerdany and abdelsalam from Northen Iraq*; Micropaleontology* V. 21(3): 364-351, Pls, 1-2.

Keen, M. C., Al-Sheikly, S. S. J., El-Sogher, A. and Gammudi, A. (1994). Tertiary Ostracoda of North Africa and the Middle East. In: *Micropaleontology and Hydrocarbon exploration in the Middle East* (ed, by: M. D. Simmons), Chapman and Hall, London: 371-388.

Kerdany, M. T. A and Abdelsalam, H. (1969). Globotruncana Falso Culcarata N.Sp. from the Queseir Area, Eastern Desert. U.A.R. Proc. 3d African Micropaleontology Coll, Cairo: 261-267. Pls, 1-2.Tf.1.

Klitzsch, E. (2000). The Structural Development of the Murzuq and Kufra Basins-Significance for Oil and Mineral Exploration. *Symposium on Geological Exploration in Murzuq Basin* (Ed. by: M. A. Sola and D. Worsley), Elsevier, Amsterdam: 143-150.

Megerisi, M. and Mamgain V. D. (1980). The Upper Cretaceous–Tertiary Formations of Northern Libya: A Synthesis. *I.R.C., Libya. Bull.* 12:85p.

Novovic, T. (1977). Sheet Nalut (NH 32-4) Geological Map of Libya, scale 1: 250,000 with *Explanatory Booklet, I.R.C.* Tripoli.

Reyment, R. A. (1963) Studies on Nigerian Upper Cretaceous and Lower Tertiary Ostracoda, Part 2: Danian, Paleocene and Eocene Ostracods. *Stockholm Contribution to Geology:*10: 1-286.

Said, R. (1978). Etude Sratigraphique et Micropaleontologique du Passage Cretace-Tertiare du Synclinan d Elles (region Siliana-Sers), Tunisie Centrale. *These Doc .3 Cycle, Univ. Paris,* V1:1-275.

Salaj, J. (1979). Geological Map of Libya, 1: 250,000, Sheet Al Qaryat Al Gharbiyah (NH 33-5) With Explanatory Booklet*, I. R C, Tripoli, Libya:* 71 p.

Salaj J. and Megresi, M. (1980). Biostratigraphy of the Upper Senonian and Paleocene of Al Qaryat Al Gharbiyah Area, Al Hammadah Al Hamra, Libya: *Journal Geol. Soc. Iraq.* 13(1): 387-398.

Salaj, J. and Nairn, A. M. (1991). Age and Depositional Environment of the Lower Tar Member of the Zimam Formation, Upper Senonian in the Northern Hammadah Al hamra, Libya. *Palaeogeography, Palaeoclimatology, and Palaeoecology,* 61(3): 121-143.

Salahi, D. (1966). (Ostracodes du Cretace superieur et du Tertiare en province d´un sondag du region de Zelten (Libya). *Revue de l´Institut Francais du Pêtrol,* 21(1): 331p.

Akad. Weten., ser. B, 75. 1, 85-95, Amsterdam.

Siddiqui, Q.A. (1971). Early Tertiary Ostracoda of family Trachyleberididae from west Bakistan, *bull, brit, Mus*, (Nat.*Hist*). *Geol.Suppl*.9 :98, 42.pls.

Swain, *et al*. (1983). Some Cretaceous Ostracoda from Nigeria. *Revista Espanola de Micropaleontologia*, 27(2): 41-65.

Treatise. (1961). On Invertebrate Paleontology (Q). *Geological society of America,* University of Kansas press.

Whatley, R. and Arias, C. F. (1993). Paleogen Ostracoda from the Tripoli Basin, Libya. *Revista Espanola de Micropaleontolgia,* 25(2): 125-154.

Witte, L. (1993). Taxonomy and Origin on Modern West African Shallow Marine Ostracoda. *Academische Pers B.V. Nieuwe Herengracht*., 31, 1011 RM Amesterdam.

Palynological Analysis of cutting samples from Well: A1-177/01, Murzuq Basin

R. El-Zaroug*, A. El-Harbi** & A. Gammudi***

Abstract: Playonological study have been utilized in order to define age and depositional environments of the penetrated sections of the well A1-177/01, which belongs to Chevron Libya Limited, located in the South Eastern Margin of Murzuq Basin. The study based on selected one hundred and four cutting samples, and despite of difficulties caused by heavy caving and reworked palynomorphs, palynological recoveries in general was good in the upper half of the studied section.

Microscope investigations revealed moderately rich to poor assemblages consisting mainly of miospores, few marine acritarches and chitinozoans, recovered from the studied samples enabled to erect six distinctive palynological assemblages. These assemblages range from Early Silurian to Early Carboniferous in age. The ages assigned to these assemblages have been determined by comparing the palynomorphs assemblages with similar assemblages recorded from Paleozoic sequences in other nearby wells in Murzuq Basin, Ghadamis Basin, North East Libya region, South east Libya (Al Kufrah Basin) and also from other parts of old Gondwana region. Paleoenvironmental interpretation is based on interpreted lithological and palynological criteria.

Keywords: Triassic, Cretaceous, Palynomorphs, Offshore Sirt Embayment.

INTRODUCTION

The studied well A1-177/01, which belongs to Chevron Libya Limited, located in the South Eastern Margin of Murzuq Basin (Fig. 1).

One hundred and four cutting samples (Table 1) were selected by Libyan Petroleum Institute (LPI) geologists for this palynological study, and despite of difficulties caused by heavy caving and reworked palynomorphs, palynological recoveries in general was good in the upper half of the studied section.

The lithostratigraphic units referred to in this report (Table 2), are based upon schemes used by Bellini and Massa (1980) and Klitzsch (1981). Reference has also been made to the Libyan Volume of the Lexicon of Stratigraphy by Burollet (1960). Paleoenvironmental interpretation is based on interpreted lithological and palynological criteria, (Table 3).

MATERIAL AND METHODS

Samples: One hundred and four cutting samples from well A1-177/01 were selected by LPI geologists.

Laboratory techniques: The samples were prepared in the laboratory of the L.P.I. according to standard palynological procedures. The preparation stages can be summarized as following:

Cleaning sample: Samples were washed using tap water and 150 µm mesh sieve to remove drilling mud.

Picking: All selected samples were sieved in 2 mm mesh sieve to eliminate any possible caved material (material larger than 2mm assumed to be caved)

Demineralization:

- Carbonate removal using hydrochloric acid (HCI 18%).
- Silicate removal using hydrofluoric acid (HF 40%).
- Sieving using 10, 18, 22 and 64 micron sieve as appropriate
- Oxidation to remove unwanted organic matter using nitric acid (HNO3 65%) for about 3-5 minutes (applied for the majority of samples)
- Removal of minerals (separation the inorganic mineral from the organic matter by using zinc chloride (ZnCl) with specific gravity 2.00.

* Tripoli University: Rzaroug@yahoo.com
&* Libyan petroleum Institute:
a_elharbi@yahoo.com, a_gammudi@yahoo.com

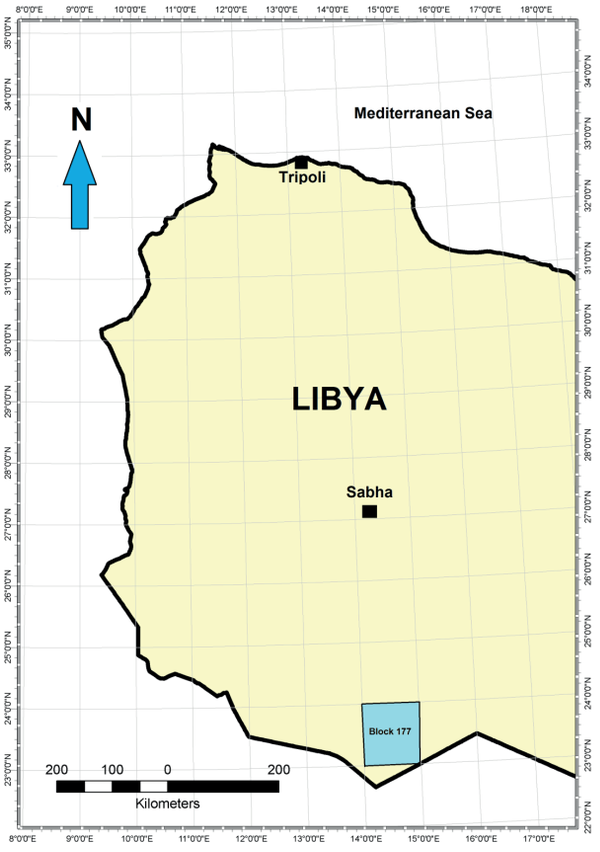


Fig. 1. Location Map of the Study Area.

The cleaned and neutralized residue is mixed with few drops of the dispersing solution (PVA) to prevent coagulation of the organic residue on the slide. This mixture spread on two 24X30mm cover slips using pipettes and allowed to dry on hot plate (25˚C). Mounting was achieved by placing one or two drops of the resin on to a clean microscope slide (76 X 26mm).

PALYNOLOGICAL RESULTS

Six palynological assemblages were identified among the studied sequences. The distribution of the common and stratigraphically significant palynomorphs is listed in the well stratigraphic chart (Fig. 2) and the identified assemblages can be described below as follows:

***Interval (ft.):* 420–1180.**

Samples analyzed: 16 Cutting samples.

Age: Lower Carboniferous, (Late Visean).

Remarks: Rich and diverse land derived organic matter, dominated by spores and herbaceous debris was recovered from this interval. Age of this interval based on the highly abundance of *Aratrispors sahariensis* and presence of *Diatomozonotriletes fragilis* Reworked Devonian and Tournasian Spores are abundant.

The above assemblage similar to what have been recorded by Clayton & Loboziak (1985) and Loboziak & Clayton (1988) from Carboniferous sediments of North East Libya, and can be assigned to the Late Visean (Clayton, 1995). The base of this assemblage is marked by first appearance down hole (last occurrence) of species *Spelaeotriletes proteau,* however the top of this assemblages cannot be seen in this well. Late Visean palynomorphs, also reported by El-Harbi (2000), from upper part sediments of Mrar Formation, Ghadamis Basin.

Palaeoenvironment: The predominance of land derived organic matter in which spores and herbaceous debris were the most common, absent of marine palynomorphs (no acritarches were observed), and the presence of butrroccocus (fresh water algae) in this intervals, suggest deposition in a non marine environment.

Interval (ft.): 1240–1690.

Samples analyzed: 12Cutting samples.

Age: Lower Carboniferous, (? Early Tournasian).

Remarks: Rich and diverse land derived organic matter, dominated by spores and herbaceous debris was recovered from this interval. The first down hole appearance (last occurrence) of *Idnotriletes explanatus*, *Cyrtospors cristifer* and *Umbonatispora baculatus* indicate an age no younger than Mid-Tournaisisn. The presence of upper most Fammenien spore *Retispora lepidophyta* and Givetian–Frasnian spores *Grandispora libyansis* & *Grandispora inculta* in the lower most part of this interval, regarded as reworked due to nature of their preservation.

The above assemblage is considered to be Tournaisian (probably Early Tournaisian) in age and almost similar in composition to palynozone 12 of Grignani *et al* (1991). Reworked Devonian and caved Visean spores are abundant.

Palaeoenvironment: The predominance of land derived material in which spores and herbaceous debris were the most common, few marine palynomorphs 1-2% (acritarches), and the presence of butrroccocus (fresh water algae) in this intervals, suggest deposition in marginal marine environment.

Interval (ft.): 1750–1910.

Samples analyzed: 4 Cutting samples.

Age: Middle Devonian &? Latest Devonian undifferentiated (Early Givetian &? Strunian).

Table 1: Samples selected for plalynological investigation

S/N	Depth/feet	S/N	Depth/feet	S/N	Depth/feet
1	420	39	2210	77	3920
2	460	40	2240	78	3980
3	510	41	2250	79	4040
4	570	42	2300	80	4100
5	630	43	2360	81	4160
6	690	44	2380	82	4220
7	760	45	2390	83	4280
8	820	46	2420	84	4340
9	880	47	2480	85	4400
10	910	48	2490	86	4460
11	920	49	2540	87	4520
12	940	50	2600	88	4580
13	1000	51	2630	89	4640
14	1060	52	2640	90	4700
15	1110	53	2650	91	4760
16	1180	54	2660	92	4820
17	1240	55	2670	93	4880
18	1300	56	2690	94	4900
19	1310	57	2720	95	4930
20	1330	58	2780	96	4960
21	1360	59	2840	97	4990
22	1410	60	2900	98	5020
23	1470	61	2960	99	5050
24	1530	62	3020	100	5080
25	1590	63	3080	102	5110
26	1630	64	3140	103	5140
27	1650	65	3200	104	5160
28	1690	66	3260		
29	1710	67	3320		
30	1730	68	3380		
31	1750	69	3440		
32	1790	70	3500		
33	1850	71	3560		
34	1910	72	3620		
35	1970	73	3680		
36	2030	74	3740		
37	2090	75	3800		
38	2150	76	3860		

Table 2: **Summary of the Stratigraphy**
The following summary tables are based on data obtained from the analyses of ditch cuttings samples. The boundaries quoted are either the bottom depths of sampled intervals or have been adjusted to suitable wire line log break (marked by the suffix (log).

Top Depth/feet	Series	Stage	Formation
420 - 1180	Lower Carboniferous	Visean	Mrar
1240 - 1690	Lower Carboniferous	Tournasian	
	Unconformity		Mrar
1700(log) - 1960	Middle Devonian ?Latest Famennian	Givetian & ?Strunian	Awaynat Wanin II & ?Tahara
	Unconformity		
1970 - 2380	Lower Devonian	?Siegenian -Emsian	Quan Kasa & ?Tadrart
	Unconformity		
2390 - 2690	Silurian	Llandovery-Wenlock	Akakus
	Unconformity		
2750 (log) - 5071	Barren Samples	indeterminate	

Table 3: Summary of the Paleoenvironments

Top Depth/feet		Paleoenvironment
420 – 1180		Non – marine
1240 – 1690		Marginal marine
	Unconformity	
1700(log) - 1960		Marginal marine
	Unconformity	
1970 – 2380		Non – marine
	Unconformity	
2390 – 2690		Outer neritic
	Unconformity	
2750 (log) - 5071	Barren Samples	indeterminate
	Unconformity	
5072 Basement (log) – 5160 T.D		

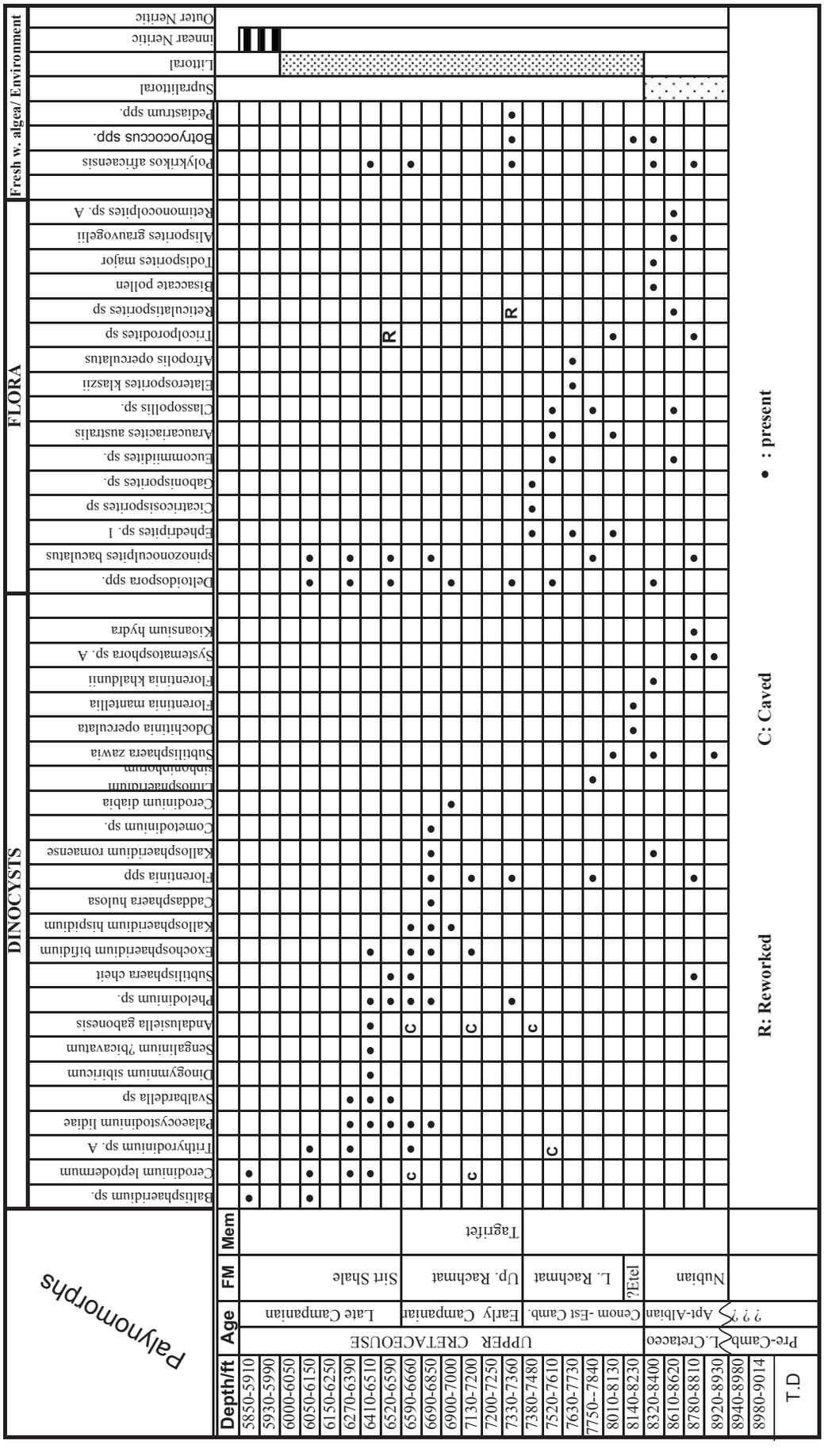


Fig. 2. Stratigraphic Chart of Well A1-177/01.

Remarks: The rare presence of Retispora lepidophyta in the intervals (1750-1850) indicates an age of latest Famennian (Strunian), but the sparsely presence of diagnostic palynomorphs such as *Acinosporites acanthomammillatus* & *A. macrospinspinosus* and the common presence of *Grandispora* inculta, *Acanthotriletes horides*, *Grandispora nauomova*, *Grandispora libyaensis & Geminospora lemuratus,* along with other spores, strongly indicate a Givetian age for this interval. However, it is hard to regard them as being reworked spores. Therefore, this interval was regarded as condensed middle and upper most Devonian deposits. Frasnian and most of the Upper Famennian index palynomorphs were not recorded from this interval, therefore, sediments of these ages might be either eroded or not deposited, thus an unconformity surface can be set between Early Givetian and Latest Devonian times.

The above assemblages is correlate very well with (AD) Oppel Zone- Interval *lem* of Streel *et al* (1987). Streel *et. al*., (1988), reported similar assemblages from Givetian sediments of North East Libya and also from the revised zonation and age of the Aouinet Ouenine III Formation, in the Ghadamis Basin western part of Libya.

Palaeoenvironment: The predominance of land derived material in which spores and herbaceous debris were the most common, few marine palynomorphs 1-2% (Acritarches), suggest deposition in a marginal marine environment**.**

Interval (ft.): 1970–2380.

Samples analyzed: 10 Cutting samples.

Age: Lower Devonian, (? Siegenian - Emsian).

Remarks: The first down hole appearance (last occurrence) of *Dictyotriletes emsensis*, *Brochotriletes macgregri* ,*Camptozonotriletes caperatus* and *Emphanisporites micronatus* indicate age of no younger than Emsian as have been dated in (McGregor, 1979). The barren sandy sequence (2100-2380) which stratigraphicaly lies between mid Silurian and Emsian times, questionably considered to be part of Tadrart Formation, and questionably assigned to a Siegenian time. The presences of Silurian spores such as *Archeozonotriletes* cf. *chulus* and *Archeozonotriletes chulus* in this interval, regarded as being reworked.

Palaeoenvironment: The predominance of land derived material in which spores and herbaceous debris were the most common, and the absence of marine palynomorphs, suggest deposition in non marine environment**.**

Interval (ft.): 2390–2690.

Samples analyzed: 14 Cutting samples.

Age: Silurian, (Late LLandovery-Wenlock).

Remarks: The analyzed samples from the above interval reveled rich chitinozoans assemblages and some acritarches species. Age of this interval based on the presence of the following Acritarchs species: *Arpylorus antiquus*, *Diexallophasis remota*, *Helosphaeridium malvernensis*, *Hoegklintia Cylindrica, Villosacapsula & Leiofusa bernesga* together with chitinozoans species such as: *Spherochitina* spp, *Angochitinia* spp, and *Ancyrochitina ancyrea*. The above assemblages can be well correlated with the LLandovery assemblages which have been reported by Hill *et al* (1985), from three wells (E1-81, A1-46 and D1-31) from North East Libya.

Palaeoenvironment: The presence of abundant marine palynomorphs, dominated by chitinozoans and acritarchs suggest an open marine environment of deposition**,** most likely outer neritic zone.

Interval (ft.): 2780–5160 T.D.

Samples analyzed: 46 Cutting samples.

Age: Indeterminate.

Remarks: All samples analyzed from the above interval prove to be barren of palynomorphs.

CONCLUSIONS

A review of miospores and acritarchs faunas of the interval 1240–1690 feet of the studied well A1-177/01 suggest precisely Early Carboniferous (? Early Tournasian) age. This interval was previously regarded as a Silurian sediments by Chevron Geologists (2009).

This conclusion is based on the highest occurrence downhole of the following characteristic species: *Idnotriletes explanatus*, *Cyrtospors cristifer* and *Umbonatispora baculatus*. Six palynological zones have been established from the Silurian and Carboniferous sediments of the well A1-177/01, on the basis of miospores, acritarchs and chitinozoans, ranging in age from Early Silurian to Early Carboniferous in age. These zones are assemblage zones and are corelatable with other assemblages reported by other authors from the Murzuq Basin, Ghadamis Basin, North East Libya region, South east Libya (Al Kufrah Basin) and also from other parts of old Gondwana region.

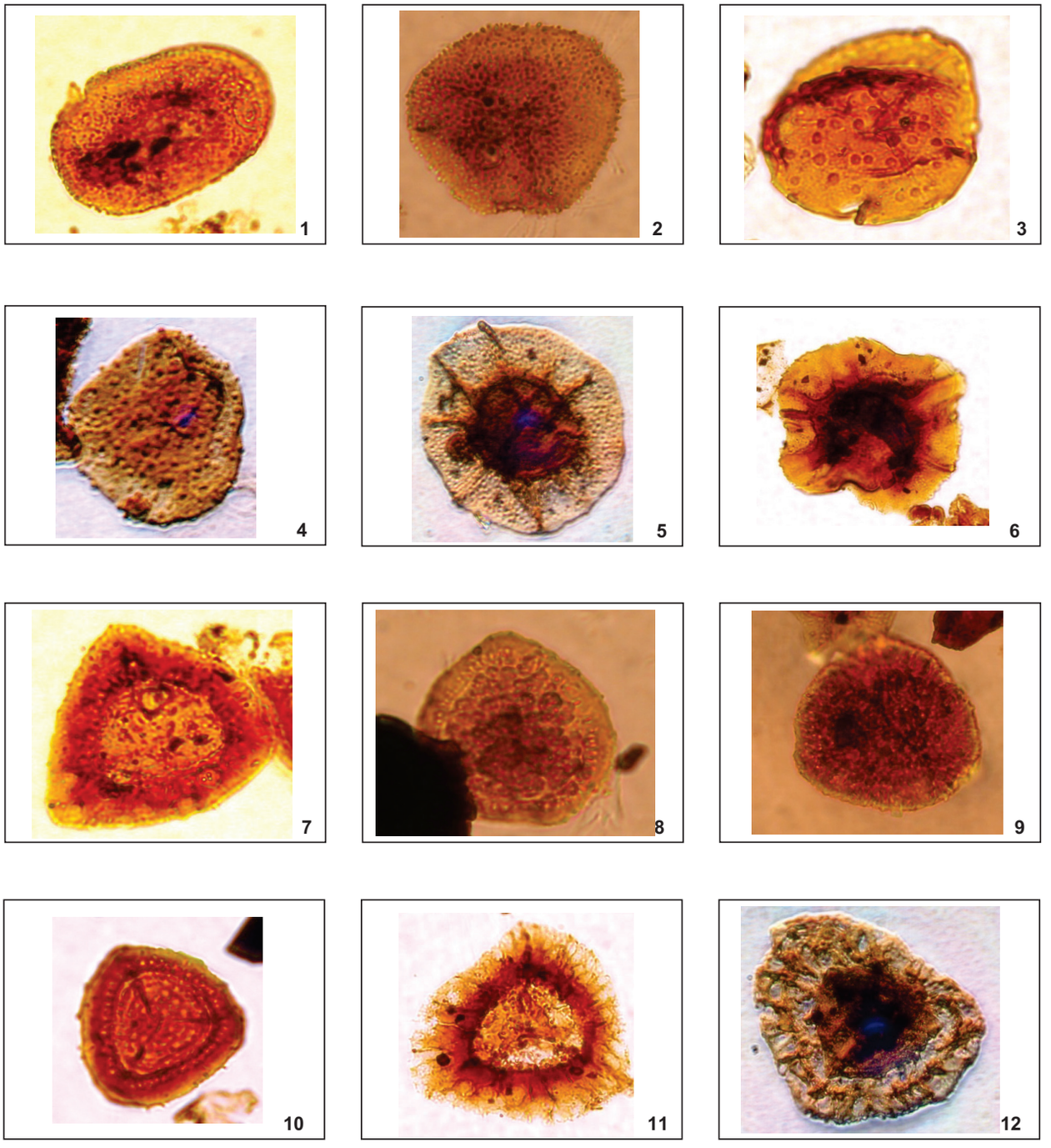


PLATE I

The species name is followed by the sample number and depth.
All figures are X800 unless otherwise indicated

Plate I - 1	Aratrisporites saharnsis, S4/570 ft
Plate I - 2.	Spelaeotriletes triangulus, S8/820 ft
Plate I - 3	Spelaeotriletes pretosus, S21/1360 ft
Plate I - 4	Spelaeotriletes pretosus, S22/1410 ft
Plate I - 5	Comptozonotriletes cyrenaicus, S8/820 ft
Plate I - 6	Comptozonotriletes cyrenaicus, S21/1360 ft
Plate I - 7	Vallatisporites vallatus, S27/1690 ft
Plate I - 8	Vallatisporites verrucosus, S8/820 ft
Plate I - 9	Vallatisporites agadesi, S1/420 ft
Plate I - 10	Vallatisporites sp, S7/760 ft, X1000
Plate I - 11	Radiizonates sp, S7/760 ft
Plate I - 12	Radiizonates genuinus, S25/1590 ft

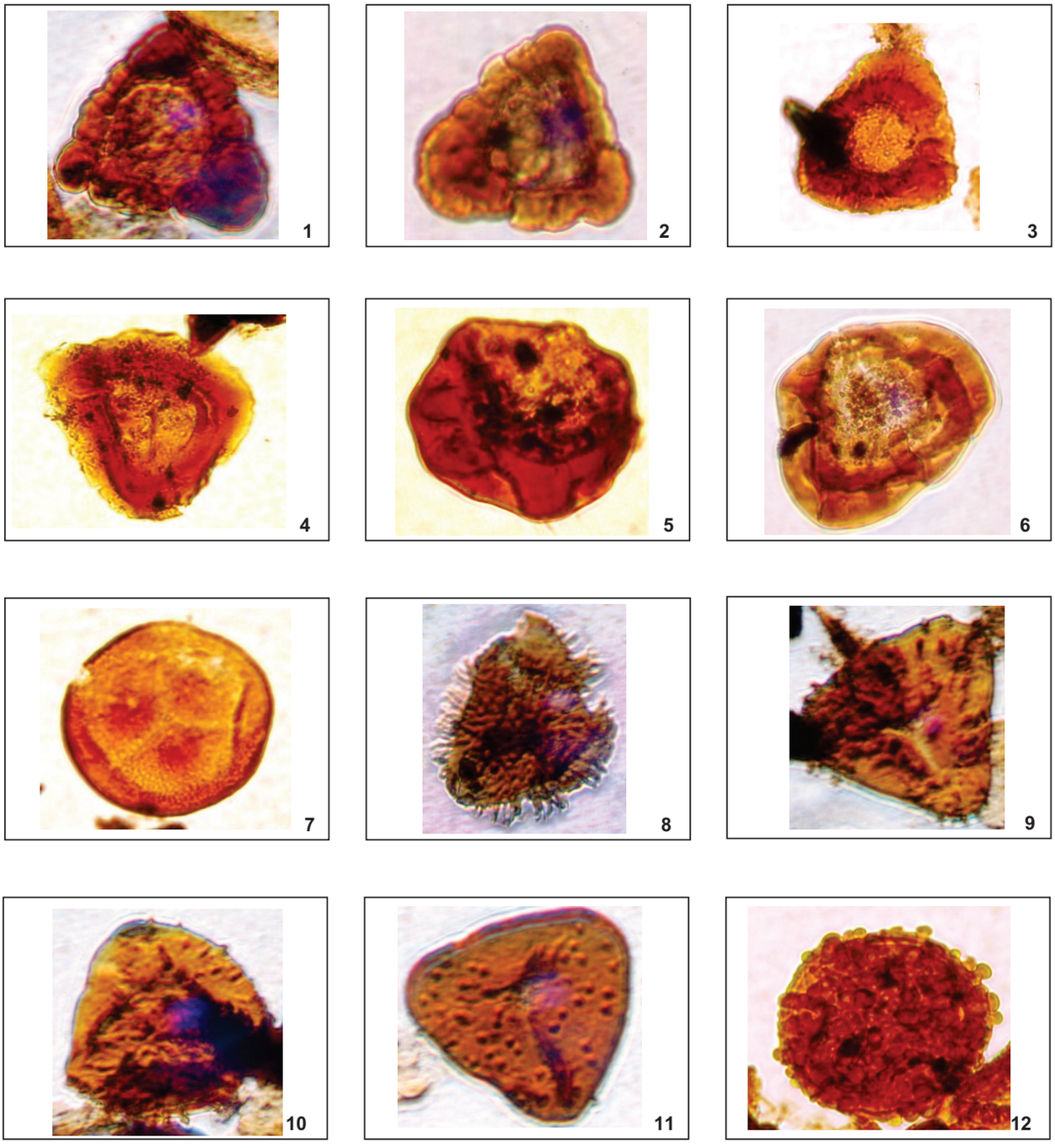


PLATE 11

The species name is followed by the sample number and depth.
All figures are X800 unless otherwise indicated

Plate II - 1	Densosporites variomarginatus, S23/1470 ft
Plate II - 2	Densosporites variomarginatus, S23/1470 ft
Plate II - 3	Cingulizonate bialatus, S25/1590 ft
Plate II - 4	Cingulizonate bialatus, S18/1300 ft
Plate II - 5	Knoxisporites pristinus, S6/690 ft
Plate II - 6	Knoxisporites pristinus, S6/690 ft
Plate II - 7	Retusotriletes crassus, S27/1690 ft
Plate II - 8	Ditomozonotriles fragilis, S27/1690 ft
Plate II - 9	Umbonatisporites baculatus, S27/1690 ft
Plate II - 10	Umbonatisporites baculatus, S27/1690 ft
Plate II - 11	Umbonatisporites sp, S26/1630 ft, X1000
Plate II - 12	Raistrickia clavata, S26/1630 ft

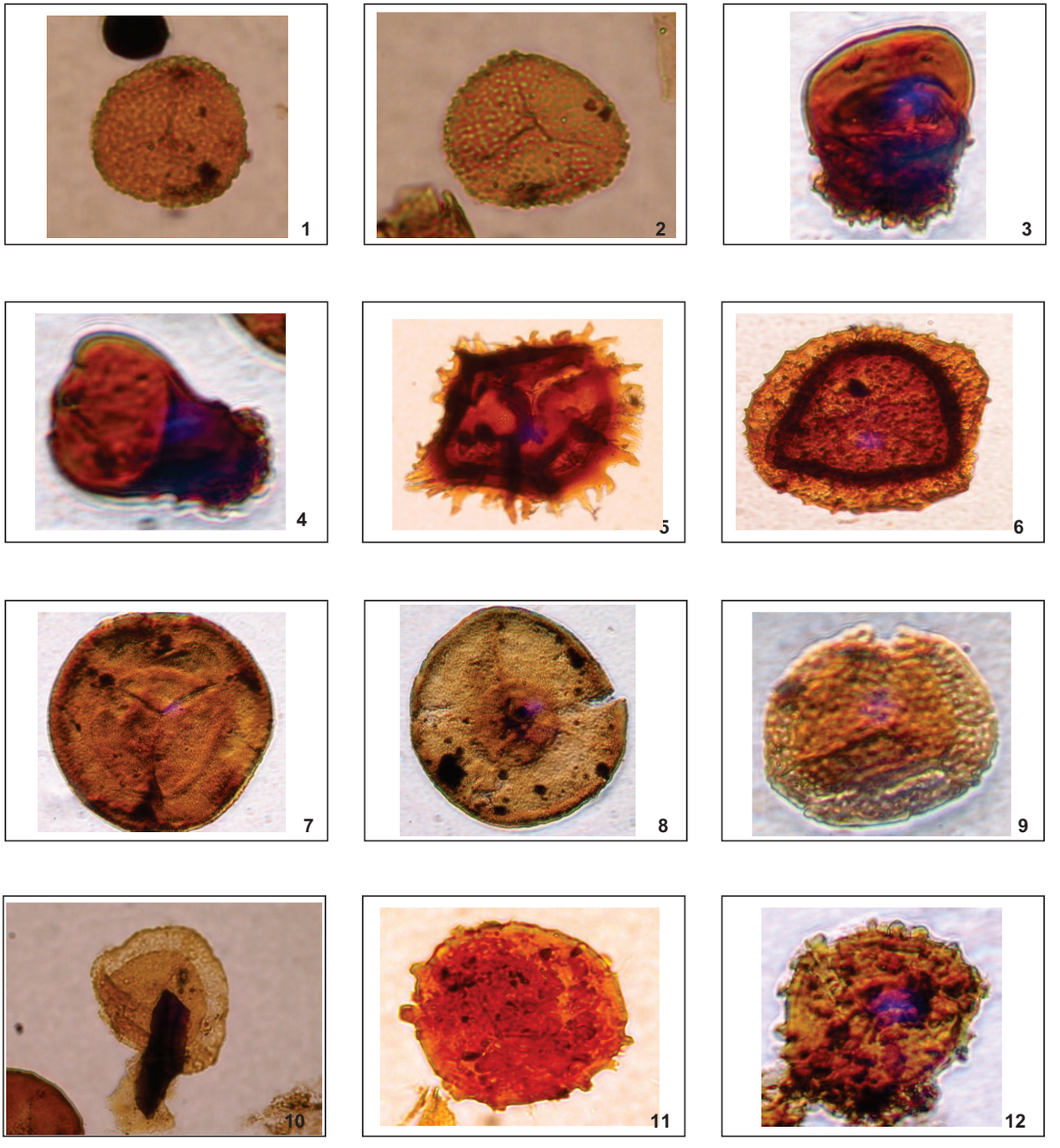


PLATE 111

The species name is followed by the sample number and depth.
All figures are X800 unless otherwise indicated

Plate III - 1	verrucosisporites fammenensis, S29/1790 ft, X1000
Plate III - 2	verrucosisporites fammenensis, S29/1790 ft, X1000
Plate III - 3	Cyrtospora cristifer, S27/1690 ft
Plate III - 4	Cyrtospora cristifer, S27/1690 ft
Plate III - 5	Dictyotiletes fimbriatus, S27/1690 ft
Plate III - 6	Indotriradites explanatus, S27/1690 ft
Plate III - 7	Spelaeotriletes giganteus, S8/820 ft
Plate III - 8	Spelaeotriletes giganteus, S8/820 ft
Plate III - 9	Retispora lepidophyta, S30/1850 ft
Plate III - 10	Retispora lepidophyta, S28/1750 ft
Plate III - 11	Pustulatisporites dolbii, S23/1470 ft, X900
Plate III - 12	Pustulatisporites dolbii, S23/1470 ft, X900

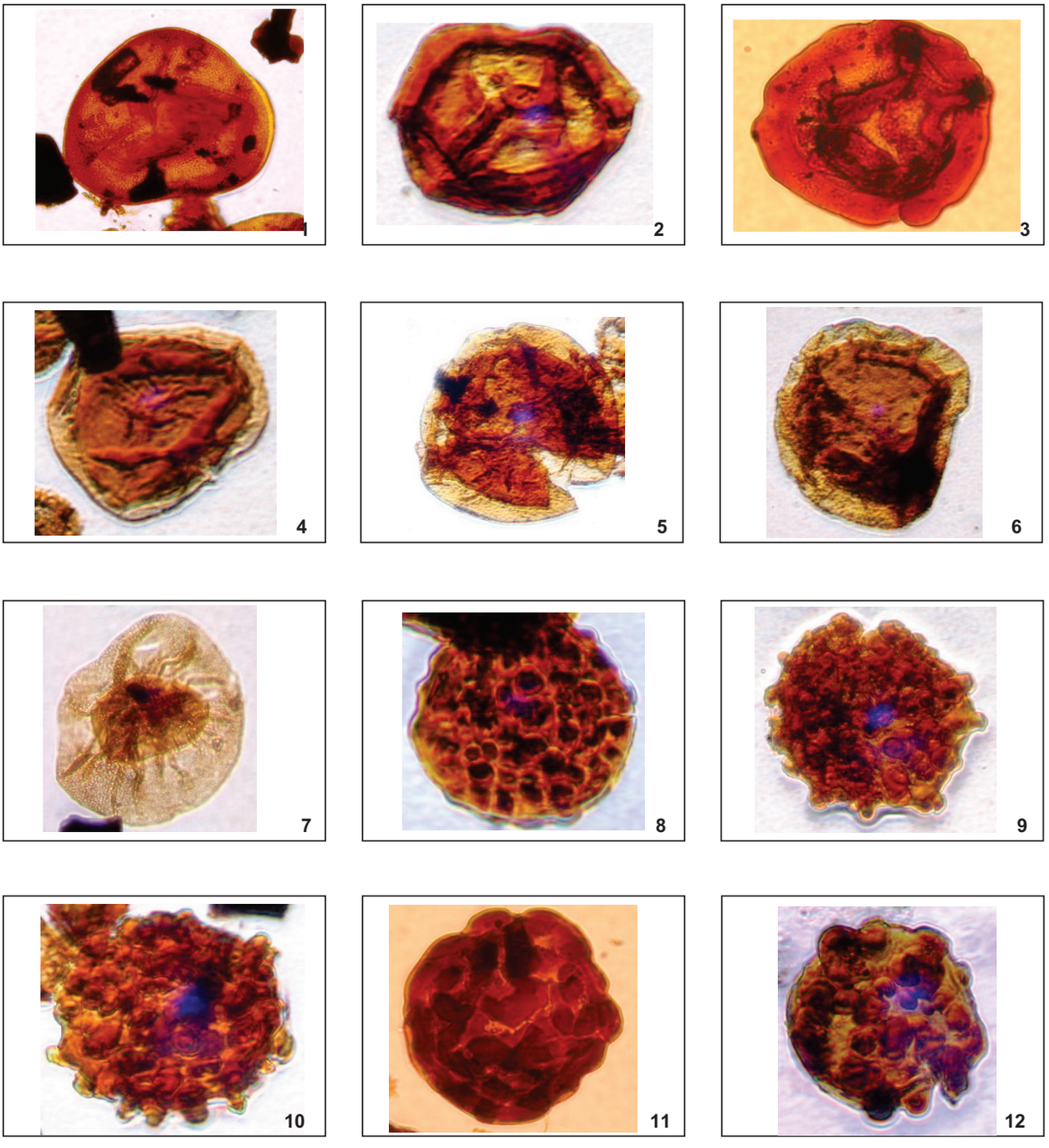


PLATE IV

The species name is followed by the sample number and depth.
All figures are X800 unless otherwise indicated

Plate IV - 1	Retusotriletes sp, S20/1470 ft
Plate IV - 2	Knoxisporites litratus, S22/1410 ft
Plate IV - 3	Lophozonotriletes rarituberculatus, S27/1690 ft
Plate IV - 4	Aurospora asperella, S18/1300 ft
Plate IV - 5	Aurospora sp, S8/820 ft
Plate IV - 6	Aurospora sp, S24/1530 ft
Plate IV - 7	Aurospora solisortus, S3/510 ft
Plate IV - 8	Verrucosisporites nitidus, S20/1470 ft
Plate IV - 9	Pustulatisporites gibberosus, S27/1690 ft
Plate IV - 10	Pustulatisporites gibberosus, S12/940 ft
Plate IV - 11	Convolutispora vermiformis, S15/1110 ft
Plate IV - 12	Verrucosisporites cf premnus, S31/1910 ft

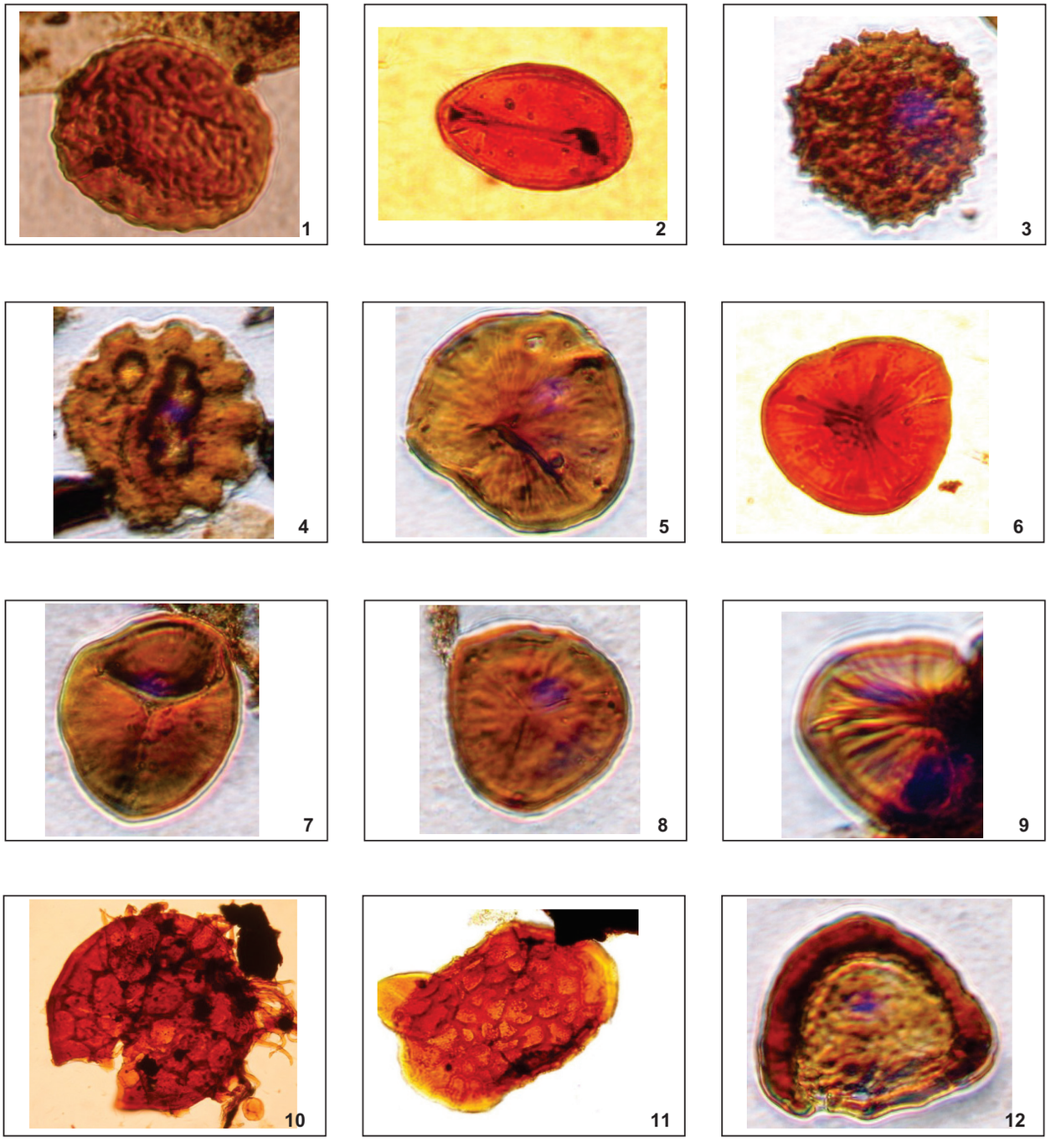


PLATE V

The species name is followed by the sample number and depth.
All figures are X800 unless otherwise indicated

Plate V - 1 Rugospora sp, S27/1690 ft, X1000
Plate V - 2 Monoletes spore, S20/1470 ft, X1000
Plate V - 3 Cristatisporites sp, S20/1470 ft
Plate V - 4 Marnhites brasiliensis, S28/1750 ft
Plate V - 5 Emphanisporites sp, S30/1850 ft
Plate V - 6 Emphanisporites rotatus, S33/2030 ft
Plate V - 7 Emphanisporiteso abscurus, S34/2090 ft, X1000
Plate V - 8 Emphanisporites cf annulatus, S30/1850 ft
Plate V - 9 Emphanisporites sp, S30/1850 ft, X1000
Plate V - 10 Courbolispora cancellata, S24/1530
Plate V - 11 Dictyotiletes trivialis, S33/2030 ft
Plate V - 12 Archeozonotriletes sp, S30/1850 ft

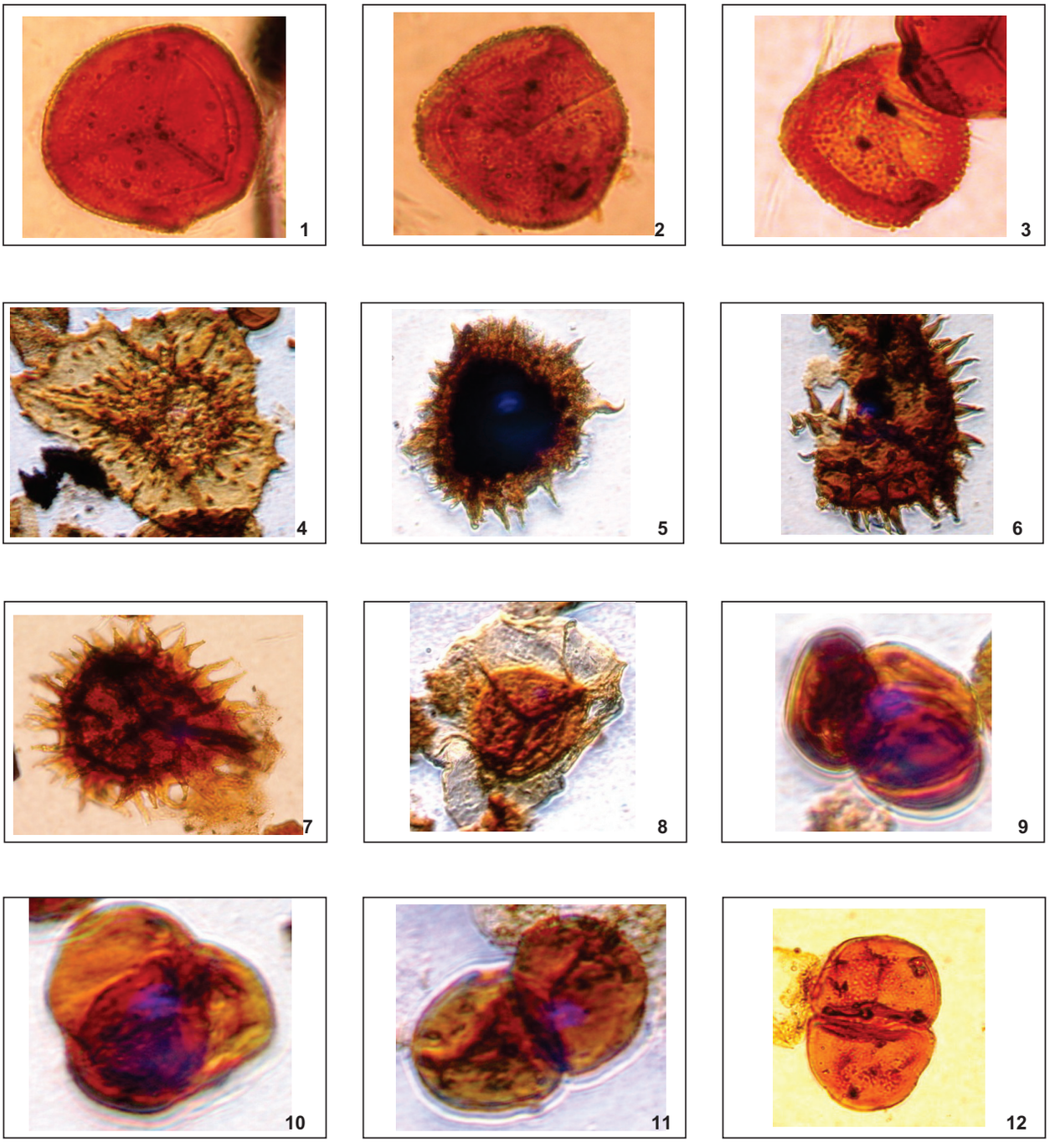


PLATE VI

The species name is followed by the sample number and depth.
All figures are X800 unless otherwise indicated

Plate VI - 1	Geminospora lemurata, S31/1910 ft, X900
Plate VI - 2	Geminospora lemurata, S31/1910 ft, X900
Plate VI - 3	Cymbosporites cyathus, S33/2030 ft
Plate VI - 4	Grandispora libyensis, S28/1750 ft
Plate VI - 5	Grandispora naumovae, S30/1850 ft
Plate VI - 6	Acanthotriletes horids, S28/1750 ft
Plate VI - 7	Ancyrosporites cf langii, S29/1790 ft
Plate VI - 8	Camptozonotiletes caperatus. S32/1970 ft
Plate VI - 9	Tetrahedraletes medinensis, S33/2030 ft
Plate VI - 10	Tetrahedraletes medinensis, S33/2030 ft
Plate VI - 11	Dyad spore, S33/2030 ft, X1000
Plate VI - 12	Dyad spore, S33/2030 ft, X900

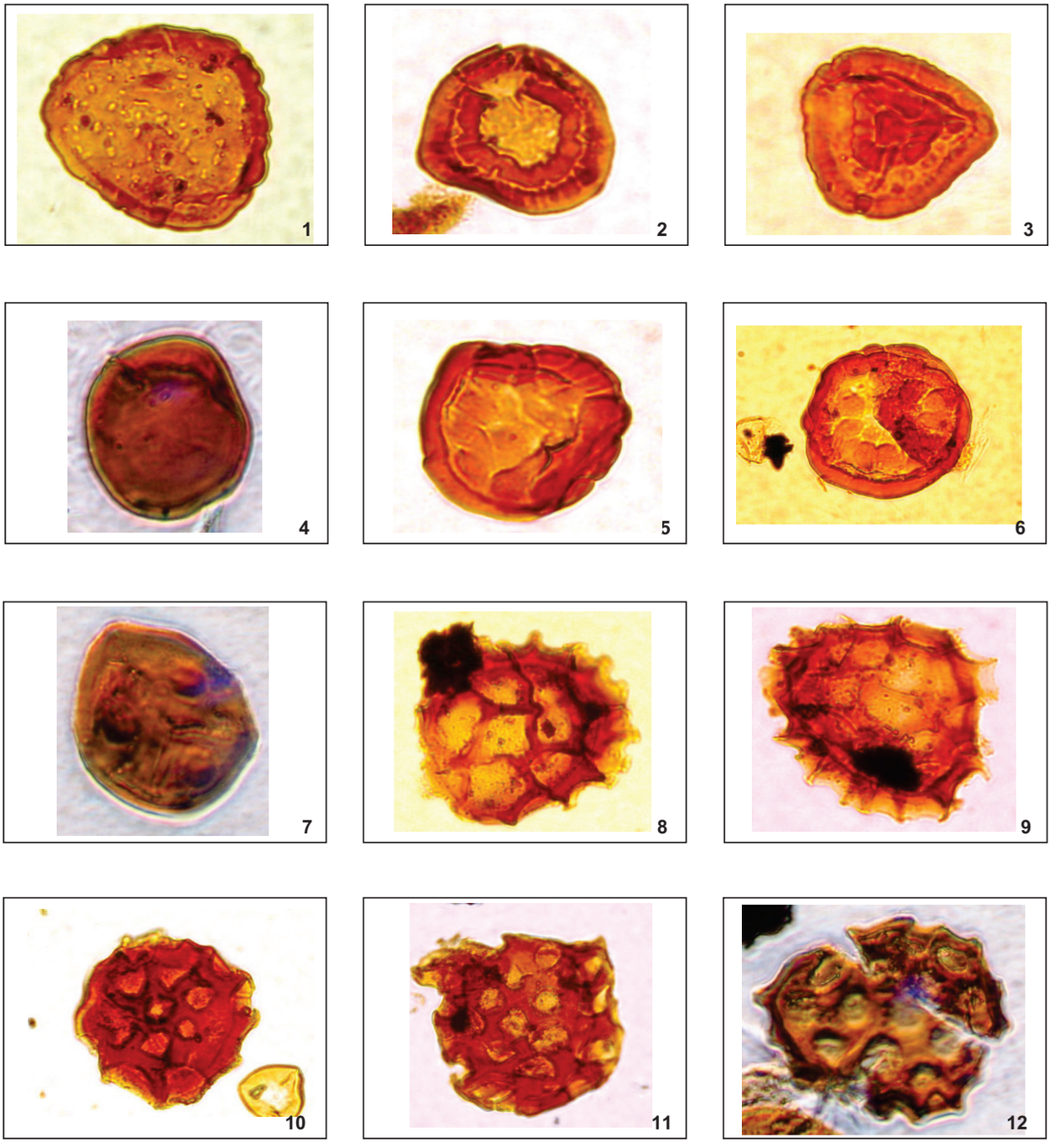
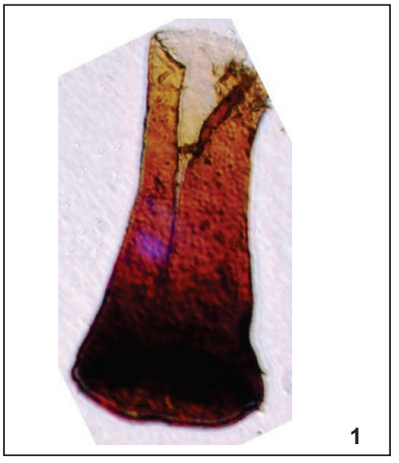
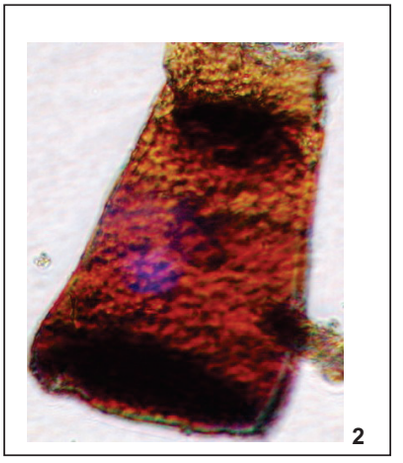


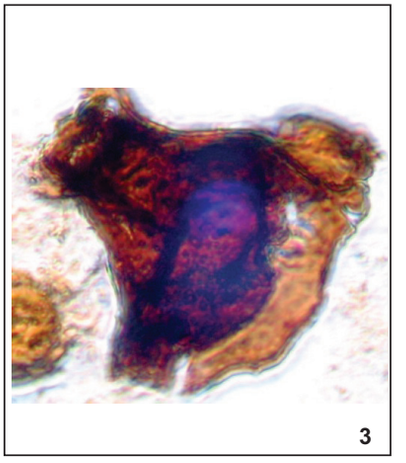
PLATE VII

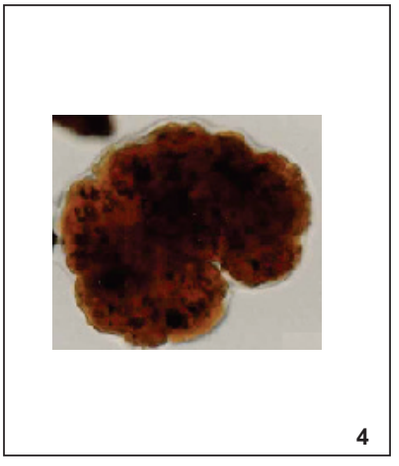
The species name is followed by the sample number and depth.
All figures are X1000 unless otherwise indicated

Plate VII - 1	Brochotriletes foveolatus, S33/2030 ft
Plate VII - 2	Synorisporites libycus, S33/2030 ft
Plate VII - 3	Synorisorites libycus, S34/2090 ft
Plate VII - 4	Archeozonotriletes sp, S33/2090 ft
Plate VII - 5	Archeozonotriletes cf chulus, S33/2030 ft
Plate VII - 6	Archeozonotriletes cf chulus, S33/2030 ft
Plate VII - 7	Synorisporites tripapillatus, S33/2030 ft
Plate VII - 8	Dictyotiletes emsiansis, S34/2090 ft, X800
Plate VII - 9	Dictyotiletes emsiansis, S33/2030 ft, X800
Plate VII - 10	Brochotriletes sp, S34/2090 ft, X800
Plate VII - 11	Brochotriletes sp, S33/2030 ft, X800
Plate VII - 12	Brochotriletes sp, S33/2030 ft, X800

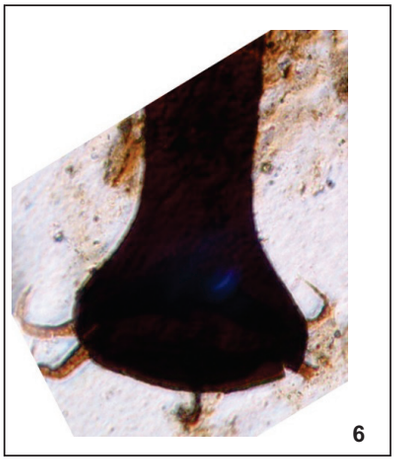


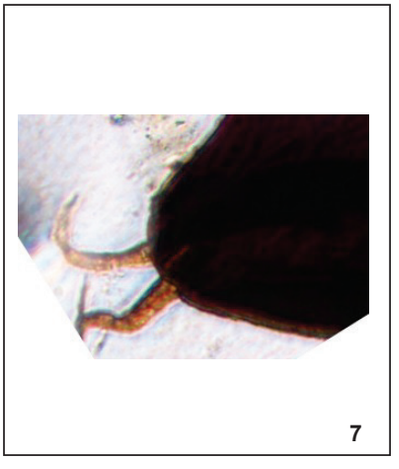












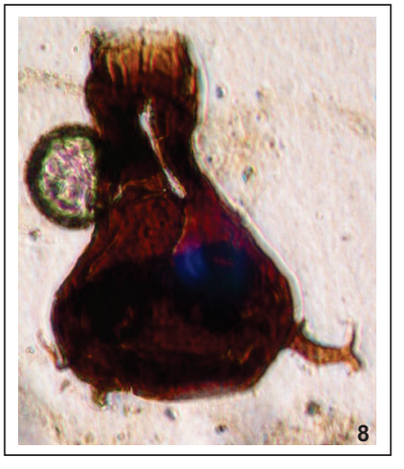
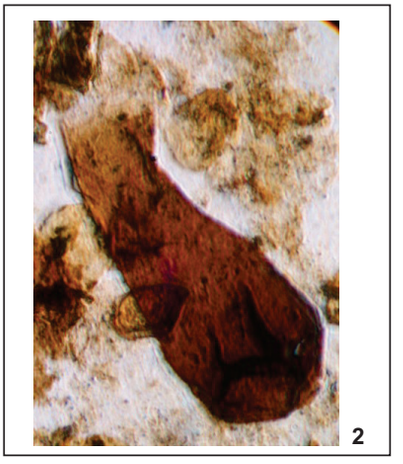


PLATE VIII

The species name is followed by the sample number and depth.
All figures are X400 unless otherwise indicated

Plate VIII - 1 Conochitina sp, S46D/2650 ft
Plate VIII - 2 Conochitina sp, S46D/2650 ft
Plate VIII - 3 Cyathochitina kuckersiana, S45C/2640 ft
Plate VIII - 4 Botryococus sp, S11/920, X800
Plate VIII - 5 Ancyrochitina ancyrea, S46C/2640 ft
Plate VIII - 6 Ancyrochitina ancyrea, S46C/2640 ft
Plate VIII - 7 Ancyrochitina ancyrea, S46C/2640 ft
Plate VIII - 8 Ancyrochitina ancyrea, S46C/2640 ft

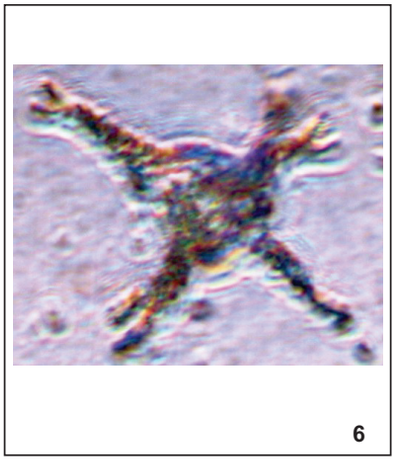

1


2


3


4


5


6

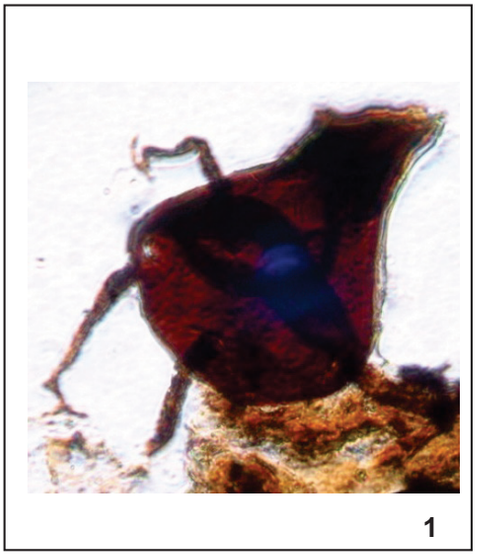

7


8

PLATE IX

The species name is followed by the sample number and depth.
All figures are X800 unless otherwise indicated

Plate IX - 1	Angochitina sp, S46C/2690 ft, X400
Plate IX - 2	Angochitina sp, S46C/2690 ft, X400
Plate IX - 3	Leiofusa bernesga, S46C/2690 ft
Plate IX - 4	Veryhachium cf oklahomenses, S45C/2640 ft
Plate IX - 5	Hoegklintia cylindrica, S46C/2690 ft
Plate IX - 6	Diexallophasis remota, S45D/2650 ft
Plate IX - 7	Helosphaeridium malvernensis, S46C/2690 ft
Plate IX - 8	Helosphaeridium malvernensis, S46C/2690 ft





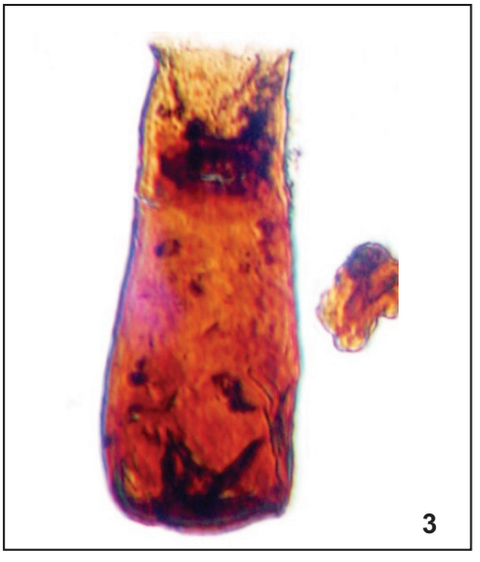




PLATE X

The species name is followed by the sample number and depth.
All figures are X400 unless otherwise indicated

Plate X - 1	Ancyrochitina ancyrea, S46C/2690 ft
Plate X - 2	Ancyrochitina ancyrea, S46C/2690 ft
Plate X - 3	Angochitina sp, S45D/2690 ft
Plate X - 4	Conochitina sp, S46D/2690 ft

REFERENCES

Bellini, E. and Massa, D. (1980). Stratigraphic Contribution to the PalaeozoicSouthern Basins of Libya. In: *The Geology of Libya* (Ed. by: M. J. Salem and M. T. Busrewil). Academic Press, London, 1: 3-56.

Burolllet, P. F. (1960). Lexigue Stratigraphique International Afrique. *Fasc. IVa, Libye. Centre. Nat. de la Rech. Sci.*, Paris: 1-62.

Clayton, G. (1995). Carboniferous Miospore and Pollen Assemblages from the Kingdom Saudi Arabia. *Review of Paleopotany and Palynology*, 89: 115-123.

Clayton, G. & Loboziak, S. (1985). Early Carboniferous (Early Visean-Serpukhovian) Palynomorphs. In: *The palyno-stratigraphy of north-east Libya* (ed. by: B. Thusu and B. Owens). *Journal of Micropalaeontology,* 4(1): *83-91, 4pl*.

El-Harbi, A. (2000). Lower Carboniferous Miospores from Surface Samples of the Mrar Formation, Ghadamis Basin, NW Libya.(abstract). *Second Symposium on the Sedimentary Basins of Libya, Geology of Northwest Libya*. Book of abstracts: p. 35.

Grignani, D., Lanzoni, E. & Elatrash. (1991). Palaeozoic and Mesozoic Subsurface Palynostratigraphy in the Al-Kufra Basin, Libya. In: *The Geology of Libya* (ed. by**:** M. J. Salem, O. S. Hammuda & B. A. Eliagoubi), Elsevier, IV: 1159-1227.

Hill, P. J., Paris, F. and Richardson, J. B. (1985). Silurian Palynomorphs. In: *The palyno-stratigraphy of north-east Libya* (ed. By: B. Thusu and B. Owens). *Journal of Micropalaeontology*, 4(1): 27-48.

Klitzsch, E. (1981). Lowere Paleozoic Rocks of Libya, Egypt and Sudan. In: L. *Paleozoic of Middle East, Eastern and Southern Africa and Antarctica* (Ed. by: C. H. Holand): 132-163.

Loboziak, S. and Clayton, G. (1988). The Carboniferous Palynostratigraphy of Northeast Libya. In: *Subsurface palynostratigraphy of Northeast Libya* (ed. by: A. El-Arnauti, B. Owens and B. Thusu), University of Garyounis Publications, Benghazi, Libya: 129-145.

McGregor, D.C. (1979). Devonian Miospores of North America. *Palynology*, 3: 31-52.

Streel, M., Higgs, K., Loboziak, S., Riegel, W. and Steemans, Ph. (1987). Spore Stratigraphy and Correlation with Funas and Floras in the Type Marine Devonian of Ardene-Rhenish Regions. *Review of Paleopotany and Palynology*, 50: 211-229.

Streel, M., Paris, F., Riegel, W. and Vanguestaine, M. (1988). Acritarch, Chitinozoan and Spore Stratigraphyfrom the Middle and Late Devonian of Northeast Libya. In: *Subsurface palynostratigraphy of northeast Libya*.(ed. by: A. El-Arnauti, B. Owens and B. Thusu). Research Center, Garyounis University. Benghazi: 111-128.

Magnetic Data for Delineating Subsurface Structures and Estimating Magnetic Sources Depth of Magnetic Intrusive in Farigh Area, Sirt Basin

Ahmed.S.Saheel *, Abdul Rahim Bin Samsudin ** and Umar Bin Hamzah **

Abstract: The studied area is characterized by having complex structures that trend mainly in the NW–SE, and E–W directions. Magnetic data is used to delineate the subsurface structures and to estimate the magnetic sources depth of the selected area in Farigh area, Sirt basin Libya. Power spectrum analysis, Horizontal gradient technique, Analytic Signal and 3D Euler deconvolution technique using standard deviation filters have been applied in order to achieve the above mentioned goals. Interpretation of the onshore magnetic anomaly of this area, suggests that the high total magnetization may be caused by an intrusive body. Analysis of the magnetic power spectra indicates the presence of four sub-anomalies at depths of 350 m, 1400 m, and 2525 m which probably related to the igneous rocks. The presence of igneous rock as basement at depth of 4740 m was confirmed by drilling J1-12. Assuming that all rock magnetization in the area is caused by induction in the present geomagnetic field, it strongly suggests that the causative structure has a remnant magnetization of declination D= 2.322^{o} and inclination (*I)* = 41.579^{o}. Based on magnetic data, the total Horizontal derivative map shows high gradient values in E-W trends related to the structures in the eastern part of the Sirte basin. An analytic signal method was applied to the aeromagnetic data to estimate locations and the minimum depths to the contact. The depth values for profiles 1,2,3,4,5 respectively 1400m,1430m, 2744m,2190m and 1415m. The depth from well J1-12 is 1400m matched to the depth results from profile 5 (1415m). The 3D Euler deconvolution map derived from magnetic data clearly indicates the location of igneous body in the study area as well as its tectonic trends and depth, which is estimated at 350 m to 1400 m below the surface. Depth of magnetic anomalies at 1400 m to 2525 m is considered as anomalies in between shallow and deep. Anomaly at depth of approximately 4740 m below the surface is interpreted as basement rock. Geologically, the magnetic survey shows that the source of anomaly is a mafic igneous rock of Early Cretaceous in age. The study also discovered a left-lateral sheared fault zone along the NW-SE of Hercynian in age which was believed to be reactivated during Early Cretaceous.

Keywords: Magnetic data, Igneous bodies, Power spectrum analysis, Horizontal gradient technique, Analytic Signal and 3D Euler deconvolution.

INTRODUCTION

The study area which is about 114 km^2 is located in the southern part of Concession 12 of Veba Oil field (Fig. 1). This report presents the results of processing and analysis of aeromagnetic field data over the southern part of the Farigh Low. The aeromagnetic survey data was acquired between February and May 2006 by Worley Parsons GPX Pty. Ltd. The survey area was between 21^{o} 05 ˙and 21^{0} 20’ East, and between 28^{0} 42’ and 28^{0} 57’ North. The survey had a traverse spacing of 500m (azimuth, 45º & 225^{o}) and a tie line spacing of 2.5km (azimuth, 135º & 315^{o}). The nominal terrain clearance of the survey aircraft was 137m. The magnetic data was supplied by the acquisition contractor in UTM zone 34N (Hayford1924) coordinates. This was the coordinate system used for all interpretation. The final High Resolution Aero Magnetic (HRAM) data was supplied in grids of 300x300m. The inclination and declination of the centre of the survey area were 41.579^{o} and 2.322^{o} respectively.

The principal aim of this study was to determine the depth and extent of the extrusive volcanic rocks within or overlying the Nubian Sandstone.

*Libyan Petroleum Institute-Tripoli-Libya, P.O.Box 6431
**School of Environment and Natural Resource Sciences, Faculty of Science and Technology, Universiti Kebangsaan Malaysia, 43600 Bangi, Selangor

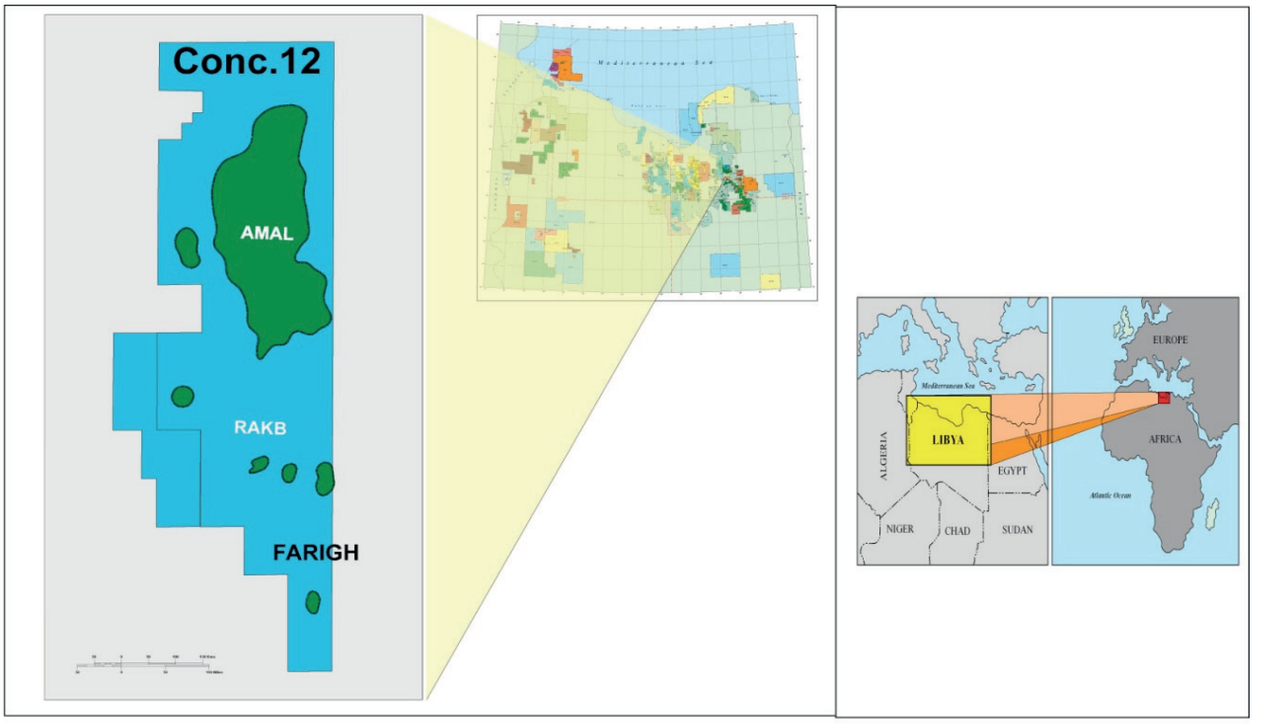


Fig. 1. Location map of the concession 12 in the Sirt basin.

Depth of the volcanic rocks was determined by using the Power spectrum analysis, Horizontal gradient technique, Analytic Signal and 3D Euler deconvolution techniques applied on magnetic data. The Horizontal gradient technique was used to locate boundaries of magnetic data. The final results revealed new information on dominant trends of the lineaments, nature of the intrusive igneous bodies, structural features, and the age of volcanic activity.

GEOLOGICAL SETTING

Farigh is located near the southern boundary of Concession 12 in the eastern part of Sirt Basin. The shallow to intermediate (2 to 3 km depth) sedimentary succession of the Sirt Basin was studied through hundreds of wells data and was divided into three major sequences (Fig. 2). In the central part of the Basin, the succession consists of a pre-rift (pre-Upper Cretaceous) sequence directly overlying the Precambrian basement, and overlain by the syn-rift (Upper Cretaceous-Upper Eocene) and the post-rift (Oligo-Miocene) sequences (Ahlbrandt, 2001). These two sequences were marine in origin and were subdivided into various rock units, but the stratigraphic order and sedimentary characteristics of the post-rift sequence and early pre-rift sequence in the deeper parts of the Basin were poorly

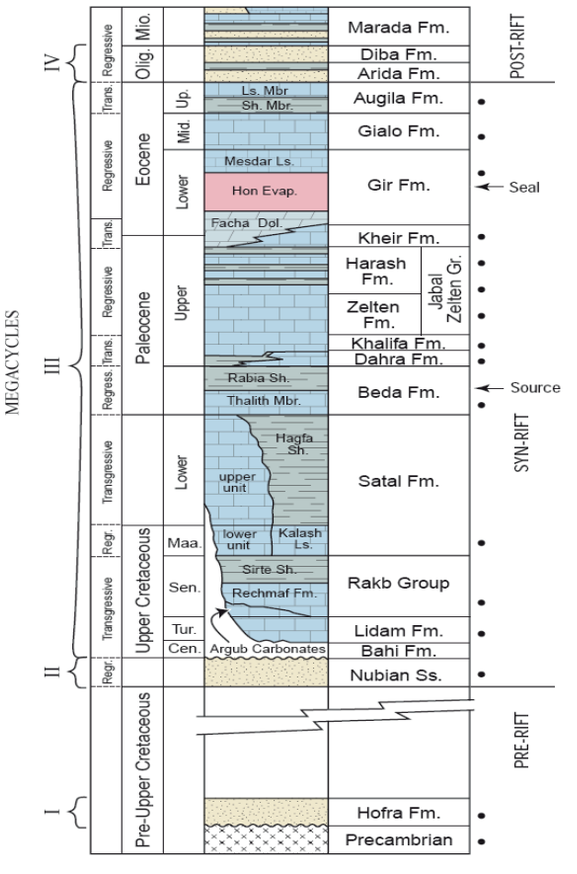


Fig. 2. Stratigraphy section of the Sirt Basin.

understood. The pre-rift (and early-rift) sequence consist of various types of continental siliciclastics deposits with some shallow marine intercalations, as well as volcanics or intrusives, ranging from Lower Paleozoic (in the case of the Gargaf Group) to Late Jurassic- Early Cretaceous (for the Nubian Sandstone and its correlatives). In the eastern part of the Sirt Basin, another sequence of siliciclastics (the Amal Group) was distinguished and entirely assigned as Triassic (Gras and Thusu, 1998). The Nubian Sandstone is best known in Egypt and Sudan, where extensive outcrops were found exposed (Klitzsch and Squyres, 1990). In the eastern part of Sirt Basin (the Sarir Arm), the Nubian was considered to be of late Jurassic to early Cretaceous in age (El-Hawat *et al* 1996) and correlated with the Sarir Sandstone (Gras and Thusu, 1998). In the Farigh area, the Nubian has been penetrated by several wells, having a maximum thickness of 2111 feet (635m), but it has not been drilled through completely. The sequence was divided into five lithological units, often with gradational contacts. All of the units did not occur in the same well. Unit 1, the youngest and often eroded and Unit 4 (131-138m) thick as drilled through at three sites contain intervals of hematitic siltstone or claystone, while all of the units contained one or more layers of pink to brown sandstones and/or white quartzite (Tawadros *et al* 2001). These lithological characteristics are reminiscent of the Triassic "Red Beds", and may have a relatively high magnetic susceptibility compared with typical sandstone due to a high iron oxide content. This may complicate the task of isolating the magnetic signature of intrusives or volcanics within the Nubian, particularly if they have limited lateral continuity, or occur close to the crystalline basement.

***Structure of the Farigh area*:** The major tectonic trends of the Arch were also believed to have controlled the post-Hercynian structure of the Sirt Basin. The Sirt Basin is widely consider to be a failed, tripartite, intra-plate rift (Ahlbrandt, 2001) that started to develop in the Triassic, undergoing multiple-phased rifting, which culminated in the late Cretaceous, followed by post-rift subsidence that ceased in Oligocene. However, in the deepest, northern parts of the Basin, such as the coastal parts of the Ajdabiya Trough, subsidence continues and the thickness of the post-Hercynian sediments may reach up to 8 km (Hallet, 2002). In general, compressional structures are rare, but diastrophic events (uplift, subsidence, tilting, faulting and intrusions) are prevalent (Goudarzi, 1980). The first phase of rifting was considered to have began in the eastern (Sarir) arm of the basin (Hameimat Trough area), culminating in the Neocomian-Barremian with a predominantly E-W orientation. The second phase of mainly NW-SE oriented rifting started within the central part of the Basin in the late Aptian (Fig. 3), migrating towards the north-northwest (Guiraud and Bosworth, 1997). Rifting was accompanied by volcanic activities (van der Meer and Cloetingh, 1993) and followed by thermal subsidence, which was shortly interrupted by inversion in the Santonian, at the peak of the Alpine orogeny (Guiraud and Bosworth, 1997). The Farigh Low is bounded to the north by large listric normal faults, which delineate the boundary between the Farigh Low and the Rakb High, and indicate the opening of the Farigh Low during Early Cretaceous time. The east-west trend of the bounding fault may be indicative of a possible earlier Hercynian faulting stage during Upper Paleozoic time.

***Hydrocarbon history in the study area*:** Drilling for oil exploration began in 1959 and after an initial dry hole, oil was discovered in basal quartzitic sandstones on the northern part of the concession 12 (Roberts 1970, see Fig. 4). The A1-12 well was drilled to a depth of 10,146 feet in the central area of the concession and penetrated a Tertiary-Cretaceous section, overlying a granitic basement with oil shows. The B1-12 well was drilled 34 km north of the first well and encountered a similar uphole section, but penetrated 600 feet of oil bearing quartzitic sandstone without reaching basement granite. Approximately 160 oil wells were drilled in the Amal B, E and N pools and the Amal Field has produced 992 million barrels of oil (February 2005) from the Amal and Maragh sandstones. The Rakb High, identified by the A1-12 well covers the central portion of the concession. The basal sandstones were neither deposited nor removed by erosion. However, reserves have been established on the Rakb High in shallower Eocene reservoirs. For the South of the Rakb High, early drilling established that the Gialo High extended onto southern part of Concession 12 and that a prospective basal sandstone trend was present between the Gialo and Rakb Highs. The Farigh Field was discovered in 1969 when the A1-12 well penetrated a thick oil column in the Nubian sandstone. The field was initially mapped as an isolated structural closure, north of the Gialo High,

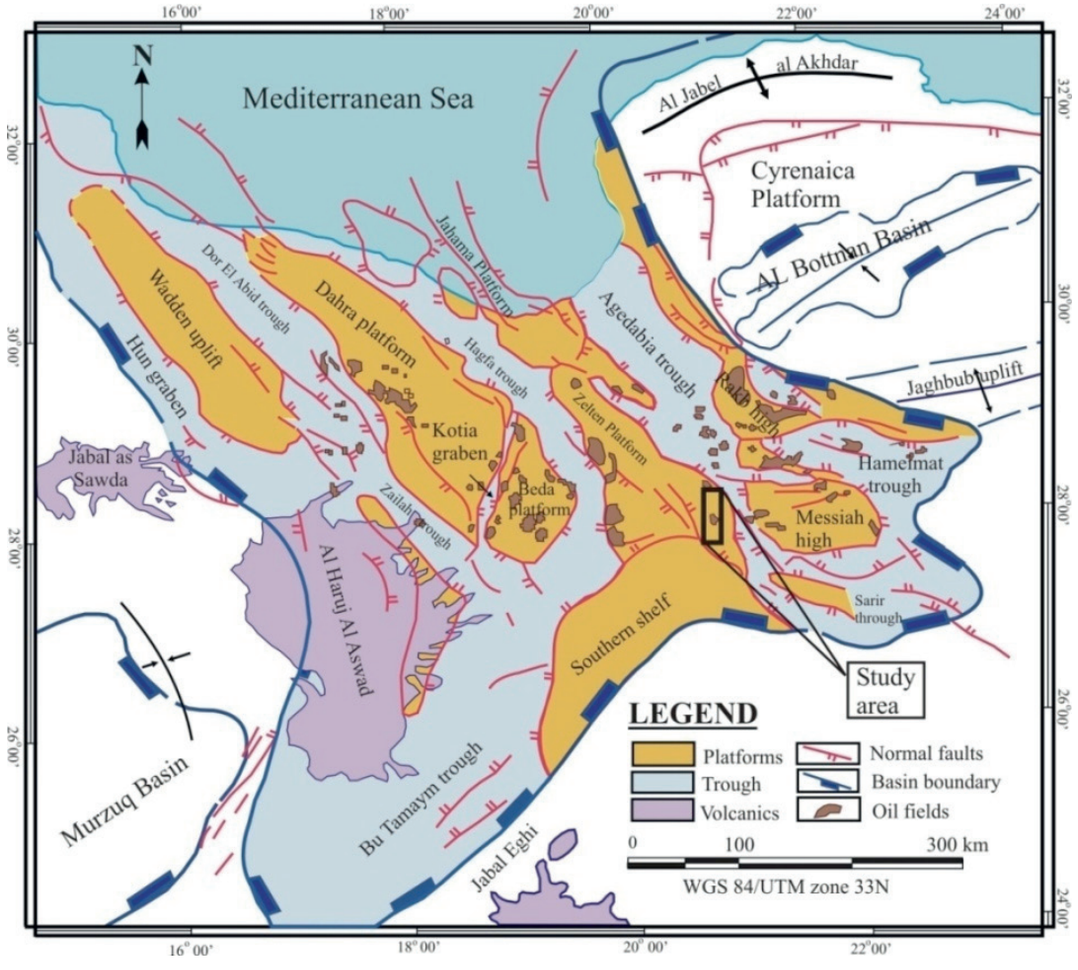


Fig. 3. Tectonic element in the Sirt Basin, (Modified after Abadi, 2002).

and extensive 2-D seismic was shot to evaluate the Concession 12 area south of the Rakb High. The most recent documented geological analysis of the Farigh area (Robertson 1970) concluded that excellent hydrocarbon potential existed in the Farigh U Lead, immediately south of the Farigh Field, and in the Farigh V Lead, 7 km north of the Farigh Field.

GEOPHYSICAL DATA

***Total Magnetic Intensity (TMI)*:** The total magnetic intensity map (TMI) of the Farigh area was calculated in an attempt to delineate its subsurface structure (Fig. 5). Majority of the Farigh area is characterized by positive magnetic anomalies. This area was clearly represented as a minimum magnetic closure (42029 to 42073 nT), and the dominant trend within the study area was NW-SE. The minimum values occurring in the north and west of the area (42030 to 42080 nT) indicate thick sediment. The high positive magnetic anomalies reflected in the eastern and southern part (42088-42161 nT) indicated the presence of highly magnetic material. This can be interpreted as an anticline structure defining the existence of outcrops of Oligocene-Miocene rocks (the oldest unit in the area) on the surface. The magnetic data showed the presence of intrusive igneous bodies in the southern part of the study area trending E-W in direction.

The magnetic data were processed and transformed into Power spectrum, Total horizontal gradient, analytic Signal and 3D Euler deconvolution (Figs. 6, 7, 8, & 9). These data contained many high frequency anomalies originated from cultural sources such as power lines, pipelines and oil wells. The Geosoft software was used to transform the Poisson equation relating the gravity and magnetic field potentials expressed by $U = -(J/G\rho)\ (\partial V/\partial I)$, where U, V, I, J, ρ and G were, respectively, magnetic potential, gravitational potential, direction of magnetization, magnetization intensity, density and Gravitational constant (Geosoft, 2009).

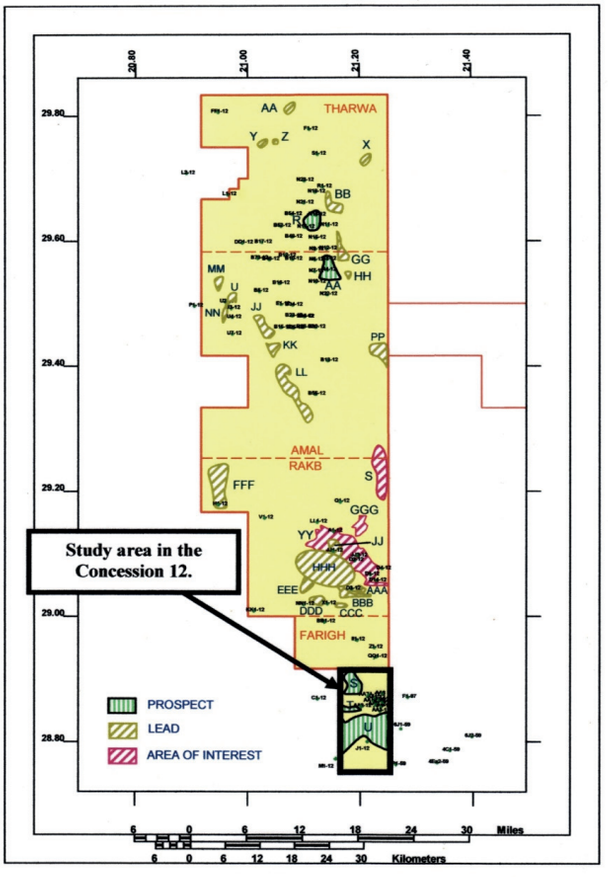


Fig. 4. Location map showing the hydrocarbon potential areas

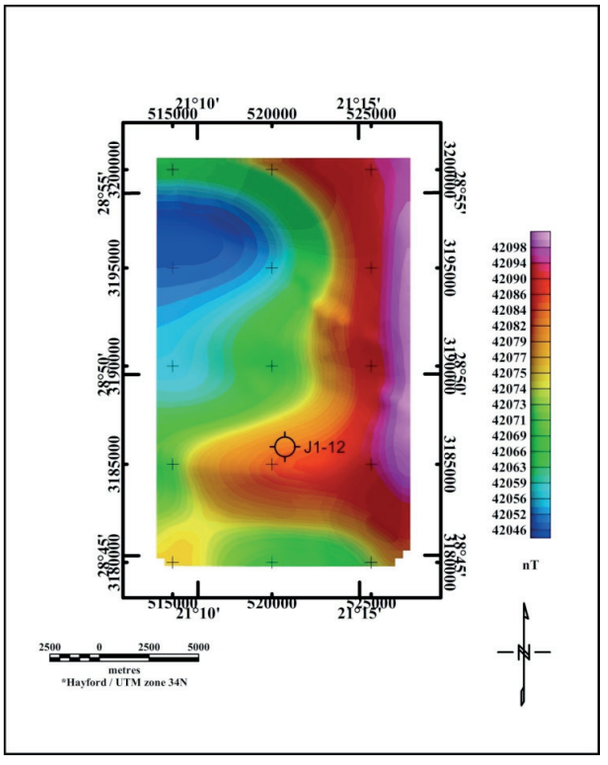


Fig. 5. Total Magnetic Intensity (TMI) map of Farigh area, using grid cell size 400m.

***Power spectrum analysis*:** The power spectrum of the reduced to the pole magnetic grid, which represented the magnitude of various frequency components of a 2D image, was computed by Fourier transform and seems in agreement with the location of the main source at the origin of the anomaly (Geosoft, 2009). The spectrum shows 4 very clear anomalies at depths below aircraft of 350m, 1400m, 2525m and 4740m. The shallowest slice (Fig. 6) at depth 350m appeared to correspond very strongly to surface features A interpreted as pipeline and wells. This data were derived from flying height of 400m above the ground. The deepest slice (Fig. 6) at depth of 4740m produced anomaly which corresponded to basement rock. The intermediate depths in the power spectrum may represent the volcanic rocks (1400m and 2525m) in Fig. 6.

***Total Horizontal gradient technique*:** Through the use of the Geosoft software, the total horizontal gradient method was applied to locate density boundaries of gravity data or susceptibility boundaries of magnetic (as Pseudogravity) data (Ma *et a*l 2006; Bilim, 2007; Pilkington, 2007). Generally, the horizontal gradient of magnetic anomaly which corresponded to a tabular body tends to overlie the edges of the body if the edges were vertical and isolated from each other (Cordell, 1979; Cordell and Grauch, 1985). These authors discussed a technique to estimate the location of abrupt lateral changes in magnetization or mass density of upper crest rocks. The main advantage of the horizontal gradient method was that it was least susceptible to noise in the data, because it only required the calculations of the two first-order horizontal derivatives of the field (Phillips, 1998). This method was also robust in delineating both shallow and deep sources, in comparison with the vertical gradient method, which was useful only in identifying shallower structures. The amplitude of the horizontal gradient (Cordell and Grauch, 1985) is expressed as:

$$HG_g = \sqrt{\left(\frac{\partial g}{\partial x}\right)^2 + \left(\frac{\partial g}{\partial y}\right)^2}$$

Where ($\partial g/\partial x$) and ($\partial g/\partial y$) are the horizontal derivatives of the magnetic data. This method is normally applied to grid data rather than profiles. Maximum magnitudes of horizontal magnetic gradient anomaly occur above geological

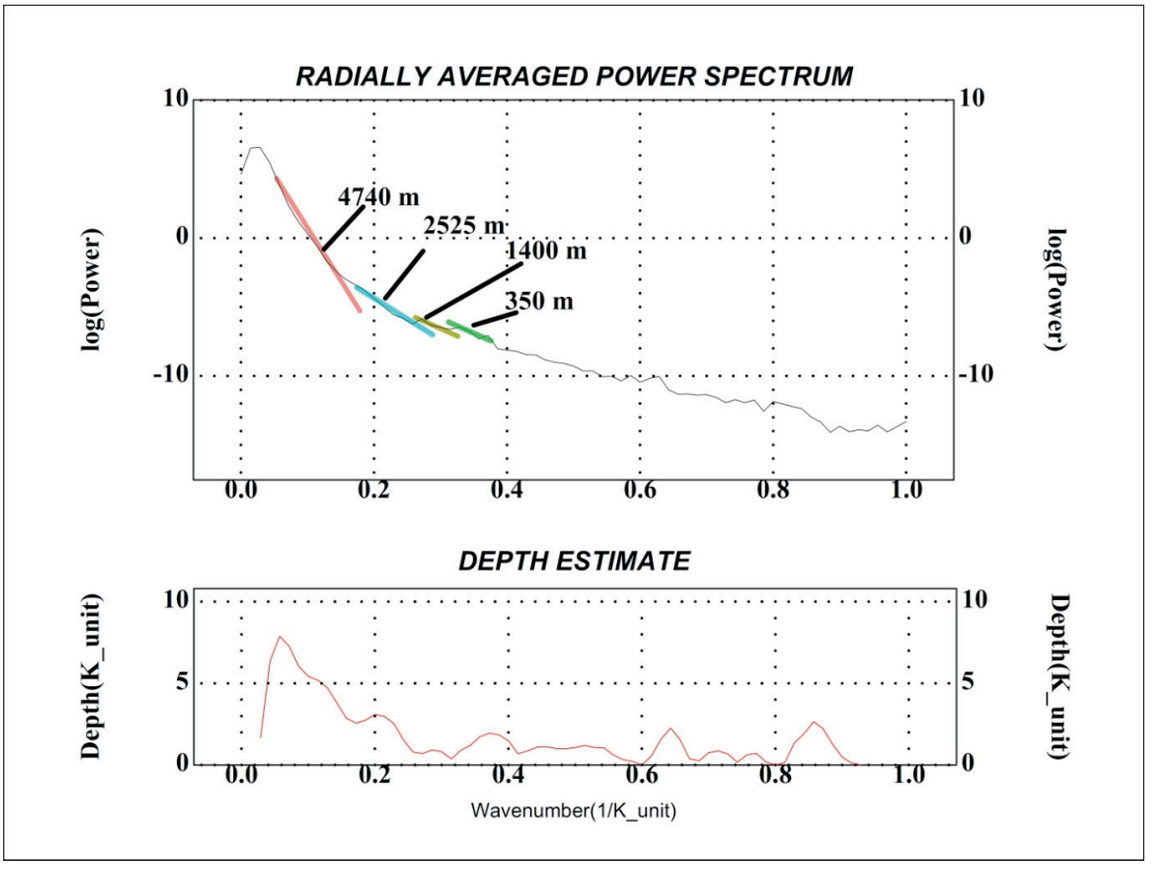


Fig. 6 Power spectrum result of study area.

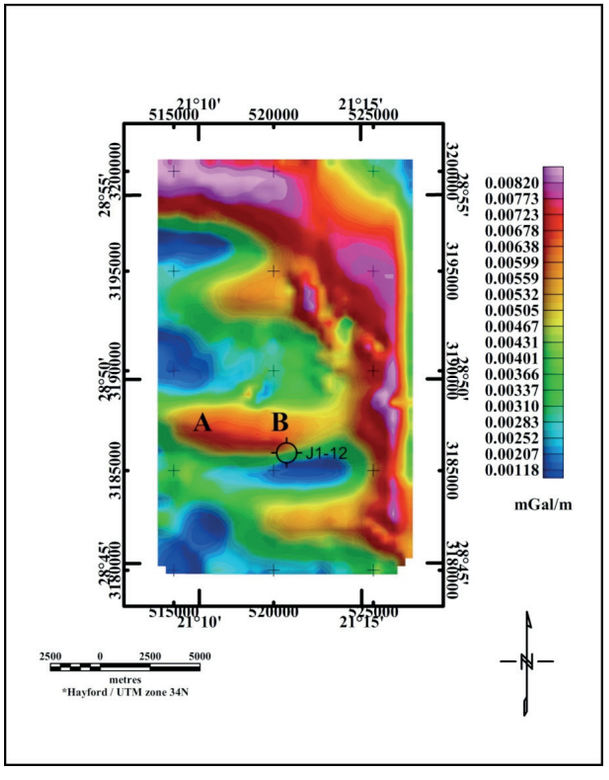


Fig. 7 Total horizontal derivative of total magnetic intensity (TMI) in the study area. The high gradient areas indicated by A and B.

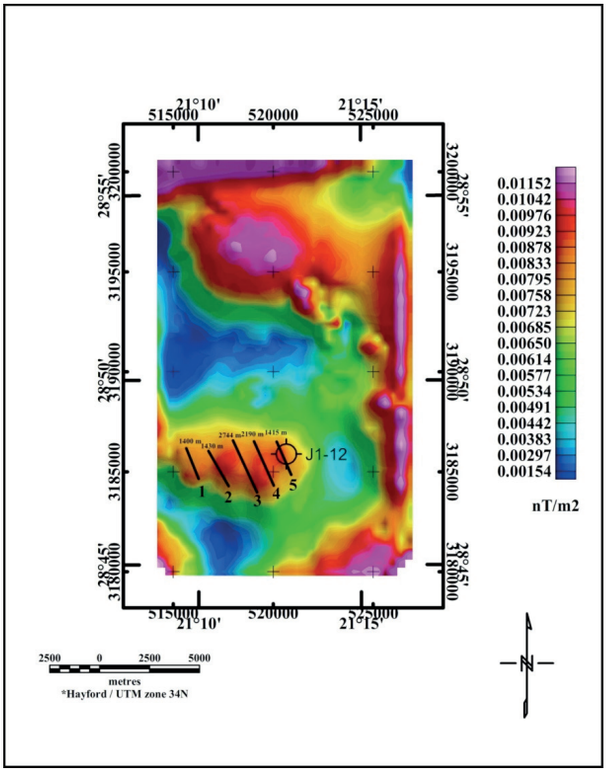


Fig. 8. Analytic signal of magnetic data of Farigh area. Lines 1–5 are the selected profiles that were used to estimate the depths from the analytic signal.

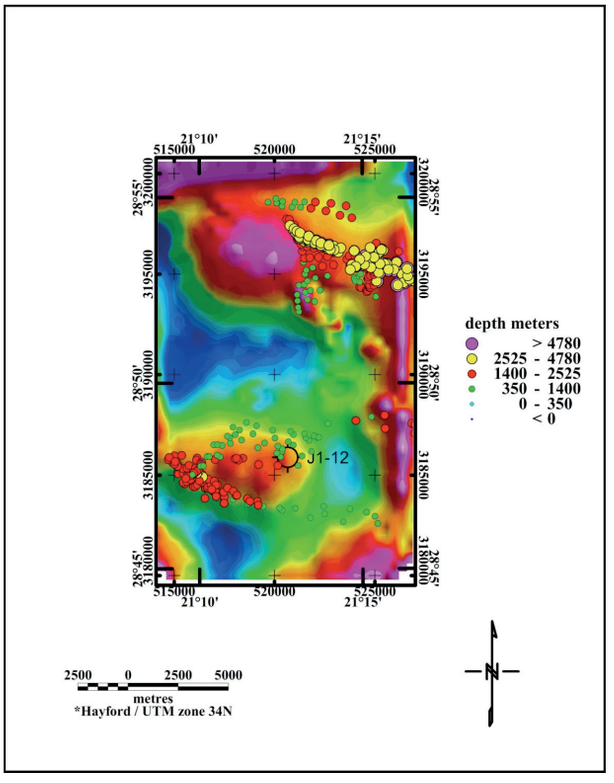


Fig. 9 3D Euler deconvolution for magnetic intensity anomaly over Farigh area. Circles indicate the depths of anomalies representing faults patterns, throws and their depths in the geological formations.

boundaries such as faults or steeply dipping lithological boundaries. Areas of steep lateral gradient have higher scalar amplitude values of horizontal magnetic gradient (Blaky and Simpson, 1986). However Fig. 7 shows the horizontal-gradient map of the study area. The magnetic field was transformed into a Pseudogravity field using an I= 41.579° and D= 2.322° . From the Pseudogravity field, the magnitude of horizontal gradient was calculated by using Geosoft software. High gradient values indicated as A and B (Fig. 7) were observed at locations that may be interpreted as the igneous bodies of the study area. The directions of the bodies were estimated in E-W direction.

***Analytic Signal Method*:** The basic concepts of the analytic signal method using 2D magnetic data were extensively discussed by Nabighian (1972, 1974, 1984) and Green and Stanley (1975). Roest *et al* (1992) showed that the amplitude (absolute value) of the 3D analytic signal at location *(x, y)* can be easily derived from the three orthogonal gradients of the total magnetic field. In the analytic signal method, it is assumed that the causative sources are magnetic contacts. The depth was estimated using the width of the analytic signal anomalies between inflection points (MacLeod *et al* 1993). The analytic signal signature of the Farigh area was calculated (Fig. 8) in the frequency domain using the fast Fourier transform technique (Geosoft, 2009). Higher values of the analytic signal are observed mainly in some regions of the study area (Fig. 8), indicating that these regions have significant susceptibility contrasts that produce identifiable signatures on the map. To estimate the depth of the contacts from the analytic signal, we selected five profiles over the regions where contrasts could be found. The depth values for profiles 1, 2, 3, 4, 5 respectively 1400m,1430m, 2744m, 2190m and 1415m. The depth from well J1-12 is 1400m matched to the depth results from profile 5 (1415m).

***Euler deconvolution technique*:** The Euler deconvolution technique is commonly used to estimate depth and location of the magnetic-gravity source anomalies. Euler deconvolution has come into wide use for automatic estimates of field source location and depth (Bournas *et al* 2003; Shepherd *et al* 2006; Chennouf *et al* 2007; Li *et al* 2008). This method was established by Thompson (1982) and has been applied essentially to real magnetic data along profiles. Reid *et al* (1990) followed up a suggestion in Thompson's paper and developed the equivalent method, which operates on gridded magnetic data. The application of Euler deconvolution to magnetic data has been carried out by several authors such as Wilsher (1987), Corner and Wilsher (1989), Klingele *et al* (1991), Marson and Klingele (1993), Fairhead *et al* (1994) and Huang *et al* (1995).

The 3-D equation of Euler deconvolution given by Reid *et al* (1990) is:

$$(x-x_o)\frac{\partial g}{\partial x}+(y-y_o)\frac{\partial g}{\partial y}+(z-z_o)\frac{\partial g}{\partial z}=\eta(\beta-g) \quad (1)$$

Equation (1) can be rewritten as:

$$x\frac{\partial g}{\partial x}+y\frac{\partial g}{\partial y}+z\frac{\partial g}{\partial z}+\mathrm{h}\,g=x_o\frac{\partial g}{\partial x}+y_o\frac{\partial g}{\partial y}+z_o\frac{\partial g}{\partial z}+\mathrm{h}\,\mathrm{b} \quad (2)$$

Where g is the magnetic or gravity anomaly detected at(x,y,z) due to a body located at (x_0,y_0,z_0). b refers to the regional field at (x,y) and h is a constant defined as " structural index" (SI), different for various geological structures. For example, in the magnetic case, SI = 3 for a sphere, SI = 2 for a

horizontal cylinder and pipes, SI = 1 for a sills and dykes, SI = 0.5 for thick step, SI = 0.0 for geological contacts and faults (Reid *et al* (1990, 2003).

Results of the Euler deconvolution of re-gidding magnetic data (400m, high resolution) in the study area (Farigh area) using a moving windows size of 10 (4km x 4km), and an SI=0.5 are shown in Figure 11. The interpretation of Euler solutions indicates that the NW-SE anomalies were truncated by NE-SW trends and characterized the whole structural setting or faults of the Farigh area. The depth of fault contacts ranged from power spectrum applied to Euler depth were 350m, 2525 m, 1400 m and 4740 m respectively. These contacts were interpreted as contacts plotted and statistically analyzed (Fig. 9). The depth levels of 1400m and 2525m (Fig. 9) were chosen to cover structural boundaries in the top of igneous bodies (especially Nubian sandstone) indicated that the depth from borehole penetrated the igneous bodies (J1-12) were matched with the results of Euler deconvolution in the study area.

DISCUSSION AND CONCLUSIONS

Total magnetic derivative results compare very well with the 3D Euler Deconvolution and tectonic elements in the study area. High magnetic gradient values delineate NW-SE and E-W fault trends which mark the faulted eastern and southern part of Sirt basin, respectively. Estimated depth of igneous body in the study area is from analytic signal. The depth values for profiles 1,2,3,4,5 respectively 1400m,1430m, 2744m,2190m and 1415m.The 3D Euler deconvolution applied to the total magnetic intensity data using structural index SI=0.5 and window size W=10 is from 350 m to 1400 m represents solutions in the shallow parts of study area. Depth of 1400 m to 2525 m is critically indicative of intermediate depth. Deeper solution at depth of 4740 m below the surface was interpreted as basement rocks. The depth 1400m from well J1-12 matched to the depth results from power spectrum in the second slop (1400m), however, the depth from analytic signal profile 5 (1415m) matched the depth from J1-12 and finally depth 1400m to 2525m from 3D Euler deconvolution using SI=0.5,W=10 also matched the depth in the J1-12.

ACKNOWLEDGMENTS

We would like to thank the National Oil Corporation of Libya and the Libyan Petroleum Institute for giving the permission to publish the present data. We would also like to thank Dr A.B. Reid for his advice on the use of Euler deconvolution.

REFERENCES

Abadi, A.M. (2002). Tectonics of the Sirt Basin: Inferences from Tectonic Subsidence Analysis, Stress Inversion, and Gravity Modeling. PhD Thesis Vrije Universiteit, Amsterdam, Netherlands.

Ahlbrandt, T. S. (2001). The Sirte Basin Province of Libya: Sirte-Zelten Total Petroleum System. *U.S. Geological Survey Bulletin,* 2202-F (Version 1.0).

Bilim, F. (2007). Investigations into the tectonic lineaments and thermal structure of Kutahya-Denizli region, western Anatolia, from using aeromagnetic, gravity and seismological data. *Physics of the Earth and Planetary Interiors*, 165 (3-4):135-146.

Blakely, R. .J. and Simpson, R. W. (1986). Locating edges of source bodies from magnetic and gravity anomalies. *Geophysics*, 51 (7): 1494-1498.

Bournas, N., Galdeano, A., Hamoudi, M. and Baker, H. (2003). Interpretation of the
aeromagnetic map of Eastern Hoggar (Algeria) using the Euler deconvolution, analytic signal and local wavenumber methods. *Journal of African Earth Sciences*, 37 (3-4): 191-205.

Chennouf, T., Khattach, D., Milhi, A., Andrieux, P. and Keating, P. (2007). Major structural trends in northeastern Morocco: The contribution of gravimetry. *Comptes Rendus–Geoscience*, 339: 383-395.

Cordell, L. (1979). Gravimetric expression of graben faulting in Santa Fe Country and the Espanola Basin, New Mexico, *Guidebook to the 30th Field Conference*, Santa Fe Country, New Mexico Geological Society (Ed), *New Mexico Geological Society, Socorro*: 59-64.

Cordell, L. and Grauch, V. J. S. (1985). Mapping basement magnetization zones from aeromagnetic data in the San Juan Basin, New Mexico. In: W. J. Hinze (Ed). The utility of regional gravity and magnetic anomaly maps: *Society of Exploration Geophysicists*: 181-197.

Corner, B. and Wilsher, W. A. (1989). Structure of the Witwatersrand basin derived from interpretation of the aeromagnetic and gravity data. In: G. D. Garlan, (Ed). Proceedings of exploration ’87, third decennial international conference on geophysical and geochemical exploration for

minerals and groundwater. *Ontario Geological Survey, Special, **3***: 532-546.

El-Hawat, A. S., Missallati, A. A., Bezan, A. M and Taleb, M. T, (1996). The Nubian Sandstone in Sirt Basin and its Correlatives. In: M. J. Salem, A. S. El-Hawat and A. M. Sbeta (Eds), *The Geology of Sirt Basin*. Elsevier, Amsterdam: 3-30.

Fairhead, J. D., Bennet, K. J., Gordon, R. H. and Huang, D. (1994). Euler: Beyond the Black Box. *64th Annual International Meeting, Society of Exploration Geophysicists*, Expanded Abstracts: 422-424.

Geosoft, Reference Manual (2009). Software for Earth Sciences Geosoft INC., Toronto, Canada.

Goudarzi, G. H. (1980). Structure-Libya. In: M. J. Salem and M. T. Buserwil, (eds.). *The Geology of Libya*. ***vol. 3***: 879-892.

Gras, R. and Thusu, B. (1998)**.** Trap architecture of the Early Cretaceous Sarir Sandstone in the eastern Sirt Basin. In: D. S. Macgreor, R.T. J. Moody and D. D. Clark-Lowes (eds), Petroleum Geology of North Africa. *Geological Society, London, Special Publication NO.* 132: 317-334.

Guiraud, R. and Bosworth, W. (1997). Senonian basin inversion and rejuvenation of rifting in

Africa and Arabia: synthesis and implications for plate scales tectonics. *Tectonophysics,* 282: 39-82.

Hallet, D. (2002). Petroleum Geology of Libya. Elsevier, Amsterdam: p487.

Huang, D., Gubbins, D., Clark, R. A. and Whaler, K. A., 1995. Combined study of Euler's homogeneity equation for gravity and magnetic field. *57th Conference and Technical Exhibition EAGE, Glasgow*, Extended Abstracts: p144.

Klitzsch, E. (1971). The structural development of part of North Africa since Cambrian time. In: C. Gray (ed.), *First Symposium on the Geology of Libya*. Faculty of Science, University of Libya, Tripoli: 253-262.

Klitzsch, E. H and Squyres, C. H. (1990). Paleozoic and Mesozoic geological history of Northeastern Africa based upon new interpretation of Nubian Strata. *AAPG Bull.*, 74: 1203-1211.

Klingele, E. E., Marson, I. and Kahle, H. G. (1991). Automatic interpretation of gravity gradiometric data in two dimensions: vertical gradient. *Geophysical Prospecting*, 39: 407-434.

Tawadros, E, Rasul, S. M, and Elzaroug, E. (2001). Petrography and palynology of quartzites in the Sirte Basin, central Libya. *Jour. African Earth Sciences*, 32: 373-390.

Van der Meer, F. and Cloetingh, S. (1993). Intraplate stresses and subsidence history of the Sirte Basin (Libya). *Tectonophysics,* 226: 37-58.

Li, C.-F., Zhou, Z., Hao, H., Chen, H., Wang, J., Chen, B. and Wu, J. (2008). Late Mesozoic tectonic structure and evolution along the present-day Northeastern South China Sea continental margin. *Journal of Asian Earth Sciences*, 31 (4-6): 546-561.

Ma, Z.-J., Gao, X.-L. and Song, Z.-F. (2006). Analysis and tectonic interpretation to the horizontal-gradient map calculated from Bouguer gravity data in the China mainland. *Chinese Journal of Geophysics (Acta Geophysica Sinica)*, 49 (1): 106-114.

Marson, I., and Klingele, E. E., (1993). Advantages of using the vertical gradient of gravity for 3-D interpretation. *Geophysics*, 58: 588-1595.

Phillips, J. D. (1998)**.** Processing and interpretation of aeromagnetic data for the Santa Cruz Basin-Patahonia Mountains area, South-Central Arizona. *U. S. Geological Survey Open-File Report*: 02-98.

Pilkington, M. (2007)**.** Locating geologic contacts with magnitude transforms of magnetic data. *Journal of Applied Geophysics*, 63 (2): 80-89.

Reid, A. B., Allsop, J. M., Granser, H., Millet, A. J. and Somerton, I. W. (1990). Magnetic interpretation in three dimensions using Euler Deconvolution. *Geophysics*, 55: 80- 91.

Reid, A. B., Fitz Gerald, D. and McInerney P. (2003). Euler Deconvolution of gravity data. *Society of Exploration Geophysicists (SEG), Annual Meeting*, 2003: 580-583.

Reid, A. B. (2003). Short note: Euler magnetic structural index of a thin-bed fault. *Geophysics*, 68: 1255-1256.

Robertson Group Comp. (1970)**.** Geological study in the concession 12. *Unpblished report*.

Shepherd, T., Bamber, J. L. and Ferraccioli, F. (2006). Subglacial geology in Coats Land, East Antarctica, revealed by airborne magnetics and radar sounding. *Earth and Planetary Science Letters*, 244 (1-2): 323-335.

Thompson, D. T. (1982). EULDPH – A new technique for making computer-assisted depth estimates from magnetic data. *Geophysics*, 47: 31-37.

Wilsher, W. A. (1987). A structural interpretation of the Witwatersrand basin through the application of the automated depth algorithms to both gravity and aeromagnetic data. *Unpublished MSc. Thesis*, University of Witwatersrand.

Petroleum System and Play Concept in the Area 113-3&4, Southern Margin of the Ghadames Basin, Libya

Takashi Sato* and Yoshihiro Watanabe*

Abstract: The Contract Area 113 Blocks 3 & 4 (Area 113-3 & 4) is located in the southern margin of the Ghadames Basin, where the glaciated Middle Ordovician Haouaz Formation and Silurian Basal Tanezzuft Hot Shale (BTHS) play important roles in the petroleum system. The newly acquired seismic data clearly indicate that the BTHS is distributed discriminatively in paleo-topographic lows surrounding Haouaz paleo-high structures. Maturation history is characterized by distinctive three heating phases and significant erosion of the post-Hercynian sediments, resulted in extremely high maturity of the BTHS in spite of its shallower present depths. In local depressions of the Area 113-3 & 4, the main hydrocarbon expulsion from the BTHS occurred in the Hercynian heating phase. The Haouaz Formation is divided into five (5) litho-stratigraphic units, Unit A to E in descending order. The Unit C sandstones have superior reservoir qualities, while those of sandstones in the other units are originally poor. Physical relationship/contacts between the Haouaz Unit C sandstones on the paleo-high structures and the surrounding BTHS are the most critical factor for formation of the Haouaz play from the viewpoint of hydrocarbon migration.

Keywords: Haouaz Formation, Silurian Basal Tanezzuft Hot Shale (BTHS), Maturity, Migration.

INTRODUCTION

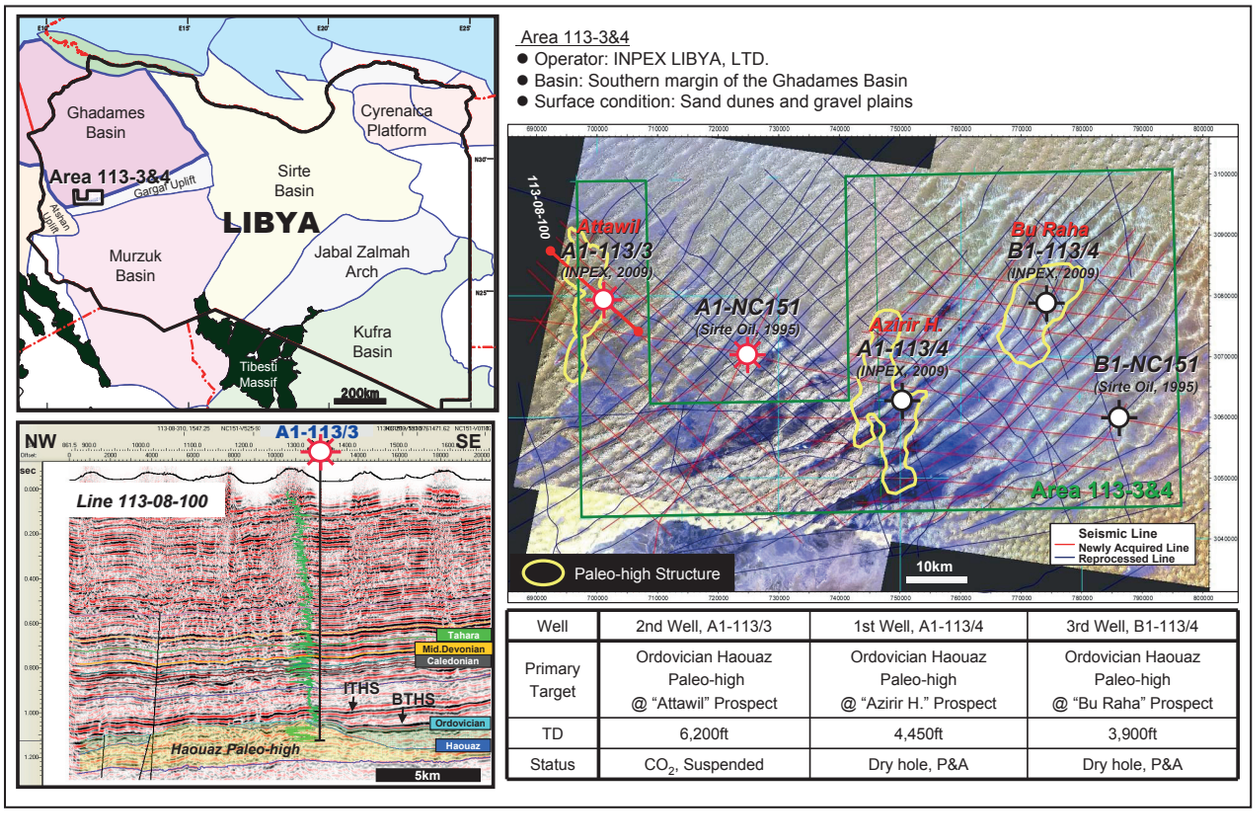
The Area 113-3 & 4 is geologically located in the southern margin of the Ghadames Basin and the southeastern corner of the Area belongs to the Gargaf Uplift that separates the Ghadames Basin from the Murzuk Basin to the south (Fig. 1).

INPEX had energetically conducted exploratory works such as reprocessing of the vintage 2D seismic data, a new 2D seismic survey, geological sample analyses, geological field excursions and integrated geological and geophysical studies since 2007. Based on these exploratory works and studies, three (3) prospects were tested through the 2009 drilling campaign (Fig. 1). The three (3) exploratory wells really validated INPEX's geological idea and/or concept, especially for the glaciated Middle Ordovician Haouaz Formation in the Area 113-3 & 4, however, they failed to demonstrate the presence of effective petroleum system aside production of unpredictable dry gas with extremely high concentration of CO_2 at the 2nd well, A1-113/3. Then an integrated post-drilling study including the reconstruction of stratigraphic framework, basin modeling study and petrographic study was carried out to bring some important speculations for the petroleum system and play concept in the southern margin of the Ghadames Basin.

GEOLOGICAL BACKGROUND

The southern margin of the Ghadames Basin is situated on the "Trans-Saharan Mega Belt", a mobile belt during Pan-African Orogeny (Lüning, *et al* 2007). The Paleozoic sediments are distributed on this Precambrian basement to dip generally northwestward in the Area 113-3 & 4. They are composed of the Cambro-Ordovician to the Carboniferous and estimated to have a total thickness of 5,000 to 7,000 ft in the Area 113-3 & 4 (Fig. 2). The Paleozoic of the Ghadames Basin is divided into some super-sequences bounded by major unconformities such as Taconic, Caledonian and Hercynian (Dardour, *et al* 2004). The post-Hercynian Mesozoic sediments, which are regionally distributed in the northern Ghadames and Murzuk basin, are believed to have been completely eroded out in the Area 113-3 & 4 at the later uplift event. The Carboniferous are widely exposed on the surface of the Area 113-3 & 4 at the present day.

*Exploration Department, INPEX LIBYA, LTD., Tripoli, Libya



Well	2nd Well, A1-113/3	1st Well, A1-113/4	3rd Well, B1-113/4
Primary Target	Ordovician Haouaz Paleo-high @ "Attawil" Prospect	Ordovician Haouaz Paleo-high @ "Azirir H." Prospect	Ordovician Haouaz Paleo-high @ "Bu Raha" Prospect
TD	6,200ft	4,450ft	3,900ft
Status	CO_2, Suspended	Dry hole, P&A	Dry hole, P&A

Fig. 1. Location map of the Area 113-3 & 4, summary of prospects tested through the 2009 drilling campaign and an interpreted seismic section showing the A1-113/3 gas structure.

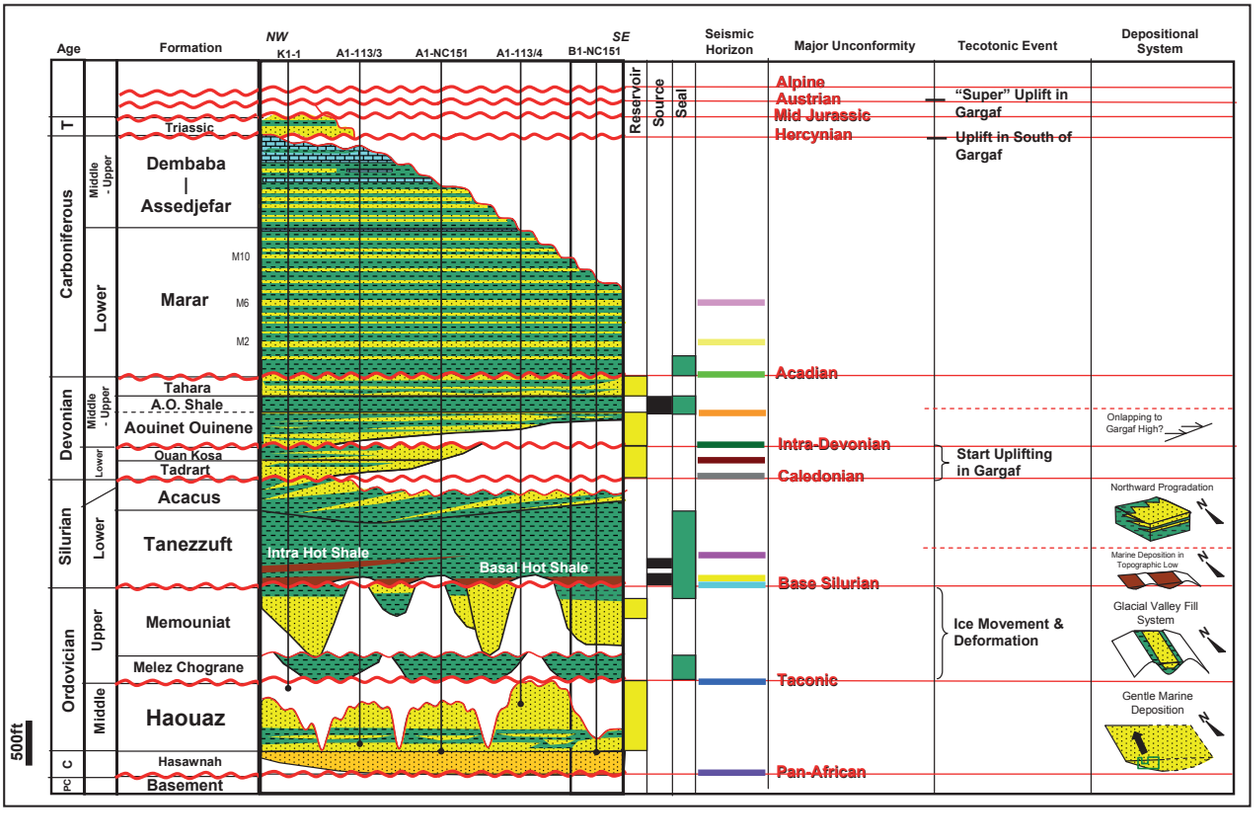


Fig. 2. Generalized stratigraphy in and around the Area 113-3 & 4

Among the Ordovician, the Haouaz paleo-high (buried-hill) structures and incised valleys resulted from glaciations in Late Ordovician are well recognized on seismic sections (Fig. 3). The shaly Melez Chograne and Memouniat Formations of the Upper Ordovician are interpreted to have been deposited with repetitious erosions to bury up paleo-topographic lows, and therefore, mal-distribution of the Ordovician sediments is resulted in a complicated well stratigraphy. The Silurian is composed of the shaly Tanezzuft and overlying sandy Acacus Formations. There are two "Hot Shale" horizons within the Tanezzuft Formation such as the Basal Tanezzuft Hot Shale (BTHS) and Intra Tanezzuft Hot Shale (ITHS). The former is distributed to surround the paleo-high formed by the Middle Ordovician Haouaz quartzitic sandstones as indicated by the amplitude anomaly of the BTHS horizon (Fig. 3). The Lower Devonian is composed of sandy Tadrart and Ouan Kosa Formations. These formations are distributed only in the west of the Area 113-3 & 4 due to the effect of the Caledonian and Middle Devonian Unconformities. The Middle to Upper Devonian consists of the Aouinet Ouinene Formation, the Aouinet Ouinene Shale (A. O. Shale) and the Tahara Formation in ascending order. The existing Carboniferous sediments thicken northwestward from approximately 800ft in the east to 3,300ft at the A1-113/3. The Lower Carboniferous Marar Formation consists mainly of shales with interbedded sandstone-rich intervals, and the overlying Assedjefar and Dembaba Formations have intercalations of carbonates.

The petroleum system of the Silurian source rock and Ordovician sandstone reservoir is proven in the Murzuk Basin. Especially El Sharara Oil Fields located in 100 km southeast of the Area 113-3 & 4 are worthy to note in that they have a particular petroleum system with the complicated stratigraphy, which is related to the paleo-high structure resulted from glacial actions in Late Ordovician (Sarkawi, 2007 and Franco, *et al* 2008). In addition, there are A1-NC151 gas discovery located in the adjacent block of the Area 113-3 & 4 and A1-113/3 CO2 rich gas accumulation in the Area 113-3 & 4 as described above. They are also interpreted to be paleo-high structures with the Middle Ordovician Haouaz sandstone reservoir.

Geological and geophysical studies reveal that the Ordovician play, which is a paleo-high related structural-stratigraphic play like El Sharara Oil Fields, is most promising in the Area 113-3 & 4.

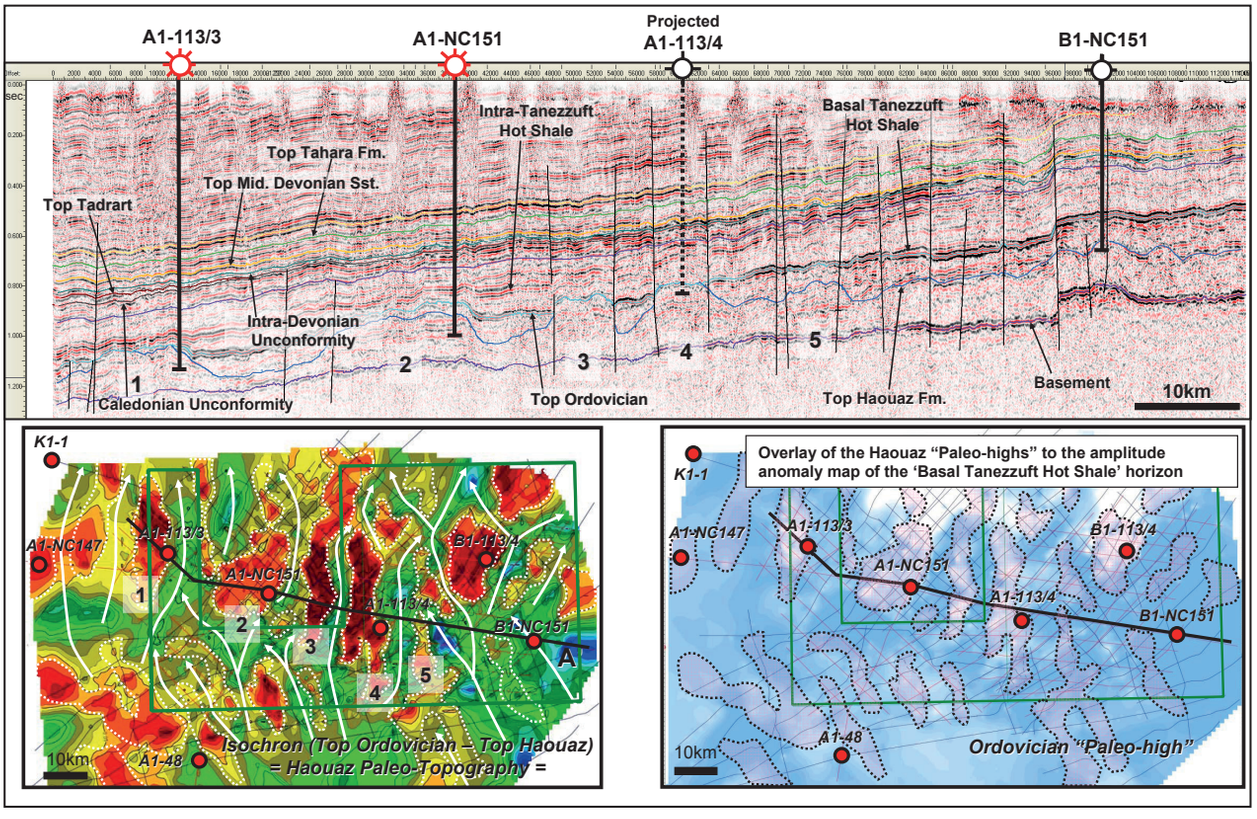


Fig. 3. A regional composite seismic line, the isochron map of Top Ordovician – Top Haouaz horizon and the amplitude anomaly map of the 'Basal Tanezzuft Hot Shale' horizon, showing the distribution of Haouaz Paleo-high and BTHS in the Area 113-3 & 4.

Isochron map between the 'Top Haouaz' and 'Top Ordovician' horizons, which is presumably assumed as the Haouaz paleo-structure map, shows the glaciated paleo-topography and presence of a lot of N-S trending paleo-high structures with 2km to 10km in width at the top of the Haouaz Formation (Fig. 3). The Melez Chograne and Memouniat shaly facies are interpreted to have been deposited to bury up the glaciated paleo-topographic lows in the Late Ordovician. They are expected to work as lateral seal, while the Silurian Tanezzuft shales as top seal for the Haouaz paleo-high structures. Matured primary source rock is the BTHS distributed to surround the Haouaz paleo-high structures (Fig. 3). Such physical relationships as onlapping of the BTHS onto the Haouaz paleo-high and direct contact of the Hot Shales with the Haouaz Formation through faults are desirable for hydrocarbon migration.

SOURCE ROCK AND BASIN MODELING

Newly acquired seismic data and geological data reveal that Tanezzuft Hot Shales are distributed within the Area 113-3 & 4. In addition, they are found to be oil-prone and are in late mature to main gas generation stage in spite of their shallower present depths. It indicates in-situ hydrocarbon generation and migration within the Area 113-3 & 4 and dispensable long lateral migration from the northwestern basin-ward, though there used to be some variations of interpretation on the kitchen area as indicated in published literatures (Echikh, K., 1998, Boote, *et al* 1998, and Seddiq and Bhaduri, 2006). Against this background, 1D basin modeling study was carried out in order to figure out the remaining unknown factors such as the timing of hydrocarbon generation and expulsion from the source rocks and expelled hydrocarbon volume. The basin modeling software, "Basin Mod 1D" by Platte River Associates was used for this study.

Source Rock Potential: The matured potential source rock within the Area 113-3 & 4 is primarily the BTHS. The geochemical data from the wells A1-113/3 and A1-113/4 indicate that the BTHS and ITHS are originally rich in Type I kerogen (Fig. 4), though very low Hydrogen Index (HI) values due to low S2 values resulted from high maturity level may suggest the possibility of admixture of Type II kerogen. The A. O. Shale is also recognized as a potential source rock containing Type II kerogen.

Heatflow History: The heat flow history is one of

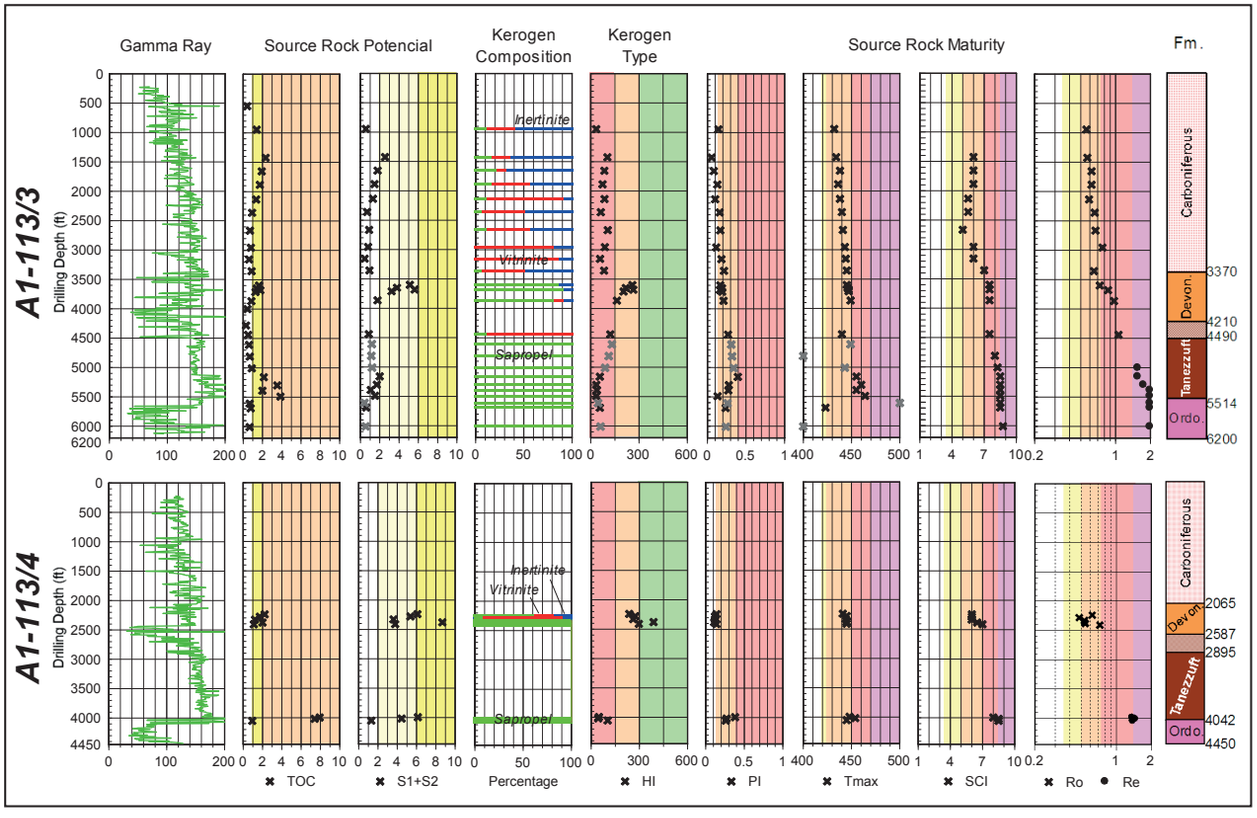


Fig. 4. Geochemical Logs of wells A1-113/3 and A1-113/4, showing source rock potential, kerogen type and maturity of the BTHS, ITHS and A. O. Shale..

key factors for the basin modeling as it is sensitive to source rock maturation. The heat flow history is interpreted to be characterized with the following three phases.

1) Post rift thermal sag after Pan-African Orogeny: The geological history of western Libya is believed to have started with the build-up of super continent Gondwana accompanied by the Pan-African Orogeny. Ghadames-Murzuk Basin was initiated on a mobile belt, called Trans Saharan Mega Belt, which appeared between the West African craton and the East Saharan craton (Lüning, *et al* 2007). At this beginning stage of the basin, it is supposed that rifting was active under high heat flow regime as indicated by volcanic rocks in the basement. Then the heat flow gradually decreased with basin evolution as sag basin until Permian.
2) Hercynian continental collision and Triassic rifting followed by thermal sag: The Hercynian Orogeny is well known as one of the largest geological events in sedimentary basins of North Africa, which was caused by the continental collision related to Pangea super continent construction in Permian (Craig, *et al* 2004). As this event was accompanied by Traissic rifting and volcanism as confirmed in northern Ghadames Basin, it is supposed that heat flow increased rapidly and then gradually decreased during the subsequent thermal sag phase.
3) Alpine volcanism to the present: The present-day geothermal gradient is reported to be very high in Gargaf region (Underdown, *et al* 2008) and is estimated to be 4.75degC/100m in the Area 113-3 & 4, based on the available well data. High geothermal gradient is probably related to the Alpine thermal activity starting in Tertiary, which is recorded as volcanic outflows in eastern Gargaf region.

Burial History: The A1-NC151, B1-NC151 and A1-113/3 well locations are control/calibration points of 1D basin modeling. Geological section penetrated by the well A1-113/3 is 6,182ft in thickness, which consists of Paleozoic succession from the Middle Ordovician Haouaz Formation to the Carboniferous Assedjefar/Dembaba Formation. There are such four (4) unconformities as Taconic, Caledonian, Intra-Devonian and Acadian in the Paleozoic succession. Eroded amounts at each unconformity are estimated based on regional well correlations with some geological assumptions, however, it is revealed through the basin modeling that these four unconformities have very minor impacts on the results, compared with the post-Carboniferous unconformities.

Huge amount of Mesozoic sediments are highly likely to have been deposited in the past and completely eroded out by the post-Carboniferous unconformities. At least four (4) unconformities, such as Hercynian, Jurassic, Austrian and Alpine, can be recognized in the southern Ghadames to Murzuk Basins, among which, the Austrian event probably shows the largest impact on uplift and erosion in the Area 113-3 & 4 as indicated by clear angular unconformity on the published geological maps of Libya (Industrial Research Centre, 1984-1985). The amount of Austrian erosion is uncertain and estimation of its eroded thickness is one of the key/sensitive issues in the basin modeling.

It is highly important that Ro profile of the well A1-113/3 show a remarkable change in trend at Devonian level. Based on this noticeable phenomenon which is likely caused by rapid and massive amounts of sedimentation in Mesozoic, several stratigraphic models with different amount of erosion by the Austrian unconformity were simulated in order to examine sensitivity of eroded thickness on maturity records and to find out the best model to fit the actual maturity and temperature profiles (Fig. 5). Consequently the eroded thickness by the Austrian unconformity was determined to be of the scale of 1,900m at the A1-113/3 well location.

Maturation: The geohistory diagram shows at the A1-113/3 well location that both ITHS and BTHS had reached into the oil window (early-mature-stage) in Devonian to Carboniferous and the main gas generation stage during the Hercynian heating phase (Fig. 6), while the A. O. Shale is suggested to have been in the mid-mature-stage since the Hercynian heating event.

Setting of Peudo-well: Overlay of the Haouaz paleo-highs to the amplitude anomaly map of the 'BTHS' horizon clearly shows that the BTHS are distributed to surround the paleo-highs. In such geological setting, hydrocarbons are expected to have been migrated from these local BTHS kitchens to nearby structures. In order to simulate the timing of hydrocarbon generation and expulsion and expelled volume in the kitchens, a pseudo-well is created. The pseudo-well PSW-1 is located in the north-south elongated BTHS kitchen between the "East Bu Raswan" and "Azirir H." structures (Fig. 7). Stratigraphic and paleo-historical model at the pseudo-well location is constructed based on

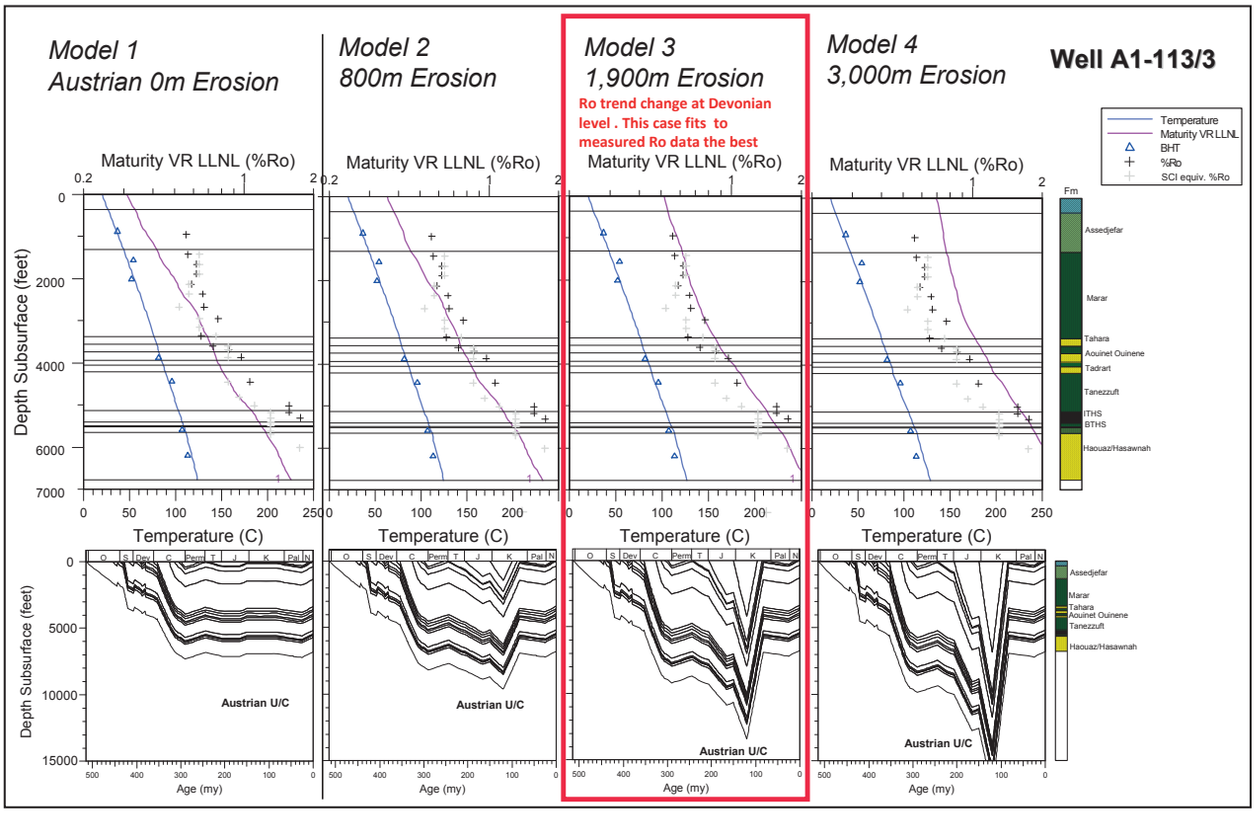


Fig. 5. Comparison of four different stratigraphic models to estimate the amount of Austrian erosion at the A1-113/3 well location, indicating eroded thickness up to 1,900m at the Austrian unconformity.

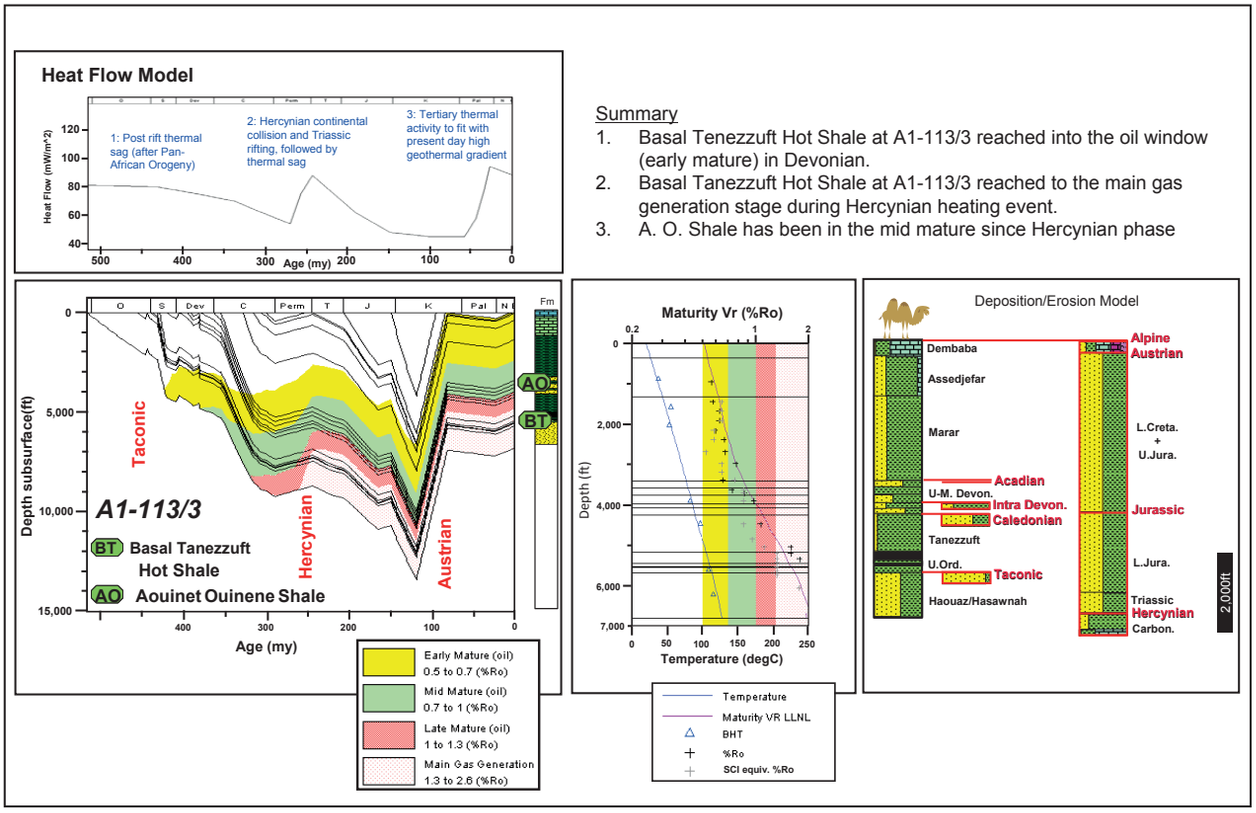


Fig. 6. The reconstructed paleohistory with maturation history at the A1-113/3 well location.

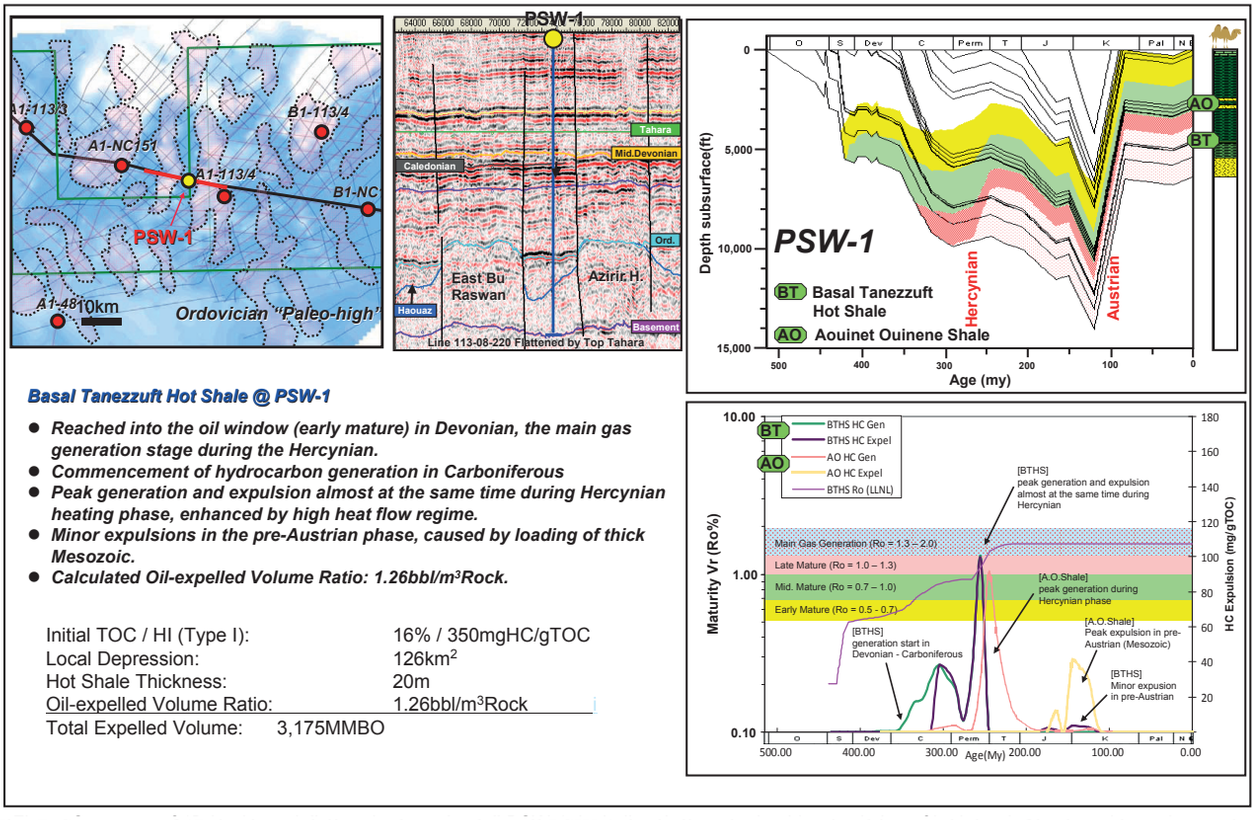


Fig. 7. Summary of 1D basin modeling at the pseudo-well PSW-1, including the maturation history, timing of hydrocarbon generation and expulsion and expelled hydrocarbon volume..

the following assumptions: 1) Present formation thickness based on post-drilling seismic/structural interpretations, 2) Almost same burial history as the well A1-113/3 but greater erosions at the Austrian event than the well A1-113/3 to be consistent with the existing geologic column and 3) Same heat flow model as the well A1-113/3.

The modeled geohistorical diagram shows that the BTHS at the pseudo-well PSW-1 reached into the oil window (early-mature-stage) in Devonian and the main gas generation phase during the Hercynian heating phase. On the other hand, the A. O. Shale is suggested to have been in the middle-mature-stage since the Hercynian heating phase.

Hydrocarbon Generation and Expulsion: The simulated hydrocarbon generation and expulsion history of the BTHS at the pseudo-well PSW-1 is summarized (Fig. 7):

- Commencement of hydrocarbon generation in Carboniferous
- Peak generation and expulsion almost at the same time during Hercynian heating phase, enhanced by high heat flow regime.
- Minor expulsions in the pre-Austrian phase, caused by loading of thick Mesozoic.
- Calculated oil-expelled volume ratio: 1.26bbl/m3 rock at PSW-1.
- Estimated total expelled oil volume: 3,175MMBO from a local depression between "Azirir H." and "East Bu Raswan" structures with assumed kitchen area of 126km2 and hot shale thickness of 20m.

RESERVOIR GEOLOGY

Stratigraphic Subdivision of the Haouaz Formation: The presence of thin Upper Ordovician Melez Chograne Formation and extremely thin BTHS and lack of the Upper Ordovician Memouniat Formation on the glaciated Haouaz Formation at the wells A1-113/3, A1-113/4 and B1-113/4 indicate these well locations are very close to the crest of each paleo-high structure drilled. Flattened images of the seismic data and difference in thickness of the Melez Chograne Formation encountered at the wells A1-113/3, A1-113/4, A1-NC151 and B1-113/4 suggest the Haouaz remnants encountered at each well location are not stratigraphically same with each other as the degrees of glacial erosion are different among the Haouaz paleo-high structures (Fig. 8). The Haouaz Formation at the well B1-NC151 is overlain by thick Melez Chograne and

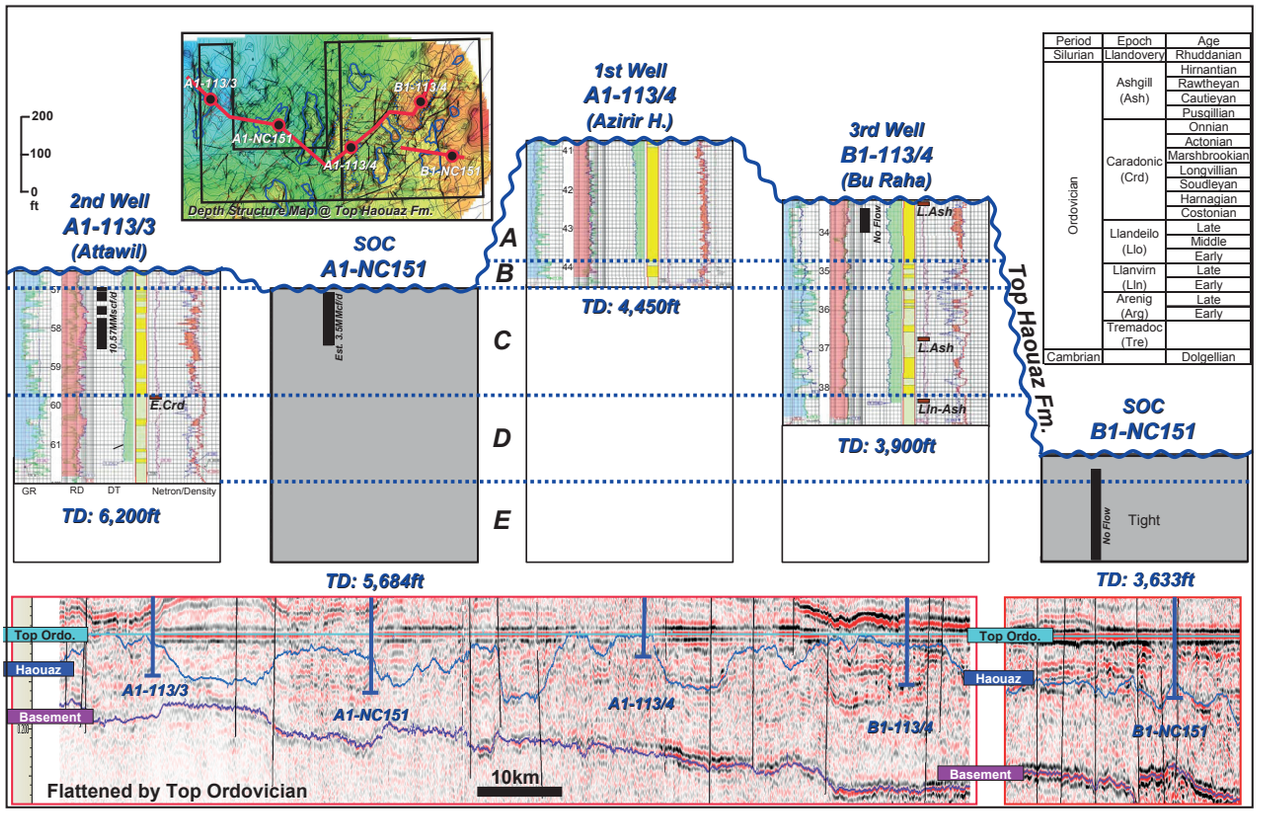


Fig. 8. Well correlations and flattened seismic sections, showing five (5) litho-stratigraphic units of the Haouaz Formation.

Memouniat Formations and relatively thick BTHS is present, indicating that the structural anomaly drilled by the well B1-NC151 is not a paleo-high structure.

The Haouaz Formation in and around the Area 113-3 & 4 is divided, based on the well correlation, seismic interpretation and biostratigraphic analysis, into five (5) litho-stratigraphic units, Unit A to Unit E in descending order, among which the Unit B and the Unit D are shaly. The uppermost parts of the Haouaz Formation are made up of the Unit A at the wells A1-113/4 and B1-113/4, the Unit B at the well A1-113/3, and the Unit C at the well A1-NC151. The Haouaz Formation penetrated at the well B1-NC151 is composed of the lower part of the Unit D and the Unit E. This litho-stratigraphic subdivision indicates that the wells A1-NC151 and A1-113/3 produced gas from the Unit C and that the Unit C may become shaly eastward though the unit was not penetrated at the well A1-113/4 and has been completely eroded out at the B1-NC151 well location.

Reservoir Property: Microscopic analysis (thin section examination) reveals that sandstones of the Unit C show the best reservoir quality. Conventional core samples taken from the Unit A at the well B1-113/4 are composed of poorly sorted sandstones which are characterized with high grain percentage up to 80% and high clay contents, indicating that reservoir properties of the Unit A sandstones have been originally very poor (Fig. 9). It is noted that point count porosities by thin section examination are much lower than CCAL porosities in the Unit A due to the dominance of micro pores between clay minerals. In contrast, SWC samples taken from the Unit C at the well A1-113/3 consist of fine-grained and well sorted quartzites which had the original porosity up to 35% without any clay content and are characterized significant quartz overgrowth (Fig. 10). SWC samples taken from the uppermost part of the Unit A at the well A1-113/4 and conventional core samples from the bottom part of the Unit C at the well A1-113/3 are silty/shaly and very fine-grained sandstones with very poor reservoir quality. The reservoir quality of the Haouaz sandstones is varied among litho-stratigraphic units and seems to be controlled by the original texture and composition rather than the latter diagenetic alteration.

It is interpreted that originally superior reservoir properties of the Unit C sandstones was deteriorated to some extent due mainly to quartz overgrowth,

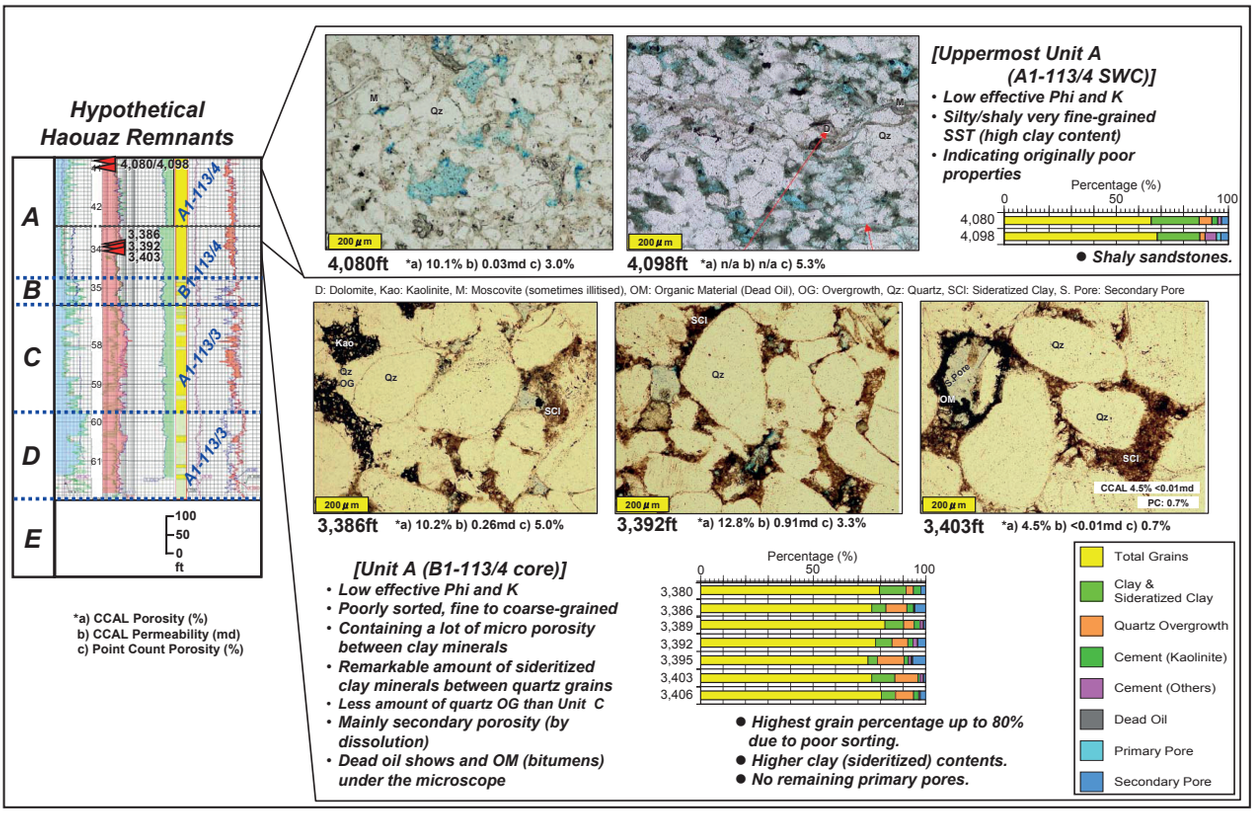


Fig. 9. Hypothetical type section of the Haouaz Formation with photomicrographs and petrographic descriptions of the Unit A.

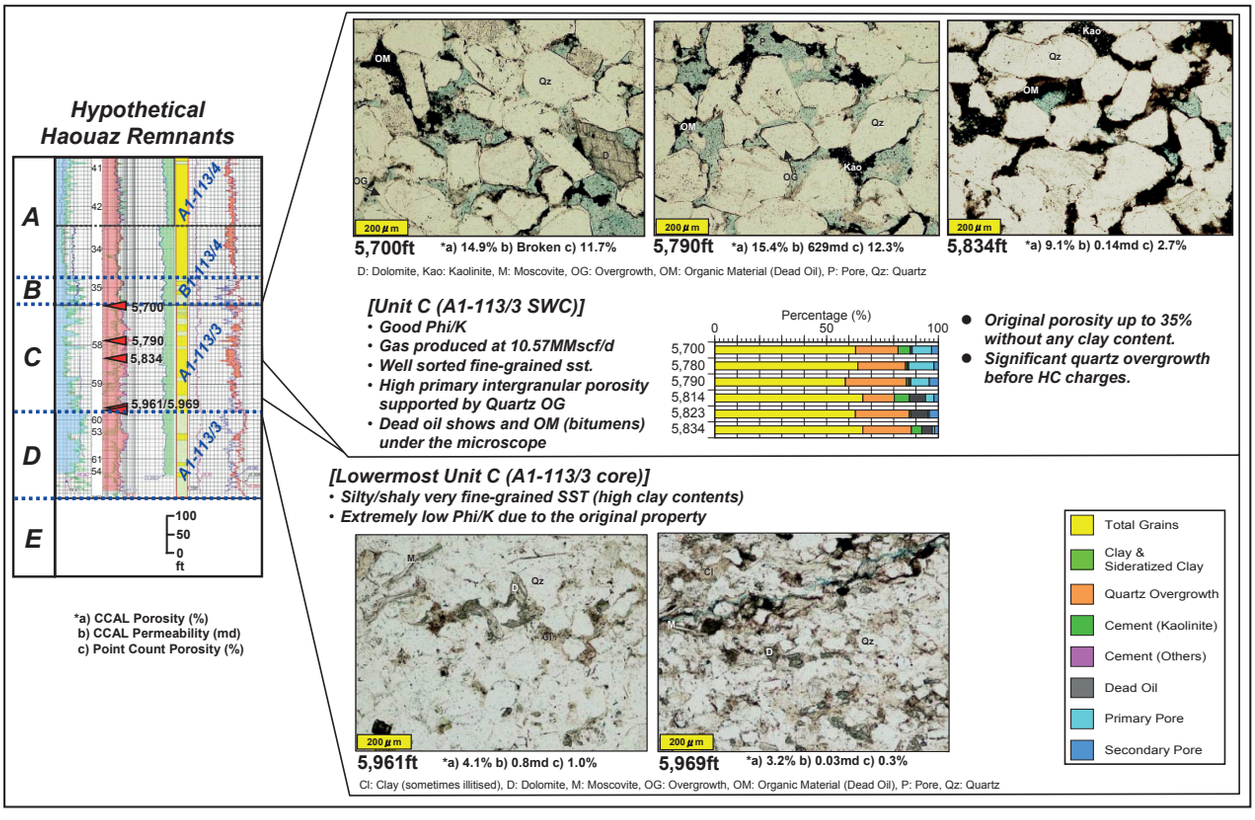


Fig. 10. Hypothetical type section of the Haouaz Formation with photomicrographs and petrographic descriptions of the Unit C.

however, have been retained by efficient hydrocarbon migration into the sandstones. On the other hand, originally poor reservoir properties of the Unit A sandstones had less chance to receive hydrocarbon charges and have become worse.

PETROLEUM SYSTEM

Diagenesis and Hydrocarbon Migration: The above-mentioned source rock and reservoir studies suggest the following diagenesis and hydrocarbon/non-hydrocarbon migration history/steps to form the A1-113/3 gas accumulation (Fig. 11).

- Deposition of well-sorted fine quartz grains of the Haouaz Unit C (original porosity up to 35%).
- Pre-Hercynian quartz overgrowth.
- Subsequent minor clay infiltration/cement.
- Oil charge into remaining intergranular pore spaces of the Haouaz Unit C during Hercynian phase from the juxtaposed BTHS.
- Replacement of oil with gas or thermal cracking (generation of dead oil stain).
- Generation of secondary pores by dissolution possibly in Austrian.
- Replacement of gas with CO_2.
- On the other hand, the following steps are interpreted for tight and no hydrocarbon-bearing Haouaz Unit A of the B1-113/4 structure.
- Deposition of poorly sorted fine to coarse quartz grains accompanied with clay (much lower original porosity).
- Pre-Hercynian quartz overgrowth.
- Sideritization of original clay.
- Subsequent clay infiltration/cement.
- Very minor oil charge in Hercynian due to negligible permeability.
- Minor dolomitic cementation and generation of secondary pores by dissolution possibly in Austrian.

Critical Factor for Haouaz Play: The main hydrocarbon generation and expulsion from the BTHS are simulated to have occurred in the Hercynian phase. Therefore direct contacts between the Haouaz Unit C sandstones on the paleo-high structures and the surrounding BTHS during Hercynian phase are most desirable to achieve an efficient hydrocarbon migration from source rock to reservoir (Fig. 12). Meanwhile, such efficient hydrocarbon migration is unlikely between the Unit A and the BTHS and under the condition of poor physical contacts due to the presence of thick and shaly Upper Ordovician. The most critical factor for formation of the Haouaz play is physical relationships between the Haouaz sandstones and the BTHS, though a certain level of trap deformation and secondary hydrocarbon migration might have occurred in and after the great Austrian uplift and tilting event.

SUMMARY AND CONCLUSION

The integrated post-drilling study including the reconstruction of stratigraphic framework, basin modeling study and petrographic study brought the following speculations for the petroleum system and play concept in the Area 113-3 & 4.

- The potential matured source rock is primarily the BTHS, which is distributed discriminatively in paleo-topographic lows surrounding Haouaz paleo-high structures.
- Maturation history is characterized by distinctive three heating phases: 1) Post-rift thermal sag after the Pan-African Orogeny, 2) Hercynian continental collision and Triassic rifting followed by thermal sag, and 3) Alpine volcanism, and by significant erosion of the post-Hercynian sediments more than 6,000ft in thickness, resulted in extremely high maturity of the BTHS in spite of its shallower present depths.
- The pseudo-well PSW-1 in the central part of the Area 113-3 & 4 simulated that the THS reached the early oil generation window in Devonian Age and the main hydrocarbon expulsion occurred in the Hercynian heating phase.
- The Haouaz Formation is divided into five (5) litho-stratigraphic units, Unit A to E in descending order. The Haouaz remnants encountered at each well location are not stratigraphically same with each other as the degrees of glacial erosion are different among the Haouaz paleo-high structures.
- The Unit C sandstones have superior reservoir qualities, while those of sandstones in the other units are originally poor. The reservoir quality of the Haouaz sandstones seems to be controlled by the original texture and composition rather than the latter diagenetic alteration.
- Physical relationship/contacts between the Haouaz Unit C sandstones on the paleo-high structures and the surrounding BTHS are the most critical factor for formation of the Ordovician play from the viewpoint of hydrocarbon migration in the southern margin of the Ghadames Basin.

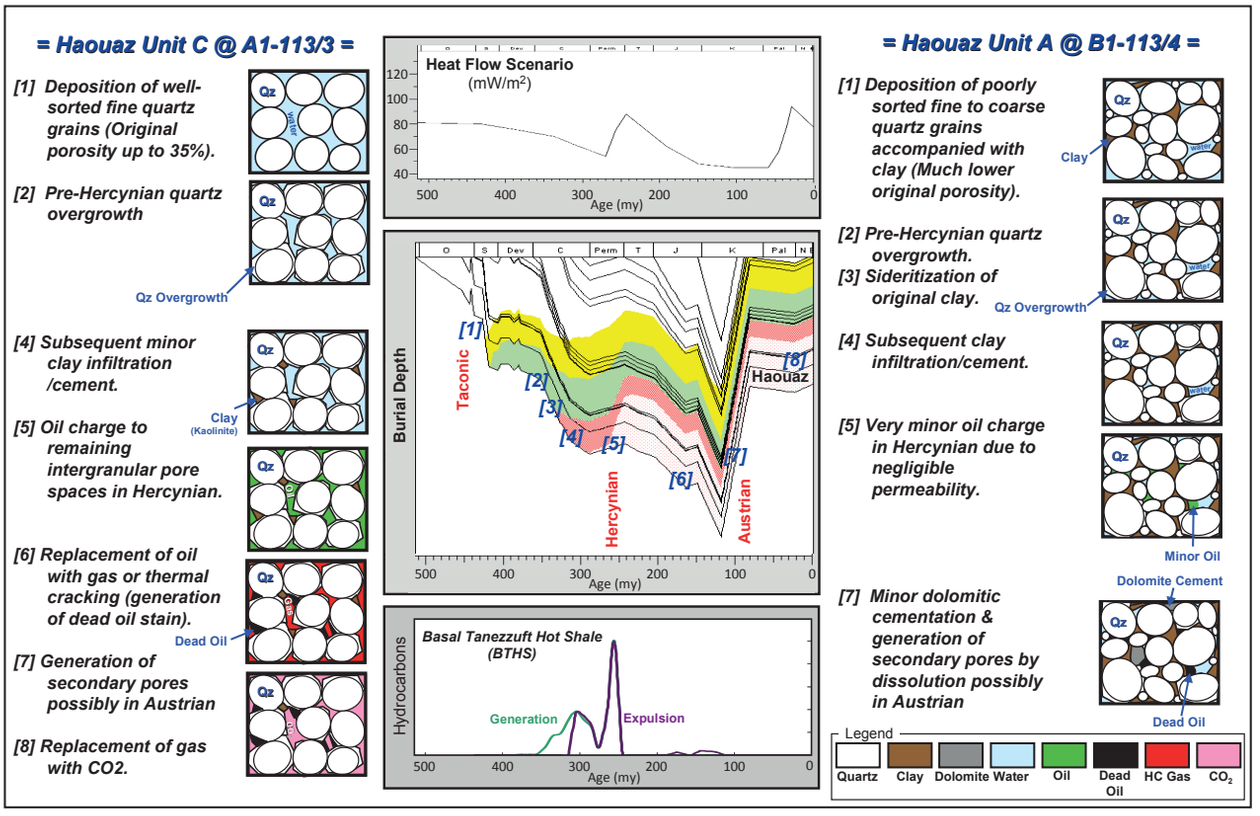


Fig. 11. Relationship of diagenesis and hydrocarbon migration for the tested Haouaz paleo-high structures.

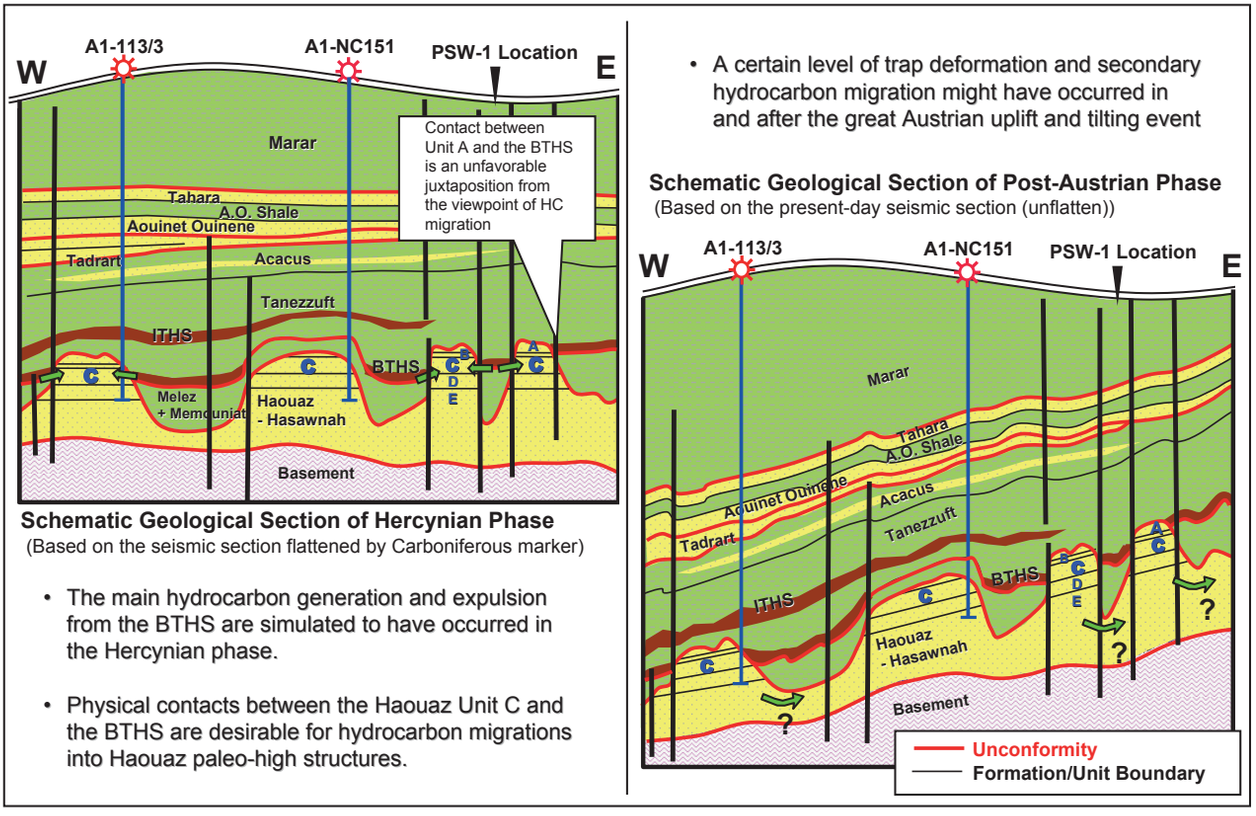


Fig. 12. Hydrocarbon migration model in the Area 113-3&4.

ACKNOWLEDGEMENT

The authors thank colleagues of INPEX LIBYA, LTD. and INPEX Corporation for their contributions and supports to release this paper.

REFERENCES

Boote, D. R. D., Clarke-Lowes, D. D. and Traut, M. W. (1998). Palaeozoic petroleum systems of North Africa. In: Macgregor, D.S., Moody, R.T., and Clark-Lowes, D.D. (eds.): Petroleum Geology of North Africa, Geological Society Special Publication 132, 7-68.

Craig, J. Rizzi, C., Said, F., Thusu, B., Luning, S., Asbali, A. I., Keely, M.L., Bell, J. F., Durham, M. J., Eales, M. H., Beswetherick S. and Hamblett, C. (2004). Structural styles and prospectivity in the Precambrian and Palaeozoic hydrocarbon systems of North Africa. In: M. J. Salem, *et al* (eds.), The Geology of East Libya, Sedimentary Basins of Libya, Third Symposium, IV: 51-122.

Dardour, A. M., Boote, D. R. D. and Baird, A. W. (2004). Stratigraphic controls on Palaeozoic petroleum systems, Ghadames Basin, Libya. Journal of Petroleum Geology, 27(2): 141-162.

Echikh, K. (1998). Geology and hydrocarbon occurrences in the Ghadamis Basin, Algeria, Tunisia, Libya. In: Macgregor, D.S., Moody, R.T., and Clark-Lowes, D.D. (eds.) Petroleum Geology of North Africa, Geological Society, London, Special Publication 132: 109-129.

Franco, A., Perona, Dwyianti, R., Yu, F., Helal, S., Suarez, J. and Ali, A. (2008). NC186 Block Murzuq Basin: Lesson learned from exploration, Abstracts of Seimentary Basins of Libya, Fourth Symposium, Geology of Southern Libya, Tripoli, Libya, 129-133.

Geological map of Libya 1:250,000 Sheet: NH 33-13 Qararat Al Marar, NG 32-3 Bi'r Anzawa, NG 32-4 Hasi Anjiwal, NG 32-7 Tikiumit, NG 32-8 Wadi Irawan, NG 32-11 Wadi Tanezzuft, NG 32-12 Al Awaynat, NG 32-15 Ghat, NG 32-16 Anay, NG 33-1 Idri, NG 33-2 Sabha, NG 33-5 Awbari and NG 33-6 Tanahmu, 1984-1985, Industrial Research Centre, Tripoli, Libya.

Lüning, S., N. M. Fello, J. Craig, D. P. Le Heron, S. Lubeseder, G. Pyke, S. Schulz, A. J. Dunford, and Abutarruma, Y. (2007). 1001 Million Saharan Nights – Petroleum Geology of Southern Libya. Documentary film, 4h 30 min, Seven Continents Science Productions, Bremen, Germany, www.seven-continents.com/libya.htm.

Sarkawi, I., Abeger, G., Tornero, J.L. and Abushaala, E. (2007). The Murzuq Basin, Libya – A Proven Petroleum System, Abstracts of 3rd North African/Mediterranean Petroleum & Geosciences Conference and Exhibition Tripoli, Libya, A11.

Seddiq, H. and Bhaduri, A. (2006). The Petroleum Geology of Libya, a Synthesis, Libya 2006 - Reservoir Optimization Conference, 20-40. Schlumberger.

Underdown, R. and Redfern, J. (2008). Petroleum generation and migration in the Ghadames Basin, north Africa: A two-dimensional basin-modeling study. AAPG Bulletin, 92,(1): 53-76.

Geochemical Evaluation of Thermal Maturity and Depositional Palaeoenvironment of Seven Cretaceous Formations from the East Sirt Basin, Libya

S. Aboglila*, K. Grice, K. Trinajstic, D. Dawson, K. Williford

Abstract: The Sirt Basin is Libya's most important petroleum province and the world's 13th largest petroleum-producing region. Several potential source rocks have been recognised within a complex geological setting, ranging in age from Precambrian to Eocene. Biomarker ratios, together with stable carbon ($\delta^{13}C$) and hydrogen (δD) isotopic compositions of individual hydrocarbons in source rock extracts (n = 21) from the East Sirte Basin were used to establish their thermal maturity and palaeoenvironmental conditions of deposition. Rock Eval pyrolysis data (OI range: 3 - 309 mg CO_2/g TOC and HI range: 115 – 702 mg/hydrocarbon/ g TOC) obtained from source rocks of the Cretaceous Sirte, Tagrifet, Rakb, Rachmat, Bahi and Nubian formations show that the organic matter (OM) is mainly dominated by Type II/III kerogen. Vitrinite reflectance data (% R_o range: 0.46 – 1.38) support variations in thermal maturity and indicate mature to post mature rocks in the Sirte and Rachmat Formations and early to mid stage maturities for the other formations. The Sirte Formation in the study area was found to be relatively more thermally mature than the Tagrifet, Rakb, Rachmat, Bahi, and Nubian Formations, reflected by δD of pristane (Pr) and phytane (Ph) (less depleted in D). A contribution of terrigenous organic matter to all formations except the Sirte Formation is evident from δD of the higher-molecular-weight *n*-alkanes. Anoxic and suboxic of the source rock deposition was identified via the pristane to phytane (Ph/Ph range 0.65 – 1.25) and dibenzothiophene to phenanthrene (DBT/P range 0.04 – 0.47) values.

Keywords*:* Sirt Basin, Source rocks, Biomarker, Pyrolysis, Kerogen, Stable isotopes.

INTRODUCTION

The Sirt Basin is one of Africa's most productive oil provinces, located in north-central Libya. It occupies an area of 600,000 km^2 (Abadi, 2002), and is the 13th largest petroleum region (Ahlbrandt, 2001), with oil equivalent recoverable in reserves of approximately 43 billion barrels (Burwood *et al* 2003) (Fig. 1). Reviews of reserves, stratigraphy structure, and petroleum geological descriptions have been reported by many authors (e.g., Ghori and Mohammed, 1996; Baric *et al* 1996; Ahlbrandt, 2001; Burwood *et al* 2003, Aboglila *et al* 2010)

Several petroleum systems have been identified, migrated-marginal to the horsts and the deeper Agedabia grabens in the offshore areas of the basin (Baird *et al* 1996, Hallett, 2002). Petroleum in the Eastern Sirt Basin occurs in Mesozoic clastic reservoirs, in stratigraphic traps superimposed on structural highs, such as those of the Sarris and Massla fields (Abadi, 2002) (Fig. 1). The main structural features are the Upper Mesozoic–Cenozoic Agedabia and the slightly older Lower Cretaceous Hameimat, Maragh and Sarir Troughs (Burwood *et al* 2003) (Fig. 1). Subsidence throughout the Mesozoic resulted in basin-fill sediments hosting source rocks (Burwood *et al* 2003). Sediments decrease in thickness from 7 km offshore in the northern Gulf or Sirte province to around 1 km near the Nubian uplift in the south (Ahlbrandt, 2001). The grabens, particularly those in the southern part of the Zallah (Abu Tumayam), Maragh (Marada) and Sirte grabens, have recently been identified as potential hydrocarbon kitchens (Hallett and El-Ghoul, 1996).

Hydrocarbons generated by Upper Eocene carbonate source rocks, particularly offshore, offers additional hydrocarbon potential (Gruenwald, 2001). Traditionally, Upper Cretaceous marine shales of the Sirte and Rachmat Formation were identified as the main source rocks for hydrocarbons in the Sirte Basin (Ghori and Mohammed, 1996;

*Corresponding Authors. Fax: +218217316202. E-mail address: Salem.aboglila@gmail.com

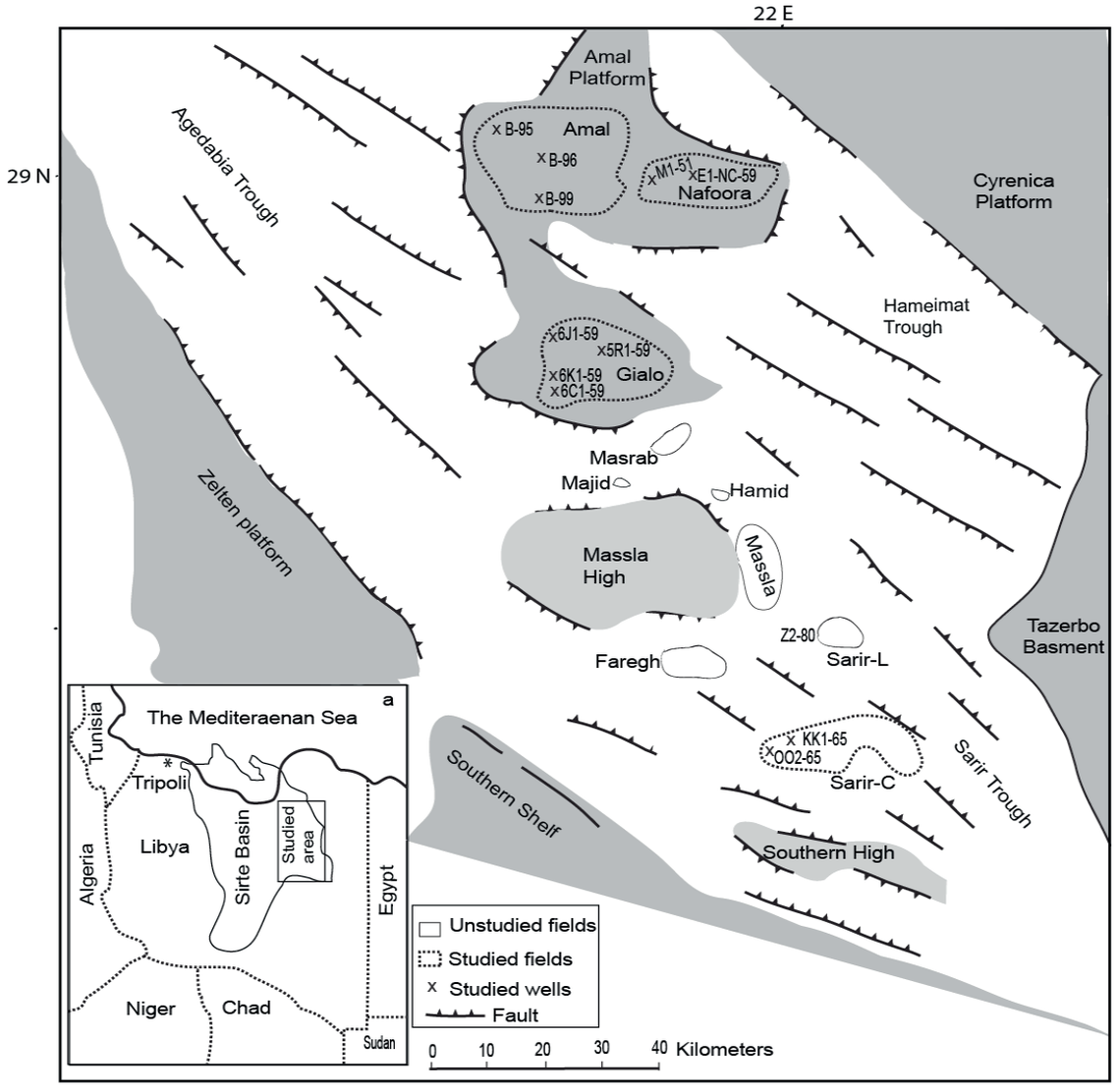


Fig. 1. Map shows the location of the Sirt Basin and its structural elements illustrate regional faults, high troughs and well samples in the studied area. Modified from Ahlbrandt (2001) and Aboglila *et al* (2010).

Baric *et al* 1996) (Fig. 2), with total organic carbon (TOC) contents ranging between 1 and 5% (El-Alami *et al* 1989). The main depocentre in the East Sirt Basin is the Agedabia Trough (Fig. 1) and due to the thickness of the section (>1400 m), source rock maturity differs between the basal and uppermost shales (Burwood *et al* 2003). Vitrinite reflectance (R_o) data indicate that the main source rocks have reached at least three levels of thermal maturity (Hallett, 2002). Basin modelling shows that in the southern part of the Agedabia Trough the Rachmat Formation entered the oil window during the Mid-Eocene, whereas the Sirte Shale started generating oil in the Late Eocene. In the north of the Agedabia Trough (Fig. 1), where it plunges steeply the sediments are post mature and have generated gas (Burwood *et al* 2003). Upper Cretaceous marine shales of the Rakb Formation and the carbonates of the Tagrifet Formation (Fig. 2) have been identified as source rock candidates in the Hameimat Trough; and the Rakb Formation is believed also to act as the seal for a number of the Sarir fields. The Nubian Formation (Triassic and Lower Cretaceous) (Fig. 2) comprises mostly continental sandstones, although some lacustrine shale horizons, located in the Faregh and Massla field of the Hameimat Trough (Fig. 1), may also act as source rocks for minor amounts of waxy oil in the southern part of the Agedabia Trough (El-Hawat *et al* 1996; Burwood *et al* 2003).

The purpose of this paper is to improve characterization of Cretaceous shale source rocks in the East Sirt Basin (Figs 1-2). An organic geochemical assessment of 99 source rock samples

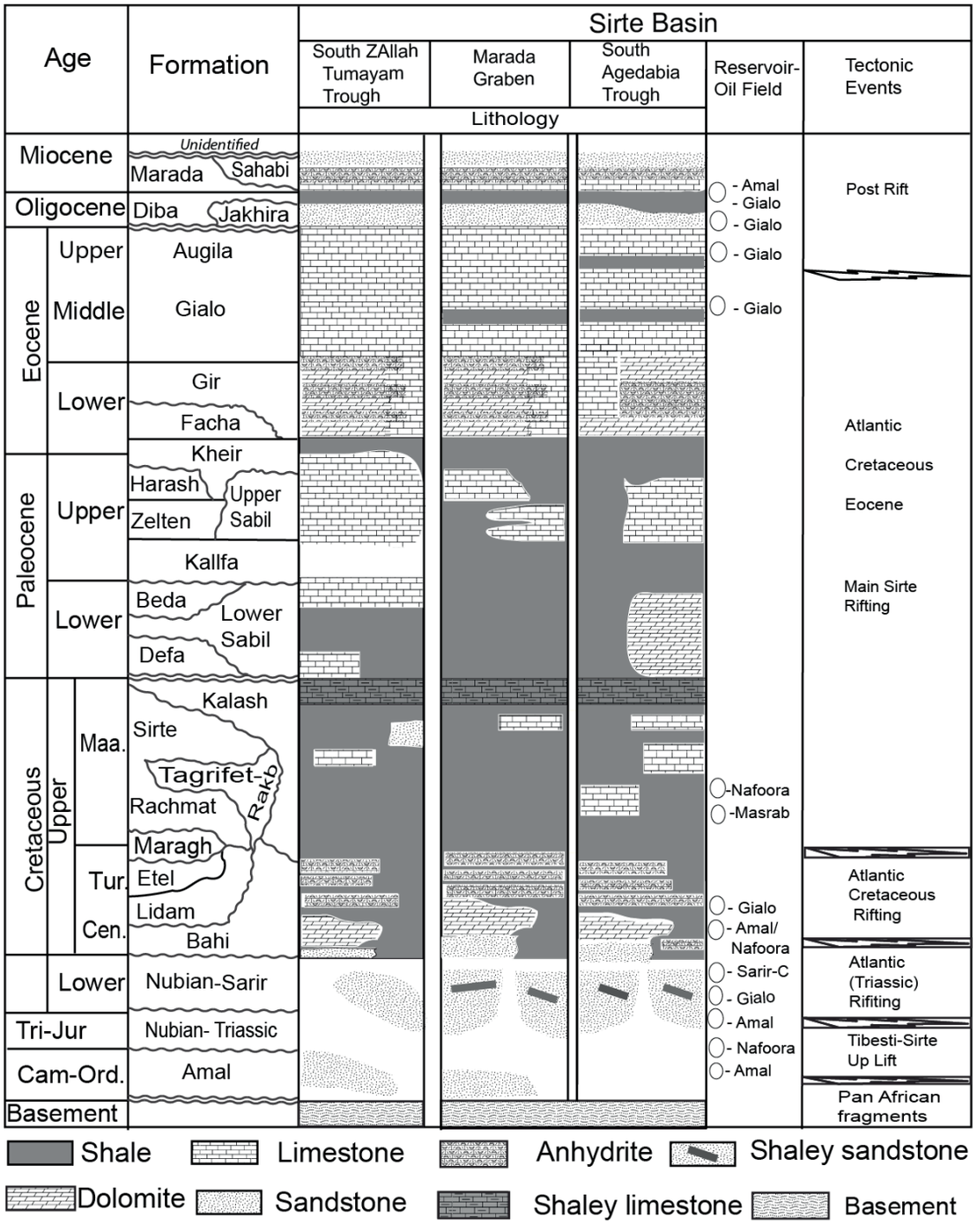


Fig. 2. Stratigraphic column of the Sirt Basin highlighting the lithologies of the formations, the reservoir units of the oil fields demonstrates age, formations, lithology, main reservoir-oil fields and its tectonic events. Modified from Barr and Weeger (1972), Burwood *et al* (2003) and Aboglila *et al* (2010).

(n = 99) was performed on seven Cretaceous formations. Twenty-one of these samples were subjected to more detailed biomarker and compound-specific stable carbon and hydrogen isotopes analyses. From these data, the relative thermal maturities and paleoenvironments of deposition of the source rocks were established.

MATERIALS AND METHODS

Geological setting: The Sirt Basin is part of one of Africa's oldest Hercynian structural provinces (Gras, 1996). Alternating episodes of uplift and subsidence commenced in the Neoproterozoic with the Pan-African orogeny that consolidated a

number of proto-continental fragments into an early Gondwanaland (Kroner, 1993). Rifting began in the Early Cretaceous, peaked in the Late Cretaceous, and ended in the Early Tertiary, resulting in the triple junction within the basin (Ahlbrandt, 2001). During the Late Jurassic and Early Cretaceous, the central Atlantic Ocean opened between northwest Africa and North America, which led to a westward shift of the African plate relative to the European plate. At this time, continental rifting was active in Africa, affecting the Northeast Brazil-Gulf of Guinea domain, southern Chad, Sudan, Kenya, the north and east of Niger, the western desert of Egypt and the southern Sirt Basin in Libya (Coward and Ries, 2003). The east-west trending structures of the Sarir and Hameimat Trough of the Sirt Basin were formed during this period (Guiraud and Maurin, 1991).

Samples: Ninety-nine samples of drill cuttings were collected by the National Oil Corporation (NOC) in Tripoli from 11 different wells (Fig. 1), located in the Amal, Gialo, Nafoora, and Sarir Fields. The attached NOC report confirmed that all samples are uncontaminated with Drilling additives. The units sampled were the Upper Cretaceous Kalash Sirte, Rakb, Tagrifet Rachmat and Bahi Formations (Fig. 2) and the Lower Cretaceous Nubian (Sarir) Formation (Fig. 2). The terms Nubian Sandstone and Sarir Formation have been used by many authors for all or part of the non-marine Lower Cretaceous units (c.f., Hallett, 2002).

Preparation of cutting samples: The cutting samples were washed with doubly distilled water and dried at room temperature prior to analysis. For more confirmation, group of random samples were sent to determine rocks contamination with drilling Fluid by gas chromatography-mass spectrometry. Following Rock-Eval pyrolysis and TOC analysis (see below), a suite of representative samples was selected for more detailed organic geochemical examination. These samples were ground to a fine powder (particle size of <150 μm) using a ring-mill (Rocklabs).

Rock-Eval pyrolysis and total organic carbon (TOC) measurements: Rock-Eval pyrolysis of powdered rock (10-50 mg) was carried out on a Girdel Rock-Eval instrument, while the TOC was measured on a Leco instrument. Samples with low TOC values (< 0.5%) were considered unsuitable for Rock-Eval pyrolysis and therefore not subjected to further analyses.

Solvent extraction and isolation of the maltenes: Twelve cuttings samples from representative formations were selected for solvent extraction based on TOC values (> 0.3%). About 10-20 g of ground sediment was extracted in an ultrasonic bath for two hours using a 9:1 mixture of dichloromethane (DCM) and methanol (MeOH). The solvent extract was then filtered and excess solvent removed by carefully heating on a sand bath (60°C) to obtain the bitumen. Asphaltenes were precipitated by mixing the bitumen with an excess of chilled *n*-heptane. The mixture was left (1 h) to settle for 1 h and later centrifuged at 2500 rpm for 5 min. The supernatant solution containing the maltenes was carefully decanted. This procedure was repeated (5x) by adding fresh *n*-heptane to precipitate the asphaltenes. Maltenes from the bitumens were fractionated using a small-scale column chromatographic method (Bastow *et al* 2007). In brief, the sample (maltenes, about 10–20 mg) was applied to the top of a small column (5.5 cm x 0.5 cm i.d.) of activated silica gel (120°C, 8 h). The aliphatic hydrocarbon (saturated) fraction was eluted with *n*-pentane (2 mL); the aromatic hydrocarbon fraction with a mixture of *n*-pentane and DCM (2 mL, 7:3 v/v,); and the polar (NSO) fraction with a mixture of DCM and MeOH (2 mL, 1: 1 v/v).

5A Molecular sieving: Aliphatic fractions of maltenes were subjected to 5A molecular sieving as described by Grice *et al (*2008). In brief, a portion of the aliphatic fraction in cyclohexane was added to a 2 mL vial, filled with activated sieves (7 mg). The vial was sealed and placed into a pre-heated aluminum block (85°C, 8 h). The solution was then cooled and decanted through a small column of silica plugged with cotton wool and pre-rinsed with cyclohexane (2 mL). The sieves were subsequently rinsed well with cyclohexane and the washings filtered through the same silica column. The combined filtrates yielded the branched/ cyclic fraction. The *n*-alkanes were recovered by hydrofluoric acid (HF) digestion of the sieve as described previously (Dawson *et al* 2005).

Gas chromatography–mass spectrometry (GC-MS): Aliphatic and aromatic fractions were analysed by GC-MS using a Hewlett Packard (HP) 5973 mass-selective detector (MSD) interfaced to a HP6890 gas chromatograph (GC). A HP-5MS (J and W Scientific) GC column (5%

phenylmethylsiloxane stationary phase) was used with helium as the carrier gas. The GC oven was programmed from 40°C to 310°C at 3˚C/min, after which it was held isothermal for 30 min. Samples were dissolved in *n*-hexane and introduced by the HP6890 autosampler into a split-splitless injector operated in the pulsed-splitless mode. Biomarker data were acquired in a full-scan mode (*m/z* 50-500). The ion source was operated in electron ionization (EI) mode at 70 eV. Selected ion monitoring (SIM) was used to identify the terpanes, steranes and triaromatic steroids by monitoring *m/z* 191, 217, 218 and 231 ions. Selected aromatic compounds were identified using *m/z* 178 (phenanthrene), *m/z* 156 (dimethylnaphthalenes) and *m/z* 184 (dibenzothiophene) ions and relative retention time data reported in the literature.

GC–isotope ratio mass spectrometry (GC-ir-MS): A HP6890 gas chromatograph (GC) equipped with a HP6890 autosampler was used in tandem with a Micromass isotope ratio monitoring mass spectrometer (ir-MS) for stable carbon and hydrogen isotope measurements. The GC-ir-MS conditions used were those detailed by Dawson *et al* (2005). In brief, the GC oven was programmed from 50°C to 310°C at 3˚C/min with initial and final hold times of 1 and 20 min, respectively. An identical capillary column to that used in GC-MS analysis was employed for GC-ir-MS. The carrier gas was He at a flow rate of 1mL/min. The ^{13}C data were obtained by integrating the masses 44, 45 and 46 in the ion currents of the CO_2 reference. CO_2 was produced from oxidation of each chromatographically separated component, after being passed through a quartz furnace packed with copper oxide pellets (heated at 850°C). The accuracy and precision of $\delta^{13}C$ measurements were monitored by analysing a mixture of organic reference compounds having known $\delta^{13}C$ ratios. Each sample was analysed at least three times, and the average $^{13}C/^{12}C$ values and standard deviations are reported in ‰ relative to a CO_2 reference gas calibrated to the Vienna Peedee Belemnite (VPDB). The δD values were obtained by integration of the mass 2 and 3 ions derived from H_2 reference, produced from pyrolysis of each chromatographically separated component, after passing through a quartz furnace packed with chromium particles (350-400 µm particle size, heated at 1050°C). The H_3^+ correction was performed by measuring mass 3 at two different H_2 reference gas pressures. Each sample was analysed at least three times, and average δD values and standard deviations are reported in ‰ relative to a H_2 reference gas calibrated to Vienna Standard Mean Ocean Water (VSMOW).

RESULTS AND DISCUSSION

Bulk geochemical parameters: Report of rocks contamination with a drilling additive confirmed the NOC report. Rock-Eval pyrolysis and TOC (%) measurements for the East Sirt Basin rock samples show quite diverse values (Table 1). TOC values from the Sirte Shale Formation range between 0.18% and 5.50%, while TOC values obtained from the Tagrifet Formation range between 0.36% and 5.16%. Three grey-greenish Rakb Shale Formation samples (Amal Field) have TOC values ranging from 1.00% to 1.42% (Table 1). Nineteen samples from the Rachmat Shale have TOC values ranging from 0.60% to 1.90%. One sample from the Bahi

Table 1. range of Rock Eval/TOC data for selected formations from the East Sirt Basin

Formation	Samples	TOC	OI	HI	Tmax	S_2	S_1	PI
Kalash	6	0.21 to 0.28	n.d.	n.d.	n.d.	n.d.	n.d.	n.d.
Sirte	47	0.18 to 5.50	3 - 185	115 - 481	427 - 437	0.27 –21.40	0.16 – 49.60	0.07 – 1.55
Tagrifet	15	0.36 to 5.16	94 - 210	242 - 612	426 - 440	2.01 – 22.80	0.26 – 51.80	0.11 – 0.79
Rakb	3	1.00 to 1.42	91 - 129	208 -415	428 - 434	2.08 – 5.90	0.30 – 1.11	0.09 -0.20
Rachmat	19	0.60 to 1.90	49 - 221	126 - 702	428 - 434	1.18 – 11.46	0.20 – 31.04	0.09 – 0.43
Bahi	1	0.9	309	413	428	2.75	3.92	0.59
Nubian	8	0.23 to 0.69	262 - 280	419 - 433	425 - 426	2.22 – 2.91	3.05 – 3.79	0.54 – 0.58

TOC (wt %): total organic carbon; HI= Hydrogen Index (S_2*100/TOC) and OI= Oxygen Index (S_3*100/TOC); Tmax (°C): maximum pyrolysis temperature yield; S_2: maximum temperature yield (mg HC/g rock); S_1: low temperature hydrocarbon yield (mg HC/g rock); PI: Production Index (S_1/S_1+S_2); n.d. not determined

Formation from M1-51 well (Nafoora Field) has a TOC of 0.90%. Eight samples from the Lower Cretaceous Nubian Formation have TOC values ranging from 0.23% to 0.69%, with the majority having < 0.5% TOC. TOC values < 0.4% indicate low source rock potential. Rock-Eval pyrolysis data for all formations, including S_1 and S_2 (mg HC/g rock), Tmax (°C), production indices (PI), hydrogen indices (HI = mg HC/g TOC) and oxygen indices (OI = mg CO_2/g TOC) were measured. The HI versus OI (Fig. 3) and TOC versus S_2 (Fig. 4) plots are used to determine source rock quality (kerogen type) and richness. The majority of the source rocks contain Type II kerogen (Peters and Moldowan, 1993), while the higher OI values of the Bahi and Nubian Formations indicate mixed Type II-III kerogen. The hydrocarbon potential of East Sirt Basin samples ranges from fair to excellent based on S_2 and TOC (Fig. 4). The Sirte and Tagrifet Formations exhibit the best (good to excellent) hydrocarbon potential. The high values (>1.0) for the S_1 peak (free hydrocarbons) and the abnormally high PI values (>0.2) are indicative of migrated bitumen in (Baird *et al* 1996, Hallett, 2002) or contamination by drilling additives, as observed in other studies (e.g. Shaaban *et al* 2006).

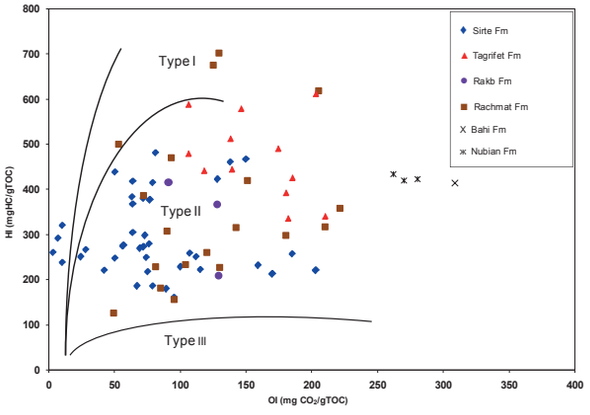


Fig. 3. Plot of hydrogen index (HI) versus oxygen index (OI) illustrating the variation of kerogen type (I, II and III) in source *rocks of the East Sirt Basin.*

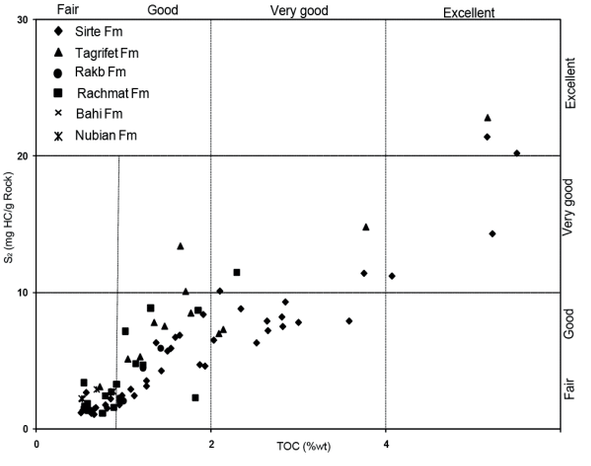


Fig. 4. Plot of Rock-Eval S2 (mg HC/g rock) versus total organic carbon (TOC, wt. %) illustrating the variation of organic richness and petroleum generation potential in source rocks of the East Sirt Basin.

Vitrinite reflectance (% R_o): Vitrinite reflectance is the most extensively used thermal maturity indicator in petroleum geochemistry (e.g. Tissot and Welte, 1984), and was used to evaluate the studied samples. These measurements show some correlation with the depths of the samples. Vitrinite reflectance data of representative samples from the deeper Sirte Formation range from 0.90 and 1.38 %R. Two samples from the deeper Rachmat Formation have %R_o of 0.81 and 0.85. Both the Sirte and Rachmat Formation samples reached the oil window (Table 2), while samples from the shallower Tagrifet, Rakb, Bahi and Nubian Formations have %R_o values ranging between 0.46 and 0.58, supporting an early to mid-stage thermal maturity (Fig. 5).

HYDROGEN AND CARBON ISOTOPIC COMPOSITION

δD of n-alkanes and isoprenoids: Fig. 6 compares the δD signatures of Pr and Ph measured in the various source rock intervals from the East Sirt Basin. Pr and Ph have been shown to become more enriched in D with increasing thermal

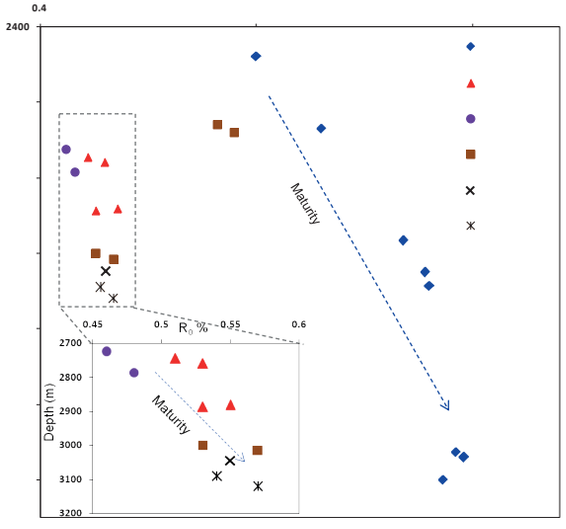


Fig. 5. Plot of vitrinite reflectance versus depth for selected source rock extracts from the East Sirt Basin.

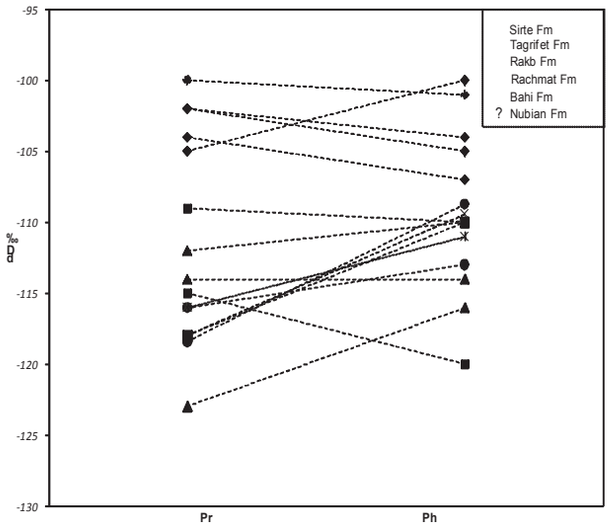


Fig. 6. Stable hydrogen isotopic compositions (δD ‰) of isoprenoid alkanes (Pr and Ph) in selected source rock extracts from the East Sirt Basin.

maturity (Dawson *et al* 2005, 2007; Pedentchouk *et al* 2006). The collected data (Table 2) indicate that δD values of isoprenoids are more positive than n-alkanes. The D enrichment in δD of Pr and Ph can attributed to H/D exchange reactions, which favour the main and minor carbons adjacent to tertiary centres (Pedentchouk *et al* 2006; Dawson *et al* 2007). Isoprenoids tend to undergo hydrogen exchange at tertiary carbons more readily than secondary or primary carbon in straight-chain *n*-alkanes. The mechanism of hydrogen exchange led to D enrichment in pr and ph has known as rearrangement of chiral centres via structural changes in pr and ph isoprenoids (Dawson *et al* 2007).

The observed enrichment of D in the Pr and Ph in these Libyan source rocks shows a strong correlation with various conventional thermal

Table 2. Vitrinite reflectance and stable hydrogen and carbon isotopic data for the source-rocks of the East Sirt Basin.

Field	Well	Formation	Depth (m)	$\%R_o$	Pr (δD‰)	Ph(δD‰)	δD‰	$\delta^{13}C$‰	ΔD‰
Galio	6C1-59	Sirte	3051-54	1.29	-100	-101	-115	-29.2	15
Galio	6C1-59	Sirte	3600-03	1.33	-105	-100	-110	-30	8
Galio	6C1-59	Sirte	3087-90	1.30	-102	-105	n.d.	n.d.	n.d.
Galio	6J1-59	Sirte	3528-31	1.36	-102	-104	-109	-30.1	6
Galio	6J1-59	Sirte	3542	1.38	n.d.	n.d.	n.d.	n.d.	n.d.
Galio	6R1-59	Sirte	2967	1.24	-104	-107	n.d.	n.d.	n.d.
Sarir-C	KK1-65	Sirte	2670	1.05	n.d.	n.d.	n.d.	n.d.	n.d.
Sarir-C	OO2-65	Sirte	2478-81	0.90	n.d.	n.d.	n.d.	n.d.	n.d.
Nafoora	M1-51	Tagrifet	2882	0.58	-123	-116	-92	-31.8	-28
Sarir-C	KK1-65	Tagrifet	2745	0.51	-114	-114	-98	-33.1	-16
Sarir-C	KK1-65	Tagrifet	2760	0.55	n.d.	n.d.	-98	-32.8	n.d
Sarir-C	OO2-65	Tagrifet	2612	0.53	-112	-110	n.d.	-32.1	n.d
Amal	B-96	Rakb	2786	0.48	-118	-109	-92	n.d.	-20
Amal	B-95	Rakb	2725	0.46	-116	-113	n.d.	n.d.	n.d.
Nafoora	M1-51	Rachmat	3015	0.57	-118	-109	-96	-30.9	-18
Nafoora	M1-51	Rachmat	3000	0.53	-109	-110	n.d.	n.d.	n.d.
Sarir-C	OO2-65	Rachmat	2681	0.85	-115	-120	-98	-31.2	22
Sarir-C	OO2-65	Rachmat	2660	0.81	n.d.	n.d.	n.d.	n.d.	n.d.
Nafoora	M1-51	Bahi	3045	0.55	-118	-109	-96	-30.7	-18
Nafoora	M1-51	Nubian	3120	0.57	n.d.	n.d.	n.d.	n.d.	n.d.
Nafoora	M1-52	Nubian	3090-93	0.54	-116	-111	-99	-31	-15

R_o= vitrinite reflectance ; δD‰ = the average of δD values of *n*-alkanes (C_{17} to C_{27}); ^{13}C‰ =the average of $\delta^{13}C$‰ values of *n*-alkanes (*n*-C_{16} to *n*-C_{27}) and ΔD‰ = Difference between average D values of Pr and Ph and average δD values of *n*-alkanes (*n*-C_{17} to *n*-C_{27}); n.d. not determined.

maturity parameters, such as % R_o. Pr and Ph in the Sirte Formation are relatively more enriched in D than isoprenoids in all other formations, having δD values ranging from -100 to -105‰ for Pr and from -100 to -104‰ for Ph. δD for the isoprenoids in the other formations range from -114 to -123‰ for Pr and -120 to -109‰ for Ph (Table 2). These δD data are consistent with the Sirte Formation being the most mature source rock of the East Sirt Basin.

The less mature rocks of the East Sirt Basin (Tagrifet, Bahi, Rakb and Rachmat Formations) contain Ph slightly more enriched in D relative to Pr (Fig. 6); possibly reflecting different sources (i.e. terrigenous plants versus algae) for Pr (cf. Dawson *et al* 2007). The *n*-alkane D profiles of these source rocks are shown in Fig. 7. The δD values of the higher-molecular-weight *n*-alkanes (C_{21}–C_{27}) from the Tagrifet, Bahi, Nubian, Rakb and Rachmat Formations are more positive (-94 to -91‰) than the lower-molecular-weight homologues in the same samples, reflecting perhaps an input to the higher *n*-alkanes from land plants. The samples from the Bahi, Nubian, Rakb, Rachmat and Tagrifet

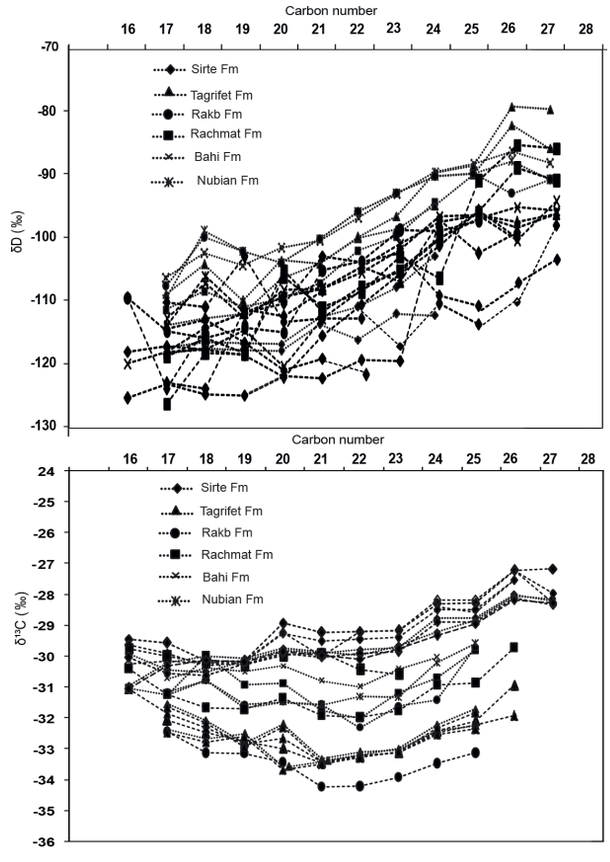


Fig. 7. Stable hydrogen isotopic (δD ‰) and stable carbon isotopic (δ13C ‰) profiles of n-alkanes in selected source-rock extracts from the East Sirt Basin.

Formations contain *n*-alkanes with average δD values from -99 to -92‰, indicating greater input of D-enriched terrigenous OM relative to the more distal (deeper) marine Sirte Formation, which has average δD for *n*-alkanes of -115‰ to -109‰. Sedimentary OM in marine source rocks typically has δD values close to -150‰ if no significant isotopic exchange has occurred during thermal maturation (Santos Neto and Hayes, 1999).

$\delta^{13}C$ of n-alkanes: The $\delta^{13}C$ values of the *n*-alkanes in the source rocks range from -29.2 to -33.1‰ (Table 2) and the *n*-alkane $\delta^{13}C$ profiles are shown in Fig. 7. Stable carbon isotope signatures of n-alkanes can be affected by many factors, such as source of OM (Hayes, 1993; Peters and Cassa, 1994) and thermal maturation (Rigby *et al* 1981; Clayton, 1991). In the Sirte Formation the average $\delta^{13}C$ values of the *n*-alkanes (C_{17}–C_{27}) are significantly heavier (-30.1 to -29.2‰) than those of the same *n*-alkanes in the other formations (-33.1 to -30.7‰). These isotopic differences could be due to differences in thermal maturation and/or source. The preferential generation and expulsion of ^{13}C-depleted hydrocarbons during source rock maturation leads to progressive enrichment of the residual kerogen in ^{13}C (Clayton, 1991). In the case of the Sirte Formation, the heavier $\delta^{13}C$ values of residual *n*-alkanes are most likely due to higher thermal maturity (Fig. 7).

MOLECULAR COMPOSITION

Thermal maturity parameters: Two well-established biomarker parameters (Peters and Moldowan, 1993, Peters *et al* 2005) were used to assess the thermal maturity of selected samples (Table 3). Ts/Ts+Tm values range from 0.41 to 0.62 and 20S/20*S*+20*R* values from 0.22 to 0.58, spanning the onset of oil generation (immature to mature). The highest maturities are displayed by the Sirte Formation in the Gialo field, in agreement with the findings of El-Alami (1996). The Sirte Formation likewise appears to be considerably more mature than other formations studied herein based on measurements of methylphenanthrene index (MPI-1) and calculated vitrinite reflectance (Rc = 0.60 MPI + 0.4: Radke and Welte, 1983). The elevated maturity of the Sirte Formation (R_c = 0.9–1%) in agreement vitrinite reflectance data (above) and from the adjacent Agedabia Trough (R_o ≈ 1.2–2%: Hallet, 2002). Although stratigraphically older, the Tagrifet, Rachmat, Rakb, Bahi and Nubian

Table 3. Geochemical parameters of thermal maturity calculated from the distribution and abundance of aliphatic biomarkers.

Field	Well	Formation	Depth (m)	Ts/Ts +T m	αααC_{29} S/S+R	C_{29} ββ/αββ + αα
Galio	6C1-59	Sirte	3051-54	0.61	0.49	0.83
Galio	6C1-59	Sirte	3600-03	0.62	0.58	1.00
Galio	6C1-59	Sirte	3087-90	0.61	0.50	n.d.
Galio	6J1-59	Sirte	3528-31	0.62	0.50	1.05
Galio	6J1-59	Sirte	3542	0.62	0.50	n.d.
Galio	5R1-59	Sirte	2967	0.58	0.46	n.d.
Sarir-C	KK1-65	Sirte	2670	0.61	0.40	0.91
Sarir-C	OO2-65	Sirte	2478-81	0.50	0.36	n.d.
Nafoora	M1-51	Tagrifet	2882	0.45	0.24	0.24
Sarir-C	KK1-65	Tagrifet	2745	0.54	0.35	0.35
Sarir-C	KK1-65	Tagrifet	2760	0.53	0.36	0.36
Sarir-C	OO2-65	Tagrifet	2612	0.46	0.22	0.22
Amal	B-96	Rakb	2786	0.41	0.24	0.24
Amal	B-95	Rakb	2725	0.39	0.17	n.d.
Nafoora	M1-51	Rachmat	3015	0.47	0.24	0.55
Nafoora	M1-51	Rachmat	3000	0.50	0.35	n.d.
Sarir-C	OO2-65	Rachmat	2681	0.58	0.36	0.58
Sarir-C	OO2-65	Rachmat	2660	0.53	0.42	n.d.
Nafoora	M1-51	Bahi	3045	0.47	0.35	0.63
Nafoora	M1-51	Nubian	3120	0.47	0.33	n.d.
Nafoora	M1-52	Nubian	3090-93	0.48	0.34	0.35

Ts/Ts+Tm= 18α (H)-22,29,30-trisnorhopane/18α(H)-22,29,30-trisnorhopane+17α(H)-22,29,30-trisnorhopane; *S*/*S*+*R*=C_{29}ααα20*S*/ C_{29}ααα20*S* + C_{29}ααα20*R*; C_{29} αββ/αββ+ααα= 5α,14β,17β-24-ethylcholstane 20*R*/ 5α,14α,17α24-ethylcholstane 20*R*.

formations within the Hameimat and Sarir Troughs (Fig. 1) are at the early stages of oil generation (R_c = 0.65–0.76%).

MOLECULAR COMPOSITION INDICATORS OF DEPOSITIONAL ENVIRONMENT.

3Ph/Ph and DBT/P values: The pristane to phytane (Ph/Ph) and dibenzothiophene to phenanthrene (DBT/P) values of the source rocks (Table 4) reveal the nature of their respective depositional settings. Their DBT/P values (0.04–0.47) are characteristic of marine shales, whereas in most samples, the Pr/Ph ratio is <1, indicating deposition under anoxic conditions. The latter are commonly associated with hypersalinity. The slightly higher Pr/Ph values (1.01–1.25) of six shales from the Sirte, Tagrifet, Rakb and Rachmat Formations (Table 4) suggest suboxic depositional conditions.

Triterpanes and steranes: The hopane, tricyclic terpane and sterane distributions of the source rocks (Fig. 8) are far from uniform, reflecting differences in the origin of their OM. For example, the relative abundance of C_{27}, C_{28} and C_{29} regular steranes vary depending on the contributions of marine or lacustrine phytoplankton, green algae and/or land plants to their kerogen (Huang and Meinshein, 1979; Volkman, 2003). The sterane distributions of most of the samples are dominated by the C_{27} homologue, usually attributed to a marine algal source. The sample

Table 4. Geochemical parameters of palaeoenvironments from the distribution and abundance of aliphatic and aromatic isoprenoids for studied formations.

Field	Well	Formation	Depth (m)	Pr/Ph	DBT/P	$C_{19}TT/C_{23}TT$	$C_{24}TeT/C_{23}TT$
Galio	6C1-59	Sirte	3051-54	0.78	0.46	0.17	0.26
Galio	6C1-59	Sirte	3600-03	0.86	0.47	0.15	0.26
Galio	6C1-59	Sirte	3087-90	1.10	0.22	n.d.	n.d.
Galio	6J1-59	Sirte	3528-31	0.68	0.36	0.08	0.35
Galio	6J1-59	Sirte	3542	0.92	0.29	0.11	0.38
Galio	6R1-59	Sirte	2967	0.92	0.27	n.d.	n.d.
Sarir-C	KK1-65	Sirte	2670	0.86	0.31	n.d.	n.d.
Sarir-C	OO2-65	Sirte	2478-81	0.77	0.13	0.10	0.28
Nafoora	M1-51	Tagrifet	2882	0.86	0.16	0.19	0.26
Sarir-C	KK1-65	Tagrifet	2745	1.13	0.19	0.1	0.31
Sarir-C	KK1-65	Tagrifet	2760	1.25	0.11	0.09	0.31
Sarir-C	OO2-65	Tagrifet	2612	0.85	0.13	0.11	0.35
Amal	B-96	Rakb	2786	1.25	0.25	0.11	0.29
Amal	B-95	Rakb	2725	1.01	0.30	n.d.	n.d.
Nafoora	M1-51	Rachmat	3015	0.70	0.13	0.17	0.29
Nafoora	M1-51	Rachmat	3000	1.12	0.11	n.d	n.d.
Sarir-C	OO2-65	Rachmat	2681	0.80	0.21	0.1	0.29
Sarir-C	OO2-65	Rachmat	2660	0.68	0.30	n.d	n.d.
Nafoora	M1-51	Bahi	3045	0.68	0.04	0.09	0.3
Nafoora	M1-51	Nubian	3120	0.68	0.28	n.d.	n.d.
Nafoora	M1-52	Nubian	3090-93	0.65	0.31	0.1	0.31

Pr= pristane/Ph= phytane; DBT= dibenzothiophene/P= phenanthrene; $C_{19}TT/ C_{23}TT= C_{19}$ tricyclic terpane /C_{19} tricyclic terpane + C_{23} tricyclic terpane; $C_{24}TeT/ C_{23}TT= C_{24}$ tetracyclic terpane /C_{24} tricyclic terpane +C_{23} tricyclic terpan *Keywords:* East Sirte

from the Tagrifet Formation in the Nafoora field is an exception, where the C_{28} sterane is co-dominant with the C_{27} and C_{29} steranes (Fig. 8). However, the Tagrifet Formation contains fossil planktonic foraminifera, bryozoans and inoceramid and rudist molluscs, clearly supporting a marine environment. A high $C_{23}/C_{19}TT$ ratio and low relative abundance of $C_{24}TeT$ are features commonly associated with marine shale and carbonate lithofacies (Aquino Neto *et al* 1983). Thus, the low C_{19} TT/ (C_{19} TT + C_{23}TT) and $C_{24}TeT/(C_{24}TT + C_{23}TT)$ in all rock samples studied (Table 4) are consistent with their interpreted marine affinity.

CONCLUSIONS

1 A variety of organic geochemical analyses were applied to set of rock extracts from the East Sirt Basin (Libya). The thermal maturity and palaeoenvironment of deposition was established using Rock-Eval pyrolysis of source rocks and biomarker ratios and compound-specific stable hydrogen and carbon isotopes of individual hydrocarbons of crude oils and source rock extracts.

2 The thermal maturities of the source rocks from the Sirte Formation were found to be

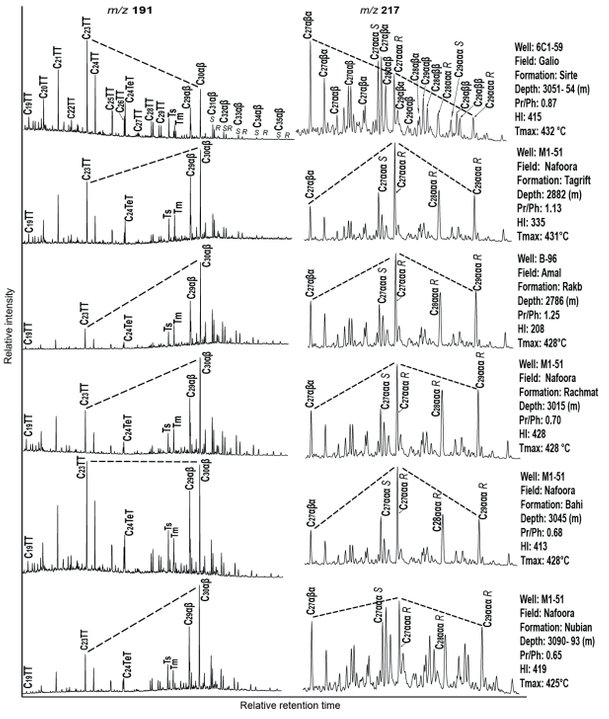


Fig. 8. Partial mass chromatograms showing distributions of tricyclic and tetracyclic terpanes and hopanes (m/z 191) and steranes (m/z 217) in various source rocks in the East Sirt Basin.

higher based on Ts/Ts+Tm (0.61 to 0.62) and $\alpha\alpha\alpha C_{29}$ 20*S*/20*S*+20*R* (0.49 to 0.58) than the Tagrifet, Rakb, Rachmat, Bahi, and Nubian formations. δD differences between *n*-alkanes and isoprenoids (Pr and Ph) are also consistent with higher levels of thermal maturity for the Sirte Formation.

3 Ph/Ph, DBT/P, triterpanes and steranes indicate anoxic to sub oxic depositional environments and variable contributions OM or from marine and lacustrine phytoplankton, green algae and/or land plants to the kerogen in the rocks.

ACKNOWLEDGMENTS

The authors thank Geoff Chidlow and Sue Wang for their assistance with GC-MS and GC-ir-MS analysis, respectively. We are grateful to the staff of the National Oil Corporation (NOC) in Tripoli and staff of the Libyan Petroleum companies (Waha, Veba and Gulf) for providing samples.

REFERENCES

Abadi, A. (2002). Tectonics of the Sirte Basin. *Unpublished PhD Dissertation*, Vrije Universiteit, Amsterdam, ITC, Enschede: p187.

Ahlbrandt, T. S. (2001). The Sirte Basin Province of Libya – Sirte-Zelten Total Petroleum System. *US Geological Survey Bulletin* 2202-F.

Aboglila, S., Grice, K., Trinajstic, K., Dawson, D., Williford, K. (2010). Use of biomarker distributions and compound specific isotopes of carbon and hydrogen to delineate hydrocarbon characteristics in the East Sirte Basin (Libya). *Organic Geochemistry* 41: 1249–1258.

Aquino Neto, F. R., Trendel, J. M., Restle, A., Connan, J., Albrecht, P. (1983). Occurrence and formation of tricyclic and tetracyclic terpanes in sediments and petroleum. In: Bjorøy, M. (Ed.), *Advances in Organic Geochemistry 1981*. John Wiley & Sons Ltd, Chichester, 659-667.

Baird, D. W., Aburawi, R. M., Bailey, N. J. L. (1996). Geohistory and petroleum in the central Sirte Basin. In: M. J. Salem, A. S. El-Hawat and A. M. Sbeta, (Eds.), *Geology of Sirt Basin* II: 3–56.

Baric, G., Spanic, D., Maricic, M. (1996). Geochemical characterization of source rocks in the NC-157 block (Zaltan platform), Sirte Basin. In: M. J. Salem, A. S. El-Hawat and A. M. Sbeta (Eds.), *The Geology of Sirt Basin*, II: 541–553.

Barr, F. T. and Weegar, A. A. (1972). Stratigraphic Nomenclature of the Sirte Basin, Libya. *Petroleum Exploration Society of Libya*, Tripoli, P.179.

Bastow, T. P., Van Aarssen, B .G. K., Lang, D. (2007). Rapid small–scale separation of saturate, aromatic and polar components in petroleum. *Organic Geochemistry* 38: 1235–1250.

Burwood, R., Redfern, J., Cope, M. (2003). Geochemical evaluation of East Sirte Basin, (Libya) petroleum systems and oil provenance. *Geological Society Special Publication*, London, 203–214.

Clayton, C. (1991). Effect of maturity on carbon isotope ratios of oils and condensates. *Organic Geochemistry* 17: 887–899.

Coward, M. P., Ries, A. C. (2003). Tectonic development of North African basins. In: T. Burnham, D. S. MacGregor, N. R. Cameron (Eds.), Petroleum Geology of Africa: New Themes and Developing Technologies, 207. *Geological Society Special Publication*, London: 61-83.

Dawson, D., Grice, K., Alexander, R. (2005). Effect of maturation on the indigenous δD signatures of individual hydrocarbons in sediments and crude oils from the Perth Basin (Western Australia). *Organic Geochemistry* 36: 95–104.

Dawson, D., Grice, K., Alexander, R., Edwards, D. (2007). The effect of source and maturity on the stable isotopic compositions of individual hydrocarbons in sediments and crude oils from the Vulcan Sub-basin, Timor Sea, Northern Australia. *Organic Geochemistry* 38: 1015–1038.

El-Alami, M. (1996). Habitat of oil in Abu Attiffel area, Sirt Basin, Libya. In: M. J. Salem, A. S. El-Hawat and A. M. Sbeta (Eds.), *The Geology of Sirt Basin* II: 337–348.

El-Alami, M., Rahouma, S., Butt, A. (1989). Hydrocarbon habitat in the Sirte Basin Northern Libya. *Petroleum Research Journal* 1: 17–28.

El-Hawat, A. S., Missallati, A. A., Bezan, A. M., Taleb, T. M., (1996). The Nubian Sandstone in Sirte Basin and its correlatives. In: M. J. Salem, A. S. El-Hawat and A. M. Sbeta (Eds.), *The Geology of Sirt Basin* II: 3–30.

Ghori, K. A. R., Mohammed, R. A. (1996). The application of petroleum generation modelling to the eastern Sirt Basin, Libya. In: M. J. Salem, A. S. El-Hawat and A. M. Sbeta (Eds.), *The Geology of Sirt Basin* II: 529–540.

Gras, R., 1996. Structural style of the southern margin of the Messlah High. In: Salem, M.J., El-Hawat, A.S., Sbeta, A.M. (Eds.), *The Geology of Sirte Basin* II. Elsevier, Amsterdam, 201–210.

Grice, K., de Mesmay, R., Glucina, A., Wang, S., (2008). An improved and rapid 5A molecular sieve method for gas chromatography isotope ratio mass spectrometry of n-alkanes (C_8-C_{30+}). *Organic Geochemistry* 39: 284-288.

Gruenwald, R. (2001). The hydrocarbon prospectivity of Lower Oligocene deposits in the Maragh Trough, SE Sirt Basin, Libya. *Jour. Pet. Geo*., 24: 213 231.

Guiraud, R., Maurin, J. C. (1991). Early Cretaceous rifts of Western and Central Africa: an overview. *Tectonophysics* 213: 153–168.

Hallett, D. (2002). Petroleum Geology of Libya. Elsevier, Amsterdam, p. 509.

Hallett, D., El-Ghoul, A. (1996). Oil and gas potential of the deep trough areas in the Sirt Basin, Libya. In: M. J. Salem, A. S. El-Hawat and A. M. Sbeta. (Eds.), *The Geology of Sirt Basin* II: 455–484.

Hayes, J. M. (1993). Factors controlling the ^{13}C contents of sedimentary organic compounds: principles and evidence. *Marine Geology* 113: 111–125

Huang, W. Y. and Meinschein, G. (1979). Sterols and ecological indicators. *Geochimica et Cosmochimica Acta*, 43: 739-745.

Kroner, A. (1993). The Pan-African belt of northeastern and eastern Africa, Madagascar, southern India, Sri Lanka and east Antarctica; Terrane amalgamation during formation of the Gondwana Supercontinent. Geoscientific research in Northeast Africa. *A. A. Balkema, Rotterdam*, Netherlands, 3–9.

Pedentchouk, N., Freeman, K. H., Harris, N. B. (2006). Different response of D values of n-alkanes, isoprenoids, and kerogen during thermal maturation. *Geochimica et Cosmochimica Acta* 70: 2063–2072.

Peters, K. E., Moldowan, J. M. (1993). The Biomarker Guide. Prentice Hall, Eaglewood Cliffs, p. 363.

Peters, K. E., Cassa, M. R. (1994). Applied source rock geochemistry. In: L. B. Magoon, W. G. Dow (Eds.). The Petroleum System-from Source to Trap. *Am. Ass. Petrol. Geol., Memoir* 60: 93–120.

Peters, K. E., Walters, C. C. and Moldowan, J. M. (2005). The Biomarker Guide. Cambridge University Press, Cambridge. P. 1151.

Radke, M. and Welte, D. H. (1983). The methylphenanthrene index (MPI): A maturity parameter based on aromatic hydrocarbons. In: M. Bjorøy (Ed.), *Advances in Organic Geochemistry* 1981. John Wiley & Sons Ltd, Chichester, 504-512.

Rigby, D., Batts, B. D., Smith, J. W. (1981). The effect of maturation on the isotopic composition of fossil fuels. *Organic Geochemistry* 3: 29–36.

Santos Neto, E. V., Hayes, J. M. (1999). Use of hydrogen and carbon stable isotopes characterizing oils from the Potiguar Basin (onshore), Northeastern Brazil. *Am. Ass. Petr. Geol., Bull*., 83: 496–518.

Shaaban, F., Lutz, R., Littke, R., Bueker, C. and Odisho, K. (2006). Source rock evaluation and basin modelling in NE Egypt (NE Nile Delta and Northern Sinai). *Jour. Petrole.* Geo., 29: 103–124.

Tissot, B. P., Welte, D. H. (1984). Petroleum formation and occurrence. Springer-Verlag, Berlin, p 699 .

Volkman, J. K. (2003). Sterols in microorganisms. *Applied Microbiology and Biotechnology*, 60: 495–506.

Effect of Pore Geometry on Reservoir Rock Properties

Hassan Sbiga*

Abstract: This study has been undertaken in three oil fields (A-Libya, B-Libya, and C-Libya) in sirte basin located in Libya. Nubian sandstone Formation is the main reservoir in the studied oil fields. Laboratory measurements methods were applied on the core samples that were selected from three different fields of Nubian Sandstone. Some of these measurements were conducted in Libyan Petroleum Institute (LPI Tripoli-Libya) laboratories in order to determine the resistivity parameters of the central graben reservoir cores and to investigate the effect of rock hetrogeneity and wettability on the resistivity parameters of Nubian sandstone reservoir rocks. The pore size distribution was estimated from generated capillary pressure curves. The samples belonged to Nubian sandstone, Sirt basin were selected to perform formation resistivity factor measurements.

The Pore size distribution and type of pores were calculated from mercury injection capillary pressure data. The results indicated that changes had been observed in formation resistivity factor and cementation exponent when overburden pressure was applied (slightly increases in cementation exponent with increasing O.B.P). Wettability played an important role in determining the fluid movement, distribution and electrical conduction during desaturation processes. Resistivity index effect has been observed after wettability measurement showing oil-wet tendency.

From the results obtained, a good relation between resistivity and type of pores (macro and micro pore system) was observed. When oil begins to penetrate micro-pore systems during the measurements, a significant change in slope of the resistivity index relationship occurs.

Keywords: Nubian Sandstone, resistivity, Heterogeneity, Micro-porosity, Electrical properties.

INTRODUCTION

The amount of hydrocarbon reserves is one of the most important parameters in the decision making process in developing a reservoir.

The interpretation of logging data is based on Archie's law. Electrical logging is the most widely used method of identifying hydrocarbon intervals in wellbore. Standard method of relating oil saturation in clay free reservoirs to electrical resistivity is based on Archie saturation equation (Archie 1942):

$$\mathrm{RI} = \frac{\mathrm{Rt}}{\mathrm{Ro}} = \mathrm{Sw}^{-n} \quad (1)$$

Where the resistivity index, *RI*, is equal to the ratio of the resistivity of the sample (*Rt*) at brine saturation (*Sw*) over the resistivity of the sample at one hundred percent brine saturation (R_o). The resistivity index is related to the saturation of the sample and the saturation exponent (***n***). The saturation exponent must be determined by experimental core analysis. The standard technique for determining the saturation exponent involves measurements in cleaned cores, usually with air as the non-wetting phase and brine phases. Thisair/brine system is only representative of the drainage conditions in strongly water wet situations. When oil displaced by water, for instance during water flooding, different distributions of fluid may prevail at the pore scale due to hysteresis effects controlled by pore geometries, initial saturation and wettability distribution at the pore scale. When the rock is compacted as a result of overburden pressure, the matrix is under stress and porosity decreases as a result of compaction, cementation factor will change. ***Wyble*** (***1958***) found a systematic decrease in the rock conductivity and an increase in formation factor as the overburden pressure increased over the range of 0 to 3500 psi using core samples. In the study carried out by Wyble, an increase in formation factor of up to **6.6** percent of original value measured at zero overburden pressure. Cementation exponent of one of the samples studied was increased from 1.87 to 2.04 as a result

*TOG2012, Researcher at Libyan Petroleum Institute, Email: hasanespiga@yahoo.com, Tel: 092 559 7511

of increasing the pressure up to 5000 psi. Porosity of sedimentary rocks can be classified according to their pore size distribution as macro- and micro-porosity. Vuggy and fracture porosities are characteristics of macro-porosity because large pore geometries are associated with vugs and fractures.

Pore system associated with macro-porosity has an average pore diameter greater than 1/16 mm (Pittman, 1971) where most of the hydrocarbon volume accumulates. Permeability is strongly dependent on the amount of macro-porosity. Micro-porosity is associated with pores whose diameter is less than 1/16 mm (Pittman, 1971). Micro-porous system is characterised by a high capillary pressure, which tends to retain high amount of irreducible water resulting in high formation electrical conductivity (low resistivity).

Wettability plays a major role in controlling the distribution of fluids within the pore space inside a rock. Keller (1953), Presented evidence that saturation exponent could be substantially different from 2.0. He found that Archie's saturation exponent (*n*) varies from 1.5 to 11.7 for the same rock, depending on how cores were treated. For the same water saturation, resistivity of an oil reservoir can vary thousand times for different wetting conditions. The wettability of sandstone cores was altered from water wet to oil wet conditions by using various chemical treatments. Keller concluded that the wettability played a great role in the fluid distribution within the rock space. By changing the relative position of the conducting fluid with respect to the rock surface, the electric behaviour of fluid filled sandstone would also change. A measurement of capillary pressure curves as a means of determining pore size distribution was first suggested by Washburn (1921). This principle was fairly accepted and the majority of the pore size distribution measurements have been determined by the mercury injection procedure.

OBJECTIVE OF THE STUDY

- Investigate the effect of rock heterogeneity and wettability on resistivity parameters of sandstone reservoir rocks, Nubian sandstone.
- Quantify experimentally pore and porosity types.
- Investigate the effect electric properties on micro-porosity rocks

METGHODOLOGY

The clean, dry samples were subjected to various analyses to determine porosity, permeability and grain density values where possible. The equations used to calculate porosity and permeability as follows:

$$\phi = \frac{V_P}{V_b} = \frac{V_P}{V_P + V_g} \quad (2)$$

$$Kg = \frac{2000 \times Pa \times Q \times \mu_g \times L}{(P1^2 - P2^2) \times A} \quad (3)$$

The samples belong to Nubian sandstone from three oil fields (Table 1); Sirt basins were selected to perform formation resistivity factor measurements.

Formation resistivity factor is calculated as the ratio of the sample resistivity to the resistivity of the water saturating it. The formation resistivity factor of a group of samples is plotted versus their porosities on log-log graph paper. The slope of the best fit line is the value of the cementation factor, "*m*" and the intercept is the value of, "*a*"

$$FF = \frac{a}{\phi^m} \quad (4)$$

The previous samples were used for the formation resistivity factor measurements at room conditions and scheduled for formation factor testing at overburden pressure (1000- 5000 psi), and formation resistivity index test either.

The wettability measurement (Amott method), was conducted on the same samples, after that the samples were selected to perform capillary pressure measurement. Mercury injection offers an alternative system for the study of capillary pressure.

Table 1. Porosity and Permeability valuesof the studied wells.

Samples#	Well Name	Ø (%)	K(mD)
03	A1-Libya	10.39	337.5
10	A1-Libya	9.01	34.11
15	A3-Libya	12.17	12.55
18	B1-Libya	14.59	1146
24	A3-Libya	8.01	9.910
29	C2-Libya	17.38	69.86
41	C1-Libya	15.34	660.4
42	A3-Libya	11.71	4.901
47	C2-Libya	17.91	279.7
53	A1-Libya	11.16	297.7
83	A2-Libya	9.56	27.73
123	A2-Libya	12.76	118.1

Mercury injection method entails injecting mercury into a clean dry sample and monitoring the injection pressure and the amount of mercury injected into the rock sample.

Pore size distribution can be calculated from mercury injection capillary pressure data; however, a broad range of pore size and type is covered by mercury injection capillary pressure. The pore throat radius is calculated as:

$$r_P = \frac{2\sigma\cos\theta}{P_C} \quad (5)$$

EXPERIMENTAL MEASURMENTS

Laboratory measurements methods were applied on the core samples that were selected from three different fields of Nubian Sandstone (Fig. 1) Some of these measurements were conducted in Libyan Petroleum Institute (LPI Tripoli-Libya) laboratories in order to determine the resistivity parameters of the central graben reservoir cores and to investigate the effect of rock hetrogeneity and wettability on the resistivity parameters of Nubian sandstone reservoir rocks.

Capillary pressure curves have been generated and the pore size distribution estimated.

RESULTS AND DISCUSSION

Twelve Sandstone core samples were selected from three oil fields (six wells) had porosities between 8.01-17.91% and permeability range from 4.90mD to 1146 mD are presented in Table 1 while the other properties such as formation resistivity factor, porosity and cementation exponent for the same samples were measured and tabulated in Table 2.

In the measured cores a well-defined relationship exists between formation resistivity factor and porosity. The formation resistivity factor was best fit to Archie's equation so that the coefficient (a) and cementation factor were determined. The data was fit to Archie equation by assuming a=1, and the value of m was calculated for each sample. The average cementation factor for all the core samples of Nubian sandstone was calculated from slope of the best fit straight line through the points. The average value of cementation factor was 1.69 and the correlation coefficient, R^2, was 1.0. In this study, both formation resistivity factor (***FF***) and cementation factor (***m***) were found increase with confining pressure for the Nubian sandstone samples.

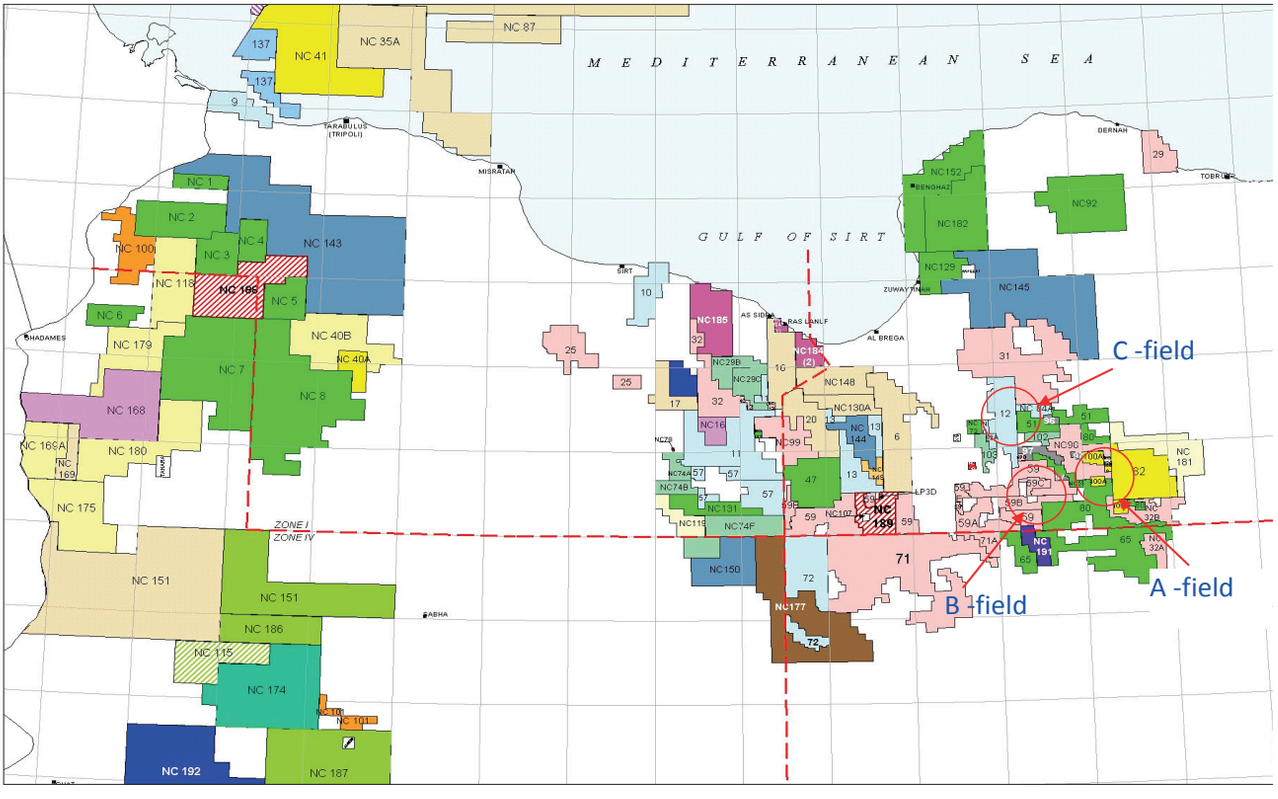


Fig. 1. Illustrate location oil fields proposed in this study

Table 2. Porosity, formation resistivity factor and cementation exponent of Nubian sandstone core samples at ambient conditions

Sample #	Porosity (%)	Formation res. Factor (F.F)	Cementation exponent "m"
03	10.39	41.6	1.65
10	9.01	52.8	1.65
15	12.17	44.6	1.80
18	14.59	23.9	1.65
24	8.01	60.4	1.62
29	17.38	20.3	1.72
41	15.34	23.3	1.68
42	11.71	41.8	1.74
47	17.91	20.0	1.74
53	11.16	36.8	1.64
83	9.56	59.0	1.74

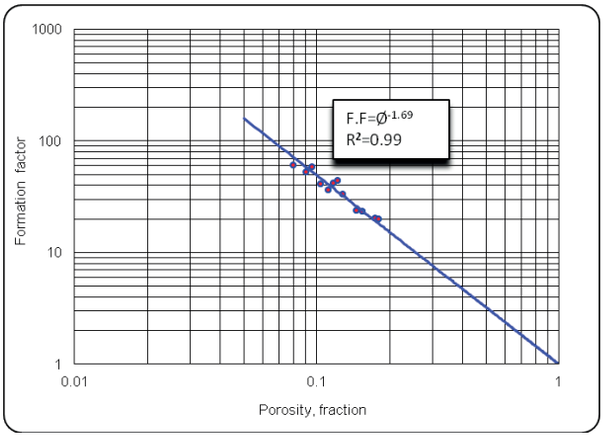


Fig. 2. Porosity versus formation resistivity factor at ambient conditions

Table 3 and Fig. 3 displaying the experimental results of the effect of overburden pressure on cementation factor. These results indicate that the cementation factor (**m**) changes at various confining pressure from 1000 to 5000 psi and the rock is compacted as a result of overburden pressure, the matrix is under stress and porosity decreases as a result of compaction , therefore, cementation factor will change.

Wettability was measured for the same samples which taken from Nubian sandstone; data in Table 4 show the results of saturation exponent (***n***) before and after wettability measurement.

(Fig. 4) shows the relation between resistivity index and water saturation before and after

Table 3. Cementation factor values at overburden pressure for the samples

Overburden pressure psi	Cementation exponent (m)
1000	1.71
2000	1.72
3000	1.74
4000	1.75
5000	1.76

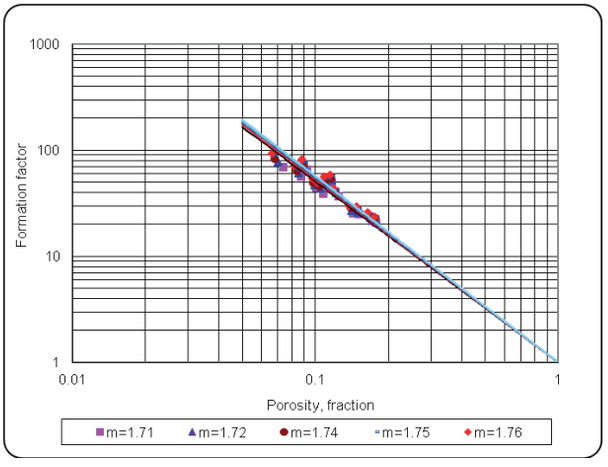


Fig. 3. Porosity versus formation resistivity factor at different overburden pressures

Table 4. Archie's saturation exponent values before and after wettability measurement

Sample #	Well Name	Saturation Exponent(n) Before wettability	Saturation Exponent(n) After wettability
03	A1-Libya	1.39	2.39
10	A1-Libya	1.75	2.60
15	A3-Libya	2.06	2.79
18	B1-Libya	1.76	2.65
24	A3-Libya	1.93	2.18
29	C2-Libya	1.79	2.59
41	C1-Libya	1.87	2.50
42	A3-Libya	2.18	2.86
47	C2-Libya	1.91	2.65
53	A1-Libya	1.78	2.43
83	A2-Libya	1.97	2.49
123	A2-Libya	1.73	2.22

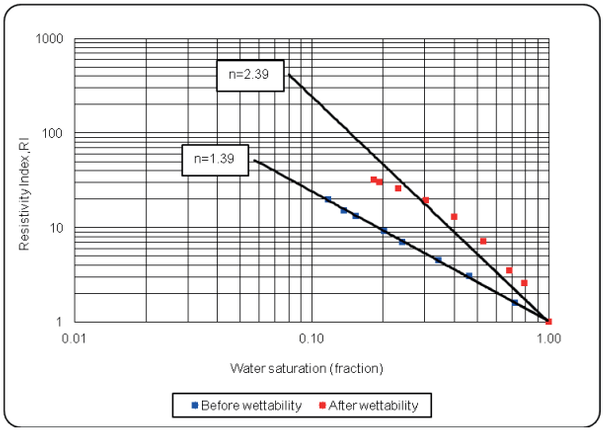


Fig. 4. Resistivity index versus water saturation before and after wettability test of sample # 3

wettability for sample #**3.** The Saturation exponent before wettability measurement was **1.39,** When wettability measurement conducted on the sample, the sample imbibed oil (tendency to oil wet), so the saturation exponent increased to **2.39**. However, slightly higher saturation exponent was obtained. The results indicate that the effect of wettability on saturation exponent (***n***) is more significant in second stage (after restoration).The increase in resistivity and saturation exponent in oil wet cores compared to water wet cores explained by (Anderson, 1986). In oil wet core, the wetting phase (oil) tends to occupy the smaller pores and to contact the majority of rock surface, while the non-wetting phase (brine) is normally located at the centre of the large pores. A fraction of the non-wetting phase (especially at low brine saturation) become disconnected and surrounded by oil which acts as an insulator to the flow of electric current. The insulation of this portion of brine prevent it from contributing to the flow of electric current and hence lead to a higher values of saturation exponent.

Fig. 5 shows the resistivity index versus water saturation and mercury saturation capillary pressure curves of sandstone sample-**3**. Excellent relation between resistivity and pore type system was observed. Note that the saturation where mercury penetration into micro-porosity occurs, a significant change in slope of the relationship between resistivity index and brine saturation of rocks containing micro-porosity as well. The change in slope may be due to micro-pores/irregular surfaces through these samples. The reason is that, as oil saturation increases, first the resistivity is dominated by the large pore network. Water saturation is still high because micro-pores hold up large water volume, high apparent saturation exponent results. Then as capillary pressure increase sufficiently to penetrate the micro- pores, water drain from micro-pores with very little influence on resistivity, then saturation exponent (***n***) decreases.

CONCLUSIONS

- The results showed that changes had been observed in formation resistivity factor and cementation exponent when overburden pressure was applied (slightly increases in cementation exponent with increasing O.B.P).
- Wettability played an important role in determining the fluid movement, distribution and electrical conduction during desaturation processes. i.e. Samples with an oil-wet tendency, for example, sample#3 have higher irreducible brine saturation and higher Archie saturation exponent values than samples with uniform water-wet surface.
- Resistivity index effect has been observed after wettability measurement showing oil-wet tendency.

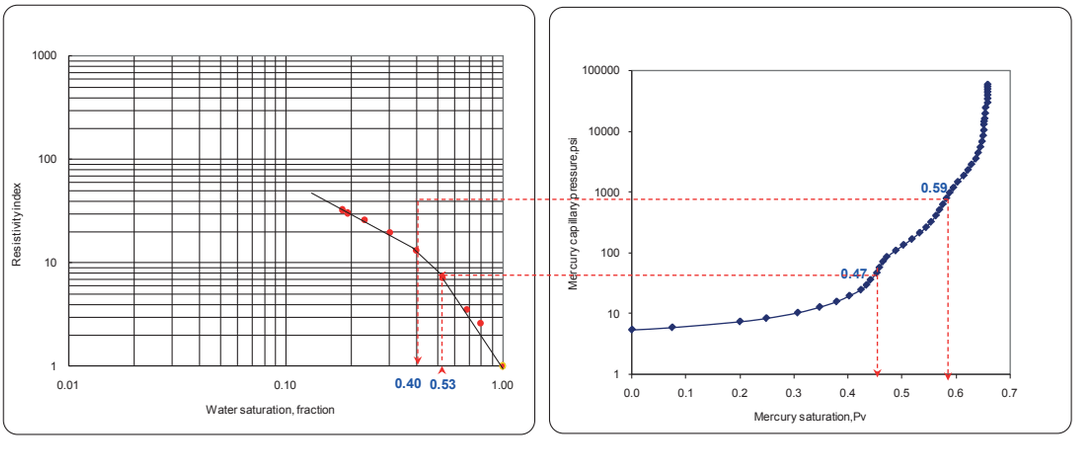


Fig. 5. Relation between resistivity and type of pore system of sample # 3

- From the results obtained, a good relation between resistivity and type of pores (macro and micro pore system) was observed. When oil begins to penetrate micro-pore systems in measurements of resistivity index versus brine saturation, a significant change in slope of the resistivity index relationship occurs.

Nomenclature

a = A constant in Archie's equation
A = Cross-Sectional area, cm^2
FF = Formation resistivity factor.
K = Permeability, mD
L = Length, cm
m = Cementation factor, dimensionless
n = Archie's saturation exponent.
P1 = Upstream Pressure, atm
P2 = Downstream Pressure, atm
Pa = Atmospheric pressure, atm
Pc = Capillary pressure, psia
ΔP = Pressure differential, atm
Q = Volumetric flow rate, cc/sec
r_p = Pore throat radius, μm
R_w = Water resistivity, Ω.m
R_t = True resistivity, Ω.m
R_o = Rock resistivity, Ω.m
RI = Resistivity index, dimensionless
S_w = Water saturation, fraction
V_p = Pore volume, cc
V_b = Bulk volume, cc
V_g = Grain volume, cc
Ø = Fractional porosity
q = Contact angle, degree
μ = Fluid viscosity, cp
s = Interfacial tension, dyne/cm

ACKNOWLEDGEMENTS

I would like to take this opportunity to thank the people that have helped me to this work. The author acknowledges very much to Proff. David Potter, who patiently supervised the evolution of my work. He provided me with the invaluable iacademic advice, excellent guidance, endless assistance, moral support and critical review that led to the completion of my work. I wish also to express my sincere thanks to Libyan Petroleum Institute for providing the necessary data.

REFERENCES

Anderson, W. G. (1986). Wettability Literature Survey- Part 3: The Effect of Wettability on Electrical Properties of Porous Media. *JPT*: 1371-1378.

Archie, G. E. (1942). The Electrical Resistivity Log As An Aid in Determining Some Reservoir Characteristics. *Trans. AIME,* V. 146: 54-62.

Burdine, N. T., Gournay, L. S., and Reichertz, P. P. (1950): Pore Size Distribution of Petroleum Reservoir Rocks. *Trans. AIME,* V. 189: 195-204.

Keller G. V. (1953). Effect of Wettability on Electrical Resistivity of Sand. *Oil and Gas Journal:* 62-65.

Swanson, B. F. (1985). Microporosity in Reservoir Rocks: Its Measurements and Influence on Electrical Resistivity. *Trans. SPWLA, 26th Ann. Logg. Symp*: 17-20.

Washburn, E. W. (1921). Note on A Method of Determining the Distribution of Pore Size in a Porous Material. *Proceedings of the National Academy of Science,* V. 7: 115-116

Wyble, D. O. (1958). Effect of Applied pressure on the Conductivity, Porosity, and Permeability of Sandstones. *Trans.AIME,* V. 213: 430-432

Log Derived Saturation Functions for Giant Carbonate Reservoirs in the Middle East

Dr. Tawfic A. Obeida*

Abstract: Fluid saturation distribution at initial reservoir conditions is vital for calculation of original oil in place (STOOIP) and reservoir simulation (dynamic models). It is a critical step in model initialization, since the subsequent step (quality of history matching) is largely dependent on the initial fluid distribution at time zero.

In many reservoirs there are limited or no SCAL (drainage capillary pressure) data available and in many cases, the available limited SCAL data has poor quality and subjective plug selection. However, log-data (open hole logs, OHL) and routine core analysis (porosity and permeability measurements) are usually more available.

The proposed method combines OHL and routine core analysis (RCA) to derive saturation functions for carbonate reservoirs with complex pore structure.

The proposed method uses a multi-regression technique to relate water saturation to height above FWL and rock quality index (RQI) for each reservoir rock type (RRT).

This method already been tested in carbonate reservoirs such as Shuaiba reservoir and Thamama-group formations.

This study used 58 core wells penetrating Thamama reservoir with permeability measurements covering six petrophysical groups. The comparison results show a good match between the calculated initial water saturation (Swi) from the dynamic model. The STOOIP calculations indicated good agreement (within 3% difference) between the dynamic and static models.

Keywords: Fluid Saturation, Reservoir Simulation, SCAL, Dynamic Model, Static Model.

INRODUCTION

Saturation functions are important and they dictate the initial fluid distribution in the reservoir. STOOIP calculation and future reserves are highly dependent on the initial oil saturation distribution at time zero. During geological time, oil migrates into geological traps and displaces the connate water which was filling the rock pore space (drainage process). The oil distributes itself within the pore space depends in many factors; height above free-water level (FWL), pore-through size, charging history, porosity, permeability and mineralogy. Unfortunately, in our reservoir models include only porosity and permeability as reservoir properties; the FWL can be calculated from depth. Other parameters are not included in the reservoir model. Historically, there are two main sources to generate saturation functions:

1 Laboratory measurements (SCAL) to establish drainage capillary pressure curve (Pc) per reservoir rock type from several plugs covering wide ranges of porosity and permeability.
2 Generate saturation function from open-hole logs (saturation-height function).

Both methods using deferent averaging methods to come up with single "average" Pc curve per RRT. These average curves used as input SCAL data in the dynamic models.

These average curves assume the water saturation is a function only of height above FWL. However, the log water saturation shows different Sw values at a given height per RRT as shown in Fig 1. That is why using a single Pc curve not be able to match initial Sw at different locations in the reservoir for a given RRT. Since a single Pc curve reflects the changes in Sw due to change in height only.

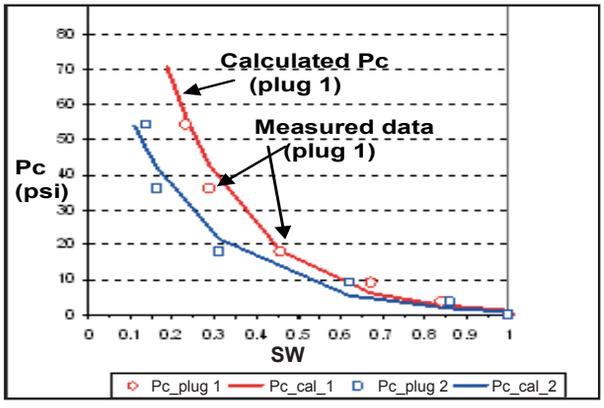


Fig. 1. Log water saturation versus height above FWL for RRT1

* ADCO, Abu Dhabi, UAE. Tawfic_obeida@yahoo.com

METHOD

The proposed method relates the initial Sw distribution to height and other reservoir properties such as porosity and permeability.

The rock quality index (RQI) is defined using porosity and permeability as shown in equation 1.

$$RQI = 0.0314\sqrt{\frac{k}{\phi}} \quad (1)$$

Where: k = permeability in mD and ϕ = porosity (fraction).

Multi-regression technique was used to relate Swi to height (H) and RQI as shown in equation 2.

$$RQI(1 - Swi_{\log}) = a + bRQI + cLn(H) \quad (2)$$

Where: a, b and c are regression parameters, they are constants for a given RRT.

H = height above FWL in feet.

The log data was filtered by RRT and all Swi data which was affected by water injection was removed to ensure that all the regression data is at initial reservoir conductions. The multi-regression was performed using spread-sheet software. To evaluate the regression quality cross-plot of the left-hand side (LHS) of equation 2 versus the right-hand side (RHS) of equation 2 were plotted. R^2 was reported for quality check. Equation 2 can be solved for H as shown in equation 3.

$$H = Exp\left\{\frac{1}{c}\left[RQI(1 - Swi) - bRQI - a\right]\right\} \quad (3)$$

The height H above FWL can be converted to capillary pressure using equation 4.

$$P_c = 0.433 * H * (\rho_w - \rho_o) \quad (4)$$

Where: ρ_w = density of water and ρ_o = density of oil.

For a given reservoir rock type or petrophysical group, if the RQI is known, then Pc can be calculated at different ranges of water saturation.

Using simple statistical methods the mean RQI can be calculated for a given rock type or petrophysical group, then from equation 3 and 4 to calculate H and Pc using mean RQI.

SCAL data was used to validate this approach which will be shown in the validation section of this paper.

The capillary pressure also can be converted to J-function as shown in equation 5.

$$J(S_w) = \frac{0.2166}{\sigma \cos\theta}\sqrt{\frac{K}{\phi}}\ Pc \quad (5)$$

Where σ = oil-water interfacial tension (dyne/cm) and θ = oil-water contact angle.

Combining equation 1 and 5, an "average" J-function can be expressed in terms of mean RQI and Pc calculated using mean RQI as shown in equation 6.

$$\overline{J(S_w)} = \frac{6.898}{\sigma \cos\theta}\left|RQI\right|_{mean} * \left|Pc\right|_{mean} \quad (6)$$

The J-function in equation 6 is the average J-function for a given RRT or petrophysical group, since it is calculated using mean RQI and mean Pc. The average J-function was used as input saturation function in the simulator for a given RRT. This method requires only one average J-function for each RRT.

Calculation of Capillary Pressure: The simulator calculates the capillary pressure after the rescaling of the average J-function according to the porosity and permeability of each grid-cell. That is the reason; the average J-function was used as an input in the dynamic model instead of normal drainge Pc curve. The simulator would not rescale input Pc. For each RRT (SATNUM), the simulator will use the average J-function for this RRT, the will calculate Pc after rescaling as shown in equation 7.

$$P_c(S_w) = \frac{\sigma \cos\theta}{0.2166}\ \overline{JF} * \sqrt{\frac{\phi}{K}}\Bigg|_{grid-cell} \quad (7)$$

The Pc calculated from equation 7 is rescaled according to $\sqrt{\frac{\phi}{k}}$ of the grid cell in the dynamic model and thus change the value of Sw accordingly. So the calculated Sw is a function of height H and cell property (porosity and permeability). However, the Sw calculated from a single Pc curve is only a function of height.

Validation of the proposed Method: Validation of proposed method was done in two stages, first stage compare the results of the proposed method (calculated Pc) with SCAL data (brine-oil Pc data at reservoir conditions) for different plugs. The second stage involves comparisons of water saturation from log data versus dynamic model results.

Comparisons with SCAL Data: Even though matching laboratory SCAL data is not an objective of this work. However, SCAL comparison is used

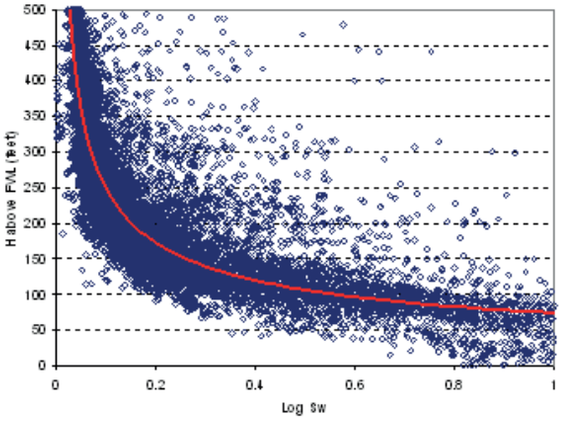


Fig. 2. Pc versus Swi comparing measured and calculated

as first stage validation of the proposed method. The calculated Pc was used to compare with oil/brine primary drainage Pc from porous-plate at reservoir conditions. For each plug sample RQI was calculated from porosity and permeability of core plug. The core samples used for comparison belong to one dominated RRT. Fig. 2 show the comparison results. The blue squares represent the laboratory measured data, the blue dotted line is the power fit of the laboratory data, the red circles represent the calculated Pc by the proposed method and the red curve is the power fit of the calculated data. All these figures indicated good agreement between the measured data and calculated values.

Comparisons with Open Hole Logs: Matching initial water saturation (Swi) from open-hole logs is our main objective of this work. Because the quality of this match has a major impact on STOOIP calculations and all the subsequent stages (history matching and predictions) coming after dynamic model initialization. All wells used for Swi comparisons should be screened to make sure all open-hole logs are reflecting Swi and not affected by injected water.

Initial water saturation match from Crest to Flank: Even though many early drilled wells are located in the crest area. However, it is important to select key wells covering the crest and flank reservoir regions, to ensure the Swi quality match. Flank wells usually are more challenging to match Swi from logs since they are drilled in the transition zone. The saturation functions should reflect the change in Swi from crest to flank before starting the history match stage. Figs. 3, 4 and 5 show initial water saturation

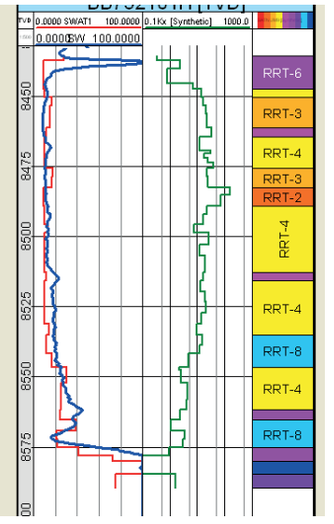


Fig. 3. Swi comparisons for crest well

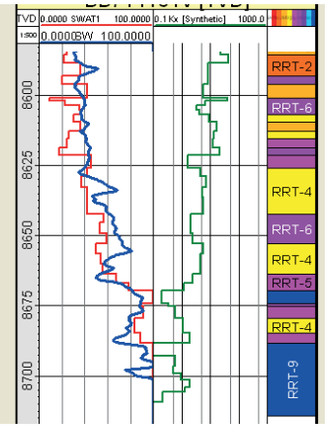


Fig. 4. Swi comparisons for mid-flank well

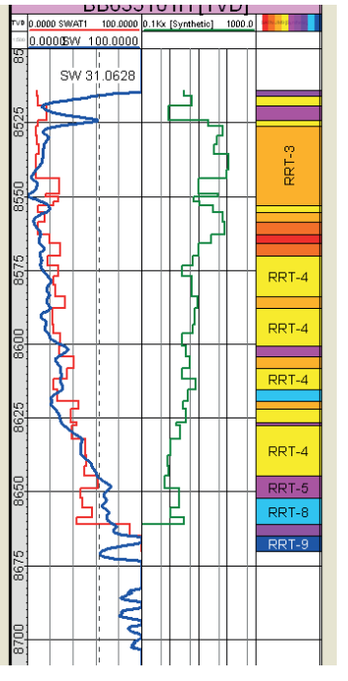


Fig. 5. Swi comparisons for flank well

match of three wells, the first well located in the crest area, the second located in mid-flank area and the third well is located in the flank area (transition zone). Fig. 3 show Swi comparison (first track) between log-Swi (blue curve) and model Swi (red curve), the second track shows permeability values (range from 0.1 to 1000 mD) and the third track shows reservoir rock type (RRT). Fig. 4 shows similar comparisons for the mid-flank well which also shows transition zone behaviour in the lower part of Swi log. Fig. 5 shows Swi comparisons for flank well.

***Limitations of the proposed method**:* The proposed method depends on permeability predictions in un-cored wells, if the model contains a good permeability predictions using neural-network for example, yield a better calculation of initial water saturations. Otherwise, the Swi calculations are not reliable. For such reservoirs where permeability data is limited or not available, a mitigation method could be used to replace the RQI variable in equation 2 with porosity and perform a similar regression. Then capillary pressure functions can be generated at different porosity ranges for a given reservoir rock type.

CONCLUSIONS

A robust method was developed to generate log-derived capillary pressure and J-functions and calculate the initial water saturation in a giant complex carbonate reservoir better than these industry standard methods. This method maybe utilized if a limited or no SCAL data is available. The limitation of the proposed method is its dependency on log-derived permeability data.

ACKNOWLEDGEMENT

The authors would like to acknowledge Abu Dhabi for Onshore Oil Operations (ADCO) for the permission and support to publish this work.

REFERENCES

Alger, R. P., Luffel, D. L. and Truman, R .B. (1989). New Unified Method of Integrating Core Capillary Pressure Data with Well logs. *SPE Formation Evaluation,* 16793: 145-152.

Amaefule, J. O., Altunbay, M., Djebbar, T., Kersey, D. and Keen, D. K. (1993). Enhanced Reservoir Description: Using Core and Log Data to Identify Hydraulic (Flow) Units and Predict Permeability in Uncored Intervals/ Wells. *SPE* 26436: 1-16.

Badarinadh, V., Suryanarayana, K., Yousef, F. Z., Sahouh, K., Valle, A. (2002). Log-Derived Permeability in a Heterogeneous Carbonate Reservoir of Middle East, Abu Dhabi, Using Artificial Neural Network. *SPE* 74345, IPCEM, Mexico, February.

Predication of Shear Velocity at Shaly Sand Reservoir Rock

Bahia M. Ben Ghawar* and Fathi S. Elburas**

Abstract: The magnitude of shear velocity (Vs) in geomechanical rocks properties leads many of petrophysics and geophysics to use and investigate simple and accurate technique for it, especially when this parameter is not measured by sonic tools. If there are no core samples available for calibration, empirical relations could be used, that based on measurable physical properties. The results emphasize the importance of local calibration before one utilizes any of the empirical relationships presented. During this study several trials, were carried out aimed to predicate shear velocity in shaly sand reservoir of late Jurassic to Late Cretaceous at southeast of Sirt Basin, Libya, by using gamma ray, compressional travel time and density logs. Therefore, a new approach by modified derived Poisson's Ratio Equation for shaly sand is introduced as an important part of shear velocity determination. This modified equation design upon deeper, highly compacted and cemented sandstone has a Poisson's ratio values range between (0.18 – 0.20), which is fairly similar to the studied reservoir condition.

Keywords: Gamma Ray; compressional travel time; porosity; bulk density.

INTRODUCTION

Several indirect methods have been used to estimate shear velocity (Vs) from full wave using acoustic logs. These methods include Stoneley wave velocity and inversion of refracted P-wave amplitude.

Historically, the primary use of the sonic log in reservoir engineering was identification of porosity, cement evaluation, mechanical properties, and formation velocities for seismic studies. This parameter Vs is an important tool to calculate rocks mechanical properties. Several techniques were published by many authors to estimate the shear velocity. Therefore, the enhancing, accuracy and reliability of the shear velocity was the main objective through this research.

Where the predication of shear velocity (Vs), for shaly sand reservoir were tested in southeast Sirt Basin, this reservoir is composed of shaly sand deposited during early rifting stages of basin formation in Late Jurassic to Late Cretaceous. The subdivided of upper part of studied (intervals) zone were subdivided according to the presence of shale layer and unknown distribution of shale contents through these zone(s). These determination and modification of the predication shear velocity depend on wireline log data, if the ultrasonic or dipole shear tools and core samples are not available. Consequently, by disclose method using shaliness index to compute Poisson's Ratio (PR) which is used to predicate shear velocity. In addition, application and comparative with published wireline log data were conduct to verify this approach. Finally, this technique is the most important requirements for an improved, accurate, simple, and economic process to determine this rock property.

There are many studies aimed to predicate the shear velocity for different rock type. Mason's (1984) introduced an approach for calculating formation S-wave velocity; was extremely dependent upon mineral composition and an idealized table of P-wave/S-wave velocity ratios. Castagna *et al* (1985) studied the relationships between compressional-wave and shear-wave velocities in elastic silicate rocks. They demonstrate simple systematic relationships between compressional and shear wave velocities. For water-saturated elastic silicate rocks, shear wave velocity is approximately linearly related to compressional wave velocity and the compressional-to-shear velocity ratio decreases with increasing compressional velocity. The results of the relationships established between Vp and Vs are

*Faculty of Engineering, Geological Engineering Department,
**Faculty of Sciences, Geophysics Department
University of Tripoli, Libya
gloriamuftah@yahoo.com; abuoras@yahoo.com

then applied to calculations of rock dynamic module. The ratio Vp/Vs is used to determine petrophysical properties. It is normally a ratio ranges from 1.4 to 2.5, although examples exist of the ratio reaching values as high as 4.0 in unconsolidated sandstones. Brie *et al* (1995); proposed the same concept of (Vp/Vs) ratio versus ΔT cross plot was intended to describe the effect of the pore fluid on the acoustic properties of the rock.

Crain's (2000) through his publication presents the main equations of elastic constants of rocks which were defined by the Wood-Biot-Gassman equations. These equations depend mainly on wire line log data.

Widarsono *et al* (2001) developed a new approach for the estimation of the elastic properties of clastic rocks in boreholes with limited log suites.

In recent studies by Vernik and Bahret (2002) related the shear and compressional velocities to built petrofacies classification with 3-D seismic inversion in deepwater turbidities reservoir.

Statistical method is presented to predict (Vs) from wireline log data in carbonate rocks introduced by Eskandari *et al* (2003).

METHODOLOGY

Elasticity is a property of matter, which causes it to resist deformation in volume or shape. Poisson's Ratio is an important elastic constant, which depend on the Shear and Compressional waves. When shear travel time is not known, which is the case in the vast majority of older wells, a value for Poisson's ratio (PR) can be estimated in shaly sand by:

$$PR = 0.125 * Vsh + 0.2 \quad (1)$$

(Crain's, 2000).

Then, the shear velocity could be calculated by:

$$\mathbf{Vs} = \frac{Vp}{\sqrt{(1 - PR) \div (0.5 - PR)}} \quad (2)$$

The two formulas are depending on the shale content and compressional sonic travel time (ΔTc). The shale content (Vsh) could be computed by many methods, through this reservoir, Gamma Ray log is the main data for its estimation.

Castagna *et al* (1985) and Han *et al* (1986) demonstrated linear relationships between compressional wave velocity Vp (km/s) and shear wave velocity Vs (km/s), see Fig. 1.

$$Vp = 5.81 - 9.42\ Ø - 2.21\ Vsh \quad (3)$$

$$Vs = 3.89 - 7.07\ Ø - 2.04\ Vsh \quad (4)$$

Where fractional porosity (Ø), and fractional clay content (Vsh) for elastic silicate rocks.

The shear wave velocity can be calculated from Christensen's equation as illustrated below; where Entwisled and McCann (1990) considered this equation in some detail and showed that it gives an over-estimate of the shear wave velocity in mud rocks and soft sediments. Indeed this equation gives over estimation of shear velocity values as illustrated in (Fig. 2).

$$\mathbf{Vs} = Vp\left[1 - 1.15\left(\frac{1/\rho + 1/\rho^3}{e^{1/\rho}}\right)\right]^{3/2} \quad (5)$$

The popular sandstone and mud rocks equations by Greenberg and Castagna (1992) given (Vs) in km/sec as follows:

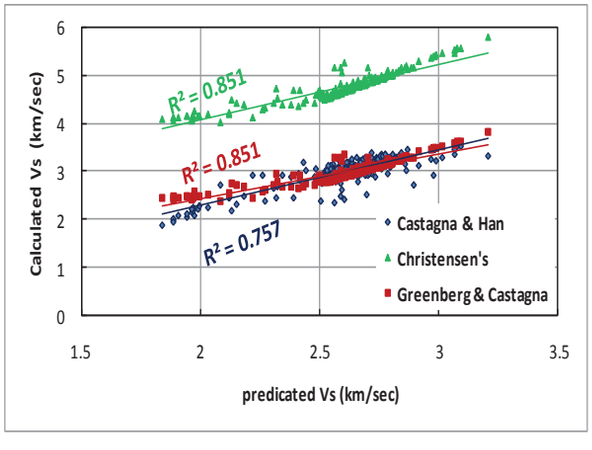


Fig. 1. Correlation between predicted Vs and calculated Vs.

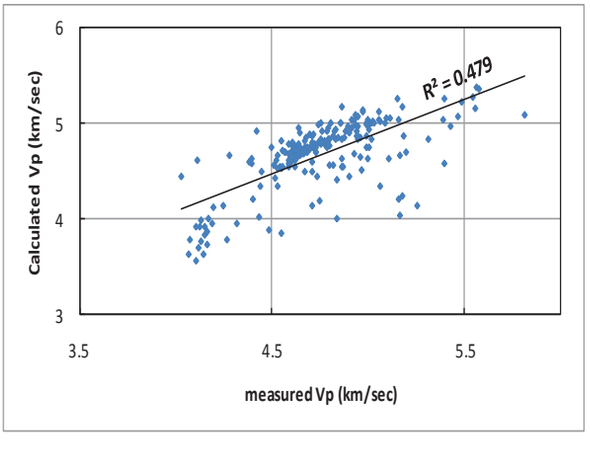


Fig. 2. Correlation between measured and calculated Vp.

$$Vs = 0.804\ Vp - 0.856 \quad (6)$$

This formula depends only on compressional velocity whereas, the other equations are depended on more than one physical parameter.

The interest of the shear interval transit time measurement has been exposed by Pickett (1963). He demonstrated that the ratio of the compressional to the shear velocities (Vp/Vs) can be used as a lithology indicator (Serra, 1984). While Crain's shown this cross –plot to indicate Poisson's ratio by lithology.

RESULTS AND DISCUSSION

Shear Velocity Verification

Practical Application at SE Sirt Basin: Application of the discussed methodology is first part of the predication Vs, and comparative of these results is a second part which gives a main reason to acceptable the Vs estimation for the southeast Sirt Basin or there are requirements for adjustment. Therefore, we assessed the repeatability of the results and then impact it for future applications such as rock mechanical parameters.

Shale layers cross the studied reservoir were easy defined as shale intervals. While clean intervals contain undefined shale distribution type as clean intervals. Consequently, the cutoff value (20 %) of shale content takes from volume of shale, which calculated within the studied reservoir (southeastern Sirt Basin). Then 20% > Vsh > 20% filter was applied to identify clean sand and shale intervals.

Fig. 1 shows the plots of predicted Vs (equation 2) with the calculated Vs by the equation 4, 5 and 6 for the studied reservoir. Castagna *et al* (1985) and Han et al (1986) give a correlation coefficient (R2) of 0.76 less than Greenberg and Castagna (1992) which is equal to 0.85. The different of the R^2 due to these different relationships are included different physical parameters. In spite of the Christensen's equation also presents good regression but has an over estimate of the shear velocity. That what makes the Christensen's equation is not suitable for studied reservoir.

Note that (Fig. 2) illustrates weak relation between the Vp derive from sonic log data correlated with that derived by the Castagna *et al* (1985) and Han *et al* (1986) equation.

The same above procedure of the predicate Vs from PR (equations 1 and 2) is applied for well has package of wire line log data (GR, ρb, Øn, Rs, Rd, "shallow and deep Resistivity", ΔTc and ΔTs). The wire line log data of the tested well has the same rock type.

Cross plot between the predicated Vs and that measured by sonic travel time is done, instead of any equations, which they are used for the estimate Vs of studied reservoir. High regression coefficient of this cross plot (Fig. 3) utilized Crain's equation (1) to find PR which is the main parameter of the shear velocity. In addition, measured compressional velocity by sonic travel time correlated with the predicated and measured shear velocity and indicate good trend as shown in (Fig. 4).

Crain's Equation Modification: The Crain's (2000) equation (1) applied on US Gulf Coast formations, needs some adjustment in other areas as he reported. Although this equation gives best regression trend in the studied reservoir at southeast Sirt Basin, but to be generalized for the whole region it requires more investigation.

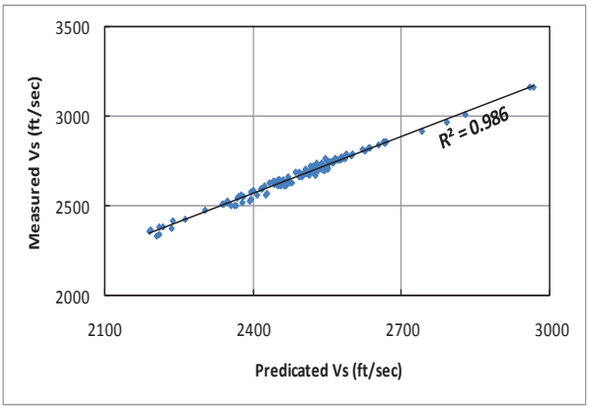


Fig. 3. Correlation between predicted and measured Vs for tested well.

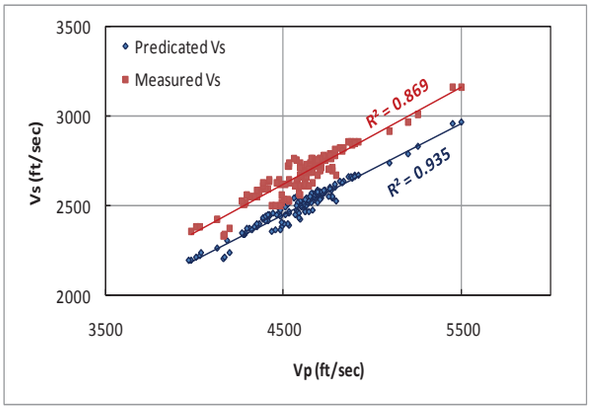


Fig. 4. Correlation between measured Vp and (predicated and measured) Vs for tested Well.

Common diagram relates Vp (km/sec) and PR indicates lithology inside certain limit. Another quick look analysis used to estimate PR by ΔTs and ΔTc (Crain's, 2000). These two conventional methods are applied as shown in (Figs. 5 and 6) respectively for studied reservoir. Comparison with the standard two diagrams appear cluster point for clean intervals which include unknown distribution of shale as mentioned before, cause to shifting from clean sandstone range into sandstone, silt and carbonate range. While the shale intervals plot in the right region of shale. Whereas, the second figure present all the clean interval points are approximately close to 0.3 and the shale intervals at suitable range of PR. Therefore, the modification of the equation (1) to estimate accurate values of PR and consequently Vs for studied reservoir is the main task through this section.

The studied reservoir in southeast Sirt Basin, Libya is not clean sandstone due to changes in depositional environment conditions and burial history of this reservoir (Abdulghader, 1996; El-Hawat, 1992 and El-Hawat *el al.* 1996). In addition to different petrophysic characteristics of this reservoir were extracted from petrophysical study

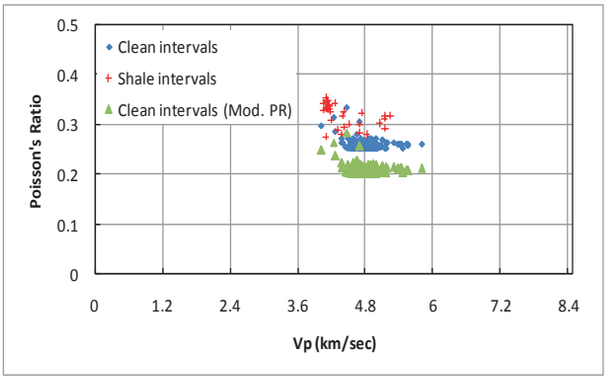


Fig. 5. Compressional velocity (Vp) versus Poisson's ratio (PR).

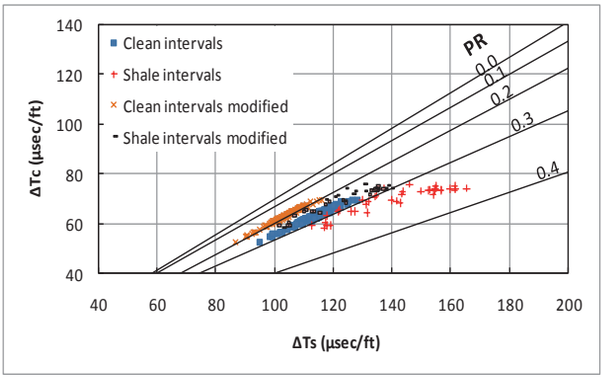


Fig. 6. Quick look analysis of Poisson's ratio (Modified after Crain's, 2000)

of this specific reservoir rock (unpublished study, 2007). Although the later result of PR (Figs. 5 and 6) is same as that observed at a common sandstone range of PR (0.2 - 0.3) (Allen and Allen, 1990), but it is unable to predicate Vs by this result (Crain's equation, 1).

Starting from a typical values of Poisson's ratio for deeper highly compacted, cemented sandstone ranging from 0.18 to 0.22 from most publications of mechanical properties of clastic rocks (Crain's, 2000). The selection of low limit (0.18) and high limit (0.22) of PR values as input constant values to calculate Vs (equation 2). The procedure worked for studied reservoir and test well data. However, comparison between the predicated Vs using variable shaliness PR with those calculated by constant values of PR are clearly noticeable in Figs. 7 and 8 respectively.

Shear velocity values through studied reservoir show conformity estimation even so the predication Vs has lower values than others. In other words, an increase in Poisson's ratio (from 0.18 to 0.22) cause decrease in shear velocity values. Consequently, the modification of Crain's equation (1) was necessary. Try and error technique used to get best modification (equation 7) of equation 1. Results of the new modified predicated Vs equation are plots with the results of equation 2, which is conduct constant values of PR. It is visible through the different Figs. 7 and 8 fitness of the Vs and located in normal range especially in clean intervals, but it couldn't reliable on the Vs results in shale intervals.

$$PR = 0.125 * Vsh + 0.2 \quad (7)$$

Repotting of the quick look diagram by the new Vs results (Fig. 6) indicates change of points toward PR line equal to 0.2.

Vs - Vp Relationship: The cross plot of the compressional and predicated shear velocities by Crain's equation (1) and the modified predicted equation (7) of Vs were compared with Vs estimation at standard PR values (0.18 and 0.22) for different studied reservoir intervals (Fig. 9). The enhancement is obvious about regression coefficient from 0.97 to 0.987 by new modified prediction equation. Therefore, an empirical relation between Vs and Vp for the studied reservoir (southeast Sirt Basin, Libya) could be:

$$Vs = 0.602\ Vp + 89.90 \quad (8)$$

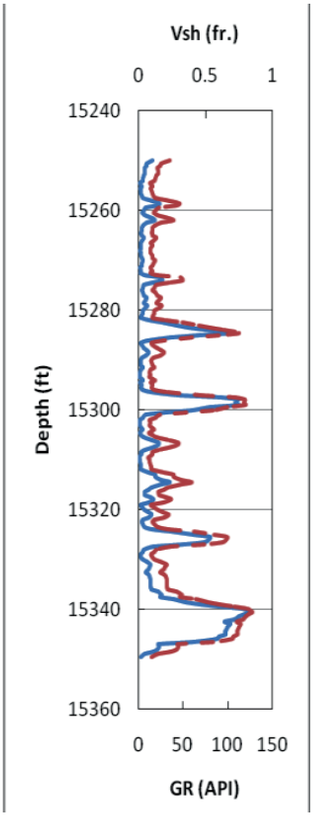


Fig. 7.a. Gamma Ray and shale content of the studied reservoir rock.

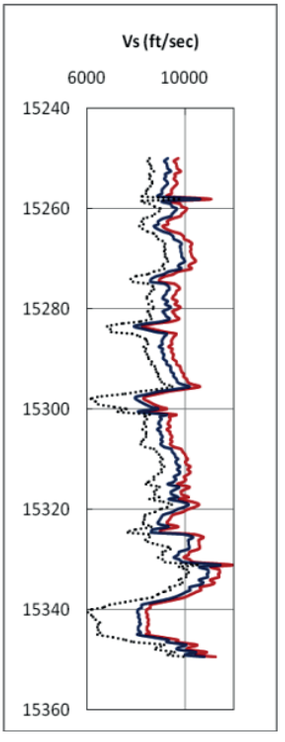


Fig. 7.b. Vs by equation no. 1 of studied reservoir.

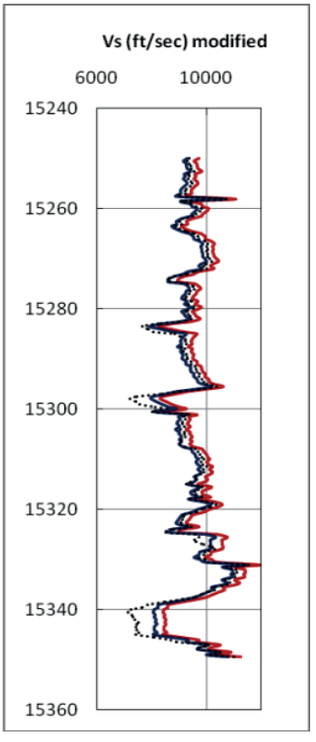


Fig. 7.c. Vs by modified equation no. 7 of the studied reservoir.

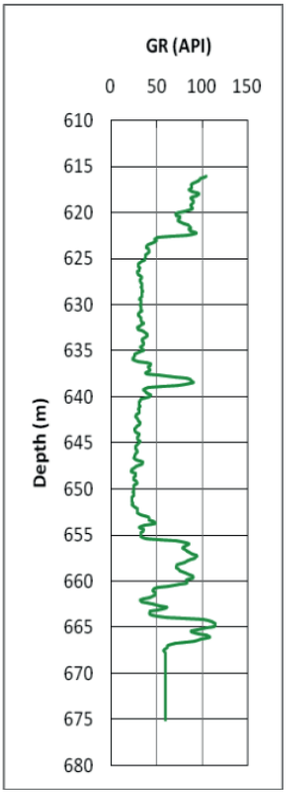


Fig. 8.a. Gamma Ray of the tested well.

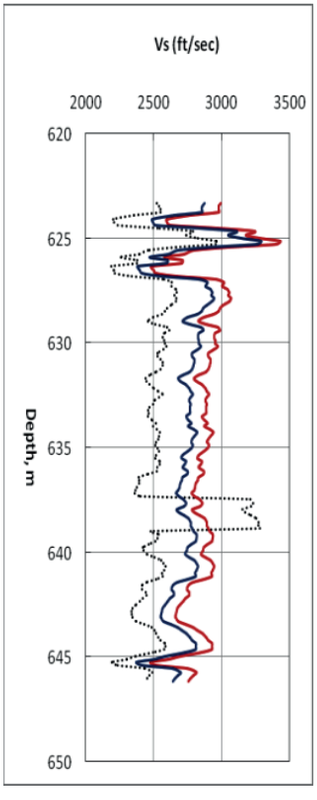


Fig. 8.b. Vs by equation no. 1 of tested well.

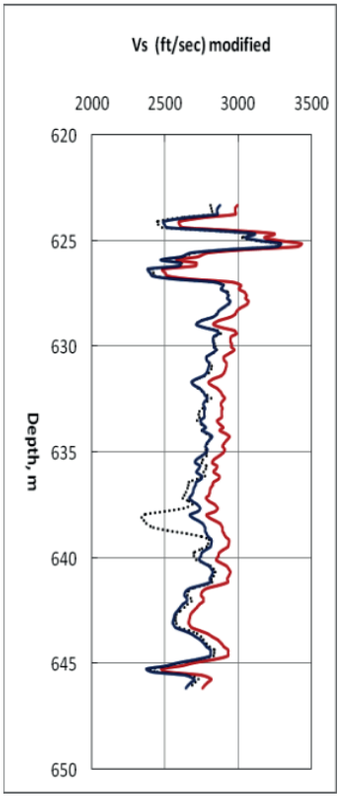


Fig. 8.c. Vs by modified equation no. 7 of tested well.

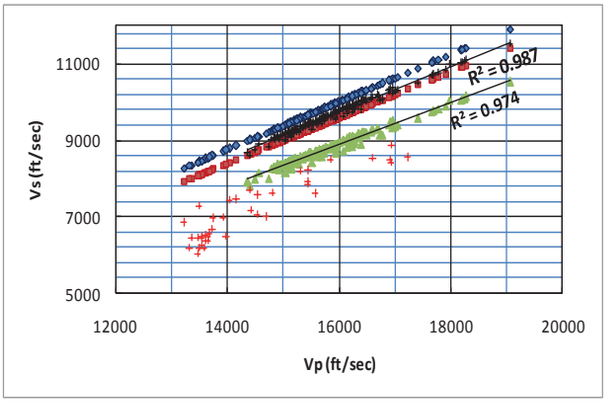


Fig. 9. Cross correlation between Vp and predicted Vs.

The application of this relation indicates good agreement in shale intervals, where as equation (7) still gives over estimation of Vs (Fig. 7c).

CONCLUSION AND RECOMMENDATION

Shear velocity (Vs) could be estimated from the popular equations if the studied rock has the same petrophysics conditions. However, presence of shale content above 20% with unknown distribution throughout the studied reservoir, cause heterogeneous of elastic reservoir rock properties (shear velocity). Therefore, the predication of the Vs of this reservoir rock type subject to some error. A present approach provides a Poisson's ratio; as one of the mechanical property, which is subsequently used to calculate Vs. This technique has been applied for selected reservoir rock in southeast Sirt Basin, Libya. Good agreement of calculated shear velocity by popular equations for sandstone rocks, except that derived from Christensen's equation.

Crain equation can be used to estimate PR for sandstone rock which has the same petrophysic characteristic. In other words, shear velocity as a function of PR could be used and gives good results at clean intervals. This equation of PR according to shale content subjected to modify for confirmation of the petrophysic studied reservoir conditions. Shear velocity by new modification of equation gives better estimation in both clean and shale intervals. According to this result, this new equation of Vs for studied reservoir can be applied without requirements to distinguish a shale intervals within the reservoir.

This approach to estimate the shear velocity within a productive part of shaly sand reservoir is strongly recommend and preferred if there are any core samples to verify an empirical equation results, in addition to study another important mechanical rock properties for this reservoir rock in the study area.

REFERENCES

Abdulghader, G. S. (1996). Depositional Environment and Diagenetic History of the Maragh Formation NE Sirt Basin, Libya. In: Geology of the Sirt Basin (eds. M. J. Salem, A. S. El-Hawat, and A. M. Sbeta), Amsterdam, Elsevier, V. 2: 263-274.

Allen, A. P., and Allen, R. John. (1990). Basin Analysis Principles and Applications. Black Scientific Publications: 223-250.

Brie, A. Pampuri, F., Marsala, A., F., Meazza, O. (1995). Shear Sonic Interpretation in Gas–Bearing Sand. SPE Paper no. 30595 presented at the SPE annual conference and exhibition, Dallas.

Castagnaj, P., Batzle, M. L. and Eastwoodr, L. (1985). Relationship Between Compressional-Wave and Shear-Wave Velocities in Elastic Silicate Rocks. Geophysics, 50(57): 1-58.

Crain, E. R. (2000). Petrophysical Handbook. Elastic Properties of Rocks: 000p.

El-Hawat, A. S. (1992). The Nubian Sandstone Sequence in Sirte Basin, Libya; Sedimentary Basins and Events. In: Geology of the Arab world (ed. by: A. Sadiq), Cairo University: 317-327.

El-Hawat, A. S., Missallati, A. A., Bezan, A. M. and Taleb T. M. (1996). The Nubian Sandstone in Sirt Basin and its Correlatives. The Geology of Sirt Basin, 3-30.

Entwisled. . C. and Mccann. D. M. (1990). An Assessment of the Use of Christensen's Equation for the Prediction of Shear Wave Velocity and Engineering Parameters. In: Geological Applications of Wireline Logs (eds. A. Hurst, M. A. Lovell & A. C. Morton) Geological Society, London, Special Publication, 48: 347-354.

Eskandari, H. , Rezaee, M. R., Javaherian, A., and Mohammadnia, M. (2003). Shear Wave Velocity Estimation Utilizing Wireline Logs for a Carbonate Reservoir, South-West Iran. Iranian Int. J. Sci. 4(2): 209-221.

Greenberg, M. L., and Castagna, J. P. (1992). Shear-Wave Velocity Estimation in Porous Rocks: Theoretical Formulation, Preliminary Verification and Applications. Geophysical Prospecting, 40: 195-209.

Han, D., Nur, A. & Morgan, F. D. (1986). Effects of Porosity and Clay Content on Wave Velocities in Sandstones. Geophysics, 51: 2093-2107.

Mason, (1984). Three-Cone Bit Selection with Sonic Logs. SPE Drilling Journal: June, 1987: 135-142.

Pickett. G. R. (1963), Acoustic Character Logs and Their Applications in Formation Evaluation. J. Petr. Tech., 15: 65-667.

Serra, O. (1984). Fundamentals of Well-Log Interpretation, Measurement of the Speed of Sound (Sonic Log), the Acquisition of Logging Data. Developments in Petroleum Science 15A: 219 P.

Vernik, D. L. Fisher, and Bahret, S. (2002). Estimation of Net–to–Gross from P and S Impedance in Deepwater Turbidities. Methods and Application in Reservoir Geophysics. Society of exploration Geophysicists, Investigation in Geophysics no. 15, the Leading Edge: 25(12): 380-387.

Widarsono, B., Wong, P. M., Saptono, F. (2001). Estimation of Rock Dynamic Roperty Profiles Through the Combination of Soft Computing, Acoustic Velocity Modeling and Laboratory Dynamic Test on Core. SPE Paper no. 68712. In: Proceedings of Asia Pacific Oil and Gas Conference and Exhibition, Jakarta, Indonesia. Society of Petroleum Engineers, Richardson, Texas: 1–10.

Neural Network Approach to Predict Average Reservoir Pressure

Saber Elmabrouk, Ezeddin Shirif and Rene Mayorga*

Abstract: The average reservoir pressure is an important parameter in petroleum engineering which is utilized in almost all reservoir and production engineering calculations. Normally, the average reservoir pressure is obtained from build-up test and can be measured only when the well is shut in. Besides that, it requires an update from time to time. It also has a great economic impact caused by shutting in the well during the entire test. However, the objective of this study is to establish a neural network model that can map certain relationship that controls previous production performance of the reservoir to predict current average reservoir pressure without shutting in the wells.

Keywords: Reservoir, Pressure, Average, Neural Network, Model.

INTRODUCTION

STraditionally, the average reservoir pressure is obtained from build-up test when the well is shut in by measuring the long-term build-up pressure. The build-up pressure eventually builds up to the average reservoir pressure over a long enough period of time. This time period depends mainly on the reservoir permeability. It may take long in low permeability reservoirs. Because reservoir pressure changes as fluids are produced from a reservoir, the average reservoir pressure should be updated from time to time. In addition, it has a great economic impact caused by shutting in the wells during the entire test.

The current state-of-the-art in production average reservoir pressure, specifically in cases of application of artificial intelligent techniques, is quite limited. In this work we established a neural network model that can map certain relationship that control previous oil, gas and water production performance of the reservoir to predict current average reservoir pressure without needing to close the wells. This method is suitable for both constant and variable flow rates. After obtaining the average reservoir pressure, it can be utilized in almost all reservoir and production engineering studies. Some of these studies include computing rock and fluid characteristics, estimating hydrocarbons in place, establishing the value of water influx, and predicting future reservoir behaviour in primary/secondary recovery and pressure maintenance projects.

Artificial neural networks (ANNs): ANNs are relatively new computation tools that have found extensive utilization in solving many complex engineering problems. A basic network shown in Fig. 1 has three layers of processors: an input layer, an output layer, and a one hidden layer in between. Each layer has a number of neurons or nods.

At first, both input data and corresponding desired output data are given to the network. As the network starts training, the input layer receives the input signals, and then starts processing the data through the hidden layers until reaching the output layer yielding the resulted outputs. These outputs are then compared with the desired outputs computing the error, which is back propagated through the system causing it to adjust the weights,

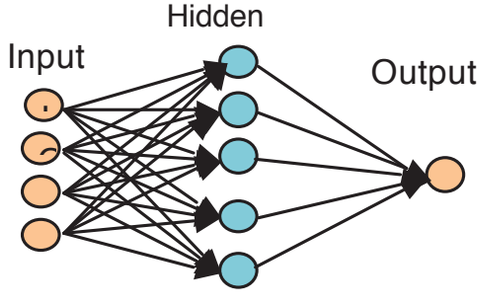


Fig. 1. A generalized artificial neural network. It has an input layer with four neurons, one hidden layer with five neurons and an output layer with one neuron.

*University of Regina, 3737 Wascana Parkway, Regina, SK, S4S 0A2

which control the network. Once a neural network is trained to satisfactory level, it may be then used as an analytical tool on other data.

The feedforward error-backpropagation is the most famous procedure for training ANNs. It is based on searching an error as a function of ANNs weights. Each iteration in the backpropagation constitutes two sweeps: forward activation to produce a solution and a backward propagation of the computed error to modify the weights (Basheer and Hajmeer 2000).

Modeling with neural networks is not an easy task. This poses considerable challenges for engineers particularly in terms of the requirement to realize sufficient robust models. The major challenges could be summarised as following:

Choosing the model structure: Once the number of input and output nods is defined by the problem, the number of hidden layers and nodes in each layer is far from clear. Therefore, the first decision we will need to make is: how many hidden layers and how many nodes in each hidden layer? In most situations, there is no way to determine the best number of hidden units without training several networks and estimating the generalization error of each. If we have too few hidden units, we will get high training error and high generalization error due to under-fitting and high statistical bias. If we have too many hidden units, we may get low training error but still have high generalization error due to over-fitting and high variance (Geman, *et al* 1992).

Selecting Training Algorithm: After the number of hidden layers and number of nods in each layer has been selected, the next step is selecting the training algorithm. The objective of the training algorithm is to determine the global minimum of the error surface. In this process, the network weights must be set so as to minimize the prediction error made by the model. This is the role of the training algorithms. The historical cases (inputs and outputs) are used to automatically adjust the weights in order to minimize this error. This process is equivalent to fitting the model represented by the network to the training data available. The error of a particular configuration of the network can be determined by running all the training cases through the network, comparing the actual output generated with the target outputs. The differences are combined together by an error function to give the network error. The most common error functions (cost functions) are the sum squares error, where the individual errors of the output units on each case are squared and summed together. Despite the wide range of learning algorithms being available to train the ANNs model, there is no single learning algorithm that works best on all learning problems. In fact, the choosing of training algorithm is based on the characteristics of the problem; consequently, training a neural network model essentially means selecting one model from the set of allowed models that minimizes the cost function.

Activation function: The specific activation function (also known as a transfer function) used at the active nodes of the feedforward ANNs is fixed before the model is trained. Activation functions are needed to introduce nonlinearity into the network. Without nonlinearity, hidden units would not make nets more powerful than just plain perceptions. In other words, the neural networks pass the output of their layers through activation functions. These activation functions scale the output of the neural network into proper ranges. There are many activation functions that we can choose from and each one has its own special virtues. We may notice that, it would be possible to use a different activation function for each layer of the neural network. As a result, we have to choose an activation function suited to the distribution of input and output values. For more details of various activation functions see Bulsari (1995).

Ultimately, the selection of the architecture of the neural network will come down to trial-and-error procedure. If the model architecture and learning algorithm are selected appropriately, the resulting ANNs can be extremely robust.

The proposed model: In this study, the ANNs model is designed to estimate the current average reservoir pressure without needing to close the wells. The network is supervised, feedforward with backpropagation. After trying several models, the [4-5-1] network was found to be the best extremely robust model. The input layer received the following parameters; cumulative oil production (Np), gas flow rate (Qg), water flow rate (Qw) and number of wells on production. The output layer has one neuron which is average reservoir pressure (Pavg). The selected model contains one hidden layer with five neurons. The error function of the proposed model was sum-of-squares.

Data preparation and acquisition: A Libyan oil reservoir located in Sirt Basin consisting of 56 oil wells was utilized in this study to develop a model to estimate the average reservoir pressure. The reservoir started its production in March 1970, and a total of 49 average reservoir pressure data points were recorded during a 39 years of production (from March 1979 to May 2009). The range of this dataset is illustrated in Table 1.

To build a robust model, the last two recorded average reservoir pressure (June 2007 and May 2009) was put beside in order to test its prediction performance after it trained properly. The rest of the dataset (47 points) were used to build the network. Besides, to avoid over fitting (overtraining), it is necessary to use early stopping technique. In early stopping, the training data points are split randomly into three sets, training, validation and test sets. The validation set (6 points) is used in learning to decide when to stop. This illustrated in Fig. 2. The Figure shows a typical plot of how the sum-of-squares error changes with the number of iterations. If the validation error increases while the training error steadily decreases then a situation of over fitting may have occurred. When the performance with the validation test stops improving, the algorithm halts. After that, the test set (7 points) was used to evaluate how good an ANNs performs on data that it has not seen before. The ranges of the aforesaid datasets are shown in Table 2.

Table 1. Range of All Used Data

Model parameter	Max	Min	Average
Pavg, psi	1188	820	924
Np, STB	492MM	492M	352MM
Qw, bbl/d	155036	3572	73280
Qg, scf/d	21902	1732	7969
No. of wells	56	12	40

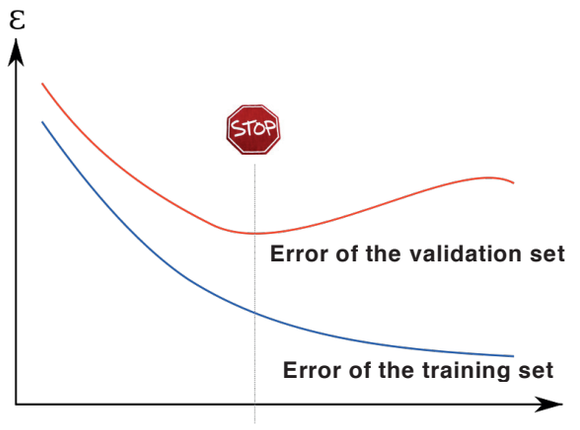


Fig. 2. Error as a function of training time. The red curve is the error on the validation set. The blue curve is the error of the training set.

Neural network architecture: The architecture of the neural network used in this study is multilayered with 4 input nodes, one hidden layer with 5 nodes, and 1 output node, [4-5-1]. The number of hidden nodes, training algorithm and activation function are determined through trial-and-error procedure.The network was trained using feedforward backpropagation with Quasi-Newton training algorithm. The neurons in the backpropagation used hyperbolic tangent as input activation function and logistic activation function in the output. A hyperbolic tangent activation function gives values that range from -1 to 1. A logistic activation function yields an output varies from 0-1.

Consequently, the proposed network provides the best minimum error for training, validation and test of the network Fig. 3, 4 and 5 respectively. It is obviously from the Figures that the network provides results very close to actual average reservoir pressure. This indicates an excellent agreement between the actual and the calculated average reservoir pressure. The statistical parameters for the prediction capability

Table 2. Range of Data using in Training Process

	Training Set			Validation Set			Test Set		
	Max	Min	Avg.	Max	Min	Avg.	Max	Min	Avg.
Pavg, psi	1188	833	933	1072	841	931	1081	853	906
Np, STB	487MM	492M	372M	387MM	618MM	378MM	393MM	563M	364MM
Qw, bpd	155036	3572	71590	114499	31453	667588	120272	22544	85388
Qg, scf/d	21902	1732	8149	17832	2458	8976	18118	1748	7965
Wells	53	12	39	49	15	36	55	37	43

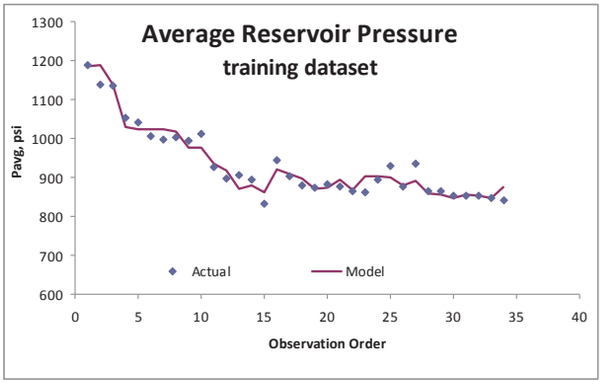


Fig. 3. Network performance, training dataset

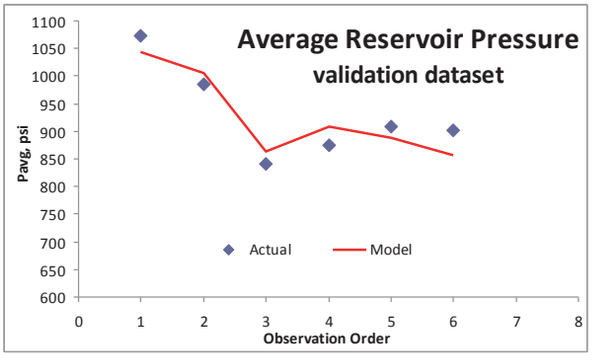


Fig. 4. Network performance, validation dataset

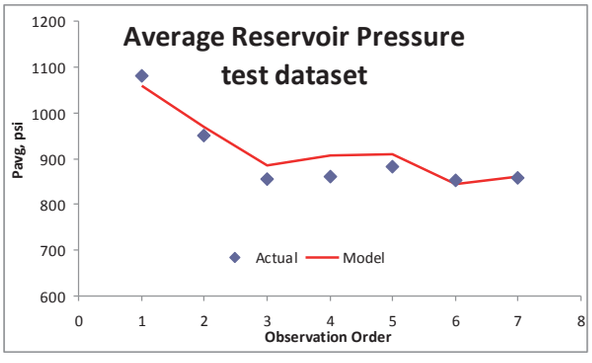


Fig. 5. Network performance, test dataset

obtained from the network are summarized in Tables 3. The proposed network provides prediction values of average reservoir pressure with an average absolute error (AAE) of 18.816 and average absolute relative error (AARE) of 2.033% indicating that the model describes the data well.

To study the prediction performance of the proposed network, two unseen points have been used to evaluate its performance Fig. 6. Table 4 summarizes the statistical error analysis. The analysis shows a small error indicating that the model is robust.

Table 3. Statistical Parameters of the Proposed Network Model

	AAE	AARE, %	MAARE, %
Training	16.814	1.792	4.48
Validation	28.23	3.061	5.027
Test	22.44	2.494	5.416
All	18.816	2.033	5.416

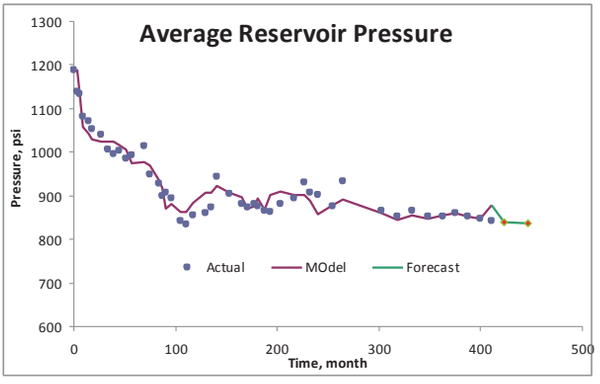


Fig. 6. Prediction of average reservoir pressure.

Table 4. Statistical Analysis for Prediction Performance

Time	wells	Model, psi	Actual, psi	AE	RAE
6/2007	56	839.32	832	2.356	0.287
5/2009	56	830.51	820	1.017	0.122

CONCLUSIONS

A neural network model was developed to predict current average reservoir pressure without needing to close the wells. The model is suitable for both constant and variable flow rates. The data in use were a set of 49 measured average reservoir pressure collected from a Libyan oil reservoir located in the Sirte Basin. The network consisted of one hidden layer with five neurons. The input layer received four parameters; cumulative oil production, water production rate, gas production rate and number of wells on production. The network was trained using feedforward backpropagation with Quasi-Newton training algorithm.

The results reflect that the application of neural network models is feasible for prediction of the current average reservoir pressure of oil reservoirs without the need to close the wells. Nevertheless, the neural network model has the ability to predict current average reservoir pressure accurately using previous reservoir production data. Further study can proceed to construct the most suitable neural network models for other oil fields.

ACKNOWLEDGMENT

We wholeheartedly thank and appreciate FGSA, University of Regina for their generous financial support.

REFERENCES

Basheer, I. A., Hajmeer, M. (2000). Artificial Neural Networks: Fundamentals, Computing, Design, and Application. Jornal of Microbiological Methods, 43: 3–31.

Bulsari, A. B. (1995). Neural Networks for Chemical Engineers, Elsevier, Amsterdam, 000p.

Geman, S., Bienenstock, E. and Doursat, R. (1992). Neural Networks and the Bias Variance Dilemma. Neural Computation, 4: 1-58.

Suchatita Gropal. (1998). Artificial Neural Networks for Spatial Data Analysis http://www.ncgia.ucsb.edu/giscc/units/u188/u188.html

Analytical Study for Physicochemical Characteristics of Bentonite Clay in Libya

Mohammad, Al. Al-Mahabis, Ibrahim, S. Shaban, Saeed*, N. Wadi and Khald, S. El.Kerikshi

Abstract: This study highlights the mechanism of formation for Bentonite clay surface properties. It investigates specific gravity and the influence of physicochemical characteristics on clay stability of structural forces on adsorbed water molecules. In particular, it describes the chemical composition, as well as cation exchange capacity (CEC). Bentonite clay is collected from the Murzuq city located 1150 km south of Tripoli i.e. southernmost town of Libya. The CEC value is leached by 500ppm Ca^{+2} at pH=8 equaled 84.5 mmoles/kg. While at pH=2, the value is (20.5 mmoles/kg). The leaching process is carried out by 500ppm K^{+} using flame emission photometer. The CEC value at pH =8 for sample is 91.5 mmoles/kg. Also the specific gravity is found to be 2.597. This value is in agreement with the obtained standard values for Wyoming (USA). The % M_xO_y of the clay is calculated by gravimetric method as follows: SiO_2, 53.75; Al_2O_3, 21.46; Fe_2O_3, 1.4; CaO, 0.97; MgO, 2.13, and agreed with the XRF analysis as follows: SiO_2, 54.93; Al_2O_3, 21.46; Fe_2O_3, 1.71; MgO, 3.18 ; CaO, 0.81; Na_2O, 5.48; K_2O, 0.54; TiO_2,0.32. The results are adequately approximate and reasonable for both methods. The percent is very limited for trace elements Pb, Cr, Cd, Cu, Fe, and Zn. In the sample, it is about 0.21%. The result of XRD analysis (intensities) for sample is presented as follows: 50% quartz, 50% kaolinite, 5% Analcine, 7.5% Illite, 5% Natrolite, 10% Nontronite, 7% Montmorillonite. The formula calculation depends on the purity of clay and consequently the structural formula for Libyan Bentonite is: $K_{0.094}Na_{1.45}Ca_{0.118}\ (Al_{2.92}Fe_{0.175}Ti_{0.033}Mg_{0.646})^{VI}(\ Al_{0.52}Si_{7.48}\ )^{IV}O_{20}(OH)_4$

Keywords: Physicochemical properties, XRD, XRF, FT-IR, Structural formula.

INTRODUCTION

Bentonite clay is an absorbent aluminum phyllosilicate. It is generally impure clay consisting mostly of montmorillonite. It is a dual layered, dual-dimensional mineral. These minerals give it a layer of cards that looks like crystalline packets and called platelets. Bentonite is a geological extract found freely in natural state. There are some nomenclatorial problems with the classification of bentonite clays. Bentonite usually forms from weathering of volcanic ash, most often in the presence of water, (Mitchell, 1993; Lagaly, 1995). However, the term bentonite, as well as similar clay called Tonsteins (Kaolin) can be used for clay beds of uncertain origin. Bentonite may also contain Feldspar, Biotite, Kaolinite, Illite, Cristobalite, Pyroxene, Zircon, and crystalline quartz. Bentonite is greasy and soap like to the touch. Freshly exposed, bentonite is white to pale green or blue and, with exposure, darkens in time to yellow, red, or brown, (Navarotsky,1994; Wright, 2003; Admis, 2005; Al-Ani, 2008). Libya has only one regional factory in Benghazi (Al-Joewf Company) that is produces 100,000 tons yearly. Libya needs 1.6 Million tons of bentonite yearly. To meet this need requires importing this substance from other countries to use it in different industrial fields, especially in drilling mud for oil and gas wells. However, some bentonite clay of Libyan origin called (as a common name) ***"White Mud"*** is found to be effective without any modification.

EXPERIMENTAL METHODS

Materials: The bentonite clay, Atomic Absorption Spectrophotometer, GBC Analysis, Model GBC 932, (Austria), FT-IR Spectrometer, (VARIAN 660-IR,USA), Flame Emission Photometer, (PFP7, JENWAY, Germany), (used for determination Na and K), XRF, Bruker AXS, (Model S-8 TIGER, 2010, Germany), XRD, Bruker AXS, (Model D-5005 TIGER, 2010, Germany), Mixer Rotating, (Edmund

* Department of Chemistry, Postgraduate studies Academy, Tripoli, Libya. *E-mail: Saeed19572001@ Yahoo.com*

Buhler, 400 rpm, Mot./min,(Germany), and pH Meter, while concentrated HNO_3 manufactured by Carlo ERBA Lab, Italy, Tripoli University. All materials stated above are used as received without any further purification.

Digestion Method: Weigh 1.0 gram of dry sample in conical flask. Added 5 ml conc. HNO_3 and covered with watch glass, Bring to slow boil on hot plate and evaporate not to dry for 30 minute. Add 10 ml conc. HNO_3, cool flask between additions evaporate on a hot plate to remove all HNO_3 before continuing treatment until all elements in sample dissolved and converted metals in the sample to nitrate completely except silica insoluble . Cooled and diluted to about 50 ml with distilled water and heat to almost boiling, then cooled at room temperature. After that, filtered and transferred to a volumetric flask 100 ml, finally it diluted to the mark, (Greenberg, *et al*, 2005).

Gravimetric Analysis

Determination of the Weight of Silica (SiO_2)

(a) Weigh 5.0gm of sample in beaker. Add 10ml of conc. HNO_3, and cover the beaker with a watch glass. Allow the acid to run down the lip of the covered beaker. After the chemical action has subsided, lift the cover. Add 5ml of acid to complete reaction. Then evaporate not to dry on hot plate for 30min. Add 50ml of distilled water. Stir the mixture with glass rod, (Welcher, 1975).

(**b) Filtration:** While preparing a mixture of hot filter through medium-texture filter paper wash dish and residue (**SiO_2**) with a minimum volume of distilled water. Save all washing to use it for later analysis.

(c) Ignition: Transfer the two filter paper and residues to platinum or porcelain crucible, dry on hot plate at 110°C, and ignite at 1000°C to constant weight. Too rapid heating may form black silica, cool in desiccators weigh, and repeat ignition and weighing until constant weight is attained. Record the weight of crucible and contents.

Determination of the Weight of $(Fe, Al)_2O_3$

(a) To the filtrate reserved in accordance with step (b) above of procedure silica should have a volume of 200 ml, and heated to boiling for 15 mins. Then treat with 10ml of NH_4OH until the brown or sometimes white color precipitate appears.

(b) Filtration: Filter and wash, two times for small precipitate to four times for large. Save all washing to use it for later analysis.

(c) Ignition: Transfer the two filter paper and residues to platinum or porcelain crucible, dry on hot plate at 110°C, and ignite at 1000°C to constant weight. Too rapid heating may form black metal oxide, cool in desiccators weigh, and repeat ignition and weighing until constant weight is attained. Record the weight of crucible and contents (Fig. 1).

Determination of the Weight of CaO

(**a)** To the filtrate reserved in accordance with procedure of $(Fe, Al)_2O_3$ having a volume 300ml, heat to boiling and add a few drops of methyl red indicator and 30ml ammonium oxalate (50g per liter). Heat the solution from 70°C to 80°C, and add NH_4OH (1:1) drop wise, until the color change from red to yellow. The precipitate is calcium oxalate (white). Allow the solution to stand without further heating for (1h), (Fig. 2).



Fig.1. Precipitation of $(Fe, Al)_2O_3$



Fig.2. Precipitation and Filtration of CaO

(b) Filtration: Filter and wash moderately with water. Save all washing to use it for later analysis.

(c) Ignition: Transfer the two filter paper and residues to platinum or porcelain crucible, dry on hot plate at 110°C, and ignite at 1000°C to a constant weight. Too rapid heating may form black calcium oxide, cool in desiccators weigh, and repeat ignition and weighing until constant weight is attained. Record the weight of crucible and contents, (Welcher, 1975).

Determination of the Weight of MgO

(a) To the filtrate reserved in accordance with procedure of CaO having a volume 400ml, heat to boiling, then add 20ml Na_2HPO_4 (100g per liter), and add 10ml NH_4OH drop by drop, cool and transfer it to magnetic movement to precipitate for 1h. Allow the solution to stand without further heating for (2h). Filter and wash it with water **(**Fig. 3**).**

(b) Ignition: Transfer the two filter paper and residues to platinum or porcelain crucible, dry on hot plate at 110°C, and ignite at 1000°C to constant weight. Too rapid heating may form black magnesium oxide, cool in desiccators weigh, and repeat ignition and weighing until constant weight is attained. Record the weight of crucible and contents.

Specific and Selective Precipitation

Principle: There are many important advantages in the use of organic reagents over inorganic reagents when used as precipitants for inorganic substances. Among these are the following: (**a**) It is often possible to attain a degree of selective not possible with an inorganic reagents; (**b**) Many organic reagents are acidic and therefore improve selectivity in precipitation reactions that can be achieved by a careful control of the hydrogen ion concentration;(**c**) The precipitates formed in reactions of organic reagents with inorganic ions are often extremely insoluble and frequently very high in molecular weight. This method is useful in many important analytical separations, like Al from Be, Mg, from alkaline and alkaline earth, at pH (4.5-5). The reagents are 0.01M Oxine (8-Hydroxyquinoline), Chloroform and 2.0N Acetic acid**,** (Welcher, 1975).



Fig.3. Precipitation of MgO

Separation of Al by Organic Solvent

(a) Procedure: Weight 3.0gm of sample in beaker, add 10ml of conc. HNO_3, and cover the beaker with a watch glass, allowing the acid to run down the lip of the covered beaker. After the chemical action has subsided, lift the cover; add 5ml of acid to complete digestion. Then, carefully evaporate to dry on hot plate for 30minute. Add 50ml of distilled water, stir the mixture with glass rod, and cooled at room temperature**.** After that make filter using filtration funnel and filter paper (40mm). Finally, the filtrate is saved in clean beaker to use later for the analytical separation, (Skoog, and *et al* 2000; Harris, 2007).

(b) Extraction: Weigh clean and dry beaker. Then extract it immediately with chloroform $CHCl_3$ using separatory funnel. Transfer extracted sample to separation funnel and add 10ml of 0.01M Oxine, followed with 20ml chloroform, close it with stopper. Shake the funnel at least 5 times. Open tap or lift the stopper to remove entrapped air, and then collect the organic layer in a beaker. Transfer the extracted layer to hot path water for drying at 70°C to evaporate and remove the chloroform (Repeat the operation three times until all the precipitation of Al is completed from aqueous phase). Finally, weigh the beaker and precipitation, (Fig. 4).

Determination of the Specific Gravity

Procedure: The specific gravity is determined by density bottle method. It is most suitable for determining specific gravity. The mass (80g) $\mathbf{M_1}$ of empty dry bottle is first taken. A 40g of sample is taken and kept it in bottle and the mass (120g) $\mathbf{M_2}$ is taken. The bottle is then filled with distilled water (or kerosene), gradually and removing the entrapped air either by applying vacuum or shaking the bottle. The mass (149.60g) $\mathbf{M_3}$ of the bottle soil and water (full on the top) is taken. Finally, the bottle is emptied completely and thoroughly washed, and clean water was filled to the top, and mass (125g)



Fig.4. Separation Al by Organic Solvent and Precipitation of Al.

M_4 is taken. Based on these four readings specific gravity is calculated .Sometimes mixed clay with amount of charcoal gives it porosity**.**

The Scanning Electron Microscopy (SEM): The SEM is a microscope that uses electrons rather than light to form an image. There are many advantages for using the SEM instead of a light microscope. The SEM method provides detailed images of individual grains of clay minerals and Electron Diffraction Spectroscopy (EDS) provides detection of major and minor elements at points on grain surfaces, allowing highly reliable identification from crystal form and composition, as well as direct observation of particle packing and size. The SEM also produces images of high resolution, which means that closely spaced features can be examined at a high magnification >3000 times or range. Preparation of the clay samples is relatively easy since most SEM require the sample to be conductive. A few thin sections of clay size fractions coated with an Au-Pd conductor are examined morphologically under (SEM) with link (EDS). The thin sections of representative samples are analyzed for semi-quantitative determination of primary and secondary minerals. Morphologies, as observed by SEM, can also be useful in identification of clay minerals, (Fig. 5a and 5b), (Atkins, 2001; Al-Ani, 2008).

RESULTS AND DISCUSSION

In this study, the results of the experiments and the resultant discussions are given under the following titles: (1) Trace elements (2) Gravimetric analysis (3) Determination of % for Metals Oxides by XRF (4) Calculation of CEC (5) FT-IR spectrum (6) Specific gravity (7) Swelling of bentonite (8) Chemical composition and structural formulate for Bentonite. The results for all measurements are in agreement approximate and reasonable with the standard value of Wyoming USA. The difference between the values may be due to errors because of the instrumental interferences or chemical analysis. Generally, elements present at high concentration can be easier and better determined by XRF, Gravimetric analysis, titration, and AAS methods provide a corpus of well tried methods of maximum accuracy.

Trace Elements: The analyte solution is aspirated into the flame and first is desolated. The resulting aerosol is thermally dissociated leading eventually to ground state atoms. Maximum sensitivity is obtained by using the flame where the atom cloud exhibits the greatest concentration, (Greenland, and Hayes, 1981). To achieve this depend upon the element concerned, the flame stoichiometry and sample matrix. For elements like Cr that tend

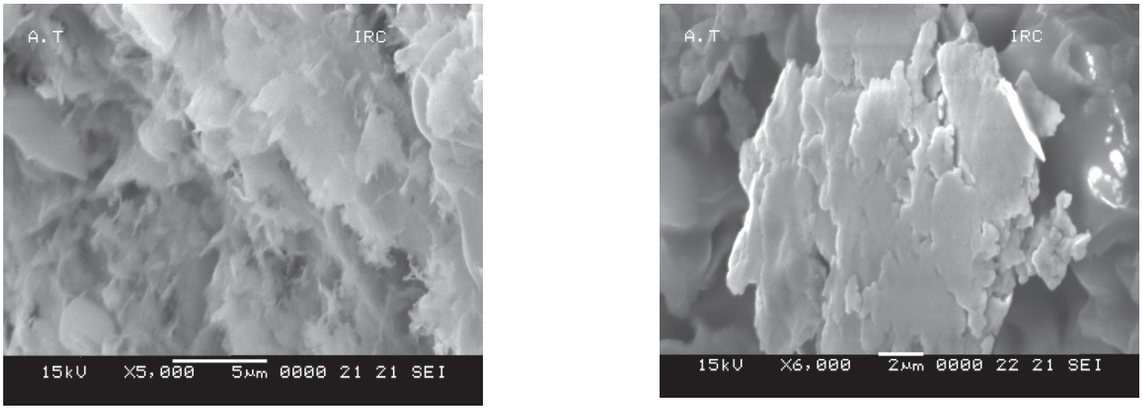


Fig.5. (a) SEM Image before Washing, (b) SEM Image after Washing and drying.

to form very stable oxides, enhanced atomization occurs within a reducing flame. In this experiment is found all trace elements very limited in the sample. The percentage of trace elements (Cd, Cr, Cu, Pb, Fe, and Zn) is found about 0.21% for this clay.

Gravimetric Analysis: Gravimetric Analysis of the clay sample, shows the results in agreement with XRF analysis approximate and reasonable, but it is found different results in measurement, due to errors that may be happened in the instrumental interferences or chemical analysis, also the digestion by HNO_3, the exchangeable cations between the 2:1 layers leave first, and replaced by the H^+ ions. Since only small quantity of (Mg^{+2}, Fe^{+3}, Al^{+3}) leaves 2:1 layer, the change in the $\%M_xO_y$ is small. The mass% of sample MW is determined as follows: SiO_2, 53.75; Al_2O_3, 21.46; Fe_2O_3, 1.4; CaO, 0.97; MgO, 2.13 ; and the results of the same sample by XRF as follows: SiO_2, 54.93; Al_2O_3, 21.46; Fe_2O_3, 1.71; MgO, 3.18 ; CaO, 0.81; Na_2O, 5.48; K_2O, 0.54; TiO_2, 0.3**,** (Table.1).

Determination of % of Metals Oxides by XRF: The most important ability is that of identifying crystalline phases rapidly and simple relatively. Its drawbacks lie in its inability to detect glassy phases and in difficulty sometimes encountered with complex patterns. XRD methods normally cannot give any direct indication of the elemental analysis of the sample. One should especially feed in chemical analytical data, to give the stoichiometry of the system, and optical microscopic finding, to give some indication of presence of glassy phases or of the probable number of separate crystalline phases in the mixture. This method is applicable only to materials with a well defined crystal structure, and hence poorly crystalline or amorphous solids cannot be identified as they don't give clear diffraction patterns. Sample preparation for XRFS is relatively easy, involving direct briquetting of ground samples or various fusion methods, (Willard, *et al* 1988).

Calculation of CEC: The CEC of the sample Murzuq white (MW) that is obtained by leaching process at pH=8 and pH=2 is calculated as follows (Table.1): 84.5 and 20.5 mmoles/kg respectively when leached by 500ppm Ca^{+2}, while CEC increased when leached by 500ppm K^+ at pH=8 as 91.5 mmoles/kg and these values were agreement with the standard value of Wyoming USA (Table. 2). Some exchange capacity for both cations and anions occurs on the edges of silicate clay crystals (Table. 3), whereas the basic cations are principally (Ca^{+2}, Mg^{+2}, K^+, Na^+). Variations in pH cause deviations from equality in the numbers of positive and negative edge charges. AEC increases at low pH=2, and CEC increases at high pH=8 (Table. 4). The likelihood of ionizing significant amounts of (OH^-) depends on the abundance of soil minerals containing (OH^-) and on pH. Relatively untreated clays have a high proportional of 2:1 layer silicate minerals in bentonite. The CEC of this clay is relatively high. Finally, the free (Fe_2O_3) and (Al_2O_3) that accumulate in the clay fraction may cause the AEC to go beyond the decreasing CEC. At pH = 8, practically all the (H^+) in the percolating water is absorbed by the soil irrespective of the salt concentration supplied. At pH =2, the influence of neutral salts increases as the pH falls, resulting in reduce soil acidification and a corresponding increase of the leached acidification. The effects of neutral salts on soil acidification are markedly influenced by the bonding energy (H^+) to the soil

Table (1) Calculation of $\%M_xO_y$ for Metals Oxides

Sample	Al_2O_3%	Fe_2O_3%	CaO%	MgO%	SiO_2%
MW	21.460	1.400	0.970	2.130	53.750

Table (2) Calculation of Concentration for Ca^{+2} by Titration with EDTA 0.01M

Sample	Volume of titrated EDTA for sample, ml	Conc. Ca^{+2} in 500ppm	Volume of titrated EDTA for blank , ml	Conc. Ca^{+2} in blank, ppm	Final Conc. of Ca^{+2} , ppm
MW at pH=2	1.5	120	7.0	560	440
MW at pH=8	5.2	416	1.2	96	320

Table (3) Calculation of K_d and CEC at pH=2 and pH=8 by leached 500ppm Ca^{+2}

Samples	K_d (L/kg)	CEC mmoles/kg
MW at pH=2	2.273	20.5
MW at pH=8	9.375	84.50*

(*) The Standard Values for Wyoming (USA), (Sparks, 2003).

Table (4) Calculation of the Concentration of K^+ from calibration curve at pH=8.

Samples	Conc. of K^+ in 500ppmK^+ at pH=8	Conc. of K^+ in blank at pH=8
MW	425	150

exchange sites. In the majority of situations, the adsorption of anions applied as neutral salts is very small, so that exchange acidity is usually greater than exchange alkalinity. If the soil becomes very acidic then (Al) associated with clay minerals may become soluble in the form (Al^{+3}) or aluminum hydroxyl cation. Soluble aluminum may also be recruited to percolation water through organic substance decomposition. These ions may then become adsorbed even in preference to hydrogen ions, present in soil solution, by the permanent (pH-independent) negative charge in soil clay mineral surfaces. The adsorbed (Al) is in equilibrium with (Al^{+3}) ions in the solution, (Higson, 2005; Harrison, and de Mora, 1996). The solution (Al^{+3}) ions can contribute to soil acidity through their tendency to hydrolyze. In this experiment, it is determined concentration of Ca^{+2} in the samples by titration with EDTA, while concentration of K^+ by flame emission photometer.

Calculation of Final Concentration of Ca^{+2} at pH=8 and pH=2

$$\textbf{Conc. of Ca in ppm} = \frac{(\mathbf{M}\times\mathbf{V})_{\mathbf{EDTA}}\times\mathbf{40}\times\mathbf{1000}}{\mathbf{V_s(ml)}}$$

V= Volume of titrated EDTA, (ml).
M= Molarity of EDTA (0.01M).
$\mathbf{V_S}$ = Volume of sample (5ml)

Calculation of K_d and CEC at pH=2 and pH=8

$$K_d = \frac{(A - B)\times V}{M_S \times B}$$

K_d= Distribution Coefficient (L/kg).
A= Initial Concentration (500) ppm
B=Final Concentration after 24h ppm
V= Volume of solution (50ml).
Ms= Mass of sample (3gm).

…….. (Al-Kateeb, 2001)

$$\mathbf{CEC = K_d \times N}$$

$N = n \times M = 2M = 2\times 0.5/111 = 9.01\times 10^{-3}$ N of $CaCl_2$
$M = N = 0.5/74.5 = 6.71\text{x}10^{-3}$ N of KCl

The distribution of each cation between clay surface and clay solution is controlled by:

1- The charge, size and hydration state of the cation.
2- The density of negative charge on the clay surface, (i.e., the greater of the charge density decrease in diameter of the hydrated cation). The order for group I and II metals cations in increasing charge density is **[$Ba^{+2} < Sr^{+2} < Ca^{+2} < Mg^{+2} < Cs^{+} < Rb^{+} < K^{+} < Na^{+} < Li^{+}$]**.
3- The ionic strength of the clay solution increases because cations are attracted to the anion but anions are repelled.
4- Selective minerals on size criteria may occur or where organic complexion (Humic and fulvic acid).
5- The cations of most common salts can be distributed in the following order according to their adsorption capacity (or energy of their adsorption at clay):

[$Fe^{+3} > Al^{+3} > H^{+} > Ba^{+2} > Ca^{+2} > Mg^{+2} > NH_4^{+} > K^{+} > Na^{+} > Li^{+}$]

Calculation of (SG) for Bentonite in sample MW

$$SG = \frac{[M_2 - M_1]}{[M_4 - M_1] - [M_3 - M_2]}$$

M_1= Weight in (g) of empty dry bottle.
M_2= Weight in (g) of bottle and dry clay.
M_3= Weight in (g) of bottle and dry clay and water required to fill it.
M_4= Weight in (g) of bottle and water required to fill it.

$$SG = \frac{[120 - 80]}{[125 - 80] - [149.60 - 120]} = 2.597 \approx 2.6$$

The IR Spectrum: The FT-IR Spectra in the Figure (1) below show the absorbance of clay samples at a various wave numbers. At 3600-3800 cm^{-1}band, the peaks for both clay samples are the same. The FT-

IR spectra in the Fig. 6 show the absorbance of the clay sample at various wave numbers. The absorption bands of Montmorillonite and Illite is 3635cm^{-1}, 3400cm^{-1}, 1640cm^{-1},1130cm^{-1},1020cm^{-1}, 920cm^{-1}, (Stuart,2004; Hollas, 2004).). Clay minerals may be differentiated by their IR- spectra through study of the bands due to the O-H and Si-O groups. In the O-H stretching region, 3800-3400cm^{-1} for clay minerals, there are 3685 cm^{-1}, 3620 cm^{-1}, 3410cm^{-1} observed. The inner hydroxyl group between the tetrahedral and octahedral sheet in a band near 3620cm^{-1} the other three hydroxyl groups at the octahedral surface form weak hydrogen bonds with oxygen's of the Si-O-Si bonds in the next layer and this result in stretching bands at 3669 cm^{-1}and 3653 cm^{-1}. In the (1300-400cm^{-1}) region, clay minerals show Si-O stretching and bending and O-H bending bands at 908 cm^{-1}, 993 cm^{-1}, 790 cm^{-1} and 748cm^{-1}. For Fig. (1), which mainly have (Al^{+3}) in octahedral position, served well resolved strong band in the 1120- 1000 cm^{-1} region, at 1114 cm^{-1} are observed, and which mainly contains, (Mg^{+2}) in the octahedral sites and (Ti^{+4}) at 747cm^{-1} and 790 cm^{-1} respectively because of the coordination number is (6), the main Si-O band is observed at 993 cm^{-1}. The O-H bending bands are strongly influenced by the layering clays. Where the octahedral sheets are mainly occupied by tetravalent central atoms, the O-H bending band occurs in the 790 cm^{-1} (Table 5). Finally, IR spectroscopy complements XRD methods (Fig. 7).

Table (5) Calculation of K_d and CEC at pH=8 by leached with 500ppm K^+

Samples	Final Conc. in 500ppm K^+	K_d , L/kg	CEC mmoles/kg at pH=8
MW	275	13.64	91.5

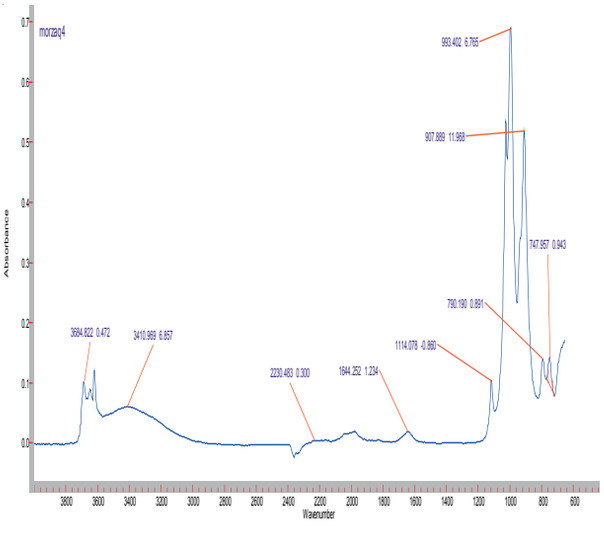


Fig.6. The FT-IR Spectrum of Bentonite Clay for Sample MW

Swelling of Bentonite: When bentonite meets water, it absorbs the water and swells up. This swelling is causes by an interaction between interlayer cations and water molecules. The bonding power between the surface negative charge and interlayer cations of montmorillonite is lower than the interaction energy between the interlayer cations and water molecules. Therefore, the gap between layers is widens as the interlayer cations attract the water molecules (Table. 6). When the interaction between the interlayer cations and water molecules becomes reaches its limit, the swelling stops. Effect of structure properties (ESP), swelling is greatest for Smectite clays that are Na^+ saturated. As the electrolyte concentration decrease, clay swelling increases. As ESP, increases, particularly above 15 times, swelling clay like montmorillonite retain a greater volume of water. Hydraulic conductivity and permeability decrease as ESP increases and salt concentration decreases. Permeability can be maintains if the EC of the percolating water is above a threshold level , which is the concentration of salt in the percolating solution, which causes a 10 to 15% decrease in soil permeability at a particular ESP. If a soil has high quantities of Na^+ and the EC is low, soil permeability, hydraulic conductivity, and the infiltration rate are decrease due to swelling and dispersion of clays and slaking of aggregates.

Chemical Composition and Structural Formulate for Bentonite: The Fig. 7 above, shows the intensities of selected XRD peaks (through 3-70 2θ) characterizing each clay minerals present in the size fraction (e.g. kaolinite 7 Å, Smectite (bentonite) 12 Å and Illite 9 Å) are measured for semi-quantitative estimate of the proportion of clay minerals present

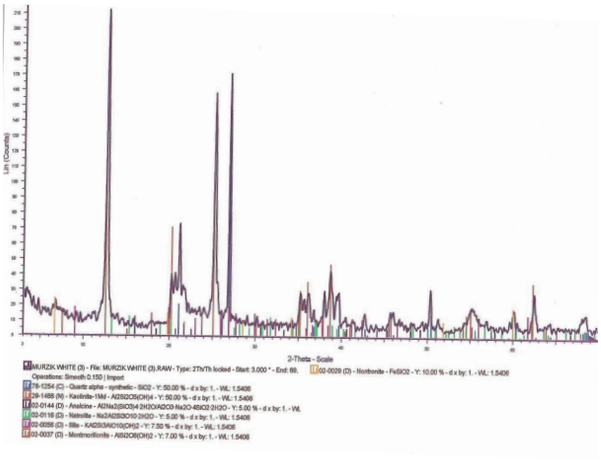


Fig.7. The XRD Analysis of Bentonite Clay for Sample MW

Table (6): Absorption Frequencies (cm^{-1}) for Metal Oxygen Stretching for Tetrahedral and Octahedral Co-ordinations.

Symbols	XO_4		XO_6	
Metal ion(X)	Isolated	Condensed	Isolated	Condensed
Al^{+3}	650-800	700-900	400-450	500-650
Fe^{+3}	550-650	550-750	300-450	400-550
Mg^{+2}	500-550	----------	----------	350-480
Ti^{+4}	650-800	----------	----------	600-650
Zn^{+2}	400-500	400-650	----------	ca. 400

Source: Pantnaik, 2004

in the size fraction < 2µm and 2-16µm. The main peak of 3.30 Å was shifted to 3.10 Å in XRD trace of the sample. Similarly second intensive peak of 14.19 Å was shifted to 14.2 Å. The shifting of other peaks was not significant. The reason for shifting may have been due to the change in crystallographic structure of quartz. XRD trace of quartz supported the results of elemental composition. The mineral related with Fe_2O_3 was not identified in the XRD pattern because it is very small amount and/or amorphous structure. The formula of 2:1 clay is mostly **$[Si_8Al_4O_{20}(OH)_4]$,** whereas:

1. g eq. cations = (Weight % / Atomic weight) × Number of charges of cation
2. There are a total of 44 positive charges and 44 negative charges in a full-cell chemical formula. Then, g eq. cation in total= (g eq. cation×44) / Normalization factor
   Normalization factor = Σ g eq. cation = 5.38
3. Finally, Atoms per unit cell = g eq. cations in total / Valance of cation. (Sparks, 2003). The structural formula of Libyan Bentonite is:

$$[\ K_{0.094}Na_{1.45}Ca_{0.118}(\ Al_{2.92}\ Fe_{0.175}Ti_{0.033}Mg_{0.646})\ ^{VI}(\ Al_{0.52}Si_{7.48}\ )^{IV}O_{20}(OH)_4\ ]$$

This type of clay was called (Na-Montmorillonite) by Wyoming, USA. The Libyan Bentonite was determined by XRD, XRF, FT-IR, and AAS (Table 7) and (Table 8).

CONCLUSIONS

1. During the addition acid at (pH=2) the partial loss of (Mg^{+2}), (Fe^{+3}) and (Al^{+3}) from the 2:1 layers increased the porosity considerably. This probability increases in previous, highly weathered, leached clay because the (Al**)** and **(**Fe) compounds accumulate in such clay, and because most of the ionized (OH^-) combines with (H^+) to form water under acid conditions.
2. Smooth grinding of clay in vibration mill produces change in its physicochemical properties. (a) The grinding for a long time, the crystallinity of the monitored minerals decreases. (b) The intensity of the vibration band in the range 400-1200cm^{-1}in the IR spectrum shows or due to gradual structural changes in the sample MW, (change in the shape and width of the absorption bands are

Table (7): Chemical Composition of Model MW

Oxides	**Molecular weight**	**(Wt. %)**	**g eq. cation**	**g eq. cation in Total**	**Atoms per unit cell**
SiO_2	60.06	54.93	3.658	29.92	7.48
Al_2O_3	101.94	21.46	1.263	10.33	3.44
Fe_2O_3	159.69	1.71	0.06425	0.525	0.175
MgO	40.30	3.18	0.158	1.292	0.646
CaO	56.08	0.81	0.0289	0.236	0.118
Na_2O	61.98	5.48	0.177	1.45	1.45
K_2O	94.20	0.54	0.0115	0.094	0.094
TiO_2	79.90	0.32	0.016	0.131	0.033
Σ % of Trace elements=0.21%			Σ =5.38		

Table (8) Contains of Libyan Bentonite

Materials	% Intensity
Quartz	50%
Kaolinite	50%
Analcine	5%
Natrolite	5%
Illite	7.5%
Nontronite	10%
Montmorillonite	7%
Zircon	120ppm
Trace elements	0.21%

observed, indicating a progressive structural degradation). (c) The reactivity of sample (MW) clay, jointed by CEC, increase during grinding because of increased surface area of clay and porosity.

3. The silicate lattices are not broken down by oxidizing acids, and to give a full break down, and thus to releases fully the associated trace elements, it is necessary to digest such samples in a mixture containing HCl and HF. This breaks the silicate lattices and release the silicon as volatile SiF_4 .With heavily polluted samples it is rarely necessary to use HCl in the digestion as pollutant material does not enter the silicate lattice, and may be extracted with other acids such as HNO_3.

REFERENCES

Adamis, Z., and Fodor, J. (2005). Bentonite and Kaolin Selected Clay Minerals, US. Environmental Protection Agency, Washington, DC, and Regional Office for the Americas of the WHO, Geneva: 50-69.

Al-Ani, T., and Sarapaa, O. (2008). Clay and Clay Mineralogy, Geological Survey in Finland, Helsinki University: 84-90.

Al-Kateeb, Al. A. (2001). Soils Pollution, Alexandria, Egypt. Unpublished Ph. D. Thesis, University of W. Virginia, USA: 186. (In Arabic).

Atkins, P., De Paula., J. (2001). Atkins' Physical Chemistry, 7th edn., Oxford University Press, Oxford: 508-595.

Atkins, P. W. and Beran, J. A. (1992). General Chemistry. *2nd edn. , Scientific American Books*, W.H. Freeman, New York: 922p.

Christian, G. D. (2004). Analytical Chemistry, John Wily and Sons Inc., printed in USA, *6th edn.*: 211p.

Greenberg, A. E., Clesceri, L .S., Eaton, A. D., and Franson, M. A. (2005). Standard Methods for the Examination of Water and Waste Water: Washington, D.C., American Water Works Association, *21st edn***:** 1368p.

Greenland, D. J. and Hayes, M. B. H. (1981). The Chemistry of Soil Processes, by John Wiley & Sons, Ltd., UK: 602p.

Harris, D. C. (2007). Qualitative Chemical Analysis, W.H. Freeman Company, New York, USA, *7th edn:* 141-147.

Harrison, R. M., and De Mora, S. J. (1996). Introductory Chemistry for the Environmental Sciences, 2ndedn., Printed in the UK at the University Press, Cambridge: 133-160.

Higson, P. J. (2005). Analytical Chemistry, Oxford University Press, UK: 210p.

Hollas, J. M. (2004). Modern Spectroscopy, John Wiley & Sons Ltd, UK: 311p.

Lagaly, G. (1995). Surface and Interlayer Reactions, Bentonites as Adsorbents, Printed in the UK: 137-144.

Mitchell, J. K., 1993, Fundamentals of Soil Behavior, John Wiley and Sons, Inc., New York, pp 437, *2nd edn.*: 32-55.

Navarotsky, A. (1994). Physics and Chemistry of Earth Materials, Cambridge University , printed in the USA: 50-70.

Patnaik, P. (2004). Dean's Analytical Chemistry Hand Book, McGraw-Hill, *2nd edn*, USA: 1280p.

Skoog, D. A., and West, D. M. (2000). Analytical Chemistry an Introduction, Thomson Learning Inc., 7th edn, USA, p 204.

Sparks, D.L., 2003, Environmental Soil Chemistry, China Translation and Printing Services Ltd., *2nd edn.*: 43-291.

Stuart, B. H. (2004). Infrared Spectroscopy Fundamentals and Applications, John Wiley and Sons, Ltd. UK: 107p.

Welcher, F. J. (1975). Standard Methods of Chemical Analysis, printed in USA, *2nd edn.*: 1053p.

Willard, H. H., and Dean, J. A. (1988). Instrumental Methods of Analysis, Wadsworth Publishing Company, Belmont, California, USA, *7th edn.*: 424p.

Wright, J. (2003). Environmental Chemistry, Printed in Rutledge by Taylor & Francis Group, UK: 163-188.

Evaluation of the Total Quality Factors Based on Deming Management Model in Oil Industry in Libya - An Empirical Study

Redha M Elhuni* and M Munir Ahmad**

Abstract: The purpose of this paper is to investigate the quality management dimensions, based on Deming Management Model, in Oil industry in Libya. Questionnaire, semi structured interview and open interview were used to collect data from random sample of 42 quality-related managers from the Libyan Oil industry. Forty-five questionnaires were provided by hand to quality-related managers from the Libyan Oil companies. A total of 42 were returned sufficiently completed, that gave us a response rate of approximately 93.33%.

The regression analysis indicated that these organizations implement total quality management practices. The findings suggest that an integrated approach is required to implement the total quality management practices in order to realize strategic quality objectives.

This study is subject to the normal limitations of survey research. The data is based on individual opinion of quality related managers, which may bring in some bias. Further research needs to be done to advance our knowledge and to further support the findings. For instance, a larger sample size and more items per Deming principle may be used in future studies to duplicate these results and to increase the internal consistency of the scales. Deming Management Model is applied to one industry in this study. Therefore, to establish the generalization of the Model within the context of Libya, it needs to be tested in other industries setting, both in public and private sectors.

The study extends the applicability of the Deming Management Model to a new industry and country. Collectively, the results of the research provide more understanding of issues relating to quality management in developing countries and a framework for enhancing organizational effectiveness. Therefore, the research can make a useful contribution.

Keywords: Total quality management; TQM; Libya oil and gas sector; Deming management model.

INTRODUCTION

The change over to TQM is currently very popular in the Libyan Oil and Gas companies (LOGCs) as a method to improve productivity, eliminate waste, reduce operation costs, and enhancing customer satisfaction. Although it is a relatively new and revolutionary approach in Libya, more and more companies are committing themselves to invest in TQM in the long term.

The problem however, is that most LOGCs today seem to be paying only lip service to TQM implementation. To what extent are executives in LOGCs aware of the impending pressures on them to conform to quality standards? Even those who may be aware, what practical steps are they take to ensure conformity?

In fact, TQM is not well defined in Libya, but is still an ambiguous concept. However, the major TQM implementation practices in LOGCs could be summarized as: Using various kinds of quality management tools such as the Quality control (QC) seven tools and statistical process control (SPC) in practice; implementing QC circles activities; analyzing and identifying quality-related costs; emphasizing quality inspection; In the meantime, many people working in LOGCs accepted education and training on quality management system such ISO.

A comprehensive review of literature indicated that the research on Libya's TQM domain, however, has not attracted much attention. As a result, couple research has been conducted in construction and manufacturing field. However, no research has been

*Libyan Petroleum Institute, Libya
**School of Science and Engineering, Teesside University, Middlesbrough,UK

conducted in Oil and Gas Sector that is progressing at a gallop pace.

Commercial oil was discovered in Libya in 1957. Today, Libya ranks 17th in the global oil production. Since 1986, the Libyan oil and gas industry has been managed by the (NOC) which is the national oil company of Libya.

The objective of the study is to assess the TQM practices of LOGCs and suggest measures for improving their competitiveness. The study was undertaken to address the lack of empirical findings concerning application of fundamentals of total quality management within Libyan Oil and Gas Companies (LOGCs).

The results will provide an objective insight to LOGCs to plan necessary steps of action to achieve and sustain quality based competitive advantage. The study will generate information that will be useful for organizational directors in evaluating TQM practices in their own companies, in Libya, using Deming Management Model to enhance organizational performance. The study would add to the continued efforts toward theory building, enhancement, wider applicability, and provide support in consolidation of knowledge.

LITERATURE REVIEW

The existing quality management philosophy has been strongly influenced by the thoughts of Deming, Juran, Crosby, Feigenbaum, and Ishikawa. Deming (1986) 14 points, Juran (1988) trilogy and 10 steps, Crosby 14 steps to quality improvement, as identified by Brocka and Brocka (1992), and Feigenbaum (1983) approach of total quality control are essential elements of a quality strategy. The holistic approach to quality management is vital for competitiveness.

Deming Management Model is based on the theory of Deming that was formulated by Anderson *et al* (1994). Deming Management Model encompasses the TQM philosophy articulated in a prescriptive set of 14 points. The 14 points in Deming Management Model are essential statements, which lay down the foundation and action plan for intra-organizational and inter-organizational behaviour. Adoption of these 14 points offer organizations with requisite strength and energy and facilitate organizations to overcome obstacles in achieving performance excellence.

The extensive readings of published materials by W. Edwards as well as other quality experts, have developed seven constructs, these seven constructs is displayed in Table 1. Insights from the readings were further developed via a three-round Delphi study using academic and practitioner experts to identify the concepts underlying Deming's 14 points (Deming, 1986). The research team then clustered these concepts into seven constructs to represent the content of the Deming management method.

The framework of Deming Management Method expresses effectiveness of the model through concerted leadership efforts toward establishment of cooperative and learning organization systems that facilitates achievement of efficient process management. The realization of process management practices enables organizations to achieve customer satisfaction through continuous improvement and employee fulfillment. The theoretical framework based on the seven constructs expressing Deming Management Method is shown in (Fig. 1).

There have been two empirical examinations of the Deming management model in the literature. First, Anderson *et al* (1995), using measures identified from the world-class manufacturing research project (Flynn, Schroeder, & Sakakibara, 1994), found exploratory support for most of the hypothesized relationships. Second, Rungtusanatham *et al* (1998) replicated the first study using manufacturing facilities located in Italy. Both the Anderson *et al* (1995) and Rungtusanatham *et al* (1998) studies supported most of the relationships in the Deming management model. However, both studies suggested that additional testing of the Deming

Table 1. Descriptive statistics.

Constructs	Mean	STDV	Cronbach's alpha (α)
Visionary leadership	4.03	0.643	0.853
Internal and external cooperation	3.96	0.664	0.822
Learning	3.71	0.682	0.875
Process Management	4.16	0.670	0.863
Continuous improvement culture	4.38	0.524	0.842
Employee involvement and participation	3.85	0.612	0.865
Customer Satisfaction	4.32	0.360	0.786

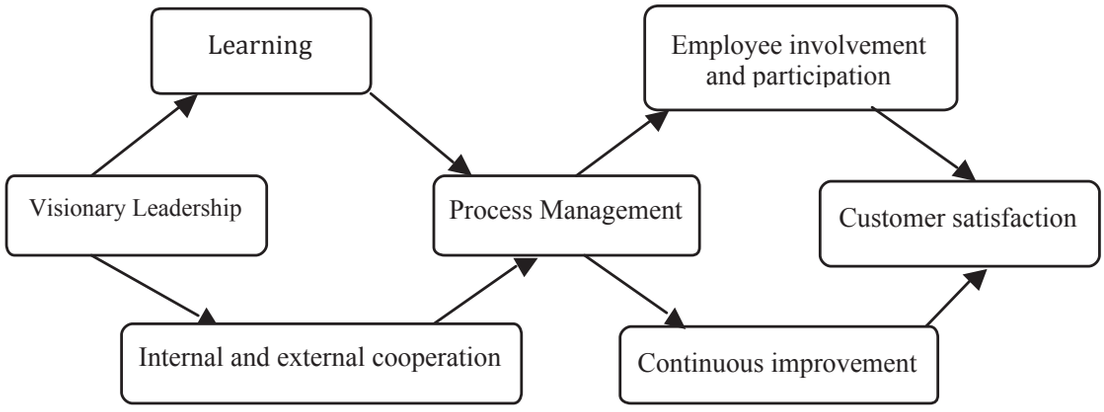


Fig.1. Proposed theory framework

management model in other industries to confirm its generalizability, and applicability across sectors, countries, industries, employee groups and time periods was necessary. Other researchers also argued that refinement efforts through testing of this theory in different contexts would contribute toward better understanding, and assist in knowledge consolidation (Sousa and Voss, 2002).

Mann and Kehoe (2004) examined the process of TQM implementation in 21 UK-based organisations with at least two years' experience of TQM and concluded that the implementation processes used were largely diverse and there appeared to be no one dominant approach. The data led them to conclude that there appeared to be no optimum approach to implementation. Newall and Dale (2002) concluded from their study of eight UK organisations (seven were manufacturers). They identified six phases: awareness; education and training; consolidation; planning, problem identification and problem solving; implementation of quality improvement plans; and assessment.

DEVELOPMENT OF HYPOTHESES

Deming Management Method Model has identified seven constructs. To develop hypotheses, these seven constructs are examined separately to explore various dimensions underlying these constructs. Review of literature has been done to find support for these constructs.

Visionary Leadership: The key role top management commitment and leadership plays in driving company-wide quality management has been recognized by practitioners and researchers as one of the major factors for achieving successful quality performance (Deming, 1986; Flynn *et al* 1994; Juran, 1988; Puffer and McCarthy, 1996). The top management element is the first step for successful implementation of TQM through leadership strategy and policies; quality planning; management by fact; and managing innovation. Top Management Commitment & Leadership encompasses the role of top management in defining a vision, mission, strategic objectives, and shared values for the organization's growth and development. In quality management context, the leaders need to emphasize the importance of transformation through open communication to achieve a shared approach to the change. Quality Gurus stressed that leadership is vital for effective implementation of total quality management initiatives. Zairi (1994) argued that in TQM environment, leaders focus on employee autonomy, recognition, coaching, and development. Rao *et al* (1999) noted that top management is responsible for quality leadership and providing support to achieve superior performance. Pierce and Niewstrom (2000) highlighted the importance of leadership in the process of ascending to world-class status, and emphasized the need for leadership to establish a high-performance culture, high-performance delivery processes and services in support of this objective.

Internal and external cooperation: Internal and external cooperation is the propensity of the organization to engage in non-competitive activities internally among employees and externally with respect to suppliers. Internal cooperation is about teamwork, unity of purpose, mutual trust and respect for all, participation at all levels and shared approach throughout the

organization. The internal cooperation construct is like human resource concept which included items such as communications, employee involvement, training and education, recognition of support for quality objectives, and employee satisfaction (e.g., Cook & Verma, 2002).

The external cooperation concept, many argue that internal customer-suppler relationship is the basic principle behind this approach. Oakland (2000) referred to this as a series of internal supplier-customer chains contributing to the company-wide quality involvement in the company.

The suppliers' interaction with customers provides opportunities for improvement of products, services, and processes. Rao *et al* (1999, p. 1052) noted that "quality-oriented companies pursue a proactive strategy in developing long term relationship with suppliers and provide support to enhance the quality of their suppliers. Evan and Lindsay (2002, p. 99) found that a "reduced supply base decreases the variation coming into the processes, thus reducing scrap, rework, and the need for adjustment to accommodate this variation." In oil industry, optimizing supplier relationships lead to reduce refining maintenance costs, eliminating defects, and conducting risk-based inspection. Slaight (1999) opined that through effective suppliers' relationship, companies can reduce procurement cost by 10% to 15%.

Learning (Training and Education): Learning is about, the organizational capability to recognize and nurture the development of its skills, abilities, and knowledge base. According to Deming (1986), learning is a continual process for the purpose of expanded knowledge with its own merit. Huq and Martin (2000 p. 97) identified that "education and training of workforce is the basic quality principle." Roth and Jackson (1995) considered operational competence of service firms as their organizational knowledge. Barret (1999) noted that learning culture fosters innovative thinking and collaborative system. Authors argue that superior Organisational performance depends on learning. Therese (2007) experienced positive impact of training and development on individuals and the organization to create value for customers. Organizations undergoing organizational transformation undertake learning in order to develop the organizational capabilities which are required for survival and success in the new context. Organizational capabilities represent 'the ability of an organization to perform a coordinated set of activities utilizing organizational resources, for the purpose of achieving a particular end result' (Helfat & Peteraf, 2003: 999). Organizations in developing economies need to develop two types of organizational capabilities. First, they need to develop the basic operational capabilities required for survival in a market economy, but missing in a centrally planned economy, for instance marketing, finance, HR and information sharing (Filatotchev *et al* 2003; Hitt *et al* 2000; Peng, 2000; Puffer, 1994). Second, since the institutional environment in transition economies is unstable, they need to develop the capability to respond quickly to changing competitive conditions, described as strategic flexibility by Hitt *et al* (1998).

Process Management: Process management is set of methodological and behavioral practices emphasizing the management of process, or means of actions, rather than results Anderson *et al* (1994). Process management emphasizes adding value to processes increasing quality levels, and raising productivity per employee. Process management also involves analysing and redesigning processes to remove problems and inefficiencies in the organization (Dahlgaarde *et al* 2002; Deming, 1986). According to them, the greatest advantage of process management is that it helps an organization to understand how things are really done, revealing problems and bottlenecks. Process management also helps to reduce lead times, decrease costs, improve overall quality, and increase customer and employee satisfaction. Process measurement is a key to the success of any process improvement and can increase understanding of how processes are operating.

Continuous improvement: The concept of continuous improvement implies constant improvement in the processes, products and services. Deming (1986) stressed the organizations to improve continuously the products and services. Anderson *et al* (1994) identified that continuous improvement is based on process management practices that yield incremental improvement and innovations in products, services, and processes. It is argued that the values driving CI are basically the values that ensure commitment to customer satisfaction. Juergensen (2000) viewed continuous improvement as an initiative that enhances success and decreases failures. Bessant *et al* (1994) found it

as a process of continuous incremental innovation. Overall performance is associated with continuous improvement (CI). According to TQM theory, the best way to improve organizational output is to continually improve performance (Corbett and Rastrick, 2000).

Employee involvement and participation: The impact of employee support in achieving quality goals has already been praised by many authors (Ahire *et al* 1996; Black and Porter, 1996; Blackburn and Rosen, 1993; Clemmer, 1990; Creech, 1994; Evans and Lindsay, 2002; Kanji and Asher, 1993; Oakland, 2000; Sun, 2000; Thiagarajan and Zairi, 1997). Middle management and shop floor employees need to be involved in the organisational process as major internal stakeholders. They need to be motivated to rise up to the challenge of adopting TQM through appropriate training packages as well as work-based incentives. Oakland (1989) concluded that employees are a source of ideas and their competency need to be harnessed to transform these ideas into reality. Deming (1986) and Feigenbaum (1983) strongly supported employees' participation in decision making. Researchers and quality experts have concluded that employee fulfillment is a multidimensional concept based on employees' total satisfaction from work environment and manifests in job satisfaction, pride of workmanship, commitment, continuous learning and innovation, and results in enhanced quality of product, processes, and services to the customers (Locke, 1976).

Customer Satisfaction: Customer satisfaction is at the heart of TQM philosophy. A proactive approach to responding to changing customer' needs are vital to attract and retain customers. By close interaction with customers, organizations can determine customers' changing requirements, trends and use them as yardstick with their competitors (Vavra, 2002). Parzinger and Nath (2000, p.356) clearly stated that "in TQM environment the job is not done until the customer is satisfied."Anderson *et al* (1994) noted that customer satisfaction is exemplified by customer driven focus. Literature review highlights that internal quality practices of organizations affect customer satisfaction (Nilsson *et al* 2001). The research found that worker awareness and mindset is positively related to customer satisfaction.

Based on the study of literature, following hypotheses emerge:

H 1. Visionary leadership has positive relationship with internal and external cooperation.
H 2. Visionary leadership has positive relationship with learning.
H 3. Internal and external cooperation has positive relationship with process management.
H4. Learning has positive relationship with process management.
H 5. Process management has positive relationship with continuous improvement.
H6. Process management has positive relationship with employee involvement and participation.
H7. Continuous improvement has positive relationship with customer satisfaction.
H8. Employee involvement and participation has positive relationship with customer satisfaction.

METHODS

Instrument Development: The present study used the questionnaire developed by Douglas and Fredendall (2004). The questionnaire was designed to suit the research objectives stated. Information obtained through the questionnaire is complemented by a second level of investigation (qualitative survey) in the form of semi-structured interviews. After a comparison of different rating scales, the researcher selected an approach that he believed would make the questionnaire easy for the respondents to answer, and thus encourage them to participate. Therefore; the questionnaire developed uses a Five points Likert scale from strongly agree (5) to strongly disagree (1) was adopted for the study.

Pilot Testing of Instrument: To validate the instrument, a sample of 6 executives, managers, and experts in TQM was used in the pilot testing. The Cronbach's alpha for different variable. This indicated that the reliability of multi-item scales corresponding to them ranged between 0.827 and 0.912. Generally, a reliability coefficient of 0.70 or more is considered to be good (Nunnally, 1978).

Sample and Data Collection: Combination of methods was used in order to improve both the reliability and validity of the data gathered. 45 questionnaires were personally distributed to quality-related managers and collected by hand in

Libya. A complete set of questionnaire including a covering letter accompanied the questionnaire. Forty two out of Forty five questionnaires were returned sufficiently completed, that gave us a response rate of approximately 93.33%. Semi-Structured Interviews with 6 case studies were conducted with managers represented different functional areas of the LOGCs. In-depth open interview with 2 case studies were conducted.

Validity of Instrument*:* The researcher believes that the instrument used in this research has content validity, since the development of the measurement items was based primarily on an extensive review of the literature and detailed evaluations carried out by academicians and practitioners. In addition different studies have used the measuring scales and validated the items of the instrument (Ahire *et al* 1996; Quazi *et al* 1998; Rao *et al* 1999; Saraph *et al* 1989). The content validity of the instrument of this study was established using two stages. First, for face validity, the instrument was presented to a panel of two quality experts who approved that the items measure the concept. In the second step, the questionnaire was given to four experts, two in academic positions and two managers working in LOGCs to ensure that the participants understand the items in the questionnaire. The response was affirmative and no ambiguity was experienced in understanding the items in the instrument. For construct validity, confirmatory factor analysis was undertaken for this study to validate the factors used in the instrument.

Data Analysis*:* Both descriptive and inferential statistics has been used to analyze the data. Statistical Package for Social Sciences (SPSS-version 17) software has been used in the analysis.

RESULTS AND ANALYSIS

Results of descriptive statistics: All the constructs drew general agreement with regard to the responses table (1). The results, based on mean score and standard deviation, reflect respondents' general agreement to the dimensions of the model. *Results of reliability and validity of data*: The Cronbach's alpha for individual variables indicated that the measure is compositely reliable and internally consistent as recommended by Nunnaly (1978).

Results of test of normality of data: The results of multi-collinearity analysis indicated that Tolerance levels (< or equal to 0.01) and Variation Inflation Factor (VIF) value (below 10) are within acceptable range. The values of Durbin Watson for all variables are also within limits ((between 1.5 and 2.7). The tests exhibit that multi-collinearity problem does not exist.

Results of factor analysis: For construct validity, to validate the underlying structure of the model, confirmatory factor analysis was conducted. Prior to the conduct of confirmatory factor analysis, Kaiser-Meyer-Olkin (KMO) static and Bartlett's Test of Sphericity was performed. The KMO value (KMO = 0.875) indicated that the degree of common variance among the seven variables was marvelous (Malhotra, 2004). The Bartlett's test of sphericity indicated a Chi square 7.205 with an observed significance level of p<

Table 2. Correlation Matrix

Variables	VL	IEC	PM	CI	EIP	CS
Visionary Leadership **(**VL**)**						
Internal and external Cooperation **(**IEC**)**	*0.647					
Learning (LG)	*0.555	*0.437				
Process Management (PM)	*0.635	*0.248	*0.298			
Continuous improvement culture (CI)	*0.242	*0.555	*0.608	*0.631		
Employee involvement and participation (EIP)	*0.546	*0.618	*0.635	*0.608	*0.622	
Customer Satisfaction (CS)	*0.175	*0.179	*0.213	*0.195	*0.186	*0.205

*Correlation is significant at p < 0.01 level (2 – tailed)

Table 3. Path Analysis

Path	R^2	Beta	T value	Significance
Visionary leadership to internal and external cooperation	0.512	0.647	13.872	**0.001
Visionary leadership to learning	0.387	0.635	13.118	**0.001
Internal and external cooperation to process management	0.340	0.555	11.048	**0.001
Learning to process management	0.340	0.555	12.687	**0.001
process management to Employee involvement and participation	0.399	0.631	13.102	**0.001
Process management to Continuous improvement	0.370	0.608	12.832	**0.001
Employee involvement and participation to Customer Satisfaction	0.254	0.307	4.213	**0.001
Continuous improvement to Customer Satisfaction	0.315	0.139	2.222	**0.001

Significance level= **, p< 0.001

.001. Based on the results, it was inferred that the relationship between the variables was strong and appropriate for factor analysis. These factors explained 72% of variance.

Results of Correlation Analysis: To determine the relationship between variables, correlation analysis was done. Table 2 indicates that all factors have positive and significant relationship. Results reflect that the correlation between variables is significant ($p < 0.001$).

Results of Regression Analysis: The result of regression equation based on path analysis is reflected in Table 3. The variable of Visionary leadership positively and significantly predicts in Internal and external cooperation, $F (1, 288) = 176.733$, $p < 0.01$, Beta = 0.647, $p< 0.01$, R Square = 0.512; continuous improvement, $F (1, 288) =158.929$, $p < 0.01$, Beta = 0.635, $p< 0.01$, R Square = 0.387; and Customer Satisfaction, $F (1, 288) =168.877$, $p < 0.01$, Beta = 0.555, $p<0.01$, R Square = 0.340. The results leadership's commitment to the total quality management creates enabling environment in the organization and fosters employee involvement and participation; customer satisfaction promote continuous improvement. Customer satisfaction was regressed on predicting variables of employee involvement and participation and continuous improvement. The combination of these variables significantly predicts customer satisfaction, $F (2,287) =73.857$, $p < 0.01$ (Beta = 0 .555, $p < 0.01$) for employee involvement and participation, (Beta = 0. 631, $p < 0.01$) for continuous improvement. The R Square = 0.340 and 0.399 depicts that these variables explain 34% and 39.9% of variance in the customer satisfaction.

DISCUSSION

The main objective of the study was to empirically examine the TQM practices in LOGCs. The results of the study provided strong empirical support to the Deming Management Model. The path analysis also provided empirical evidence for the support of the theoretical relationship proposed in 8 hypotheses. The crucial role of visionary leadership in pursuing companywide quality policies has been well established.

Visionary leadership pursues a partnership with employees, customers, and other stakeholders. The study indicated positive and statistically significant relationship with customer satisfaction. Kanji and Moura (2001) acknowledged that outstanding leaders can contribute heavily to total quality by creating inspiring innovative environment.

Employee involvement and participation manifest in individual's job satisfaction, job commitment and the pride of accomplishment of products, services quality, and possession of knowledge for initiating improvement in processes. The study found positive and statistically significant relationship with customer satisfaction. Sureschandar *et al* (2001) found evidence of strong relationships between employee perception of employee well-being and customer perception of service quality and satisfaction. Rienzer and Testa, (2003) acknowledged that the benefits for internal customers' satisfaction (employee

satisfaction) provide greater support for continuous improvement.

Continuous improvement is one of the essential factors in TQM success. Rapid changes in technology and customers' requirements require a flexible approach toward aligning organizational products, processes and services to meet and exceed ever changing customers' needs. The results highlight positive and statistically significant relationship with customer satisfaction.

The findings of this study highlight the important role of the leadership in driving the total quality management practices in LOGCs. The findings supported the studies regarding the dominant role of leadership in planning and implementing TQM practices (Pun & Hui, 2002; Tata & Prasad, 1998; Singh *et al* 2007; Zairi, 1994).

The findings support the idea that effects of visionary leadership on customer satisfaction is dependent on creating and sustaining a quality focused organizational culture (Waldman & Gopalakrishnan, 1996).

CONCLUSIONS

The aim of the study was to examine the total quality management practices of Libyan Oil and Gas Companies (LOGCs). The results have reflected that these organizations implement TQM practices. There is, however, lack of a structured mechanism for self evaluation of these practices. These companies need to focus on these important issues to identify gaps, and strive for continuous improvement to achieve competitiveness.

The study provides a significant contribution in the application of Deming Management Model to oil industry in a different cultural context. The sound theoretical and empirical support for different variables in the oil and gas industry advocates that researchers and academician should include these dimensions in the study and research. The study indicates that Deming Management Model is equally applicable to oil industry and reinforces the belief in the effectiveness of the Model.

The success of TQM practices depend on a supporting organizational culture. In Libyan business environment, the cultural dimension becomes even more important for the success of TQM initiatives. The response to TQM initiatives in different cultural context has been studied. There is a need to further study the cultural dimensions in Libyan organizations and its compatibility to TQM philosophy, identifying the bottlenecks for adaptation of this philosophy of change and initiating the required response to enhance organizational competitiveness.

The model also offers opportunities for its further development based on the study and exploration of additional paths. In order to manage quality dimensions effectively, identification of barriers in planning and implementation of TQM practices is essential in Libyan organizations. This aspect should be investigated with a view to adopt a proactive response strategy to eliminate these barriers to realize the objectives of TQM practices.

This study offers strong evidence of continued significance of quality management as a priority issue for developing countries to remain competitive in domestic and global markets. The results of this research indicate that quality management practices have been well embedded in the managerial practices of organizations in developing countries.

REFERENCES

Ahire, S. L., Golhar, D. Y., & Waller, M. A. (1996). Development and Validation of TQM Implementation Constructs. *Decision Sciences,* 27(27): 23-56.

Anderson, J. C., Rungtusanatham, M., & Schroeder, R. G. (1994). A Theory of Quality Management Underlying the Deming Management Method. *Academy of Management Review,* 19(3): 472–509.

Anderson, J., Rungtusanatham, M., Schroeder, R., & Devaraj, S. (1995). A Path Analytic Model of A Theory of Quality Management Underlying the Deming Management Method: Preliminary Empirical Findings. *Decision Sciences,* 26: 637-658.

Anderson, M., & Sohal, A. S. (1999). A Study of Relationship Between Quality Management Practices and Performance in Small Business. *International Journal of Quality & Reliability Management,* 16 (9): 859-77.

Barrett, F. (1999). Creating Appreciative Learning Cultures. *Organizational Dynamics, Autumn*: 36-49.

Bessant, J., Caffyn, S., Gilbert, J., Harding, R., & Webb, S. (1994). Rediscovering Continuous Improvement. *Technovation,* 14 (1): 17-29.

Black, S. A, Porter, L. J. (1996). Identification of the Critical Factors of TQM. *Decision Sciences,* 27(1): 1-21

Blackburn, R. and Rosen, B. (1993). Total Quality and Human Resource Management: Lessons Learned

from Baldbridge Award-Winning Companies. *Academy of Management Executive,* 7(3): 49-66.

Brocka, B., & Brocka, M.S. (1992). Quality Management: Implementing the Best Ideas of the Masters, Richard D. Irwin, Homewood, IL. Clemmer, J. (1990). Firing on All Cylinders. *Judy Piatkus Publishers*, London.

Cook, L. S., & Verma, R. (2002). Exploring the Linkages Between Quality System, Service Quality, and Performance Excellence: Service Providers' Perspectives. *Quality Management Journal,* 9(2): 44–56.

Corbett L. M. and Rastrick K. N. (2000). Quality Performance and Organisational Culture: A New Zealand Study. *International Journal of Quality & Reliability Management,* 17(1): 14-26.

Creech, B. (1994). The Five Pillars of TQM: How to Make Total Quality Management Work for You. New York, NY: Truman Talley Books/Dutton.

Dale, B. G. (2003). Managing Quality (*4th ed*.). Hertfordshire: Prentice Hall. 676 p.

Deming, W. E. (1986). Out of the Crisis: Quality Productivity and Competitive Position, Cambridge University Press, Cambridge. 508p.

Deming, W. E. (1993). The New Economics for Industry, Government, Education. Cambridge: *Massachusetts Institute of Technology, Center for Advanced Engineering Study*.

Dahlgaard F. F.; Poksinska, B.; Antoni, M. (2002). The State of ISO 9000 Certification: A Study of Swedish Organizations. *The TQM Magazine,* 14(5): 297-306.

Evans, J. R., & Lindsay, W .M. (2002). The Management and Control of Quality (*5th ed*). South-Western, USA.

Feigenbaum, A. V. (1983). Total Quality Control (*3d Ed*) New York, McGraw-Hill. 896p.

Filatotchev, I., Wright, M., Uhlenbruck, K., Tihanyi, L. & Hoskisson, R. E. Governance. (2003). Organizational Capabilities, and Restructuring in Transition Economies. *Journal of World Business.* 38: 331-47.

Flynn, B. B., Schroeder, R. G. and Sakakibara, S. (1994). A Framework for Quality Management Research and an Associated Measurement Instrument. *Journal of Operations Management,* 11(4): 339-366.

Hitt, M. A., Dacin, M. T., Levitas, E., Arregle, J. L. & Borza, A. (2000). Partner Selection in

Emerging and Developed Market Contexts: Resource-Based and Organizational Learning Perspectives. *Academy of Management Journal,* 43: 449-67.

Hitt, M. A., Keats, B. W. & DeMarie, S. M. (1998). Navigating in the New Competitive Landscape: Building Strategic Flexibility and Competitive Advantage in the 21st Century. *Academy of Management Executive.* 12: 22-42.

Huq, Z., & Martin, T. (2000). Workforce Cultural Factors in TQM/CQI Implementation in hospital. *Health Care Management Review,* 25(3): 80-103.

Helfat CE, Peteraf MA. (2003). The Dynamic Resource-Based View: Capability Lifecycles. *Strategic Management Journal,* 24: 997-1010.

Juergensen, T. (2000). Continuous Improvement: Mindsets, Capability, Process, Tools and Result. *The Juergensen Consulting Group, Inc., Indianapolis,* IN. 598p.

Juran, J. M. (1988). Juran on Planning for Quality. Cambridge MA: Productivity Press. A *Life Cycle Approach (5th ed), Homewood*, IL, Irwin. 634p.

Kanji, G. K. and Asher, M. (1993). Total Quality Management Process-A Systematic Approach. Advances in Total Quality Management Series. Carfax Publishing, Abingdon.

Kanji, G. K., & Moura, P. (2001). Measuring Leadership Excellence. *Total Quality Management,* 12(6): 701-718.

Locke, E. A. (1976). The Nature and Causes of Job Satisfaction. In: *Handbook of industrial and organizational psychology* (ed. by: M. D. Dunnette). Chicago: Rand McNally: 1297-1349.

Mann R. S, Kehoe D. F. (2004). The Implementation of Total Quality Management (paper 2). *Quality World Technical Supplement*, 12(2): 11-23.

Newall D, Dale BG. (2002). The introduction and development of a quality improvement process: a study. *International Journal of Production Research*, 29(9): 1747-1760.

Nilsson, L., Michael, D., Johnsonb, Gustafssonc, a. (2001). The Impact of Quality Practices on Customer Satisfaction and Business Results: Product Versus Service Organizations. *Journal of Quality Management,* 6(1): 5-27.

Nunnally, J. C. (1978). Psychometric Theory (*2d. ed*.), McGraw-Hill, New York; 640p.

Oakland, J. S. (1989). Total Quality Management, Butterworth-Heinemann, Oxford.

Oakland, J. S. (2000). Total Quality Management-Text with Cases (*2d Edition*). Butterworth-Heinemann, Oxford: 380p.

Oakland, S. and Oakland, J. S. (2001). Current People Management Activities in World-Class Organizations. *Total Quality Management,* 12(6): 773-88.

Parzinger, M. J., & Nath, R. (2000). A Study of the Relationships Between Total Quality Management Implementation Factors and Software Quality. *Total Quality Management,* 11(3): 353–371.

Peng, M. W. (2000). Business Strategies in Transition Economies. Thousand Oaks, CA, Sage: 322p.

Puffer, S. M. (1994). Understanding the Bear: A Portrait of Russian Business Leaders. *Academy of Management Executive,* 8: 41-54.

Puffer, S. M. and McCarthy, D. J. (1996). A Framework for Leadership in a TQM Context. *Journal of Quality Management*, 1(1): 109-130.

Pun, K., & Hui, I. (2002). Integrating the Safety Dimension into Quality Management Systems: A Process Model. *Total Quality Management,* 13(3): 373-391.

Quazi, H.A., Jemangin, J., Kit, L.W., Kian, C.L. (1998). Critical Factors in Quality Management and Guidelines for Self-Assessment, the Case of Singapore. *Total Quality Management,* 9(1): 35-55.

Rao, S. S., Solis, L. E., & Raghunathan, T. S. (1999). A Framework for International Quality Management Research: Development and Validation of a Measurement Instrument. *Total Quality Management,* 10(7): 1047–1075.

Roth, A. V. and Jackson, W. E. (1995). Strategic Determinants of Service Quality and Performance: Evidence from the Banking Industry. *Management Science,* 41: 1720-733.

Rungtusanatham, M., Forza, C., Filippini, R., & Anderson, J. (1998). A Replication Study of Theory of Quality Management Underlying the Deming Management Method: Insights from an Italian Context. *Journal of Operations Management,* 17: 77-95.

Saraph, J. V., Benson, P. G., & Schroeder, R. G. (1989). An Instrument for Measuring the Critical Factors of TQM. *Decision Sciences,* 20(4): 810-29.

Singh, P .J, Chua, M.W., & Sum, C. C. (2007). Deming Management Method: Applying Theory to Public Sector Organizations and Testing Refinements. [Online] Available: http://www.ecom.unimelb.edu.au/downloads/nus_symposium/Singh_paper.pdf

Slaight, T. H. (1999). Strategic Sourcing: Not a Squeeze Your Vendor Process. *Telecommunication,* 33(3): 59-62.

Sousa, R., & Voss, C. (2002). Quality Management re-Visited: A Reflective Review and Agenda for Future Research. *Journal of Operations Management,* 20(1): 91-109.

Sun, H. (2000). A Comparison of Quality Management Practices in Shanghai and Norwegian Manufacturing Companies. *International Journal of Quality & Reliability Management,* 17(6): 636-660.

Sureshchandar, G. S., Rajendran, C., & Kamalanabhan, T. J. (2001). Customer Perceptions of Service Quality: A Critique. *Total Quality Management,* 12(1): 111-124.

Taguchi, G. (1979). Introduction to Off-Line Quality Control. *Japanese Standards Association*. Tokyo. 857 p.

Therese A. J. (2007). Total Quality Management and Performance, the Role of Organization Support and Co-Worker Support. *International Journal of Quality and Reliability Management.* 24(6): 617-627.

Thiagarajan, T. and Zairi, M. (1997). A Review of Total Quality Management in Practice: Understanding the Fundamentals Through Examples of Best Practice Applications, Part 1. *The TQM Magazine,* 9(4): 270-86

Tata, J., & Prasad, S. (1998). Cultural and Structural Constraints on Total Quality Management Implementation. *Total Quality Management,* 9 (8): 703-10.

Vavra, T. G. 2002. Customer Satisfaction Measurement Simplified: A Step-by-Step Guide for ISO 9001:2000 Certification. Milwaukee; WI: ASQ Quality Press.

Waldman, D. A., & Gopakakrishnan, M. (1996). Operational, Organizational, and Human Resource Factors Predictive of Customer Perceptions of Service Quality. *Journal of Quality Management,* 1(1): 91-107.

Wilsey, M. D. (1995). Leadership and Human Motivation in the Workplace. *Quality Progress,* 28(11): 85-88.

Zairi, M. (1994). Leadership in TQM Implementation: Some Case Examples. *The TQM Magazine,* 6(6): 9-16.

Zhang, Z. (2000). Developing A Model of Quality Management Methods and Evaluating Their Effects on Business Performance. *Total Quality Management,* 11(1): 129-37

Effect of Plastic Deformation on the Corrosion Behavior of Super1Duplex Stainless Steel

A. Elhoud*

Abstract: The effect of plastic deformation of super duplex stainless steel on the subsequent corrosion behavior in 3.5% sodium chloride solution was investigated. Potentiodynamic corrosion measurements were conducted at temperature of 90°C. Deformation at levels of 8 and 16%plastic strain showed high intensity of deformation bands. The presence of such deformations was highly sensitive to corrosion attack in the tested environment. The results confirmed the significant effect of deformed surfaces, as the plastic deformation level increased the corrosion resistance of super duplex stainless steel decreased.

Keywords: Super duplex stainless steel, Plastic deformation, Potentiodynamic

INTRODUCTION

Duplex stainless steels have become more attractive than single phase austenitic and ferritic grades in many applications owing to their high strength and corrosion resistance in chloride containing media. Like other stainless steels this alloy relies on surface passive films for their excellent corrosion resistance. The fine austenite-ferrite microstructure of these materials promotes an excellent combination of toughness and mechanical resistance, desirable for many applications in the chemical and petrochemical industries (Tavares, *et al* 2005). Plastic or cold deformation is invariably present in components used in plant due to fabrication techniques used in machining, bending and rolling. Stress present due to cooling from high temperatures during welding and welding in constrained geometries cause deformation in materials and high stress/strains (Kain, *et al* 2004). Cold working generally introduces deformation substructures like dislocation networks, twins, deformation bands, cell structures and emerging slip steps at thesurface (Kamachi, 2000). Structure transformation, which occurs in metals under plastic deformation bycold work, is accompanied by considerable changes in the most important physical andmechanical properties. Crystal defects, metallurgical structure, and composition affect the properties of the protective passive films, such as thickness, strength solubility, and porosity,and hence the susceptibility to localized breakdown and pitting of the alloy (Barbucci, 2002).

Stainless steels are fit for cold work and mechanical treatment, allowing controlled modulation of the mechanical resistance, but corrosion properties can be modified in an uncontrolled way. The corrosion resistance of stainless steels can be significantly affected by metallurgical parameters such as cold working, alloy composition, inclusions, heat treatment, sensitization, precipitation (Hamad, 2006). It has been reported that structure nonhomogeneity encourages localized corrosion of passivable metals. In particular, the detrimental effect of plastic deformation on the corrosion resistance of stainless steel has been shown. Thus, cold working has been found to lower the critical pitting potential of austenitic stainless steel in 0.1M HCl and in solution simulating seawater (Barbucci, 2002).There are studies reporting detrimental influence of cold work on the pitting corrosion resistance of AISI 304 (18Cr-8Ni), 316L (17Cr-12Ni-2Mo) and 301 (17Cr-7Ni) type austenitic stainless steels (Hamad, 2006); Mazza,1979).

In duplex stainless steels and due to the presence of a massive second phase during processing makes deformation more complicate and the microstructure is a decisive limiting factor of plastic behavior. In addition to the work hardening and softening mechanisms required to deform each phase, the ferrite/austenite boundaries play an important

*Libyan Petroleum Institute, Gargarish Road Km 7, P. O. Box 6431, Tripoli-Libya. Email: aelhoud@gmail.com

role in duplex microstructure; the accommodation of macroscopic deformation depends on plastic characteristics of both phases (Reis, 2000). When the ferrite and austenite phases in duplex stainless steel are jointly deformed, the distribution of strains among the phases is no longer uniform. When straining begins in duplex stainless steels, strain concentrations appear in the softer ferrite (Reis, 2000). As deformation increases, strain gradients may decrease as a result of accommodation mechanisms such as recovery and recrystalization, cracking formation, as well as interphase and grain boundary sliding. On cold working strain induced martensite and residual stress are significantly introduced on the surface, which affects the localized corrosion resistance by increasing the number of active anodic sites on the surface. Thus it is the aim of this paper to discuss the effect of the associated substructural development of the two phases of ferrite and austenite on corrosion resistance of duplex alloy.

SAMPLES AND TEST PROCEDURES

The chemical composition of the investigated super duplex stainless steel in weight percentage is 0.02%C, 24.84%Cr, 6.54%Ni, 0.45%Mn, 2.07%W, 0.34 % Si , 3.10%Mo, 0.28%N and the rest is iron. The as-received specimens were solution annealed at 1050ºC for 1 hour and water quenched. Specimens were machined in cylindrical tensile shape of 100mm length and 5mm diameter; a specimen schematic view is showing in Fig. 1. Before straining, specimens were mechanically polished starting with coarse grain emery paper of 200, 400, 600, 800 and 1200 and then followed by alumina paste in order to get a mirror like surface, then rinsed with acetone and dried by hot air. Specimens were strained in axial tension to the required plastic strain percentage at a constant rate of 0.2mm/ min using a tensile test machine. Metallographic observation using optical and scanning electron microscopy was carried out on strained and unstrained specimens after electrochemical etching in 10% oxalic acid solution.

After straining, electrochemical corrosion behaviour of the specimens was investigated using potentiodynamic polarization measurements in 3.5% sodium chloride according to ASTM G 5. The electrochemical cell was a conventional three electrode cell comprises the working (specimen), the reference electrode silver / silver chloride (Ag/AgCl) and platinum counter electrode. All electrochemical measurements were made at temperature (90°C) using **Princeton Potentiostat/Galvanostat (263A)**. Before potentiodynamic measurements, the electrodes were immersed in a glass corrosion cell filled with 700ml of the investigated electrolyte. The open circuit potential became stabilized after 30min. The potentiodynamic curves measurement were recorded at a potential scan rate of 1 mV /s starting from 100Mv below the open-circuit potential (OCP). The potential scan continued while the corrosion current density was monitored. Analysis from the polarization curves were made to determine the breakdown potential at which the current increased with time and exceeded 1mA.

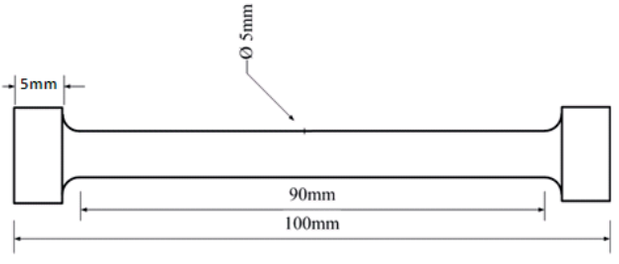


Fig. 1. Schematic of the test specimen.

LABORATORY OBSERVATIONS

Surface Texture: The morphology of the surfaces after straining was carefully examined using scanning electron microscopy (SEM). Examples of unstrained and strained surfaces texture are shown in (Fig. 2a-c). It can be seen that the unstrained specimen has uniform texture as shown in Fig. 2a. In the case of deformation, the deformed textures are composed of elongated grains and shear bands crossing the grains. The presence of shear bands was found on 8% and 16% strained specimens, (Figs. 2b & c). However, the percentage of shear bands is higher in the specimen strained to 16% (Fig. 2c).

Etched Surface Texture: Samples after straining were polished to mirror for metallographic examination. By contrast on the oxalic acid etched surfaces shown in Fig. 3(a, b), there was a significant difference between undeformed and deformed surfaces on ferrite (a) and austenite (g) grains. Change in surface texture at ferrite phase (a) when deformation conducted at 16% plastic strain is shown in (Fig. 3b).

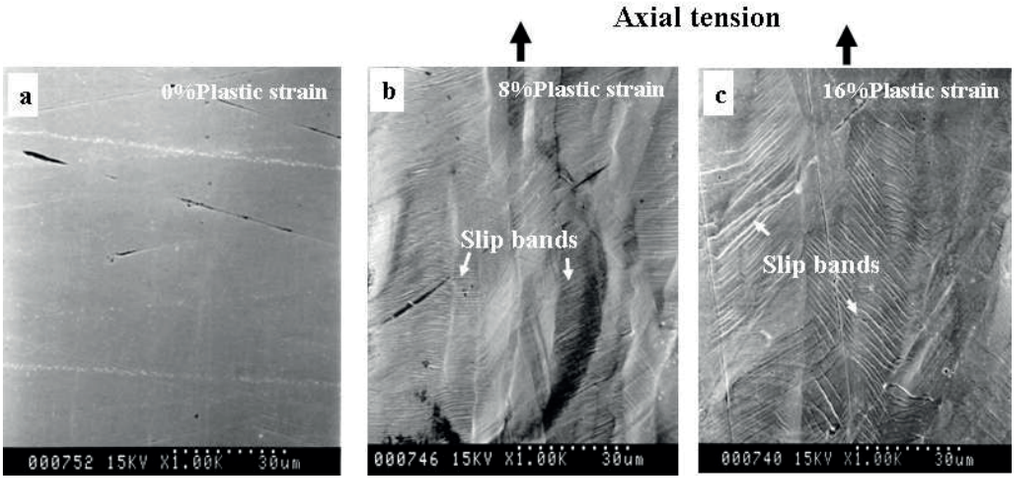


Fig. 2. SEM photographs of unstrained, 8% and 16% plastic strain super duplex alloy surfaces.

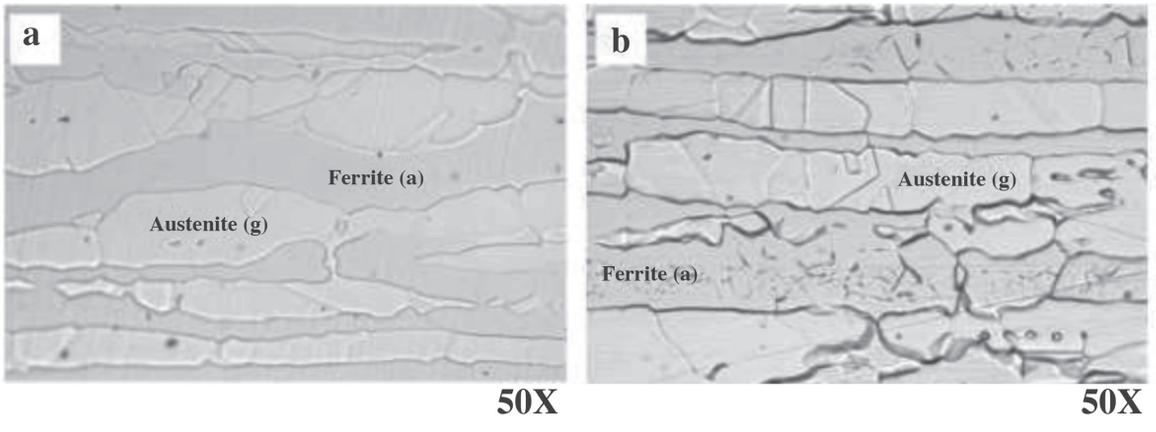


Fig. 3. Microstructure of super alloy in annealed condition; a) - Solution annealed with no plastic deformation, b) - 16% plastic strain. *10% Oxalic acid etching.*

The same etched surfaces were evaluated using scanning electron microscope. Deformation marks on ferrite (a) and austenite (g) grains can be seen clearly at higher magnification (Figs. 4a & b) of 16% plastic strain specimen. In the centre there is a cross-grid network of screw deformation bands. The Figure also illustrates that the deformation in ferrite has formed a well defined slip band structure. The features of the structures in the ferrite grains were similar to those reported in the literature (Chiu, 2006). Small voids coupled with the slip bands exist in austenite phase. Dislocations are also located and clustered near to the ferrite austenite interface as shown in Fig. 4b. Generally the more densely populated bands are within the grains that were more susceptible to deform.

***Electrochemical Tests**:* The potentiodynamic results at 90ºC in 3.5% sodium chloride solution are shown in (Fig. 5). The results show the effect of metallurgical changes caused by plastic deformation on the pitting corrosion potential of super duplex stainless steels. Specimens had different corrosion resistance to the corrosive. The pitting corrosion resistance of the annealed (zero cold work) samples decreased after cold work (plastic deformation). The passivity region of the annealed samples is much wider than those with plastic deformation. The wider passivity range manifested the delay in pitting corrosion as indicated by pitting potential value. The difference in pitting corrosion values at two cold work levels is slight compared to the annealed condition samples.

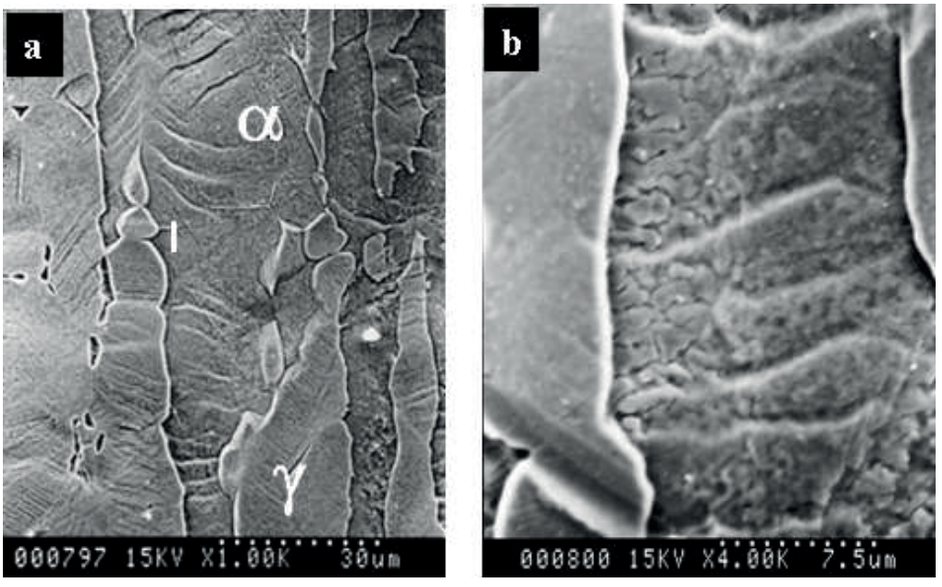


Fig. 4. SEM photographs; a) - 16% plastic strain, b) high magnification at local I. *10% Oxalic acid etching* .

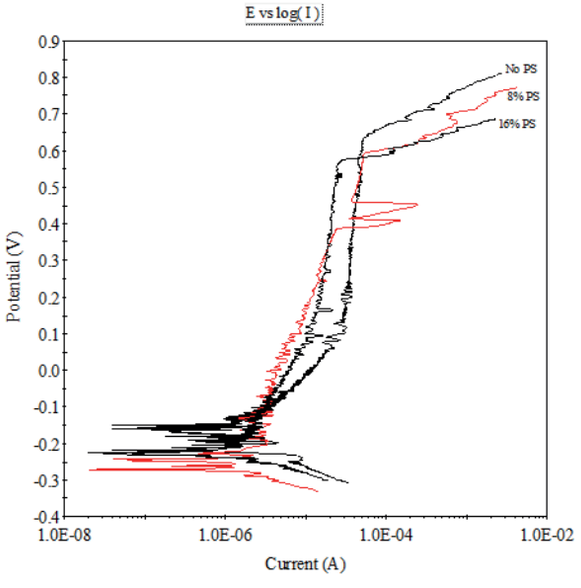


Fig. 5. Potentiodynamic polarization curves of super duplex alloy in 3.5% sodium chloride at 90ºC.

Corrosion morphology: Corrosion morphology results showed that the plastic strain produced defects that acted as anodic sites for pitting corrosion initiation. The intense slip bands formed in the grains promoted rapid dissolution during the corrosion test. Figs. 6a-c) shows the corrosion morphology of 8% plastic strain specimen. The results illustrate an isolated shallow pit with edges indicating that the ferrite grains are the candidate propagation path as can be seen at higher magnification images in (Figs. 6b & c).

The morphology of corrosion was transformed to preferentially attack along the ferrite grains on 16% plastic strain specimen as illustrated in (Figs. 7a-c). Moreover, the fraction of cluster pits increased at grains containing shear bands or deformation marks. The presence of such clusters of attack specimen can be attributed to the sharp increase in shear bands on ferrite grains. Shear bands and deformation marks had poor corrosion resistance.

DISCUSSIONS

Plastic deformation resulted in a wide variety of slip bands in the deformed structure. Moderately and low intense slip bands were formed in the structure plastically deformed at 8% plastic strain. For specimens strained to 16% plastic strain, slip bands of higher intensity were produced. Intense slip bands were always produced in the ferrite grains and at austenite grain. This depends on the stacking fault energy of each phase. The value of stacking fault energy (SFE) plays an important role in the deformation process. Low SFE in nitrogen austenitic stainless steels promotes planar dislocation slip and twining, while a high concentration of nitrogen interstitials increases the friction stress against dislocation motion and twining nucleation (Jandova, 2004).

The deformation marks and dislocation structure in the straining course of the dual phase austenite-ferrite stainless steel are illustrated in the optical

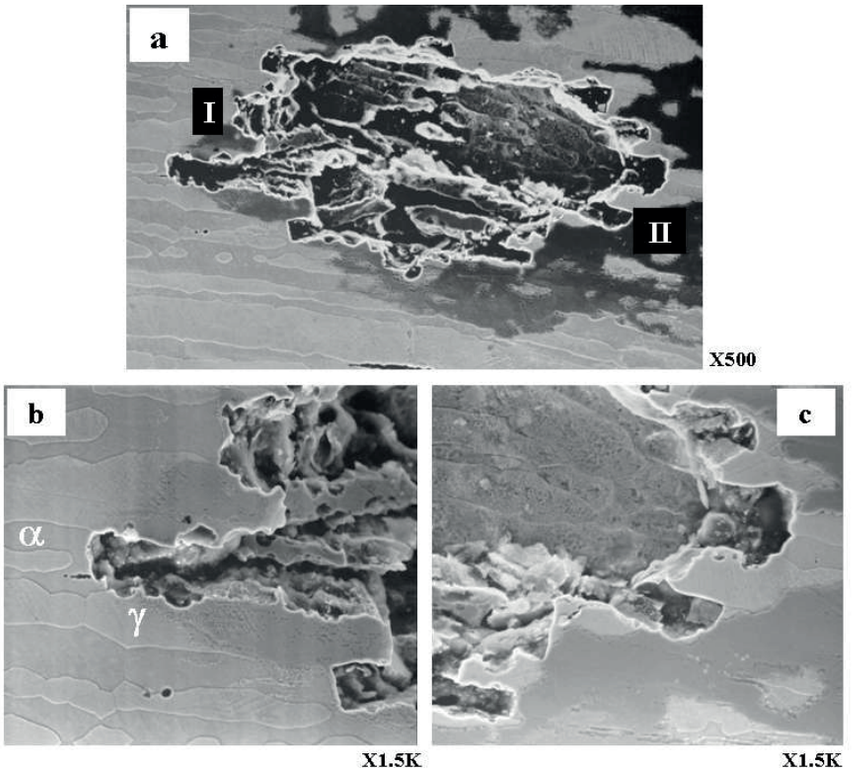


Fig. 6. Pitting corrosion attack on 8% plastic deformed super duplex alloy in 3.5% sodium chloride solution at 90ºC; a)- General view for a shallow pit , b and c)- Higher magnification at the pit propagation edges.

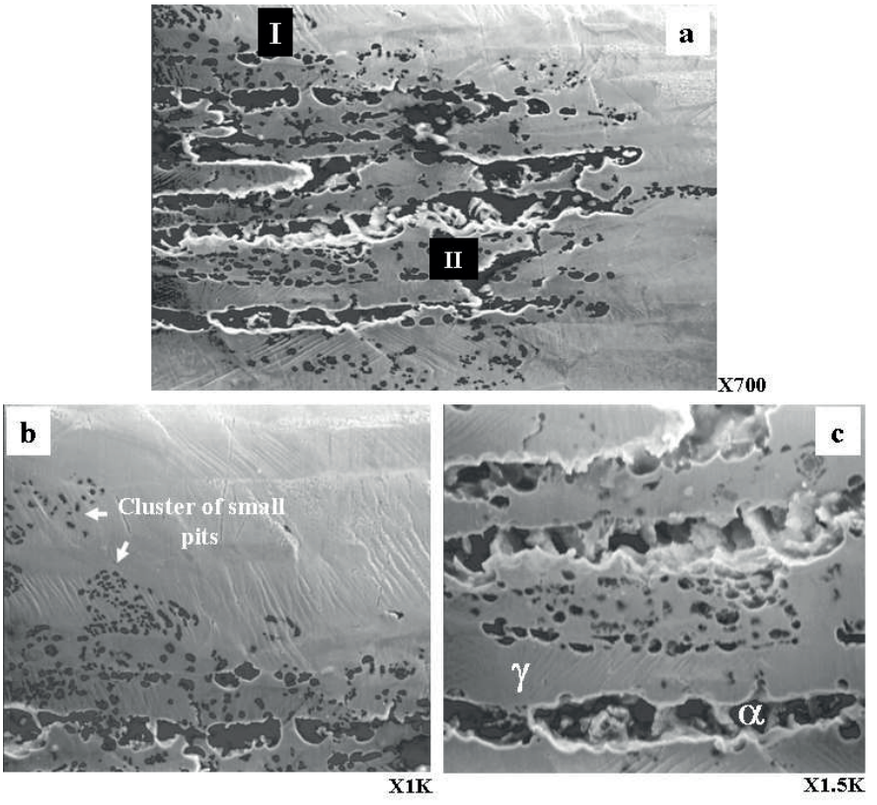


Fig. 7. Pitting corrosion attack on 16% plastic deformed super duplex alloy in 3.5% s sodium chloride solution at 90ºC; a)- General view for severe attack, b)- high magnification at circumferential pit side and at the deformation bands and c)- High magnification inside the pit along the grains.

and scanning electron microscope results in (Figs. 3 and 4a & b). The dislocation behavior at less plastic deformation is controlled and accommodated by the softer austenite phase. At high plastic strain the presence of slip bands is related to the plastic deformation of the two phases in the alloy especially ferrite. The ferrite phase accommodates more dislocation than the austenite phase at high plastic deformation. The high plastic deformation produces dislocation angles, which were more obvious in the ferrite phase. Deformation structure observed in the study are in good agreement with results found by (Mateo *et al* 1969) on the substructure evaluation after cyclic stress – strain tests on duplex alloy. After exposure to the corrosive environment, slip bands on ferrite grains were observed as nucleation and preferential sites for corrosion attack by chloride. As demonstrated previously that the strain-induced martensite and the residual stresses are significantly introduced on the surface, which affects the localized corrosion resistance by increasing the number of active anodic sites on the surface (Elayaperumal, 1972; Randak & Trautes, 1987). The susceptibility of cold worked 18 Cr – 10 Ni – 2 Mo steel to pitting corrosion in a NaCl solution was reported with the number of pits generally increasing with increase in the deformation, except in the 15 %deformation where low pit count and large average pit size were reported (Newman, 1987). In this study it was found that cold work of super duplex stainless steel to plastic strain values of 8% and 16% had an adverse effect on the corrosion resistance of the alloy in 3.5% sodium chloride solution. The results of this study further support the significant effect of plastic strain on the corrosion resistance of stainless steels. The results also indicate that the corrosion resistance of super duplex stainless steel was highly affected by the metallurgical structural changes caused by the plastic deformation. Dislocations and slip bands inside the microstructure work as corrosion initiation sites.

CONCLUSIONS

Straining in axial tension caused severe deformation of the passive film and the grains. The presence of deformation has a significant effect on the corrosion resistance of the super duplex stainless steel alloy. Corrosion resistance, as measured by pitting potential, was decreased by plastic deformation. Defects caused by deformation worked as anodic sites promoted corrosion dissolution rate. Deformation bands acted as acceleration preferential locations for new pits. Transformation to severe corrosion attack was along the most highly deformed grains which were mainly ferrite. Deformation on ferrite phase was more pronounced, This causing ferrite to be preferentially attacked by chloride.

REFERENCES

Barbucci, A., Cerisola, G., and Cabot P. L. (2002). Effect of Cold Working in the Passive Behaviour of 304 Stainless Steel in Sulfate Media. *Journal of the electrochemical society* 149 (12): B534-B542.

Chiu P. K., Wang, S. H., Yang, .J R., Weng, K. L. and Jason Fang (2006). The Effect of Strain Ratio on Morphology of Dislocation in Low Cycle Fatigued SAF 2205 DSSm. *Materials Chemistry and Physics* 98: 103-110.

Elayaperumal, K., De, P. K. and Balachandra, J. (1972). Passivity of Type 304 Stainless Steel Effect of Plastic Deformation. *Corrosion* 28: 269-273.

Hamad, A. S., Krjalainen, L. P. and, Somani, M. C. (2006). Electrochemical Corrosion Behaviour of a Novel Submicron-Grained Austenitic Stainless Steel in an Acidic NaCl Solution. *Materials Science and engineering* A43: 211-217.

Jandova, D., Rehor, J. and Novy, Z. (2004). Microstructural Changes Taking Place During the Thermo-Mechanical Processing and Cold Working of Steel 18Cr18Mn0.5N. *Journal of Materials Processing Technology* 157-158: 523-530.

Kain, V., Chandra, K., Adhe, K. N., De, P.K. (2004). Effect of Cold Work on Low-Temperature Sensitization Behaviour of Austenitic Stainless Steels. *Journal of Nuclear Materials* 334: 115-132.

Kamachi Mudali, U., Shankar, P., Ningshen, S., Sanjay, Rai and Dayal, R. K. (2000). Pitting Corrosion Studies on Cold Worked Nitrogen-Bearing Austenitic Stainless Steels. *7th International symposium on electrochemical methods in corrosion research, EMCR2000*, Budapest, Hungary.

Mateo, A., Llanes, L., Iturgoyen, L. and Anglada, M. (1996). Cyclic Stress-Strain Response and Dislocation Substructure Evolution of a Ferritic-Austenitic Stainless Steel. *Acta mater*, 44 (3): 1143-1153.

Mazza, B., Pedeferri, P., Sinigagila, D., Cigada, A., Fumagalli, G., Re, G. (1979). Electrochemical and Corrosion Behaviour of Work-Hardened Commercial Austenitic Stainless Steels in Acid Solutions. *Corrosion Science* 19: 907-921.

Randak. A. and Trautes Werks, F. W. (1987). The Effect od Alloyed Nitrogen or Dissolved Nitrate Ions on the Anodic Behavior of Austenitic Stainless Steel in Hydrochloric Acid. *Korros Corrosion Science* 27(8): 827-838.

Reis, G. S., Jorge, A. M., Balancin, O. (2000). Influence of the Microstructure of Duplex Stainless Steels on their Failure Characteristics During Hot Deformation. *Materials Research* 3(2): 31-35.

Tavares, S. M., Terra, V. F., Parada, J. M., and Cindra Fonseca M. P. (2005). Infuence of the Microstructure on the Toughness of a Duplex Stainless Steel, UNSS311 803. *Journal of Materials Science* 40: 145-154.

Incompatibility of Injection Water with Formation Waters from Different Depths

Mhamed A. Kahrwad, Majeda Erraies and Omar Mkhatresh*

Abstract: This paper aims to evaluate the damage that might occur as a result of incompatibility between injection and reservoir waters under reservoir and surface conditions. The amount of scale formed was determined at surface and reservoir conditions and different mixing ratios for five produced water samples which have been collected from locations DD and EE and tested for parameters of (Temperature, pH, O_2, CO_2 and H_2S) at site and metal content of these water samples (i.e. A, B, C, D, E and produced water) as shown in Table (1). Five water samples (i.e. A, B, C, D, E and produced water) have been tested for water-water compatibility test with different mixing ratios at surface and reservoir temperatures. Each mixture was kept for twenty four hours at desired temperature. The mixtures were filtered through cellulose nitrate filter paper with pore size of 0.45µm. The formed precipitates were collected, dried at 95 ºC and weighed to calculate the amount of deposits. The filtrates were immediately analyzed by Inductively Coupled Plasma (ICP) to determine the cations such as (Ca^{2+}, Sr^{2+}, Ba^{2+} and total Fe) that might react with anions (i.e. SO_4^{2-}, CO_3^{2-} and HCO_3^-) to form mineral scale. These tests demonstrated that $CaCO_3$ and $SrSO_4$ could be precipitated in different amounts depending on mixing ratios and conditions of temperature and pressure. Also, the scale predications have been performed using Multiscale software (7.1) to predict the tendency of scale formation and to compare that with the laboratory work which includes mixing of injection water with formation waters from different depths at surface and reservoir conditions of temperatures & pressures. This prediction covers the type, extent and location of all scale depositions that are expected to form during water injection period. Tests were conducted to identify the main scaling compounds when produced water mixed with the formation water. The basis of positive evidence of scaling encountered in the laboratory tests, a computer simulation program has been carried out to support the incompatibility of these brines when mixed at desired conditions.

Keywords: Water-Water compatibility, mineral scales, scale predictions

INTRODUCTION

The injection of water or gas into the oil-bearing reservoir is to increase the recovery factor and maintain the reservoir pressure. In water flooding, the injected water will react with both the water already in the pore space of the rock (formation water) and with the mineral in the rock itself. This reaction will create scale formation. Sulfate scale (i.e. gypsum $CaSO_4$, anhydrite $CaSO_4.2H_2O$, Celcitie $SrSO_4$, barite $BaSO_4$) may result from changes in temperature and/or pressure while water flows from one location to another, but the major cause of sulfate scale is the chemical incompatibility between the injected water, with high concentration of sulfate ion and formation waters, with high concentrations of calcium, barium and strontium ions. Changes in temperature, pressure, pH and CO2/H2S partial pressure could contribute in forming a scale (Amer Badr, *et al* 2009, Mackay, 2003). Scale also can deposit when two incompatible waters are mixed and super-saturation is reached (Vetter, *et al* 1982). It is important to treat the injection water with a scale preventive chemical to prevent precipitation in the immediate area of the injection wellbore (Charles, 2007).

Water-Water Compatibility Tests: Seven produced water samples have been collected from A and B oilfields and tested for parameters of (Temperature, pH, O_2, CO_2 and H_2S) at laboratories as shown in table (1) The metal content analysis of

*Production Chemistry Department, Libyan Petroleum Institute (LPI), P.O. Box 6431, Tripoli, Libya. E-mails: oasmkhatresh@gmail.com mhamed_lpi@yahoo.co.uk

Table (1) Water Chemistry of the brines used in the study (mg/L).

	A	B	C	D	E	F	Produced water
Na+	61200	32500	42500	28750	62000	70000	37750
K+	1000	1200	1100	700	2000	200	900
Ca++	7120	2640	4400	2480	5200	4760	4080
Mg++	1507	1118	1458	826	1847	1239	1142
Ba++	<0.0003	<0.0003	0.02	0.14	0.45	0.34	0.25
Sr++	518	125	467	337	1750	412	497
Fe(total)	0.088	3.9	0.1	0.19	0.04	0.04	0.02
CL-	111766	58324	77721	51240	111422	121051	68779
SO4--	480	450	660	550	220	570	720
HCO3-	281	647	317	488	268	244	305
CO3-	0	0	0	0	0	0	0
PH	6.02	6.51	6.4	6.17	6.34	5.91	6.54
Dissolved Solids evap@180Cº	189360	101450	133200	89008	189950	199300	117800

these water samples (i.e. C, D, E, F and produced water) were carried out according to standard methods.

Six water samples (i.e. C, D, E, F and produced water) have been tested for water-water compatibility test with different mixing ratios at surface and reservoir temperatures. Each mixture was kept for twenty four hours at desired temperature. The mixtures were filtered through cellulose nitrate filter paper with pore size of 0.45µm. The formed precipitates were collected, dried at 95 ºC and weighed to calculate the amount of deposits. The filtrates were immediately analyzed by Inductively Coupled Plasma (ICP) to determine the cations such as (Ca^{2+}, Sr^{2+}, Ba^{2+} and Fe) that might react with anions (i.e. SO_4, CO_3 and HCO_3) and form mineral scale.

In this study compatibility tests were performed between produced water which become injection water and mixed with different depths of formation waters (C, D, E, F and produced water) under surface and reservoir conditions. These compatibility tests showed different results based on the operating conditions as follows:

At surface temperature: Fig. 1 shows the amount of scale in (mg/L) as a result of mixing injection water with D formation water under surface temperature. The increasing in the amount of scale as injection water amount increases. This is confirmed in (Fig. 2) where the concentration of calcium increases as injection water increase. In (Fig. 2) blue columns represent calcium content before test and red columns represent calcium content after test. The drop in calcium ions (i.e. difference between blue and red columns) at each mixing ratio is scale based calcium ions. D formation water contains lower TDS (89,008 mg/L) than injection water (117,800mg/L).

E formation water shows high amount of scale which decreases as injection water increases as in (Fig. 3). Fig. 4 confirms the decrease in the calcium concentrations as the volume of injection water increase where the total dissolved solids in injection water is lower than in E.

Figs. 5 & 6 show the results of mixing A water with injection water under surface temperature where the amount of scale and calcium concentrations before and after test are clearly dropped as injection water volume increase (i.e. lower total dissolved solids). In (Figs. 7 & 8) the same trend of F results comparing with E & A waters (i.e. scale amount and calcium ions decreasing as injection water increase).

At reservoir Temperature: Fig. 11 shows scale amount of mixing of E formation water with injection water under reservoir temperature. The amount of scale is decreasing as injection water increase where TDS is lower than formation

water. In Fig. 12 a slight decline in calcium concentrations comparing with Figs. (3 & 4).

C and D water shows a slight decrease in the amount of scale at reservoir temperature as injection water volume increase (Figs. 9, 10, 13, 19 and 20). The change in calcium concentration is slightly dropped in Fig. 14 comparing with Fig. 2 at surface temperature.

Observations from Figs. 15, 16, 17 and 18 show no significant effect of temperature on scale formation as compared between surface and reservoir temperatures. Scale amount under reservoir temperature is less than scale amount under surface temperature which strongly affects the scale solubility; also slightly decrease in calcium concentrations comparing with high drop in calcium concentrations at surface temperature.

SCALE PREDICTION

The predictions of scales have been performed using Multiscale software (7.1) under surface and reservoir conditions of temperature and pressure. This prediction calculate the saturation ratio which gives the indication whether scale is likely to form if SR above zero or not. In (Fig. 21) saturation indices as result of mixing of A formation water with injection water under surface conditions. Saturation indices are increasing as A formation water increase where Celestite scale is likely to form associated with Anhydrite & Gypsum. Fig. 22 shows a stable result for sulfate scales as result of mixing of F with injection water. Fig. 23 shows increasing in potential of Celestite as injection water increase (i.e. high TDS). E shows very high potential of celestite to form (i.e. high content of strontium ions in formation water) associated with gypsum and anhydrite (Fig. 24). Fig. 25 shows a slight decrease in saturation ratios as a result of mixing C with injection water.

Under reservoir conditions Fig. 26 shows a slight increase in scale potential where the major scale (Celestite) is associated with gypsum and anhydrite in most cases. Celestite and anhydrite are highly expected to form as F formation water increase (Fig. 27). Fig. 28 E shows very high potential of celestite to form under reservoir conditions of temperature and pressure (i.e. high content of strontium ions in formation water). Gypsum and anhydrite are decreasing as E formation water increase. C under reservoir conditions showed lower potential of saturation ratio than surface conditions (Fig. 29).

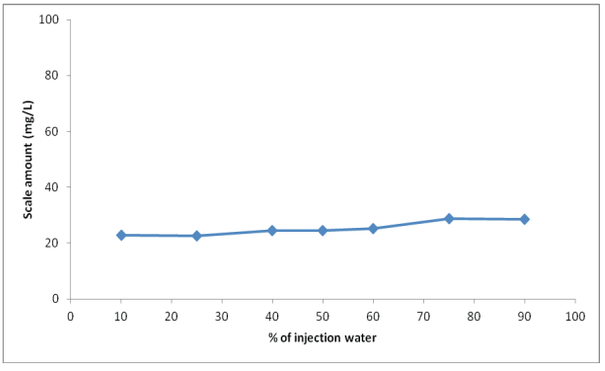


Fig. 1. Scale amount (mg) D mixing ratio at 106 ºF.

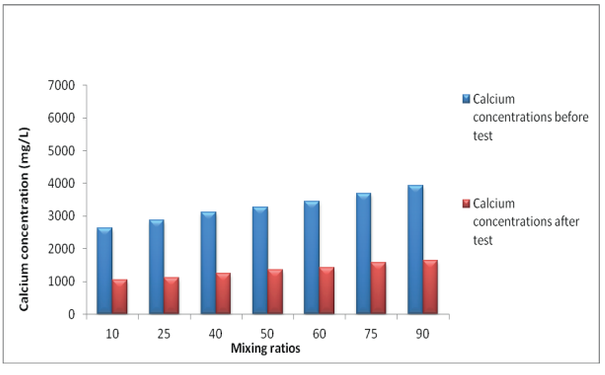


Fig. 2: Calcium concentration (mg/L) in filtrate for D after test at 106ºF.

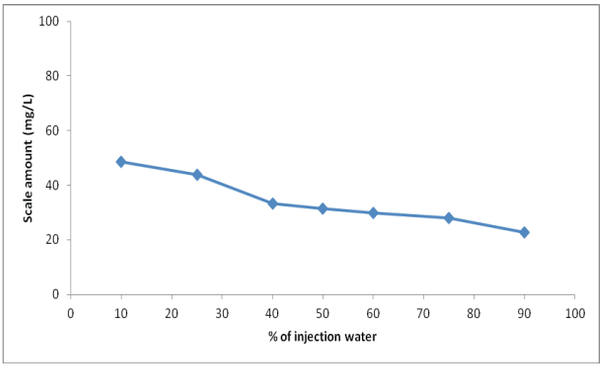


Fig. 3. Scale amount (mg) of E mixing ratio at 113 ºF.

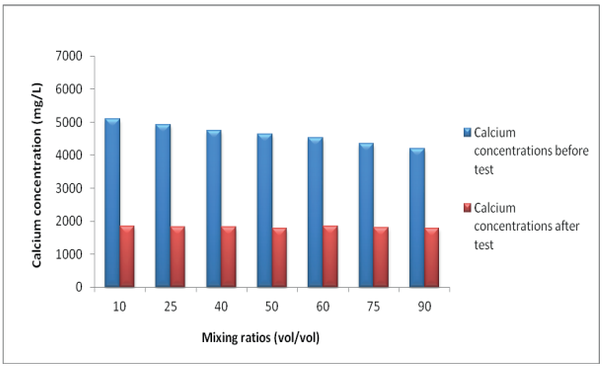


Fig. 4. Calcium concentration (mg/L) in filtrate for E after test at 113º

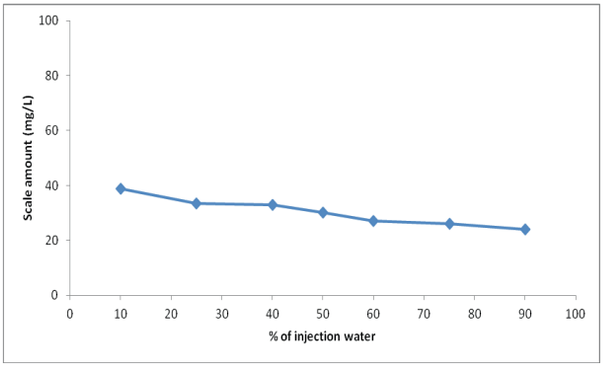


Fig. 5. Scale amount (mg) of A mixing ratio at 136ºF.

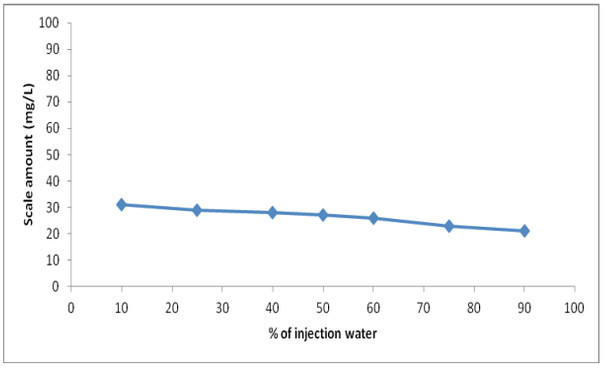


Fig. 9. Scale amount (mg) of C mixing ratio at 154 ºF.

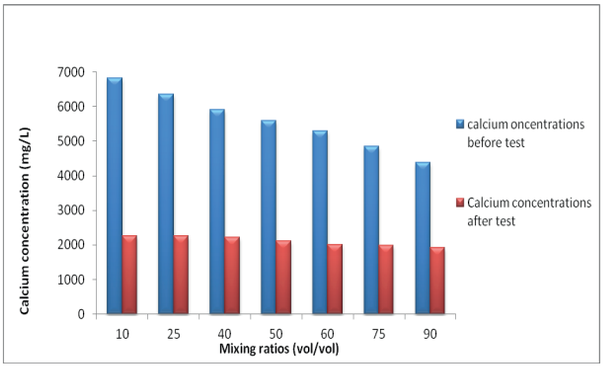


Fig. 6. Calcium concentration (mg/L) in filtrate for A after test at 136ºF.

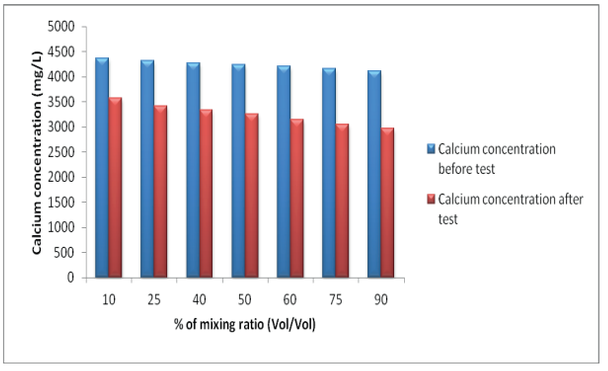


Fig. 10. Calcium concentration (mg/L) in filtrate for C after test at 154ºF.

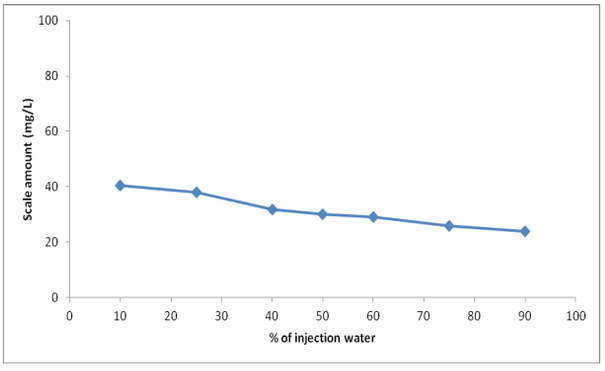


Fig. 7. Scale amount (mg) of F mixing ratio at 149 ºF.

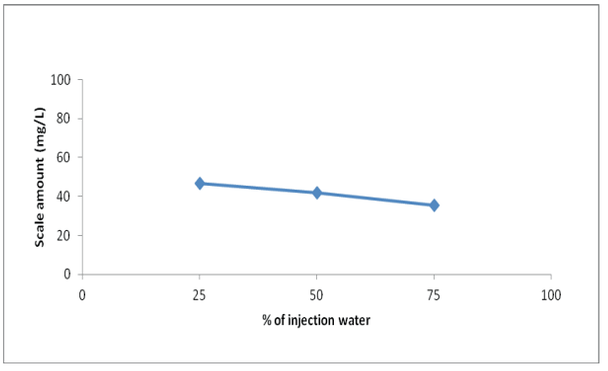


Fig. 11. Scale amount (mg) of E mixing ratio at 197ºF.

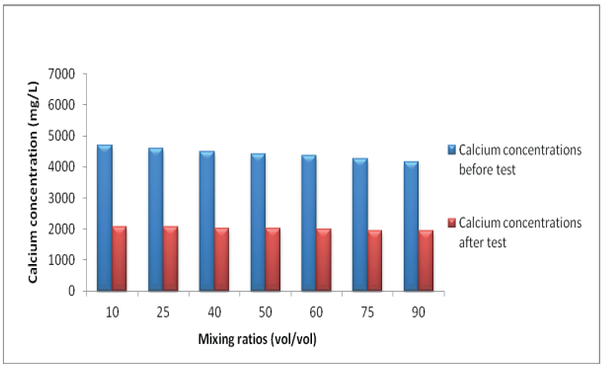


Fig. 8. Calcium concentration (mg/L) in filtrate for F after test at 149ºF.

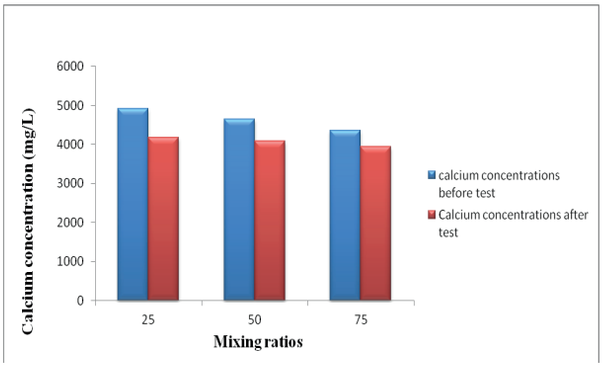


Fig. 12. Change in Calcium concentrations (mg/L) in filtrate for E before & after test at 197ºF.

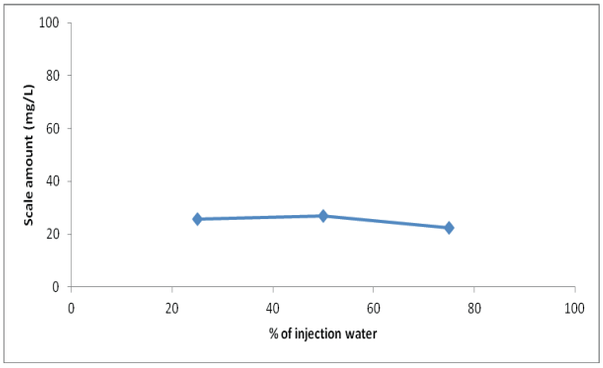


Fig. 13. Scale amount (mg) of D mixing ratio at 165ºF.

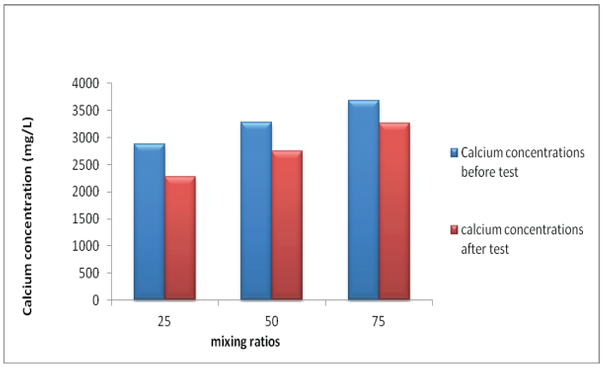


Fig. 14. Calcium concentration (mg/L) in filtrate for D mixing ratio at 165ºF.

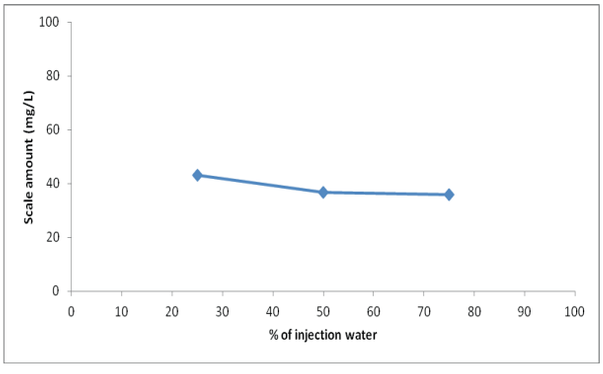


Fig. 15. Scale amount (mg) of F mixing ratio at 215ºF.

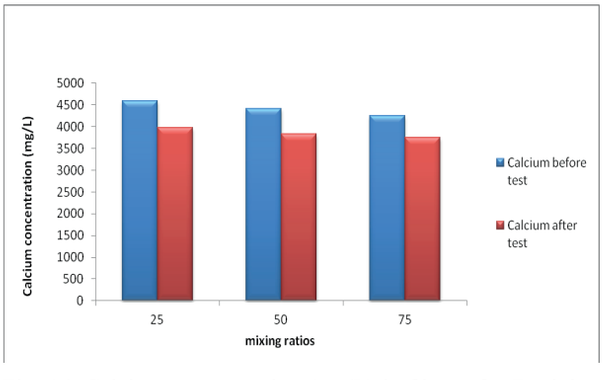


Fig. 16. Calcium concentration (mg/L) in filtrate for F mixing ratio at after test at 215ºF.

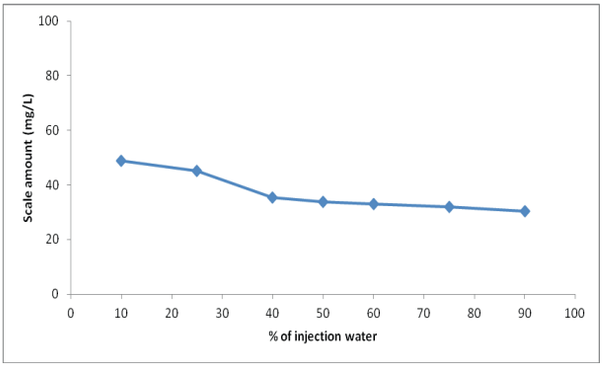


Fig. 17. Scale amount (mg) of A mixing ratio at 226 ºF.

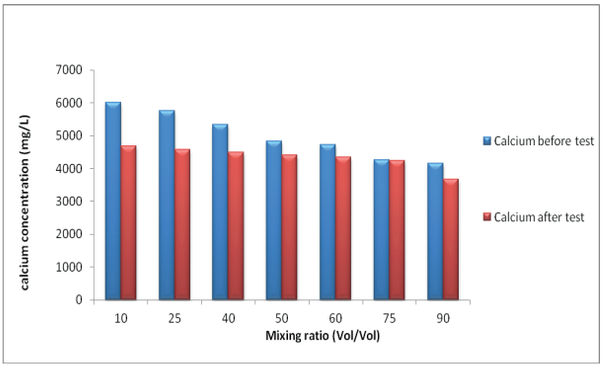


Fig. 18. Calcium concentration (mg/L) in filtrate for A mixing ratio at after test at 226ºF.

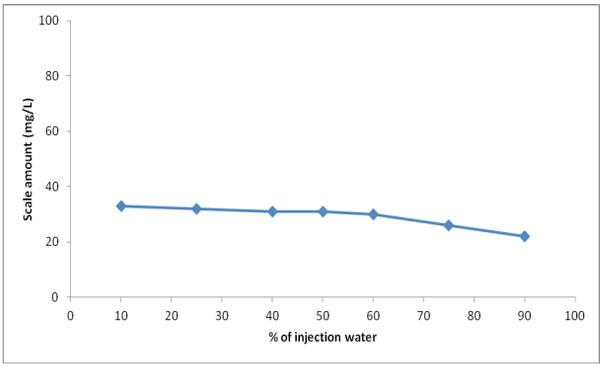


Fig. 19. Scale amount (mg) of C mixing ratio at 162ºF.

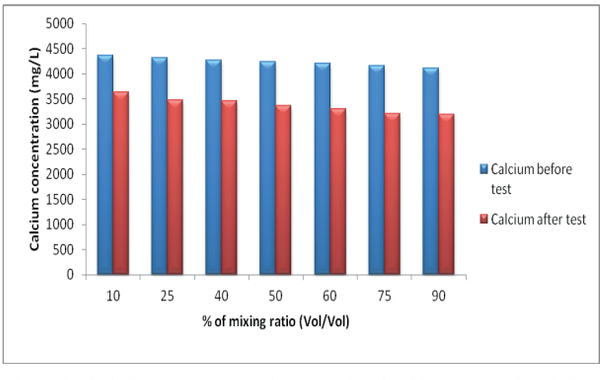


Fig. 20. Calcium concentration (mg/L) in filtrate for C mixing ratio at after test at 162ºF.

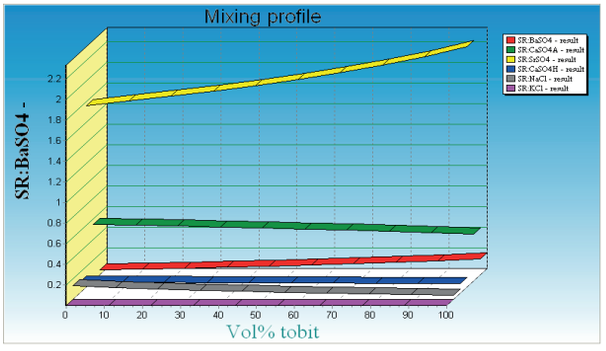


Fig. 21. Saturation indices for sulfate scales at surface conditions of temperature and pressure (A).

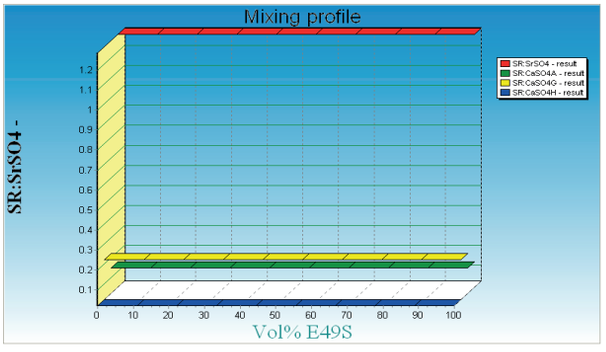


Fig. 22. Saturation indices for sulfate scales at surface conditions of temperature and pressure.(F).

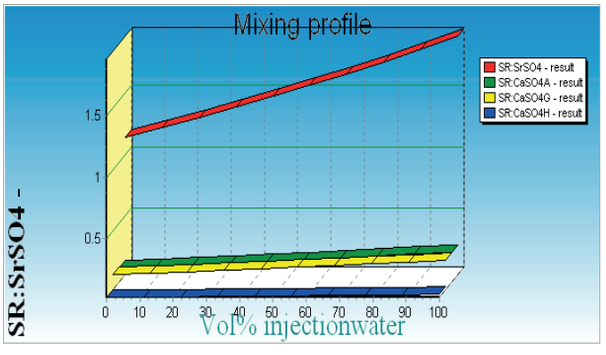


Fig. 23. Saturation indices for sulfate scales at surface conditions of temperature and pressure.(D).

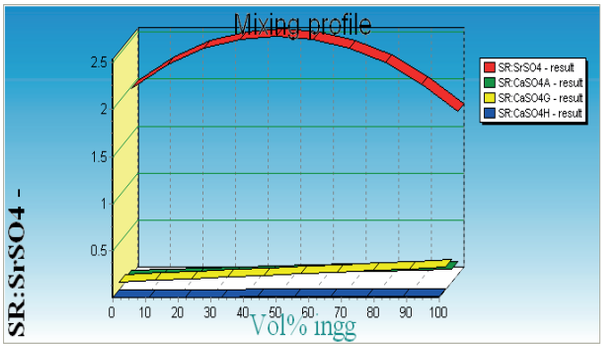


Fig. 24. Saturation indices for sulfate scales at surface conditions of temperature and pressure.(E).

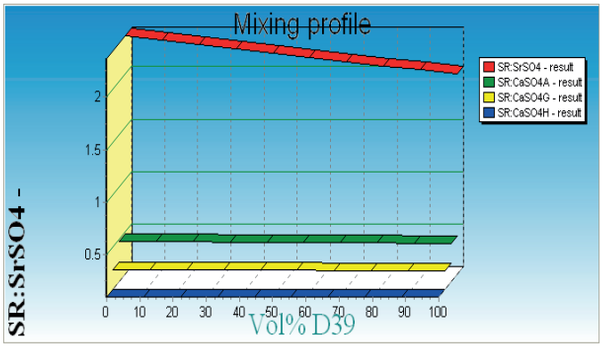


Fig. 25. Saturation indices for sulfate scales at surface conditions of temperature and pressure.(C) Under reservoir conditions.

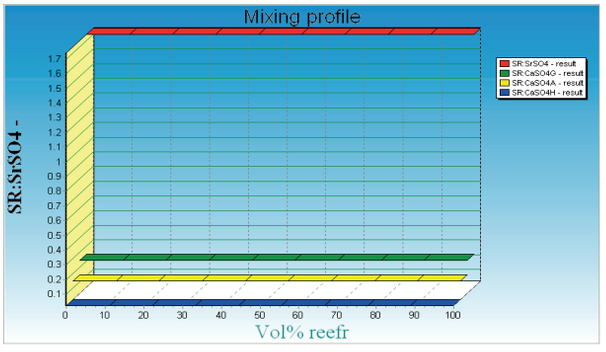


Fig. 26. Saturation indices for sulfate scales at reservoir conditions of temperature and pressure(A).

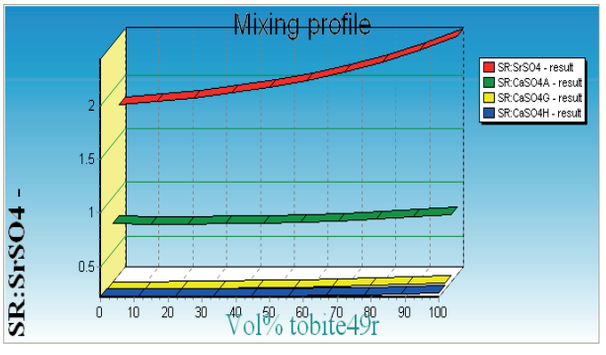


Fig. 27. Saturation indices for sulfate scales at reservoir conditions of temperature and pressure (F).

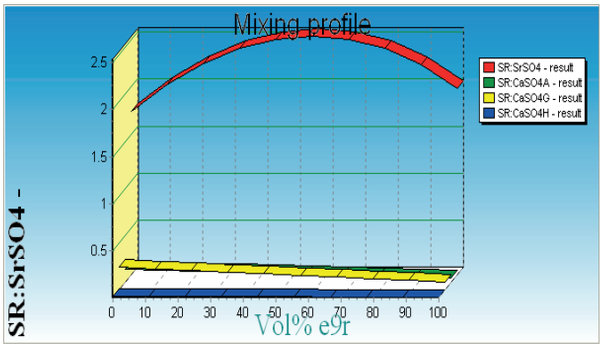


Fig. 28. Saturation indices for sulfate scales at reservoir conditions of temperature and pressure (E).

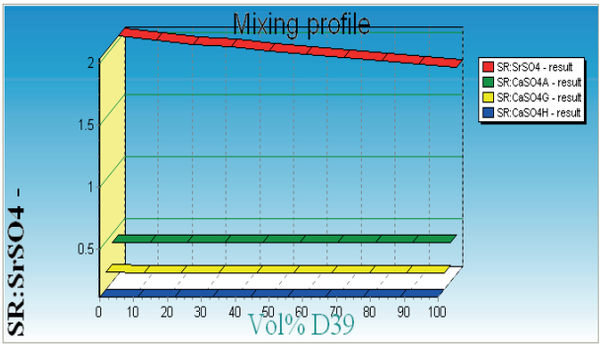


Fig. 29. Saturation indices for sulfate scales at reservoir conditions of temperature and pressure.(C).

CONCLUSIONS

Tests were conducted to identify the main scaling compounds when produced water mixed with the formation water. These tests demonstrated that $CaCO_3$ and $SrSO_4$ could be precipitated in different amounts depending on mixing ratios and conditions of temperature and pressure. On the basis of positive evidence of scaling encountered in the laboratory tests, a computer simulation program has been carried out to support the incompatibility of these brines when mixed at desired conditions.

a. The effect of temperature is observed on amount of scale for all mixing ratios where the amount of different types of scales are higher under surface conditions than reservoir conditions

b. A complex scale was observed under surface conditions as Celestite, Anhydrite and Gypsum.

c. Under reservoir conditions Carbonate and Celestite are most likely to occur.

REFERENCES

Bin Merdhah, A. B. and Yassin, A. M. (2009). Scale Formation due to Water Injection in Malysian Sandstone Cores. *American Journal of Applied Science,* 6 (8): 1531-1538.

Charles, C. F. (2007). Applied Water Technology. *Gulf Publication Comp*.: 594p.

Mackay, E. (2003). Predicting in situ sulfate scale deposition and the impact of produced ion concentrations. *Institute of Chemical Engineers Trans IChemE,* Vol 8:*, Part A*.

Vetter, J. O., Kandarpa, V., and Harouaka, A. (1982). Prediction of Scale Problems due to Injection of Incompatible Waters. *Journal of Petroleum Technology.* 34: 273-284.

TQM Implementation in Libyan Oil and Gas Sector

Redha M. Elhuni* and M. Munir Ahmad**

Abstract: This paper investigates quality factors that are absolutely essential for successful implementation Total Quality Management (TQM) in Libyan oil and gas companies (LOGCs). Eleven quality factors with forty-two elements where identified based on literature search to develop a questionnaire to carry out the survey in order to identify the quality factors that are seen by LOGCs to be critical to the success of TQM implementation. Forty-five questionnaires were provided by hand to quality-related managers from the Libyan Oil and Gas sector. A total of forty-two were returned sufficiently completed, that gave us a response rate of approximately 93.33%. The empirical analysis demonstrates several key findings: The analysis indicated that twenty-four quality factors are found to be critical and absolutely essential for successful TQM implementation. These factors classify into three levels of criticality. All of the factors were found to be supported by similar studies and cited literatures. These factors will direct an organisation towards business excellence and enhancing success of TQM practices in the oil and gas sector.

Keywords: Total quality management, Critical success factors, Libya, Oil and gas.

INTRODUCTION

In a global market, knowing how the best organizations conduct their business is a critical element of successful competition. The international paradigms of management that cross national boundaries, the new information revolution, the introduction of new technologies, and the shift towards customer-focused strategies have made competition stronger than ever.

Organisations and governments can no longer perform their functions with bureaucratic rules, inadequate resource planning, or inefficient managerial approaches. They are challenged by the need for a better quality of products, services, improved performance standards, and greater responsiveness in order to be competitive in the global market.

Quality has been an important issue for organisations for many years. The early focus on quality evolved from inspection to quality control and later to quality assurance. During the 1990s, TQM evolved as a common term among organisations in different parts of the world. TQM has developed in many countries into a holistic framework (e. g. National quality or internationally recognized awards such as the Deming award, MBNQA and EFQM) aimed at helping organizations achieve excellent performance, particularly in customer and business results.

Companies in developed and developing economics need to transform their traditionally bureaucratic style of management to a high value-added, proactive, and efficient one. For such a transformation the adoption of effective quality strategies and practices is considered as one of the crucial factors for success.

In the continued global changes, companies need to continually improve this is where TQM come into play, and companies taken TQM for many different reasons. For some the focus is upon reducing the cost of operation, others focus on improving customer and/or employee satisfaction, some see it as a way of changing the corporate culture and style. Many look to TQM as a step further than their achievement of IS09000 certification. Most, though are looking for a way to improve their businesses make them more profitable and competitive and more enjoyable to work with.

LITERATURE REVIEW

Many countries have established their quality award programs based on Deming Prize, MBNQA, and EQA awards. Respectively, many quality awards have been developed in Europe the last 15 years. Their purpose is the improvement of the competitiveness of

*Libyan Petroleum Institute, Libya
**School of Science and Engineering, Teesside University, Middlesbrough, UK

various types of organizations. Most of the European countries have initially used the ISO quality assurance standards in order to promote development and production procedures. The followed stage was the implementation of methods of self-assessment and systems of quality management, basically through quality awards schemes, serving the ultimate goal of the alteration of the quality's philosophy and the improvement of competitiveness of small- and medium-sized firms.

The first published paper to address the determination of the critical quality factors of TQM was by Saraph, *et al* 1989. This study involved thorough analysis of the literature (writing of the gurus, experts, and academics). They extracted 120 organisational prescriptions for effective TQM. Using judgmental process (Saraph *et al* 1989) categorised these prescriptions into eight critical factors was established utilising the one hundred and twenty prescriptions. A questionnaire survey directed to twenty firms in Minnesota, USA was used to validate the instrument. Using a likert scale of five points (1 very low and 5 very high), respondents were asked to rate the level of practicing the factors in their firms. Using the responses of 162 managers, and applying reliability and detailed item analysis, Saraph *et al* was able to validate the following eight factors as critical quality factors (1) Role of top management and quality policy, (2) Role of the quality department, (3) Training, (4) Product/ service design, (5) Supplier quality management, (6) Process management, (7) Quality data and reporting, (8) Employee relations.

Baker and Strabird (1993) were the first to publish a research paper applying the instrument developed by Saraph *et al* 1989. The study was directed to the food processing industry in California, USA. The study aimed at assessing the level of CF's that are present, and to identify the organisational characteristics that are conducive to these CF's. The results of this study empirically reinforced the emphasis on the top management's role and behaviour and quality policy in the efforts of quality management. Another result of this study is that organisation-wide sharing of responsibility is more conducive to quality management implementation than a centralised approach.

The instrument of Flyn *et al* (1994) represented significant departure from the pioneer instrument of Saraph *et al* 1989. The instrument was administrated at the plant level in view of the fact that quality programmes are most often implemented at that level. Seven major dimensions of quality management and eleven constructs were identified mainly from the practitioner and empirical literature. The study was based on a sample of forty two manufacturing plants from the machinery, transportation components and electronics industry located in the USA. The constructs identified by this study include quality leadership, feedback, inter-fanctional design process, supplier relationship, quality improvement rewords, selection of teamwork potential and teamwork, customer interaction, process control, cleanliness and organisation.

Thiagarajan and Zairi (1997) present a comprehensive review of the literature in a three-part series of articles. This is done by discussing critical factors in key areas of TQM which are often stressed in implementation case studies, and supported by quality gurus and writers. Such critical factors are considered conducive to the success of TQM implementation. The authors take 98 companies as examples of best practices of TQM implementation, based on the Malcolm Baldrige National Quality Award (MBNQA) the European Quality Award (EQA) and the Deming Prize for assessing organizational excellence. The criteria used are found to reflect the most important components of effectiveness and competitiveness. Thiagarajan and Zairi (1997) emphasize the key elements of quality management implementation taken from the experts on quality and examine them against TQM implementation in companies with quality awards. The key elements of TQM can be summarised as follows: Leadership, Internal stockholders' management, Employees' involvement, Middle management role, Training and education, Reward and recognition, Teamwork, The role of employees' unions, Policy and strategy, Resource management, Communication for quality, Managing suppliers, System and process management. Accredited quality management system, Organising for quality, Managing by process Benchmarking, Self-assessment, Cost of quality, Quality control techniques, Measuring customers wants and satisfaction, Issues in implementation, TQM and national culture, TQM failures, Gestation period, Hard and soft quality management.

Another study conducted by Al-Khalifa and Aspinwall (2008). The study had presented the results of a study on Critical Success Factors for Total Quality Management (TQM) implementation in UK organisations. A survey instrument (10 Success Factors) developed by Yusof and Aspinwall for use in the automotive sector was used after some modification. The findings have supported Yusof

study and validated the instrument as a reliable tool. The results indicated that the Manufacturing sector in UK is embarked towards quality excellence. Suggestions were made to replicate the study in some developing countries.

A study by Dayton (2001) used data from American industrial companies to determine whether the ten TQM critical factors (i.e. people and customer management, supplier partnerships, communications, customer satisfaction, external interface management, strategic quality management, teamwork structures for improvement, operational quality planning and quality improvement systems) identified by the Black and Porter (1996) study could be considered as important TQM CSFs by USA small and large companies. From his conclusion he identified the strategic quality management as the most important TQM critical factor.

Baidoun (2003), conducted an empirical study of critical factors for TQM in Palestinian organisations. The main focus of the study was to identify the critical quality factors for effective TQM implementation and to understand how they were implemented by Palestinian organizations. His study identified nineteen quality factors were perceived as being critical for the successful implementation of TQM. These factors were identified and classified into three tiers of criticality. Nine of them were addressed in the early stages of the implementation process.

Many other researchers have also investigated the critical success factors of implementing TQM (Allen and Kilmann, 2001; Dean and Bowen, 1994; Douglas and Judge, 2001; Easton and Jarrell, 1999; Nilsson *et al* 2001; Reed *et al* 2000; Waldman 1994; Sila *et al* 2002). These writers produced more or less the same factors as the previous studies. The common conclusion from these studies is that each organization has a set of critical success factors to which it must pay attention, and that the implementation process is firm-specific (Ghobadian *et al* 2005).

METHODOLOGY

Based on this literature review of the quality factors, 42 factors were derived to construct the questionnaire of this study. The questionnaire survey targeting the oil and gas organisations aims at identifying the perception of these organisations of each of the 42 quality factors as to its level of criticality in successful implementation of TQM.

Frequency distribution is most appropriate for the data organisation as it allows the typical value (point of centre tendency) and it can be seen how typical this value isWeisberg (1992).The use of mode as the measure of central tendency for this level of investigation is proved appropriate as all of the quality factors response distributions appear on one category, illustrated as a single peak in the bar charts representing the response distribution of each the 42 quality factors. According to the scale used in the questionnaire (four-point scale), there are only four possible range values. A zero value of the range occurs when all respondents give a quality factors the same rating (that is, 1, 2, 3, or 4) where the maximum and minimum rating will be thesame. The range analysis tells little about the general agreement on the importance of a quality factor. Therefore, Variation ratio will help separating the quality factors with majority the consensus from other quality factors with no majority consensus as perceived by some respondents as of no consequences to the success of failure of the implementation process of TQM.

VR is calculated using the following simple formula:

VR= 1- frequency distribution of the mode

Where:
Variation ratio = 0 means unanimity (all respondents rated the quality factor as critical).
Variation ratio $\leq$ 0.5 means majority consensus (more than 50% of respondents rated the quality factor as critical).
Variation ratio > 0.5 means no majority consensus in rating a quality factor as critical.
However, the variation ratio doesn't take into account the full distribution of responses. To do so, index of diversity does take full distribution into account when dealing with non-metric data. The Index of diversity shows the degree of concentration of responses in a few large categories, and it can be considered as a surrogate measure of agreement amongst respondents concerning the response distribution of each of the quality factor.

In mathematical terms:
Index of diversity = 1- (P_{21}+P_{22}+….+P_{2k})

Where Pk= the proportion of responses in category k and k is the number of categories.

This means:

Index value close to zero will imply near unanimity; Index value close to 0.5 is when there is equal clustering around two large categories; and a

value close to 0.75 (4-1/4) will indicate high level of disagreement.

Sample selection: This study has focused on the most important sector of Libyan industry, namely the oil and gas sector. This sector constitutes an important and influential part of the entire Libyan industrial economy. The reason for this selection, that these companies have at least adopted ISO 9001, which is shared with their international counterparts.

Questionnaire design and administration: The questionnaire developed in this study consisted of two parts. The first part of the questionnaire (8 questions) was intended to determine fundamental issues, business information; such as the number of years a respondent is involved in quality management, the position of the respondent in the company, size of the organisation, business category, organisation ownership, and whether the company had implemented TQM. The second part consists of 42 variables or statements, which were extracted from the published literature of leading TQM practitioners and academics in order to enable the participants to evaluate and measure the implementation of quality initiatives in their organizations. The questionnaire developed uses a 4-point Likert scale (Critical, Important, Minor Importance, Don't Know) for rating the level of criticality of factors important to successful TQM implementation among Libyan oil and gas organisations.

Respondents Rate: 42 out of 45 questionnaires were returned sufficiently completed, with a response rate of approximately 93.33%, which is considered large enough to establish a representation and credible data for analysis. The questionnaire with a covering letter was directed to individuals who were considered quality-related managers from the Libyan oil and gas sector as they are in a position to answer the questions and to indicate how they perceive each of quality factors, as to their level of importance to the successful implementation of TQM, and to study the effects of TQM implementation on overall business performance.

Questionnaire reliability: Data were entered into a computer, the SPSS 17 reliability program was performed separately for the all factors. An internal consistency analysis was performed on the set of 42 factors. Table 1 lists Cronbach's alpha for different TQM implementation factors. This indicated that the reliability of multi-item scales corresponding to them ranged between 0.827 and 0.912. Generally, a reliability coefficient of 0.70 or more is considered to be good (Nunnally, 1967). The instrument developed for measuring TQM implementation using CSFs was considered to be reliable.

Table1. Internal Consistency Analysis

Quality Factor	No. of Question	Cronbach'salpha
1.Top management commitment & leadership	2	0.898
2. Vision and Quality Policy	4	0.827
3.Employee Participate	8	0.912
4. Customer Focus	2	0.881
5. Training & Education & Reward	3	0.875
6. supplier Management	3	0.902
7. Continues Improvement	10	0.891
8. Process Control	4	0.863
9. Cost of Quality	1	0.893
10. Information Technology	1	0.888
11. Culture	4	0.896

RESULTS AND ANALYSIS

Profile of the respondents: Table 2 presents the demographic profile of the respondents.The survey represented various types of organisations working in oil and gas sectors. The breakdown of these organisations is 29 % from the upstream operation, 16 % from oiland gas production, 5% from refinery and petrochemical, 24 % from oil services, and 26 % from consultation in oil and gas sector. Regarding the organisations size in terms of number of employees, about 34 % of the organisations participating were large- sized have more than 500 employees,43% were medium-sized have less than 250 employees, and 23% small size have less than 5o employees. Regarding principle ownership, about 43% of the organisations were public, 33% were private, and 24% were sharing organisations.

Analysis of responses: A total of 41 quality factors were stacked on critical and important categories, while one quality factor was returned as of minor importance by the majority of the respondents. This factor related to employees union support of the organisation's quality initiative (Figs. 1 & 2).

The Modal Category: The mode provides a summary of how respondents perceive the criticality of the QF to the success of the implementation

Table 2. Demographics of respondents of the survey

	Number of respondents	Percentage of respondents
Business Category		
Upstream operation	12	28.57
Oil & Gas production	7	16.67
Refinery & Petrochemical	2	4.76
Service	10	23.81
Consultancy	11	26.19
Year of experience		
Less than a year	12	28.57
1 to < 5 years	26	61.90
>5 years	4	9.52
Number of Employee		
Less than 50	10	23.81
Less than 250	18	42.86
More than 500	14	33.33
Position		
Quality Engineer	18	42.86
Quality manager	8	19.05
Consultant	8	19.05
Technical Engineer	5	11.90
Deputy general Manager	2	4.76
General Manager	1	2.38
Principle Ownership		
Public	18	42.86
private	14	33.33
Sharing	10	23.81
Techniques		
ISO 9001:2000	30	71.43
ISO 14000	8	19.04
TQM	none	0
Other	4	9.53

process of TQM in their organisations. Based on the identification of the mode for each quality sample, 24 factors were identified as critical, 17 factors were identified as important and only one factor was identified as minor importance which is related to employee's union support to the organisation's quality initiative, and no factor was identified as don't know. These modal categories are presented in the Table 3.

Range Analysis: Range analysis is used to indicate how the perceived importance of a quality factor varies in practice. This investigation reveals that the response distributions of the quality factors include only two possible types of ranges, which are (1 & 2). Nine distributions exhibit a range value of 1 that grouped into one category (critical) and the other Thirty-three distributions exhibit a range value of 2 which dispersed into the three categories. However, in the instances of a value of one or two of the range tells little about the general agreement on the importance of a quality factor.Therefore it is very important to look for other complementary measures of spread to achieve the objectives of this investigation.

From Tables 2 and 3, the quality factors with a range value of one were returned as critical impact the successful of implementation of TQM. The remaining 33 quality factors have a range value of two. Form these quality factors, the majority consensus returned 17 factors as important and 1 factor as minor important. Therefore, it will be rational not to analyse these 18 quality factors and to treat all of them as non-essential quality factors in the implementation of TQM in Libyan context. This support the conclusion from literature, that there is little agreement essentiality of many of the quality interventions to the success of TQM implementation. This reflects the need for classifying the quality factors in terms of their criticality.

Variation ratio and Index of diversity: Variation ratio helps to separate the quality factors with majority consensus from others with no majority consensus, and the index of diversity shows the degree of concentration of responses in a few large categories. Table 4 shows the computed variation ratio and the index of diversity for 24 quality factors returned by respondents as critical.

Table 5 shows that the index of diversity values supports the level of agreement identified by the variation ratio. The value of the index of diversity did not reach the maximal value of 0.75. This implies agreement among the respondents concerning the criticality of these quality factors.

The variation ratio values, however, identified 16 quality factors to have majority consensus (those with VR value of 0.5 or less), and 8 quality factors of no majority consensus (VR > 0.5).The findings, therefore, represent the fundamentals to construct the group's structure of the critical quality factors.

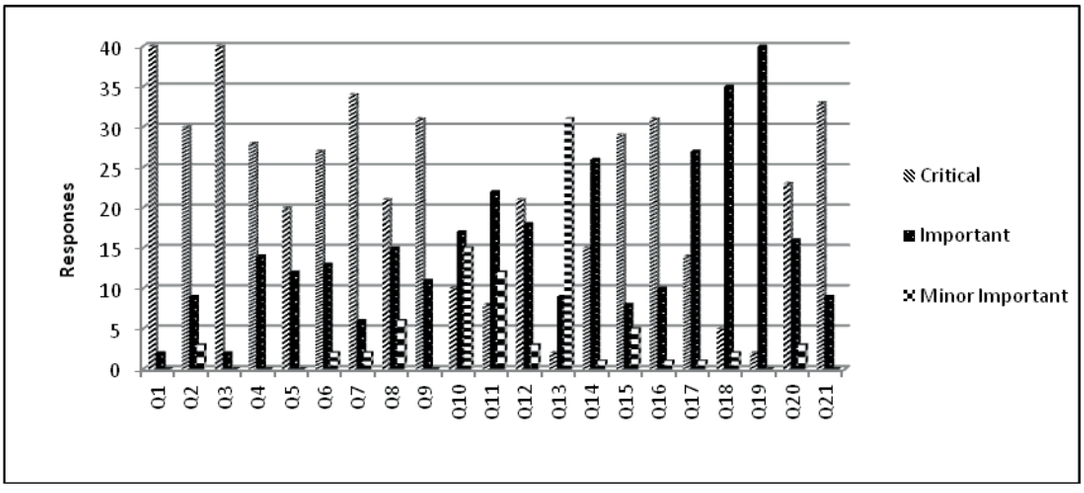


Fig. 1. Critical Quality Factors Frequency distribution

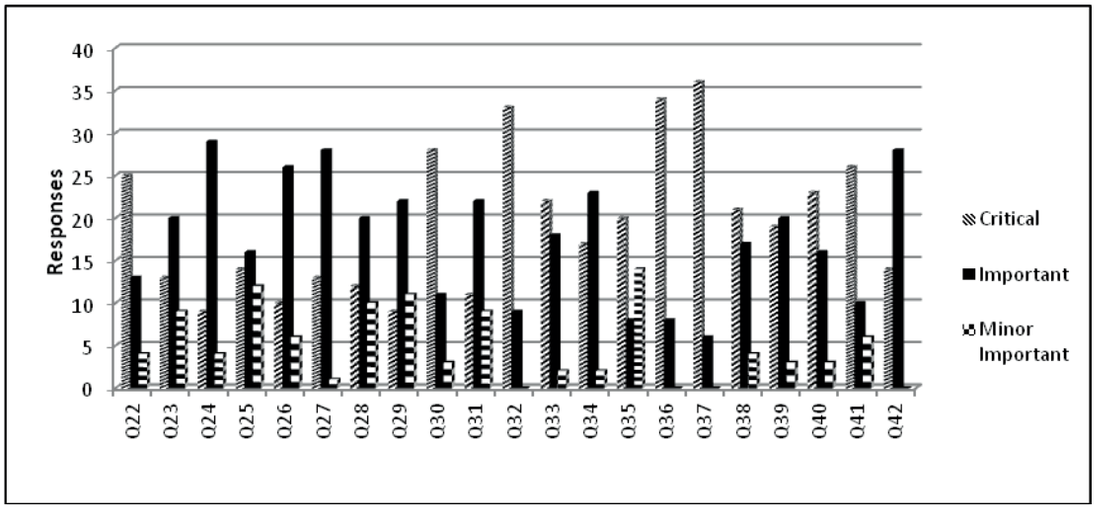


Fig. 2. Critical Quality Factor Frequency distribution

CLASSIFICATION OF THE IDENTIFIED CRITICAL QUALITY FACTORS

In the process of classifying and ordering the CQF's the use of range and the variation ratio well provide an opportunity for objective judgement. The sorting and ordering of the 24 CQF's using VR and DI provide a hierarchical structure in a descending order of criticality which is presented in table 5. These CQF's become essential. The CQF's classifying into three levels according to the range and the variation ratio presents the CQF's ranked in a descending order of their variation ratio.

The range and calculated variation ration values impose a three levels structure. A four level structure might prevail if several factors were returned with a range value of zero, and others with range value of one and two, and the calculated variation ratio values were between zero and greater than 0.5. Many researchers in the process of developing their TQM models ordered the hierarchical structure of critical quality factors into three tiers of importance (Ramirez and Loney, 1993; Ali, 1997; Thiagarajan *et al* 2001). The criteria to be used to stratification the CQFs is as follows

Level 1 critical quality factors: Those are quality factors that have a range value of 1 with the highest consensus level. They are essential to successful TQM implementation as perceived by all respondents to impact on the success of implementation. The low value of VR and range value of 1 indicate that there is uniformity in this level of quality factors amongst organisations concerning the criticality of these factors. These CQF's should be treated as basic components of the TQM implementation model and must be considered with priority in the early stages of implementation process.

The nine critical quality factors in level 1 are:

Table3. Quality factors' Modal Categories

Q. No.	Quality Factor
Modal Category - Critical	
Q1	1- Senior executive assume active responsibility evaluation and improvement of management system, and leading quality drive.
Q2	2- Visibility of senior executive commitment to quality and customer satisfaction.
Q3	3- Clear, consistent communication of mission statement and objectives defining quality values expectations and focus.
Q4	4- Comprehensive policy development and effective deployment of goals.
Q5	5- Top management push decision-making to the lowest practical level.
Q6	6- Effective top-down and bottom-up communication.
Q7	7- Elements of quality management structure are in place to manage the organisation's quality journey.
Q8	8- The entire organization understands that each individual and each process has internal customer and suppliers.
Q9	9- The entire workforce understands, and is committed to the vision, values, and quality goals of the organization.
Q12	10- Supervisors, unit heads and divisional managers assume active roles as facilities of continuous improvement, coaches of new methods, mentors and leaders of empowered employees.
Q15	11- Training objectives of the organisation corresponded with the main objectives of the organisation.
Q16	12- Training for employee to improve interactive skills (such as communication skills, effective meeting skills, and empowerment and leadership skills).
Q20	13- Systematic review and analysis of key process measures that have a direct impact on value-addition to customer satisfaction.
Q21	14- Problem-solving and continuous improvement processes based on facts and systematic analysis.
Q22	15- Application of total quality approach to the management of support services and business processes.
Q30	16- Cost of quality process to track rework, waste, rejects, and for continuous improvement.
Q32	17- A formal documented quality management system in place.
Q33	18- Reliance on reasonable few dependable suppliers who are evaluated and selected based on their capability and commitment to product and service quality, and value for money.
Q35	19- Comprehensive identification of customers and customers' needs and alignment of processes of satisfy the needs.
Q36	20- The use of customer surveys and feedback process, and tracking of other key measures to asses' customer satisfaction.
Q37	21- The use of Information Technology (IT) considered as important tool in achieving strategic objective.
Q38	22- Quality forms part of our organisation culture.
Q40	23- We have a culture of continuous improvement.
Q41	24- I look upon change as a challenge.
Modal Category - Important	
Q10	25- The use of employee surveys and tracking of other key measures to assess employee support of, and involvement in the quality initiative.
Q11	26- Employee suggestion scheme in place, with target time scales for management response.
Q14	27- System for recognition and appreciation of quality efforts and success of individuals and teams.
Q17	28- Informal benchmarking and other forms of information acquisition and sharing with organisation in different sectors and industries to identify best practices for improvements and opportunities.
Q18	29- Competitive benchmarking made against primary competitors.
Q19	30- Benchmarking help improve system and processes.
Q23	31- The use of self-assessment tools and other mechanisms to track and improve performance gaps in the implementation and effectiveness of system, processes and practices.
Q24	32- The outcomes of the self-assessment are linked to the business planning processes.
Q25	33- People who conduct the self-assessment receive relevant training.
Q26	34- A team approach (such as quality circles, cross-functional teams) to problem solving and continuous improvement.
Q27	35- The use of statistical processes control to control variability and improve processes.
Q28	36- Process performance outcome is measured.
Q29	37- Measurement of process performance is based on defined standards.
Q31	38- Zero defects as the quality performance standards.
Q34	39- Long term relationship and working partnership with key suppliers.
Q39	40- Our organisation's culture enhances productivity.
Q42	41- Employees fully understand the need to change from the status (existing situation) to a Total quality management philosophy.
Modal Category –Minor Important	
Q13	42- Employees' union support of the organisation's quality initiative.

Table 4. Category quality factors by range value

Range value	No. of factors	Quality factors	category
1	9	Q1, Q2, Q3, Q4, Q9, Q21, Q32, Q36, Q37	Critical
2	33	Q5, Q6, Q8, Q10 to Q20, Q22 to Q31, Q33 to Q35, Q38 to Q42	Critical, Important, minor important

Table 5. Variation ratio and index of diversity

Sq.	Quality Factor		Variation Ratio	Index of Diversity	Classification into levels
	Range =I	Range =II			
1	Q1		0.048	0.091	1
2	Q3		0.048	0.091	1
3	Q37		0.143	0.172	1
4	Q36		0.190	0.267	1
5	Q21		0.214	0.277	1
6	Q32		0.214	0.297	1
7	Q9		0.262	0.347	1
8	Q2		0.286	0.384	1
9	Q4		0.333	0.394	1
10		Q7	0.337	0424	2
11		Q6	0.357	0.481	2
12		Q40	0.452	0.494	2
13		Q22	0.457	0.510	2
13		Q16	0.462	0.522	2
14		Q30	0.464	0.577	2
15		Q8	0.500	0.622	2
16		Q5	0.505	0.632	3
17		Q12	0.510	0.679	3
18		Q15	0.542	0.669	3
19		Q20	0.610	0.670	3
20		Q33	0.667	0.684	3
21		Q35	0.673	0.710	3
23		Q38	0.686	0.732	3
24		Q41	0.710	0.740	3

1. Q1: Senior executive assume active responsibility evaluation and improvement of management system, and leading quality drive.
2. Q2: Visibility of senior executive commitment to quality and customer satisfaction.
3. Q3: Clear, consistent communication of mission statement and objectives defining quality values expectations and focus.
4. Q4: Comprehensive policy development and effective deployment of goals.
5. Q9: The entire workforce understands, and is committed to the vision, values, and quality goals of the organization.
6. Q21: Problem-solving and continuous improvement processes based on facts and systematic analysis.
7. Q32: A formal documented quality management system in place.
8. Q36: The use of customer surveys and feedback process, and tracking of other key measures to asses' customer satisfaction.
9. Q37: The use of Information Technology (IT) considered as important tool in achieving strategic objective.

Level 2 critical quality factors: Those are quality factors that have a range value of 2, but their variation ratio value is 0.5 or less, they are absolutely essential as perceived by majority of the organisations, while some organisations perceive them to be of no consequence with regard to the success of implementation. These CQF's are suggested to be addressed immediately after addressing the level 1 quality factors in the TQM implementation framework. These seven quality factors are:-

1- Q7: Elements of quality management structure are in place to manage the organisation's quality journey.
2- Q40: We have a culture of continuous improvement.
3- Q6: Effective top-down and bottom-up communication.
4- Q22: Application of total quality approach to the management of support services and business processes.
5- Q30: Cost of quality process to track rework, waste, rejects, and for continuous improvement.
6- Q8: The entire organization understands that each individual and each process has internal customer and suppliers.
7- Q16: Training for employee to improve interactive skills (such as communication skills, effective meeting skills, and empowerment and leadership skills).

Level 3 critical quality factors: Those are quality factors that have a range value of 2, but their variation ratio value is greater than 0.5 which indicates low majority consensus (low level of agreement). They have the lowest impact on the implementation process of TQM. These eight quality factors are:

1. Q5: Top management push decision-making to the lowest practical level.
2. Q20: Systematic review and analysis of key process measures that have a direct impact on value-addition to customer satisfaction.
3. Q12: Supervisors, unit heads and divisional managers assume active roles as facilities of continuous improvement, coaches of new methods, mentors and leaders of empowered employees.
4. Q33: Reliance on reasonable few dependable suppliers who are evaluated and selected based on their capability and commitment to product and service quality, and value for money.
5. Q41: I look upon change as a challenge.
6. Q35: Comprehensive identification of customers and customers' needs and alignment of processes of satisfy the needs.
7. Q38: Quality forms part of our organisation culture.
8. Q15: Training objectives of the organisation corresponded with the main objectives of the organisation.

DISCUSSION

The identification and analysis of CQFs for successful implementation of TQM are based on feedback received from the questionnaire survey carried out. The findings of this study are based on the perception of managers from the Libyan oil sector. Respondents were asked to rate given quality factors they perceive to be critical for the successful implementation of TQM in their organizations'. The findings from investigation identified 24 CQFs for a successful implementation of TQM in the Libyan oil sector. These factors were classified into three levels of criticality, as perceived by respondents from the companies of oil sector. Level 1 CQFs have been found to be fundamental components to be addressed in the early stages of the implementation. (40 out of 42 respondents) was achieved returning the factor of (senior executive assume active responsibility evaluation and improvement of management system, and leading quality drive) as critical.This is in conjunction with previous studies (Saraph *et al* 1989; Mann, 1992; Ramirez and Loney, 1993; Flyn *et al* 1994; Black and Portor, 1996; Thiagarajan, 1996; Ali, 1997; Ahire *et al* 1996; Tamimi, 1998; Rao *et al* 1999; Zhang et al, 2000; Thiagarajan *et al* 2001), and all major quality awards. The importance of top management commitment and leadership has got agreement in opinions amongst all quality gurus and every author of TQM (Zairi 1996).Problem-solving and continuous improvement processes based on facts and systematic analysis is an essential factor of TQM implementation (Oakland, 2000; Kanji, 1998) and a formal documented quality management system to be one of the essential factors. As for level 2 critical quality factors, elements of quality management structure are in place to manage the organisation's quality journey. Training and education is needed for empower employees and to improve interactive skills (such as communication, effective meeting, empowerment and leadership skills), and other technical skills (Deming, 1986; Rao *et al* 1999; Oakland, 2000).

To improve customer satisfaction, systematic review and analysis of key processes (Rao *et al* 1996). Application of total quality approach to the management of support services and business processes and Cost of quality process to track rework, waste, rejects, and for continuous improvement (Zhang *et al* 2000; Kanji, 1998; McAdam and Kelly, 2002) are all important.

However, for level 3 critical quality factors, these factors have the lowest impact on the implementation process of TQM. The emphasis is on organisational operations related to establishing a systematic review and analysis of key process measures that have a direct impact on value-addition to customer satisfaction. This is apparent from reliance on reasonable few dependable suppliers who are evaluated and selected based on their capability and commitment to product and service quality, and value for money to comprehensive identification of customers and customers' needs and alignment of processes of satisfy the needs.

CONCLUSION

Quality is an important consideration for executive thinking. The increased awareness of senior executive, who has recognised that quality is an important strategic issue is reflected as an important focus for all levels of the organisation (Crosby,1989, Oakland, 2000). This required defining and implementing several factors. These quality factors for successful

implementation of TQM cited in the literature are not formulated on the basis of empirical research (Black and Porter, 1996). Various quality factors are identified by various writers based on their own experiences in working as consultants, managers or researchers. Munro(2004:49) also indicated that TQM is an everywhere organizational phenomenon that has been given little empirical research attention.Knowledge of TQM in developing economics especially in Arab countries is almost totally lacking. The attention given to research in developed nations, confused by the acknowledged limitations of most of the research findings across national boundaries have made any efforts to readily learn and transfer empirically sound knowledge to developing economies all the difficult. This research tried to make the distance between the theory and practice of TQMimplementation and increasing its effectiveness in a developing country with different culture, andsocialist economy.

The results of this investigation suggest that addressing the 24 CQFs as main structure of quality management process increases its opportunity of success in Libya oil and gas sector. The discussion of the finding reveals that almost of 24 CQFs identified in this investigation share the value covered by MBNQA 2000, and EQA 2000.

TQM as a generic philosophy of management has been proved through the finding of the survey questionnaire as all quality factors identified as important in the developed countries (Thiagarajan and Zairi, 1997) were returned as critical or important by LOGCs except one factor (Employee union support of the organisation's quality initiative). For future research, a framework can be developing for successful TQM implementation in Libyan context based on the three levels of 24 CQFs identified and according to their degree of critical.

However, this study confirms that there are differences in the order and degree of emphasis of the quality factors. This is evident by making comparative of the identified CQFs in this study with other similar studies (Baidoum 2003, Thiagarajan and Zairi, 1997, Thiagarajan *et al* 2001). This is the evident that TQM organisations aim to excel in certain areas, regardless of their place of incorporation and supporting the saying that culture does not influence the approaches to TQM implementation.

Finally, the study assessed information only from the perspective of the participating organisations. Thus, it offers one dimensional focus. However, in the business practice, such TQM the success depends on its ability to satisfy the interested of multiple stakeholders. So, considering to gathering information from various stakeholders such as employees, customers, suppliers and even competitors it may be appropriate and this can be overcome using multiple methods to collect datain future research.

REFERENCES

Ahire, S. L., Golhar, D.Y. and Waller, M. A. (1996), Development and Validation of TQM Implementation Constructs. Decision Sciences, 27(1): 23-56.

Ali, M. (1997). An Empirical Study of Total Quality Management in the Middle East: A Proposed

Model for Implementation. Unpublished PhD Thesis, University of Bradford, Bradford, UK: 312p.

Al-Khalifa, K. and Aspinwall, E. (2008). Critical Success Factors of TQM: A UK Study. International Journal of Productivity and Quality Management, 3(4): 430-443.

Allen, R. S. and Kilmann, R. H. (2001). The Role of the Reward System for a Total Quality Management Based Strategy. Journal of Organizational Change Management, 14(2): 110-131.

Baidoun, S. (2003). An Empirical Study of Critical Factors of TQM in Palestinian Organizations. Logistics Information Management, 16(2): 156-171.

Baker, G. and Starbird, S. (1993). Managing Quality in California Food Processing Firms. Agribusiness, 8(2): 155-164.

Black, S. and Porter, L. (1996). Identification of Critical Factors of TQM. Decision Sciences, 27(1): 1-21.

Crosby, P. (1979), Quality is Free: The Art of Making Quality Certain, Penguin Books, New York, NY. 265p.

Dayton, N.A. (2001). Total Quality Management Critical Success Factors, a Comparison: the UK

Versus the USA. Total Quality Management, 12(3): 293-298.

Dean, J. W. Jr and Bowen, D. E. (1994). Management Theory and Total Quality: Improving Research and Practice Through Theory Development. Academy of Management Review, 19(3): 392-418.

Deming, W. E. (1986). Out of the Crisis: Quality Productivity and Competitive Position. Cambridge University Press, Madras: 508p.

Douglas, T. J. and Judge, W. Q. (2001). Total Quality Management and Competitive Advantage: the Role of Structural Control and Exploration. Academy of Management Journal, 44: 158-169.

Easton, G. S. and Jarrell, S. L. (1999). The Effects of Total Quality Management on Corporate Performance, An Empirical Investigation. Journal of Business, 71(2): 253-307.

Flyn, B., Schroeder, R. and Sakakibara, S. (1994). A Framework for Quality Management Research and an Associated Measurement Instrument. Journal of Operations Management, 11(4): 339-366.

Ghobadian, A., Gallear, D., Woo, H. and Liu, J. (2005). Total Quality Management-Impact, Introduction and Integration Strategies. The Chartered Institute of Management Accounts, London.

Kanji, G. K. (1998). Measurement of Business Excellence. Total Quality Management, 9(7): 633-643.

Kanji, G. K. and Asher, M. (1993). Total Quality Management Process: A Systematic Approach. Advances in Total Quality Management Series, Carfax, Abingdon.

McAdam, R. and Kelly, M. (2002). A Business Excellence Approach to Generic Benchmarking in SMEs. Benchmarking. International Journal, 9(1): 7-27.

Mann, R. S. (1992). The Development of a Framework to Assist in the Implementation of TQM. Unpublished PhD Thesis, University of Liverpool, Liverpool, UK 387P.

Munro, R. (2000). Linking Six Sigma with QS-9000. Quality Progress: 47-53.

Nilsson, L., Johnson, M. D. and Gustafsson, A. (2001). The Impact of Quality Practices on Customer Satisfaction and Business Results: Product Versus Service Organizations. Journal of Quality Management, 6: 5-27.

Nunnally, J. (1978). Psychometric Theory (2d ed.). McGraw-Hill Inc., New York, NY: 640p.

Oakland, J. S. (2000). Total Quality Management-Text with Cases (2d ed.), Butterworth-Heinemann, Oxford: 380p.

Ramirez, C. and Loney, T. (1993). Baldrige Award Winners Identify the Essential Activities of a
Successful Quality Process. Quality Digest 5: 38-40.

Rao, A., Carr, L., Dambolena, I., Kopp, R., Martin, J., Rafii, F. and Schlesinger, P.H. (1996). Total Quality Management: A Cross-Functional Perspective, Wiley, New York, NY.

Rao, S., Solis, L. and Raghunathan, T. (1999). A Framework for International Quality Management Research: Development and Validation of a Measurement Instrument. Total Quality Management, 10(7): 1047-1075.

Reed, R., Lemak, D. J. and Mero, N. P. (2000). Total Quality Management and Sustainable Competitive Advantage. Journal of Quality Management, 5(1): 5-26.

Saraph, J. V., Benson, P. G. and Schroeder, R. G. (1989). An instrument for Measuring the Critical Factors of Quality Management. Decision Sciences, 20(4): 810-829.

Sila, I. and Ebrahimpour, M. (2005). Critical Linkages Among TQM Factors and Business Results. International Journal of Operations & Production Management, 25(11): 1123-1155.

Tamimi, N. (1998). A Second Order Factor Analysis of Critical TQM Factors. International Journal of Quality and Reliability Management, 14(1): 71-79.

Thiagarajan, T. (1996). An Empirical Study of Total Quality Management (TQM) in Malaysia: A Proposed Framework of Generic Application. Unpublished PhD Thesis, University of Bradford, Bradford, UK: 447p.

Thiagarajan, T. and Zairi, M. (1997). A Review of Total Quality Management in Practice: Understanding the Fundamentals Through Examples of Best Practice Applications: Part 1. The TQM Magazine, 9(4): 270-286.

Thiagarajan, T., Zairi, M. and Dale, B. (2001). A Proposed Model of TQM Implementation Based on An Empirical Study of Malaysia Industry. International Journal of Quality & Reliability Management, 18(3): 289-306.

Waldman, D. (1994). The Contributions of Total Quality Management to a Theory of Work Performance. Academy of Management Review, 19: 510-536.

Weisberg, H.F. (1992). Central Tendency and Variability. Sage University Paper Series on Quantitative Applications in the Social Series on Quantitative Applications in the Social Sciences, Sage, Newbury Park, CA: 7-83.

Zairi, M. (1996). Managing Excellence: Leadership. The TQM Magazine, 11(4): 215-220.

Zhang, Z., Waszink, A. and Wijngaard, J. (2000). An Instrument for Measuring TQM Implementation for Chinese Manufacturing Companies. International Journal of Quality and Reliability, 17(7): 730-755.

Characterization of Post-Pyrolysis Tyre Char as a pigment in Aqueos Ink-Jet Printing Inks: Using Different Analytical and Spectroscopy Technique

Tareg.O.Mansour*

Abstract: Disposal of used tyres is becoming an increasingly important environmental issue and the recycling is a more environmentally friendly solution than mass accumulation.

A process known as pyrolysis enables the recovery of potential useful products from the rubber portion of used tyre ,such as pyrolytic oil, gas and a carbon black pigment (CB_p).Therefore the study was aimed to assess whether the recovered carbon could be used as a pigment in aqueous based inkjet printing inks.

The (CB_p) contained a higher concentration of inorganic compounds than commercial carbon black,mainly due to the various additives incorporated in the manufacture of the original tyre.The contamination is reflected by the high content of the ash present in the (CB_p).

A characterization of the recovered carbon black was performed and a possible reduction of the ash content by an acid-base demineralization treatment and physical separation techniques were investigated,thereby improving its quality.

In this study we evaluate the properties and performance of the recoverd carbon char as a pigment in water-based ink-jet links.The success of this project could help resolve a major environmental issue and thus be a benefit to us all.

The post-pyrolysis car tyre CBp (obtained from coalite ,Debyshire, UK) which was stored under room temperature and pressure and ground to a mean partical size of 20μmThe samples were characterized and evaluated by using different analytical and spectroscopy technique, such as X-ray Flourscence Spectroscopy.

Keywords: *Pyrolysis, carbon black, pigment, tyre.*

INTRODUCTION

Increasing numbers of used tyres have become a problem. The most common way of dealing with them is recycling, which entails great economic losses and environmental pollution (Dhir, *et al* 2001). Recent data show that in the European Union, 2.5 million tons of used tyres appear each year, equivalent to 80% of new tyres are made up of different materials: organic ones of a polymeric type, such as natural or synthetic rubber, inorganic ones, and metals. This complex structure makes recycling difficult (Williams, *et al* 1995). A possible solution to treat used tyres not as waste, but as an energy resource (Williams, *et al* 1998).

Carbon Black is a particular form of industrial carbon produced by thermal cracking or decomposition of a hydrocarbon raw material. More than 90% of carbon black is produced using the oil furnace process,which involves injucting an aromatic petroleum distillate into preheated closed furnace and then cooling and collecting the carbon aggregates that have been formed.by controlled mainuplating of reactor conditions it is possible to vary particle size,aggregate size,and surface chemistry to creat a board range of carbon black properties to be used in awide range of applications (Pakdel, *et al* 1992) The recovery of carbon black product is different in structure ,morphology and chemical composition in comparison with virgin carbon blacks Typically carbon black properties that best describe the high performance level of both automotive tyres and pigment based inkjet inks (Williams, *et al* 2002).

The post-pyrolysis car tyre (CBp) (obtained from coalite, Debyshire, UK) is carrying out recovery of used car tyres, based on the separation of the polymeric and metal contents .in this case

*Environmental Department, Libyan petroleum institute, P.O.Box: 6431, Tripoli – Libya.
Corresponding author: (E-mail: twarfali@ yahoo.com)

of used car tyres, the company has set up a pilot pyrolysis plant where used tyres are subjected to thermal decomposition into two fractions, solid and gas, both of which can be used as fuel for generating energy.

EXPERIMENTAL

Samples of the Post pyrolysis char were collected in special containers, the determination of ash content used to quantify the amount of non-organic mineral matter present in a sample, Ball mill with assorted milling balls, Laboratory furnace, crucible,measuring cylinder, Semi-quantitive XRF, Ash content, Chemicals and reagents.

Qemscan is the most powerful process mineralogical tool currently employed in the mineral industry for quantitative evaluation of minerals and inorganic substances.

The samples was analysed using the partical mineral analysis mode.this was where the electron beam is rastered over individual particles at a pre-determined beam stepping interval (pixel spacing) and a mineralogical map of each particle was obtained.

RESULTES AND DISCUSSION

Ash content in (Fig. 1) show that CBp has a substantially higher ash content than the two commercial carbon black grades (CB01 and CB02) that are currently available for inkjet applications.

The results in (Fig. 2) show that CBp has a substantially lower carbon content than the two commercial carbon black grades (CB01 and CB02) that are currently available for inkjet applications.

The proximate analysis of CBp,and two commercial grades of carbon black designed specially for inkjet printing.

Semi-quantitave XRF: The results in the Table 1 show that the major contaminats found in CBp are the elements Si,S,Fe,Ca and Zn.The carbon content was calculated by difference, giving around 85%.

The results in Fig. 3 below show the main contaminant elements: silica,Sulfur and Zinc, whilist carbon content is calculated around 85%. The main major compounds identified in the used tyre cahar from pyrolysis process as tentatively

Table 1. Results of semi-quantitave XRF analysis performed on the CBp.

Element	Concentration %	Element	Concentration %
Na	0.209	Ca	1.05
Mg	0.123	Ti	0.0291
Al	0.205	Fe	1.08
Si	3.51	Co	0.0295
S	3.98	Cu	0.0696
Cl	0.0990	Zn	3.56
K	0.104	Br	0.0679

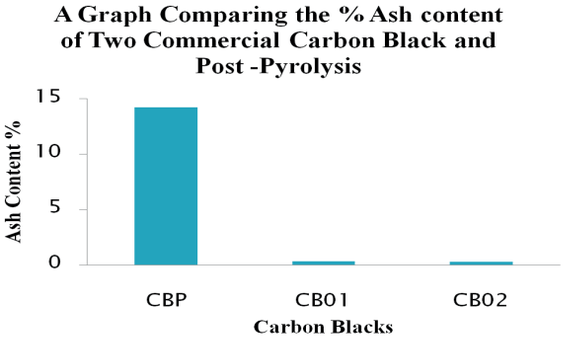


Fig. 1. Ash content (%).

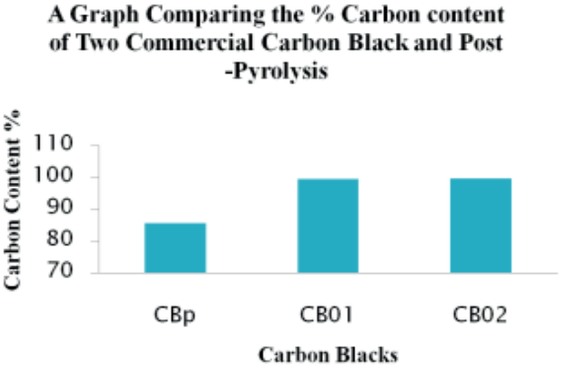


Fig. 2. Comparison of two commercial carbon and post pyrolysis.

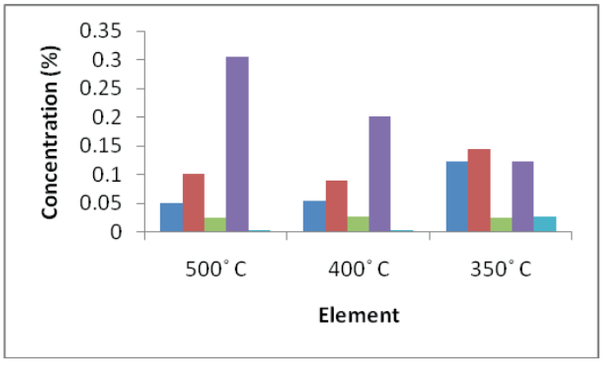


Fig. 3. Elements at different temperatures.

identified by GC-MS chromatograms are shown in Figs. 4, 5, and 6.

Generally, it has been suggested that the pyrolysis of used tyres may be successful new recycling method when tyres are no longer suitable for their orginal applications.that are usually dumped in landfill sites, burnt in cement kilns ,or turned to tyre crumb. It has been suggested that pyrolysis of used car tyres may be successful new recycling method. When tyres are no longer suitable for their original application.

The results from this study show that the CBp recovered from tyre pyrolysis has a carbon content around 85%,which is much lower than that of most commercial grades of carbon black used in the printing industry. The ash content of the CBp was determined to be higher than that of the commercial grades.

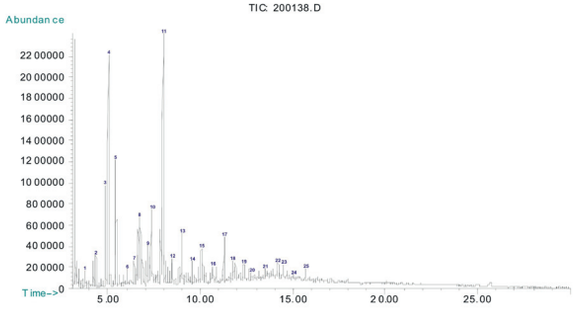


Fig. 4. GC-MS Chromatogram for carbon black char at 500ºC.

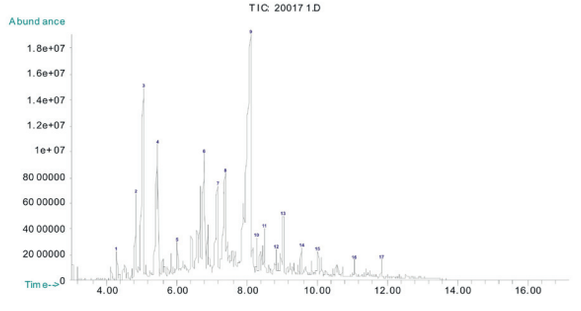


Fig. 5. GC-MS Chromatogram for commercial carbon black 01 at 400ºC.

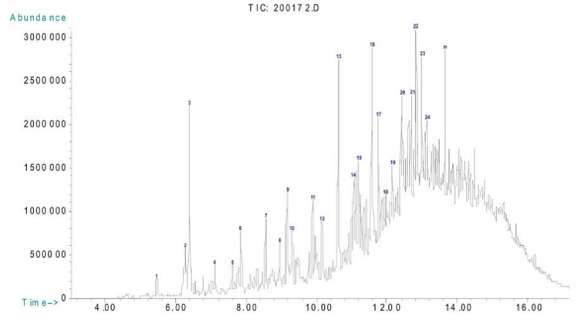


Fig. 6. GC-MS Chromatogram for commercial carbon black 02at 350ºC.

CONCLUSIONS

The pyrolysis of used car tyres has been thoroughly researched during the preceding 20 years on a small laboratory scale. Initial results from tyre pyrolysis were deemed sufficiently promising to lead to scale up. This current project had access to samples from a pilot plant obtained at different temperatures.

Pyrolysis may be an interesting option of waste tyres recycling. There are many technological variants of the process. As a result of waste tyres pyrolysis one may obtain valuable chemical semi-products or fuels. The full utilization of the waste tyres pyrolysis products is possible after their further processing.

ACKNOWLEGEMENT

The author is gratefully acknowledge the support of Libyan Petroleum Institute for this work.

REFERENCES

Dhir, R. K., Limbachiva. M. C. and Paine, K. A. (2001). Recycling and Reuse of Used Car Tyres. London, Telford Publishing,**10**: 1445-1449.

Pakdel, H., Roy, C., Aubin, H. Jean, G. and Cowlombe, S. (1992). Pyrolysis of Scrap Tyres and Conversion of Chars to Activated. carbonEnvironment Sci Technology, 25: 1646-1649

Williams, J. and Brindle, A. J. (2002). Effect of Pigmentation on Organic Coating Characteristics. Journal of Paint TechnologyFuel, 81: 30-34

Williams, P. T., Besler, S., Taylor, D. T. and Bottrill, R. P. (1995). The Pyrolysis of Automative Tyre Waste. Energy, 68: 11-21.

Williams, P. T., Bottrill, R. B. and Cunliffe, A. M. (1998). Haracterization of Pyrolytic Carbon Blacks from Commercial Tyre Pyrolysis Plants. Process, 76: 291-302.

Rheology and Pipeline Start up Pressure of Raguba Crude Oil

A.I. Amhamed* and H. Benkreira**

Abstract: Waxy crude oil is a valuable soft that undergoes long journeys from the well to the terminals through thousand of miles of pipeline in various parts of the globe that include deserts, arctic areas and sub-sea beds. Under such conditions, pipeline cease pumping with serious consequences both in cost of interruption of production and damages to the pipeline.

This paper describes research carried out on Libyan waxy crude oil namely (Raguba) to study (1) the rheology of this crude oil under various conditions and (2) the start-up pressure of this oil when temperatures decrease below the gel point. The rheological data to be presented are extensive in that they cover a range of conditions of temperature below and above gel and pour point and cooling histories (from very low to rapid cooling, 0.1 to 6.5°C/min representative of conditions under pipeline operations). Steady and unsteady states rheological tests were carried out under controlled shear stress and shear rate using an MCR-501 Anton Paar rheometer. Experiments were also carried out to measure the extent of visco-elasticity. As for the start-up pressure measurement, the paper describes a laboratory pipeline rig developed for the purpose of conditioning the oil (setting a measured cooling history) and measuring the corresponding start-up pressures after a range of stoppage time of 1, 2, 4 and 6 hours.

The data obtained shows a good agreement between the yield stresses measured in the rheological tests and the start-up pressure tests but only when conditioning of the oil in the pipeline rig is duplicated in the rheological tests. The data also give practical guidelines on the minimum pressures required after certain time of pipeline stoppage. The data are useful in practice as they reduce excessive waste of power during pumping the oil.

Keywords: Rheology, Waxy crude oil, Gel point, shear rate, shearing time, cooling rate, yield stress.

INTRODUCTION

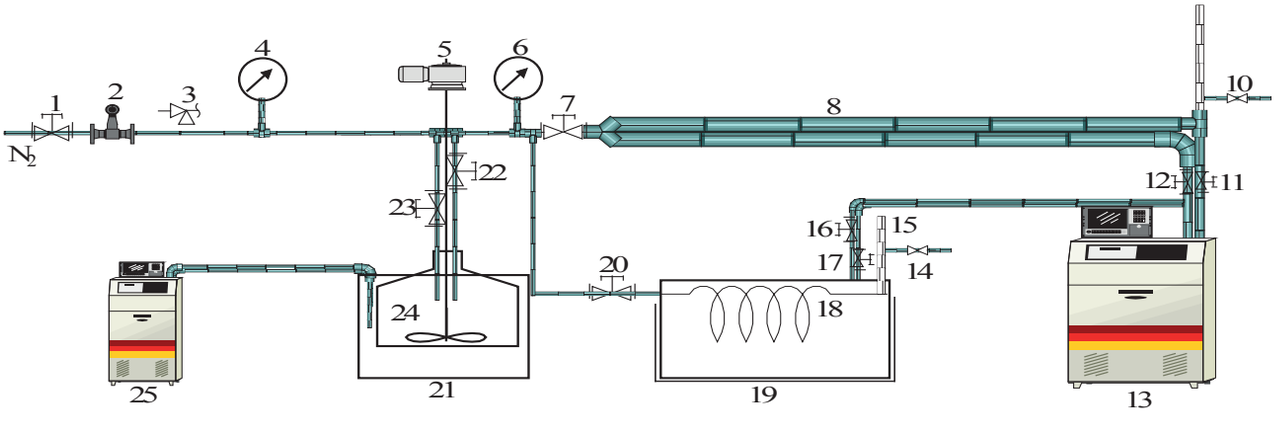
Waxy crude oils present challenging transportation problems especially when sudden drop in temperature arise to the oil gelling, effectively crystallising the paraffin and heavy hydrocarbons molecules. Pipelines transporting waxy crude oils may be shut down regularly for normal operational reasons and occasionally for emergency reasons, such as power failure, line damage, or even earth-quake, etc. In this case, the warm crude oil in the pipeline may be cooled statically below its pour point, leading to a strong waxy crystal interlocking network forming in the oil. Typical pipeline of 1m in diameter and 500 km long carries 1 million barrels of oil per day, such transport is expensive in terms of pumping cost ($million/year) and in any events that may lead to pumping failure and re-start add further to these costs and inevitably to the price of oil. Such event is related to the composition of the crude oil which if it contains sufficient wax which can gel or solidify in the pipe when the temperature drops below the gel point. One may think that the temperature has to drop significantly for oils to gel but this is not always the case. Libyan crude oils for example and these are the ones considered in this study, can gel at temperature 3, 5, or even 39^{0}C which are normal temperatures in winter at night times in Libya. In such conditions, pumping failures can be frequent and re-starting pumping costs become critical to the cost of operating the pipeline. Waxy crude oils are not limited to Libya and are common to many fields (North Sea and Canada are two examples) particularly new explored fields, so the waxy crude oils re-start problem is universal and of great interest to the petroleum industry. Rheological properties are important to pumping and re-start

* Corresponding author: Sirte Oil Company, for Production Manufacturing of Oil and Gas, Marsa El-Brega-Libya. Tel: 00218914209385 Fax:00218213605117, email:kgabaili@yahoo.co.uk
** University of Bradford Richmond Rd, Bradford BD71DP Westyorkshire, UK e-mail: H. Benkreira@bradford.ac.Uk

pressures estimation and require thus careful evaluation. This is one aspect of this paper and furthermore, using the most advanced rheological instruments to characterize these oils and establish their time-shear dependent viscous properties, yield stresses and viscoelasticity. Another important aspect of this paper is the careful measurement of the start-up pressures after gelling which we have established in our laboratory using a purpose built small-scale pipeline rig. The final and may be most important achievement of this paper is reconciling the measured start-up pressures with the predicted start-up pressures using the rheological data in a simple analytical model. Previous studies have not been able to achieve such a fit because they have not -as we shall show- considered the important need of duplicating the deformation-flow conditions in the rheological tests and in the pipeline tests. The yielding of the gelled oil, which is a fracture process of waxy crystals interlocking network, is the critical mechanism to track down and measure carefully and unless it is achieved in the rheological tests and in the pipeline test from the same *history* point, there should be no expectation that model predictions (regardless of how comprehensive the model may be) should match the measurements.

Waxy crude oils deform and eventually flow much in the same way as materials with a structure, for example polymer melts or concentrated suspensions. In other words, the yielding is not sudden (there is more than a single yield stress) but gradual, which must begin at a critical minimum stress which is best defined as the elastic lower limit yield stress, τ_e. Above this lower limit, the gelled oil will deform elastically and reversibly until it reaches the upper elastic limit yield stress $\tau_{s,}$ 'static' (start of flow from rest) when irreversible creeping begins. Beyond this point, the structure disintegrates rapidly but requiring little extra stress to give way eventually at $\tau_{d\ ,}$ to flow or dynamic flow, mostly by shear in this instance. Both $\tau_{s,}$ and $\tau_{d,}$ can be labeled 'dynamic' (determined during flow) in relation to the 'static' definition of the yield stress $\tau_{s,}$ the static and dynamic yield stresses are shown in Fig. 1. This three-yield-stress description is now accepted as being the most appropriate (Chang *et al* (1999;), Bonnecaze and Brady, (1992); Benkreaira and Amhamed, (2008) superseding the *"myth"* or no yield stress debate sparked of by Barnes and Walter, (1985).

We propose in this work to perform rheological tests along the three-yield-stress model and apply the model in a simple analytical way to predict start-up pressures in a laboratory pipeline under isothermal conditions. We shall ignore in our work compressible effects which occur in practice as a result of the crude oil shrinking upon gelling when cooled and developing gas voids in the pipe.



1,7,10,11,12,14,16,17,20,22,23- VALVE
2- REGULATOR
3- RELIVE VALVE
4,6- PRESSURE GAUGE
5- MIXER
8- LAGGED PIPE
9,15- GRADUATED RECEIVER
13,25- TEMPERATURE CONTROLLER
18-COILED PIPE
19,21- WATER BATH
24- OIL BOTTLE

Fig. 1. Static and dynamic yield stresses of waxy crude oils (ref.17)

EXPERIMENTAL METHOD

The sample source was the Ragouba field of Sirte oil Company and was drawn from the well-head. Its specific physical properties as quoted by the operating company are given in Table1, which include wax content and pour point. The pour point is useful indicator of gel or wax formation temperatures and will guide us in the design of our rheological and pumping experiments. The oil sample was collected near the well-head by the company personal into two 5 litre tins. These two tins were then transported to the University of Bradford in England. The oil in the five litre tins was transferred and mixed into a ten-litre container. Samples, which were used in experimental work, were taken from the 10 litres tin by preheating in hot water. The experiments started with establishing the rheological properties of the oils using advanced rheometers capable of detecting yield values then measuring start-up pressures in a suitably designed pipeline rig.

Table 1. Physical characteristics of Ragouba Waxy Crude.

Test	Method	value
API gravity@60°F	Calculated	41.86
Wax content (wt%)	UOP46/64	6
Pour point, °C	IP 15/D97	7
Asphalten content (wt%)	IP 143/84	0.1
Total Sulphur (wt%)	IP 61/84	0.03

Rheology of waxy crude oils: The rheological tests were performed using Anton Paar MCR301 and MCR 501 operated at controlled shear stress or shear rates. The rheometers are provided with an air bearing with digitally controlled shear stress CSS (10^{-7} Pa to 3000 Pa) and control shear rate CSR (10^{-6} min^{-1} to 3000 min^{-1}) tests. The shear tests were performed using a cone and plate geometry (diameter 5cm and cone angle 1°) and the dynamic storage G' and the loss G'' moduli were measured in a plate-plate geometry with an appropriately roughened upper plate to avoid slip during the test. A peltier device accurately controlled the temperature to within +/- 0.1 ^{0}C. Prior to the measurement of the rheological properties, a strict protocol for the preparation of the sample was followed to ensure a tractable history and one that could be reproduced in the pipeline rig.

Sample preparation: The oil was retrieved from the two 5 litres original containers and transferred to a single stirred vessel fitted with a hot water jacket. The oil was heated to 48^{0}C and stirred for 20 minutes. Samples were poured into a half-litre stirred glass container then heated to 80^{0}C for two hours while stirring. After this treatment, the oil was left to cool quiescently at room temperature for at least 48 hours before testing. Such a procedure, also used by other researchers [7-10], removes the fluid memory and this was confirmed by a series of repeat experiments in the rheometers. In all the subsequent text we shall refer to this oil as the no-memory base stock or sample.

Determination of gel point: In these experiments, the oscillatory test is used to examine the gelation temperature. The amplitude sweep test has to be done to determine the linear viscoelastic range (LVE) of the sample. In the liner viscoelastic (LVE) range at low amplitudes, each of the G' and G" shows a constant plateau value. The strain was kept at 1%, frequency 1 Hz and the gap was set at 0.5mm. The initial temperate in all these tests was fixed at 35°C; final test temperature was 5°C .The tests were performed at different cooling rates of 0.5, 1, 3, 5 and 6.5°C/min, full details of test can be seen in Table2. The storage G' and the loss G'' module are also recorded.

Table 2. Oscillatory test conditions for Ragouba waxy oil

Sample	Initial Temp., ºC	Final Temp.,ºC	Cooling rate °C/min	Frequency Hz	Strain %
Ragouba Oil	35 35 35 35 35	5 5 5 5 5	6.5 5.0 3.0 1 0.5	1	1

Effect of static cooling rate on rheological properties: For these experiments, 70-100 ml samples were loaded onto the rheometer plate, pre-set at the rheological temperature desired. The sample was left to rest for 15 minutes on the plate to form its equilibrium structure.The temperature is pre-set above the gel point.The sample is cooled statically from 30 to 5°C using different cooling rates. When the sample reaches 5°C, the rheological properties are measured at dynamic conditions over a range of shear rates from 1 to 1000 s^{-1}. This procedure (Table3) was repeated at 15 and 25 °C using a fresh sample for each run.

Pipeline Rig measurements: As for the start-up pressure test, a new laboratory pipeline rig developed for purpose of conditioning the oil and measuring the corresponding start-up pressure after a range of stoppage time of 1 to 2, 4, and 6 hours. In this measurement the oil cooled dynamically and statically in two stages in order to mimic the actual conditions in the field. The essential pressure to restart flow in a full-scale pipeline blocked with gilled waxy crude oil is calculated by a force balance equation:

$$\Delta P = 4L\tau_y / D \qquad (1)$$

This formal comes from the simplified idea that the force pushing the gel $\Delta P \frac{\pi D^2}{4}$ must be equal to the shear resistance along the wall $\pi D\ \tau_y$ [20].

The main assumption is that the value of yield stress τ_y is constant along the length of the pipeline. Where D is the internal diameter of the pipeline, ΔP is the applied pressure differential and L is the length of the pipeline. Fig. 2 shows the lab model pipeline assembly used in the present research. The experimental rig which consists of a straight jacketed pipeline, 9 m long and 6.5 mm inside diameter copper tube or 17 m long coiled pipeline of 6.5 mm inside diameter copper tube having 21 circular rings immersed in a tank. In both cases nitrogen gas is used to pump the oil. The pressure drop between two ends of the pipeline can be measured by means of a pressure gauge/manometer. The first water bath will be used for cooling the sample whilst the oil agitated by Rushton turbine impeller at a controlled temperature. The dynamic cooling is carried out in a 2-litre aluminium pot. The second stage cooling is under static conditions (i.e. whilst the oil stationary in the pipe) in either the coil pipeline or straight pipeline.

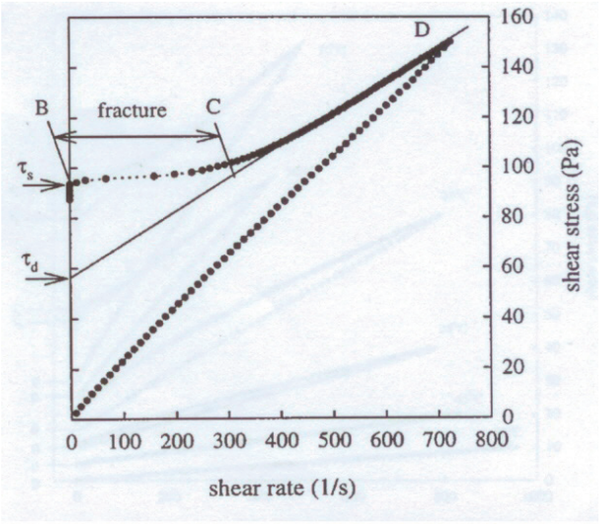


Fig. 2. The start-up pressure pipeline rig. Items 25 and 13 are temperature controller. , Nitrogen gas is used to pump, 8 is a straight pipeline (9m x 6.5mm ID) and 18 an alternative coiled pipeline (17m x 6.5mm ID).

EXPERIMENTAL PROCEDURE

(i) About 0.65 - 1 litre of crude oil is poured into the pot, which is connected to the 6.5 mm pipeline; the oil was kept for 30 min. under stirring (80 rpm).

(ii) Then the oil was dynamically cooled with preset rate of cooling to a final temperature, and left for 30 min. at this temperature.

(iii) The oil was introduced into the pipeline by use of Nitrogen gas from the bottle flask, and cooled statically to the test temperature under a specified rate of cooling. At this temperature, the oil is held for a certain period of time of 1, 2, 4 and 6 hours to simulate static condition.

Table 3. Parameters of cooling test for Raguba waxy crude oil.

Sample	Overhead temperature (ºC)	Test temperature (ºC)	Cooling rate, ºC/min.
Raguba Waxy Crude Oil	30 30 30	5 15 25	6.5, 1, 0.5, 0.1 “ “

(iv) Finally, by applying Nitrogen gas pressure, shear force was increased in steps of 0.25 psi until continues movement of oil occurs, i.e. when 4-8 ml of oil flows out of the model pipeline within 10-20 minutes. The shear stress applied at this stage is equivalent the value of yield stress. Data for this test is shown in Table 4.

Table 4. Heating and cooling conditions for Raguba crude oil.

Raguba waxy Crude Oil	Conditions
Dynamic cooling Initial Temperature, °C Final Temperature, °C Rate of cooling °C/min.	 50 40 0.16,0.6,1
Static cooling Initial temperature, ° C Final temperature, °C Rate of cooling °C/min Hold up time , h	 40 3.5, 5.5, 10 0.16,0.6,1 1, 2, 4, 6

RESULT AND DISCUSSION

Gel point: The experimental results obtained of Ragouba crude oil are shown in Fig. 3(a), (b), (c), (d) and (e) where the storage G' and the loss G'' moduli are plotted versus temperature during cooling. For this crude oil, the crossing of moduli occurs at 26 to 16.1°C according to the used cooling rate. This may be called the gel temperature (T_g). At a temperature below the gel point, the value of G' is higher than the value of G''. This indicates the formation of a rigid network even above the pour point. Fig. 3(e) shows the effect of cooling rate on the gel point. For this sample, it can be seen that the gel point decreases as the cooling rate increased for the temperature range studied. It has to be said that the pour point may not be a precies indication of gel point which is strongly dependent on cooling rate. This is expected as crystallisation is crucially controlled by cooling rate.

A very slow cooling rate will allow crystals to form and grow whilst a fast cooling rate will prevent this occurring. Clearly relying on the pour point to inform operation and design of pumping waxy crude oil is not recommended as we observe gel points to be larger than pour points. There is however an important difference to make. Gelation temperature only means that wax is beginning to form, it does not mean that all the wax has solidified. In other words whereas pour point is related to "flow" as measured crudely, it is still an indication of flow. While Gel point is not and flow in the pipeline may not be hampered until well below the gel point when all the wax has solidefied.

Effect of cooling rate on rheological properties during static conditions: In general, the cooling rate is expected to influence the rheology by the possibility of modifying the wax crystal size distribution. Moreover, it is well known that relatively low temperatures adversely affect the rheological properties of waxy crudes. This is because it modifies the oils rheological behaviour to a non-Newtonian character at a certain temperature. Under static cooling, an interlocking crystal network is built up in the waxy crude causing adverse flow properties. This is a real problem in pipeline when the oil cools down quiescently on a prolonged shutdown. Therefore, we tried to apply the same field conditions, which may help to understand the rheological flow properties at static conditions. Fig. 4 shows the effect of static cooling rate on the flow properties of Raguba waxy oil

A low cooling rate could help the growth of large crystals, which could give rise to the pumping problems Venkatesan *et al* (2002) & Chang *et al* (1999). Very rapid cooling could form a rigid interlocking crystal structure, causing a high yield pressure and resistance to flow. In case of Raguba waxy crude oil, by plotting the resultant equilibrium flow curves, the low cooling rate gives to approximately same equilibrium flow curves of viscosities at same temperature, telling that the low cooling rate has no influence on the flow properties of Ragouba crude oil. As the rapid cooling rate, e.g. 6.5ºC/min has a clear influence on the viscosity of this oil. It has to be said that there is an increase in viscosity due to the build up of a rigid interlocking crystal structure. In addition, viscosity reduction is due to structural breakdown in the shear field, which starts at about 10 s^{-1}.

Yield stress measurements

Measurements by Rheometers: The reproducibility of yield stress measurements has been found to be poor due to many reasons, e.g. the confused definition of yield stress, limitation of the instruments, methods, the procedure of the test and the poor control of the thermal conditions of the test (Bonnecaze *et al* (1992); Venkatesan *et al* 2002). Nowadays, due to

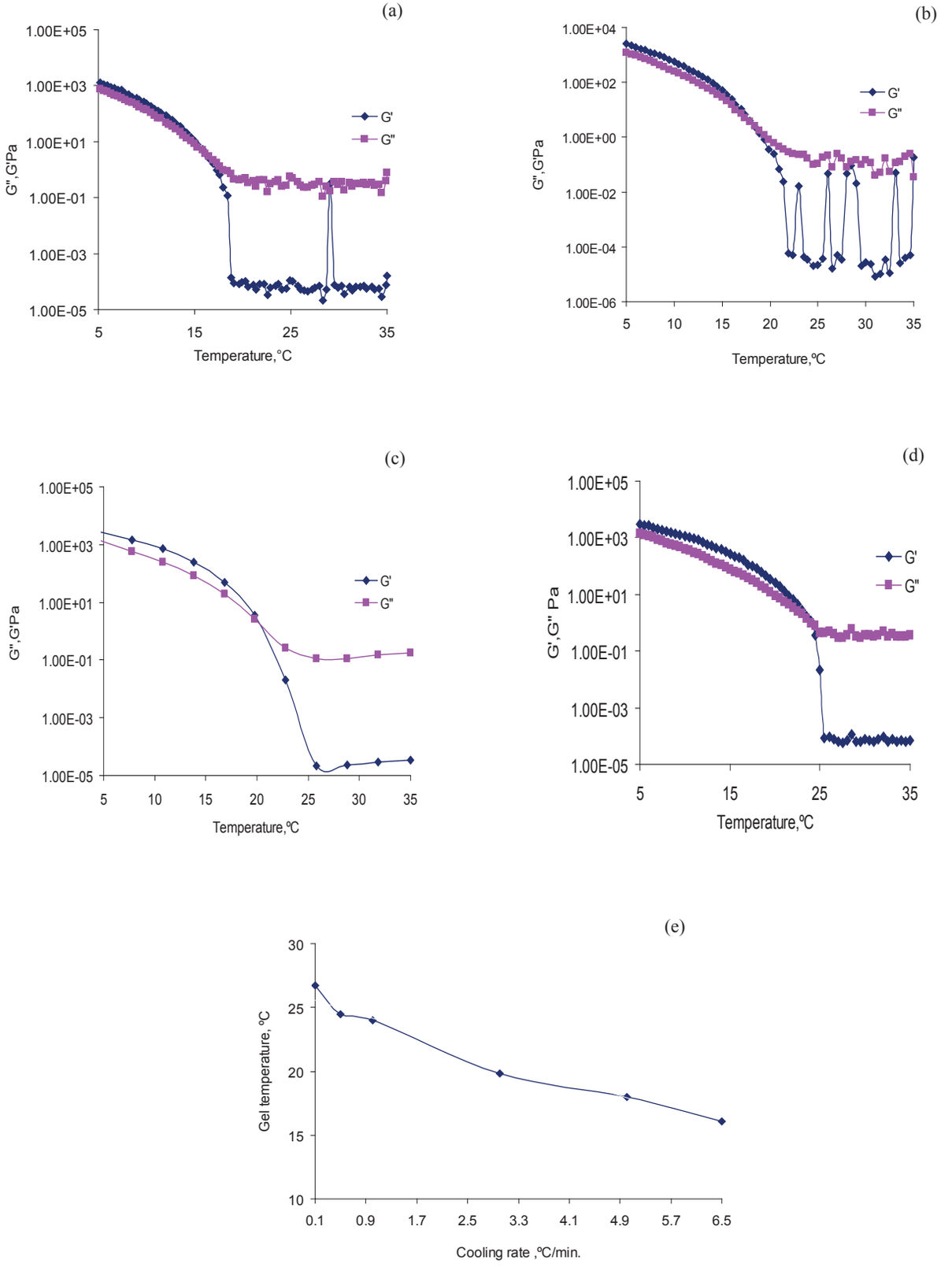


Fig. 3. Gel point temperature of Raguba oil at various cooling rate, (a) 0.1º/min.,(b) 0.5º/min, (c) 5º/min., (d) 6.5º/min. and (e) deviation of gel point against the cooling rate.

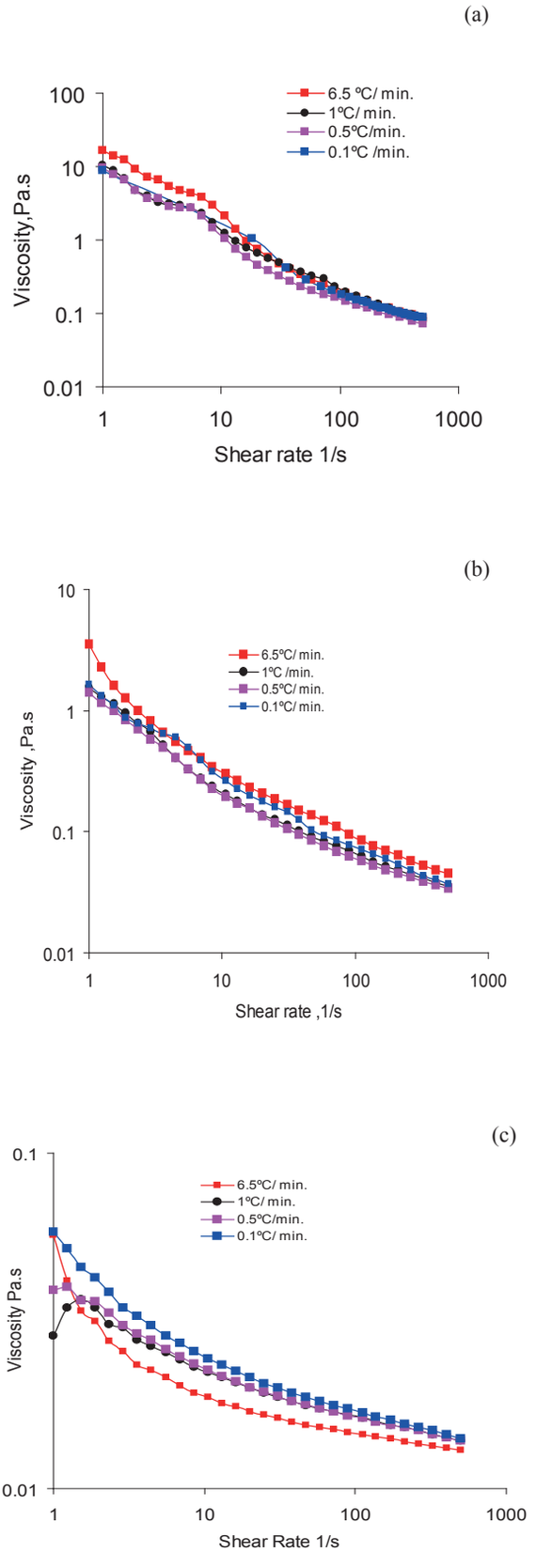


Fig. 4. Variation of Viscosity with Cooling Rate for Raguba Oil. (a)T= 30→5ºC ,(b) T=30→15ºC and (c) T=30→25ºC.
note: Viscosity measured at 5, 15 and 25ºC, respectively.

the availability of controlled stress rheometers with cone and plate geometries, the true yield stress of waxy crude oil using direct method can be easily determined. In these measurements, a fundamental problem with concept of yield stress fluids is the complexity in determining the yield stress value. There is no single method that has been commonly established as the standard for measuring the yield stress. It is to be stated that it is not unusual to get a different values of yield stress for the same material, prepared and tested in the same laboratory even by using same Rheometer, and obtained by using different methods (Moller *et al* 2006; Barnes 1999; Nguyen and Boger, 1992; Naguyen *et al* 2006). The apparent yield point, which is determined as the limit of elastic range, is not material constant and depends on time, pre-treatment and the test conditions (Mezger, 2002). In this research work, direct method is used to determine the yield stress of this sample according to a prescribed procedure. So the yield stress data covered are:

1. Time dependency yield stress.
2. Instantaneous yield stress.
3. Yield stress beginning from an equivalent state in the pipeline.

The yield stress is the value that shows a critical massive change in viscosity. Fig. 4 shows this clearly for the Ragouba oil tested where time dependency of yield stress or its instantaneous threshold is monitored. Conceptually, this method of identifying the yield is feasible and from an engineering perspective reasonable but nevertheless a value must be determined and there lies the problem. Which value in the changes of viscosity is the most representative of a true yield stress? Mathematically, it could "pin" the yield stress as the value in the viscosity curve which shows an inflection point or the first point at which the viscosity begins to drop. It does observe in the data however, that the viscosity goes through a reduced region before plummeting down completely to a very low value. We can thus distinguish between:

1. A lower yield stress or the beginning of shear flow
2. An upper yield stress or the value where shear flow is fully "on", i.e. beyond this point the structure has fully disintegrated and the "solid" part of the oil has disappeared.

Thus the lower yield stress is the most appropriate as it is that indicates the start of shear flow.

Having defined all the terms and their meaning

we can note the following observations on the results. Yielding is strongly time dependent. For example, at 5^0C and 15 minutes, Ragouba oil will yield at 20, 30, 40 and 50 Pa over a range of time. For the same temperature and 2 hrs as shutdown time sample will yield at higher value of yield stress starting from 30, 40, 50 and 100 Pa as can be seen in Fig. 4. The main conclusion is that we have already defined a series of yield stress not just one!

Yielding in the critical region, i.e. in the narrow region where the viscosity begins to drop considerably occurs in a range of time, i.e. in a range of stresses.

On an instantaneous basis, i.e. when we remove time dependency, yielding must occur over a range of stresses and there will be, as we indicated above, a lower yield stress and an upper yield stress. Because shear flow will begin at the upper value, this value is the "true" yield stress at least from an engineering perspective. A corollary to the above observations is that below the lower limit, the crude oil behaves as an elastic solid. In other words, if we remove the stress it should revert back to its original state. i.e. it is now shear- flowing.

The data obtained from rheological measurements on Ragouba waxy crude oil, which fully conditioned and measured by an Anton Paar rheometer are shown in Fig. 5, these measurements were performed at 5 ºC with 15 min. and 2 hrs as shutdown time. It can be seen from the data that after yielding point, the viscosity dropped by six to five orders of magnitude, which indicates that the viscosity of oil could be reduced to low value and oil could be pumped at certain conditions even below the pour point.

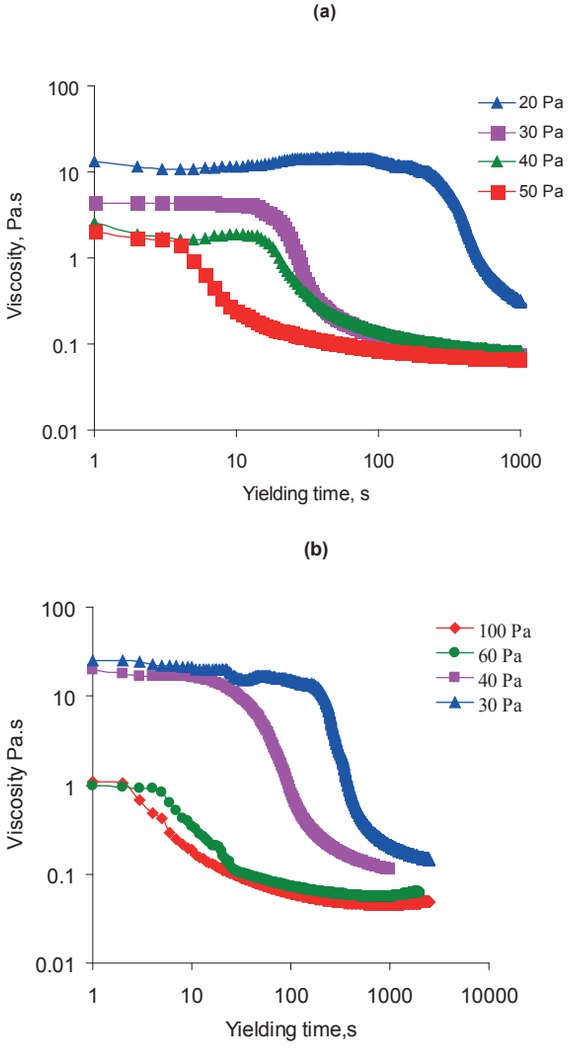


Fig. 5. Yielding time measurements for Raguba oil.
(a) T = 5ºC, 15min. shut downtime;
(b) (b) T = 5ºC, 2hrs shut downtime.

Yield stress measurements from pipeline rig: The aim is to use the pipeline rig in order to measure start-up pressure and use the simple force balance model Equation 1 to calculate the yield stress and compare this stress with the stress measured using the rheometer. This is effectively our experimental work underpinning of the theoretical work it assumes here the rheological measurements are in fact the theoretical information or more precisely the fundamental information.

The experimental equipment and procedure in terms of measurements are described above, but the important details here are the conditions under which the stresses (start-up pressures) are measured. We aim all along to replicate the conditions covered in the rheometer measurement, i.e. start temperature, end temperature, cooling rate, hold up–time but very importantly to start from a base line where the memory of the sample being pumped is erased before it was placed in the pipeline and proceeding with mimicking the conditions that would occur in a typical shut –down. The results of these experiments are presented in Figs. 6 to 9. Here it is interested to compare the stresses measured in the pipeline with rheological results obtained from Rheometers.

The ultimate aim is to demonstrate that rheological tests carried out carefully are able to replicate the performance in the pipeline. This is indeed the main aim of our research and many previous researches in this field. The lower yield stress and upper yield stress are discussed earlier and could only distinguish between the two because of the accuracy in stepping up in stresses at very small steps in our rheometer. Also, the cooling

equipment connected to the rheometer is very effective so a range of scenarios could be applied. As far as the pipeline rig, the creative feature is the way we erase the memory and condition the sample in a purpose made holder-mixer under controlled temperature conditions. It is the key to the experimental protocol.

The results presented in Figs. 6-9 reveal the following points:

1. The yield stress (Start up Pressure) was significantly reduced by increasing the test temperature.
2. The change of yield stress will be insignificant when the change of temperature occurs at or above the pour point temperature. In this region the oil behaves slightly Newtonian due to presence of a small amount of wax crystals.
3. The data obtained shows that yield stress decreases with an increase in test temperature.

The yield stress for the first hour was 4 Pa and increases to 7.77 Pa after two hours of shut downtime. Data obtained shows that the yield stress even after 4 or 6 hours of shut downtime remains constant at about 8 Pa. This data enables us to say that there is no extra power required to restart up the Raguba pipeline after six hours of shutdown at a low cooling rate and a 2.5ºC below the pour point.

The data also show that the high cooling rate gives higher values of yield stresses. This is due to the different morphology developed by the paraffin crystals during different rates of rapid cooling. Moreover, the increased yield stresses for this oil indicate that they contain C_{36} and C_{32} components. This component leads to an increase of yield stress with increasing cooling rate (Benkreaira *et al* 2008).

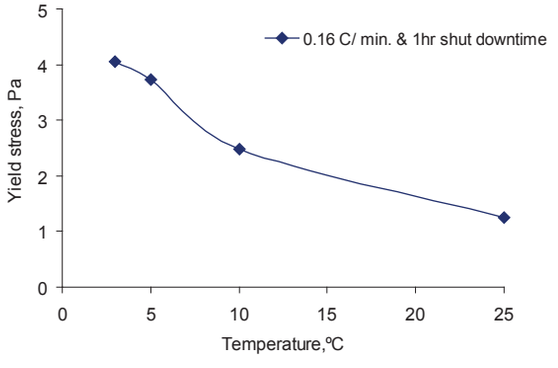


Fig. 6. Effect of test temperature on yield stress values for Raguba oil.

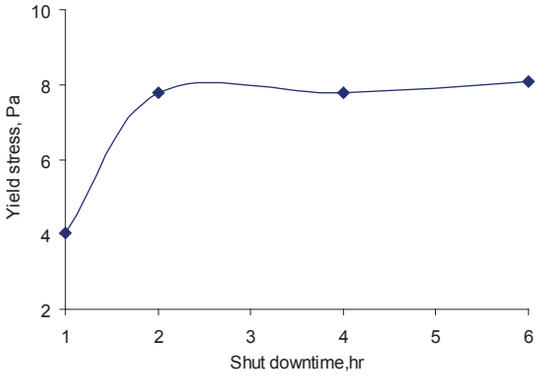


Fig. 7. Effect of shut downtime on yield stresses values of Raguba waxy oil at 0.16 ºC/min. and 3.5ºC.

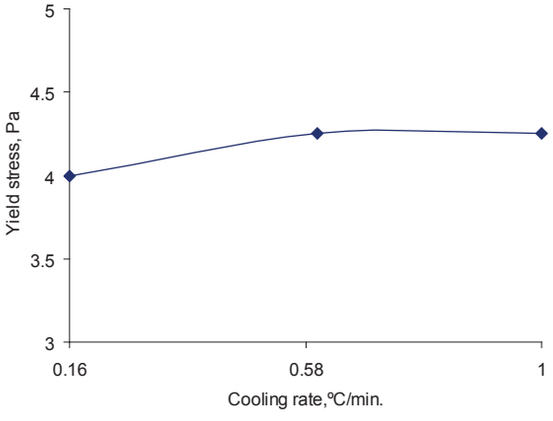


Fig. 8. Effect of cooling rate on yield stresses values of Raguba waxy oil. (3.5 ºC, 1 hr shutdown time).

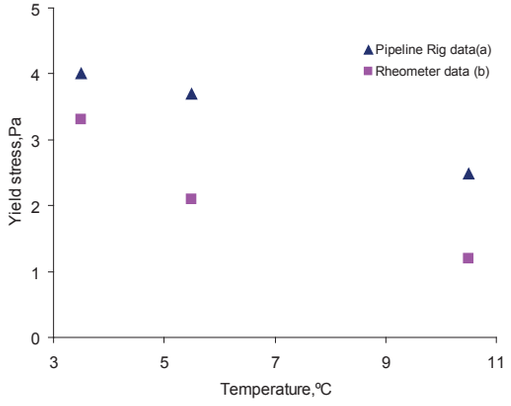


Fig. 9. yield stresses measurements for Raguba oil in Pipeline rig and MCR 501 Rheometer. 3.5 ºC and 1hr shut downtime.

CONCLUSIONS

It is to conclude that Ragouba waxy crude oil is a shear-sensitive and slightly time-dependent non-Newtonian fluid below the gel point temperature. It behaves as a strong non-Newtonian at and below the pour point temperature. The cooling temperature adversely affects the rheological properties of waxy crudes in such a manner that it modifies their rheological behaviour to a non- Newtonian character on approaching a certain temperature. The effect of cooling rate was investigated, the data obtained shows that the low cooling rate gives almost identical equilibrium flow curves of viscosities, suggesting that low cooling rate has no influence on the flow properties of Raguba oil, whilst the rapid cooling, 6.5ºC/min has a clearly influenced the viscosity especially at low shear rate. The effect of rapid cooling rate is strongly related to low shear rate, because at high shear rate the effect is negligible.

In the second class of experiments, which is done using pipeline rig, it is found that the value of yield stress decreased with increased test temperatures, and increases with increased rate of cooling and hold up time. Moreover, a good agreement found between yield stresses measured using the rheometer with those measured in the pipeline rig via the measurements of start-up pressures at certain conditions. From data comparsion, it is clear there is a good agreement. This gives confidence in the prediction using the rheometer which is cheaper option than using a pipeline rig data for restarting pressure estimation. The data obtained also give practical guidelines on the minimum pressures required after certain time of pipeline stoppage. The data are helpful in practice as they reduce excessive waste of power during pumping processes

REFERENCES

Barnes, H. A. & Walter, K. (1985). The Yield Stress myth. *Rheol. Acta*, 24: 323-326.

Barnes, H. A. (1999), The Yield Stress Review. *Journal of Non-Newtonian Fluid Mechanics*, 81(1-2): 133-178.

Benkreaira, H. and Amhamed, A. (2008). Rheology and Start Up Pressure of Waxy Crude Oils, *18Th International Congress of chemical and process Engineering*, August, , Pruge, Czech Republic.

Bonnecaze, R. T. & Brady, J. F. (1992). Yield Stresses in Electrorhelogical Fluids. *J. Rheol,* 36:73-115.

Chang, C., Nguyen, O. D. & Ronningsen, H. P. (1999). Isothermal Start-up of Pipeline Transporting Waxy Crude Oil. *Journal of Non-Newtonian Fluid Mechanics,* 87: 127-154.

Mezger, T. G. (2002). The Rheology-Handbook. Hannover, Germany: 252.

Moller, P. C. F., Mewis, J. and Bonn.,D. (2006). Yield Stress and Thixotropy: On the Difficulty of Measuring Yield Stresses in Practice. *Soft Matter* **2**: 274-283.

Naguyen, Q. D., Akroyd, T., Danial, C. De Kee. X., Zhu, L. (2006). Yield Stress Measurements in Suspensions: An Inter-Laboratory Study. *Korea-Australia Rheol. J.,* 18(1): 15-24.

Naguyen, Q. D. and Boger. D. V. (1992). Measuring the Flow Properties of Yield Stress Fluids. *Annul. Rev. Fluid Mech.,* 24: 47-88.

Venkatesan, R, Singh. P, and S. Fogler H. (2002). Delineating the Pour Point and Gelatine Temperature of Waxy Crude Oils. *SPE Journal,* V. 7(4): 349-352.

Study of Paraffin Wax Effect on Base oil flow Behavior

M. Abu-shaala* and M. EL-Bousiffi**

Abstract: Some of Libyan crude oils are known to have moderate to high content of paraffin wax. Problems related to paraffin wax are adding to the cost of barrel. In this work, the flow behavior of blends made from two types of base oil (N150, N500) have been experimentally studied, the blends were formulated in order to simulate Libyan waxy crude oils, and to exclude any effects of asphalten, resins and sediments which are normally present in crude oil. The main equipment used in this study is a rotational viscometer, measurements were performed by measuring the rheological properties (shear rate, shear stress, yield stress, and viscosity) of the blends at four different wax concentrations [2%, 5%, 8% and 10%wt] and measurements performed at six different temperatures in the range (15 - 60ºC). The flow behavior of the blends found to vary with temperature ranging from Newtonian to Non-Newtonian flow behavior, the apparent viscosity found to increase with decreasing temperature. Furthermore, the measured yield stress of blends found to increase with increasing wax content and decreasing temperature

Keywords: Waxy oil; Rheology Behavior; Temperature; Yield Stress; Shear rate

INTRODUCTION

The waxy crude oils have been a field of study, due to the severe difficulties that it causes in pipelining, storage. Evaluation of the flow properties of oils containing wax is complex and initially, poor agreement was found between different studies. However, substantial progress has been made thanks to the continues improvement of measuring techniques which made systematic study of the physical parameters affecting the rheology manageable. The role of the shear history on the flow properties is carefully considered. At high temperatures, the crude oils containing linear paraffin's behave like Newtonian. Heated base oil is mixed with wax flaks and carefully homogenized in the bulk of oil. The reason for selecting base oil in this study is to excluded any interference of different materials present in the crude oil. Various studies have been conducted on the rheological properties of different crude oils most of these studies have reported the existence of Non-Newtonian behavior for certain crude oils. (E.G. Barry, 1971) used North Africa oil to investigate the flow behavior, some of these crudes found to behave as Newtonian fluids at higher temperature and as a Non-Newtonian for lower temperature. (AL-Zhrani and AL-Fariiss 1998) investigated the viscosity of Saudi crude oil and has provided a mathematical model described the viscosity. (El-bousiffi, *et al* 2006) reported the flow behavior of Sarir Abu attifel crud oils, some experimental results were obtained on the rheology of Sarir and Abu attifel crude oils. Rotational viscometer is utilized, the temperature dependence of rheological properties and thixotropy of these crudes were investigated.

In this work, two types of base oils are used (i.e, N150, N500) from Azzawiya refinery, mixing with various amount of wax to develop a rheological understanding of these oils.

Experimental: A number of 10 samples were prepared and characterized

Material: Two types of base oils namely (N150 and N500) were used to prepare the blends. The physical properties of the base oils are listed in table (1, 2) paraffin wax flaks (melting point 57°C) were added to the base oil at various concentrations ranging from 2%wt to 10%wt.

Blend Preparation method: The following procedure was followed to prepare the blends:

The paraffin wax was melted in a beaker at 67°C. The temperature was maintained at 10 degrees above the wax melting point (57°C), for 1 h. The base oil

*mhm_chmcl@yahoo.com
**m.elbousiffi@lpilibya.com

was then slowly mixed with the melted wax under continuous stirring conditions until a pre-specified concentration was attained. Additions of base oil to the paraffin wax were made on the basis of percentage by weight of paraffin in the mixture. For this work, concentrations of 2, 5, 8, 10wt% of wax in the base oil were selected.

Equipments: Equipments used to measure the physical properties (density (ASTM D 5002) by density meter, pour point by cooling according to (ASTM D 5853), wax appearance temperature by DSC Differential scanning calorimeter (DSC 822 Module)) and the viscosity (Dynamic and Kinematic) are measured by Stabinger viscometer (SVM3000).

RESULTS AND DISCUSSION

Base oil properties: The physical properties measurement for base oil N150 and N500 and blends included: Density, Pour point, Wax appearance

Table 1. Physical properties of the base oil.

Base oil	Density(gm/cm^3) at 15°C	Pour Point (°C)	WAT (°C) Cooling rate=5°C/min	Kinematic viscosity (mm^2/s) at T=40°C
N150	0.8770	-15	-11.14	31.049
N500	0.8880	-12	-11.8	103.31

Table 2. Physical properties of the N150 base oil and blends.

Blend (N150)	Density (gm/cm^3) at 15°C	Pour Point (°C)	WAT (°C) Cooling rate=5°C/min
N150 Base oil	0.8770	-15	-11.14
2%wax	0.8536	-9	18.18
5%wax	0.8514	21	26.51
8%wax	0.8494	27	30.03
10%wax	0.8479	30	32.74

Table 3. Physical properties of the N500 base oil and blends.

Blend (N500)	Density (gm/cm^3) at 15°C	Pour Point (°C)	WAT (°C) Cooling rate=5°C/min
N500 Base oil	0.8880	-12	-11.8
2%wax	0.8860	3	21.06
5%wax	0.8856	24	28.28
8%wax	0.8832	30	39
10%wax	0.8816	36	42

Table 4. The viscosity and density for base oil N150 and blends at T=40°C.

Blend (N150)	Density (gm/cm^3)	Kinematic viscosity (mm^2/s)	Dynamic viscosity (mPa.s)
N150 Base oil	0.8618	31.049	26.757
2%wax	0.8603	30.306	26.071
5%wax	0.8581	29.065	24.942
8%wax	0.856	27.985	23.955
10%wax	0.8544	27.309	23.33

Table 5. The viscosity and density for base oil N500 and blends at T=40°C.

Blend (N500)	Density (gm/cm^3)	Kinematic viscosity (mm^2/s)	Dynamic viscosity (mPa.s)
N500 Base oil	0.8623	40.157	34.626
2%wax	0.8606	37.939	32.652
5%wax	0.8579	35.087	30.101
8%wax	0.8546	31.578	27.14
10%wax	0.8535	31.296	26.713

Table 6. The viscosity and density for base oil N150 and blends at T=60°C.

Blend (N500)	Density (gm/cm^3)	Kinematic viscosity (mm^2/s)	Dynamic viscosity (mPa.s)
N500 Base oil	0.8740	103.31	90.293
2%wax	0.8721	95.262	83.081
5%wax	0.8698	86.326	75.086
8%wax	0.8673	78.56	68.134
10%wax	0.8652	74.132	64.142

Table 7. The viscosity and density for base oil N500and blends at T= 60°C.

Blend (N150)	Density (gm/cm^3)	Kinematic viscosity (mm^2/s)	Dynamic viscosity (mPa.s)
N150 Base oil	0.8496	14.717	12.503
2%wax	0.8476	14.887	12.618
5%wax	0.8458	14.055	11.888
8%wax	0.8439	13.69	11.553
10%wax	0.8423	13.437	11.318

temperature (WAT) and viscosity (Dynamic and Kinematic). (Tables 1, 2, 3, 4, 5,6 and 7). As can be seen from listed properties that the main difference between the two base oils is the viscosity (Dynamic and Kinematic), and density, other properties such as pour point, WAT are almost similar.

Base oil carbon number distribution: The carbon number distribution for both oils N150,and N500, was determined using 3800 gas chromatograph and listed in Table (8) as can be seen N150 consisted of mainly (C_{20}-C_{35}) however N500 consisted mainly of (C_{25}-C_{35}) and this explains the increase in viscosity of base oil N500 compared with N150.

Furthermore, the percentage weight of C_{30} and higher in N500 base oil are in higher values than corresponding components in N150.

Flow behavior of base oils N150, N500: The flow behavior of base oils (N150, N500) are determined and graphically presented in Fig. 1 to Fig. 4, the flow behavior of base oils found to be Newtonian. Which is represent by constant viscosity as shown in Fig. 3 and Fig. 4.

Flow behavior of base oils N150, N500 blends: The flow behavior of blends (2%, 5%, 8% and 10%wt) prepared from N150, and N500 are determined and graphically presented in Fig. 5 to Fig. 28. Blends were made from base oil N150 are placed at the lift side of the page while blends mad from base oil N500 are placed at the right side of the page. From Figs. 5, 6 the shear rate vs. shear stress ,the magnitude of yield stress is increasing with wax concentration in all blends made from (N150 and N500), as can be seen from the Figs. 5, 6 the magnitude of yield stress at low shear is appeared as a Peak (i.e. maximums shear stress), but this peak was increasing as wax concentration increased at T=15ºC ,where the maximum shear stress for the blend (10%) wax is significant for blends made from (N150 and N500) and as can be shown in the Figs. 5, 6 for the two types blends of shear stress is disappearing with wax concentration decreasing, then the curve is declining with increasing shear rate until to shear rate of (7.5 1/s for 8% and 10% wax) after this value of shear rate the magnitude of shear stress as shown become stable even with increasing shear rate in Figs. 5, 6.

In other hand, the flow curve of the blends in this study can be dividing into two parts:-

1. Flow curve without (maximum yield stress).
2. Flow curve with (maximum yield stress).

Flow curve without (maximum yield stress): In this part, the measurement results of the base oils and 2%wt wax are graphical presented as a straight line, passing through the origin point of the graph which indicates base oils and blends with 2%wt wax for N150; N500 behaves as a Newtonian at temperatures considered.

Flow curve with (maximum yield stress): Blends with 8%wt and 10%wt wax prepared from N150 and N500 exhibited a maximum shear stress at shear rate higher than 0 1/s and at temperatures less than 30ºC.

Yield stress of blends: For blends made from base oil N150 and N500 the yield stress is found to increase with increasing wax concentration in the blend. Regarding the effect of temperature on yield stress, where the yield stress is decreasing with increasing temperature of the blends (Figs. 29 & 30).

Tables 9 and 10 below list the yield stress at minimum and maximum shear rate at (0 and 100 1/s) and maximum stress.

Table 8. carbon distribution for base oil N150, N500 blends.

Component	Base oil N150	Base oil N500	Paraffin wax
C_{20}	5.31	-	0.154
C_{21}	5.097	-	0.688
C_{22}	5.727	-	2.033
C_{23}	4.861	-	4.21
C_{24}	9.081	-	7.671
C_{25}	8.067	2.883	10.767
C_{26}	9.314	3.132	14.769
C_{27}	9.685	6.254	15.01
C_{28}	7.255	2.897	14.559
C_{29}	9.589	7.675	11.829
C_{30}	6.458	12.608	8.398
C_{31}	3.447	9.418	5.37
C_{32}	2.349	13.982	2.772
C_{33}	2.011	8.727	1.191
C_{34}	1.037	17.129	0.517
C_{35}	0.32	10.283	0.029

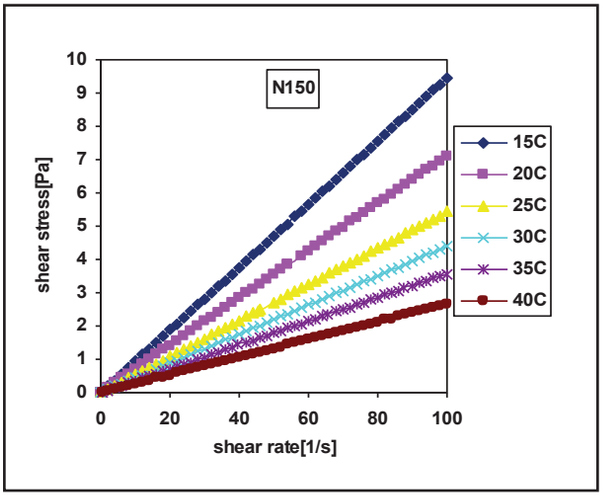


Fig. 1. Shear rate vs. shear stress for base oil N150 at different temperature.

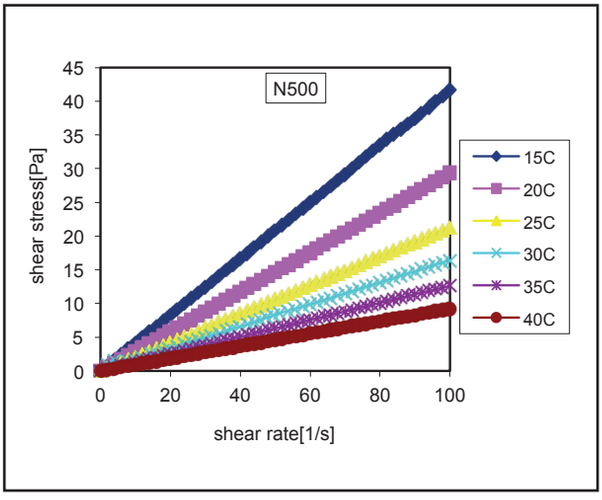


Fig. 2. Shear rate vs. shear stress for base oil N500 at different temperature.

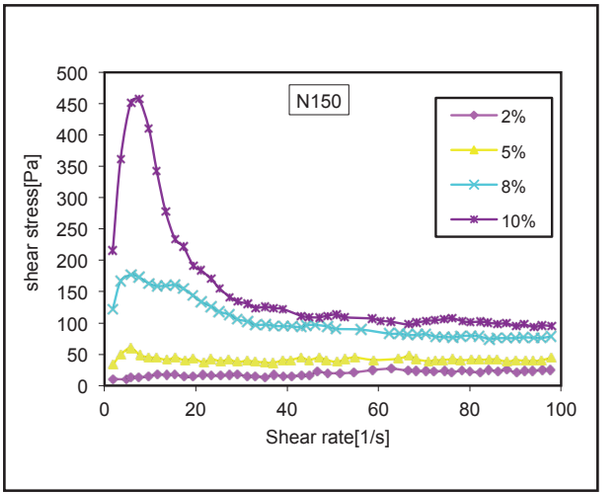


Fig. 3. Shear rate vs. apparent viscosity for base oil N150 at different temperature.

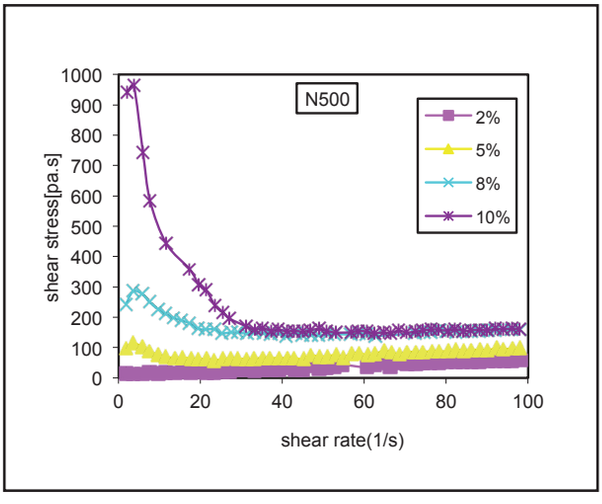


Fig. 4. Shear rate vs. apparent viscosity for base oil N150 at different temperature.

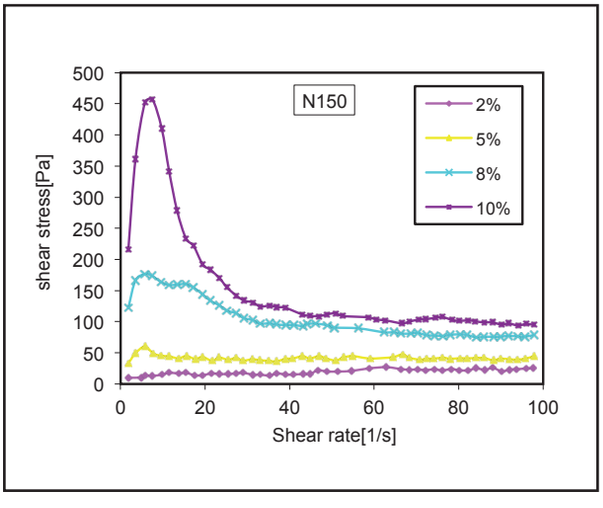


Fig. 5. Shear rate vs. shear stress for N150 blends, at T=15°C.

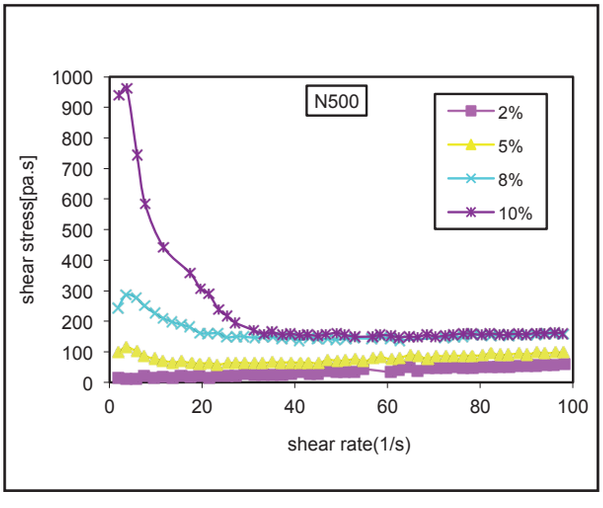


Fig. 6. Shear rate vs. shear stress for N500 blends, at T=15°C.

Table 9. Yield stress for N150 blends at different temperature and wax content.

Temperature	Wax content	Yield stress [Pa]	Shear stress at 100 [1/s]	Shear rate at Max. shear stress [1/s]	Max. shear stress [Pa]	Type of behavior
15°C	2%	10.2	25.22	-	-	Newtonian
	5%	32	44.5	5.73	60	Non-Newtonian
	8%	122.4	78.72	5.76	176.6	Non-Newtonian
	10%	215.2	94.72	7.522	457.2	Non-Newtonian
20°C	2%	0.825	7.92	-	-	Newtonian
	5%	6.2	21.4	-	-	Non-Newtonian
	8%	69.04	57.51	7.395	101.4	Non-Newtonian
	10%	122.1	82.48	7.4	323.3	Non-Newtonian
25°C	2%	0.067	5.22	-	-	Newtonian
	5%	1.236	10.2	-	-	Non-Newtonian
	8%	15.67	19.3	13.87	22	Non-Newtonian
	10%	66.81	28.85	3.956	96.55	Non-Newtonian

Table 10. Yield stress for N500 blends at different temperature and wax content.

Temperature	Wax content	Yield stress [Pa]	Shear stress at 100 [1/s]	Shear rate at Max. shear stress [1/s]	Max. shear stress [Pa]	Type of behavior
15°C	2%	11.65	58.9	-	-	Newtonian
	5%	115	98.04	3.57	114.9	Non-Newtonian
	8%	285.8	158.2	3.56	285.8	Non-Newtonian
	10%	962	160.1	3.7	962.2	Non-Newtonian
20°C	2%	2.57	31.75	-	-	Newtonian
	5%	33	65.3	-	65.44	Non-Newtonian
	8%	113.3	102.9	3.5	126.8	Non-Newtonian
	10%	253.8	136.2	5.76	321.5	Non-Newtonian
25°C	2%	0.4164	19.98	-	-	Newtonian
	5%	4.821	35.82	-	-	Non-Newtonian
	8%	48.15	52.76	1.967	48.15	Non-Newtonian
	10%	126	64.17	1.963	126	Non-Newtonian

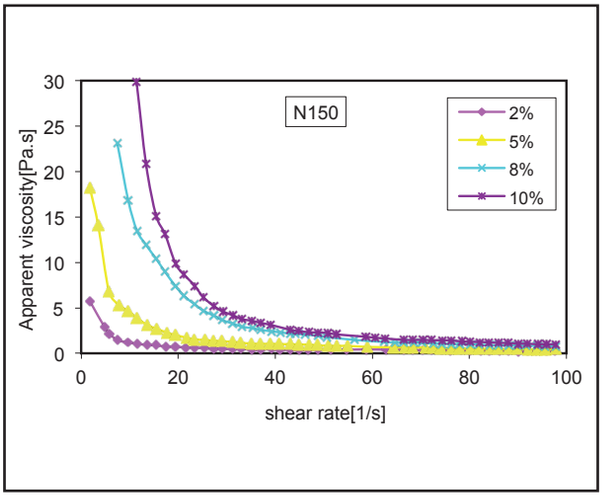


Fig. 7. Shear rate vs. apparent viscosity for N150 blends, at T=15°C.

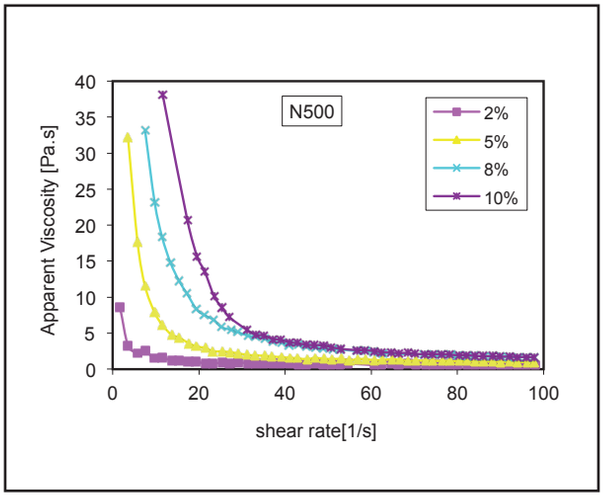


Fig. 8. Shear rate vs. apparent viscosity for N500

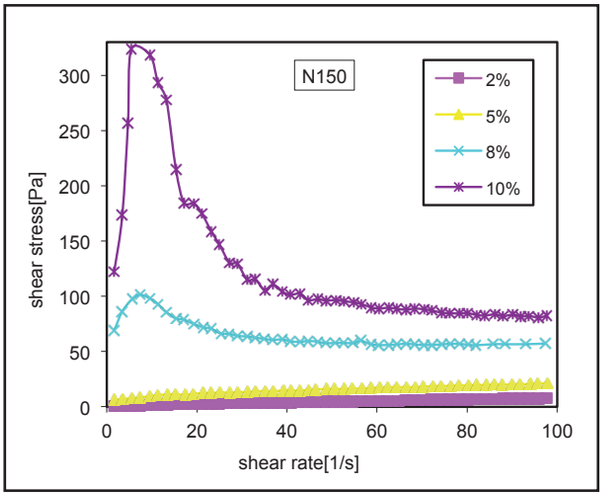


Fig. 9. Shear rate vs. shear stress for N150 blends, at T=20°C.

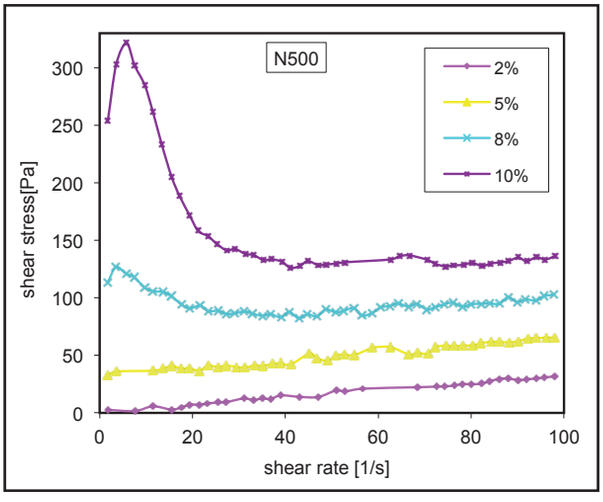


Fig. 10. Shear rate vs. shear stress for N500 blends, at T=20°C.

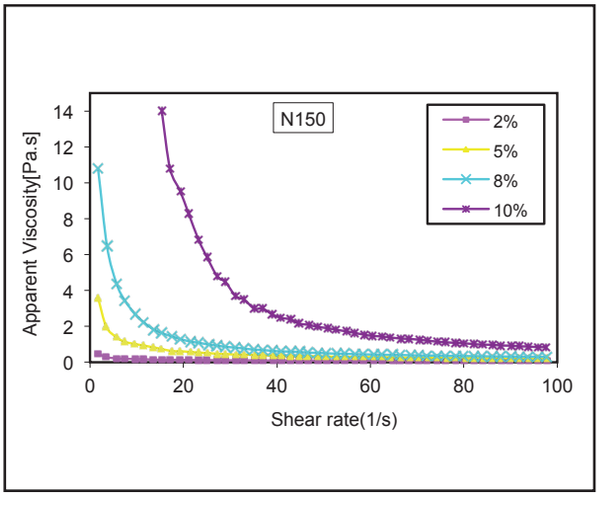


Fig. 11. Shear rate vs. apparent viscosity for N150 blends, at T=20°C.

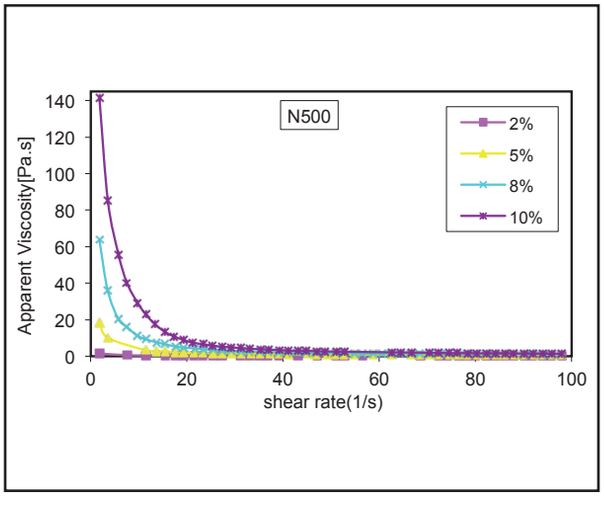


Fig. 12. Shear rate vs. apparent viscosity for N500 blends, at T=20°C.

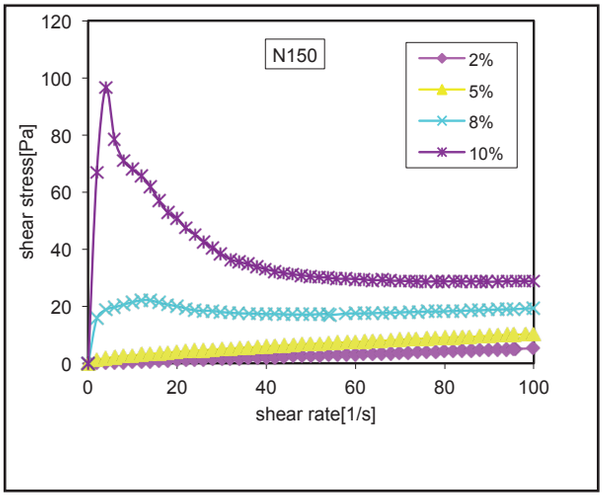


Fig. 13. Shear rate vs. shear stress for N150 blends, at T=25°C.

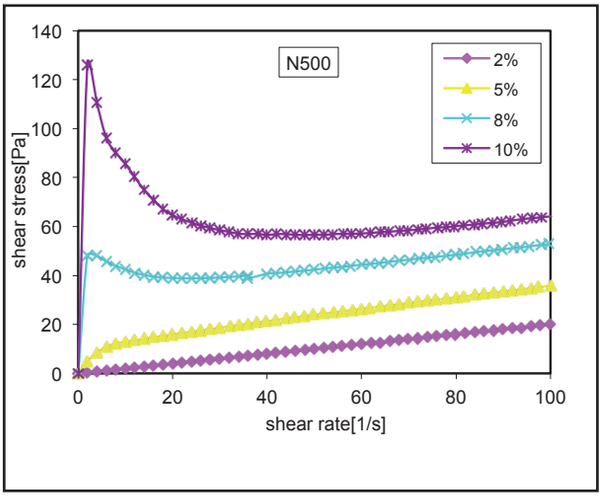


Fig. 14. Shear rate vs. apparent viscosity for N500 blends, at T=25°C.

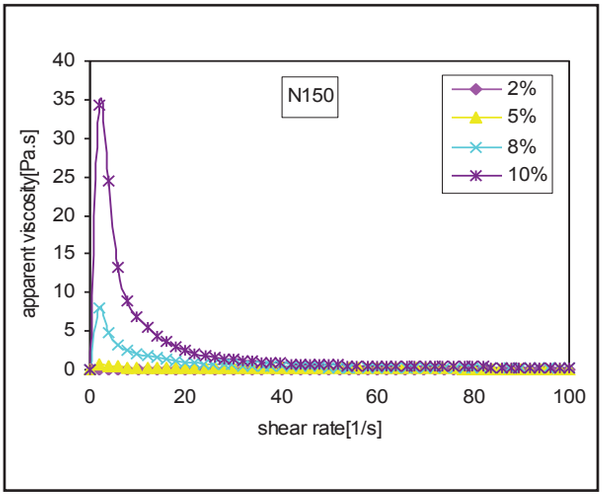


Fig. 15. Shear rate vs. apparent viscosity for N150 blends, at T=25°C.

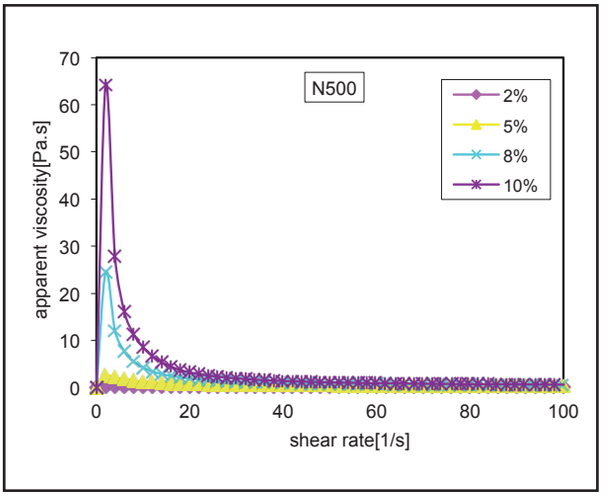


Fig. 16. Shear rate vs. apparent viscosity for N500 blends, at T=25°C.

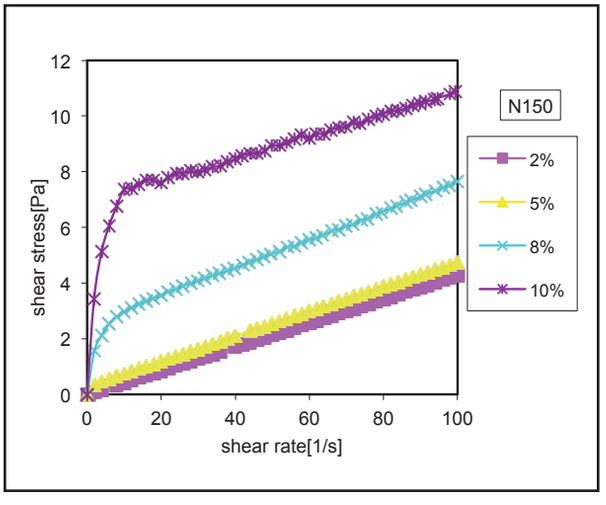


Fig. 17. Shear rate vs. shear stress for N150 blends, at T=30°C.

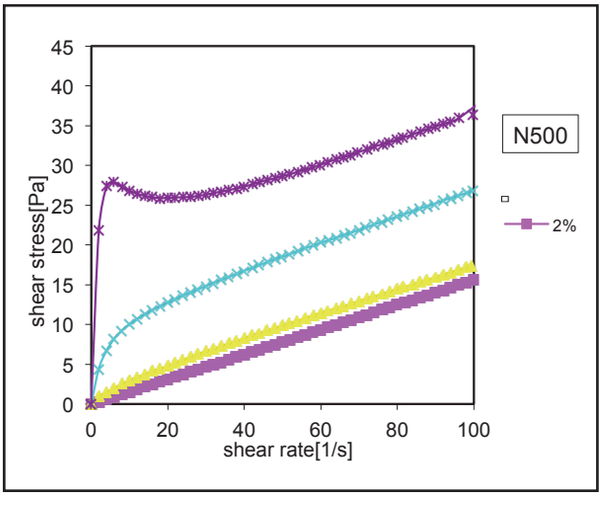


Fig. 18. Shear rate vs. shear stress for N500 blends, at T=30°C.

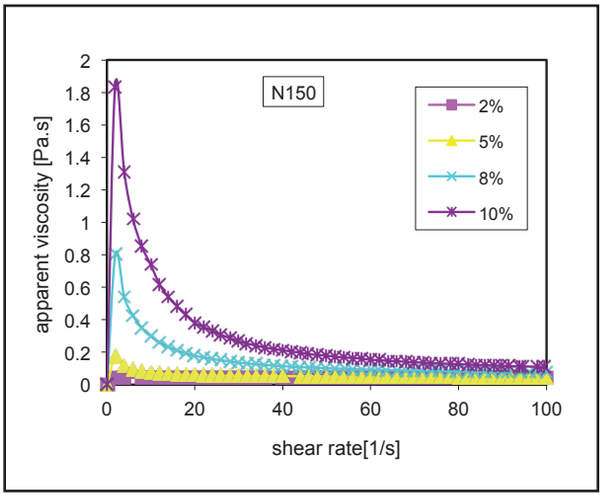


Fig. 19. Shear rate vs. apparent viscosity for N150 blends, at T=30°C.

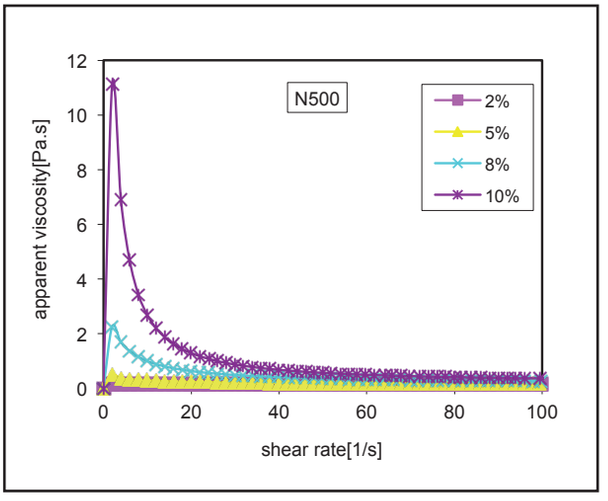


Fig. 20. Shear rate vs. apparent viscosity for N500 blends, at T=30°C.

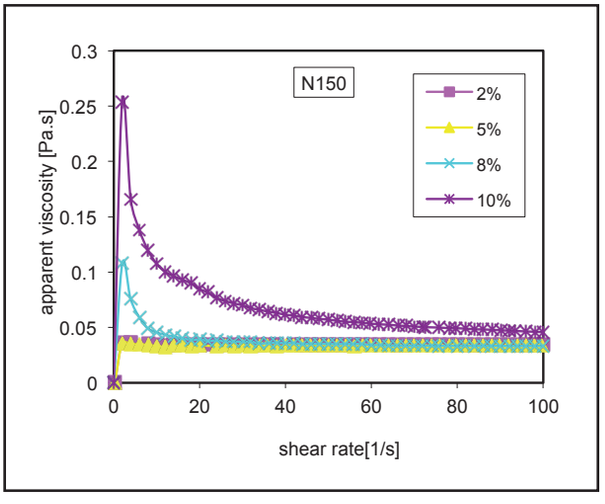


Fig. 21. Shear rate vs. shear stress for N150 blends, at T=35°C.

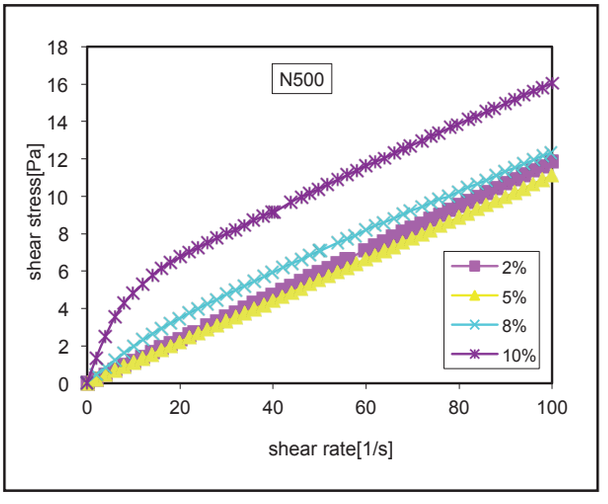


Fig. 22. Shear rate vs. shear stress for N500 blends, at T=35°C.

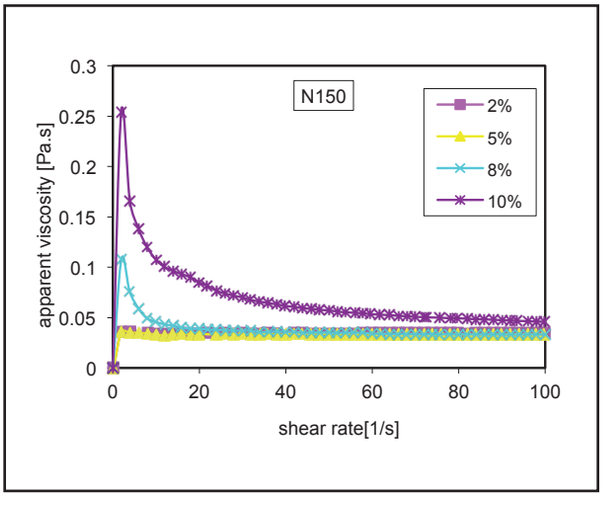


Fig. 23. Shear rate vs. apparent viscosity for N150 blends, at T=35°C.

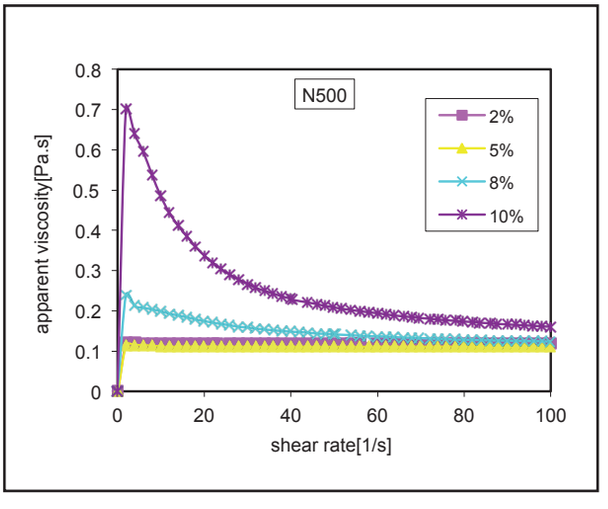


Fig. 24. Shear rate vs. apparent viscosity for N500 blends, at T=35°C.

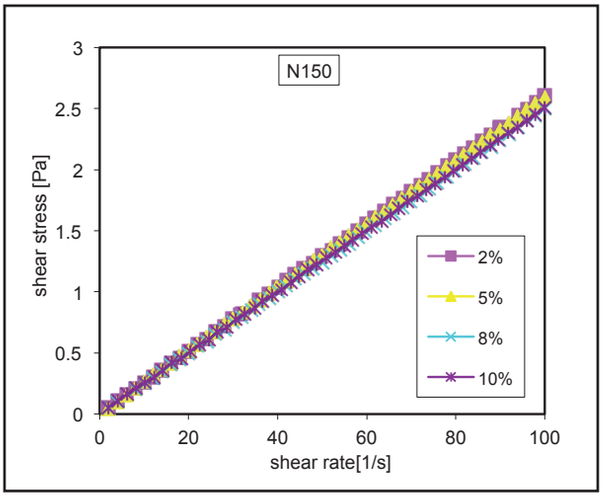


Fig. 25. Shear rate vs. shear stress for N150 blends, at T=40°C.

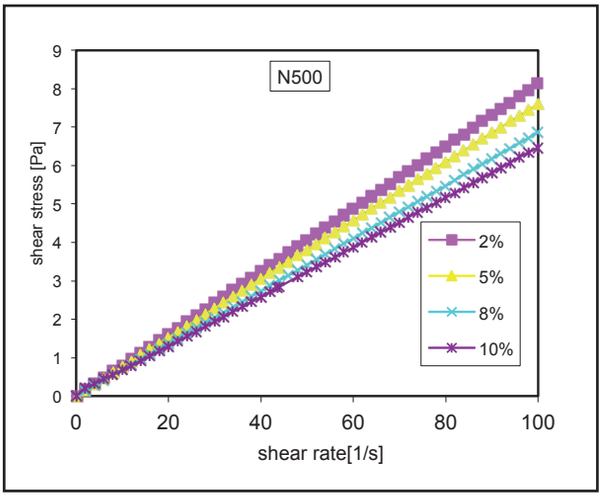


Fig. 26. Shear rate vs. shear stress for N500 blends, at T=40°C.

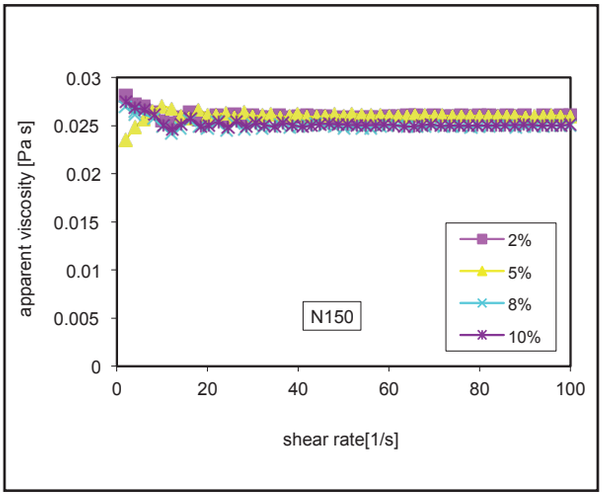


Fig. 27. Shear rate vs. apparent viscosity for N150 blends, at T=40°C.

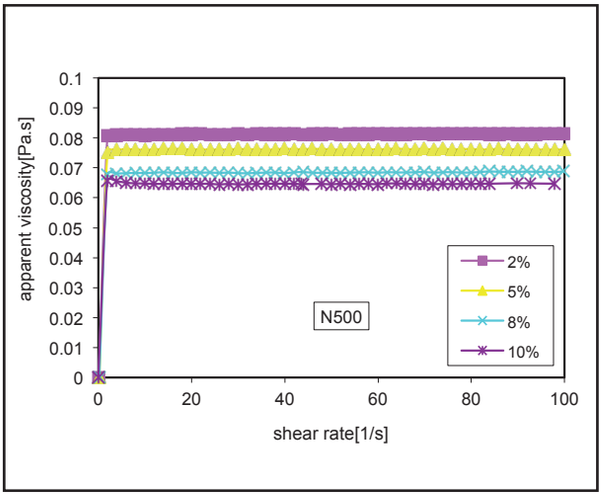


Fig. 28. Shear rate vs. apparent viscosity for N500 blends, at T=40°C.

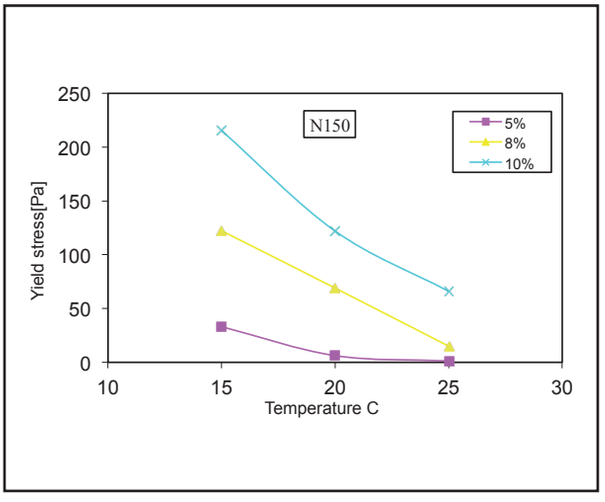


Fig. 29. Yield stress at different temperature for N150 blends

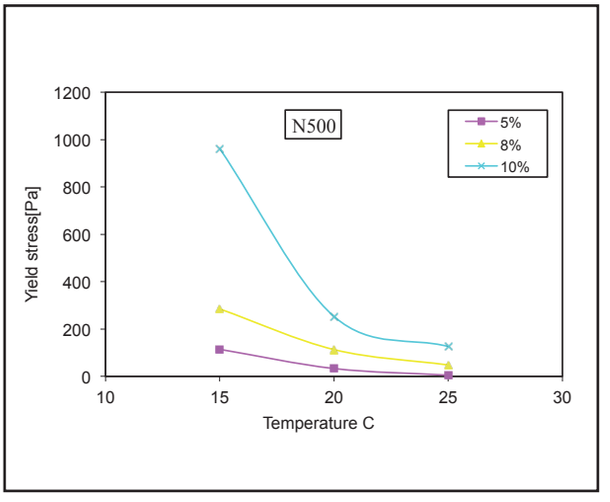


Fig. 30. Yield stress at different temperature for N500 blends

CONCLUSIONS

- Blends from base oil and wax flaks were prepared with wax content ranging (2-10 %wt). Simulating waxy crude oils.
- The flow behaviors of the produced blends were measured using rotational viscometers at temperature (15-60°C).
- The increase of wax content found to alter the flow behavior from Newtonian to non Newtonian with yield stress specially at low temperatures.
- Experimental results indicate that wax content and temperature are the main parameters affecting the viscosity and flow behavior.

REFERENCES

Barry, E. G. (1971). Pumping of non-Newtonian waxy crude oils, *J. Inst. Pet*., (Mobile and Development Corporation, NJ) 57 554.

Al-Zahrani, S. M. and Al-Fariss, T. F. (1998). A general model for the viscosity of waxy oils. *Chemical Engineering and Processing* 37: 433–437.

El-bousiffi, M., Mohamed, F. and Abu Shuwerb, F. (2006). Rheological Properties of Waxy Crude Oils: *An Experimental Study*: 13p.

Rashaida, A. (2005). Flow of A non-Newtonian Bingham plastic fluid over a rotating disk, Unpublished *PhD Thesis Dissertation*, University of Saskatchewan, Canada.

Thermodynamic Analysis for Nitric Acid Plant

Mohammed E. Said* and Basma N. Dakhil

Abstract: A thermodynamic energy analysis based on the first and second laws were performed for small size nitric acid plant with a capacity of (20000 tons/ year) to produce (50 to 60) % nitric acid.

The lost work available energy to produce work was calculated for each unit and the total lost work of the plant was determined and found to be about (3.5MW), the lost work of the reactor unit represents (59.326%) of the total lost work. This means that irreversibility which causes lost work is severe for the reactor. Any improvement of the operating condition which reduces irreversibility of the reaction would improve the efficient use of energy of the overall plant, that is, reduce lost work or available energy for work.

This method of analysis can be used to pinpoint location of excess energy use in the chemical processes. However, it is the role of process engineers to recommend ways to reduce such waste of energy to the minimum possible and yet keep the process feasible.

Keywords: Nitric acid, thermodynamic, energy analysis, energy losses, plant efficiency.

INTRODUCTION

Nitric acid is an important chemical species for many industries. It is widely used in the production of fertilizers, explosives, etching of metals, wood finishing, and cleaning of food and diary equipment. On industrial scale, Ostwald's method is used to produce aqueous acid at about 60%by oxidizing ammonia with air. The following sequence of reactions takes place:

$$2NH_3\,(g) + 5/2\,O_2 = 2NO(g) + 3H_2O(g)$$
$$2NO(g) + O_2 = 2NO_2(g)$$
$$3NO_2(g) + H2O(l) = 2HNO_3(aq) + NO(g)$$

The production cost of nitric acid has a considerable effect on the cost of other products which use nitric acid as a raw material or otherwise. Therefore, any attempt to reduce the overall cost of nitric acid plants will contribute to the reduction of the cost of other products such as fertilizers (Chilton, 1931).

This study applies basic thermodynamic analysis to a 60% 20,000 ton/year nitric acid plant in order to assess energy utilization of this plant. The aim of this analysis is to evaluate energy losses (lost work) at each process step that otherwise could be partially recovered as useful energy instead of being wasted. It is then up to process engineers to come up with bright ideas to develop new process synthesis for new plants or carry out modifications on existing plants that cuts the energy cost of these plants. That is, this analysis pinpoint locations in the process where excessive energy losses take place, and therefore, concentrate efforts to reduce these losses. However, since real processes must always result in some energy losses, the target should be to reduce these losses while evaluating the economics of any process modifications which leads to the least feasible minimum cost design.

BASIC THEORY

Thermodynamic analysis of chemical processes is based on application of the combined equation derived from first and second laws of thermodynamics. For a steady state process, neglecting changes in potential and kinetic energies, the first law (energy balance) reduces to:

$$\Delta H = Q + W_s$$

And the second law (entropy balance) is given by:

$$\Delta S_{fs} - Q/T_0 = \Delta S^t \geq 0$$

* Chemical Engineering Department, Tripoli University Tripoli-Libya
Correspondence author: Email – 17fb@gmail.com.said

Where, ΔS_{fs} is the entropy change of the flowing streams, ΔS^t is the total system and surrounding entropy changes, and T_0 is the ambient temperature.

For a completely reversible (ideal) process Q is given by:

$$Q_{rev} = T_0 \Delta S_{fs}$$

Therefore, substituting this into the first law equation gives:

$$W_{s(rev)} = \Delta H - T_0 \Delta S_{fs}$$

Since the ideal work ($W_{id} = W_{s(rev)}$) and the real work ($W_{real} = W_s$) the lost work (W_{lost}) is defined as:

$$W_{lost} = W_{real} - W_{id}$$

Substituting W_{real} and W_{id} by their values above leads to:

$$W_{lost} = T_0 \Delta S^t \geq 0$$

This last equation states that the lost work (energy available for work) is either zero for ideal processes and positive for practical (real) processes. This equation is used to calculate the lost work for each step or equipment of the chemical process and then summed up to give the total lost work of the plant (Smith *et al* 2001).

RESULTS

The first step of this analysis is to carry out detailed calculations of the material and energy balances on the plant flow sheet Fig. 1. The results are given in Table 1. Then entropy changes for each process step (unit operation) are carried out using well known thermodynamic relations (Perry's Chemical Engineers Handbook, 2008). However, in order to use these relations hypothetical paths from the initial to the final state must be devised so that these relations may be applied. An example to illustrate this point is given by Fig. 2 for the absorption unit which produces the aqueous acid. reaction. Table 2 summarizes the lost work of the plant units. Fig. 3 and Fig. 4 compare the lost work calculated for different units percent-wise and in quantities of kW, respectively.

DISCUSSION AND CONCLUSION

The results of the thermodynamic analysis carried out for the nitric acid plant considered here indicate clearly that about 85% of lost work calculated for the whole plant comes from the ammonia oxidation reactor and the waste heat boiler to generate steam. This leads to the conclusion that the major source of the plant inefficiencies is located at these two equipments, and therefore, any process alteration regarding these two units may improve their efficiencies and reduce lost work of the plant. It is then the role of the process engineer to devise these alterations and check their improvements on the efficiency of the plant and evaluate these alterations economically to determine the most efficient and cost effective one. In this plant, since the oxidation reaction is exothermic, a possible alteration is to divide the reactor into zones so that the reaction may proceed progressively with intermediate cooling to reduce irreversibility which causes lost work.

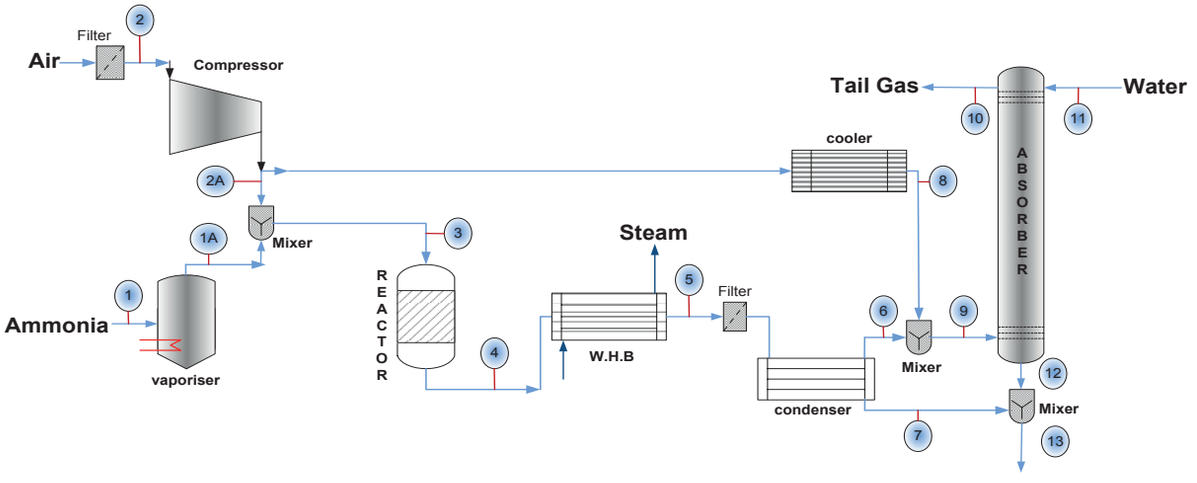


Fig. 1. Plant flow sheet.

Table 1. Mass balance {flows (Kg / hr)}

Line No. stream / Component	1 Ammonia Feed	1A Ammonia Vapor	2 Filtered Air	2A Oxidizer Air	3 Oxidizer Feed	4 Oxidizer Out let	5 W.H.B Out let	6 Condenser Gas	7 Condenser Acid	8 Secondary Air	9 Absorber Feed	10 Tail Gas	11 Water feed	12 Absorber Water	13 Product Acid
NH_3	731.0	731.0	----	----	731.0	----	----	----	-----	-----	----	----	----	----	----
O_2	----	----	3063.9	2628.2	2628.2	935.7	935.7	275.2	-----	408.7	683.9	371.5	----	----	----
N_2	----	----	9990.8	8644.7	8644.7	8668.8	8668.8	8668.8	-----	1346.1	10014.7	10014.7	----	----	----
NO	----	----	----	----	----	1238.4	1238.4	202.5	-----	----	202.5	21.9	----	----	----
NO_2	----	----	----	----	----	-----	----	967.2	-----	----	967.2	----	----	-----	----
HNO_3	----	----	----	----	----	----	----	----	850.6	-----	----	----	----	1704.0	2554.6
H_2O	----	----	----	----	----	1161.0	1161.0	29.4	1010.1	----	29.4	26.3	1376.9	1136.0	2146.0
Total	731.0	731.0	13027.7	11272.9	12003.9	12003.9	120039	10143.1	1860.7	1754.8	11897.7	10434.4	1376.9	2840.0	4700.6
Press (bar)	8	8	1	8	8	8	8	8	1	8	8	1	8	1	1
Tem (c^0)	15	20	15	230	204	907	234	40	40	40	40	25	25	40	43

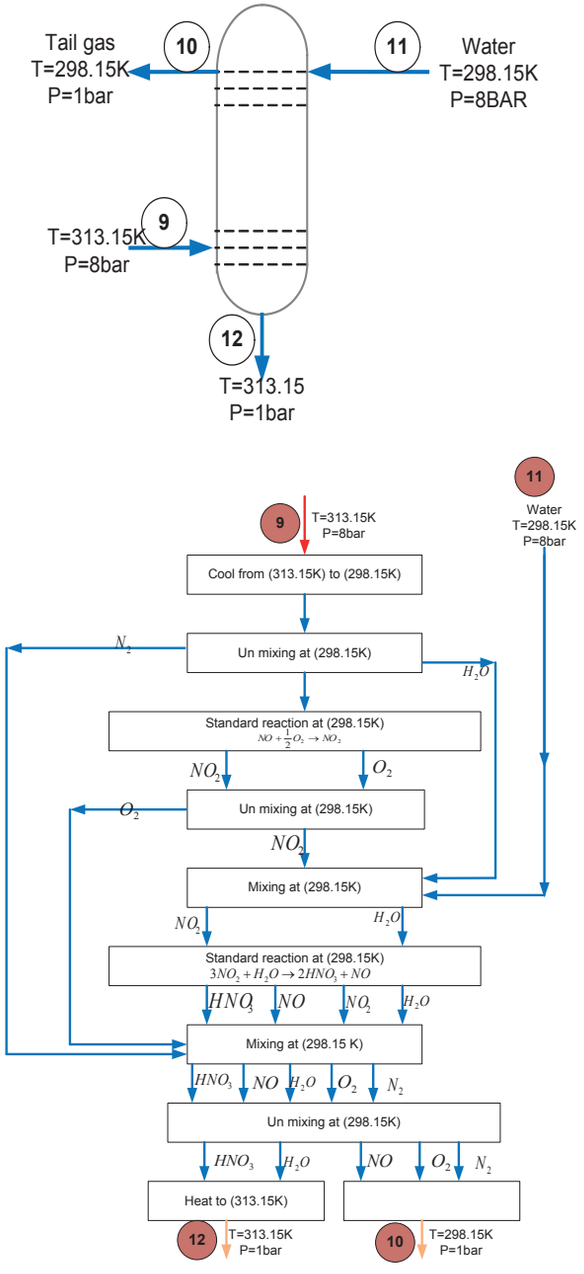


Fig. 2. Hypothetical path for ΔS calculation of the absorber

Table 2. (Summary of lost work the plant)

Unit	lost Work (Kw)	% of total
Reactor	2304.22	59.326
W.H.B	969.59	24.96372
Mixer(1)	230.841	5.943388
Mixer(2)	165.8335	4.269661
Absorbed	81.67	2.102731
Mixer(3)	79.7445	2.053156
Cooler	21.5879	0.555817
Condenser	12.263	0.315731
Compressur	10.617	0.273352
Vaporiser	7.6298	0.196442

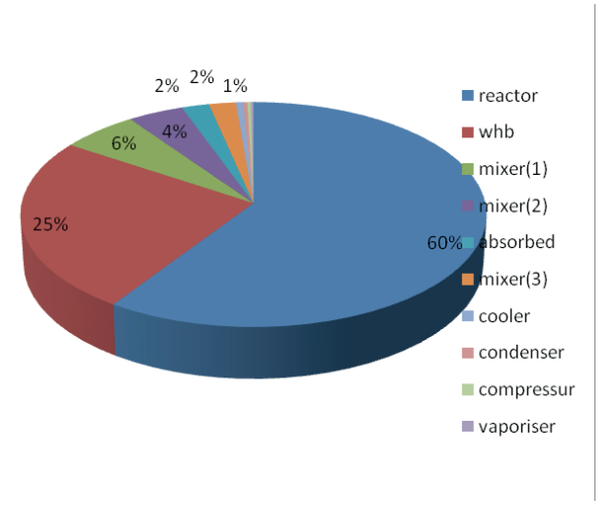


Fig. 3. Lost work percentage comparison

However, the increase in capital cost as a result should be compared to the savings on energy from lost work reduction. For the waste heat boiler unit, In general, maximizing feed water inlet temperature and reducing generated steam temperature will lead to less irreversibility, lower lost work, and higher thermal efficiency. On the other hand, the generated steam will be of lower quality.

Finally, the following concluding remarks regarding this thermodynamic method of analysis can be summarized:

1 Lost work analysis is a powerful tool to evaluateprocess designs from the standpoint of energy utilization.
2 The method locates major sources of wasteful energy, but gives no hints on process changes to reduce them.
3 It directs the attention of the process engineer to the steps or equipments where process modifications can lead to considerable energy savings.
4 For newly designed plants, application of the analysis can result in highly efficient and environment-friendly processes.

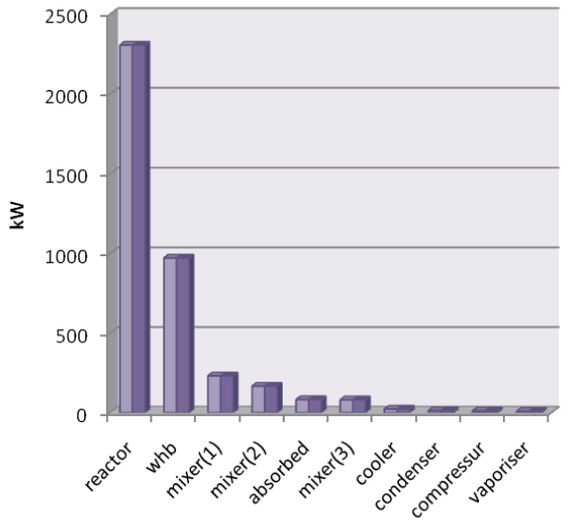


Fig. 4. Lost work (kW) comparison)

5 For existing plants, however, any feasible process modifications based on this analysis must be assessed considering plant layout, safety, controllability, etc.

RFERERENCES

Chilton, C. H. (1931). The Manufacture of Nitric Acid by the Oxidation of Ammonia. *American Institute of Chemical Engineers, Ind. Eng. Chem,* 23(8): 860-865.

Smith, J. M. Van Ness, H. C. and Abbott, M. M. (2001). Introduction to Chemical Engineering Thermodynamics, Sixth Edition. McGraw-Hill: 316p.

Perry's Chemical Engineers Handbook (2008). *8th Edition*, McGraw-Hill: 2640p.

A Study of Precipitation and Flocculation of Calcium Carbonate and Magnesium Hydroxide in Alkaline Flooding

Wei Tian*, Ezeddin Shirif**, Mingzhe Dong***

Abstract: Precipitation of multivalent ions has been recognized as a major problem in oilfield operations. In alkaline flooding, precipitation of calcium carbonate and magnesium hydroxide, known as alkaline scaling, is a major concern, despite its vital role in increasing heavy oil recovery. In this study, several types of polymers were examined to investigate their potential of minimizing the total suspended solid from injection water. It was found that certain polymers successfully reduce 99% of suspended solid from water which strongly assist flow injection system and prevent scale formation in surface and subsurface equipments.

Keywords: Alkaline Flooding, Calcium Carbonate, Precipitation, Flocculation

INTRODUCTION

The precipitation of insoluble deposits is an undesirable phenomenon in oilfield and industry technology. The noted concern has been given serious attention since precipitation and scale problems have caused considerable damage in surface and subsurface facilities. The precipitated material, which forms during injection or production processes, gets accumulated and settled on pipeline walls and which eventually forms a thick impermeable layer of scale. Moreover, the issue becomes more crucial in oilfield operations when precipitation and scale problems lead not only to formation damage but also to a decline in oil production, emergency shutdown, and production intervals (Moghadasi *et al* 2003), (Voloshin *et al* 2003; Al-Rawajfeh *et al* 2005).

Alkaline scale is known as the precipitation and deposition of calcium carbonate ($CaCO_3$) and magnesium hydroxide $Mg(OH)_2$ in alkaline solution (Cowan and Weintritt 1976). This precipitation is formed due to several factors. The main factor is the crystallization of the inversely soluble salts calcium carbonate, magnesium hydroxide and calcium sulphate, in declining rank. In alkaline flooding, as a result of increasing pH value from as high as 13.5 to near 7 at various points within the reservoir, some active hydrated material initially develops and converts to be less active and in more crystalline form. This process with adequate reactive surface, first results in precipitation of magnesium hydroxide and then calcium carbonate as the magnesium form is less soluble than the calcium form in a pH range of 9 to 11. The overall reactions mechanism governing the alkaline scale can be expressed as follows. A substantial amount of OH- ions in presence of CO_2 results in a strong alkaline aqueous solution.

$$CO_3^{2-} - H_2O \leftrightarrow CO_2 + 2OH^- \quad 2.1$$

$$Ca^{2+} + CO_3^{2-} \leftrightarrow CaCO_3 \quad 2.2$$

$$Mg^{2+} + 2OH^- \leftrightarrow Mg(OH)_2 \quad 2.3$$

Chemical techniques are known to be the most effective scale removal and prevention treatments in oilfield and industry operations. These include chemical precipitation, acid injection, addition of anti-scaling compounds and polyelectrolyte.

For the purpose of controlling the alkaline scale (calcium carbonate and magnesium hydroxide), several methods such as acid injection, acid forming salts, acid forming gases and polyelectrolyte techniques have been reported in the literature. Acid injection methods are based mainly on lowering the pH, in order to eliminate the scale. Different types of acids including sulphuric acid and hydrochloric acid have been proposed and used. However, using a

*Petroleum Systems Engineering, University of Regina, SK, Canada.
**Chemical and Petroleum Engineering, University of Calgary, AB, Canada.
***Correspondence author: Email – Ezeddin.Shirif@uregina.ca

strong acid such as hydrochloric acid may cause other problems like corrosion which results in increased cost of operation or production. Thus, strong acids are not recommended (York and Schorle, 1966). Some other methods were used to control alkaline scale such as the addition of acid forming salts (Ferric chloride, sodium acid, ferric sulphate and aluminium chloride). In this work, an experimental study focusing on precipitation calcium carbonate and Magnesium hydroxide has been done. The study focuses on the removal of scale forming constituents from injection water.

EXPERIMENTAL

In this study, a series of four major experiments have been conducted, Graduate Cylinder Test and Sedimentation Column Test have been carried out to study the capability of polymers in settling the solid particles from injection (brine/alkaline/polymer) water. Permeability measurements have also been done to investigate the potential of polymer in increase flow process, Flocculation Flow Test has been done to study calcium carbonate and magnesium hydroxide precipitation mechanism in dynamic process. All experiments were conducted at ambient temperature (22± 0.5°C) using sodium hydroxide solution at a constant concentration of 0.4 wt%.

Fluids and Chemicals: Pelican brine samples were collected from a heavy oil reservoir in Western Canada. The samples were analyzed by the Saskatchewan Research Council analytical lab and formulated in the lab for experimental use. The analyses of formation brine are shown in Table 1. In addition, four anionic polymers and six cationic polymers have been selected for study. Types and specification of those polymers are shown in Table 2.

Measurement of Total Suspended Solid: The main task in this study was to determine the total suspended solid for such a composition (brine/alkaline) solution, which will help in investigating capability of polymer in removing the suspended material. The base value for the total suspended solid (mg/kg) was obtained theoretically and experimentally.

The theoretical value was calculated according to the following chemical reaction;

Table 1. Analysis of Pelican Brine Composition.

Properties	Percentage (%)
Ph @ 20 °C	7.27
Chloride, mg/l	15600
Sulfate, mg/l	2
Sodium, mg/l	8900
Calcium, mg/l	380
Magnesium, mg/l	280
Iron, mg/l	0.62
Potassium, mg/l	80
Total dissolved solids, mg/l @ 110 ° C @ 180 ° C	 28020 27560
Bicarbonate as $CaCO_3$, mg/l	1360
Sulfide as H_2S, mg/g	120

Table 2. Specification of utilized Polymers.

Polymer Name	Polymer Type	Mw (MM)	Cationic Degree (%)	Hydrolysis Degree (%)
AN 934 PGO	Anionic	20	-	35
AN 934 PG1	Anionic	20	-	35
AN 910 PGO	Anionic	13	-	10
FA 920 PGO	Nonionic	10	-	<1
C 5045	Cationic	10	45-50	-
C 3035	Cationic	5-6	30-40	-
C 5015	Cationic	10	15-20	-
C 3098	Cationic	5-6	90-100	-
DC 4015	Cationic	7-8	15-20	-
DC 4070	Cationic	7-8	70	-

$$Mg^{2+} + 2\left(OH^{-}\right) = Mg(OH)_2 \quad (1)$$

$$HCO_3^{-} + (OH)^{-} = H_2O + CO_3^{2-} \quad (2)$$

$$Ca^{2+} + CO_3^{2-} = CaCO_3 \quad (3)$$

$$Ca^{2+} + HCO3^{-} + (OH)^{-} = H_2O + CaCO_3 \quad (4)$$

By calculating the reaction constant K_1, K_2, K_3, and K_4 and solubility constant Ksp, both the total suspended solid TSS (mg/kg) & total dissolved solid TDSW (mg/kg) were found to be 1600 mg/kg and 0.0284 mg/kg respectively.

The experimental measurement was studied at room temperature with a constant alkaline (0.4wt %) and polymer concentration (0.5-3 ppm). A Watman filtration paper number 41, with a fast flow property, was dried for two hours in a 105^{o}C oven and weighed until the net weight was obtained. Then the paper was carefully dropped onto a metal desk on the filtration apparatus. After all the liquid was filtrated, the wet paper was immediately measured after the last drop of liquid passed. It was then placed in an oven for drying, for two hours. The paper was weighted again and measurement was repeated twice for this step in order to reduce errors. Total suspended solid was calculated using a calculation method, as shown in Table 3.

To calculate the removal efficiency of precipitation solid, the total volume of suspended solid per litre was obtained, theoretically and experimentally. Those values were 1600 mg/kg and 1440 mg/kg, respectively. The theoretical value 1600 mg/kg was taken into consideration to calculate the removal efficiency because of possible errors appearing in the experimental result. There are two possible reasons for this error. First, during the filtration process, some particles stick on the wall of the filtration cylinder and do not form sediment on the precipitation cake. Secondly, some fine precipitation particles could pass through the filtration paper.

Settlement Test: Two main experiments were performed to select the best polymer, concentration and mixing technique. Firstly, screening test experiments were carried out in a 250 ml graduate cylinder. A volume of 200 ml, 0.4 wt% NaOH solution was used for each set of the test at different polymer concentration (1, 2, 3 and 5 ppm). Both polymer, Alkaline and brine solution were prepared at desirable concentration and a given amount of brine was added to a 1 litre plastic bottle during each experiment. Then a measured volume of alkaline solution was transferred to the bottle with a syringe. Afterward, cylinder was turned ten times from horizontal position to vertical position and left for two minutes, and then a certain volume of polymer was added to the aqueous solution with a syringe. The bottle was turned ten times from vertical to horizontal and finally the solution was poured into a graduate cylinder for measurement. Measurement starts when the interface of the precipitation begins to settle in the graduate cylinder. Both time and volume were continuously recorded until precipitation remained constant at the bottom of the cylinder. Fig. 1 shows graduate cylinder test and the experimental procedure.

Secondly, Sedimentation Test experiments were carried out at three different settlement times, 60, 35 and 45 minutes, respectively. Also, two types of mixing were used in this test. First, when settlement times were 60 and 35 minutes, a bottle-rolling technique (10 + 10) was used. Secondly, when settlement time was 40 minutes, a rotating technique was used (2 minutes mixer+15 minutes rotating at 10.5-11 rpm using a speed reducer device). Furthermore, at each settlement time,

Table 3. Measurement of total suspended solid.

Sample	Polymer (C) ppm	Vol.(kg)	W (B)	W.dry (B+P)	W.wet (B+P)	W.dry (B+P+S)	TS (g)	TDS (g)	TSS (mg/kg)
Brine+NaOH	0	0.5298	34.1981	34.3389	34.7408	34.3608	0.0219	0.0108	21
AN 934 PG1	3	0.5100	36.8713	37.0073	37.3854	37.0238	0.0165	0.0103	12
C 5015	3	0.5119	34.1963	34.3350	34.7646	34.3533	0.0183	0.0117	13
AN 934 PG1	0.5	0.5247	36.8696	37.0073	37.3692	37.0255	0.0182	0.0097	17
C 5015	0.5	0.5102	28.4493	28.5926	29.0016	28.6114	0.0188	0.0111	15

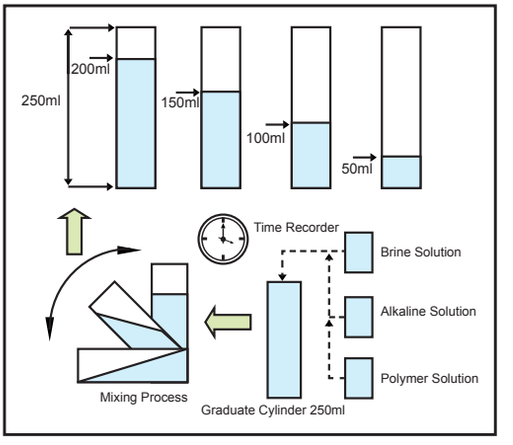
B: Beaker P: Paper S: Sedimentation TS: Total solid
TDS: Total Dissolved Solid TSS: Total Suspended Solid

the removal efficiency of each type of polymer was investigated (AN 934 PG1 and C 5015) at three polymer concentrations (0, 0.5 and 3 ppm). Total suspended solid and settlement time for each polymer concentration was obtained. Fig. 2 illustrates sedimentation column test apparatus and procedure.

Permeability Test: The objective of this test is to understand the capability of polymer in increasing the flow process. Polymer particles combine with small precipitation particles and form larger particles. Consequently, the solution liquid travels between particles and the process becomes much faster. Permeability of precipitation cake was measured at constant pressure and at volumes of solution ((3 kg, 750 gram). Both, concentrations of alkaline solution and polymer were constantly maintained at 0.4% and 3 ppm, respectively. After mixing, the solution was left overnight for settlement and the following day the solution was carefully and repeatedly added to the filtration cylinder. This test was undertaken for 40-60 hours until all the liquid filtrated through a filter paper. During the test, data for pressure, time and filtrated volume were recorded at regular intervals by using a constant rate slow pump filtration. A pressure gauge was used to measure pressure values during the experiment.

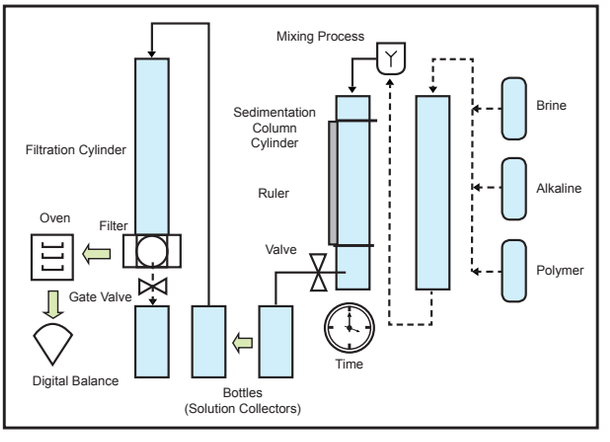


A



B

Fig. 1. Settlement Test. (A) Graduate Cylinder equipment; (B) Test Procedure.



A



B

Fig. 2. Sedimentation Test. (A) Test Procedure; (B) Test Apparatus.

Flocculation Flow Test: Efficiency of polymer usage during injection flow process was evaluated throughout this test. By giving sufficient mixing time to alkaline and polymer solution, polymer particles were allowed to communicate and get attached with other particles forming large flogs. Two sets of flocculation experiments were accomplished, a screening test with only alkaline and brine and then with a polymer AN 935 PG1 at 3 ppm. Measurement of total suspended solid and removal efficiency was performed and good results were obtained. Fig. 3 shows experimental set up for Flocculation Flow Test.

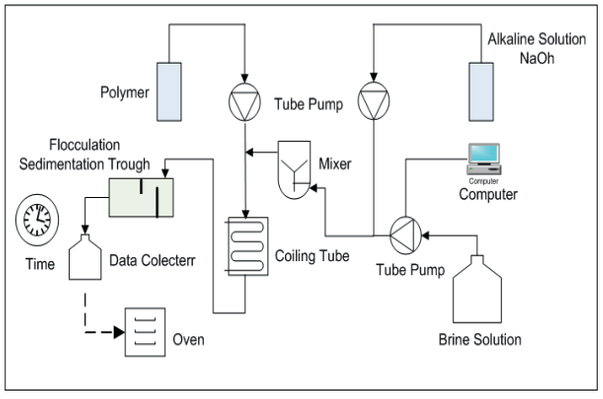
A flocculation sedimentation trough model was designed to measure the removal efficiency of suspended solid from clear liquid. Precipitation settled in a flocculation sedimentation trough and clear liquid was collected from the model output. A premixing tube (DI 7/16" and V 46.3 ml) was used to mix the suspension liquid brine and alkaline before settlement in the trough. The test was carried out at serious flow rates and two different techniques were developed for flocculation mixing positions (Flat & Wave). At last, data for removal efficiency of anionic polymer was determined.

RESULTS AND DISCUSSION

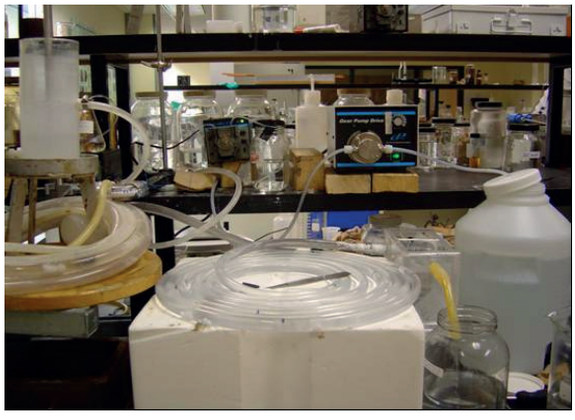
Selection of Polymers: In this study, Graduate Cylinder Test, and Sedimentation Column Measurement were carried out to screen best polymers for Pelican injected water brine. Two polymers (AN 935 PG1 & C 5035) were selected out of ten. Those polymers have provided the faster settlement time as shown in Fig. 4. During screening test, time was regularly recorded at certain reading volumes (150 ml, 100 ml, and 150 ml (again 150 ml)). Those volumes were plotted against time at where precipitation surface was, and then the sedimentation speed was obtained using the following equation:

Results show the settlement rate has the best settlement efficiency when 3 ppm polymer concentration is used, as described in Fig. 5. At constant polymer concentration (3 ppm), the settlement rate achieves its optimum value, as compared with other concentrations. This polymer concentration is a proper concentration that could be used in future experiments to demonstrate the polymer potential of precipitation removal of calcium carbonate and magnesium hydroxide from injection water. Among two different mixing techniques, results of sedimentation experiments show that rotating technique using speed reducer device at 10.5-11 rpm provide good mixing status. Moreover, values acquired of total suspended solid confirm proper polymer concentration is 3 ppm as showing in Fig. 6.

Permeability Measurement: Filtration test results indicate the polymer accelerates the flow process. As the size of particles increase, more and wide channels are created through the precipitation cake. Thus, the cake permeability becomes higher. However, when all precipitation sediment is on the filtration cake, the permeability reaches its minimum value. The effect of polymer can be seen through a comparison where no polymer is added to a solution and at 3 ppm polymer concentration.



A



B

Fig. 3. Flocculation Flow Test. (A) Test Procedure; (B) Experimental Set up.

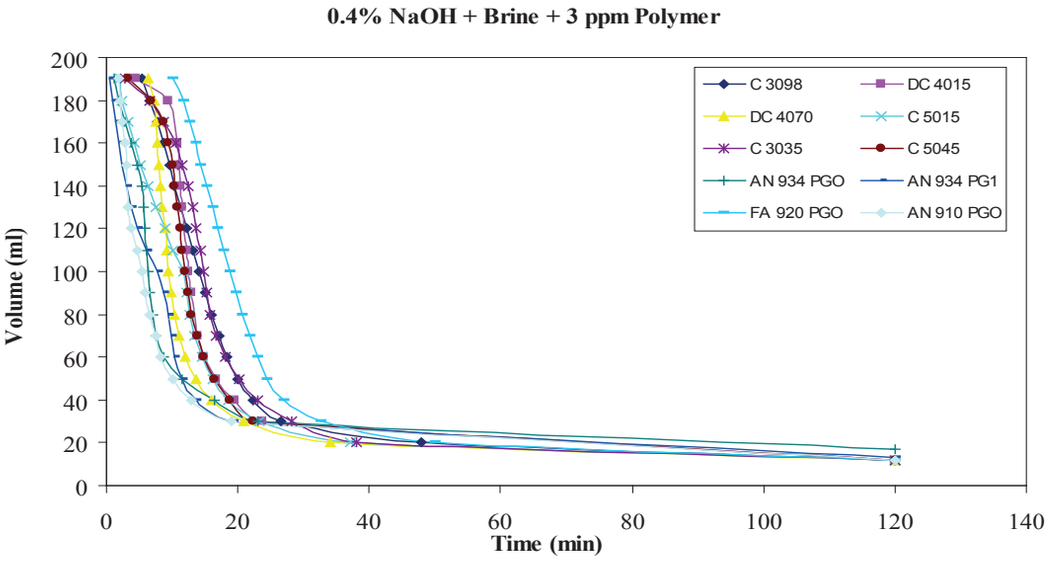


Fig. 4. Settlement rate of polymers at 3 ppm polymer concentration.

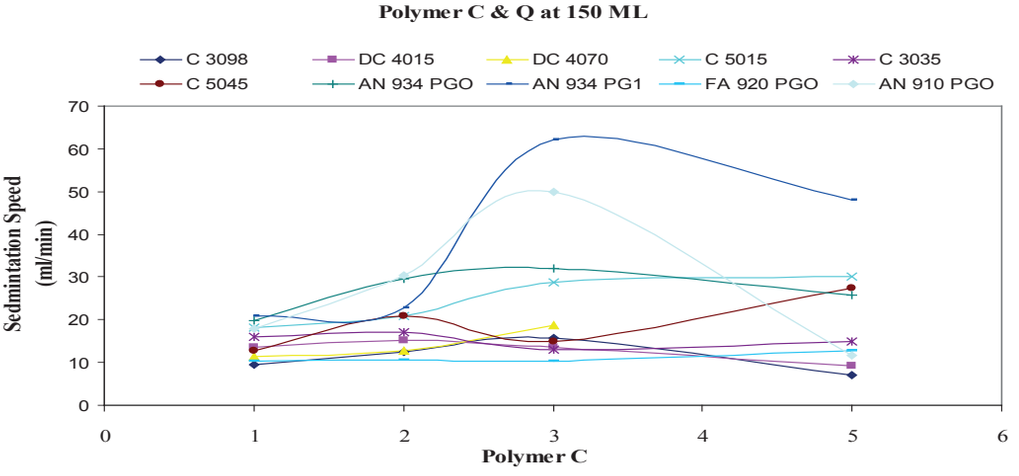


Fig. 5. Sedimentation Rate for all Polymers at a Constant Volume of 150 ml.

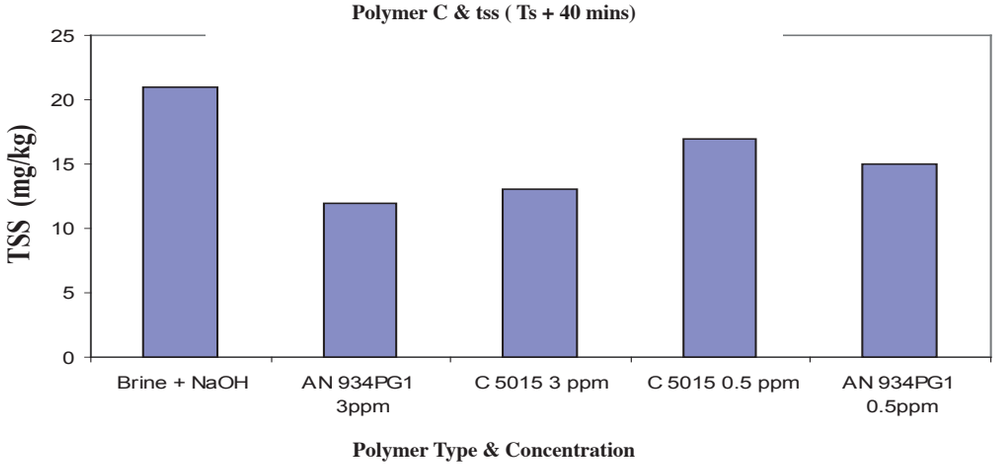


Fig. 6. Total Suspended Solid Data at a Sedimentation Time of 40 Minutes.

The filtration permeability is higher in presence of polymer than when no polymer added. However, the permeability declines during the filtration process as more sediment particles settle on the filtration paper and the cake's thickness increases. Fig. 7 illustrates permeability measurements for 3 kg solution.

Flocculation & Removal Efficiency Test: To represent the injection flow process, flocculation flow experiments were performed to investigate the polymer potential of increasing the removal efficiency and to reduce the total suspended solid from the clear liquid. Results show that at a low flow rate, the amount of solid particles increase slowly with increase of flow rate, until it reaches a certain value called critical flow rate. Beyond critical flow rate, solid particles in the clear liquid tend to increase rapidly. This phenomenon is represented in flocculation screening test where no polymer was added to solution. Afterward, in second test when polymer was added to the suspension liquid, 99% removal efficiency of suspended solid in clear liquid was obtained. This percentage indicates the success of using polymer for injection water treatment. Results also clearly demonstrate the necessity of using certain techniques of polymer handling in order to achieve high removal efficiency values. Fig. 8; represent removal efficiency of Anionic polymer.

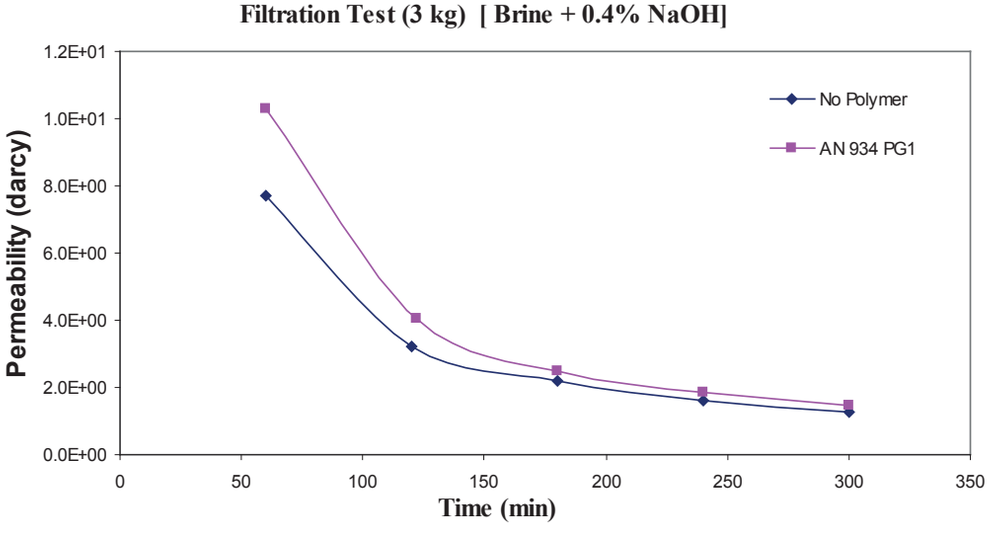


Fig. 7. Permeability Measurement for 3 kg solution.

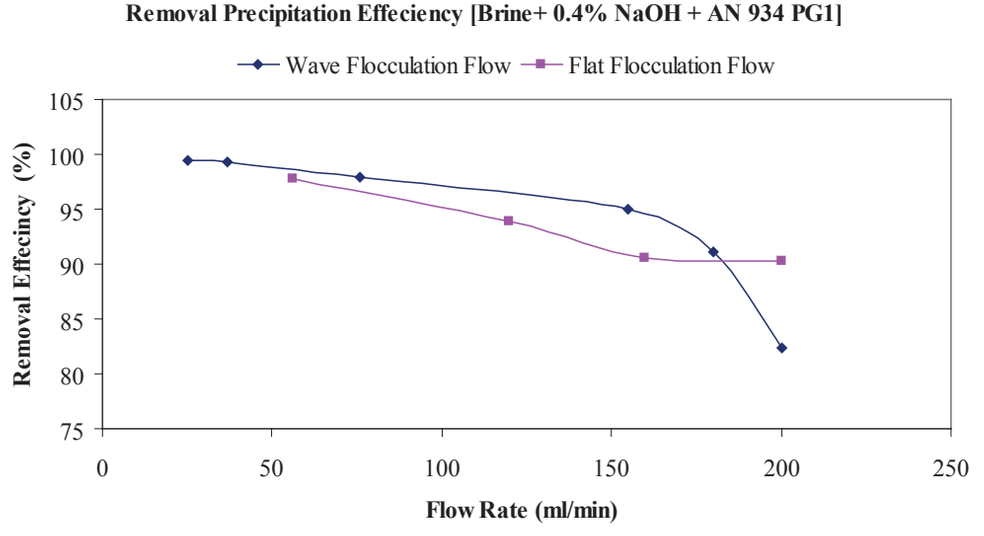


Fig. 8. Removal Efficiency of Anionic Polymer AN 934 PG1.

CONCLUSIONS

Based on the presented results, the following conclusions can be drawn:

1) Experiments of settlement and sedimentation rates indicate anionic polymers have better precipitation removal efficiency than cationic polymers and are highly recommended for use in practical implementation.
2) The prerequisite experimental setup for all precipitation tests was designed to measure the feasibility of polymer by reducing the total suspended solid from injection water.
3) The maximum removal efficiency was achieved by using Anionic polymer AN 934 PG1 at 3 ppm concentration and it reached 99%.

REFERENCE

Al-Rawajfeh, A., Glade, H. and Ulrich J. (2005). Scaling in Multiple Effect Distillers: The Role of CO_2 Release. *Desalination:* 209-219.

Cowan, J. and Weintritt, D. J. (1976). Water Formed Scale Deposit. *Gulf Publishing Company, Houston, Texas*: 596p.

Moghadasi, J., Jamilahmadi, M., Muller-Steinhagen, H. and Sharif A. (2003). Scale Formation in Iranian Oil Reservoir and Production Equipment During Water Injection. *SPE Paper No. 80406*.

Voloshin, A. I., Ragulin, V. V., Tyabyeva, N. E., Diakonov I. I and Mackay E .J. (2003). Scaling Problems in Western Siberia. *SPE Paper No.80407*.

York, J. L. and Schorle, B. J. (1966). Principles of Desalination (*Chapter 10)*. In: K. S. Spiegler (ed.): 497-514.